URINARY PROTHROMBIN FRAGMENT 1:

A potential role-player in the protection of South African blacks from calcium oxalate kidney stone disease

Dawn Webber

Thesis presented for the Degree of

DOCTOR OF PHILOSOPHY

In the Department of Chemistry

UNIVERSITY OF CAPE TOWN

August 2003

ACKNOWLEDGEMENTS

I am deeply indebted to many people, but especially to the following, without whom this thesis could not have been completed.

Professor Allen Rodgers... for inspiring me to undertake the challenge of stone research and protein biochemistry, and for being a constant source of encouragement and knowledge,

Dr Ed Sturrock... for agreeing to train a chemist in the demanding area of biochemistry, for his expert supervision, and most especially for his good humour,

Professor Rose Ryall... for generously sharing her considerable expertise on UPTF1 with me and for her supervision during my visit to her laboratory,

Dr Pauline Rudd... for her keen interest in and supervision of my research during my visit to her laboratory,

Ms Shameez Allie... for her enthusiastic assistance with practical and intellectual problems during my thesis, but just as importantly for her moral support and friendship,

Mrs Diane Pinnock, Mrs Gretchen Baretta and Mrs Jeanette Durbach... for their generous assistance and encouragement in the laboratory every day,

Ms Sylva Schwager... for teaching me about proteins and biochemistry, and for her assistance with setting up the protein purification method,

Mrs Catherine Radcliffe, Dr Tony Merry and Dr Louise Royle... for teaching me about the fascinating field of glycobiology,

Ms Magali Chauvet... for her enthusiastic assistance with the proteolysis experiments and FESEM work,

All of my colleagues... in the Kidney Stone, Medical Biochemistry and Glycobiology Laboratories, for their genuine interest and support during the daily trials of laboratory work,

And to the following individuals for offering their services,
Professor Wolf Brandt... protein sequencing, *Dr David Harvey...* glycan MALDI-TOF MS, *Dr Jerry Rodrigues...* amino acid analysis, *Dr Louise Royle...* glycan QTOF MS, *Ms Sylva Schwager...* protein MALDI-TOF MS, and *Dr Mark Wormald...* glycan modeling,

My parents and sister... for sustaining me in other areas of my life, and especially to René for her encouragement and expert advice both as a sister and a fellow researcher,

And finally to my husband Colin... for his unfailing belief in my potential which sustained and uplifted me throughout this journey.

PUBLICATIONS

Durrbaum D, Rodgers AL, Schwager SLU, and Sturrock ED. 2000. Characterisation and preliminary inhibitory study of urinary prothrombin fragment 1 (UPTF1) from two population groups in South Africa. In: Rodgers AL, Hibbert BE, Hess B, Khan SR, and Preminger GM, editors. Urolithiasis 2000. University of Cape Town, Cape Town, 153-155.

Durrbaum D, Rodgers AL, and Sturrock ED. 2001. A study of crystal matrix extract and urinary prothrombin fragment 1 from a stone-prone and stone-free population. *Urol Res* 29: 83-88.

Durrbaum D, Rodgers AL, and Sturrock ED. 2001. Urinary prothrombin fragment 1: black or white? In: Kok DJ, Romijn HC, Verhagen PCMS, and Verkoelen CF, editors. Eurolithiasis: 9th European Symposium on Urolithiasis. Shaker Publishing, Netherlands, 205-206.

Webber D, Rodgers AL, and Sturrock ED. 2002. Synergism between urinary prothrombin fragment 1 and urine: A comparison of inhibitory activities in stone-prone and stone-free population groups. *Clin Chem Lab Med* 40:930-936.

Webber D, Rodgers AL, and Sturrock ED. 2003. Intracrystalline UPTF1 in black and white South Africans: Does it decide their fate? *Urol Res* 31:91.

Webber D, Rodgers AL, and Sturrock ED. 2003. Selective inclusion of proteins into urinary calcium oxalate crystals: Comparison between stone-prone and stone-free population groups. *J Crys Growth*, accepted for publication July 2003, in press.

CONFERENCES

Poster & oral summary, 9th International Symposium on Urolithiasis, Cape Town, February 2000

"Characterisation and preliminary inhibitory study of urinary prothrombin fragment 1 (UPTF1) from two population groups in South Africa"

Poster, 9th European Symposium on Urolithiasis, Rotterdam, September 2001

"Urinary prothrombin fragment 1: black or white?"

Invited speaker, FASEB (Federation of the American Society of Experimental Biology) Summer Research Conference on Calcium Oxalate in Biological Systems, Vermont, August 2002

"UPTF1 in black and white South Africans: More questions than answers"

Poster, 10th European Symposium on Urolithiasis, Istanbul, June 2003

"Intracrystalline UPTF1 in black and white South Africans: Does it decide their fate?"

OVERSEAS STUDENTSHIPS

Urology Laboratory, Department of Surgery, Flinders Medical Centre, Adelaide, Australia
Supervisor: Professor Rosemary Ryall
October – November 2001

Glycobiology Institute, Department of Biochemistry, University of Oxford, England
Supervisor: Dr Pauline Rudd
March – June 2003

SUMMARY

The incidence of kidney stones amongst South Africa's black population is rare. This is in contrast to the white population, whose stone rate is similar to that in Western society. Urine composition alone does not account for these differences. This thesis presents a study of the inhibitory role of the protein, urinary prothrombin fragment 1 (UPTF1), and its biochemical characterisation in both population groups.

In a preliminary study, the urine composition and inhibitory activity of urine and urinary macromolecules from healthy white and black subjects was compared using a spectrophotometric sedimentation assay, zeta potential measurements and particle size analysis. Results suggested greater inhibition by urinary macromolecules in the black group.

UPTF1 was isolated from calcium oxalate (CaOx) crystals and purified by reverse phase (RP)-high performance liquid chromatography (HPLC) from the urine of healthy white (WF1) and black (BF1) subjects. The identity of the purified proteins was confirmed by Western blotting, N-terminal protein sequencing, matrix-assisted laser desorption ionisation time-of-flight (MALDI-TOF) mass spectrometry (MS), amino acid analysis and 2D sodium dodecyl sulphate-polyacrylamide gel electrophoresis (SDS-PAGE); these analyses did not indicate differences in the protein backbone from the two groups. However, alkaline amino acid analysis showed the presence of more γ-carboxyglutamic acid (Gla) residues in BF1. The *N*- and *O*-linked glycans were released by enzymatic and chemical reactions, respectively, and sequenced using exoglycosidase digestions in tandem with RP and weak anion exchange HPLC, as well as MS. These analyses demonstrated a high proportion of sialylated glycans on UPTF1 and a greater number of sialic acid residues on BF1. Molecular modeling located the glycans on the protein's kringle domain and identified a potential mode by which crystallisation could be inhibited.

The inhibitory activity of crystal matrix extract (CME) from healthy white and black subjects, of which UPTF1 is the major component, was compared in synthetic urine. Using Coulter Counter and [^{14}C]-oxalate deposition analysis, and scanning electron microscopy (SEM), CME was shown to inhibit CaOx crystal nucleation, growth and aggregation. These effects were greatest in the presence of the black group's CME. The activity of the purified proteins, WF1 and BF1, were compared in a similar study and were shown to inhibit CaOx crystal growth and aggregation. The inhibitory effects were greatest in the presence of BF1. The activities of WF1 and BF1 were also compared in crystal slurries, prepared with either exogenous CaOx monohydrate (COM) or dihydrate (COD) crystals, using a spectrophotometric sedimentation assay and zeta potential measurements. The relative effects

of WF1 and BF1 were similar, but the potential of UPTF1 to inhibit COM rather than COD aggregation was significantly greater.

The activities of WF1 and BF1 were also compared in urine. A cross-over design was employed in which ultrafiltered urine from both population groups was dosed with WF1 and BF1 (at physiological concentrations). Coulter Counter and [^{14}C]-oxalate deposition analyses, in conjunction with SEM, showed that both proteins promoted CaOx crystal nucleation, but inhibited its growth and aggregation. A synergistic relationship between UPTF1 activity and urine composition was demonstrated, and BF1 was found to be a more efficient inhibitor than WF1 in their endogenous urines.

Possible differences in urine crystal morphology and the proteins included therein were investigated in healthy white and black subjects, as well as in white stone-formers. Urinary CaOx crystals were precipitated and examined using SEM, and their hydrate compositions were determined by x-ray powder diffraction (XRD). The protein and UPTF1 content of the urines and crystals were analysed by SDS-PAGE and Western blotting. A higher proportion of COM crystals were observed in the black subjects, compared with mainly COD in the white group. More of the black subjects' crystals included UPTF1 than amongst the whites.

Pure COM and COD crystals were precipitated from same urine of healthy white and black subjects, and similarly characterised and analysed for their protein content. COM crystals from black subjects contained mainly UPTF1 but also osteopontin (OPN), whereas the same CaOx hydrate from white subjects included only UPTF1. COD crystals from both population groups included mainly OPN. The total amount of intracrystalline protein (per mg CaOx) was greater in the black subjects.

In order to compare their response to dissolution and proteolysis, CaOx crystals from healthy white and black subjects were incubated in saturated and unsaturated CaOx buffers along with proteases. Crystals were examined by field emission SEM. Differences in the response of the typical CaOx hydrates from the two population groups were observed and these were consistent with a greater protective role in the black population.

In this thesis, differences in the activity and structure of UPTF1 from black subjects compared with whites were demonstrated. Different CaOx hydrates typically predominated in the two groups and these were associated with differences in the nature and amount of urinary proteins included therein, as well as their susceptibility to dissolution and proteolysis. All of these trends implicated UPTF1 either directly or indirectly, and were consistent with the rarity of stones amongst the black population. Thus UPTF1 appears to be a potential role-player in the protection of the black population from CaOx kidney stone disease.

ABBREVIATIONS

α_1-m.....	α_1-microglobulin
2AB.....	2-Aminobenzamide
Abs.....	*Arthrobacter ureafaciens* sialidase
ACN.....	Acetonitrile
Amf.....	Almond meal fucosidase
Amps.....	Ammonium persulphate
ANOVA.....	Analysis of variance
Asn.....	Asparagine
BC.....	Black control subject
BF1.....	Urinary prothrombin fragment 1 from black control subjects
Bkf.....	Bovine kidney fucosidase
BMM.....	Black subject's macromolecular urine extract
BSA.....	Bovine serum albumin
BSF.....	Black stone-former
Btg.....	Bovine testes galactosidase
BU.....	Black subject's urine
BUF.....	Black subjects' ultrafiltered urine
CaOx.....	Calcium oxalate
CME.....	Crystal matrix extract
CMP.....	Crystal matrix protein
COD.....	Calcium oxalate dihydrate
COM.....	Calcium oxalate monohydrate
COT.....	Calcium oxalate trihydrate
DTT.....	Dithiothreitol
EDTA.....	Ethylenediaminetetraacetic acid
FESEM.....	Field emission scanning electron microscopy
Gal.....	Galactose
Gla.....	γ-Carboxyglutamic acid
Glc.....	Glucose
GlcNAc.....	N-Acetyl glucosamine
Glu.....	Glutamic acid
GluH.....	*Streptococcus pneumoniae* glucosaminidase
GU.....	Glucose unit
Hex.....	Hexose
HRP.....	Horse radish peroxidase
HPLC.....	High performance liquid chromatography
HSA.....	Human serum albumin
I_A.....	% Inhibition of aggregation (sedimentation rate experiments)
IA.	Iodoacetamide
IgG.....	Immunoglobulin
Jbh.....	Jack bean hexosaminidase
Jbm.....	Jack bean mannosidase
kDa.....	Kilodaltons
mag.....	Magnification
MALDI-TOF.....	Matrix-assisted laser desorption ionisation time-of-flight
Man.....	Mannose
MM.....	Macromolecular urine extract

MS	Mass spectrometry
MSL	Metastable limit
Nani	*Streptococcus pneumoniae* sialidase
NaOx	Sodium oxalate
n.d	No date
Neu5Ac	N-Acetylneuraminic acid
NP	Normal phase
OPN	Osteopontin
PAGE	Polyacrylamide gel electrophoresis
PNGase F	Peptide N-glycanase F
PT	Prothrombin
PTF1	Prothrombin fragment 1
PTF2	Prothrombin fragment 2
PTF1+2	Prothrombin fragment 1+2
QTOF	Quadropole time-of-flight
R^2	Square of the Pearson product moment correlation coefficient
RI	Tiselius risk index
RP	Reverse phase
RS	Relative supersaturation
RT	Room temperature
SBP	Sub boiling point distilled
SDS	Sodium dodecyl sulphate
SE	Standard error
SEM	Scanning electron microscopy
Ser	Serine
Spg	*Streptococcus pneumoniae* galactosidase
SU	Synthetic urine
TEMED	N,N,N'N'-tetramethylethylendiamin
TFA	Trifluoroacetic acid
TGA	Thermogravimetric analysis
THM	Tamm-Horsfall Mucoprotein
Tris	Tris(hydroxymethyl)-aminomethane
UPTF1	Urinary prothrombin fragment 1
WAX	Weak anion exchange
WC	White control subject
WF1	Urinary prothrombin fragment 1 from white control subjects
WMM	White subject's macromolecular urine extract
WSF	White stone-former
WU	White subject's urine
WUF	White subjects' ultrafiltered urine
XRD	X-ray powder diffraction
ZP	Zeta potential

TABLE OF CONTENTS

Acknowledgements..... i
Publications..... ii
Conferences & overseas studentships..... iii
Summary..... iv
Abbreviations..... vi

CHAPTER 1: Introduction

1.1 Stone formation in South Africa..... 1
1.2 Epidemiological factors..... 4
1.3 Physical chemistry of stone formation and inhibitors..... 5
1.4 Urinary proteins..... 7
1.5 Urinary prothrombin fragment 1..... 11
1.6 Urinary protein studies in black South Africans..... 16
1.7 Objectives..... 17
1.8 Thesis outline..... 18
1.9 References..... 19

CHAPTER 2: Composition & inhibitory properties of urine & urinary macromolecules

2.1 Introduction..... 25
2.2 Methods..... 26
Inhibitory activity of urine..... 26
2.2.1 Urine collection and treatment..... 26
2.2.2 Preparation and characterisation of calcium oxalate monohydrate crystals..... 27
2.2.2.1 X-ray powder diffraction..... 27
2.2.2.2 Thermogravimetric analysis..... 28
2.2.2.3 Scanning electron microscopy..... 28
2.2.3 Sedimentation rates..... 28
2.2.3.1 Preparation of COM crystal slurries and slurry / urine mixtures..... 28
2.2.3.2 Measurement of COM crystal sedimentation rates..... 29
2.2.3.3 Verification of sedimentation rates method..... 30
2.2.3.4 Statistical analysis..... 30
2.2.4 Zeta potentials..... 30
2.2.4.1 The concept of zeta potential..... 30
2.2.4.2 Preparation of COM crystal slurry / urine mixtures..... 31
2.2.4.3 Measurement of zeta potentials..... 31
2.2.4.4 Statistical analysis..... 31
Inhibitory activity of macromolecular urine extracts..... 31
2.2.5 Urine collection, preparation and treatment..... 31
2.2.6 Determination of urinary protein concentration..... 32
2.2.7 Preparation of synthetic urine and metastable limit determination..... 32
2.2.8 Particle size distribution determination..... 33
2.3 Results..... 34
Inhibitory activity of urine..... 34
2.3.1 Characterisation of calcium oxalate monohydrate crystals..... 34
2.3.2 Sedimentation rates..... 36
2.3.3 Zeta potentials..... 37

Inhibitory activity of macromolecular urine extracts 39
2.3.4 Urine protein concentration 39
2.3.5 Synthetic urine metastable limit 40
2.3.6 Particle size distributions 40
2.3.7 Average urine compositions 42
2.4 Discussion 42
2.5 References 44

CHAPTER 3: Crystal matrix extract

3.1 Introduction 47
3.2 Methods 48
3.2.1 Urine collection and treatment 48
3.2.2 Isolation of CME 48
3.2.3 Characterisation of CME 49
3.2.3.1 SDS-PAGE 49
3.2.3.2 Western blotting 50
3.2.4 Synthetic urine study 50
3.2.4.1 Urine preparation and treatment 50
3.2.4.2 Effect of CME on particle number, volume and size 51
3.2.4.3 Effect of CME on [^{14}C]-oxalate deposition 51
3.3 Results 51
3.3.1 Urine composition 51
3.3.2 Isolation and characterisation of CME 52
3.3.3 Synthetic urine study 53
3.3.3.1 Effect of CME on particle number and volume 53
3.3.3.2 Effect of CME on particle size 54
3.3.3.3 Effect of CME on [^{14}C]-oxalate deposition 56
3.4 Discussion 57
3.5 References 60

CHAPTER 4: UPTF1 purification & characterisation

4.1 Introduction 63
4.2 Methods 64
4.2.1 Purification of UPTF1 64
4.2.2 Western blotting 65
4.2.3 Protein MALDI-TOF mass spectrometry 65
4.2.4 Protein sequencing 65
4.2.5 Amino acid analysis 65
4.2.6 Gla analysis 66
4.2.7 2D SDS-PAGE 66
4.2.8 Glycan analysis 67
4.2.8.1 The concept of glycosylation 67
4.2.8.2 Protein preparation 67
4.2.8.3 Extraction of *N*-linked glycans 68
4.2.8.4 Extraction of *O*-linked glycans 69
4.2.8.5 Exoglycosidase digestions 69
4.2.8.6 Normal phase HPLC 70
4.2.8.7 Weak anion exchange HPLC 71
4.2.8.8 MALDI-TOF and Quadropole TOF mass spectrometry 71
4.2.8.9 Molecular modeling 71

4.3 Results 72
4.3.1 Purification of UPTF1 72
4.3.2 SDS-PAGE and Western blotting 73
4.3.3 Protein MALDI-TOF mass spectrometry 73
4.3.4 Protein sequencing 74
4.3.5 Amino acid analysis 74
4.3.6 Gla analysis 75
4.3.7 2D SDS-PAGE 76
4.3.8 Glycan analysis 76
***N*-linked glycans** 76
4.3.8.1 NP-HPLC of glycan pools 76
4.3.8.2 Exoglycosidase digestions 78
4.3.8.3 Weak anion exchange HPLC 84
4.3.8.4 MALDI-TOF and QTOF mass spectrometry 87
4.3.8.5 Summary of *N*-linked glycans 87
***O*-linked glycans** 90
4.3.8.6 NP-HPLC of glycan pools and exoglycosidase digestions 90
4.3.8.7 Weak anion exchange HPLC 93
4.3.8.8 Summary of *O*-linked glycans 94
Molecular modeling 95
4.3.8.9 Molecular model of UPTF1 95
4.4 Discussion 97
4.4.1 Primary structure 97
4.4.2 Post-translational modifications 98
4.5 References 101

CHAPTER 5: UPTF1 crystallisation studies in inorganic solutions & urine

5.1 Introduction 105
5.2 Methods 106
5.2.1 Synthetic urine study 106
5.2.1.1 Urine preparation and treatment 106
5.2.1.2 Effect of UPTF1 on particle size 106
5.2.1.3 Effect of UPTF1 on [^{14}C]-oxalate deposition 106
5.2.1.4 Statistical analysis 106
5.2.2 Ultrafiltered urine study 106
5.2.2.1 Urine collection and treatment 106
5.2.2.2 Cross-over experiment 107
5.2.2.3 Effect of UPTF1 on particle number, volume & size 108
5.2.2.4 Effect of UPTF1 on [^{14}C]-oxalate deposition 109
5.2.2.5 Statistical analysis 109
5.2.3 Sedimentation rates 109
5.2.3.1 Effect of UPTF1 on COM crystal slurries 109
5.2.3.2 Effect of UPTF1 on COD crystal slurries 109
Preparation of COD crystals 109
Measurement of sedimentation rate 109
5.2.3.3 Statistical analysis 110

5.2.4 Zeta potentials 110
5.2.4.1 Effect of UPTF1 on COM crystal slurries 110
5.2.4.2 Effect of UPTF1 on COD crystal slurries 111
5.2.4.3 Statistical analysis 111
5.3 Results 111
5.3.1 Synthetic urine study 111
5.3.1.1 Metastable limit 111
5.3.1.2 Effect of UPTF1 on particle size 112
5.3.1.3 Effect of UPTF1 on [^{14}C]-oxalate deposition 114
5.3.2 Ultrafiltered urine study 115
5.3.2.1 Urine composition and metastable limit 115
5.3.2.2 Effect of UPTF1 on particle number & volume 116
5.3.2.3 Effect of UPTF1 on particle size 118
5.3.2.4 Effect of UPTF1 on [^{14}C]-oxalate deposition 120
5.3.3 Sedimentation rates 122
5.3.3.1 Effect of UPTF1 on COM crystal slurries 122
5.3.3.2 Characterisation of CaOx crystals 123
5.3.3.3 Effect of UPTF1 on COD crystal slurries 125
5.3.3.4 Comparative effect of UPTF1 on COM & COD crystal slurries 126
5.3.4 Zeta potentials 127
5.3.4.1 Effect of UPTF1 on COM crystal slurries 127
5.3.4.2 Effect of UPTF1 on COD crystal slurries 127
5.3.4.3 Comparative effect of UPTF1 on COM & COD crystal slurries 128
5.4 Discussion 129
5.4.1 Synthetic urine study 129
5.4.2 Ultrafiltered urine study 130
5.4.3 Sedimentation rates and zeta potentials 132
5.4.4 Conclusions 133
5.5 References 135

CHAPTER 6: UPTF1 in urine & calcium oxalate urine crystals

6.1 Introduction 137
6.2 Methods 137
6.2.1 Urine treatment 137
6.2.2 Crystal preparation 138
6.2.3 Characterisation of urine crystals 138
6.2.4 Preparation of urine and crystals for protein analysis 138
6.2.5 SDS-PAGE 139
6.2.6 Western blotting 139
6.3 Results 139
6.3.1 Urine composition 139
6.3.2 X-ray powder diffraction 140
6.3.3 Scanning electron microscopy 141
6.3.4 Protein analysis 145
6.3.4.1 White control subjects 145
6.3.4.2 Black control subjects 147
6.3.4.3 White stone-formers 149
6.4 Discussion 151
6.5 References 155

CHAPTER 7: UPTF1 inclusion in calcium oxalate monohydrate & dihydrate crystals

7.1 Introduction 157
7.2 Methods 157
7.2.1 Urine treatment 157
7.2.2 Crystal preparation 158
7.2.3 Characterisation of urine crystals 158
7.2.4 Crystal preparation for protein analysis 158
7.2.5 SDS-PAGE 159
7.2.6 Western blotting 159
7.3 Results 159
7.3.1 Urine composition 159
7.3.2 X-ray powder diffraction 159
7.3.3 Scanning electron microscopy 164
7.3.4 Protein analysis 165
7.4 Discussion 169
7.5 References 173

CHAPTER 8: Proteolysis & partial dissolution of calcium oxalate urine crystals

8.1 Introduction 175
8.2 Methods 176
8.2.1 Preparation of CaOx urine crystals 176
8.2.2 SDS-PAGE 177
8.2.3 Western blotting 177
8.2.4 Proteolytic digestion and partial dissolution of crystals 178
8.3 Results 179
8.3.1 Urine composition 179
8.3.2.SDS-PAGE and Western blotting 179
8.3.3 FESEM of control crystals 180
8.3.3.1 Crystals from ultrafiltered urine 180
8.3.3.2 Crystals from filtered urine & ultrafiltered urine dosed with UPTF1 182
Crystals from white subjects 182
Crystals from black subjects 184
8.3.4 FESEM showing proteolysis 185
8.3.4.1 Crystals from white subjects 185
8.3.4.2 Crystals from black subjects 186
8.3.5 FESEM showing proteolysis and dissolution 188
8.3.5.1 Effect of cathepsin D 188
8.3.5.2 Effect of thrombin 191
8.3.5.3 Effect of Proteinase K 192
8.3.6 FESEM showing dissolution 194
8.4 Discussion 196
8.5 References 199

CHAPTER 9: Discussion, conclusions & a future outlook 201

Tables and figures 205

Appendices

Appendix A (chapter 1)..... A1
Appendix B (chapter 3)..... A10
Appendix C (chapter 4)..... A23
Appendix D (chapter 5)..... A35
Appendix E (chapter 6)..... A55
Appendix F (chapter 7)..... A66
Appendix G (chapter 8)..... A78
Appendix H A79

CHAPTER 1: INTRODUCTION

Approximately 12 % of males in the Western world will have at least one kidney stone episode during their lifetime. The figure is only 5 % amongst females (Blacklock 1982). The incidence of urolithiasis is similar in South Africa's white population. However, in the black population it is extremely rare (Modlin 1967, Whalley *et al.* 1998). The exceptionally low incidence of stones in this group is well recognised and recent studies suggest that, while it may have increased slightly (Beukes *et al.* 1987), the average figure is still below 1 % (Whalley *et al.* 1998). The juxtaposition of a stone-prone and virtually stone-free population group provides a model scenario for the study of stone formation.

1.1 Stone formation in South Africa

The first recorded case of renal calculi in a black South African was in 1927. Vermooten (1937) reviewed the Johannesburg General Hospital records for the period 1922 – 1935 and reported that of 217 000 admissions, 273 white patients were treated for renal calculi compared with only one black patient. An x-ray of the black patient, a 30-year-old female, indicated the presence of a shadow in her ureter. The physician suspected that this was due to a ureteral calculus; however, further examination was refused and thus the diagnosis could not be confirmed. Analysis of the typical diet ingested by the black population revealed that the diet was acid-ash based and contained high amounts of vitamin A and low levels of calcium (Vermooten 1937). This finding was of interest since a previous study reported a significant reduction in stone incidence following an intervention with a similar diet (Higgins 1935, cited by Vermooten 1937).

Subsequently, a few proven cases of renal calculi in members of the black population were reported. The first such case was in 1948 (Lopis and Kaplan 1948) and a further two cases were reported three years later (Muskat 1951). However, the black patients afflicted in these cases were all born north of the South African border. Wise and Kark (1961) observed that calculi appeared to be more common in these areas than in South Africa itself, suggesting that geographical as well as racial factors may be implicated in the black South African's protection from stone disease.

Data obtained from a Durban hospital between 1951 and 1959 confirmed previous reports of the remarkably low incidence of stones amongst the black population in South Africa. Of the nearly half a million patients affected, only seven were locally-born blacks

(Wise and Kark 1961). This corresponds to an incidence of 0.001 %. Even more striking is that only one of these cases involved a diagnosis as a primary calculus. Although predisposing factors such as urinary obstruction and bilharzia were equally common amongst South Africa's Indian and black populations, primary and secondary calculi were still a hundred times less prevalent amongst blacks (Wise and Kark 1961).

Modlin (1967) recorded the first comprehensive study of renal calculi amongst South African blacks. He hypothesised that urine composition may be responsible for the disparate stone incidences amongst the white and black populations. Comparison of their average twenty-four hour urine excretions indicated a significantly higher volume, osmolality, ionised calcium and sodium level in this group, while their total calcium, phosphate and citric acid levels and urinary pH were lower than the white population. Modlin (1967) suggested that the higher sodium/calcium ratio in blacks might be an important factor in their protection from stone disease. He argued that sodium competed successfully with calcium ions in hydroxyapatite, thus preventing further growth by epitaxy and aggregation. A more recent study reported the same sodium/calcium trend in white and black subjects (Meyers *et al.* 1994).

No further studies investigated the intriguing rarity of kidney stones amongst the black population until nearly twenty years later. Rodgers and De Klerk (1986) analysed urine specimens from four black stone-formers and detected a considerably lower sodium/calcium ratio for this group than that which has been reported by Modlin (1967) in black control subjects. This supported Modlin's hypothesis that a high sodium/calcium ratio may play a protective role in the black population. Crystalluria studies showed similar particle size distributions in white and black (male) control subjects (Rodgers and De Klerk 1986). However, interesting qualitative differences were observed with the aid of scanning electron microscopy. While conventional crystalluria such as calcium oxalate dihydrate (COD) crystals was observed in the urine of white subjects, black control subjects' urines were composed of copious crystalline salt deposits. These deposits were composed mainly of NaCl and KCl along with some mixed deposits containing Na, P, S, Cl, K and Ca ions. With the exception of KCl, these deposits were not observed amongst the black stone-formers. These observations were in agreement with the black control group's higher sodium/calcium ratio (Modlin 1967, Rodgers and De Klerk 1986, Meyers *et al.* 1994) and suggested a direct or indirect protective role for urinary salts in the black population.

The ultrastructure (Rodgers and De Klerk 1986) and composition (Beukes *et al.* 1987) of stones from black patients is similar to that of white stone-formers. Thus similar mechanisms of stone formation probably apply to the black population as to other ethnic groups. In a study of 1002 stones collected in the Bloemfontein area over a 15-year period, 10 % of which were from black patients, Beukes and co-workers reported that the only difference in the stone composition of white and black patients was in the percentage of COD and struvite (Beukes *et al.* 1987). The incidence of COD stones was three-fold higher amongst white stone-formers, whereas struvite had a five-fold higher incidence amongst blacks.

Several studies have compared urine composition data of white and black subjects in order to identify differences which might account for the latter's lower stone incidence. The two most consistently reported differences are the black population's lower calcium (Meyers *et al.* 1994, Whalley *et al.* 1998, Craig *et al.* 2000, Rodgers and Lewandowski 2002) and citrate excretions (Meyers *et al.* 1994, Whalley *et al.* 1998, Lewandowski *et al.* 2001, Craig *et al.* 2000), followed by their lower sodium (Meyers *et al.* 1994, Whalley *et al.* 1998) and phosphate levels (Whalley *et al.* 1998, Rodgers and Lewandowski 2002). Paradoxically, a low citrate excretion is associated with an increased risk of stone formation and thus urine composition alone does not appear to adequately account for the rarity of stones amongst South Africa's black population. However, several intrinsic factors have been reported in black subjects that may account for their relative protection from stone disease. These factors are: a lack of correlation between sodium and calcium/cystine excretions since the black population's higher urinary sodium is not associated with unfavourably high levels of urinary calcium and cystine (Whalley *et al.* 1998); a possibly lower oxalate absorption rate than the white population (Whalley *et al.* 1998, Lewandowski *et al.* 2001); and a possible different renal handling mechanism with respect to calcium and oxalate (Rodgers and Lewandowski 2002).

A recent comparative study of white and black stone-formers demonstrated that while their urine compositions were similar, lithogenic risk factors such as metabolic disorders were less common and less severe amongst the black group (Whalley *et al.* 1999), thereby adding further intrigue to the phenomenon. In addition, the observation that none of the black stone-formers had a family history of urolithiasis suggested that genetic factors were less important in this population group. It is worth mentioning that the clinic at which the study was conducted attended only twenty-two black patients during the

ten-year period of the study, illustrating the remarkably low incidence of stones amongst this group. Despite the fact that health care is less accessible to South Africa's poorer black communities, the rarity of stone episodes amongst this group is sufficiently noteworthy to warrant interest and attention.

1.2 Epidemiological factors

In order to understand the processes involved in stone formation and thus appropriately address its study, a brief summary of its epidemiology is required. The difference in stone incidence in South Africa's two population groups suggests that race may be a factor. In addition to the black population in South Africa, several other groups have also been reported to show stone rarity, namely the Indians of Mexico, Peru, Ecuador and Bolivia (Finlayson 1974), Eskimoes (cited by Rodgers and Spector 1981) and Australia's aboriginal population (Scott 1990). Although they do not show the rarity to stone formation as the afore-mentioned groups, African Americans also show a lower incidence of kidney stones than the white population (Finlayson 1974, Soucie *et al.* 1994). It is surprising that, with the exception of the South African studies already mentioned, none of these populations have been the subject of intense investigation.

Diet has frequently been cited as a possible explanation for the remarkably low stone incidence amongst South African blacks, and is an obviously important epidemiological factor. Thus, although a detailed discussion of diet is beyond the scope of this thesis, a brief summary of some of the key issues concerning diet is warranted. The increased consumption of animal protein in modern society (Blacklock 1982, Robertson and Peacock 1983) has been cited as a potential factor contributing to stone formation. However, most studies have focused on the role of dietary calcium and oxalate, both of which have an important role to play in determining CaOx stone-forming potential. The most recent evidence suggests that an increase in dietary calcium (*e.g.* from dairy products) should be advised since it reduces urinary oxalate levels by binding oxalate in the gut (Curhan *et al.* 1993, 1997). Conversely, it appears that dietary oxalate should be *reduced* since the ingestion of oxalate-rich foods, such as rhubarb, spinach and beets, is associated with an unfavourable increase in urinary oxalate excretion (Massey *et al.* 1993).

A factor related to dietary advice is that of fluid intake. Many scientists and clinicians regard this as the most important factor in controlling stone formation (Pak *et al.* 1980, Vahlensieck 1986). It is apparent that an increase in urine volume will decrease the concentration of stone-forming salts. Mineral water containing calcium and magnesium has been shown to have both therapeutic and prophylactic merit (Rodgers 1997). This is consistent with an earlier proposal that soft water, which contains low levels of

magnesium, may be associated with increased rates of stone formation in the south-eastern United States (Rodgers and Spector 1981).

Blacklock (1982) proposed that dietary factors may be related to familial trends, and other authors have cited the possible role of genetic factors too. This is supported by a study in which a significantly higher frequency of renal calculi was observed amongst first-degree relatives of stone-formers than their more distant relatives (Resnick *et al.* 1968). However, Finlayson (1974) proposed that environmental factors might mediate genetic ones. Subsequently, comparisons of stone incidence based on geographical location have been extensively reported. It is likely that differences between stone rates amongst countries are related, in part, to their levels of development and economy (Blacklock 1982).

Variations in stone patterns within countries suggest that other factors, such as climatic variation, play a role. Increases in heat and humidity are often associated with an increase in stone risk (Blacklock 1982, Robertson and Peacock 1983, Scott 1990), possibly due to increased exposure to ultraviolet radiation and dehydration (Blacklock 1982). The south-eastern United States is an example of a so-called stone belt where the incidence of stones is significantly greater than elsewhere in the country. This is probably due to the region's excessive heat (Scott 1990), but also a lifestyle favouring the ingestion of large amounts of oxalate-rich iced tea (Rodgers and Spector 1981). Other epidemiological factors include infection, metabolic disorders and occupation, since higher rates of stone formation are found amongst those involved in less active occupations (Finlayson 1974).

1.3 Physical chemistry of stone formation and inhibitors

According to Robertson and Peacock (1983), most epidemiological factors induce changes in one or more urinary risk factors. These workers identified six important CaOx stone risk indicators on the basis of their ability to distinguish stone-formers from controls: increased calcium, oxalate and uric acid excretions; elevated pH; decreased volume; and decreased excretion of a group of inhibitors. The result of such changes would be an increase in urinary CaOx supersaturation, a prerequisite for crystalluria and thus CaOx stone formation (Robertson and Nordin 1982).

However, while urinary supersaturation is undoubtedly required for stone formation, it is insufficient in itself since both healthy and stone-forming subjects' urines are supersaturated and contain crystals (Werness *et al.* 1981). Even in the unlikely event of the precipitation of all urinary oxalate and extremely rapid crystal growth, renal stone

disease is unlikely to occur via free crystalluria (Finlayson and Reid 1978). Thus particle retention, perpetuated by injury of the renal epithelium and the subsequent adhesion of crystals to the sticky glycocalyx, is both necessary and sufficient for stone formation (Finlayson *et al.* 1984).

Crystallisation begins with the formation of nuclei in a supersaturated solution. This is a mechanism by which such a solution sheds its free energy as solid material (Hess and Kok 1996). Since urine is seldom sufficiently concentrated to ensure a reasonable rate of spontaneous or homogeneous nucleation, it is probable that nucleation usually takes place on a foreign surface, *i.e.* heterogeneous nucleation (Finlayson *et al.* 1984; Hess and Kok 1996). Once a crystal nucleus has reached a critical size, new crystal components are added to reduce the overall free energy. This mechanism is known as crystal growth. A third mechanism of crystal formation is the rapid sticking together of existing crystals to form larger particles, referred to as aggregation (Hess and Kok 1996). The latter mechanism is likely to be the more decisive one since growth is usually slow (Robertson and Nordin 1982) and thus aggregation is required to form crystals of a clinically relevant size (Kok *et al.* 1990). Furthermore, calculations based on nephron dimensions, supersaturation and growth rates, and the size increasing effects of crystal aggregation, indicate that the crystal size required for particle retention (as described above) is largely dependent on aggregation (Kok and Khan 1994).

Three major theories have been expounded to explain the physical processes of stone formation. The first is the heterogeneous nucleation and epitaxy theory. As explained earlier, heterogeneous nucleation occurs in urine. This process can occur via epitaxial growth. Evidence for the latter mechanism is found in the characteristic mixture of crystalline salts detected in kidney stones due to the close fit of their crystal lattices, *e.g.* calcium oxalate (CaOx) and uric acid (Lonsdale 1968). Secondly, the matrix theory proposes that, similar to the organic matrix of all stones, the secretion of a matrix substance into urine provides a surface for mineralisation (Robertson and Nordin 1982, Ryall 1989). However, the growth of stones in ultrafiltered urine suggests that a matrix substance is not required for stone development (Ryall 1989), although it may still be important in determining the stone's physical properties.

A third theory of stone formation draws on the discovery that urine from healthy subjects retarded the calcification of rat cartilage, whereas stone-formers' urine did not (Howard and Thomas 1958). The premise of the inhibitor theory is that inhibitory substances in normal urine prevent or reduce crystallisation. The corollary to this

hypothesis is that stones occur due to the absence of such ions in the stone-formers' urine (Robertson and Nordin 1982, Ryall 1989).

The study of small molecules such as pyrophosphate, citrate and magnesium as well as macromolecules, which include glycosaminoglycans and proteins (Worcester 1996), are of considerable interest in view of their possible role in the inhibition of physical processes which direct stone formation. It is believed that inhibitors reduce crystal nucleation by chelating to calcium or oxalate ions, thereby reducing their supersaturation and thus the precipitation of CaOx crystals (Ryall 1997). Inhibition of growth is more likely to occur via the binding of inhibitor molecules to crystal surfaces, thus blocking growth in this direction (Fleisch 1990). Crystal aggregation may be inhibited by a change in the electrical surface charge of crystals which in turn alters their attractive and repulsive forces (Fleisch 1990), or by steric hinderance in the case of large molecules (Ryall 1997).

1.4 Urinary proteins

Of the classes of inhibitors described, macromolecules are the most widely investigated today. Indeed, they may be responsible for most of the inhibitory activity measured in urine (Worcester 1996). Interest in the role of proteins in the pathogenesis of stones originated with the discovery that the organic matrix of kidney stones constitutes 2.5 % of its dry weight and is distributed throughout its structure (Boyce and Garvey 1956). A significant proportion of the matrix (about 64 %) is protein (King and Boyce 1959). Any material associated with a stone, and particularly in such a large proportion, is likely to have participated in its formation. However, while this finding may offer valuable insight into the mechanisms involved, analysis of the matrix has been problematic due to its poor solubility (Boyce *et al.* 1962). Another difficulty associated with the study of the stone matrix has been the uncertainty of its origin. The proteins and macromolecules included may be those usually present in urine or they may have been released from the urinary tract's epithelial lining as a results of injury caused by the stone itself (Doyle *et al.* 1991).

Leal and Finlayson (1977) reported that physical adsorption alone could not account for the association of macromolecules with CaOx stones, implying that a specific mechanism must be involved. This finding provided support for the importance of accessing information on the role of these molecules in stone formation. Fortuitously, Morse and Resnick (1988) proposed a novel approach to the matrix dilemma, studying CaOx crystals which they precipitated from urine by adding calcium chloride and sodium oxalate (NaOx). The proteins associated with these crystals, which were visualised by

two-dimensional gel electrophoresis, were representative of normal urinary macromolecules and not those derived from secondary processes. Of particular interest was the finding that only a few of the numerous urinary proteins observed in urine was included in the CaOx crystals derived from the sample (Morse and Resnick 1988).

Recent technological advancements in the fields of protein biochemistry and molecular biology have greatly increased scientists' ability to address the role of proteins in kidney stone formation. A summary of some of the important findings to date is presented here.

Tamm-Horsfall Mucoprotein (THM), the most abundant protein in human urine, is synthesised in the kidney and excreted at between 20 and 200 mg per day. Monomeric THM has a molecular weight of 80 kDa, but the protein tends to self-associate (Worcester 1996), a property to which its dual functionality has been attributed (Ryall 1997). The effect of THM on CaOx crystallisation has been extensively studied and a variety of conclusions reached, depending on the solution characteristics of the test media. At low ionic strength and high pH conditions, the protein is an effective inhibitor of aggregation, however, the inhibition decreases as these conditions are reversed (Hess *et al.* 1989). Its effect on aggregation is enhanced by the presence of citrate ions, but an increase in calcium concentration results in the promotion of aggregation by THM (Hess 1991). It has little effect on nucleation (Worcester 1996) or growth (Yoshioka *et al.* 1989, Grover *et al.* 1998), and can actually promote nucleation at high ionic strength and low pH (Worcester 1996). All of the afore-mentioned studies used inorganic solutions or seeded systems. However, THM's ability to inhibit aggregation has been confirmed in ultrafiltered urine at a concentration in its physiological range (Ryall *et al.* 1991). The small amount of THM present in calcium stones (Hess 1991) and its absence from CaOx crystals suggests that the protein does not adsorb to crystal surfaces (Doyle *et al.* 1991). In fact, steric hinderance has been proposed as the mechanism by which it reduces crystal aggregation (Ryall *et al.* 1991). Molecular abnormalities in THM from stone-formers have been reported due to its polymerization and decreased solubility (Hess 1991) and yet, surprisingly, the same urinary concentration of THM has been reported in healthy and stone-forming subjects (Ryall 1997). A recent study demonstrated THM's ability to coat exogenous CaOx monohydrate (COM) crystals incubated in whole urine, and thereby prevent their adhesion to renal cells (Kumar *et al.* 2003). THM also reduces COM crystal endocytosis by its action on renal epithelial cells (Lieske *et al.* 1999). Thus along with its ability to retard crystal aggregation, THM may play an important role in the prevention of stone formation.

Nephrocalcin was named in recognition of its analogy with the bone protein osteocalcin. Analogous to THM, it is known to polymerise and thus ranges in size from 14 kDa, the monomeric form, to 60 – 68 kDa as a tetramer (Ryall 1997). Approximately 1 - 20 mg is excreted in urine each day (Worcester 1996). Inhibition of nucleation, growth (Worcester 1996) and aggregation (Hess *et al.* 1989) has been shown to result from the presence of nephrocalcin in inorganic test solutions. Its effect on crystal growth is reportedly due to the blocking of potential growth sites via its binding to crystal surfaces (Worcester 1996); aggregation is reduced by induction of a negative charge on crystal surfaces (Hess *et al.* 1989). The protein's crystal binding ability also facilitates its role in the prevention of COM crystal adhesion to renal cells (Lieske *et al.* 1999). Nephrocalcin contains two to three γ-carboxyglutamic acid (Gla) residues per molecule (Ryall 1997). These residues are probably responsible for its inhibitory activity since nephrocalcin isolated from stone-formers' urine and CaOx stones lacks Gla and exhibits diminished activity (Hess *et al.* 1989). Post-translational modifications such as phosphorylation and glycosylation may also be involved (Worcester 1996). Nephrocalcin's activity in urine has yet to be demonstrated.

Another protein that has not yet been tested in urine is osteopontin. It was first named uropontin in recognition of its analogy with the bone mineral protein osteopontin (Shiraga *et al.* 1992). However, many subsequent authors have preferred the name osteopontin (OPN) and thus this trend will be followed in the present thesis. Urinary OPN presents as multiple bands by gel electrophoresis, probably due to its degradation by urinary proteases (Ryall *et al.* 2001a); the major band has been observed alternatively at 50 (Hoyer 1994) and 67 kDa (Ryall *et al.* 2001a) by different workers using gel electrophoresis. Its urinary concentration has been reported at 3 mg/l, assuming a molecular weight of 50 kDa (Ryall 1997). Inhibition of COM crystal nucleation and growth has been effected by OPN in an inorganic system. This activity is reduced after dephosphorylation, suggesting that this post-translational modification may be important for its activity (Worcester 1996). OPN also acts as an inhibitor of COM crystal aggregation (Asplin *et al.* 1998) and its presence results in a phase transition from COM to COD crystals (Worcester 1996). In addition to its inhibition of crystallisation, OPN appears to reduce COM crystal adhesion to renal cells by coating the crystal surface (Lieske *et al.* 1999). This was confirmed recently when OPN was detected on the surface of exogenous COM crystals incubated in whole urine (Kumar *et al.* 2003). The binding ability of OPN is presumably also responsible for its inclusion in CaOx crystals, where it is found

preferentially in COD (Ryall *et al.* 2001a). Surprisingly though, greater amounts of OPN have been observed in COD stones compared with those composed principally of COM (Hoyer 1994).

A complex urinary protein that has received much attention is inter-α-inhibitor, a 220 kDa protein (Atmani *et al.* 1996a) composed of two heavy chains covalently linked by the glycosaminoglycan chondroitin sulphate to a light chain (Dawson *et al.* 1998b). Most studies have focused on the 35 kDa light chain known as bikunin, previously referred to as uronic-acid-rich protein in view of its composition (Atmani *et al.* 1993). The inclusion of bikunin and its fragments in urine and CaOx crystals has been reported (Dawson *et al.* 1998b); however, it was only detected in one of ten CaOx stones analysed (Dawson *et al.* 1998a). Bikunin inhibits crystal nucleation, growth (Worcester 1996) and aggregation in inorganic systems (Atmani and Khan 1999), and the protein isolated from stone-formers' urine exhibits reduced activity to that obtained from control subjects (Atmani *et al.* 1996a). Of further interest is the demonstration that bikunin reduces the adhesion of COM crystals to renal cells (Ebisuno *et al.* 1999). This was recently confirmed when exogenous COM crystals were incubated in whole urine and bikunin was detected on the crystal surface (Kumar *et al.* 2003). Much less has been reported on bikunin's parent molecule, inter-α-inhibitor. However, crystallisation studies in inorganic systems indicate inter-α-inhibitor's ability to inhibit both crystal growth (Atmani *et al.* 1996a) and aggregation (Dean *et al.* 1999). Recently, the inclusion of its two heavy chains has been demonstrated in urine, CaOx crystals (Dawson *et al.* 1998b) and CaOx stones (Dawson *et al.* 1998a). Crystallisation studies using a seeded inorganic system also demonstrated that the lighter of the two heavy chains inhibit crystal growth and aggregation, although these effects were small (Dean *et al.* 1999).

The final protein discussed, albumin, is also the second most abundant in urine. Albumin resolves as a 67 kDa protein by gel electrophoresis and is excreted at an average concentration of 2.40 and 2.66 mg per day in control and stone-forming subjects, respectively (Cerini *et al.* 1999). Urinary albumin has been shown to be a powerful nucleator in an inorganic test solution and results in a phase transition from COM to principally COD crystals. Promotion of nucleation, regarded as a protective mechanism due to its reduction in urinary supersaturation, was more pronounced in control subjects' urine. Polymeric forms of albumin were observed more frequently in control subjects than stone-formers; the 67 kDa monomeric form was observed in both groups (Cerini *et al.* 1999). The effect of serum-derived albumin has also been tested in inorganic systems

where it appears to inhibit crystal aggregation (Ryall *et al.* 1991), but demonstrates no effect on growth (Grover *et al.* 1998). Albumin is included in CaOx crystals (Atmani *et al.* 1996b), where it is found in greater quantities amongst stone-formers (Atmani and Khan 2002), and in CaOx stones (Hoyer 1994). Unlike the other proteins described above, albumin does not affect COM crystal binding to renal cells (Lieske *et al.* 1999).

Finally, the protein urinary prothrombin fragment 1 has received much attention and has attracted considerable interest. Since this protein was ultimately selected for rigorous investigation in the project described in this thesis, a detailed description of its properties follows.

1.5 Urinary prothrombin fragment 1

With the intention of studying proteins associated with the early stages of urinary crystallisation, Doyle and co-workers precipitated CaOx crystals from urine as described previously (page 7; Morse and Resnick 1988) using one-dimensional (instead of two dimensional) gel electrophoresis (Doyle *et al.* 1991). They, too, observed the selective inclusion of urinary proteins into CaOx crystals, and demonstrated that a 31 kDa protein was predominant. Believing that this protein had not been previously described, it was named crystal matrix protein (or CMP) in recognition of its origin. Although CMP appeared to be a minor constituent of urine, it clearly exhibited a remarkable affinity for CaOx crystals. Furthermore, higher levels of CMP were found in crystals from female subjects when compared with male subjects (Doyle *et al.* 1991). However, the same concentration was detected in the urine of males and females, probably reflecting differences in the crystal binding affinity of CMP in men and women (Dawson and Ryall 1994). The possibility that CMP may be associated with the female population's lower stone incidence and the manifest potential of a urinary protein directly involved in the crystallisation process to influence the course of stone formation, led to further intensive scrutiny of CMP.

Crystallisation studies of the crystal matrix extract (CME), of which CMP is the principal component, demonstrated this potential. In an inorganic solution and ultrafiltered urine, CME inhibited CaOx crystal growth and aggregation; the greater effect was on the latter mechanism (Doyle *et al.* 1995). The reduction in crystallisation induced by CME in the range 0.08 - 1.25 mg/l for the inorganic solution and 1.25 – 10.0 mg/l for the ultrafiltered urine was dose dependent. One of the most noteworthy features of this study was the considerable reduction in crystal growth (65 %) measured in the inorganic solution

at the highest CME concentration. Under comparable conditions, previous macromolecule studies reported growth inhibition of less than 5 % (Edyvane *et al.* 1986). The highly efficient inhibition of both crystal growth and aggregation by CME could not be accounted for by the cumulative effects of other previously reported proteins likely to be associated with the matrix extract. Thus, this observation suggested that the activity of CME might be largely attributable to its principal component, CMP (Doyle *et al.* 1995).

In order to clarify the identity of the 31 kDa protein, CMP was isolated and purified from CaOx crystals by column chromatography and reverse phase (RP)-high performance liquid chromatography (HPLC) (Stapleton *et al.* 1993b). Protein sequencing of the first eleven N-terminal amino acids by Edman degradation showed an 82 % sequence homology with the N-terminus of human prothrombin (PT). The relationship between CMP and PT was confirmed by Western blotting with a commercial PT antibody. This finding established the first link between urolithiasis and blood coagulation proteins. Suzuki and co-workers independently confirmed CMP's relationship with PT by amino acid composition analysis and Western blotting, but mistakenly identified CMP as the PT activation peptide, PT fragment 1+2 (PTF1+2) (Suzuki *et al.* 1994). However, subsequent comparison with a standard preparation containing both PTF1+2 and PT fragment 1 (PTF1), clarified the identity of CMP as a urinary form of PTF1 (Stapleton and Ryall 1995a). The protein appeared as a double band by gel electrophoresis in contrast to the sharp, single band of serum-derived PTF1, probably due either to alterations in the protein's molecular structure in the kidney or the action of other urinary components.

In order to affirm the role of the F1 fragment of PT in stone formation and its possible prevention, the anatomical location (Stapleton *et al.* 1993a) and gene expression (Stapleton *et al.* 1998) of the protein was investigated. Immunohistochemical studies of human renal tissue samples and several other organs showed that its distribution was limited to the most lithogenic regions of the kidney, namely the epithelial cells of the thick ascending limb of the loop of Henle, the distal convoluted tubule of the nephron and the maculae densae of involved nephrons, where it was found in greater quantities amongst stone-formers. PTF1 was also observed in the liver although with different characteristics to the kidney (Stapleton *et al.* 1993a). It was initially speculated that urinary PTF1 might be derived from the glomerular filtrate of plasma PT (Stapleton and Ryall 1995a). However, a polymerase chain reaction study demonstrated the presence of PTF1 mRNA (messenger ribonucleic acid) in human kidney, spleen and liver sections. Expression in the liver was greater than in the kidney (Stapleton *et al.* 1998). This confirmed that PTF1 was

produced by the human kidney and, along with its precise location within the renal system and its abundant and selective incorporation into urinary CaOx crystals, strongly suggested that this protein played an important role in determining the course of stone formation. Recent studies have demonstrated PT expression in rat kidney and liver, suggesting that in the absence of human tissue specimens, rats may be an appropriate choice for the investigation of possible therapeutic measures (Grover *et al.* 1999). In recognition of the human protein's identity, yet its subtle differences with the analogous fragment from plasma, CMP was renamed urinary prothrombin fragment 1, or UPTF1.

Another important requirement if a protein is to fulfill a regulatory role in stone formation, is that it be present in the end product of this process, namely, the stone itself. Any protein involved in the physical process of stone formation, or its inhibition, is likely to be associated with it. The presence of UPTF1 in CaOx-containing stones satisfies this requirement (Stapleton *et al.* 1996). The absence of any detectable UPTF1 in struvite stones suggests that this association with CaOx stones may be elucidative rather than merely a product of injury (and the subsequent release of the plasma protein PT) caused by the stone. Furthermore, the higher urinary pH in which struvite stones are usually observed suggests that the adsorption of UPTF1 onto the crystal surface may be pH dependent (Stapleton *et al.* 1996).

Another vital property of UPTF1 provides convincing evidence that this protein might play an important role in stone formation. A study on the effect of UPTF1 on CaOx crystallisation in ultrafiltered urine demonstrated that it was a powerful inhibitor of both crystal growth and aggregation (Ryall *et al.* 1995). UPTF1 decreased crystal aggregation as well as the amount of CaOx deposition in a dose-dependent manner at nanomolar concentrations (1.25 - 10 mg/l or 40.3 - 322 nmol/l, assuming a mass of 31 kDa). The lowest concentration tested in the crystallisation study equates approximately with the highest urinary concentration previously reported in healthy subjects using a radioimmunoassay (Bezeaud and Guillin 1984). Using this assay, UPTF1 was detected in all thirty-seven urines tested with concentrations in the range 0.9 - 35.3 nmol/l. At its estimated physiological concentration of 1.25 mg/l, UPTF1 inhibited crystal growth and aggregation by 25 and 22 %, respectively (Ryall *et al.* 1995).

In order to gauge the relative activity of UPTF1, inhibition experiments were conducted comparing PTF1 with three other urinary proteins: THM, human serum albumin (HSA), and α_1-microglobulin (α_1-m) (Grover *et al.* 1998). All except THM were derived from commercially available sources; THM was purified from urine due to its relative

abundance. The proteins were chosen due to their presence in CaOx stones and, except for THM, their association with CaOx crystals. Using an inorganic system and final concentrations of 32 nmol/l (which equates to 1 mg/l UPTF1), the proteins reduced crystal aggregation in order of decreasing magnitude: PTF1, THM, HSA and α_1-m. Only PTF1 reduced crystal growth. These results not only confirmed the effectiveness of UPTF1 as an inhibitor of CaOx crystallisation, but also demonstrated its superiority on a molar basis in comparison with other potentially important urinary proteins (Grover *et al.* 1998).

UPTF1's considerable effect on CaOx crystallisation is of interest in light of the elevated levels observed in the kidneys of stone-formers. It is possible that UPTF1 is produced as a protective response in the stone-formers. UPTF1 from this group may also be functionally defective, or perhaps not all of the PTF1 produced by their kidneys is released into their urines (Stapleton and Ryall 1995b). Indeed, the amino acid composition of UPTF1 from stone-formers is different to the protein from control subjects (Stapleton *et al.* 1998).

Prior to its identification as UPTF1, amino acid composition analysis of CMP suggested the presence of several unusual amino acids referred to as Gla (Stapleton *et al.* 1993b, Suzuki *et al.* 1994). Gla is formed by the addition of an extra carboxyl group to glutamic acid during post-translational modification of vitamin K-dependent proteins (of which PT is one). The Gla domain of UPTF1 contains ten such residues and is located at the N-terminal region of the molecule. By way of its calcium binding ability, the Gla domain of UPTF1 is responsible for its exceptional affinity for CaOx crystals (Stapleton and Ryall 1995b).

A study of several Gla-containing proteins by Romberg and co-workers showed the necessity of the Gla domain to their activity (Romberg *et al.* 1986). In order to investigate the possibility of such a structure-function relationship in UPTF1, *in vitro* activity studies were carried out using the intact PT molecule as well as several of its activation products (Grover and Ryall 1999). PTF1, PT fragment 2 (PTF2) and thrombin were tested in parallel with their parent molecule, PT, in an inorganic solution at final concentrations of 16.13 nmol/l (this equates to a final PTF1 concentration of 0.50 mg/l). PTF1 was the most effective inhibitor of crystal growth and aggregation, followed by PT. The two fragments that lacked the PT Gla domain, namely PTF2 and thrombin, were the least effective inhibitors, suggesting that the inhibitory effects of PT and PTF1 could be attributed to their Gla domain (Grover and Ryall 1999). The existence of this relationship in (ultrafiltered) urine was later confirmed (Grover and Ryall 2002). It has been proposed that the superior

activity of PTF1 compared to PT was due to the former's greater charge/mass ratio (Grover and Ryall 1999, Grover and Ryall 2002).

The extent of γ-carboxylation in UPTF1 from urine and CaOx crystals has been investigated by two-dimensional gel electrophoresis and Western blotting (Buccholz *et al.* 1999). Most urine samples analysed in the study contained two isoforms of UPTF1 in the low pI range (2.5 – 3.0), whereas the crystals incorporated these two charged variants as well as another three at slightly higher pI values. It is likely that the highly charged variants were present at lower concentrations in the urine samples and thus could not be detected by Western blotting. These results showed that most UPTF1 is found in a highly charged state corresponding to a high degree of γ-carboxylation. Another study reported an approximate pI value of 4 for UPTF1 (Stapleton *et al.* 1996).

Although the Gla domain of UPTF1 imparts its considerable inhibitory properties, the domain's strong binding affinity for CaOx crystals also results in frequent underestimation of the protein's urinary concentration (Ryall *et al.* 2000). Crystalluria often occurs during urine collection as well as during storage (at 4 ^{0}C and –20 ^{0}C) prior to analysis. Thus, unless these crystals are dissolved before the assay, any UPTF1 associated with these crystals will be excluded from the protein determination (Dean *et al.* 2000). Attempts to address this difficulty with measures such as ten-fold post-void urine dilution have been unsuccessful and thus no analytical method is currently available for the quantitation of UPTF1.

The pilot study in which UPTF1 (or CMP as it was then known) was discovered was the first to suggest that the protein may be closely associated with CaOx crystals (Doyle *et al.* 1991). Several years later, Fleming and co-workers fractured CaOx crystals precipitated from filtered urine, and demonstrated the presence of extensive channeling throughout their internal structure by field emission scanning electron microscopy (FESEM) (Fleming *et al.* 1999). The internal detail was more evident after treatment with Proteinase K, but was not observed in the presence of a protease inhibitor cocktail or with crystals precipitated from ultrafiltered urine (Fleming *et al.* 2000). Thus, it may be assumed that the erosion observed with the crystals derived from filtered urine must have resulted from the removal of protein, and thus that proteins form part of the internal ultrastructure of CaOx crystals, *i.e.* the proteins, including UPTF1, are intracrystalline (Fleming *et al.* 1999). Similar FESEM results obtained by incubation of crystals in urine, showing the erosion of crystal margins and surface fissures, demonstrated that the formation of crystals in urine might be a reversible process (Fleming *et al.* 2000).

The visual evidence obtained by FESEM was recently confirmed by empirical data using x-ray synchrotron diffraction (Fleming *et al.* 2003). Higher nonuniform strain was observed in urinary CaOx crystals compared with crystals composed of pure mineral or those obtained from ultrafiltered urine. These results conclusively demonstrated the presence of intracrystalline proteins in urinary CaOx crystals.

Studies of intracrystalline proteins in other biomineralisation systems provide insight into possible roles of UPTF1. Such proteins have been shown to direct crystal composition and shape, as well as to influence physicochemical features such as crystal binding ability and aggregability (Ryall *et al.* 2000). Crystals containing proteins distributed in continuous channels may also be more susceptible to digestion and degradation by intracellular proteases, thus providing a potential mechanism for their disintegration, dissolution and even removal by opsonins (Ryall *et al.* 2000, 2001b).

Several studies have reported the rapid binding of COM (Riese *et al.* 1988, Lieske *et al.* 1995, Verkoelen *et al.* 1995) and COD (Lieske *et al.* 1996) crystals to cultured renal epithelial cells, and crystal adhesion to the renal epithelium is now widely regarded as a possible mechanism of stone formation. A recent study reported the presence of PTF1+2, which contains the sequence of PTF1, on the surface of exogenous COM crystals incubated in whole urine. This demonstrated the ability of PTF1 to reduce COM crystal adhesion to renal cells by coating the crystal surface (Kumar *et al.* 2003). However, if crystals are endocytosed, their possible dissolution within lysosomal bodies (at acidic pH levels) may represent a protective mechanism (Lieske *et al.* 1999). Ryall has proposed that crystal binding to the cell surface, and their possible internalisation and disintegration, will be influenced by the nature and concentration of intracrystalline proteins (Ryall *et al.* 2000). Thus, by implication, UPTF1 may have a vital role to play in this process.

In addition, the different affinity of UPTF1 for COM and COD crystals is of interest. While COM crystals contain mainly UPTF1, the protein's concentration in COD intracrystalline space is reduced considerably (Ryall *et al.* 2001a). Since COM crystals exhibit a greater binding affinity for renal cells than COD (Wesson *et al.* 1998), the differential expression of UPTF1 in these crystals may be of relevance to the understanding of the crystal-cell binding mechanism.

1.6 Urinary protein studies in black South Africans

Research available to date on urinary proteins, as described, suggests that this field may offer insight into the pathogenesis of stone formation. The composition of urine and

lithogenic risk factors have not been conclusively shown to account for South African blacks' relative protection from stone disease, other factors are likely to be involved. The role of urinary proteins is an obvious area to be investigated. Indeed, studies involving THM and albumin have already commenced.

THM isolated from the urine of white and black subjects have been shown to inhibit CaOx crystal nucleation in the black group's urine, but had no effect on nucleation in the white group's urine (Craig *et al.* 1999). This suggests that the black population's urine milieu may enhance the inhibitory capacity of THM. Zeta potential measurements have demonstrated that THM (Craig *et al.* 2001) and albumin (Mensah *et al.* 2003) from black subjects carry higher negative charges than the same protein obtained from white subjects. Thus these proteins in black subjects will exert stronger repulsive forces, which may result in greater inhibition of aggregation. This was confirmed by COM crystal sedimentation studies in which THM and albumin derived from black subjects demonstrated greater inhibition of COM crystal aggregation than the corresponding protein obtained from white subjects (Craig *et al.* 2001, Mensah *et al.* 2003). Comparison of the molecular weight, amino acid composition and tryptic digestion patterns of THM from white and black subjects have not revealed differences which might account for their distinct activities (Craig *et al.* 2000).

It seems possible that the more potent inhibitory activity of urinary proteins in South African blacks may contribute to their lower stone incidence. In particular, UPTF1 appears to be a likely candidate in this context. The growing body of evidence that has emerged over the past twelve years on UPTF1 strongly suggests that it may play a key role in an understanding of the processes involved in stone formation and, indeed, the requirements for its prevention. Thus, in view of the protein's apparent potential and the intriguing rarity of kidney stones amongst the black population in South Africa, a unique research opportunity presented itself.

1.7 Objectives

The hypothesis of this thesis was that differences in the physical structure and/or inhibitory properties of UPTF1 from the white and black populations in South Africa contribute to their disparate incidences of kidney stones, and, specifically, the rarity of stones amongst the black population. The objectives of the thesis can be stated as follows:

- To investigate the urine composition and relative inhibitory activity of urine and urinary macromolecules of healthy white and black subjects towards CaOx crystallisation;
- To isolate the CME from the urine of healthy white and black subjects;
- To compare the protein composition and inhibitory activity of the CME from healthy white and black subjects;
- To isolate and purify UPTF1 from the urine of healthy white and black subjects;
- To characterise UPTF1 from healthy white and black subjects; and
- To compare the inhibitory activity of UPTF1 from healthy white and black subjects in both inorganic media and urine.

In addition to the above-mentioned objectives, several other avenues of investigation emerged during the course of the study. Thus the following supplementary objectives were identified:

- To compare the morphology of urinary CaOx crystals in healthy white and black subjects and white stone-formers, and the proteins included therein;
- To compare the relationship between urinary crystal morphology and UPTF1 in healthy white and black subjects; and
- To compare the susceptibility of urinary CaOx crystals from healthy white and black subjects to proteolysis and dissolution.

1.8 Thesis outline

The results of the urine composition and urine inhibitory activity studies are presented in chapter 2. These results suggested that urinary macromolecules might provide insight into the rarity of kidney stones in South Africa's black population. Thus a detailed investigation of the CME (chapter 3) and its principal protein component, UPTF1 (chapters 4 – 8), from both population groups was conducted. The primary structure of UPTF1 from healthy white (WF1) and black (BF1) males was rigorously characterised. In addition, the glycosylation of WF1 and BF1 was compared with UPTF1 isolated from white and black stone-formers (chapter 4). The inhibitory activities of WF1 and BF1 were compared in inorganic media as well as in ultrafiltered urine (chapter 5). The latter study employed a cross-over design in which each protein was tested in both population groups' urine. Chapter 6 presented investigations of the apparent differences in morphology of urinary crystals between the two population groups, along with the relative amounts of UPTF1 and other proteins in urine and CaOx crystals precipitated therein. Furthermore, by preparation

of pure COM and COD crystals from the same urine, the relationship between crystal morphology and UPTF1 was explored in both population groups (chapter 7). Finally, the possibility that differences in the susceptibility of urinary crystals to proteolysis and dissolution was investigated in the white and black populations (chapter 8). A summary of the major findings and conclusions drawn from these studies are presented in chapter 9.

1.9 References

1. Asplin JR, Arsenault DA, parks JH, Coe FL, and Hoyer JR. 1998. Contribution of human uropontin to inhibition of calcium oxalate crystallization. *Kidney Int* 53:194-199.

2. Atmani F and Khan SR. 2002. Quantification of protein extracted from calcium oxalate and calcium phosphate crystals induced in vitro in the urine of healthy controls and stone-forming patients. *Urol Int* 68:54-59.

3. Atmani F and Khan SR. 1999. Role of urinary bikunin in the inhibition of calcium oxalate crystallization. *J Am Soc Nephrol* 10:S385-S388.

4. Atmani F, Lacour B, Drueke T, and Daudon M. 1993. Isolation and purification of a new glycoprotein from human urine inhibiting calcium oxalate crystallisation. *Urol Res* 21:61-66.

5. a) Atmani F, Mizon J, and Khan SR. 1996. Inter-alpha-inhibitor: a protein family involved in the inhibition of calcium oxalate crystallization. *Scan Micros* 10:425-434.

6. b) Atmani F, Opalko FJ, and Khan SR. 1996. Association of urinary macromolecules with calcium oxalate crystals induced in vitro in normal human and rat urine. *Urol Res* 24:45-50.

7. Beukes GJ, De Bruiyn H, and Vermaak JH. 1987. Effect of changes in epidemiological factors on the composition and racial distribution of renal calculi. *Br J Urol* 60:387-397.

8. Bezeaud A and Guillin M-C. 1984. Quantitation of prothrombin activation products in human urine. *Br J Haem* 58:597-606.

9. Blacklock NJ. 1982. Epidemiology of urolithiasis. In Williams DI and Chisholm GD, editors. Scientific foundations of urology. William Heinemann Medical Books Limited, London, 235-243.

10. Boyce WH and Garvey FK. 1956. The amount and nature of the organic matrix in urinary calculi: a review. *J Urol* 72:213-227.

11. Boyce WH, King JS Jr, and Fielden ML. 1962. Total non-dialysable solids (TNDS) in human urine. XIII. Immunological detection of a component peculiar to renal calculous matrix and to urine of calculous patients. *J Clin Inves* 41: 1180-1189.

12. Buchholz NP, Kim DS, Grover PK, Dawson CJ, and Ryall RL. 1999. The effect of warfarin therapy on the charge properties of urinary crystallization of calcium oxalate in undiluted human urine. *J Bone Miner Res* 14:003-1012.

13. Cerini C, Geider S, Dussol B, Hennequin C, Daudon M, Veesler S, Nitsche S, Biostelle R, Berthezene P, Dupuy P, Vazi A, Berland Y, Daghorn J-C, and Verdier J-M. 1999. Nucleation of calcium oxalate crystals by albumin: involvement in the prevention of stone formation. *Kid Int* 55:1776-1786.

14. Craig T-A, Rodgers AL, and Brandt W. 2001. Inhibition of calcium oxalate (CaOx) crystallisation by Tamm-Horsfall Mucoprotein (THM) from two different population groups. In: Kok DJ, Romijn HC,

Verhagen PCMS, and Verkoelen CF, editors. Eurolithiasis: 9th European Symposium on Urolithiasis. Shaker Publishing, Netherlands, 59-60.

15. Craig T-A, Rodgers AL, and Brandt W. 2000. Comparison of Tamm-Horsfall Mucoprotein (THM) in normal and stone-forming caucasian and african males in South Africa. In: Rodgers AL, Hibbert BE, Hess B, Khan SR, and Preminger GM, editors. Urolithiasis 2000. University of Cape Town, Cape Town, 119-120.

16. Craig T-A, Rodgers AL, and Brandt W. 1999. Inhibitory properties of Tamm-Horsfall Mucoprotein isolated from two different population groups. In: Borghi L, Meschi T, Briganti A, Schanchi T and Novarini A, editors. Proceedings of the 8th European Symposium on Urolithiasis. Editoriale Bios, Cosenza, 261-263.

17. Curhan GC, Willett WC, Rimm EB, and Stampfer MJ. 1993. A prospective study of dietary calcium and other nutrients and the risk of symptomatic kidney stones. *N Engl J Med* 328:833–838.

18. Curhan GC, Willett WC, Speizer FE, Spiegelman D, and Stampfer MJ. 1997. Comparison of dietary calcium with supplemental calcium and other nutrients as factors affecting the risk for kidney stones in women. *Ann Int Med* 126:497–504.

19. a) Dawson CJ, Grover PK, Kanellos J, Pham H, Kupczyk, Oates A, and Ryall RL. 1998. Inter-alpha-inhibitor in calcium stones. *Clin Sci* 95:187-193.

20. b) Dawson CJ, Grover PK, and Ryall RL. 1998. Inter-alpha-inhibitor in urine and calcium oxalate urine crystals. *Br J Urol* 81:20-26.

21. Dawson CJ and Ryall RL. 1994. Factors affecting the inclusion of crystal matrix protein into calcium oxalate crystals: centrifugation, sieving and sex. In: Ryall RL, Bais R, Marshall VR, Rofe AM, Smith LH, and Walker VR, editors. Proceedings of the 7th international symposium on urolithiasis. Plenum Press, New York, 316.

22. Dean CJ, Kanellos J, Pham H, Gomes M, Oates A, Grover PK, and Ryall RL. 1999. Calcium oxalate crystallisation in vitro effect of inter-alpha-inhibitor and derivatives. In: Borghi L, Meschi T, Briganti A, Schanchi T and Novarini A, editors. Proceedings of the 8th European Symposium on Urolithiasis. Editoriale Bios, Cosenza, 291-293.

23. Dean CJ, Macardle P, and Ryall RL. 2000. The effect of the presence of calcium oxalate crystals on the measurement of prothrombin fragment 1 in urine. In: Rodgers AL, Hibbert BE, Hess B, Khan SR, and Preminger GM, editors. Urolithiasis 2000. University of Cape Town, Cape Town, 150-152.

24. Doyle IR, Marshall VR, Dawson CJ, and Ryall RL. 1995. Calcium oxalate crystal matrix extract: the most potent macromolecular inhibitor of crystal growth and aggregation yet tested in undiluted human urine in vitro. *Urol Res* 23:53-62.

25. Doyle IR, Ryall RL, and Marshall VR. 1991. Inclusion of proteins into calcium oxalate crystals precipitated from human urine: a highly selective phenomenon. *Clin Chem* 37:1589-1594.

26. Ebisuno S, Nishihata M, Inagaki T, Umehara M, and Kohjimoto Y. 1999. Bikunin prevents adhesion of calcium oxalate crystal to renal tubular cells in human urine. *J Am Soc Nephrol* 10:S436-S440.

27. Edyvane KA, Hibberd CM, Harnett RM, Marshall VR, and Ryall RL. 1986. Macromolecules inhibit calcium oxalate crystal growth and aggregation in whole human urine. *Clin Chim Acta* 167:239

28. Finlayson B. 1974. Renal lithiasis in review. *Urol Clin N Am* 1:181-212.

29. Finlayson B, Khan SR, and Hackett RL. 1984. Mechanisms of stone formation - an overview. *Scan Micros* 111:1419-1425.

30. Finlayson B and Reid F. 1978. The expectation of free and fixed particles in urinary stone disease. *Inves Urol* 15:442-448.

31. Fleisch H. 1990. Role of inhibitors and promoters of crystal nucleation, growth and aggregation in the formation of calcium stones. In Renal tract stone. Metabolic basis and clinical practice. Wickham JEA and Buck AC. editors. Longman Group UK Limited, London. 295-306.

32. Fleming DE, Doyle IR, Evans N, Marshall VR, Parkinson VM, and Ryall RL. 1999. Proteins associated with calcium oxalate crystals formed in human urine are intracrystalline. In: Borghi L, Meschi T, Briganti A, Schanchi T and Novarini A, editors. Proceedings of the 8th European Symposium on Urolithiasis. Editoriale Bios, Cosenza, 359-361.

33. Fleming DE, Grover PK, Chauvet MC, Marshall VR, and Ryall RL. 2000.An unexpected role of urinary proteins in the prevention of calcium oxalate urolithiasis. In Rodgers AL, Hibbert BE, Hess B, Khan SR, and Preminger GM, editors. University of Cape Town, Cape Town, 169-171.

34. Fleming DE, Van Riessen A, Chauvet MC, Grover PK, Hunter B, van Bronswijk W, and Ryall RL. 2003. Intracrystalline proteins and urolithiasis: a synchrotron X-ray diffraction study of calcium oxalate monohydrate. *J Bone Miner Res* 18:1282–1291.

35. Grover PK, Moritz RL, Simpson RJ, and Ryall RL. 1998. Inhibition of growth and aggregation of calcium oxalate crystals in vitro. A comparison of four human proteins. *Eur J Biochem* 253:637-644.

36. Grover PK and Ryall RL. 1999. Inhibition of calcium oxalate crystal growth and aggregation by prothrombin and its fragments in vitro. *Eur J Biochem* 263:50-56.

37. Grover PK and Ryall RL. 2002. Effect of prothrombin and its activation fragments on calcium oxalate crystal growth and aggregation in undiluted human urine in vitro: relationship between protein structure and inhibitory activity. *Clin Sci* 102:425-434.

38. Grover PK, Stapleton AMF, and Ryall RL. 1999. Prothrombin gene expression in rat kidneys provides an opportunity to examine its role in urinary stone pathogenesis. *J Am Soc Nephrol* 10:S404-S407.

39. Hess B. 1991. The role of Tamm-Horsfall glycoprotein and nephrocalcin in calcium oxalate monohydrate crystallisation processes. *Scan Micros* 5:689-696.

40. Hess B and Kok DJ. 1996. Nucleation, growth, and aggregation of stone-forming crystals. In Kidney stones: Medical and surgical management. Coe FL, Favus MJ, Pak CYC, Parks JH, and Preminger GM, editors. Lippincott-Raven Publishers, Philadelphia, 3-32.

41. Hess B, Nakagawa Y, and Coe FL. 1989. Inhibition of calcium oxalate monohydrate crystal aggregation in urine proteins. *Am J Physiol* 257:F99-F106.

42. Howard JE and Thomas WC. 1958. Some observations on rachitic rat cartilage of probably significance in the etiology of renal calculi. *Trans Am Clin Climatol Assoc* 70:94-102.

43. Hoyer RJ. 1994. Role of uropontin in urinary calcium stone formation. In: Ryall RL, Bais R, Marshall VR, Rofe AM, Smith LH, and Walker VR, editors. Proceedings of the 7th international symposium on urolithiasis. Plenum Press, New York, 253–258.

44. King JS and Boyce WH. 1959. Analysis of renal calculous matrix compared with some other matrix minerals and with uromucoid. *Arch Biochem Biophys* 82:455-461.

45. Kok DJ and Khan SR. 1994. Calcium oxalate nephrolithiasis, a free or fixed particle disease. *Kidney Int* 46:847-854.

46. Kok DJ, Papapoulos SE, and Bijvoet OLM. 1990. Crystal agglomeration is a major element in calcium oxalate urinary stone formation. *Kidney Int* 37:51-56.

47. Kumar V, Farell G, and Lieske JC. 2003. Whole urinary proteins coat calcium oxalate monohydrate crystals to greatly reduce their adhesion to renal cells. *J Urol* 170:221-225.

48. Leal JJ and Finlayson B. 1977. Adsorption of naturally occurring polymers onto calcium oxalate crystal surfaces. *Inves Urol* 14:278-283.

49. Lewandowski S, Rodgers A, and Schloss I. 2001. The influence of a high-oxalate / low-calcium diet on calcium oxalate renal stone risk factors in non-stone forming black and white South African subjects. *Br J Urol* 87: 307-311.

50. Lieske JC, Deganello S, and Toback FG. 1999. Cell-crystal interactions and kidney stone formation. *Nephron* 81:8-17.

51. Lieske JC, Toback FG, and Deganello S. 1996. Face-selective adhesion of calcium oxalate dihydrate crystals to renal epithelial cells. *Calcif Tissue Int* 58:195-200.

52. Lieske JC, Leonard R, and Toback FG. 1995. Adhesion of calcium oxalate monohydrate crystals to renal epithelial cells is inhibited by specific anions. *Am J Physiol* 268:F604-F612.

53. Lonsdale K. 1968. Epitaxy as a growth factor in urinary calculi and gallstones. *Nature* 217:56–58.

54. Lopis S and Kaplan SA. 1948. Renal calculus in the Bantu. *Clin Proc* 7:103-108.

55. Massey LK, Roman-Smith H, and Sutton RA. 1993. Effect of dietary oxalate and calcium on urinary oxalate and risk of formation of calcium oxalate kidney stones. *J Am Diet Assoc* 93:901-906.

56. Mensah P, Rodgers AL, and Sturrock ED. 2003. Inhibitory effect of urinary albumin from black and white South Africans on calcium oxalate monohydrate crystal aggregation. *Urol Res* 31:91.

57. Meyers AM, Whalley N, Zakolski WJ and Shar T. 1994. Chemical composition of the urine in the normal black and white population. In: Ryall RL, Bais R, Marshall VR, Rofe AM, Smith LH, and Walker VR, editors. Proceedings of the 7th international symposium on urolithiasis. Plenum Press, New York, 422.

58. Modlin M. 1967. The aetiology of renal stone: A new concept arising from studies on a stone-free population. *Ann Roy Coll Surg Eng* 40:155-178.

59. Muskat DA. 1951. The problem of nephrolithiasis with special reference to the Bantu. *S Afr J Clin Sci* 2:18-38.

60. Morse RM and Resnick MI. 1988. A new approach to the study of urinary macromolecules as a participant in calcium oxalate crystallization. *J Urol* 139:869-873.

61. Pak CYC, Smith LH, Resnick MI, and Weinerth JL. 1980. Dietary management of idiopathic calcium urolithiasis. *J Urol* 131:850–852.

62. Resnick M, Pridgen DB, and Goodman HO. 1968. Genetic predisposition to formation of calcium oxalate renal calculi. *New Engl J Med* 278:1313-1318.

63. Riese RJ, Riese JW, Kleinman JG, Wiessner JH, Mandel GS, and Mandel NS. 1988. Specificity in calcium oxalate adherence to papillary epithelial cells in culture. *Am J Physiol* 255:F1025-F1032.

64. Robertson WG and Peacock M. 1983. Review of risk factors in calcium oxalate urolithiasis. *World J Urol* 1:114-118.

65. Robertson WG and Nordin BEC. 1982. Physico-chemical factors governing stone formation. In Scientific foundations of urology. Williams DI and Chisholm GD, editors. William Heinemann Medical Books Ltd, London, 194-267.

66. Rodgers A and Spector M. 1981. Human stones. *Endeavour* 5:119-126.

67. Rodgers AL. 1997. Effect of mineral water containing calcium and magnesium on calcium oxalate urolithiasis risk factors. *Urol Int* 58:93–99.

68. Rodgers AL and De Klerk DP. 1986. Crystalluria and urolithiasis in a relatively stone-free population. *Scan Elec Micros* 3:1157-1167.

69. Rodgers AL and Lewandowski S. 2002. Effects of 5 different diets on urinary risk factors for calcium oxalate kidney stone formation: evidence of different renal handling mechanisms in different race groups. *J Urol* 168:931-936.

70. Romberg RW, Werness PG, Riggs BL, and Mann KG. 1986. Inhibition of hydroxyapatite crystal growth by bone-specific and other calcium binding proteins. *Biochem* 25:1176-1180.

71. Ryall RL. 1989. The formation and investigation of urinary calculi. *Clin Biochem Revs* 10:149-157.

72. Ryall RL. 1997. Urinary inhibitors of calcium oxalate crystallisation and their potential role in stone formation. *World J Urol* 15:155-164.

73. a) Ryall RL, Chauvet MC, and Grover PK. 2001: A space oddity. In: Kok DJ, Romijn HC, Verhagen PCMS, and Verkoelen CF, editors. Eurolithiasis: 9th European Symposium on Urolithiasis. Shaker Publishing, Netherlands, 273-274.

74. b) Ryall RL, Fleming DE, Doyle IR, Evans NA, Dean CJ, and Marshall VR. 2001. Intracrystalline proteins and the hidden ultrastructure of calcium oxalate urinary crystals: implications for kidney stone formation. *J Struc Biol* 134:5-14.

75. Ryall RL, Fleming DE, Grover PK, Chauvet M, Dean CJ, and Marshall VR. 2000. The hole truth: intracrystalline proteins and calcium oxalate kidney stones. *Mol Urol* 4:391-402.

76. Ryall RL, Grover PK, Stapleton AMF, Barrell DK, Tang Y, Moritz RL, and Simpson RJ. 1995. The urinary F1 activation peptide of human prothrombin is a potent inhibitor of calcium oxalate crystallization in undiluted human urine in vitro. *Clin Sci* 89:533-541.

77. Ryall RL, Harnett RM, Hibberd CM, Edyvane KA, and Marshall VR. 1991. Effects of chrondriotin sulphate, human serum albumin and Tamm-Horsfall mucoprotein on calcium oxalate crystallisation in undiluted human urine. *Urol Res* 19:181-188.

78. Scott R. 1990. The epidemiology of urolithiasis. In Renal tract stone. Metabolic basis and clinical practice. Wickham JEA and Buck AC, editors. Longman Group UK Limited, London, 19-28.

79. Shiraga H, Min W, VanDusen WJ, Clayman MD, Miner D, Terrell CH, Sherbotie JR, Foreman JW, Przysiecki, Nielson EG, and Hoyer JR. 1992. Inhibition of calcium oxalate crystal growth in vitro by uropontin: Another member of the aspartic acid-rich protein superfamily. *Proc Natl Acad Sci USA* 89:426-430.

80. Soucie JM, Thun MJ, Coates RJ, McClellan W, and Austin H. 1994. Demographic and geographic variability of kidney stones in the United States. *Kid Int* 46:893-899.

81. Stapleton AMF, Dawson CJ, Grover PK, Hohmann A, Comacchio R, Boswara V, Tang Y, and Ryall RL. 1996. Further evidence linking urolithiasis and blood coagulation: Urinary prothrombin fragment 1 is present in stone matrix. *Kidney Int* 49:880-888.

82. a) Stapleton AMF and Ryall RL. 1995. Blood coagulation proteins and urolithiasis are linked: crystal matrix protein is the F1 activation peptide of human prothrombin. *Br J Urol* 75:712-719.

83. b) Stapleton AMF and Ryall RL. 1995. Crystal matrix protein - getting blood out of a stone. *Min Elect Metab* 20:399-409.

84. a) Stapleton AMF, Seymour AE, Brennan JS, Doyle IR, Marshall VR, and Ryall RL. 1993. Immunohistochemical distribution and quantification of crystal matrix protein. *Kid Int* 44:817-824.

85. b) Stapleton AMF, Simpson RJ, and Ryall RL. 1993. Crystal matrix protein is related to human prothrombin. *Biochem Biophys Res Comm* 195:1199-1203.

86. Stapleton AMF, Timme TL, and Ryall RL. 1998. Gene expression of prothrombin in the human kidney and its potential relevance to kidney stone disease. *Br J Urol* 81:666-672.

87. Suzuki K, Moriyama M, Nakajima C, Kawamura K, Miyazawa K, Tsugawa R, Kikuchi N, and Nagata K. 1994. Isolation and partial characterisation of crystal matrix protein as a potent inhibitor of calcium oxalate crystal aggregation: evidence of activation peptide of human prothrombin. *Urol Res* 22:45-50.

88. Vahlensieck W. 1986. Review: The importance of diet in urinary stones. *Urol Res* 14:283–288.

89. Verkoelen CF, Romijn JC, de Bruijn WC, Boeve ER, Cao L, and Schroder FH. 1995. Association of calcium oxalate monohydrate crystals with MDCK cells. *Kid Int* 48:129-138.

90. Vermooten V. 1937. The occurrence of renal calculi and their possible relation to diet. *J Am Med Assoc* 109:857-859.

91. Werness PG, Berghert JH, and Smith LH. 1981. Crystalluria. *J Crystal Growth* 53:166-181.

92. Wesson JA, Worcester EM, Weissner JH, Mandel NS, and Kleinman JG. 1998. Control of calcium oxalate crystal structure and cell adherence by urinary macromolecules. *Kidney Int* 53:952-957.

93. Whalley NA, Martins MC, Van Dyk RC, and Meyers AM. 1999. Lithogenic risk factors in normal black volunteers, and black and white recurrent stone formers. *Br J Urol* 84:243-248.

94. Whalley NA, Moraes MFBG, Shar TG, Pretorius SS, and Meyers AM. 1998. Lithogenic risk factors in the urine of black and white subjects. *Br J Urol* 82:785-790.

95. Wise RO and Kark AE. 1961. Urinary calculi and serum calcium levels in Africans and Indians. *S Afr Med J* 35:47-50.

96. Worcester EM. 1996. Inhibitors of stone formation. *Sem Nephrol* 16:474-486.

97. Yoshioka T, Koide T, Utsunomiya M, Itatani H, Oka T, and Sonada T. 1989. Possible role of Tamm-Horsfall glycoprotein in calcium oxalate crystallisation. *Br J Urol* 64:463-467.

CHAPTER 2: COMPOSITION & INHIBITORY PROPERTIES OF URINE & URINARY MACROMOLECULES

2.1 INTRODUCTION

The remarkable difference between the incidence of kidney stones amongst South Africa's white and black populations is now well recognised. Thus identification of urinary parameters or inhibitory properties which distinguish the stone-prone white group from the stone-free black group is an intriguing challenge. As outlined in chapter 1, studies to date have addressed urine composition and have reported several noteworthy findings. Examples are the black population's lower urinary calcium (Modlin 1967, Whalley *et al.* 1998, Rodgers and Lewandowski 2002), citrate (Modlin 1967, Meyers *et al.* 1994, Whalley *et al.* 1998, Lewandowski *et al.* 2001), phosphate and urate excretions (Rodgers and Lewandowski 2002), higher urinary oxalate excretion (Lewandowski *et al.* 2001) and higher urinary pH (Rodgers and Lewandowski 2002). Paradoxically, the low citrate and higher oxalate are associated with an increased risk of stone formation.

Howard and Thomas (1958) first reported the inhibitory properties of human urine more than forty years ago. They demonstrated that urine from healthy subjects inhibited the calcification of rat cartilage more effectively than that of stone-formers. However, to date no studies have compared the inhibitory properties of the white and black populations' urine in an attempt to explain the latter group's low stone incidence.

Robertson described CaOx urolithiasis as the result of an inequality between the opposing forces of supersaturation and inhibitory activity in urine (Robertson *et al.* 1976). Several workers have suggested that it is inhibitory activity that distinguishes stone-forming and healthy individuals (Ryall *et al.* 1986, Kok *et al.* 1990, Asplin *et al.* 1999) since both groups' urines are supersaturated with calcium salts (Werness *et al.* 1981). A study by Asplin confirmed this postulate, showing that inhibition experiments were good discriminators between stone-forming and healthy individuals whereas routine urine chemistry and supersaturation data were similar in the two groups (Asplin *et al.* 1999).

Since crystal aggregation is acknowledged as more important than growth in determining stone formation (Kok *et al.* 1990, Hess and Kok 1996), adequate control of this process would appear to be essential for protection against stone formation. Thus, an

objective of this thesis was to investigate the two population groups with respect to urinary inhibition of aggregation and then to compare these trends with their urine compositions and supersaturation levels. In this chapter, crystallisation experiments involving urine and macromolecular urine extracts from black and white subjects are described.

2.2 METHODS

Inhibitory activity of urine

2.2.1 Urine collection and treatment

Twenty-four hour urine samples were collected in plastic bottles containing a boric acid preservative (5 g per 24-hr urine). The subjects were five black and five white males (respective ages 21 - 25 and 19 - 27 years) on their free unrestricted diet and with no previous history of kidney stones. Urines testing positive for haematuria or nitrite using urinalysis test strips (Medi Test Combi 5N, Macherey-Nagel) were excluded. Each urine was filtered through a 0.75 μm pre-filter followed by a 0.45 μm nitrocellulose filter paper before use.

Aliquots of each sample were retained for urinalysis. Calcium, magnesium, sodium and potassium were analysed using a Varian 1275 Model (Australia) flame atomic absorption spectrometer (Willis 1967, Trudeau and Freier 1967, Fernandez and Kahn 1971). Oxalate and citrate were quantified using enzymatic assays: oxalate was analysed using oxalate decarboxylase and an ascorbate oxidase spatula was used to remove *L*-ascorbic acid (Chiriboga 1963), while citrate was determined by citrate lyase conversions to oxaloacetate (Gruber and Möllering 1966). Inorganic phosphorus was determined using ammonium molybdate (Dryer and Routh 1963), creatinine was determined using picric acid (Rock *et al.* 1986) and uric acid using uricase (Fossati *et al.* 1980). Analytical kits were used for these determinations (Boehringer Mannheim; oxalate kit: Sigma). Chloride was determined using a chloride sensitive electrode.

The urinary relative supersaturations of CaOx, brushite and uric acid were calculated using the programme EQUIL2 (Werness *et al.* 1985). The terms relative supersaturation and supersaturation are used synonymously in the literature and this approach was adopted in the present thesis. Urine composition data was analysed statistically by analysis of variance (ANOVA) and the results considered statistically significant if $p \leq 0.05$. Average values and their standard errors (SE) are reported. The

reasonable assumption was made that the two groups had equal variances and thus the variances were pooled.

2.2.2 Preparation and characterisation of calcium oxalate monohydrate crystals

COM crystals were prepared according to Pak *et al.* (1975). Equal volumes of 0.010 mol/l $CaCl_2$ and 0.010 mol/l NaOx solutions were mixed at a constant rate of 1 ml/min using a peristaltic pump while stirring. The mixture was then stirred for 7 days at 10 ^{0}C after which the crystals were collected by filtration (0.22 μm). The crystals were dried at 37 ^{0}C for at least one hour and then verified by x-ray powder diffraction (XRD) and thermogravimetric analysis (TGA). The crystals were also viewed by scanning electron microscopy (SEM).

2.2.2.1 X-ray powder diffraction

The crystal powder pattern was measured using a Philips PW1050/25 goniometer with nickel filtered CuKα radation (λ = 1.51418 Å) produced at 40 kV and 25 mA. Ideally, the specimen should be a homogeneous powder of constant particle size in which the material has no preferred orientation as this reduces the likelihood of erroneous relative intensities (Jenkins and de Vries n.d., Glasser 1977). Since fine grinding greatly reduces the contribution of this factor (Klug and Alexander 1974), the sample was ground with a pestle and mortar prior to analysis.

The powder was placed in an aluminium holder and a scan of the relative intensity of reflected x-rays as a function of the Bragg angle (2θ) was recorded between angular limits of 12-40 ^{0} for each sample. The angle which coincided with the maximum of the prominent peaks was converted to its corresponding d-spacing using a standard table for Cu Kα radiation (Parrish and Mack 1963). These d-spacings were then compared with standard reference values (Table 2.1, page 28) for COM, COD and CaOx trihydrate (COT) crystals (Sutor and Scheidt 1968, Deganello *et al.* 1981).

Intensities can be influenced by several factors such as crystal motion (Klug and Alexander 1974), the theta angle and the path distance of x-rays (Jenkins and de Vries n.d.). A detailed calculation of the corrected intensity is possible by taking into account many of these factors, but this practice is seldom used for routine analyses such as the determination of crystal phases (Jenkins and de Vries n.d.). The accuracy of the method is thus limited to no more than 5 % (Glasser 1977).

In the present study the percentage composition of the crystals was determined semi-quantitatively on the basis of calculated d-spacings and estimation of relative peak intensities, rather than by detailed calculation.

2.2.2.2 *Thermogravimetric analysis*

For thermogravimetric analysis, crystals (4 mg) were heated from 40 ^{0}C to 200 ^{0}C at a rate of 10 ^{0}C per minute (Perkin Elmer PC7 system). A plot of weight percentage versus temperature was obtained from which the percentage change in weight was determined. This mass loss was then correlated to the number of water molecules in the original compound.

Table 2.1: Interplanar spacings and relative intensities of powder patterns of calcium oxalates

* Calcium oxalate monohydrate:		* Calcium oxalate dihydrate:		** Calcium oxalate trihydrate:	
d-spacing (Å)	*Relative intensity*	*d-spacing (Å)*	*Relative intensity*	*d-spacing (Å)*	*Relative intensity*
5.93	100	8.70	12	7.87	40
5.79	25	6.31		6.70	20
4.64	7	6.15	100	5.50	100
4.52	6	4.40	45	5.28	40
3.78		3.89	14	4.99	60
3.76	13	3.67	8	4.79	20
3.65	100	3.58	1	4.02	20
3.00	10	3.38	2	3.75	20
2.97	46	3.15	3	3.67	40
2.91	12	3.09		3.62	60
2.89	10	3.07	18	3.58	10
2.84	14	2.81	20	3.43	20
2.51	2	2.77		3.35	10
2.48	30	2.75	85	3.26	20
2.41	5	2.41	14	2.84	100
2.37	2	2.39	14	2.77	80
2.34	90	2.33	10	2.74	40
				2.69	40
				2.66	20
				2.64	40

** Sutor and Scheidt 1968; ** Deganello et al. 1981*

2.2.2.3 *Scanning electron microscopy*

Crystals (0.1 mg) were retrieved on filter papers (0.22 µm) which were glued onto aluminium stubs and coated with a single layer of Au/Pd. The crystals were examined using a Leica S440 scanning electron microscope (Leica Cambridge Ltd , Cambridge, England) operating at an accelerating voltage of 10 kV, a working distance of 10 – 15 mm and a probe current of 20 - 30 pA.

2.2.3 Sedimentation rates

2.2.3.1 *Preparation of COM crystal slurries and slurry / urine mixtures*

COM crystal slurries were prepared for sedimentation experiments by the addition of 0.8 mg/ml COM crystals to a buffer containing 0.010 mol/l tris(hydroxymethyl)-

aminomethane(Tris).HCl, 0.090 mol/l NaCl (pH 7.2) (Hess *et al.* 1989). Crystal slurries were equilibrated overnight (at least 16 hours) at 37 ^{0}C with stirring (1100 rpm) to ensure that equilibration saturation had been achieved.

After filtration, urine samples from white and black subjects (referred to as WU and BU, respectively) were dialysed (10 kDa membrane cut-off) extensively against the same buffer used to prepare the slurries and passed through a 0.22 μm filter. The slurries were then mixed with the appropriate volume of urine to achieve a final dilution of 1:2 (urine to crystal volume) and equilibrated for 2 hours at 37 ^{0}C at 1100 rpm.

2.2.3.2 Measurement of COM crystal sedimentation rates

The equilibrated mixtures were transferred to a 10 mm glass cuvette and placed in a spectrophotometer (Unicam Helios, Merck, Johannesburg) fitted with a water circulation system and a stirrer attachment. The absorbance was then monitored at 620 nm and 37 ^{0}C for 10 minutes (Hess *et al.* 1989). Such plots will henceforth be referred to as an OD_{620} plot; a typical example is shown in Figure 2.1 below.

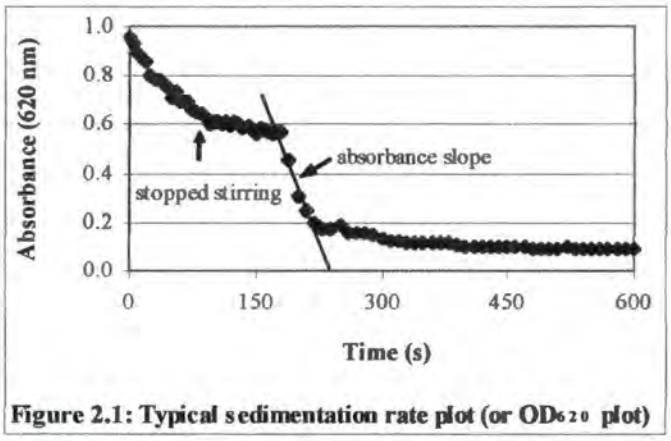

Figure 2.1: Typical sedimentation rate plot (or OD_{620} plot)

Crystal aggregation was induced by slow stirring at 722 rpm until the system was stable and equilibrium had been reached again, demonstrated by a stable absorbance for at least 10 seconds. Stirring was then stopped so that the sedimentation rate of crystals indicated by a decrease in absorbance could be monitored. Since no further growth or dissolution was possible in the system because it was at equilibrium, the slope of the linear decrease in absorbance (shown by a straight line in Figure 2.1 and henceforth referred to as the absorbance slope) could be directly related to the degree of crystal aggregation of the sample. The degree of aggregation of each test mixture (*i.e.* urine - slurry dilution) was calculated by the ratio of the slope of the test sample's (S_T) absorbance *vs.* time graph and the slope of the equivalent graph for the control COM slurry (S_C). The percentage

inhibition of aggregation (I_A) was determined from the formula: $I_A = 100 - [100 \times (S_T/S_C)]$ (Hess *et al.* 1989).

2.2.3.3 Verification of sedimentation rates method

Since the sedimentation method had not been previously employed in the author's laboratory, a series of urine : crystal dilutions (1:1, 1:2, 1:4, 1:8, 1:16) was tested using a single 24-hour urine obtained from a white male (27 years). These results were compared with those published by Hess *et al.* (1989) in order to verify the methodology. For these experiments, a slow stirring speed of 722 rpm was used since the experimental data obtained was most similar to published data obtained by Hess and co-workers at 500 rpm (Hess *et al.* 1989).

2.2.3.4 Statistical analysis

The slope of each absorbance versus time plot was determined by linear regression analysis. The square of the Pearson product moment correlation coefficient (R^2) corresponding to the slope is reported for these analyses. The average slopes for the WU and BU-dosed COM slurries were compared statistically by ANOVA, and standard errors are reported. Results were considered statistically significant if $p \leq 0.05$.

2.2.4 Zeta potentials

2.2.4.1 The concept of zeta potential

The extent of adhesion between particles can be defined as the difference between the sum of the cohesive van der Waals and viscous binding forces and the repulsive electrostatic forces between them (Finlayson 1976). The latter is defined as the electrical potential at the interface of a layer of chemically adsorbed ions on a crystal surface and the diffuse double layer of oppositely charged ions surrounding this, more frequently referred to as zeta potential (Scurr and Robertson 1986a). Zeta potential is regarded as the main driving force favouring disaggregation (Hess and Kok 1996). Curreri *et al.* (1979) were the first to postulate that small molecular weight molecules that inhibited crystal aggregation may do so by modification of the crystal zeta potential. Finlayson (1976) later suggested that polyanionic macromolecular inhibitors also employ this mechanism. However, the presence of hydrophilic regions in these molecules (for example, proteins) results in competition by viscous binding forces and the electrostatic forces, thereby increasing the

probability of crystal adhesion rather than repulsion (Scurr and Robertson 1986b). It has been shown that trends towards more negative zeta potentials correlate well with an increase in inhibition of aggregation in certain molecules (such as heparin, THM and macromolecular extracts isolated from urine) (Scurr and Robertson 1986b). Practically, zeta potential may thus be regarded as an indicator of the potential of a compound to reduce aggregation by the action of its repulsive negative charge.

2.2.4.2 Preparation of COM crystal slurry / urine mixtures

COM crystal slurries were prepared for zeta potential experiments by the addition of 0.3 mg/ml COM crystals to a 0.010 mol/l sodium acetate buffer (pH 5.7). The ratio of urine to crystal slurry volume used was 1:2. Crystal slurries were then treated in the same way as described for the sedimentation experiments (paragraph 2.2.3.2) except that slurries were incubated at 25 ^{0}C (since the instrument measures zeta potential at this temperature).

2.2.4.3 Measurement of zeta potentials

After equilibration, the surface charge of each crystal slurry was determined in triplicate by measuring its zeta potential (mV) using a Zetasizer 4 (Malvern, England). The average percentage decrease in zeta potential of each test sample (Z_T), *i.e.* slurry / urine mixture, relative to its COM slurry control (Z_C) was calculated using the following formula: $100 \times [(Z_T - Z_C)/Z_C]$.

2.2.4.4 Statistical analysis

The average zeta potential of the WU and BU-dosed slurries were compared by ANOVA and standard errors are reported. The results were considered statistically significant if $p \leq 0.05$.

Inhibitory activity of macromolecular urine extracts

2.2.5 Urine collection, preparation and treatment

Twenty-four hour urine samples were collected from ten black and ten white males (respective ages 20 - 25 and 19 - 21 years) with no previous history of stone disease and were treated as described in paragraph 2.2.1 (page 26). An aliquot of each urine was retained for protein determination. Of the 20 urines, ten randomly-chosen urines (five black and five white subjects) were used for further experiments. These samples were

dialysed (10 kDa membrane cut-off) extensively against distilled water and freeze-dried to yield the macromolecular urine extract (MM). Each MM was reconstituted in a minimum volume of distilled water for use in the inhibitory activity study. The protein concentration of each MM was redetermined prior to the activity study since protein may have been lost during dialysis.

2.2.6 Determination of urinary protein concentration

The protein concentration of each urine was determined using the Bradford method (Bradford 1976). An aliquot of each sample (800 µl) was added to a Bio-Rad protein assay solution (200 µl) (Bio-Rad) and incubated at room temperature for 5 minutes. The absorbance was measured at 595 nm and compared to a triplicate standard curve obtained using bovine serum albumin in the range 1 µg/ml - 10 µg/ml. The slope of the standard curve and R^2 value corresponding to the slope were determined by linear regression analysis.

2.2.7 Preparation of synthetic urine and metastable limit determination

A synthetic urine (SU) was prepared according to the method of Burns and Finlayson (1980) for an inhibitory activity study. Six salts were dissolved in the given sequence in distilled water at the following final concentrations: 0.106 mol/l NaCl, 0.0323 mol/l NaH_2PO_4, 0.00321 mol/l $Na_3C_6H_5O_7.2H_2O$, 0.00385 mol/l $MgSO_4.7H_2O$, 0.0170 mol/l Na_2SO_4 and 0.0637 mol/l KCl. Care was taken to ensure that each salt had dissolved completely before the next one was added to the mixture. A separate solution of $CaCl_2.2H_2O$ was added to the mixture with stirring at a final concentration of 5.75 mmol/l followed by the slow addition of a NaOx solution at a final concentration of 0.318 mmol/l. The pH was adjusted to 6.2 by addition of 0.148 g NH_4Cl and 716 µl of 5 mol/l NH_4OH per 100 ml of SU. The final solution was stored at 4 ^{0}C for a maximum of 5 days and filtered through a 0.22 µm filter paper before use.

Difficulties were encountered with the above preparation. Firstly, the solution frequently became (irreversibly) cloudy during the preparation stage if the NaOx solution was added too quickly or the pH was allowed to exceed 6.2 while adjusting with NH_4OH. Secondly, the solution remained stable for a maximum period of only 5 days before salts began to precipitate (indicated by an opaque appearance).

The CaOx metastable limit (MSL) of the synthetic urine was determined. This is the concentration at which a solution of CaOx is in a state of metastability or supersaturation and above which spontaneous crystallisation will occur (Ryall *et al.* 1985).

A measure of the MSL is obtained by challenging the urine to crystallise with increasing doses of NaOx and monitoring the effect on particle number. A low MSL indicates relative ease of crystallisation.

The CaOx MSL of the synthetic urine was measured using a Coulter Counter I (Beckmann, Johannesburg) fitted with a 140 µm orifice (2.8 - 90.0 µm particle size range) according to the method described by Ryall *et al.* (1985). For this determination, 8 ml aliquots of synthetic urine were incubated in plastic Coulter cups in a shaking water bath (100 rpm) at 37 ^{0}C. The samples were dosed with 80 µl NaOx of increasing concentrations, ranging from 15 mmol/l to 195 mmol/l in increments of 15 mmol/l. After a 30-minute incubation period, the particle number at each concentration was measured in duplicate and a plot of particle number versus NaOx concentration was constructed. From this plot, the exogenous NaOx concentration above which spontaneous crystallisation occurred (indicated by a sudden increase in particle number) was determined and was taken as a measure of the urine's MSL. A typical plot is shown in Figure 2.2 below. The MSL is equivalent to 120 mmol/l NaOx and thus a concentration exceeding this value (at 1 % of the urine volume) would be required to induce spontaneous crystallisation.

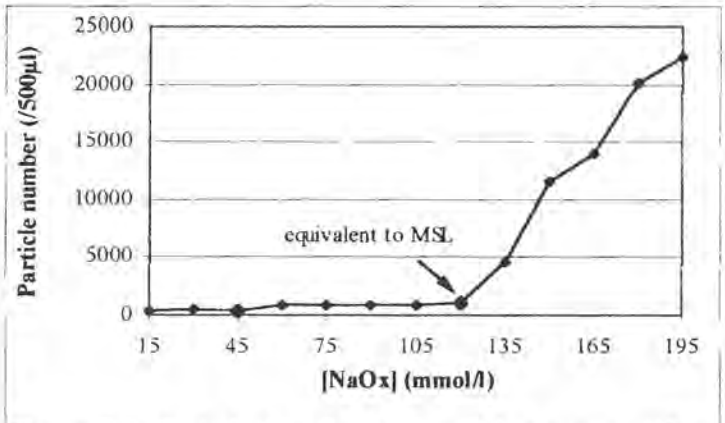

Figure 2.2: Typical plot of particle number versus sodium oxalate concentration to determine metastable limit (MSL)

2.2.8 Particle size distribution determination

Aliquots of synthetic urine (10 ml each) were pipetted into glass conical flasks and dosed with 100 µl NaOx at a concentration 30 mmol/l in excess of the previously determined MSL to produce adequate crystallisation (Ryall *et al.* 1985). Five aliquots were retained as control samples, five were dosed with MM obtained from white subjects (referred to as WMM) and five were dosed with MM obtained from black subjects (referred to as BMM). Control and MM-dosed urines were dosed with the same NaOx concentration. The final MM concentration was equivalent to the protein concentration of the filtered urine from

which the MM was derived. The control and MM-dosed urines were then incubated at 37 ^{0}C in a shaking water bath (100 rpm) for 120 minutes after which the particle size distributions were measured using a Coulter Counter I.

2.3 RESULTS

Inhibitory activity of urine

2.3.1 Characterisation of calcium oxalate monohydrate crystals

The composition of the CaOx crystals prepared according to the method described by Pak *et al.* (1975) was verified by XRD, TGA and SEM. The XRD pattern of the crystals together with the d-spacings (Å) of prominent peaks is shown in Figure 2.3. The assignment of these peaks is shown in Table 2.2. All peaks corresponded with known COM reflections (refer to Table 2.1 on page 28 for a standard reference table).

Figure 2.3: X-ray powder diffraction pattern of CaOx crystals prepared according to Pak *et al.* (1975)

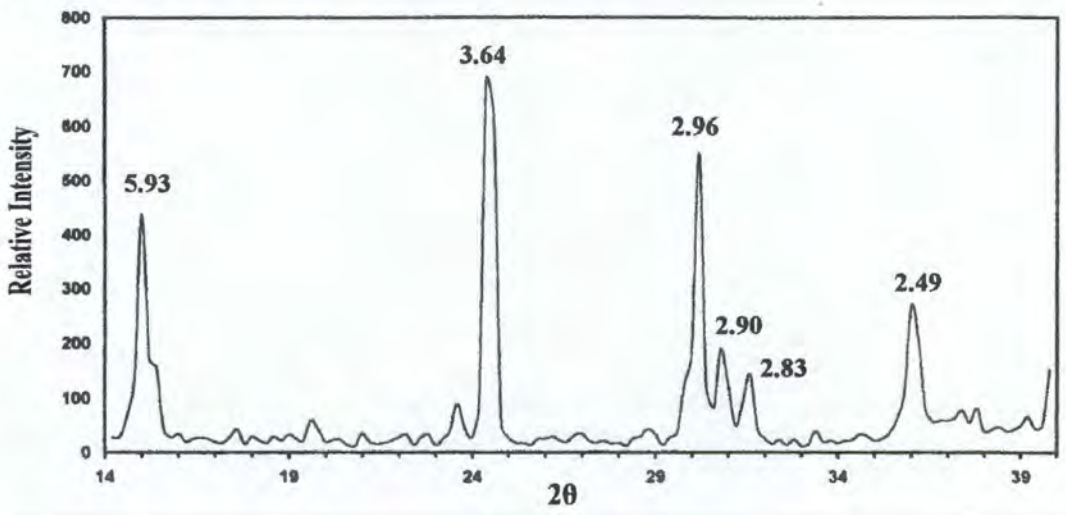

Table 2.2: X-ray powder diffraction peak assignments and percentage composition of CaOx crystals prepared according to Pak *et al.* (1975)

d-spacing (Å)	Assignment	
5.90	COM	100% COM
3.64	COM	
2.96	COM	
2.90	COM	
2.83	COM	
2.49	COM	

The TGA spectrum of these crystals is shown in Figure 2.4 and indicates the decrease in weight (%) of the crystals as a function of temperature. The experimental mass loss of 12.24 % (at an onset temperature of 103.4 ^{0}C) corresponded closely with the theoretical value of 12.32 % for the loss of one water molecule associated with a single CaOx molecule. XRD and TGA thus confirmed that the crystals were composed of 100 % COM, as required for the slurry studies.

Figures 2.5.1 - 2.5.2 show scanning electron micrographs of the CaOx crystals at different magnifications. Small crystals (~4 μm in diameter) of ill-defined morphology were observed and were thus inconclusive in demonstrating CaOx hydrate morphology.

Figure 2.4: Thermogravimetric analysis of CaOx crystals prepared according to Pak *et al.* (1985)

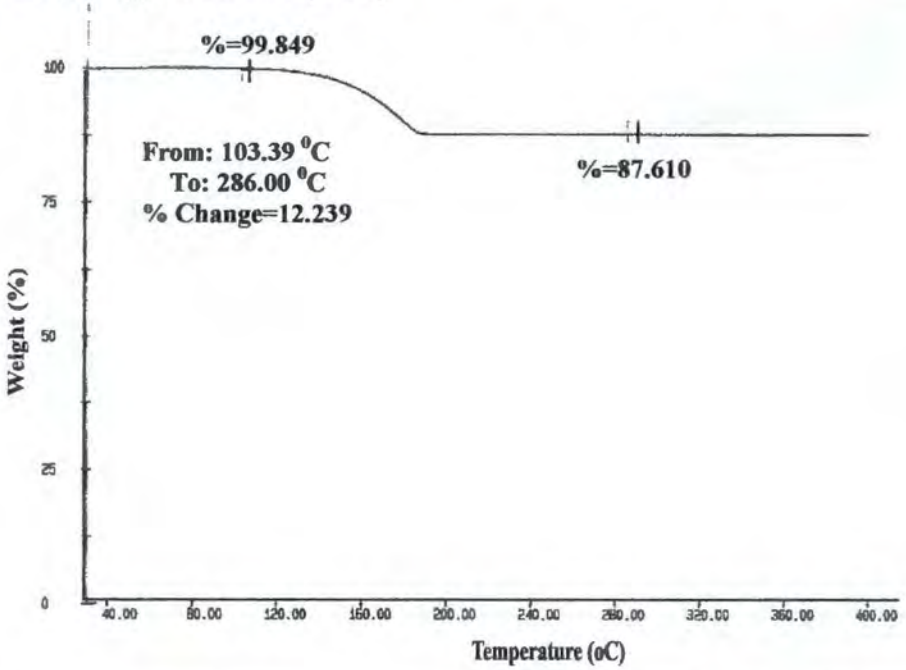

Figure 2.5: Scanning electron micrographs of calcium oxalate crystals prepared according to Pak *et al.* (1975). The photographs were taken at the following magnifications: 10K (Fig 2.5.1) and 12K (Fig 2.5.2).

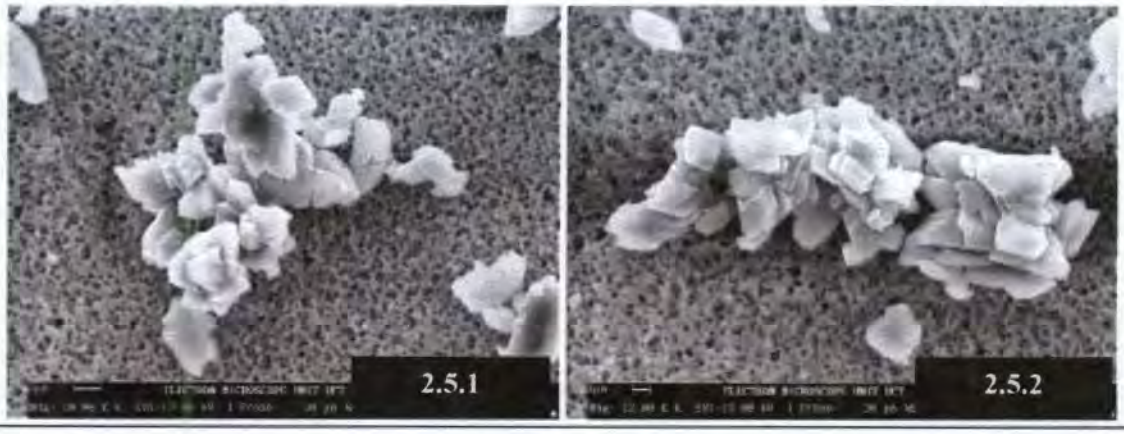

2.3.2 Sedimentation rates

Figure 2.6 shows the OD_{620} plots of a COM crystal slurry before and after the addition of urine at various dilutions. A gradual increase in the absorbance slope was observed as the urine to crystal ratio was increased from 1:1 to 1:16. The absorbance slopes and corresponding percentage inhibition of aggregation relative to the COM slurry control for and corresponding percentage inhibition of aggregation relative to the COM slurry control for each dilution are presented in Table 2.3. The data demonstrated that inhibition of aggregation (I_A) decreased as the ratio of urine to crystal slurry increased.

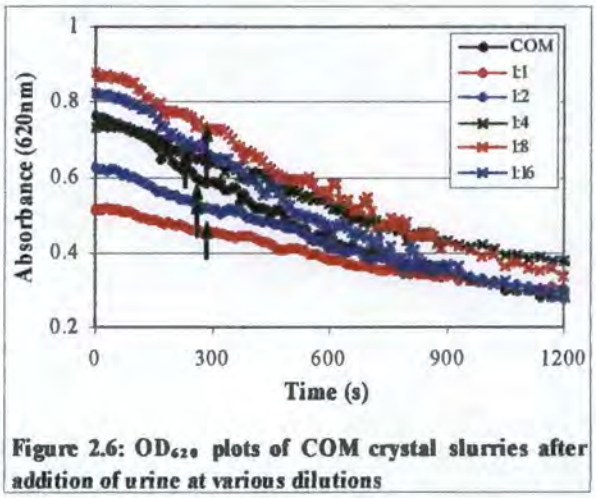

Figure 2.6: OD_{620} plots of COM crystal slurries after addition of urine at various dilutions

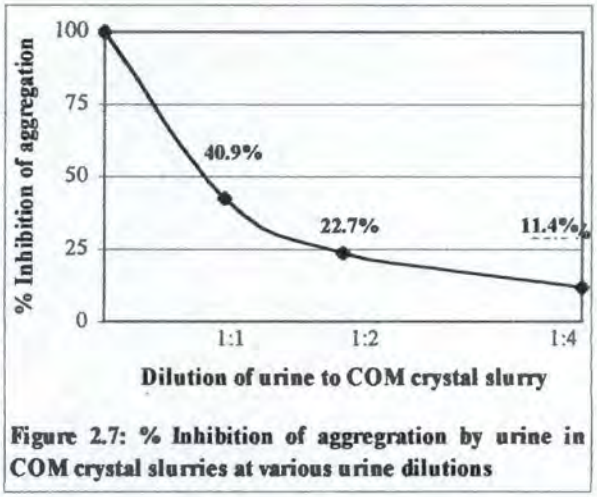

Figure 2.7: % Inhibition of aggregration by urine in COM crystal slurries at various urine dilutions

Table 2.3: Absorbance slopes and inhibition of aggregation (I_A %) of COM crystal slurry by urine at various dilutions

	COM slurry	Urine to COM crystal slurry dilution: 1:1	1:2	1:4	1:8	1:16
Absorbance slope ($x\text{-}10^{-5}s^{-1}$)	44	26	34	39	77	65
R^2	0.97	0.97	0.98	0.97	0.95	0.95
I_A %		40.9	22.7	11.4	-75.0	-47.7

This trend is clearly shown in Figure 2.7. The concentration dependent increase in I_A was similar to that reported by Hess *et al.* (1989), except that a sharper decrease in inhibition between 1:1 and 1:4 dilutions was observed by Hess (approximate I_A: 65 % for 1:2 and 50 % for 1:4 dilutions) than in the present study. However, the trends were sufficiently similar to verify that the method provided adequate results using the author's system. The 1:8 and 1:16 dilutions were omitted from the I_A plot in Figure 2.7 and were not considered for use in further experiments since negative inhibition data was obtained (suggesting promotion of aggregation).

Figure 2.8 shows a plot of the average rate of decrease in absorbance (620 nm) of a COM crystal slurry in the absence and presence of urine from white and black subjects at a urine to crystal dilution of 1:2. The individual experiments from which these averages were

obtained are shown in Appendix A (COM: Figure A1, page A4; COM+WU: Figures A2.1 - A2.5, page A5; COM+BU: Figures A3.1 – A3.5, page A6). It was apparent from Figure 2.8 that the sedimentation rate of the COM crystal slurry was considerably reduced by the addition of urine from both white and black subjects (indicated by a more gradual slope), while the effect of the two group's urine appeared to be similar in this regard (indicated by the equal slopes). The absorbance slope and inhibition of aggregation data for each white and black subject is shown in Tables 2.4 and 2.5, respectively. All subject's urine reduced the absorbance slope of the COM crystal slurry and thus inhibited crystal aggregation. The average inhibition exhibited by the white subjects (83.2 %) did not differ significantly from the black subjects (85.4 %) ($p > 0.05$). No noteworthy inter-group differences were apparent.

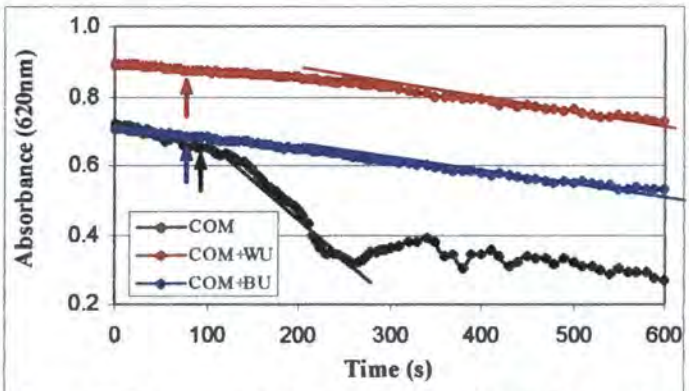

Figure 2.8: Average OD_{620} plot of COM crystal slurries. Before and after addition of urine from white (WU) and black (BU) subjects at a 1:2 dilution

Table 2.4: Absorbance slopes and inhibition of aggregation (I_A %) of COM crystal slurries before and after addition of white subjects' urine (WU) at a dilution of 1:2

Sample	Absorbance slope ($x\text{-}10^{-5} s^{-1}$) (R^2)	I_A (%)
COM	266 (0.981)	
COM+WU1	29 (0.979)	89.1
COM+WU2	45 (0.939)	83.1
COM+WU3	48 (0.935)	82.0
COM+WU4	57 (0.915)	78.6
COM+WU ave:	45 (0.927) ± 4.8	83.2

Table 2.5: Absorbance slopes and inhibition of aggregation (I_A %) of COM crystal slurries before and after addition of black subjects' urine (BU) at a dilution of 1:2

Sample	Absorbance slope ($x\text{-}10^{-5} s^{-1}$) (R^2)	I_A (%)
COM	266 (0.981)	
COM+BU1	35 (0.937)	86.8
COM+BU2	47 (0.956)	82.3
COM+BU3	32 (0.930)	88.0
COM+BU4	41 (0.886)	84.6
COM+BU ave:	39 (0.935) ± 4.8	85.4

2.3.3 Zeta potentials

The zeta potentials of a COM crystal slurry before and after addition of urine from white and black subjects at a urine to crystal dilution of 1:2 are presented in Tables 2.6 and 2.7, respectively. The individual values from which the averages were calculated are shown in Appendix A (white subjects: Table A1.1, page A1; black subjects: Table A1.2, page A1).

Table 2.6: Average zeta potential (ZP) of COM crystal slurries before and after addition of white subjects' urine (WU) at a dilution of 1:2

Sample	ZP ave. ± SE (mV)	% Increase in negative charge wrt COM	p-value wrt COM	n-value
COM	-17.9 ± 0.14			6
COM+WU1	-29.0 ± 0.57	62.5	< 0.01	3
COM+WU2	-29.6 ± 0.25	65.8	< 0.01	3
COM+WU3	-30.0 ± 0.12	67.9	< 0.01	3
* COM+WU4	-17.2 ± 0.74	-3.6	> 0.05	3
COM+WU ave:	-29.8 ± 2.89	65.4		

** Excluded from average since no change in ZP wrt COM (p>0.05)*

Table 2.7: Average zeta potential (ZP) of COM crystal slurries before and after addition of black subjects' urine (BU)

Sample	ZP ave. ± SE (mV)	% Increase in negative charge wrt COM	p-value wrt COM	n-value
COM	-17.9 ± 0.14			6
COM+BU1	-22.9 ± 0.35	28.3	< 0.01	3
COM+BU2	-23.5 ± 0.088	31.8	< 0.01	3
COM+BU3	-23.3 ± 0.17	30.7	< 0.01	3
COM+BU4	-23.4 ± 0.22	30.9	< 0.01	3
COM+BU ave:	-23.2 ± 2.89	30.4		

All of the subjects' urine (except WU4), significantly decreased the zeta potential of the COM slurry from -17.9 mV to values ranging from -22.9 to -30.0 mV ($p < 0.01$). There were no intra-group differences. However, there was a significant inter-group difference between the average zeta potentials ($p < 0.05$). The average decrease in zeta potential of the COM crystal slurry achieved by the white subjects' urine was 65.4 %, compared with 30.4 % after addition of the black subjects' urine (Figure 2.9).

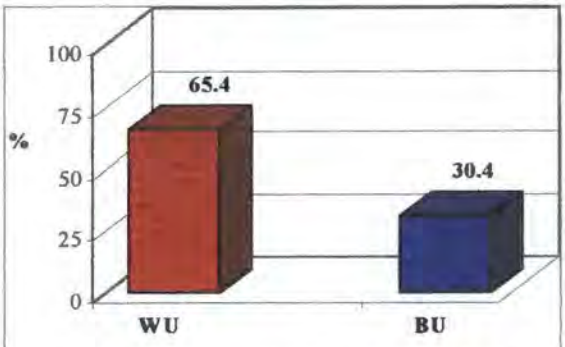

Figure 2.9: Comparison of % decrease in ZP of COM crystal slurry after addition of white (WU) and black (BU) subjects' urine at a dilution of 1:2

Inhibitory activity of macromolecular urine extracts

2.3.4 Urine protein concentration

The absorbance of a series of bovine serum albumin (BSA) concentrations measured using the Bradford protein assay are presented in Table 2.8. The standard curve and linear regression data corresponding to these results are shown in Figure 2.10.

Table 2.8: Bradford protein assay standard curve data using bovine serum albumin (BSA)

BSA (µg/ml)	Absorbance (595nm)	SE
1	0.0651	0.0037
2	0.1150	0.0140
3	0.1521	0.0018
4	0.2114	0.0077
5	0.2610	0.0085
6	0.3222	0.0061
7	0.3449	0.0118
8	0.4083	0.0096
9	0.4519	0.0165
10	0.5039	0.0093

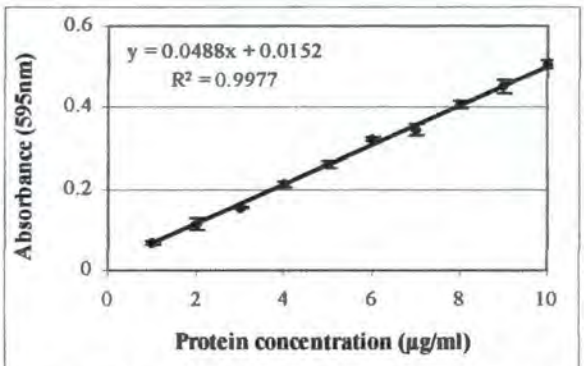

Figure 2.10: Standard curve for Bradford protein assay using bovine serum albumin

The urinary protein concentration and corresponding daily urinary protein excretions in white and black subjects, calculated using the BSA standard curve, are shown in Table 2.9. A large within-group variation was observed in both population groups. The protein concentrations ranged from 12.8 - 69.2 mg/l and 15.6 - 95.2 mg/l amongst the white and black subjects, respectively. Daily protein excretions ranged from 26.8 – 85.0 mg/day and 24.1 - 110 mg/day for the white and black subjects, respectively. Comparison of the average values showed that the black subjects' urinary protein concentration tended to be higher than the white subjects (38.4 *vs.* 33.2 mg/l). In contrast, the black subjects' daily

protein excretion tended to be lower than the white subjects (50.7 *vs.* 58.3 mg/day). However, these trends were not statistically significant ($p > 0.05$). The average protein excretion values obtained were within the reported urinary values of 40 - 80 mg/day (Free 1986).

Table 2.9: Protein concentration (mg/l) and excretion (mg/day) of white and black subjects' urine

Sample	Protein concentration (mg/l)	Protein excretion (mg/day)	Sample	Protein concentration (mg/l)	Protein excretion (mg/day)
WU5	35.7	74.2	BU5	22.5	45.8
WU6	58.5	67.8	BU6	38.3	55.9
WU7	24.2	33.9	BU7	51.1	48.0
WU8	21.2	35.4	BU8	27.4	57.9
WU9	14.3	38.8	BU9	95.2	50.4
WU10	19.1	40.7	BU10	36.3	85.0
WU11	69.2	110	BU11	37.2	32.2
WU12	52.5	74.1	BU12	31.9	70.8
WU13	25.0	52.9	BU13	28.6	34.2
WU14	12.8	55.2	BU14	15.6	26.8
WU ave ± SE:	33.2 ± 6.69	58.3 ± 7.09	***BU ave ± SE:***	38.4 ± 6.69	50.7 ± 7.09

Average protein concentration: WU vs. BU $p>0.05$; average protein excretion: WU vs. BU $p>0.05$

2.3.5 Synthetic urine metastable limit

The average CaOx MSL plot of the synthetic urine, shown as particle number versus NaOx concentration, is presented in Figure 2.11. The data for this plot is shown in Appendix A, Table A2 (page A1). The MSL was equivalent to 45 mmol/l NaOx as shown by the enlarged data point (final urinary NaOx concentration: 0.45 mmol/l).

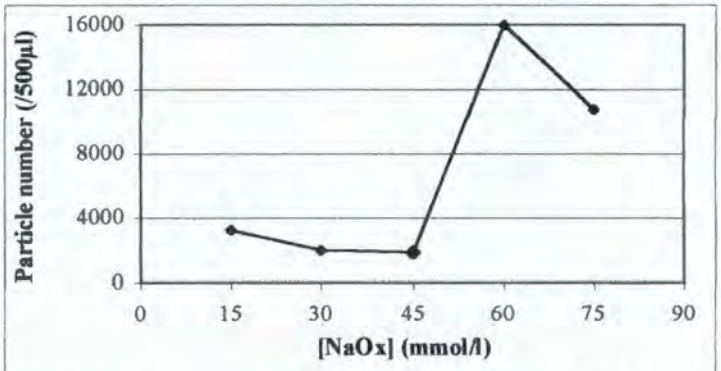

Figure 2.11: Average of particle number versus sodium oxalate concentration in synthetic urine

2.3.6 Particle size distributions

Figure 2.12 shows the average particle volume-particle size distributions at 120 minutes after addition of a NaOx load in excess of the MSL. A decrease in the average particle size was observed after addition of macromolecular urine extracts from both white and black

subjects as indicated by a shift in the mode of the protein-dosed distributions to smaller values relative to the synthetic urine.

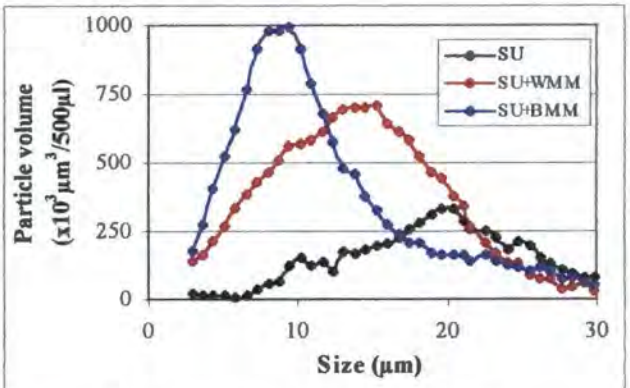

Figure 2.12: Average particle size distributions. Synthetic urine before and after addition of macromolecular urine extracts from white (WMM) and black (BMM) subjects. SU: 20.2µm, SU+WMM: 13.8µm, SU+BMM: 9.32µm

The size distributions for each subject from which these averages were calculated are shown in Appendix A (SU: Figures A4.1-4.5, page A7; SU+WMM: Figures A5.1-5.5, page A8; SU: Figures A6.1-6.5, page A9). The individual particle size values for the white and black subjects (giving rise to the peak of each curve above) are reflected in Table 2.10.

Table 2.10: Particle size (µm) of synthetic urine before and after addition of macromolecular urine extracts from white (WMM) and black (BMM) subjects

Sample	Particle size (µm)	% Decrease wrt SU
SU	21.5, 21.1, 20.4, 18.9, 18.9	
SU ave ± SE:	20.2 ± 0.823	
SU+WMM5	14.6	27.7
SU+WMM6	9.47	53.1
SU+WMM7	15.3	24.3
SU+WMM8	16.8	16.8
SU+WMM9	13.1	35.2
SU+WMM ave ± SE:	13.8 ± 0.823	31.7
SU+BMM5	9.47	53.1
SU+BMM6	10.2	49.5
SU+BMM7	8.74	56.7
* SU+BMM8	10.2, 21.5	49.5, -6.44
SU+BMM9	8.01	60.4
SU+BMM ave ± SE:	9.32 ± 0.823	53.9

** Size distribution was bimodal; smaller size was used for SU+BMM average calculation.*
SU+WMM ave vs. SU+BMM ave: $p<0.05$

All of the macromolecular urine extracts tested, regardless of the population group from which they were derived, induced a decrease in the average particle size of the synthetic urine. Comparison of the average size values for each population group showed that the urine extracts derived from the black subjects resulted in a significantly greater decrease in

the average particle size than the white subjects ($p < 0.05$). After addition of WMM and BMM, the average size in the synthetic urine decreased from 20.2 μm to 13.8 μm and 9.32 μm, respectively. These values correspond to particle size decreases of 31.7 and 53.9 % in the presence of WMM and BMM, respectively.

2.3.7 Average urine compositions

The average composition values (mmol/24 hour) and physicochemical parameters of the 24-hour urines from white and black subjects (n=14) are shown in Table 2.11 below (the results for the urine and MM inhibitory activity studies have been combined). The composition of each subject's urine from which the averages were derived is shown in Appendix A (white subjects: Table A3.1, page A2; black subjects: Table A3.2, page A3). It was noteworthy that the magnesium, phosphate and uric acid excretions were significantly lower in the black population group ($p < 0.05$).

Table 2.11: Average composition (mmol/24hour) and physicochemical parameters of white (WC) and black (BC) subjects' urine (n=14)

Variables	WC	BC	SE
pH	6.20	6.30	0.0930
Volume (ml/24hr)	1774	1536	139
Calcium (mmol/24hr)	3.05	2.20	0.374
Chloride (mmol/24hr)	151	132	13.6
Citrate (mmol/24hr)	3.04	3.57	0.358
Creatinine (mmol/24hr)	15.9	13.7	1.12
*Magnesium (mmol/24hr)	3.82	2.64	0.397
Oxalate (mmol/24hr)	0.17	0.15	0.014
*Phosphate (mmol/24hr)	31.2	18.2	2.46
Potassium (mmol/24hr)	59.9	44.4	5.57
Sodium (mmol/24hr)	152	142	21.9
Sulphate (mmol/24hr)	20.1	15.6	1.61
*Uric acid (mmol/24hr)	3.84	2.76	0.284
RS Brushite	0.680	0.500	0.150
RS Calcium oxalate	1.51	1.57	0.273
RS Uric acid	1.30	0.920	0.231

RS: Relative supersaturation
**Difference is statistically significant: $p<0.05$*

2.4 DISCUSSION

The present study investigated whether urine composition and inhibitory activity studies would discriminate between South African white subjects who are stone-prone, and black subjects in whom stone incidence is extremely rare. The rationale for adopting this approach arose from a report which suggested that a combination of such data is required

to distinguish between stone-formers and controls rather than using urine composition and relative supersaturation values alone (Tiselius *et al.* 1995).

Urine composition trends in the present study were inconclusive. Magnesium, phosphate and uric acid excretions were significantly lower in the black population group (other trends were not significant). The same phosphate and uric acid trends were reported recently by Rodgers and Lewandowski (2002) and are consistent with stone incidence in this group. The lower urinary magnesium, however, is inconsistent with a low risk of stone formation (Takasaki 1972) and is an example of the contradictory trends in urine composition that have been reported amongst the black population (Modlin 1967, Whalley *et al.* 1998, Lewandowski *et al.* 2001). These results suggest that the extremely low stone incidence in South African blacks cannot be explained in terms of urine composition alone.

In the present study, zeta potential measurements revealed that filtered, dialysed urine from white subjects induced a significantly greater negative charge in the COM crystal slurry than that from black subjects, implying that stronger repulsive forces will operate between crystals in the former, eventually leading to a greater probability of disaggregation. However, as has been documented previously, competing cohesive forces are also involved (Hess and Kok 1996). These tend to negate the effect of the repulsive zeta forces. The results of the sedimentation experiments bear testimony to this. These showed that there was no difference in the degree of aggregation inhibition between the urines of the two population groups, despite the stronger repulsive forces induced by the macromolecules in urines from white subjects. It is thus concluded that the cohesive forces associated with macromolecules in the latter were stronger than those arising in the urines from black subjects.

At first glance, these results seem somewhat surprising, given that the incidence of stones in the black population is far lower than in the whites. However, attention is drawn to the use of dialysed urine as opposed to whole urine. An extrapolation of results and interpretations from the one medium to the other is clearly inappropriate. If the hypothesis that inhibition of aggregation is greater in the urine of black subjects is valid, then one can speculate that the same interplay between cohesive and repulsive forces occurs in whole urines, and that the former are stronger in the urinary macromolecules of whites than blacks. This would give rise to repulsive forces and disaggregation of greater magnitude in black subjects.

The zeta potential and sedimentation results also suggest fundamental differences in the properties of the macromolecules larger than 10 kDa in the urine of the two

population groups. It is possible that the macromolecules in white subjects' urine carry more negatively charged functional groups, while their suggested stronger cohesive forces indicate a greater probability to polymerise. The tendency of THM to self-associate has been associated with a decreased effect on crystal aggregation (Hess *et al.* 1989). Thus, a higher degree of polymerisation of macromolecules may induce a lower inhibition of aggregation in the white population.

The addition of macromolecular urine extracts from both white and black subjects to the synthetic urine resulted in a considerable decrease in the average particle size. This change, which may be ascribed to inhibition of aggregation and/or reduced crystal growth, was significantly more pronounced in the black subjects. Further studies are required to elucidate the specific mechanisms of crystallisation inhibition. However, since inhibition of aggregation was demonstrated in the afore-mentioned zeta potential and sedimentation experiments, it seems reasonable to conclude that this was the operative mechanism. Indeed, this conclusion would be consistent with the white population's urinary macromolecules' greater potential to polymerise, as described above. Similar to the black group in the present study, other studies have found that smaller particle sizes are a consistent feature of control subjects' urine compared with stone-formers (Robertson and Nordin 1982). Thus this may be an important factor in the black population's lower stone incidence. It is surprising that only a moderate correlation between protein concentration and particle size was observed (0.55). This may suggest that specific macromolecular components, rather than the total amount of urinary macromolecules, are important in determining inhibition of crystallisation.

Albeit that small sample sizes were used, the results of these experiments provide some evidence to suggest that the inhibitory properties of the urine from white and black subjects are indeed different. Further studies are required to study the mechanisms of crystallisation in more detail. The interesting findings with regard to macromolecules from white and black subjects, and specifically the potentially greater inhibition in the black subjects, suggest that urinary macromolecules might provide insight into the rarity of stones amongst the black population.

2.5 REFERENCES

1. Asplin JR, Parks JH, Chen MS, Lieske JC, Toback FG, Pillay SN, Nakagawa Y, and Coe FL. 1999. Reduced crystallisation inhibition by urine from men with nephrolithiasis. *Kid Int* 56:1505-1516.

2. Bradford MM. 1976. A rapid and sensitive method for the quantitation of microgram quantities of protein utilizing the principle of protein dye-binding. *Anal Biochem* 72:248-254.

3. Burns JR and Finlayson B. 1980. A proposal for a standard reference artificial urine in *in vitro* urolithiasis experiments. *J Urol* 18:167-169.

4. Chiriboga J. 1963. Some properties of an oxalic oxidase purified from barley seedlings. *Biochem Biophys Res Comm* 11:277-282.

5. Curreri P, Onoda GY, and Finlayson B. 1979. An electrophoretic study of calcium oxalate monohydrate. *J Colloid Interface Sci* 69:170-182.

6. Deganello S, Kampf AR, and Moore PB. 1981. The crystal structure of calcium oxalate trihydrate: $Ca(H_2O)_3(C_2O_4)$. *Am Miner* 66:859-865.

7. Dryer RL and Routh JI. 1963. Determination of serum inorganic phosphorus. *Clin Chem* 4:191-195.

8. Fernandez FJ and Kahn HL. 1971. Clinical methods for atomic absorption spectroscopy. *Clin Chem Newsl* 3:24-26.

9. Finlayson B. 1976. Physicochemical aspects of urolithiasis. *Kidney Int* 13:344-360.

10. Fossati P, Prencipe L, and Berti G. 1980. Use of 3,5-dichloro-2-hydroxybenzenesulphonic acid/4-aminophenazone chromogenic systems in direct enzymatic assay of uric acid in serum and urine. *Clin Chem* 26:227-231.

11. Free HM, editor. 1986. Modern urine chemistry. Ames Division, Miles Laboratories, Indiana.

12. Glasser LSD. 1977. Crystallography and its application. Van Nostrand Reinhold, London.

13. Gruber W and Möllering H. 1966. Citrat-lyase und bestimmung von citrat. *Biochemische Zeitschrift* 346:85-88.

14. Hess B and Kok DJ. 1996. Nucleation, growth, and aggregation of stone-forming crystals. In Kidney stones: Medical and surgical management. Coe FL, Favus MJ, Pak CYC, Parks JH and Preminger GM, editors. Lippincott-Raven Publishers, Philadelphia, 3-32.

15. Hess B, Nakagawa Y, and Coe FL. 1989. Inhibition of calcium oxalate monohydrate crystal aggregation in urine proteins. *Am J Physiol* 257:F99-F106.

16. Howard JE and Thomas WC. 1958. Some observations on rachitic rat cartilage of probably significance in the etiology of renal calculi. *Trans Am Clin Clim Assoc* 70:94-102.

17. Jenkins R and De Vries JL. n.d. An introduction to x-ray powder diffractometry. Philips, Eindhoven.

18. Klug HP and Alexander LE. 1974. X-ray diffraction procedures for polycrystalline and amorphous materials. Wiley, New York.

19. Kok DJ, Papapoulos SE, and Bijvoet OLM. 1990. Crystal agglomeration is a major element in calcium oxalate urinary stone formation. *Kidney Int* 37:51-56.

20. Lewandowski S, Rodgers A, and Schloss I. 2001. The influence of a high-oxalate / low-calcium diet on calcium oxalate renal stone risk factors in non-stone forming black and white South African subjects. *Br J Urol* 87:307-311.

21. Meyers AM, Whalley N, Zakolski WJ and Shar T. 1994. Chemical composition of the urine in the normal black and white population. In: Ryall RL, Bais R, Marshall VR, Rofe AM, Smith LH, and Walker VR, editors. Proceedings of the 7th international symposium on urolithiasis. Plenum Press, New York, 422.

22. Modlin M. 1967. The aetiology of renal stone: A new concept arising from studies on a stone-free population. *Ann Roy Coll Surg Engl* 40:155-178.

23. Pak CYC, Ohata M, and Holt K. 1975. Effect of diphosphonate on crystallization of calcium oxalate in vitro. *Kidney Int* 7:154-160.

24. Parrish W and Mack M. 1963. Data for x-ray analysis: charts for the solution of Bragg's equation. Centrex, Eindhoven.

25. Robertson WG and Nordin BEC. 1982. Physicochemical factors governing stone formation. In Scientific foundations of urology. Williams DI and Chisholm GD, editors. William Heinemann Medical Books Ltd, London, 194-267.

26. Robertson WG, Peacock M, Marshall RW, Marshall DH, and Nordin BEH. 1976. Saturation-inhibition index as a measure of the risk of calcium oxalate stone formation in the urinary tract. *New Engl J Med* 294:249-252.

27. Rock RC, Walker WG, and Jennings CD. 1986. Nitrogen metabolites and renal function. In Textbook of Clinical Chemistry. Tietz NW, editor. WB Saunders, Philadelphia, 1278-1280.

28. Rodgers AL and Lewandowski S. 2002. Effects of 5 different diets on urinary risk factors for calcium oxalate kidney stone formation: evidence of different renal handling mechanisms in different race groups. *J Urol* 168:931-936.

29. Ryall RL, Hibberd CM, Mazzachi BC, and Marshall VR. 1986. Inhibitory activity of whole urine: a comparison of urines from stone formers and healthy subjects. *Clin Chim Acta* 154:59-68.

30. Ryall RL, Hibberd CM, and Marshall VR. 1985. A method for studying inhibitory activity in whole urine. *Urol Res* 13:285-289.

31. Scurr DS and Robertson WG. 1986. Modifiers of calcium oxalate crystallisation found in urine. II. Studies on their mode of action in an artificial urine. *J Urol* 136:128-131.

32. Scurr DS and Robertson WG. 1986. Modifiers of calcium oxalate crystallisation found in urine. III. Studies on the role of Tamm-Horsfall mucoprotein and of ionic strength. *J Urol* 136:505-507.

33. Sutor DJ and Scheidt S. 1968. Identification standards for human urinary calculus components, using crystallographic methods. *Br J Urol* 40:22-28.

34. Takasaki E. 1972. The magnesium:calcium ratio in the concentrated urines of patients with calcium oxalate calculi. *Inves Urol* 10:147–150.

35. Tiselius H-G, Bek-Jensen H, Fornander A-M, and Nilsson M-A. 1995. Crystallisation properties in urine from calcium oxalate stone formers. *J Urol* 154:940-946.

36. Trudeau DL and Freier EF. 1967. Determination of calcium in urine and serum by atomic adsorption spectrophotometry. *Clin Chem* 13:101-114.

37. Werness PG, Brown CM, Smith LH, and Finalyson B. 1985. EQUIL2: a basic computer program for the calculation of urinary supersaturation. *J Urol* 134:1242-1244.

38. Werness PG, Berghert JH, and Smith LH. 1981. Crystalluria. *J Crys Growth* 53:166-181.

39. Whalley NA, Moraes MFBG, Shar TG, Pretorius SS, and Meyers AM. 1998. Lithogenic risk factors in the urine of black and white subjects. *Br J Urol* 82:785-790.

40. Willis JB. 1967. Determination of calcium and magnesium in urine by atomic absorption spectroscopy. *Anal Chem* 33:556-559.

CHAPTER 3: CRYSTAL MATRIX EXTRACT

3.1 INTRODUCTION

Investigators studying the anomaly of black South African's apparent stone immunity have focussed considerable attention on urine composition. However, the role of urinary proteins has not yet been rigorously investigated. As described in chapter 1, approximately 64 % of the organic matrix of kidney stones consists of protein (King and Boyce 1959) and thus characterisation of this component and its role in stone formation is of considerable interest. The incorporation of proteinaceous material into kidney stones may occur during the primary event of crystal formation as well as during cellular trauma resulting from abrasion of the renal epithelium by the stone (Doyle *et al.* 1991). Morse and Resnick (1988) were the first to study proteins in CaOx crystals freshly precipitated from urine, thus precluding the possibility that their presence was due to secondary, injurious events. This mixture of proteins derived from CaOx crystals is now commonly referred to as the crystal matrix extract or CME (Doyle *et al.* 1991).

Since then, numerous investigators have identified proteins associated with urine crystals and have reported their inhibitory properties, albeit mainly in inorganic solutions. The proteins identified are albumin (Ryall *et al.* 1991, Cerini *et al.* 1999) nephrocalcin (Hess *et al.* 1989, Worcester 1996), UPTF1 (Ryall *et al.* 1995, chapter 5), inter-α-inhibitor (Atmani *et al.* 1996, Dean *et al.* 1999) and OPN (Worcester 1996, Asplin *et al.* 1998).

Doyle and co-workers studied the CME from urine and reported remarkable inhibitory activity in both an inorganic solution and undiluted urine compared with previous studies of other proteins (Doyle *et al.* 1995). They also reported the inclusion of a previously unknown protein as the major component of the matrix extract (Doyle *et al.* 1991). This protein was later identified as the urinary form of prothrombin fragment 1 (Stapleton and Ryall 1995). This protein is the topic of further discussion in Chapters 4 - 8.

This chapter reports the isolation of the CME from the urine of white and black subjects and a comparison of their protein composition and inhibitory activities. This allowed an assessment of whether the proteins associated with the respective extracts might contribute to the black group's low stone incidence.

3.2 METHODS

3.2.1 Urine collection and treatment

Twenty-four hour urine samples were collected from white and black subjects with no previous history of kidney stones and pooled according to population group. The number of urines that were pooled varied between batches but was usually between 5 and 10. Urines were tested for haematuria and infection and filtered as described in paragraph 2.2.1 (page 26). They were discarded if the tests were positive. Urine composition data (mmol/l) and physicochemical parameters were obtained for the pooled urines as previously described (paragraph 2.2.1, page 26); no relative supersaturation values were computed since these are not appropriate for pooled urines. Urine composition data was analysed statistically by analysis of variance (ANOVA) and the results considered statistically significant if $p \leq 0.05$. Average values along with their standard errors (SE) are reported

The CaOx MSL of each urine pool was determined as outlined in paragraph 2.2.7 (page 32). Some of the MSL experiments were performed using a turbidimeter instead of a Coulter Counter (due to availability). This instrument measures the turbidity or cloudiness of a sample, and a sharp increase in this parameter is comparable to a sudden increase in particle number. Thus the same analysis as that described for the Coulter Counter experiment is applicable in these experiments.

3.2.2 Isolation of CME

The CME was isolated from the pooled urines according to a method previously described (Doyle *et al.* 1991). The urines were incubated in a shaking water bath (100 rpm) at 37 ^{0}C and CaOx crystallisation was induced by the addition of NaOx at 30 mmol/l in excess of the previously determined MSL (0.1 ml NaOx / 100 ml urine). Additional loads of NaOx were added after 1 and 2 hours. After a total incubation time of 3 hours, the crystals were collected by filtration (0.22 µm filters) and washed thoroughly with 0.1 mol/l sodium hydroxide followed by distilled water. The crystals were dried at 37 ^{0}C for at least 1 hour and then demineralised by stirring in 100 ml per gram of 0.25 mol/l ethylenediaminetetraacetic acid (EDTA) (pH 8.0). The solution was filtered through a 0.22 µm filter and dialysed extensively against distilled water at 4 ^{0}C. The dialysate was freeze-dried and stored at -20 ^{0}C for later use; it is referred to as the CME. The CME

prepared from the urine of white and black subjects are henceforth referred to as WE and BE, respectively.

3.2.3 Characterisation of CME

Aliquots of the pooled urine samples as well as the CMEs each population group were retained for protein analysis by gel electrophoresis and Western blotting.

3.2.3.1 SDS-PAGE

Aliquots of filtered urine (1 ml) and CME (0.5 mg) from each population group were prepared for analysis by sodium dodecyl sulphate (SDS)-polyacrylamide electrophoresis (PAGE). The urine samples were dialysed against distilled water and freeze-dried for SDS-PAGE. The CME were dissolved in a minimum volume of distilled water, diluted 1:4 with five times concentrated (5x) SDS reducing buffer [0.147 mol/l Tris.HCl (pH 6.8), 5 % SDS, 25 % glycerol, 0.0025 % Bromophenol Blue and 12.5 % β-mercaptoethanol], and heated at 100 ^{0}C for 5 minutes before loading. Proteins were resolved by electrophoresis on 15 % polyacrylamide mini gels [37 % (v/v) of a 40 % acrylamide in 0.2 % bisacrylamide solution, 0.373 mol/l Tris.HCl (pH 8.8), 27 % distilled water, 0.10 % SDS, 0.1 % ammonium persulphate (Amps), 0.10 % N,N,N'N'-tetramethylethylendiamin (TEMED)] with a 6 % stacking gel [16 % (v/v) of a 40 % acrylamide in 1.8 % bisacrylamide solution, 0.123 mol/l Tris (pH 6.8), 46 % distilled water, 0.25 % SDS, 0.25 % Amps, 0.16 % TEMED] using a Tris-HCl running buffer [15 % glycine, 3 % Tris, 1 % SDS, pH 8.3]. Samples were run at 50 mA for 50 - 60 minutes. A low range molecular weight marker was included (Bio-Rad).

The protein bands were then detected by silver staining. Briefly, gels were fixed for 45 minutes [50 % methanol, 12 % acetic acid, 0.05 % formaldehyde] and then washed three times with 50 % ethanol (10 minutes per wash) before a 1-minute pretreatment step [0.02 % sodium thiosulphate pentahydrate]. The gels were then rinsed with distilled water and incubated in a solution of silver nitrate [0.2 % silver nitrate, 0.075 % formaldehyde] for 20 minutes. Following further rinsing with distilled water, the gels were developed [6 % sodium carbonate, 0.05 % formaldehyde, 0.008 % sodium thiosulphate pentahydrate] and then further development was prevented by addition of a stop solution [50 % methanol, 12 % acetic acid].

3.2.3.2 Western blotting

Equal amounts of each sample were used for Western blotting. Following electrophoresis, gels were soaked in blotting buffer [24.9 mmol/l Tris, 0.192 mol/l glycine, 20 % methanol, pH 8.3] for 15 minutes prior to assembly in the Bio-Rad Mini Trans-Blot apparatus. Proteins were then transferred onto a nitrocellulose membrane in blotting buffer at 100 V for 1 hour, with cooling, followed by immunodetection. Non-specific sites on the membranes were blocked with blocking buffer [9.97 mmol/l Tris and 147 mmol/l NaCl (pH 8.0), 6 % fat-free skim milk powder, 0.05 % Tween-20] for 1 hour. The blot was then probed for UPTF1 using a 1:500 dilution of a monoclonal UPTF1 antibody (provided by Professor Rosemary Ryall, Flinders Medical Centre, South Australia) in the blocking buffer for 90 minutes with agitation, followed by four washes with blocking buffer, each for a period of 5 minutes. The monoclonal antibody was then probed with a 1:1000 dilution of a rabbit anti-mouse/HRP (horse radish peroxidase) conjugated secondary antibody in blocking buffer for 1 hour. After extensive washing with blocking buffer, the HRP conjugate was detected with a solution containing 4-chloro-1-napthol (Sigma) [0.05 % (w/v) in 17 % ice-cold methanol, 0.042 % hydrogen peroxide and 83 % Tris-buffered saline (9.97 mmol/l Tris, 147 mmol/l NaCl, pH 8.0)] for approximately 15 minutes.

3.2.4 Synthetic urine study

3.2.4.1 Urine preparation and treatment

A synthetic urine was prepared as previously described (paragraph 2.2.7, page 32) and two replicate crystallisation studies were conducted independently to assess and compare the effect of the CME from both population groups on CaOx crystallisation. The CaOx MSL of the synthetic urine was measured (refer to paragraph 2.2.7, page 32) and the urine was divided into three equal aliquots that were either left untreated or dosed with WE or BE at final concentrations of 5 mg/l. The concentration is greater than the approximate physiological value reported (Doyle extracted 24.0 mg CME from 12.5 l urine, *i.e.* 1.9 mg/l) (Doyle *et al.* 1995).

3.2.4.2 Effect of CME on particle number, volume and size

Since it has previously been shown that CME does not alter the MSL (Doyle *et al.* 1995), and the amount of CME was limited, equal NaOx loads (30 mmol/l in excess of the MSL of the control urines, 0.1 ml NaOx per 100 ml urine) were added to the synthetic urine and protein-dosed samples to induce crystallisation. This was followed by incubation at 37 ^{0}C in a shaking water bath (100 rpm) for 60 minutes. The effects of WE and BE on the particle number and particle volume were measured at 15-minute intervals using a Coulter Counter I (140 µm orifice, 2.8 - 90.0 µm particle size range, 64 channels). After 60 minutes, an aliquot (2 ml) of each sample from one such experiment was filtered (0.22 µm) and prepared for examination by scanning electron microscopy as described elsewhere (paragraph 2.2.2.3, page 28).

In a separate experiment, synthetic urine and protein-dosed urines were incubated at 37 ^{0}C for 120 minutes after which the particle size distributions were measured using the Coulter Counter I.

3.2.4.3 Effect of CME on [^{14}C]-oxalate deposition

Experiments were carried out as described for the kinetics studies above except that 3.125 µCi / 100 ml "hot" [^{14}C]-oxalic acid (NEN, Boston, USA) was added to each flask prior to addition of the "cold" NaOx. The incubation period was 120 minutes. Samples were filtered into concentrated HCl (10 % v/v) at 30-minute intervals to prevent further crystallisation. Thereafter, duplicate 1 ml aliquots of the latter were added to 10 ml scintillation fluid (Zinsser Analytic, Frankfurt, Germany). Each sample was counted for 10 minutes in a scintillation counter (1900 CA Tri-Carb Liquid Scintillation Analyser, Packard-Instrument Co. Inc., Meriden CT, USA). A measure of the percentage precipitated [^{14}C]-oxalate at each time interval was obtained by the following calculation: $100 - 100x (CPM_{x\ min} / CPM_{0\ min})$ where CPM is counts per minute (Ryall *et al.* 1995).

3.3 RESULTS

3.3.1 Urine composition

The average composition of pooled urines from white and black subjects is shown in Table 3.1.

Table 3.1: Average urine composition (mmol/l) and physicochemical parameters of pooled urines from white (WC) and black (BC) subjects (n = 7)

Variables	WC	BC	SE
Number of urines pooled	9.4	10.6	0.96
pH	6.26	5.91	0.0937
Volume (ml)	14564	15340	1961
*Metastable limit (mmol/l)	38.6	87.8	5.32
*Calcium (mmol/l)	2.74	1.24	0.234
Chloride (mmol/l)	231	120	90.7
*Citrate (mmol/l)	2.38	1.52	0.215
Creatinine (mmol/l)	21.1	8.36	7.80
Magnesium (mmol/l)	3.11	2.59	0.429
Oxalate (mmol/l)	0.277	0.287	0.080
*Phosphate (mmol/l)	19.6	12.5	1.05
*Potassium (mmol/l)	34.9	20.9	64.5
Sodium (mmol/l)	144	187	17.7
Uric acid (mmol/l)	2.44	2.00	0.150

Significant difference: WC vs. BC, $p<0.05$

The data of each pooled urine is shown in Appendix B (white subjects: Table B1, page A11; black subjects: Table B2, page A12) along with the data and plot for each pooled urine's MSL determination (white subjects: Tables B3.1 – 3.7, pages A13 – A14 and Figures B1.1 – 1.5, page A19; black subjects: Tables B4.1 – 4.7, pages A15 - A17 and Figures B2.1 – 2.5, page A20). The synthetic urine's MSL was the same as reported in chapter 2 (page 40). The black subjects' average urinary calcium, citrate, phosphate and potassium concentrations were significantly lower than the white subjects, while their average MSL was significantly higher ($p < 0.05$).

3.3.2 Isolation and characterisation of CME

The entire volume of the pooled urines detailed in paragraph 3.3.1 was used for the isolation of CME. A portion of these extracts was then retained for the crystallisation study described in the present chapter, while the remainder was used for the isolation and purification of UPTF1 (described in chapter 4). Typical protein patterns of the white and black subjects' pooled urine and CME are shown in Figure 3.1.

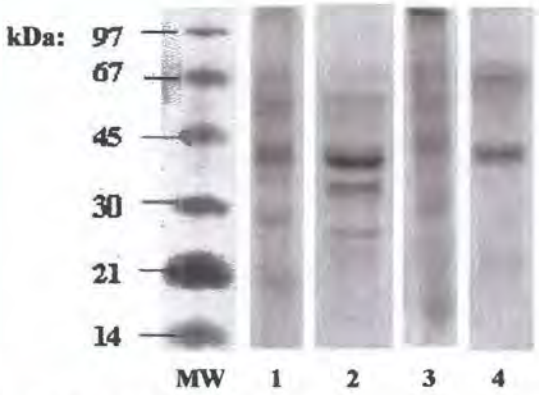

Figure 3.1: SDS-PAGE of urine and CMEs from white and black subjects. The patterns were obtained from *MW:* low molecular weight marker; *1:* white subjects' urine (1 ml); *2:* WE (0.5 mg); *3:* black subjects' urine (1 ml); *4:* BE (0.5 mg).

Figure 3.2: Western blot of CMEs from white and black subjects immunoblotted for prothrombin. The patterns were obtained from *1:* WE (0.5 mg); *2:* BE (0.5 mg).

The urine samples from white (lane 1) and black subjects (lane 3) both contained several bands with molecular weights ranging from 17 kDa to 64 kDa. However, it was noteworthy that both population groups' CME samples contained only a few bands, with the most prominent one at 42 kDa (lanes 2 and 4). In addition to this major band, WE also contained two other prominent bands at lower molecular weights, namely 26 and 37 kDa. In contrast, BE had another prominent band at a higher molecular weight, namely 62 kDa.

A Western blot of the CME samples from both population groups is shown in Figure 3.2 above. The blot identified the major band in both samples as UPTF1. The CME from black subjects (lane 2) appeared to contain more UPTF1 per milligram of CME than that from the white subjects (lane 1).

3.3.3 Synthetic urine study

3.3.2.1 Effect of CME on particle number and volume

Figures 3.3 and 3.4 (Appendix H, page A79) show the average increase in particle number and particle volume during a 60-minute time course after addition of a NaOx load. These trends were demonstrated in two independent experiments. The data from the separate particle number experiments and the corresponding plots are shown in Appendix B (Table B5,

page A18; Figures B3.1 – 3.2, page A21). The analogous particle volume results are also shown in Appendix B (Table B6, page A18; Figures B4.1 – 4.2, page A21).

Two features of the plots are apparent: firstly, CME from both population groups caused a notable decrease in particle number and particle volume relative to the control and secondly, the extent of the decrease was greater in the urine dosed with BE. The common point of maximum inhibition of particle number and volume occurred at 30 minutes. The average particle numbers after 30 minutes were 14 094, 9 225 and 8 408 /500µl in the SU and WE and BE-dosed urines, corresponding to decreases of 34.5 % and 40.3 % in the latter two urines, respectively. The average particle volumes after the same time period were 1.862, 1.482 and 1.123 x 10^6 μm^3 /500µl in SU, WE-dosed and BE-dosed urines, respectively. These values corresponded to decreases in volume of 20.4 % and 39.7 % in the WE and BE-dosed samples, respectively.

3.3.2.2 Effect of CME on particle size

Figure 3.5.1 shows the average particle volume – particle size distributions of the synthetic urine and extract-dosed urines at 120 minutes after addition of a NaOx load. The plots for the two independent experiments are shown in Appendix B (experiment 1: Figures B5.1.1 – 5.1.2, experiment 2: Figures B5.2.1 – 5.2.2, page A22). A decrease in the average particle size of synthetic urine was observed after addition of WE and BE, indicated by a shift in the mode of the CME-dosed distributions to significantly smaller values compared to the control sample (Figure 3.5.1). A magnified view of the SU+WE and SU+BE curves at lower particle volumes indicated the presence of a second, smaller peak in the range 7 - 20 µm (Figure 3.5.2). In this range, there was a slight shift towards smaller sizes in the BE-dosed urine compared with the WE-dosed one.

The average particle sizes of the above curves (as well as the values from the two independently performed experiments) are presented in Table 3.2 below. The two values listed for each CME-dosed curves are indicative of their bimodal distributions. The addition of both CMEs induced a decrease in the average particle size from 15.30 to 2.91 µm, corresponding to an 81.0 % decrease in size. The second (larger) peak in each extract-dosed urine had an average size of 11.29 and 9.84 µm after addition of WE and BE, respectively. These values represent size decreases of 26.2 and 35.7 % by WE and BE, respectively, relative to the

average particle size in the control synthetic urine. This trend was observed in experiment 1, while in experiment 2 the larger mode was the same in the two extract-dosed urines.

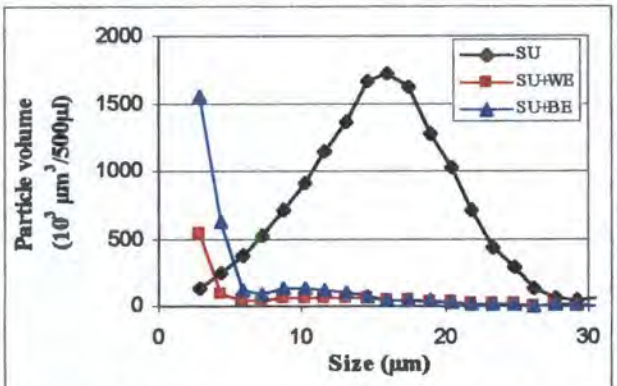

Figure 3.5.1: Average particle size of synthetic urine. Before and after addition of CME from white (WE) and black (BE) subjects at final concentrations of 5 mg/l

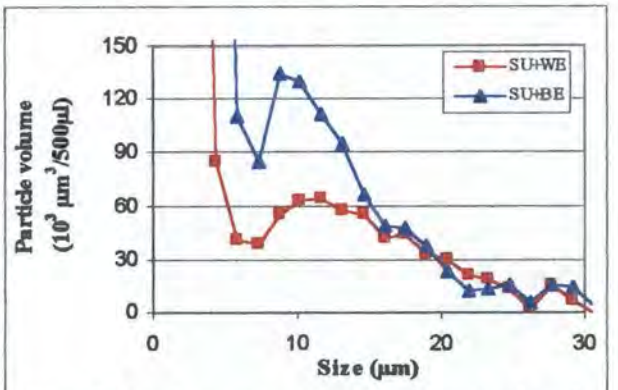

Figure 3.5.2: Average particle size of synthetic urine after addition of CME. From white (WE) and black (BE) subjects at final concentrations of 5 mg/l

Table 3.2: Particle size (µm) of synthetic urine before and after addition of CME from white (WE) and black (BE) subjects at final concentrations of 5 mg/l

Sample	Experiment 1	Experiment 2	Average
SU	14.57	16.02	15.30
SU+WE	2.91, 13.11	2.91, 9.47	2.91, 11.29
SU+BE	2.91, 10.20	2.91, 9.47	2.91, 9.84

Figure 3.6 shows scanning electron micrographs of CaOx crystals precipitated from synthetic urine before and after addition of the CME. Differences were not observed between the synthetic urines dosed with WE and BE. Thus, in the context of the microscopy study, the two crystal extracts are henceforth collectively referred to as CME. In the control synthetic urine, coffin-shaped COM crystals and COM aggregates were typically observed (Figure 3.6.1). The addition of CME resulted in the formation of bipyramidal COD crystals. Single CODs together with a few COD aggregates were characteristically observed. An example of the latter is shown in Figure 3.6.3. Survey views of the synthetic urine and extract-dosed urine illustrated a marked decrease in the number of single and aggregated crystals after addition of CME (Figure 3.6.4) compared to the control urine (Figure 3.6.2).

Figure 3.6: Scanning electron micrographs of CaOx crystals deposited in synthetic urine. The crystals were precipitated from synthetic urine: mag 7.7 K (Fig 3.6.1), mag 1.2 K (Fig 3.6.2); and synthetic urine dosed with CME at a final concentration of 5 mg/l: mag 12 K (Fig 3.6.3), mag 1.2 K

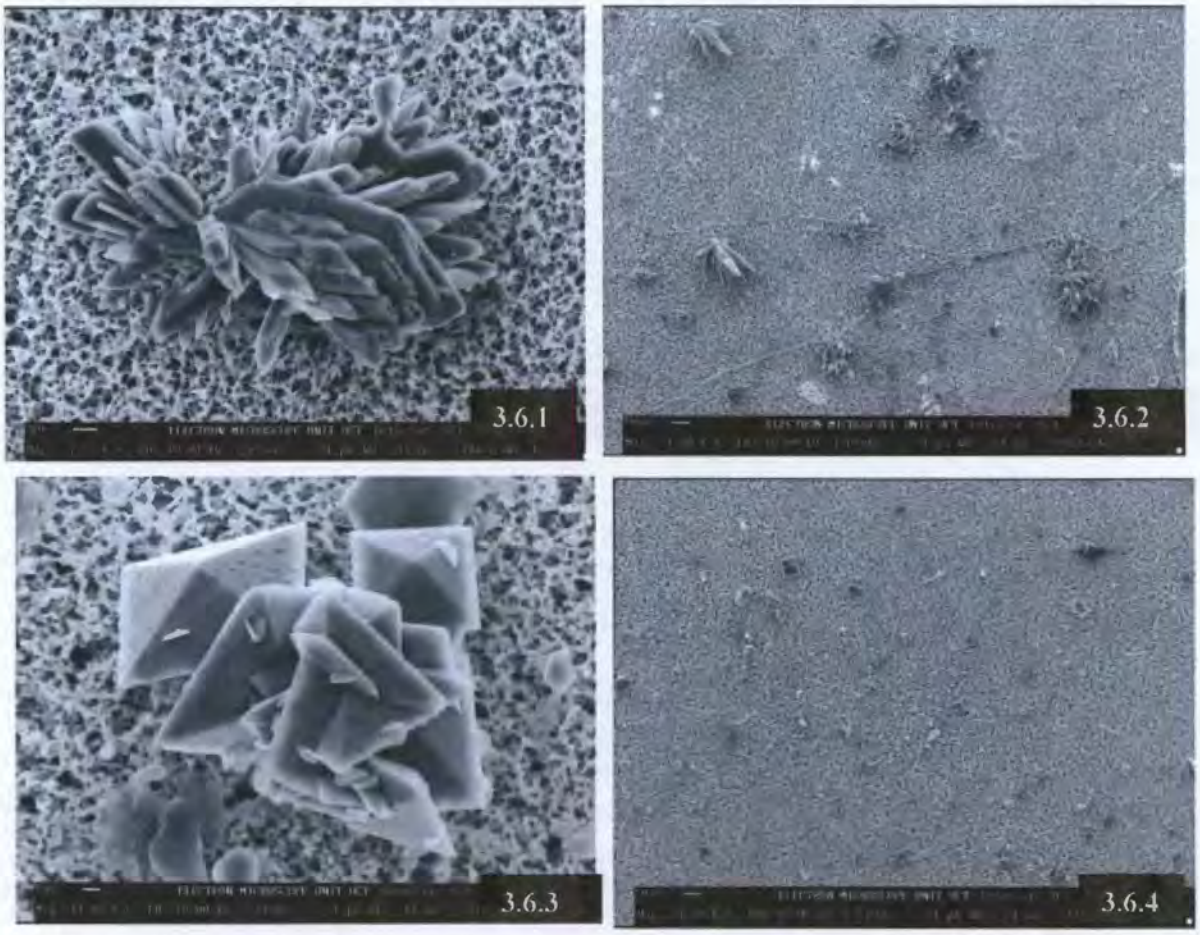

3.3.2.3 Effect of CME on [^{14}C]-ox deposition

Figure 3.7 shows the average increase in the quantity of precipitated [^{14}C]-oxalate during a 120-minute time course after addition of a NaOx load to synthetic urine. The plots for the two independent experiments are shown in Appendix B (experiment 1: Figure B6.1, experiment 2: Figure B6.2, page A22). The corresponding data are given in Table B7 on page A18.

The CMEs from both population groups induced a significant decrease in the amount of deposited material relative to the control synthetic urine. The deposition in the BE-dosed urine was less than the WE-dosed urine until 60 minutes (in both independent experiments),

after which the two samples were not significantly different. Inspection of the data at 30 minutes, the time point at which the particle number and volume data were analysed, showed that the average amount of precipitated material decreased from 29.0 % in the synthetic urine to 12.4 and 5.0 % after addition of WE and BE, respectively. These values corresponded to inhibition of CaOx deposition of 57.2 and 82.8 % by WE and BE, respectively.

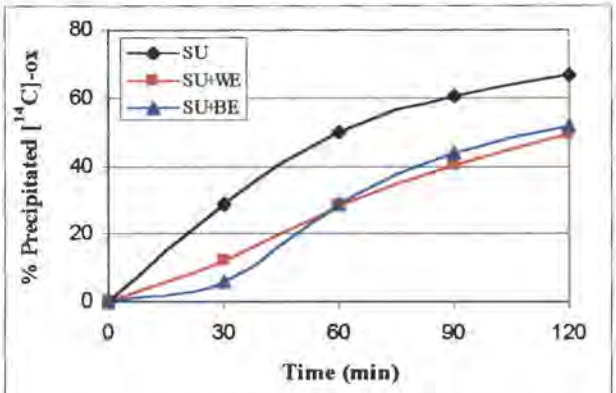

Figure 3.7: Average [^{14}C]-ox deposition rate in synthetic urine. Before and after addition of CME from white (WE) and black (BE) subjects at final concentrations of 5 mg/l

3.4 DISCUSSION

In the study described in this chapter, particle numbers, volumes and sizes were measured using a Coulter Counter. Interpretation of such data should take into consideration the characteristics of "particles", measured in the present study, as opposed to "crystals". Thus the particles themselves could be crystals, proteinaceous material or a combination of both. However, as discussed below, the [^{14}C]-oxalate deposition and SEM data clearly depicted crystal formation. As such, the association of particle formation with crystal formation in the discussion below is justified.

The molar compositions of pooled urines used for the preparation of the CMEs are presented for reference purposes. A portion of the CMEs was subsequently used for the purification of UPTF1 (described in chapter 4), which was used in several experiments throughout this thesis. In the synthetic urine crystallisation study, a decrease in particle number was observed after addition of the CME from both white and black population groups.

This observation could be interpreted as either reduced crystal nucleation or promotion of aggregation. However, the observed decrease in particle size is inconsistent with the latter. Further evidence supporting a decrease in crystal nucleation is the decreased particle volume and amount of CaOx deposition, and the notably fewer crystals after the addition of the CME from both population groups revealed by scanning electron microscopy. Furthermore, lower particle volumes, in conjunction with the decrease in CaOx deposition, were consistent with inhibition of growth. Thus the results collectively suggest the CME from both population groups is an inhibitor of crystal nucleation, growth and aggregation in the synthetic urine, particularly during the early stages of the crystallisation process, during which time the changes in particle parameters were the greatest in comparison to the synthetic urine. The greater decrease in the particle number and volume and amount of CaOx deposition by BE suggests that the black population's matrix extract may be a more efficient inhibitor than that derived from white subjects. Inhibition of nucleation by CME has not been previously demonstrated.

In an earlier study, CME was shown to be an inhibitor of CaOx growth and aggregation rather than nucleation (Doyle *et al.* 1991). However, the study by Doyle and co-workers differed substantially from the present one as it was conducted using a seeded crystallisation system and undiluted ultrafiltered human urine. Doyle and co-workers postulated that the observed inhibitory properties were largely attributable to UPTF1, the major component of the extract. The synthetic urine employed in the present study contained several more components than Doyle's seeded system, but far fewer than the complex milieu of real urine. The disparate complexity of the test solutions and, to a lesser extent, the different concentrations of CME used, are likely explanations for the CME's different inhibition mechanisms in these media. A further explanation might be the possible variation in the composition of CME from different urines. This possibility is explored in chapter 6 of this thesis.

Despite the shortcomings of synthetic solutions in mimicking real urine, the synthetic urine used in the present study satisfied the requirement of a neutral test solution in which to compare protein extracts derived from the two population groups. The use of real urine from either group may have influenced the relative effects. The important point that emerged, however, was that CME appears to have the capacity to inhibit all three crystallisation

mechanisms. In addition, the extent of such inhibition is dependent on the choice (and therefore chemical composition) of the test solution.

A noteworthy observation of the present study was the preferred nucleation of COD in the presence of the crystal extracts. Another possibility is that COD was preferentially stabilised in the presence of CME. This observation is perhaps surprising in light of the fact that COM is thermodynamically more stable COM (Werness *et al.* 1979). On the other hand, it is consistent with the inhibitory properties demonstrated by both CMEs. According to Cerini and co-workers, the higher positive charge of COD (due to a greater number of calcium ions per unit cell) leads to repulsive forces between crystals and thus disaggregation (Cerini *et al.* 1999). Furthermore, the concomitant lower negative charge of COD crystals diminishes crystal adhesion to the cell surface due to the surface's overall negative charge (Asselman and Verkoelen 2002), thereby reducing the retention of COD crystals in the collecting ducts (Cerini *et al.* 1999). Thus, the formation of COD induced in the presence of CME may be regarded as a favourable primary step ultimately leading to secondary inhibitory processes.

Of significance in the present study was the observation that the crystal extract derived from black subjects tended to inhibit crystal nucleation to a greater extent than that from white subjects, particularly during the initial stages of crystallisation (*i.e.* first 30 minutes). Indeed, the percentage difference between WE and BE (at 30 minutes) with respect to the inhibition of particle numbers, particle volumes and [^{14}C]-oxalate deposition was respectively 6, 19 and 26 % respectively. Furthermore, the BE-dosed synthetic urine contained particles of slightly smaller size. This suggested a possible superior inhibitory capability that may be related to the black population group's relative stone immunity.

Differences in the protein composition of the two population groups' CME (shown by gel electrophoresis), influenced in part by the different urine compositions from which these extracts were derived, are likely contributors to the different activities observed. Recognising that UPTF1 is the major component of both crystal extracts, it was tempting to speculate that the observed inhibitory effects were due to the former. While this is possible in light of Ryall's UPTF1 study in which the protein's potent inhibitory activity was demonstrated (Ryall *et al.* 1995), several other proteins as well as non-proteinaceous material such as lipids could contribute to the extracts' inhibitory activity. However, even if the activity of CME could be directly attributed to UPTF1, these results cannot be readily extrapolated to activity in real urine or even to a physiological function in actual stone formation. Nevertheless, the present

study provided sufficient evidence to suggest that an investigation of UPTF1, rather than the crude CMEs tested here, from blacks and whites in real urine was warranted. A crystallisation study of UPTF1 in real urine, as well a comprehensive structural study of UPTF1 from black and white subjects, should assist in clarifying the contribution, if any, of this inhibitor to the low stone incidence of black South Africans.

3.5 REFERENCES

1. Asplin JR, Arsenault DA, Parks JH, Coe FL, and Hoyer JR. 1998. Contribution of human uropontin to inhibition of calcium oxalate crystallization. *Kidney Int* 53:194-199.

2. Asselman M and Verkoelen CF. 2002. Crystal-cell interaction in the pathogenesis of kidney stone disease. *Curr Opin Urol* 12:271-276.

3. Atmani F, Mizon J, and Khan SR. 1996. Inter-alpha-inhibitor: a protein family involved in the inhibition of calcium oxalate crystallization. *Scan Micros* 10:425-434.

4. Cerini C, Geider S, Dussol B, Hennequin C, Daudon M, Veesler S, Nitsche S, Biostelle R, Berthezene P, Dupuy P, Vazi A, Berland Y, Daghorn J-C, and Verdier J-M. 1999. Nucleation of calcium oxalate crystals by albumin: involvement in the prevention of stone formation. *Kidney Int* 55:1776-1786.

5. Dean CJ, Kanellos J, Pham H, Gomes M, Oates A, Grover PK, and Ryall RL. 1999. Calcium oxalate crystallisation in vitro effect of inter-alpha-inhibitor and derivatives. In: Borghi L, Meschi T, Briganti A, Schanchi T and Novarini A, editors. Proceedings of the 8th European Symposium on Urolithiasis. Editoriale Bios, Cosenza, 291-293

6. Doyle IR, Marshall VR, Dawson CJ, and Ryall RL. 1995. Calcium oxalate crystal matrix extract: the most potent macromolecular inhibitor of crystal growth and aggregation yet tested in undiluted human urine in vitro. *Urol Res* 23:53-62.

7. Doyle IR, Ryall RL, and Marshall VR. 1991. Inclusion of proteins into calcium oxalate crystals precipitated from human urine: a highly selective phenomenon. *Clin Chem* 37:1589-1594.

8. Hess B, Nakagawa Y, and Coe FL. 1989. Inhibition of calcium oxalate monohydrate crystal aggregation in urine proteins. *Am J Physiol* 257:F99-F106.

9. King JS and Boyce WH. 1959. Analysis of renal calculous matrix compared with some other matrix minerals and with uromucoid. *Arch Biochem Biophys* 82:455-461.

10. Morse RM and Resnick MI. 1988. A new approach to the study of urinary macromolecules as a participant in calcium oxalate crystallization. *J Urol* 139:869-873.

11. Ryall RL, Grover PK, Stapleton AMF, Barrell DK, Tang Y, Moritz RL, and Simpson RJ. 1995. The urinary F1 activation peptide of human prothrombin is a potent inhibitor of calcium oxalate crystallization in undiluted human urine in vitro. *Clin Sci* 89:533-541.

12. Ryall RL, Harnett RM, Hibberd CM, Edyvane KA, and Marshall VR. 1991. Effects of chrondriotin sulphate, human serum albumin and Tamm-Horsfall mucoprotein on calcium oxalate crystallisation in undiluted human urine. *Urol Res* 19:181-188.

13. Stapleton AMF and Ryall RL. 1995. Blood coagulation proteins and urolithiasis are linked: crystal matrix protein is the F1 activation peptide of human prothrombin. *Br J Urol* 75:712-719.

14. Werness PG, Duckworth SC, and Smith LH. 1979. Calcium oxalate dihydrate crystal growth. *Inves Urol* 17:230-233.

15. Worcester EM. 1996. Inhibitors of stone formation. *Sem Nephrol* 16:474-486.

CHAPTER 4: UPTF1 ISOLATION & CHARACTERISATION

4.1 INTRODUCTION

The inhibitory activity of the CME derived from the urine of black subjects was greater than that of the extract from white subjects when tested in an inorganic solution (chapter 3). Since UPTF1 is the major protein included in matrix extracts from both population groups, and is reported to be a potent inhibitor of CaOx crystallisation (Ryall *et al.* 1995), further study of this protein was required.

Several studies have compared the expression level (Hedgepeth *et al.* 2001, Atmani and Khan 2002) and/or structure (Nakagawa *et al.* 1987, Knorle *et al.* 1994) of proteins in stone-formers and normals in order to identify key factors in stone formation and its prevention. A similar approach in South Africa's stone-prone and stone-free populations appears to be prudent. Thus in this chapter, possible structural differences in UPTF1 from white and black subjects were investigated.

The two features of UPTF1 most relevant to a discussion of its activity are the Gla domain and its glycosylation. The Gla domain of UPTF1 contains ten Gla residues responsible for the protein's exceptional binding affinity for CaOx crystals (Stapleton and Ryall 1995) and has already been identified as the region of UPTF1 that determines its inhibitory activity (Grover and Ryall 1999). Furthermore, nephrocalcin from stone-formers lacks the Gla residues present in the inhibitory protein from healthy subjects' urine (Nakagawa *et al.* 1987), thus supporting the importance of Gla residues in protein activity.

No detailed characterisation of the glycosylation of UPTF1 has been carried out, despite the fact that the *N*- and *O*-linked glycans account for about 45 % of the protein's molecular weight (based on a comparison of the observed mass of 31 kDa on SDS-PAGE with the calculated mass using the amino acid sequence of 17 kDa). However, two previous studies have investigated carbohydrate structures on bovine PT, which has a high percentage of homology with human PT. Mizuochi identified three biantennary, complex type structures which he noted were highly sialylated (Mizuochi *et al.* 1979). Harlos later produced a model of these oligosaccharides on the bovine protein crystal structure (Harlos *et al.* 1987).

Co- and post-translational modifications such as glycosylation are known to alter protein function and are therefore also important in determining protein activity (Worcester

1996, Rudd and Dwek 1997). In a study of THM by Knorle, the protein isolated from stone-formers' urine, which is also known to be a poor inhibitor of crystallisation, was less highly glycosylated than THM from normals (Knorle *et al.* 1994).

An objective of this thesis was therefore to isolate and purify UPTF1 from the urine of white and black subjects and compare their biochemical properties. On this basis, an assessment could be made as to whether differences in the amino acid sequence and structure of UPTF1 or post-translational modification might account for the black population's low incidence of kidney stones. For the glycosylation study, CaOx stone-formers were included for comparison with the control subjects.

4.2 METHODS

4.2.1 Purification of UPTF1

UPTF1 was purified from the CME according to methods previously published and described in chapter 3 (Ryall *et al.*1995; paragraph 3.2.2 on page 48). The CME was suspended in a minimum amount of distilled water, centrifuged at 11000 *g* for 3 minutes and the supernatant was loaded onto a P2 BioGel desalting column. Fractions of approximately 1 ml each were collected and the absorbance was measured at 280 nm. The protein eluted in the void volume and this was freeze-dried prior to HPLC.

UPTF1 was isolated by RP-HPLC with a Vydac C4 column (1.0 ml/min) using a linear gradient of 0 - 42 % acetonitrile (ACN) in 0.1 % trifluoroacetic acid (TFA) over 62 minutes as detailed below.

Table 4.1: RP-HPLC gradient used for UPTF1 purification

Time (min)	Solvent A (%)	Solvent B (%)
0	100	0
15	100	0
50	14	86
55	14	86
56	0	100
61	0	100
62	100	0

Solvent A: 0.1 % TFA; Solvent B: 0.1 % TFA in 70 % ACN

The protein peaks were collected (absorbance was monitored at 280 nm) and analysed by SDS-PAGE and visualised by silver staining. The fraction containing UPTF1 was dialysed extensively against a phosphate buffer (145 mmol/l NaCl, 8.21 mmol/l K_2HPO_4, 1.84 mmol/l KH_2PO_4, pH 7.3) at 4 ^{0}C and the protein concentration was

determined using the Bradford method (Bradford 1976; paragraph 2.3.4, page 39). The purity of the dialysed material was confirmed by SDS-PAGE (refer to paragraph 3.2.3.1, page 49 for details) after which it was aliquoted into plastic eppendorf tubes and stored at -20 ^{0}C for later use. UPTF1 purified from white and black subjects' urine is henceforth referred to as WF1 and BF1, respectively.

4.2.2 Western blotting

The proteins presumed to be WF1 and BF1 were immunoblotted with a monoclonal UPTF1 antibody as described in paragraph 3.2.3.2 (page 50) to confirm their identity.

4.2.3 Protein MALDI-TOF mass spectrometry

Purified WF1 and WF1 were analysed by matrix-assisted laser-desorption-ionisation time-of-flight (MALDI-TOF) mass spectrometry according to methods previously described (Schwager *et al.* 1998). The protein samples were reduced and the cysteine residues were protected with vinyl pyridine followed by hydrolysis with endoproteinase Lys-C and Asp-N (2 % w/w) that cleave peptide bonds C- and N-terminally to lysine and aspartic acid, respectively. Whole or HPLC fractionated digests were analyzed by MALDI-TOF mass spectrometry, and the mass measurements (equivalent to mass/charge or m/z) were correlated with calculated masses of UPTF1 peptide fragments. Mass spectra were generated from a sinapinic acid matrix (10 mg/ml) using a PerSeptive Voyager Elite Biospectrometry Workstation (PerSeptive Biosystems, Framingham, Massachusetts).

4.2.4 Protein sequencing

The N-terminal protein sequence of WF1 and BF1 were determined by automated Edman degradation (Brandt *et al.* 1984). Only the first five amino acids were identified to confirm the identity of the protein as UPTF1.

4.2.5 Amino acid analysis

The amino acid composition of WF1 and BF1 was determined by acid hydrolysis using an Amino Acid Analyser (Millipore) with a cation exchange resin and post-column fluorescence using orthophthaldialdehyde.

4.2.6 Gla analysis

The composition of WF1 and BF1 with respect to Gla was determined by alkaline hydrolysis (Price 1983) using the same Amino Acid Analyser described above. The alkaline conditions prevented the conversion of Gla to glutamic acid (Glu) residues which occurs under the acidic conditions frequently used for amino acid analyses. A DL- γ-Gla standard (Sigma) was included.

Since Gla is quantitatively converted to Glu during acid hydrolysis, the sum of Gla and Glu in the alkaline hydrolysate equals the Glu content of the acid hydrolysate (determined as per paragraph 4.2.5 above). Thus the molar ratio of Gla to Glu residues was used to determine the Gla content of WF1 and BF1 (Price 1983),

i.e. number of Gla residues = [mols Gla/(mols Glu + mols Gla)] x (number of Glu).

4.2.7 2D SDS-PAGE

UPTF1 from white and black subjects (5 μg each) was resolved using 2D SDS-PAGE using a MultiPhor II system (Gorg *et al.* 1988). Immobiline dry strips (pH 3-10 non-linear, 18cm, Amersham) were used for the isoelectric focusing separation in the first dimension. These were rehydrated in a urea solution [8 mol/l urea, 0.5 % Triton X-100, 0.5 % Pharmalyte 3-10, 0.2 % dithiothreitol (DTT), few grains of bromophenol blue] prior to use. Samples were diluted 1:4 in a urea mixture [9 mol/l urea, 1 % DTT, 2 % Pharmalyte 3-10, 0.5 % Triton X-100, few grains of bromophenol blue] to denature the proteins, prior to loading at the acidic end of the strip. The samples were covered with silicone oil and run at 500 V for 5 hours after which the voltage was increased to 3200 V (maximum setting) for 18 - 20 hours (for isoelectric focusing). (The first dimension resolved the proteins according to charge.)

For the second dimension, the strips were then placed in equilibration solution 1 [0.5 % DTT, 50 mmol/l Tris-HCl (pH 6.8), 6.0 mol/l urea, 30 % glycerol, 1 % SDS] for 10 minutes with agitation followed by a further 10 minutes in equilibration solution 2 [4.5 % iodoacetamide (IA), 50 mmol/l Tris-HCl (pH 6.8), 6.0 mol/l urea, 30 % glycerol, 1 % SDS, few grains of bromophenol blue] with agitation. The Immobiline strips containing WF1 and BF1 were run on separate gels and resolved by molecular weight using 15 % acrylamide gels as previously described (refer to paragraph 3.2.3.1, page 49). The samples were electrophoresed at 25 mA until the dye had run off the strips and then at 80 mA until the dye front had reached the bottom of the gels (approximately 4 hours). A low molecular

weight protein standard was included on each gel. Protein spots were visualised by silver staining (paragraph 3.2.3.1, page 49).

4.2.8 Glycosylation analysis

4.2.8.1 Theory of glycosylation

Glycosylation is a process whereby oligosaccharides are attached to proteins and occurs within the endoplasmic reticulum and Golgi apparatus of cells (Rudd and Dwek 1997). Proteins usually emerge from the biosynthetic pathway as a mixture of glycosylation variants referred to a glycoforms and the profiles are usually characteristic of the tissue in which the protein is expressed. There are three main classes of covalently-bonded glycosidic linkages to proteins, two of which are explored in the present study.

N-glycosylation is a co-translational modification that occurs during protein folding and is available to all proteins that contain the sequon asparagine-Xaa-serine/threonine where Xaa represents any amino acid other than proline. The *N*-glycosylation process is initiated by the transfer of a specific oligosaccharide unit (namely $Glc_3Man_9GlcNAc_2$ where Glc: glucose, Man: mannose, Ac: acetyl) to the nitrogen atom in the side chain of certain asparagine residues. In contrast, the addition of *O*-linked glycans is a post-translational process. It is initiated by the transfer of a single monosaccharide (usually GlcNAc) to the oxygen atom on appropriate serine or threonine side chains (Rudd and Dwek 1997).

Monosaccharides may be conveniently represented by geometric symbols (Figure 4.1, page 68). A type of line drawing and short-hand notation has also been devised to readily communicate complex oligosaccharide structures. An example of a biantennary complex type structure is given below to illustrate this scheme (devised by Glycobiology Institute, University of Oxford).

4.2.8.2 Protein preparation

Previously purified UPTF1 from pooled urines of healthy white and black males was used (12 µg each) for extraction of the *N*-linked glycans. In addition, 24-hour urine samples were collected from eight healthy white males (ages 20 - 27) and seven healthy black males (ages 21 - 26) so that possible intra-group differences could be investigated. The CME was isolated from these urines as previously described (paragraph 3.2.2, page 48) and used for the analysis of the *N*-linked glycans on UPTF1.

Figure 4.1: Graphical representations of monosaccharides and their linkages

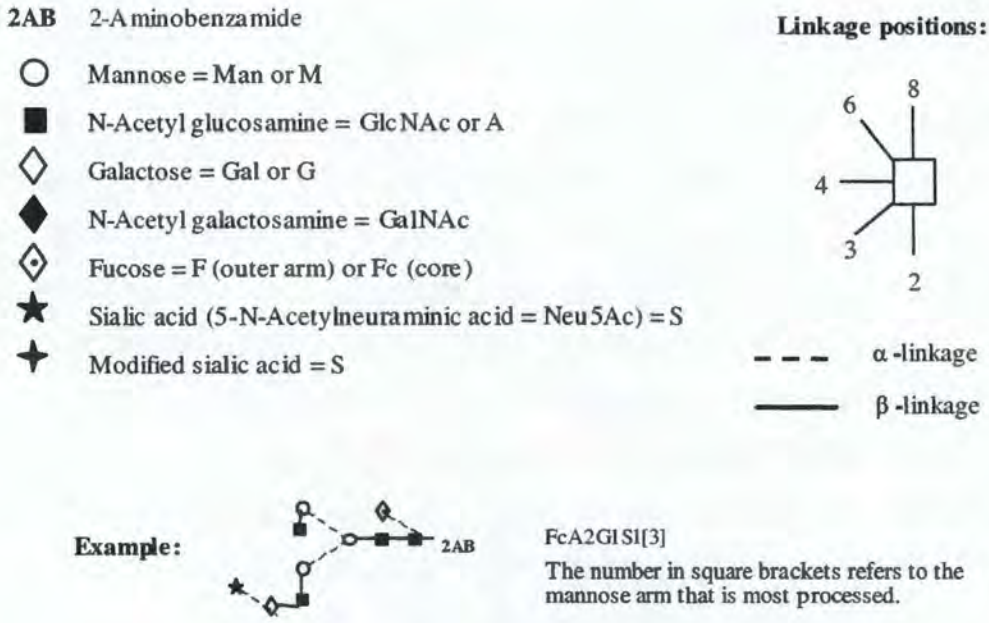

Twenty-hour urine samples were collected from six white CaOx stone-formers (ages 35 - 65) and one black CaOx stone-former (age 35). All of these subjects had either passed a stone or had one surgically removed during the nine months prior to commencement of the study. The CME was isolated from each of these urines and used for analysis of the *N*-linked UPTF1 glycans. The purified UPTF1 from pooled urines of healthy white and black males and white CaOx stone-formers (50 µg each) was used for analysis of the *O*-linked glycans. Glycans from each group are denoted by the following abbreviations: white controls = WC; black controls = BC; white stone-formers = WSF; black stone-former = BSF. Samples obtained from pooled urine samples are denoted as "pool".

4.2.8.3 Extraction of N-linked glycans

MilliQ water has been found to contain traces of polymers and organic contaminants that give a high background signal on mass spectrometry. All glycan samples were therefore prepared in fresh MilliQ water purified by distillation at sub-boiling point (referred to as SBP H_2O).

All of the protein samples were resolved by electrophoresis on 12.5 % polyacrylamide mini gels after reduction (50 mmol/l DTT) and alkylation (10 mmol/l IA). Up to four wells of each sample were run to provide sufficient glycans for analysis. The

protein bands were stained with Coomassie Brilliant Blue and then destained. The band corresponding to UPTF1 (prominent band at ~31 kDa) was excised, cut into 1 mm^3 pieces and frozen at -20 ^{0}C for at least 2 hours before further processing. The gel pieces were then washed with sodium hydrogen carbonate (20 mmol/l, pH 7.0) and ACN to remove excess SDS, and vacuum dried. The *N*-linked glycans were released overnight by *in situ* deglycosylation with peptide N-glycanase F (PNGase F) (Roche) at 37 ^{0}C. The released glycans in the supernatant were combined with several washings of the remaining gel pieces (alternate washings with ACN and SBP H_2O) and desalted using an activated anion exchange resin. The glycans were filtered to remove any remaining resin and dried under vacuum. The extracted glycans were fluorescently labeled with 2-aminobenzamide (2AB; Oxford GlycoSciences, Abingdon, United Kingdom) by reductive amination for 2 hours at 65 ^{0}C and the excess label was removed by ascending paper chromatography. The labeled glycans were then washed off the paper, dried and dissolved in 200 µl SBP H_2O. Refer to Appendix C (pages A23 – A27) for further details of the extraction procedure of *N*-linked glycans (Küster *et al.* 1997, Radcliffe *et al.* 2002)

4.2.8.4 Extraction of O-linked glycans

Proteins were dialysed overnight against a 0.1 % TFA solution, freeze-dried and cryogenically dried for 2 nights before manual hydrazinolysis. The *O*-linked glycans were then chemically released by incubation with anhydrous hydrazine at 60 ^{0}C for 6 hours and the excess hydrazine removed by evaporation. An acid-washed tube was included from this stage of the procedure as a blank sample. Glycans were then re-N-acetylated and cleaned up by application to an activated anion exchange resin column followed by descending paper chromatography. Finally, the glycans were eluted from the paper and dried under vacuum. The *O*-linked glycans were then 2AB labeled and dissolved in a final volume of 200 µl SBP H_2O as described in paragraph 4.2.8.2 above. Refer to Appendix C (pages A28 – A30) for further details on the release of *O*-linked glycans (Patel *et al.* 1993, Royle *et al.* 2002).

4.2.8.5 Exoglycosidase digestions

Aliquots of the *N*- and *O*-linked glycan pools (1 and 2 %, respectively) were vacuum dried and incubated overnight with arrays of exoglycosidases at 37 ^{0}C. The specificity and final concentration of the exoglycosidases are presented in Table 4.2 (on the next page). Following digestion, exoglycosidases were removed with SBP H_2O using Micropure-EZ filters, vacuum dried and dissolved in 20 µl SBP H_2O for analysis by normal phase

(NP)-HPLC. Control digests were included in which glycans were incubated in the buffer and SBP H_2O. Refer to Appendix C (page A28) for further details. The results were used to determine the sequence, monosaccharide type and linkage of glycan residues (in conjunction with mass spectrometry).

4.2.8.6 Normal phase HPLC

Aliquots (1 % in 20 µl SBP H_2O) of the glycan pools before and after exoglycosidase digestion were added to 80 µl ACN and analysed by NP-HPLC according to the low salt buffer system as previously detailed (Guile *et al.* 1996) using a 4.6 x 250 mm GlycoSep-N column (Glyko, England) (HPLC details: Appendix C, page A27). A 2AB-labeled dextran hydrolysate ladder standard consisting of glucose oligomers was used to calibrate the system. Since the number of glucose residues (GU units) of the dextran peaks are known, these were used to calculate the GU values of the unknown glycan structures. These values were then compared with a database so that preliminary assignments on the structure of each glycan peak could be made. The area of each glycan peak was calculated and expressed as a percentage of the total glycan pool.

Table 4.2: Specificity and final concentration of exoglycosidases

Enzyme	Source	Abbrev.	Specificity	Conc.
Sialidase	Arthrobacter ureafaciens	Abs	Releases α2-3 and 2-6 linked non-reducing terminal sialic acids	1 U/ml
	Streptococcus pneumoniae sialidase	Nani	Releases α2-3 linked non-reducing terminal sialic acids.	1 U/ml
Fucosidase	Almond meal	Amf	Releases α1-3 and 1-4 linked non-reducing terminal fucose residues. Digests outer arm fucose.	2 mU/ml
	Bovine kidney	Bkf	Releases α1-6 linked non-reducing terminal fucose residues more efficiently than α1-2, 1-3 and 1-4 fucose. Digests core fucose.	1 U/ml
Galactosidase	Bovine testes	Btg	Releases β1-3 and 1-4 linked non-reducing terminal galactose residues more efficiently than β1-6 linked residues.	1 U/ml
	Streptococcus pneumoniae galactosidase	Spg	Releases β1-4 linked non-reducing terminal galactose residues.	80 mU/ml
Hexosaminidase	Streptococcus pneumoniae glucosaminidase	GluH	Releases β1-2, 3, 4 and 6 linked GlcNAc but not GalNAc residues. Does not remove bisecting GlcNAc residues.	4.5 U/ml
	Jack bean	Jbh	Releases β1-2, 3, 4 and 6 linked GlcNAc and GalNAc residues. Does not remove bisecting GlcNAc residues.	50 mU/ml
Mannosidase	Jack bean	Jbm	Releases α1-2, 3 and 6 linked mannose residues more efficiently than α1-3 linked mannose residues.	50 U/ml

4.2.8.7 Weak anion exchange HPLC

Glycan pools (1 % in 100 µl SBP H_2O) were separated according to charge by weak anion exchange (WAX)-HPLC using a Vydac 301VHP575 column (7.5 x 50 mm) (Anachem Limited, Luton, England) (Zamze *et al.* 1998). A bovine serum fetuin standard was included which has previously been characterised (Merry *et al.* 2002). Fractions were collected, washed with SBP H_2O to remove the solvents, dried under vacuum and analysed by NP-HPLC. These profiles were then compared with the total glycan pool obtained on NP-HPLC. An aliquot of the glycan pools were also analysed by WAX-HPLC following overnight digestion with Abs (which converts charged sialylated glycans to neutral glycans). Refer to Appendix C (page A27) for further details.

4.2.8.8 MALDI-TOF and Quadropole TOF mass spectrometry

MALDI-TOF mass spectra were recorded using a Micromass TofSpec 2E reflection time-of-flight mass spectrometer (Micromass Limited, Manchester, England) with a saturated solution of 2,5-dihydroxybenzoic acid in ACN as the matrix. Additional mass data was also obtained using a hybrid quadropole TOF (QTOF) mass spectrometer fitted with a nanospray source (Waters-Micromass Limited, Manchester, England).

4.2.8.9 Molecular modeling

Molecular modeling was performed on a Silicon Graphics Fuel work station using InsightII and Discover Software (Acelrys, San Diego). The figures were produced using the programme Molscript. Since UPTF1 is an intracrystalline urinary protein, the Ca-bound bovine PTF1 crystal structure (Brookhaven database) was used as the basis for modeling. The bovine (SWISSPROT, P00735, residues 44 – 199) and human (SWISSPROT, P00734, residues 44 – 198) sequences were aligned using BLAST (www.ncbi.nlm.gov/BLAST). *N*- and *O*-linked glycan structures were generated using the database of glycosidic linkage conformations and *in vacuo* energy minimisation to relieve unfavourable steric interactions. Predicted glycan sites were used in the model (www.cbs.dtu.dk/Services/NetNGlyc and www.cbs.dtu.dk/Services/NetOGlyc). The Asn-GlcNAc linkage conformations were based on the observed range of crystallographic values, the torsion angles around the Asn Cα-Cβ and Cβ-Cγ bonds then being adjusted to eliminate unfavourable steric interactions between the glycans and the protein surface.

4.3 RESULTS

4.3.1 Purification of UPTF1

Results obtained at various stages of the UPTF1 purification process are shown below. The first step of protein purification was the desalting of the CME by column chromatography. A typical absorbance plot of the fractions collected from the column is shown in Figure 4.2 below. The first peak eluted corresponded to the protein while the salt peak was eluted later.

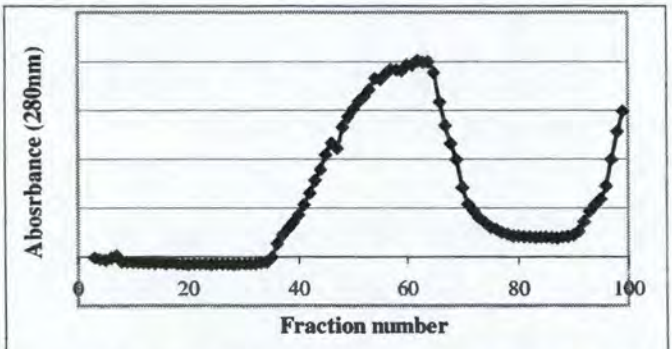

Figure 4.2: Typical absorbance plot obtained of a CME sample on a desalting column

UPTF1 was then separated from the mixture of proteins contained in the desalted CME by RP-HPLC as shown in Figure 4.3 below. Typically, a mixture of proteins was eluted from 33 to 43 minutes followed by UPTF1 at 44 minutes (shown by an asterisk).

Figure 4.3: Typical HPLC chromatogram of desalted crystal matrix extract

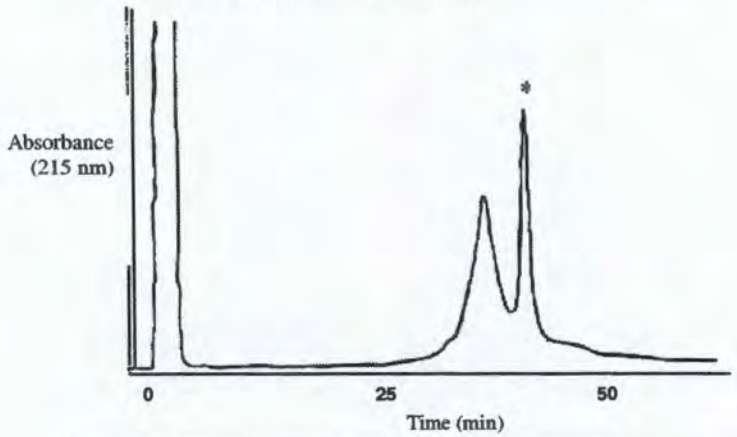

4.3.2 SDS-PAGE and Western blotting

The HPLC purified protein was analysed by SDS-PAGE (Figure 4.4) and Western blotting (Figure 4.5). The SDS-PAGE showed that a single band was present in the protein samples from both white (lane 1) and black (lane 2) subjects after HPLC with apparent molecular weights of 42 kDa. Both of these protein bands cross-reacted with the monoclonal UPTF1 antibody (Figure 4.5) and their identity was thus confirmed as UPTF1. The faint band in lane 1 at a slightly higher molecular weight than UPTF1 (indicated by an arrow) indicated the presence of a small amount of PTF1+2 in the WF1 sample. This fragment of PT is also known to cross react with the monoclonal antibody (Stapleton *et al.* 1996).

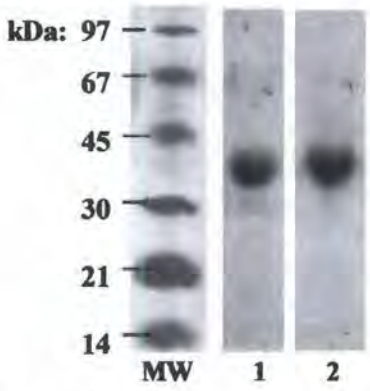

Figure 4.4: SDS-PAGE of UPTF1 from white and black subjects. The protein patterns obtained are from *MW:* low molecular weight marker; *1:* WF1 (2μg); *2:* BF1 (2μg).

Figure 4.5: Western blot of UPTF1 from white and black subjects. The protein patterns obtained are from *1:* WF1 (2μg); *2:* BF1 (2μg).

4.3.3 MALDI-TOF mass spectrometry

The spectra of WF1 and BF1 (Table 4.3) revealed $[M+H]^+$ ions at *m/z* corresponding closely with the calculated values of 1207.4 and 1617.8 of the Lys-C derived peptides Ala-1—Lys-10 and Tyr-44—Lys-56. Ions at 766.2, 2000.4 and 1118.6 corresponding to Lys-C derived peptide Asp-38—Lys-43 and Asp-N derived peptides Asp-130—Gln-145 and Asp-146—Arg-155 were also observed in BF1 (Asp: aspartic acid; Gln: glutamine; refer to Table 4.4 on page 74 for the other abbreviations). Peptide 1-10 contains two potential Gla residues, which exist in both the carboxylated and uncarboxylated forms in both WF1 and BF1. The high percentage of Glu residues in peptide 11-37 and the glycosylation of peptides 57-97 and 97-107 hindered the determination of their masses. The mass spectral data were consistent with the reported sequence of UPTF1. The 14 % and 34 % of WF1 and BF1, respectively, that was successfully mapped did not reveal any apparent differences.

Table 4.3: MALDI-TOF of observed $[M+H]^+$ ions of UPTF1 generated by endoproteinase Lys-C or Asp-N (cysteines were protected with vinyl pyridine)

Amino acid residues	Calculated m/z	Observed m/z	
		WF1	*BF1*
1-10	1207.4	1207.5	1207.7
1-10 [a]	1251.4	1252.1	1252.2
1-10 [b]	1295.4	1296.1	1296.2
11-37 [c]	3209.4		
38-43	765.8		766.2
44-54	1374.6		1375.5
44-56	1617.8	1618.1	1618.3
57-97	4791.5		
97-107	1124.2		
130-145	1999.3		2000.4
146-155	1118.3		1118.6

[a] *Peptides contains one and* [b] *carboxylated glutamic acid residue;* [c] *High percentage of glutamic acid residues (30%);* [d] *Glycosylated peptide*

4.3.4 Protein sequencing

The first five amino acids at the N-terminus of WF1 and BF1 were alanine-asparagine-threonine-phenylalanine-leucine. These results are in agreement with Walz *et al.* (1977) and thus confirmed the identity of the purified proteins as UPTF1 and that there were no differences at the N termini.

4.3.5 Amino acid analysis

The results of an amino acid analysis of WF1 and BF1 by acid hydrolysis are shown in Table 4.4.

Table 4.4: Amino acid composition of WF1 and BF1 as determined by acid hydrolysis

Amino Acid	Number of residues:		
	Calculated value	*WF1*	*BF1*
Asparagine (Asn)	14	16	16
Threonine (Thr)	18	18	17
Serine (Ser)	9	11	12
Glutamic acid (Glu)	22	23	23
Proline (Pro)	9	9	9
Glycine (Gly)	9	10	9
Alanine (Ala)	12	12	13
Cystine (Cys)	10	10	10
Valine (Val)	8	8	8
Methionine (Met)	1	1	1
Isoleucine (Ile)	4	3	3
Leucine (Leu)	8	8	8
Tyrosine (Tyr)	5	4	3
Phenylalanine (Phe)	4	4	4
Tryptophan (Trp)	3	3	3
Histidine (His)	3	5	3
Lysine (Lys)	4	4	5
Arginine (Arg)	12	8	8

The amino acid composition of UPTF1 from both population groups was similar to the calculated data, thus confirming their identity as UPTF1. These data are similar to the amino acid composition obtained by Walz *et al.* (1977) of human PT.

4.3.6 Gla analysis

The results of alkaline hydrolysis and subsequent amino acid analysis of WF1 and BF1 are shown in Table 4.5 below. The number of Gla residues in WF1 and BF1 was determined as 10 and 13, respectively, using the number of Glu residues as 23 (from acid hydrolysis treatment).

Table 4.5: γ-Carboxyglutamic acid and glutamic acid composition of WF1 and BF1 determined by alkaline hydrolysis

	WF1	BF1
Moles Gla	5.370138	5.013123
Moles Glu	6.818915	4.083367
Number Gla residues	$10.1 \approx 10$	$12.7 \approx 13$

The same trend was observed in a second experiment although the number of Gla residues differed (WF1: 9, BF1: 8). Such inter-experimental variation is commonly observed in amino acid analyses.

4.3.7 2D SDS-PAGE

The 2D map of UPTF1 from white and black subjects (5 µg each) is shown in Figures 4.6.1 and 4.6.2, respectively. Only the region in which protein spots were detected is shown. Both WF1 and BF1 were present as three distinct spots (shown in red since they were not clear on the gel) at molecular weights of approximately 40 kDa. These spots represent charged variants of UPTF1 at low pI values (near the acidic end of the gel). The relative size of the middle spot suggested that this charged variant is the most abundant of the three.

Figure 4.6: 2D SDS-PAGE of UPTF1 from white (4.6.1) and black subjects (4.6.2)

4.3.8 Glycan analysis

N-linked glycans

4.3.8.1 NP-HPLC of glycan pools

The *N*-linked glycans were enzymatically released from SDS-PAGE purified UPTF1. A typical protein pattern is shown in Figure 4.7 (Appendix H, page A79). The four bands at 31 kDa corresponding to UPTF1 were combined for glycan extraction. Two of the white stone-formers had two bands near 31 kDa; these were excised and processed separately. They were later found to have similar profiles on NP-HPLC (suggesting that both bands were UPTF1) and the glycans were thus combined.

Figures 4.8 (page 77) and 4.9 (page 78) show the NP-HPLC profiles of the pool of *N*-glycans from control and stone-forming subjects, respectively. The GU values, which reflect the relative size of the glycans, are shown on the x-axis. The intragroup and intergroup similarity of the glycan profiles is apparent by inspection. The peak areas for each glycan pool are shown in Appendix C (WC: Table C1, page A31; BC: Table C2, page A32; WSF and BSF: Table C3, page A33). They confirmed the considerable correlation between samples. The peak numbers indicated in these tables correspond to those shown in Figure 4.16 (page 88).

Owing to the similarity of the *N*-linked glycan profiles, WC6 was chosen as a representative sample (since it contained the largest glycan pool) and used for further characterisation. The WCpool and BCpool glycan profiles were slightly different to those obtained from the individuals' profiles for white and black subjects, particularly near the GU values of 7.16 and 7.88. This may be due to the fact that the pooled samples' *N*-glycans were released from purified UPTF1 whereas the individuals' samples were obtained from the crystal matrix extract by SDS-PAGE. However, since the individuals' samples were so similar, this was not regarded as significant.

Preliminary assignments were made by comparing the GU values of peaks with a database of *N*-linked structures. These were confirmed, and some additional assignments were made, by following the progression of each peak with a series of exoglycosidase arrays in conjunction with mass spectrometry and WAX-HPLC analyses.

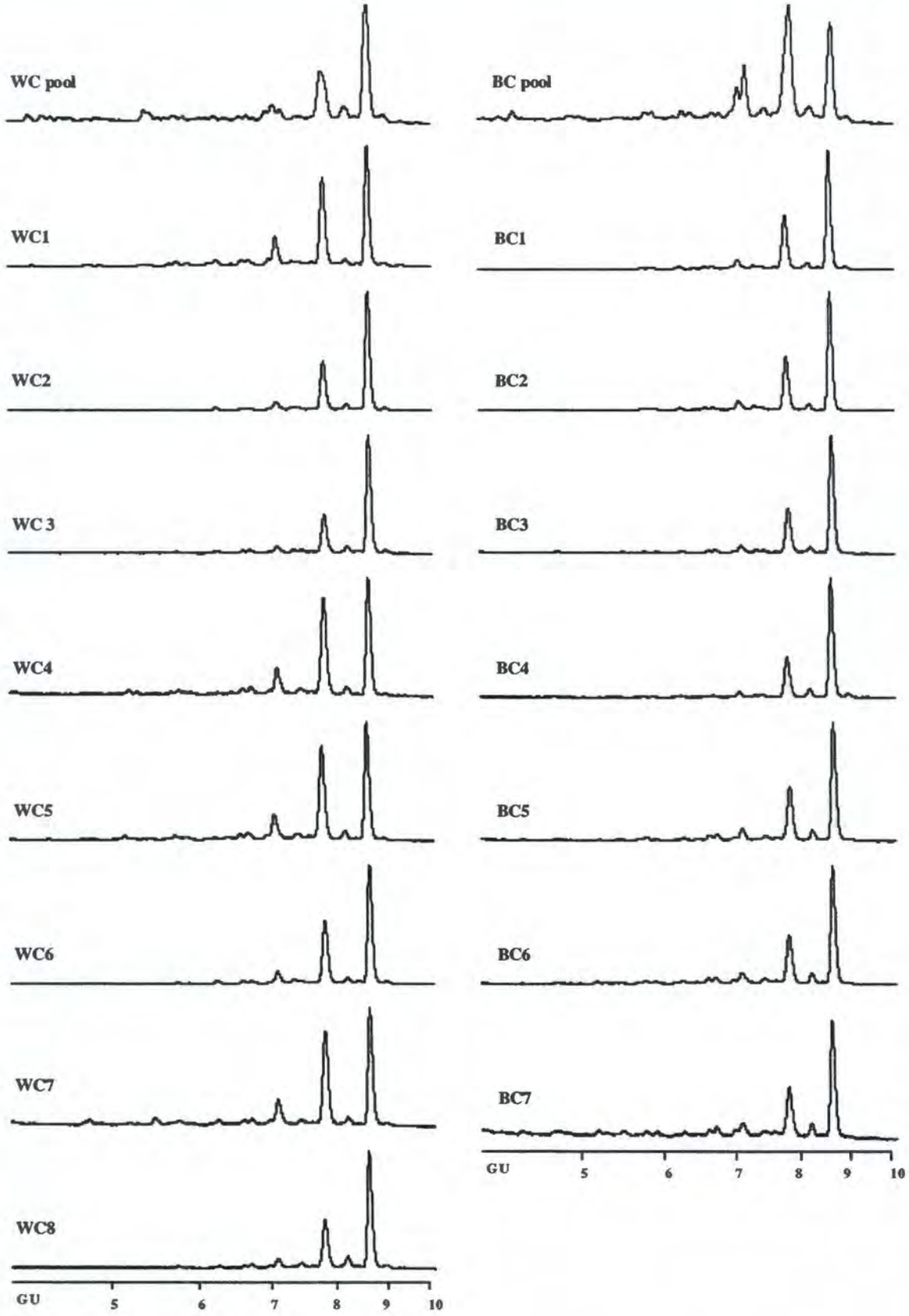

Figure 4.8: NP-HPLC profiles of N-linked glycans on UPTF1 pooled from white (WC pool) and black (BC pool) control subjects as well as from several individual white (WC1-8) and black (BC1-7) subjects. Refer to Tables 4.6 (WC) and 4.7 (BC) for peak areas.

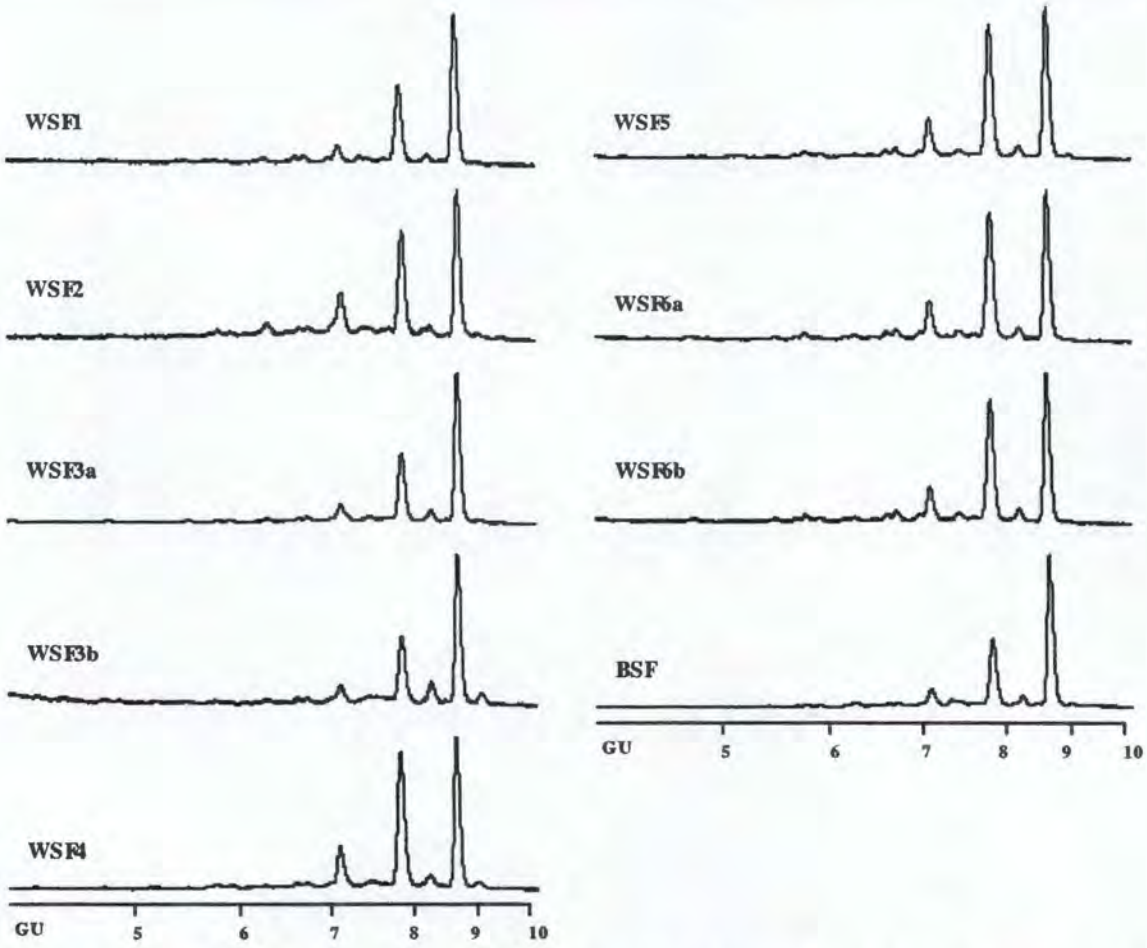

Figure 4.9: NP-HPLC profiles of N-linked glycans on UPTF1 from several white stone-formers (WSF1-6) and one black stone-former (BSF). Refer to Table 4.8 for peak areas. WSF3 and WSF6 had two bands (shown as "a" and "b") presumed to be UPTF1 on SDS-PAGE and thus these were processed separately.

4.3.8.2 Exoglycosidase digestions

Table 4.6 (pages 79 – 81) shows the peak areas expressed as a percentage of the total WC6 *N*-glycan pool before (undig) and after a series of exoglycosidase arrays. One peak present in the undigested glycan pool was absent in the control digest (peak 6) while another was significantly reduced (peak 18). The most likely explanations would be loss of this glycan structure during incubation at 37 ^{0}C due to its lability or during filtration following the overnight digestion. However, these theories were tested and ruled out by additional experiments (data not shown) and thus no plausible explanation can be provided. The control digest HPLC profile was therefore used for comparison with the exoglycosidase array profiles. Although this could not be confirmed, the structure at peak 6 was provisionally assigned as A2 on the basis of its relative elution position and comparison of its GU value (5.70) with a database.

Table 4.6: NP-HPLC analysis of *N*-linked glycans on UPTF1 from white control subject WC6

PEAK ID	MAJOR STRUC-TURE	GU	% AREA:										
			Undig	Control digest	Exoglycosidase(s) added to undigested glycan pool								
					Abs	*Abs Amf*	*Abs Amf Btg*	*Abs Amf Btg GluH*	*Abs Amf Btg GluH Bkf*	*Abs Amf Btg GluH Bkf Jbm*	*Abs Amf Spg*	*Abs Bkf*	*Bkf*	*Jbm*
	Man1	2.66								99.3				0.2
	[a] A1[6]-M	3.87												0.1
	[a] A1[3]-M	4.15												0.1
1	Man3	4.43	0.2	0.2	0.3	0.2	0.9	93.9	94.6			0.7	0.6	
	ni	4.60					1.5				0.8			
	ni	4.74					0.6				0.4			
	S	4.78						0.9	0.8	0.2				
2	A1[6]	4.91	0.1	0.3	0.2	0.4	0.7				0.4	1.0	0.2	
	FcMan3							1.9						
	S								0.5	0.2				
	[a] A1G1[6]-M													0.5
	A1	5.00					3.9				4.5			
3	A1[3]	5.06	0.1	0.1	0.2	0.3						0.9	0.2	
	[a] A1G1[3]-M													0.5
	M	5.21						0.8	0.8					
	[b] A2	5.26					2.4				2.7			
	ni	5.31	0.2	0.2	0.2	0.5					0.3	1.4		
	M	5.38					0.4	0.7	0.9					
	A2	5.50					83.3				82.9			
	M	5.59						0.7	1.3			0.9		
	M, S									0.1				
	ni	5.63			0.4	0.3								
6	[c] A2	5.70	0.5				0.4				0.6			
	M, S									0.2				
7	A1G1[6]	5.83	0.3	0.2	1.2	1.2						2.6	0.4	
8	A1G1[3]	5.90	0.6	0.6	2.3	2.2					2.4	4.9	1.1	
	FcA2						1.6							
	[a] A1G1S1[6]-M													1.3
9	[d] A1G1S1[3]	6.03	0.8	0.7									1.2	
	[a] A1G1S1[3]-M													1.9
	ni	6.15			0.7	0.7	0.7				1.0	2.0		
11	A2G1[6]	6.28	0.3	0.1	1.3	1.1					1.3	2.9	0.4	0.5

Table 4.6: NP-HPLC analysis of *N*-linked glycans on UPTF1 from white control subject WC6 (continued)

PEAK ID	STRUC-TURE	GU	% AREA:											
			Undig	Control digest	Exoglycosidase added to undigested glycan pool									
					Abs	*Abs Amf*	*Abs Amf Btg*	*Abs Amf Btg GluH*	*Abs Amf Btg GluH Bkf*	*Abs Amf Btg GluH Bkf Jbm*	*Abs Amf Spg*	*Abs Bkf*	*Bkf*	*Jbm*
12	A2G1[3]	6.37	1.6	0.4	1.4	1.4						3.5	0.6	0.6
	ni						0.8							
	S, G, M	6.49						0.9	0.9					
	ni				0.7	0.7					0.5	1.2		
13	[d] A2G1S1	6.58	0.8	0.5										
	ni				0.8	0.6	0.3					1.2	1.1	0.8
14	A1G1S1[6]	6.70	1.4	0.7								1.4	1.8	0.6
	Ni	6.75			0.9	0.7								
15	A1G1S1[3]	6.80	1.8	1.1		0.7						0.9	2.9	1.5
	Ni				0.8									
	S, G, M	6.90					0.9				1.1			
16	[e] A2G2	7.07	1.0	1.8	1.7	1.7						2.0	1.8	1.6
17	A2G2	7.16	5.8	7.6	77.4	82.4					0.5	69.7	8.4	7.0
	undig						0.3							
18	A2G1S1[6]	7.36	2.3	0.8									1.3	0.9
19	A2G1S1[3]	7.49	2.1	2.6								1.0	3.2	2.7
	[f] FcA2G2	7.58			1.0	0.9								
20	A2G2S1[6]	7.70	1.6	1.4									2.1	1.7
	[f] FcA2G2	7.75			1.1	1.0								
	ni											0.6		
21	A2G2S1[3]	7.88	27.3	32.8									29.0	28.6
	A2G2F	7.98			3.7									
	ni					0.6								
	F, G	8.18			0.4	0.3						0.7		
23	[d] A2G2S2	8.25	3.3	5.0								0.2	5.2	5.3
24	[d] A2G2S2	8.40	2.1	1.1									0.9	1.0
	F, G				0.4	0.3								
25	A2G2S2	8.56	43.3	39.3							0.1		35.9	40.4
	S, G, M				0.8	0.6						0.2		
	F, G	8.72			0.3	0.2								
26	[d] A2G2FS2	8.91	1.6	2.2									1.7	2.0
	F, G				0.3	0.2								
27	FcA2G2S2	9.26	0.4	0.6										0.4

Table 4.6 - Notes:

a –[M] indicates the loss of a β1-6 mannose. These structures are indicated on the Jbm digest shown in Figure 4.13.

b This could possibly be a bisected A2 structure. Digestion with Sph should be used to test this possibility (unavailable at time of study).

c Likely to be an A2 structure based on its GU value (5.70) and its relative position in the glycan pool profile. However, this could not be confirmed since the peak was absent in the control digest.

d Likely to be sialic acid residues other than Neu5Ac (N-Acetyl substitution at C-5) which is the most commonly observed. Characterisation of the molecular structures of these sialic acids requires further investigation.

e This structure digests similarly to A2G2 (at peak 17). The difference in structure or linkage which could account for the slightly lower GU value is not known.

f Both structures appear to be FcA2G2 on the basis of their digestions and the difference in GU values could be consistent with one of them being bisected. Digestion with Sph should be used to test this possibility (unavailable at time of study).

F, G: These structures could not be fully characterised since they were observed after Abs digestion but could not be correlated with peaks present in the undigested glycan pool. It is thus probable that they co-eluted with the major peaks observed by NP-HPLC. They are likely to be fucosylated (since peaks moved after Abs+Bkf digestion compared with Abs alone) and contain β1-4 galactose linkages (since peaks moved following Abs+Amf+Btg and Abs+Amf+Spg digestion compared with Abs+Amf).

M: These structures contain mannose glycans since the peaks moved following addition of Jbm.

S: These structures are likely to be sulphated since they remained after the array of exoglycosidases.

S, G, M: These structures could not be fully characterised however it is apparent that they emerged as subsequent digestion products of the peak at GU 8.56 after Abs digestion. It is probable that the peak co-eluted with another major peak observed in the undigested glycan pool. It is likely that the structure is sialylated (it elutes with the disialylated structures after Abs digestion on WAX-HPLC), galactosylated (peak moved following addition of Btg and Spg), mannose-containing (peak moved following addition of Jbm) and sulphated (since it remained after the array of exoglycosidases).

ni: These structures could not be identified.

Undig: This is likely to be an A2G2 structure that was incompletely digested by the addition of Btg.

The NP-HPLC profiles of the exoglycosidase arrays are shown in Figures 4.10 - 4.13. The complete array is shown in Figure 4.10 (page 82). The change in elution times of relevant peaks following digestion is shown with arrows. For example, the peak corresponding to A2G2FS2 (control digest profile) was digested with a sialidase to A2G2F. Addition of a fucosidase, which digests outer arm fucose residues (Amf), produced the structure A2G2. This was digested to A2 by a galactosidase (Btg) and finally the *N*-linked structure was reduced to the trimannosyl core Man3 by a hexosaminidase (GluH).

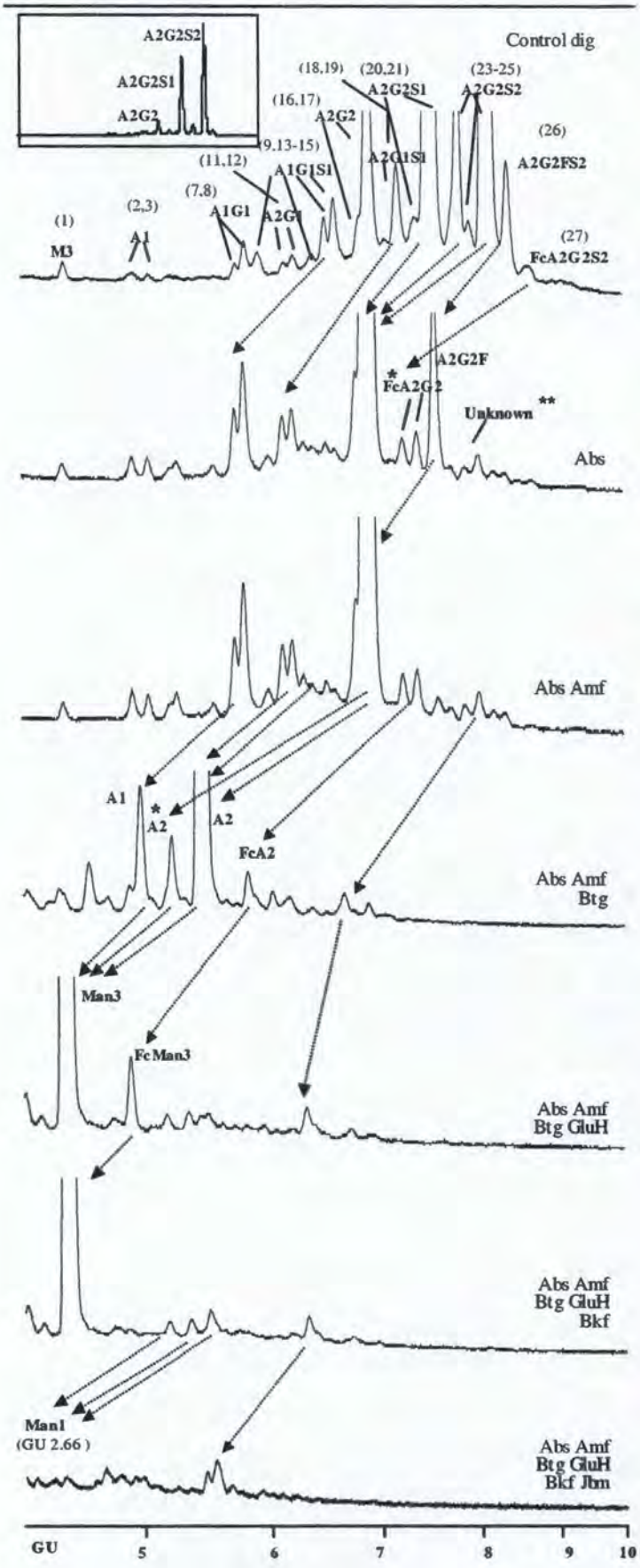

Figure 4.10: NP-HPLC profiles of a UPTF1 *N*-glycan pool from white control subject WC6 before and after treatment with an array of exoglycosidases. Refer to Table 4.9 for summary of structures and Table 4.6 for peak areas. *These structures may be bisected. **Refer to notes with Table 4.6 for discussion.

The identification of the two fucosylated structures (peaks 26 and 27) was confirmed by comparison of a digest with a fucosidase alone and in combination with a sialidase (Figure 4.11). Bkf digested FcA2G2S2 (peak 27) to A2G2S2, but A2G2FS2 (peak 26) was unaffected. However, Abs+Bkf digested A2G2FS2 to A2G2. This confirms the presence of outer arm fucose, which would be inaccessible to the fucosidase due to the presence of the sialic acid residue, rather than core fucose in the structure at peak 26.

Additional galactosidase digestions confirmed the linkage of galactose residues (Figure 4.12) together with the corresponding peak areas (Table 4.6). The majority of terminal galactose were β1-4 linked since very similar profiles were obtained with Btg which digests β1-3 and β1-4 linked galactose more efficiently than β1-6 residues, compared with Spg which digests only β1-4 linked galactose residues. The A2G1 structure was partially digested

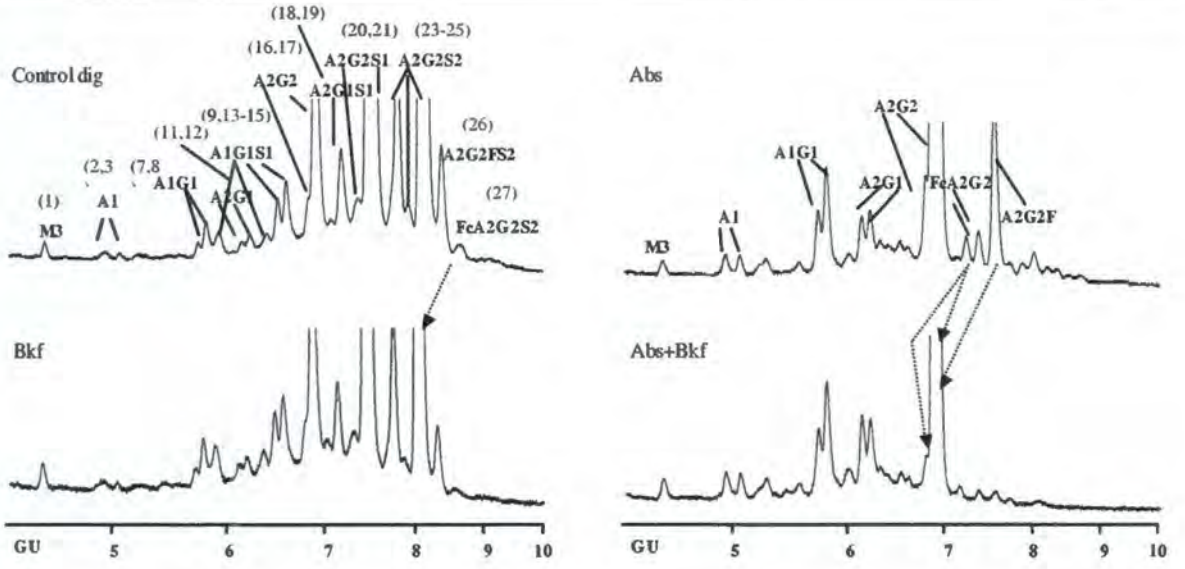

Figure 4.11: NP-HPLC profile of a UPTF1 *N*-glycan pool from white control subject WC6 before and after treatment with a fucosidase, alsoused in combination with a sialidase.

by both Btg and Spg and is therefore a mixture of β1-3 (~20 %), β1-4 (~50 %) and β1-6 (~30 %) linked galactose structures. Since A2G1S1 is a derivative of A2G1, it contains the same mixture of galactose linkages. Five monoantennary *N*-linked structures were identified by preliminary assignments, namely Man3, A1, A1G1, A2G1 and A1G1S1. All of these structures, when digested with a mannosidase (Figure 4.13), shifted to earlier elution times and thus confirmed that at least one of the mannose residues in their trimannosyl core was unprocessed.

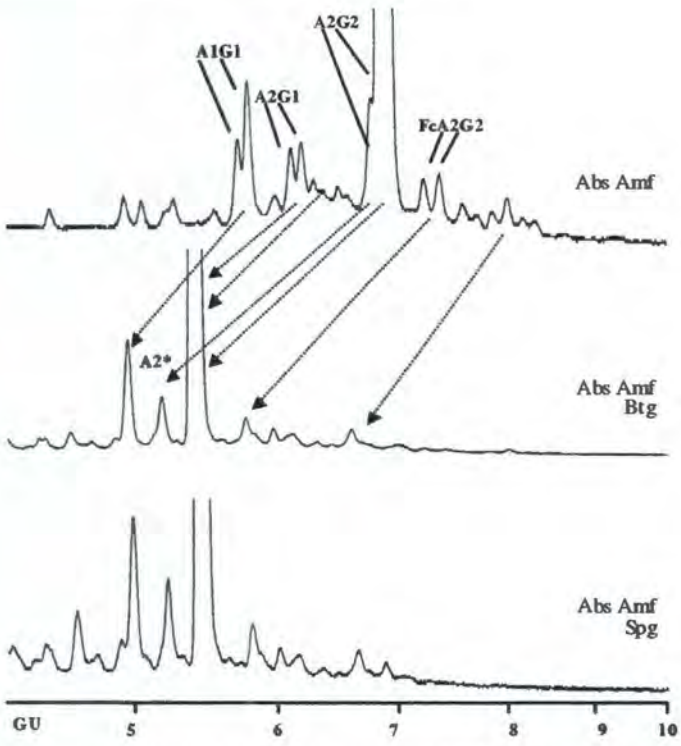

Figure 4.12: NP-HPLC profile of a UPTF1 *N*-glycan pool from white control subject WC6 before and after digestion with two galactosidases, Btg and Spg, (in combination with other exoglycosidases) to determine the galactose linkages. *This may be a bisected A2 structure.

The sialic acid residues were found to be α2-6 linked since all of the sialylated structures digested with Abs, which is specific for α2–3 and α2–6 linked terminal sialic acids, but the profile

following digestion with Nani, which digests only α2-3 linkages, was identical to the undigested glycan pool (data not shown).

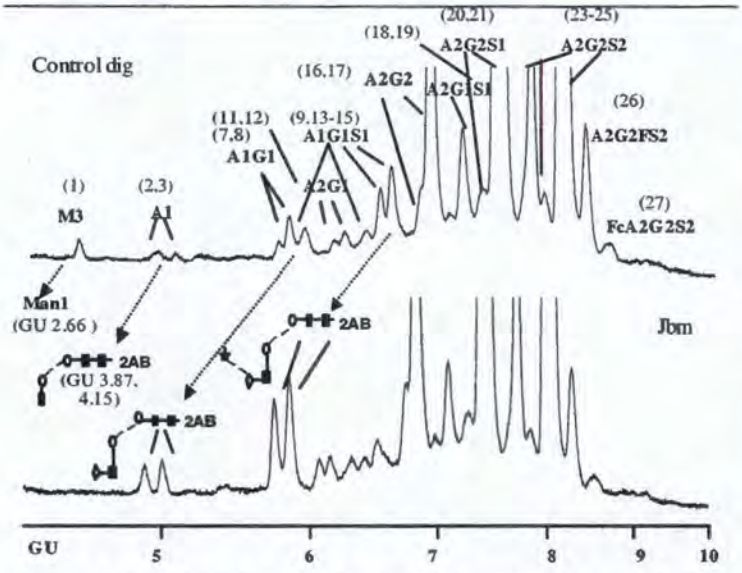

Figure 4.13: NP-HPLC profile of a UPTF1 *N*-glycan pool from white control subject WC6 before and after digestion with a mannosidase.

Digestion with the combination Abs+Amf+Btg+ Jbh produced an identical HPLC profile to that with GluH substituted for Jbh (the latter is shown in Figure 4.6; the Jbh digest profile is not shown). Since GluH releases GlcNAc but not GalNAc residues while Jbh releases both, it can be concluded that the *N*-linked glycan pool does not contain GalNAc residues.

4.3.8.3 Weak anion exchange HPLC

WAX-HPLC was used to separate the WC6 *N*-linked glycan pool into neutral, mono- and disialylated fractions, both before and after digestion with Abs. These HPLC profiles are presented alongside a fetuin standard (Figure 4.14). The undigested glycan profile shows that a high proportion of the *N*-linked structures are sialylated, which is consistent with the proposed assignments. The presence of a small amount of charged glycans after Abs digestion suggests that there may be structures other than the

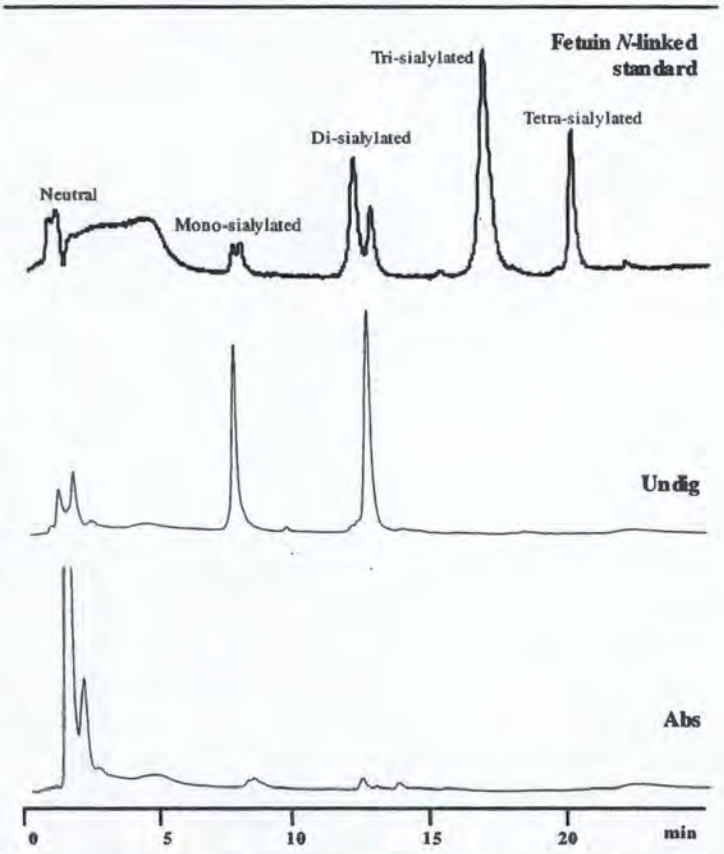

Figure 4.14: WAX HPLC profile of *N*-linked glycans on UPTF1 from white control subject WC6 before and after digestion with a sialidase. A profile of an *N*-linked fetuin standard is included for comparison.

sialylated ones which also be charged, however further studies are required to confirm this proposal. It could also indicate incomplete sialidase digestion. The WAX-HPLC fractions were collected and analysed by NP-HPLC for comparison with the total glycan pool (Figure 4.15). This analysis showed that in addition to those structures previously assigned to each peak, other structures had also co-eluted at the same GU values. The percentage of neutral, mono- and disialylated structures present in each peak is shown in Table 4.7.

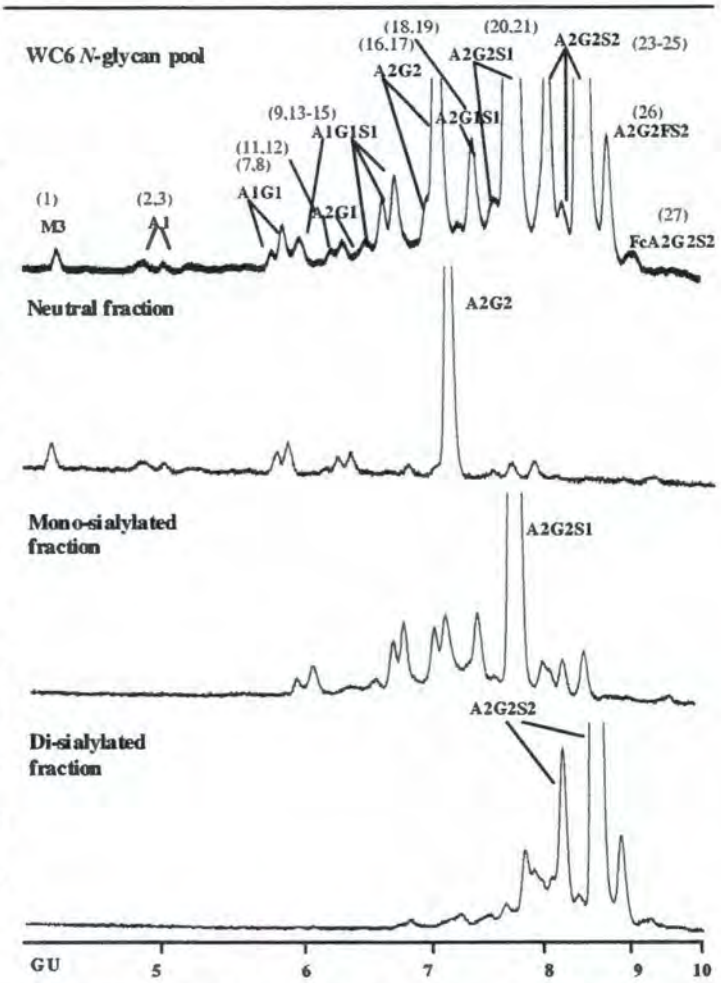

Figure 4.15: NP-HPLC profiles of UPTF1 *N*-glycan pool from white control subject WC6 before and after separation by WAX HPLC.

Table 4.7: Analysis of WAX-HPLC fractions on NP-HPLC of *N*-linked glycans on UPTF1 from white control subject WC6

Peak ID	Peak area (%)	GU	% PEAK AREA: Neutral fraction	Monosialylated fraction	Disialylated fraction
1	0.2	4.43	100		
2	0.1	4.95	100		
3	0.1	5.08	100		
7	0.3	5.84	100		
8	0.6	5.92	57.8	42.2	
9	0.8	6.08		100	
11	0.3	6.30	100		
12	0.4	6.40	100		
13	0.8	6.60		100	
14	1.4	6.75		100	
15	1.8	6.84		79.5	20.5
16	1.0	7.12	8.3	91.7*	
17	5.8	7.19	57.3	30.9*	11.8*
19	2.1	7.48		83.4	16.6
20	1.6	7.81	13.4	45.7	40.8
21	27.3	7.92	0.5	87.2	12.3
23	3.3	8.29			100
24	2.1	8.57		44.5	55.5
25	43.3	8.66		2.0	98.0
26	1.6	8.96			100
27	0.4	9.24			100

**Since these peaks did not move on NP-HPLC following Abs digestion, they are likely to be neutral fractions which were carried over in the mono- and disialylated fractions (probably due to the large sample amount present).*

Table 4.8: Mass data of *N*-linked glycans on UPTF1 from white control subject WC6

Peak ID	GU	Mass MALDI-TOF MS $[M+Na]^+$		Mass QTOF MS $[M+2H]^+$		Composition				Structure
		Observed	Calc.	Observed	Calc.	Hex	HexNAc	Neu5Ac (Na)	Fuc	
2	4.91	1256.6	1256.5			3	3	0		A1[6]
3	5.06									A1[3]
7	5.83	1418.6	1418.5			4	3	0		A1G1[6]
8	5.90									A1G1[3]
11	6.28	1621.7	1621.6			4	4	0		A2G1[6]
12	6.37									A2G1[3]
14	6.70	1731.6	1731.6	925.3	925.4	4	3	1		A1G1S1[6]
15	6.80									A1G1S1[3]
17	7.16	1783.6	1783.7	881.2	881.3	5	4	0		A2G2
20	7.70	2096.6	2096.7	1026.9	1026.9	5	4	1		A2G2S1[6]
21	7.88									A2G2S1[3]
25	8.56	2409.6	2409.8	1172.3	1172.4	5	4	2		A2G2S2
*26, 27	8.91, 9.26	2242.8	2242.8			5	4	1**	1	A2G2FS2
		1929.9	1929.7			5	4	0**	1	FcA2G2S2
				1245.5	1245.3	5	4	2	1	

**The mass data are in agreement with both of these peaks since no distinction can be made between core and outer arm fucosylation.*

*** Sialic acid residues frequently decompose on MALDI-TOF MS.*

4.3.8.4 MALDI-TOF and QTOF mass spectrometry

Mass spectral data obtained by MALDI-TOF MS and QTOF MS is shown in Table 4.8 (page 86). Refer to Appendix C for the chromatograms recorded (Figures C1 – C2, page A34). From the observed masses, the number of hexose (Hex; includes Man, Gal), N-Acetyl substituted hexose (includes GlcNAc), Neu5Ac (the most commonly observed sialic acid residue) and fucose residues are computed. The most probable structure corresponding to this composition is then chosen as the assigned structure, taking into consideration the exoglycosidase and WAX-HPLC analyses. The mass data recorded was consistent with the previously assigned structures. The fucosylated structures could not be differentiated by mass spectrometry since no distinction can be made between outer arm (peak 26) and core fucose (peak 27, Figure 4.16) and the composition of the remaining residues was the same (Hex: 5, HexNAc: 4, Neu5Ac: 2).

4.3.8.5 Summary of N-linked glycans

Table 4.9: Summary of *N*-linked glycans on UPTF1 from white control subject WC6 (refer to Figure 4.16 for structures)

Peak ID	GU	% Area	Major structure
1	4.43	0.2	Man3
2	4.91	0.1	A1[6]
3	5.06	0.1	A1[3]
6	5.70	0.5	A2
7	5.83	0.3	A1G1[6]
8	5.90	0.6	[a] A1G1[3]
9	6.03	0.8	[b] A1G1S1[3]
11	6.28	0.3	A2G1[6]
12	6.37	1.6	A2G1[3]
13	6.58	0.8	[b] A1G1S1
14	6.70	1.4	A1G1S1[6]
15	6.80	1.8	A1G1S1[3]
16	7.07	1.0	[c] A2G2
17	7.16	5.8	A2G2
18	7.36	2.3	A2G1S1[6]
19	7.49	2.1	A2G1S1[3]
20	7.70	1.6	A2G2S1[6]
21	7.88	27.3	A2G2S1[3]
23	8.25	3.3	[b] A2G2S2
24	8.40	2.1	[b] A2G2S2
25	8.56	43.3	A2G2S2
26	8.91	1.6	[b] A2G2FS2
27	9.26	0.4	FCA2G2S2

[a] *The secondary structure that elutes at this GU is A1G1S1[6] (42% of peak area as shown by WAX-HPLC).*
[b] *These structures are likely to have sialic acid residues other than Neu5Ac which is most commonly observed.*
[c] *This structure digests similarly to A2G2 (at peak 17). It could be a bisected A2G2 structure, however a further digest with Sph is required to confirm this.*

The final structures assigned to each peak in the total *N*-linked glycan pool are summarised in Figure 4.16 (page 88). Three major structures were identified which collectively

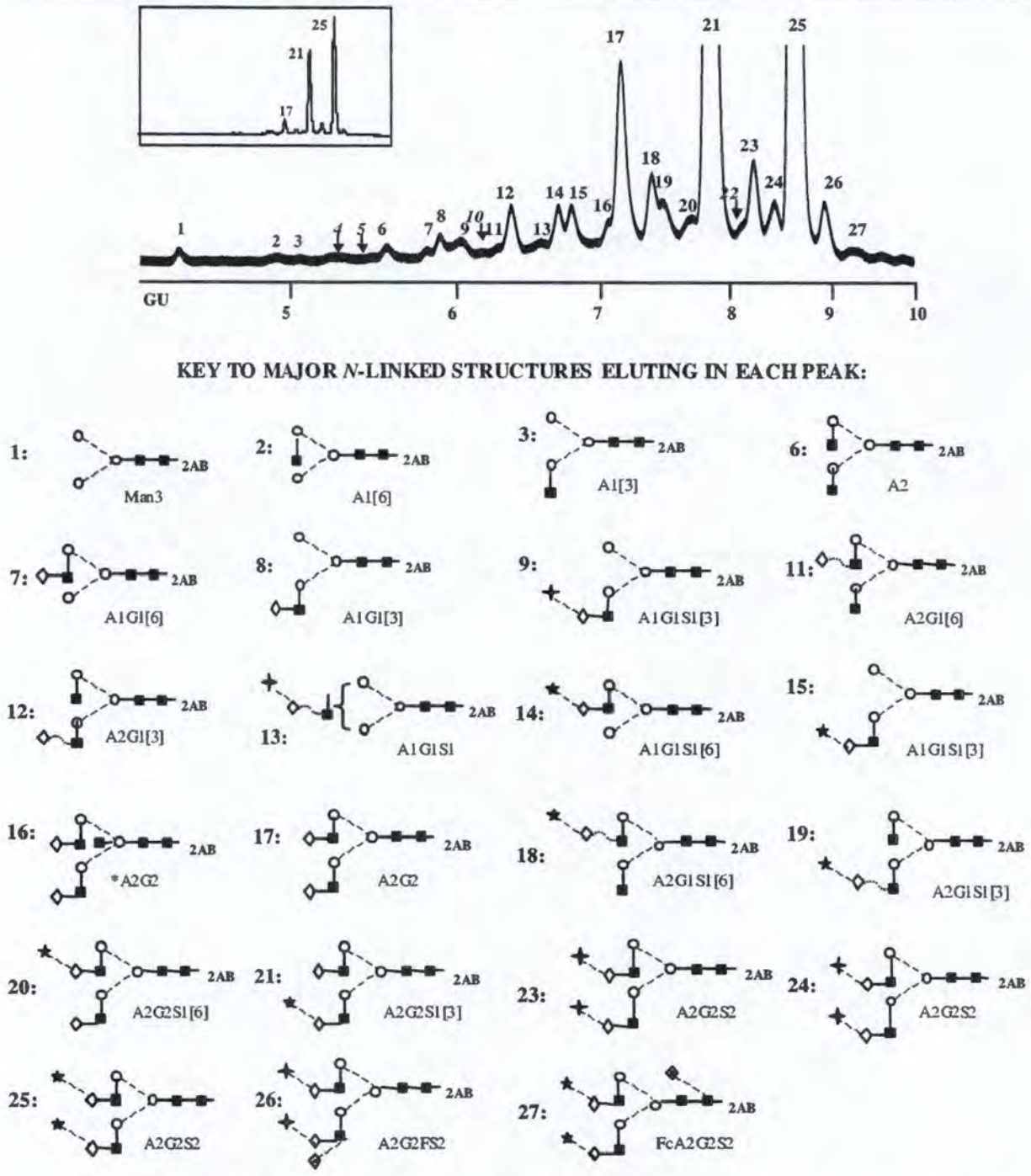

Figure 4.16: NP HPLC profile of an undigested UPTF1 *N*-glycan pool from white control subject WC6. Italicised numbers on the HPLC profile indicate structures observed in glycan pools other than WC6 (these were not identified). The four-pointed stars used in structures 9, 13, 23 and 24 indicate sialic acid residues other than Neu5Ac which is most commonly observed. *This structure has not been confirmed since no exoglycosidase was available to remove a bisecting GlcNAc residue.

accounted for 76 % of the *N*-linked glycan structures: A2G2 (6 %), A2G2S1[3] (27 %) and A2G2S2 (43 %). These structures as well as the remaining *N*-glycans are listed together with their GU values and percentage of the glycan pool in Table 4.9 (page 87). Approximately 95 % of the structures were sialylated, 5 % were galactosylated and 3 % were fucosylated (Table 4.10). All of the structures were complex type oligosaccharides; 93 % of these were biantennary and 95 % were charged.

Table 4.10: Percentage composition of *N*-linked glycans on UPTF1 from white control subject WC6

PERCENTAGE COMPOSITION:						
Charge of structures:		**Antennae:**		**Major structures:**		
Charged	***Uncharged***	***Monoantennary***	***Biantennary***	***Sialylated***	***Galactosylated***	***Fucosylated***
94.5	5.5	6.9	92.9	94.5	5.3	2.6

Owing to the high proportion of sialylated structures, further analysis of all of the *N*-linked glycan samples was carried out with respect to this monosaccharide. The percentage of mono- and disialylated structures for each of the control and stone-forming subjects' *N*-glycan pools is summarised in Table 4.11

Table 4.11: Percentage of mono- and disialylated N-linked glycans on UPTF1 from white and black control subjects and white stone-formers

Sialylation	**WC1**	**WC2**	**WC3**	**WC4**	**WC5**	**WC6**	**WC7**	**WC8**	**WC Ave**
Mono:	44.0	34.2	29.4	48.9	47.3	40.2	44.7	33.0	**40.2**
Di:	45.2	59.6	66.9	43.7	42.5	54.3	44.1	62.1	**52.3**
Total:	89.2	93.8	96.3	92.6	89.7	94.5	88.7	95.1	**92.5 ± 2.0**
	BC1	**BC2**	**BC3**	**BC4**	**BC5**	**BC6**	**BC7**		**BC Ave**
Mono:	15.0	11.8	11.2	9.0	15.8	7.5	20.4		**15.0**
Di:	78.7	82.9	83.4	87.6	77.8	74.7	63.7		**78.4**
Total:	93.7	94.7	94.5	96.6	93.6	82.2	87.7		**93.4 ± 2.0**
	WSF1	**WSF2**	**WSF3**	**WSF4**	**WSF5**	**WSF6**			**WSFAve**
Mono:	15.3	20.2	16.9	18.6	16.8	16.5			**17.3**
Di:	77.2	63.8	74.6	70.8	73.6	72.7			**72.5**
Total:	92.5	83.9	91.4	89.5	90.3	89.2			**89.5 ± 2.0**
	BSF								**BSF**
Mono:	15.5								**15.5**
Di:	76.9								**76.9**
Total:	92.4								**92.4 ± 2.0**

Total sialylation: WC vs. BC p=0.32, WC vs. WSF p=0.08
Mono- and disialylation: WC vs. BC p<0.01, WC vs. WSF p<0.01

The total percentage of sialylated structures was not statistically different for the four groups, however the relative proportions of mono- and disialylated structures were of interest. The latter constituted 52 % of the white control subjects' *N*-glycans compared with 78 % amongst black control subjects. The white stone-formers' glycans contained 72 % disialylated structures. Both the black control and white stone-forming subjects had significantly higher proportions of disialylated structures than the white controls. No statistical comparison could be made with the black stone-former due to the small sample size, however the percentage of disialylated structures (77 %) was also higher than the white control subjects.

O-linked glycans

4.3.8.6 NP-HPLC of glycan pools and exoglycosidase digestions

Figure 4.17 shows NP-HPLC profiles from the undigested WSF glycan pool followed by a series of exoglycosidase digestions. The peak areas are shown in Table 4.12 (page 91). Several structures could be readily identified by comparison with the previously characterised fetuin standard as well a database of *O*-linked structures (Royle *et al.* 2002) and thus the exoglycosidase digestions (as well as WAX-HPLC) were used to confirm these assignments.

The structure observed at a GU value of 2.22 in the fetuin and WSFpool sample (5.5 %) is the product of a base catalysed β-elimination reaction referred to as peeling. This occurs during hydrazinolysis (depending on the conditions used) and leads to the elimination of terminal (core) GalNAc residues on susceptible oligosaccharides (Merry *et al.* 2002).

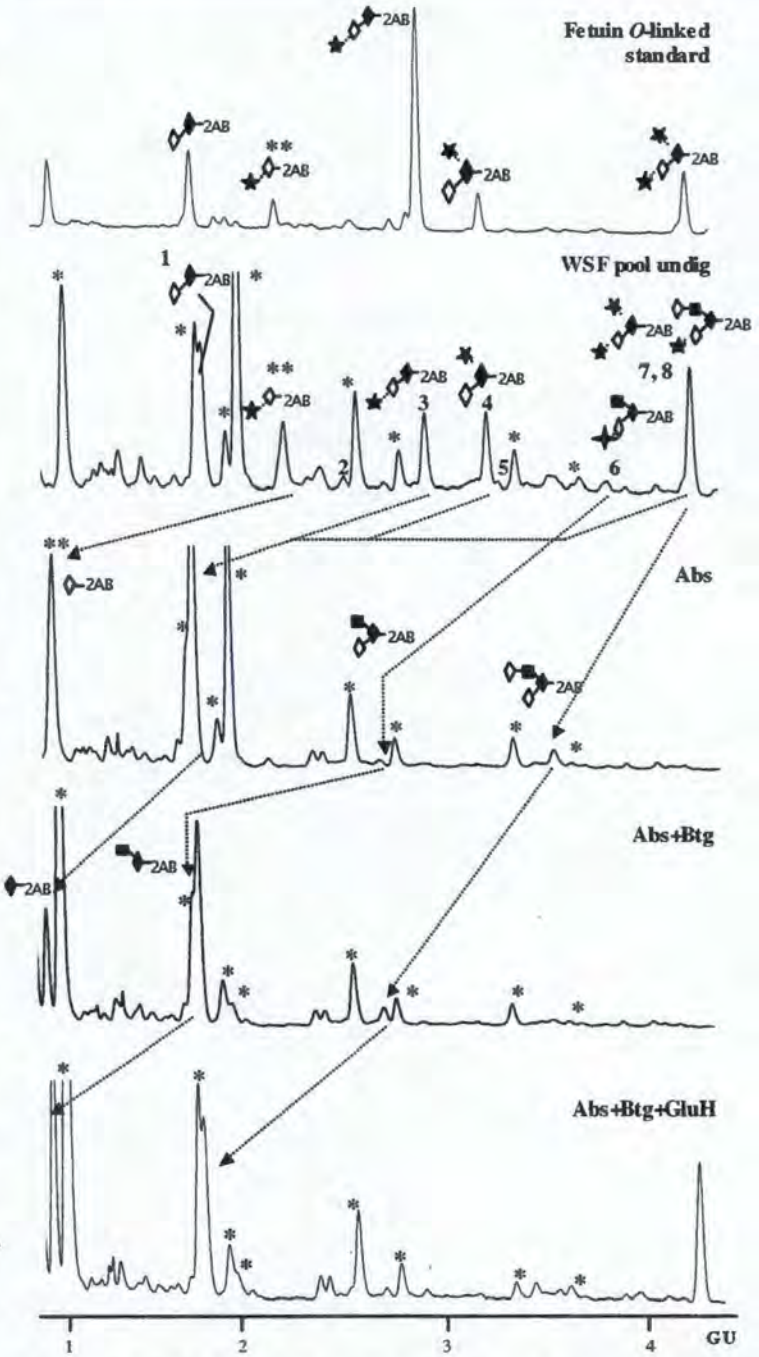

Figure 4.17: NP-HPLC profiles of *O*-linked glycans on UPTF1 pooled from 3 white stone-formers following arrays of exoglycosidase digestions. An *O*-linked fetuin standard is included above for comparison. *Contaminant peaks. **Peeled product. The peak at GU 4.40 after addition of GluH is an *N*-linked structure, some of which are released during hydrazinolysis.

Table 4.12: NP-HPLC analysis of *O*-linked glycans on UPTF1 pooled from 3 white stone-formers

PEAK ID	STRUCTURE	GU	% AREA:			
			Undig	Exoglycosidase added		
				Abs	*Abs Btg*	*Abs Btg GluH*
		0.92			7.9	14.3
		1.00		7.9	22.0	22.6
	Contaminant		12.0	12.0	12.0	12.0
	ni	1.21				
	ni	1.35	2.9	2.4	2.7	2.9
	ni	1.48	2.8	3.2	3.5	3.0
	ni	1.73	1.3	2.3	1.7	1.2
		1.78			1.2	3.1
	Contaminant		5.5	5.5	5.5	5.5
1	 "Core 1"	1.81	8.7	22.9	17.6	11.8
	Contaminant	1.94	3.1	3.9	4.9	4.2
	Contaminant	1.99	18.4	19.5	2.5	1.9
	Incomplete digestion	2.18		2.4		
	[a] 	2.22	5.5			
	ni	2.39	2.1	1.8	1.6	1.6
	ni	2.44	3.1	1.6	2.6	1.5
2	[b] Sialylated	2.52	2.0			
	Contaminant	2.58	5.6	5.9	5.8	5.6
		2.72		1.4	2.3	1.1
	Contaminant	2.78	2.8	2.8	3.2	3.0
3		2.91	4.7			
4		3.22	4.5			
5	[c] 	3.29				
	Contaminant	3.37	1.1	3.0	3.0	1.6
	ni	3.49				1.8
		3.58	2.2	2.6		
	Contaminant	3.68	2.8			1.3
6		3.88	2.1			
7, 8		4.38	6.8			

[a] *This is a degradation product of the hydrazinolysis reaction and is referred to as a "peeled" product.*

[b] *WAX-HPLC showed that this structure is charged and it digests with Abs, suggesting the presence of sialic acid. Further studies are required to identify the structure (e.g. liquid chromatography – mass spectrometry).*

[c] *This structure has a slightly higher GU value than peak 5 and digests with Abs, suggesting that it may be the same structure as peak 5 but with a modified sialic acid (i.e. not Neu5Ac which is the most commonly observed sialic acid residue).*

Contaminant: *These peaks corresponded to those observed in the blank O-linked sample.*

ni: *not identified*

It is not possible to determine the *O*-linked structure from which this peeled product originated and thus is a limitation of the analysis. In addition, structures corresponding to those eluted in the blank sample's NP-HPLC profile were observed in the undigested glycan pool. These are unavoidable byproducts of the sample preparation procedure and have been indicated by asterisks on the HPLC profiles to prevent their confusion with genuine *O*-linked structures.

The NP-HPLC profiles of undigested *O*-glycan pools from the control subjects appeared similar to the WSF sample (Figure 4.18). However, closer inspection showed that the core 1 structure (Gal-GalNAc, peak 1) was absent from the control subjects and there were larger amounts of the structures from peaks 2 and 5 (P2 and P5) (in fact they were not initially identified in the WSF sample due to the small amount in the undigested pool).

Since the *O*-glycan pools from white and black control subjects contained the same structures, only the former was used for exoglycosidase digestions. In an attempt to identify the additional structures (P2 and P5), WC pool was digested with Abs followed by Btg. Both structures digested with the sialidase and are therefore sialylated *O*-glycans. Structure P5 digested to core 1 with Abs, which was further digested to the GalNAc monosaccharide with Btg. The digestion pattern is therefore the same as that of structure 4 and the GU value is only slightly higher (GU 3.29 versus 3.22). It is therefore likely that this *O*-glycan has the same basic structure but with a modified sialic acid. Previous studies of *N*-glycans have shown that this monosaccharide is the most likely to show variation in GU values and thus the same may be true of sialylated *O*-glycans (Guile *et al.* 1996). Further characterisation using liquid chromatography-mass spectrometry is

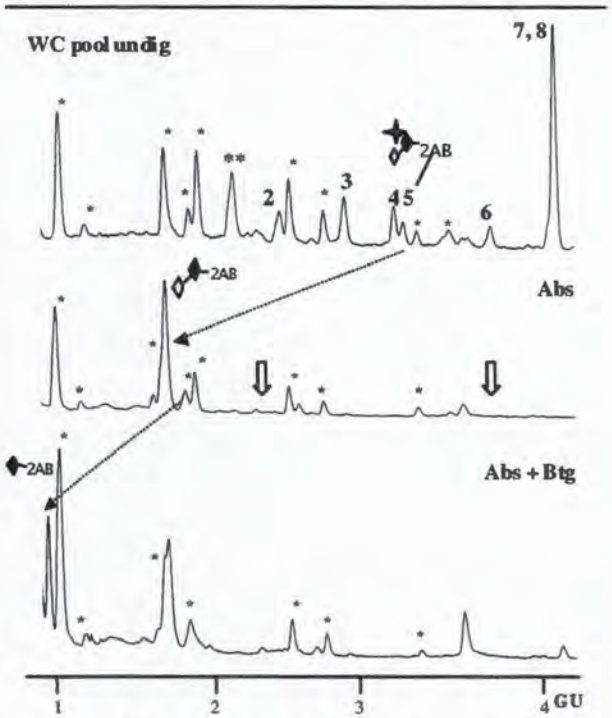

Figure 4.18: NP-HPLC profiles of *O*-linked glycans on UPTF1 pooled from 3 white control subjects before and after exoglycosidase digestions. The numbers correspond to the same structures observed in WSF pool. Structure 2 has not been identified but clearly digests with Abs. Peak 5 probably corresponds to a core 1 structure with a modified sialic acid (*i.e.* not Neu5Ac). The open arrows (Abs profile) the GU value at which peaks 2 and 5 appeared in the undigested sample. *Contaminant peaks. **Peeled product.

required to verify the proposed structure. Structure P2 was characterised further in the present study and also does not appear in the existing *O*-glycan database. Further studies in which the peak is collected during NP-HPLC and analysed may aid identification of this structure.

4.3.8.7 Weak anion exchange HPLC

WAX-HPLC was used to separate the WSF and WC *O*-linked glycan pools by charge density, both before and after digestion with Abs (Figure 4.19). These HPLC profiles are presented alongside a fetuin standard which has been previously characterised (Royle *et al.* 2002). Three structures observed in both glycan pools correlated with peaks in the fetuin standard and thus confirmed the assignment of the sialylated core 1 structures 3, 4 and 8. A peak at 8 min in both samples as well as two further peaks in WC (10, 14 min) could not be identified, however digestion with Abs confirms that they are sialylated structures. The presence of a small amount of glycans after Abs digestion in both WSF and WC samples suggested that charged structures other than the sialylated ones may be present. Two structures (eluted at 12.5 and 16min) in WC were resistant to the sialidase (shown by solid arrows in Figure 4.19) and one of these (12.5 min) also remained after Abs digestion in the WSF sample. Incomplete digestion by the sialidase seemed unlikely here (as

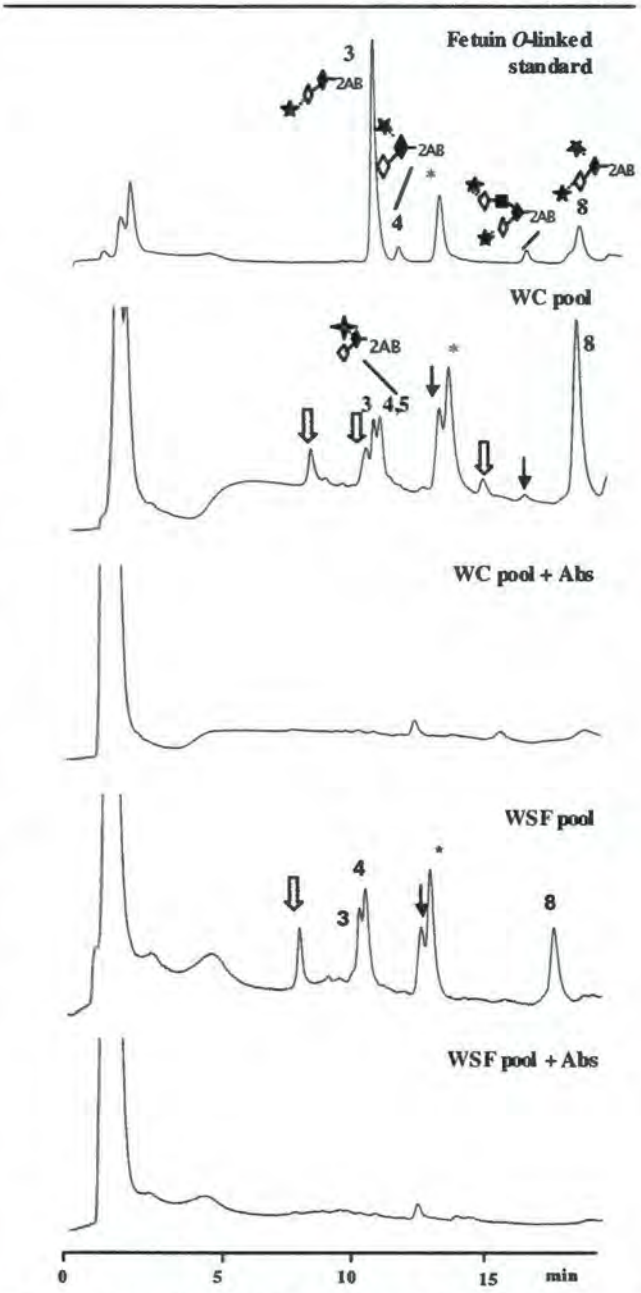

Figure 4.19: WAX-HPLC profiles of *O*-linked glycans on UPTF1 pooled from white control (WC) subjects and white stone-formers (WSF) before and after Abs digestion. An *O*-linked fetuin standard is included for comparison. Solid arrows indicate structures which did not digest with Abs and open arrows indicate structures which could not be identified.

proposed for the WC6 *N*-linked glycans) as less material was present before digestion. Thus these peaks may represent previously unreported *O*-linked glycan structures.

4.3.8.8 Summary of O-linked glycans

The final structures assigned to each peak in the total *O*-linked glycan pools are summarised in Figure 4.20. These structures are listed together with their GU values and the percentage of the total glycan pool in Table 4.13. All of the fully characterised *O*-links in the two control groups' samples were core 1 structures and all of these were sialylated. Of these structures, two had a GlcNAc residue β1-6-linked to the GalNAc core. In addition, the white stone-formers' sample also had a large proportion of the core 1 structure (28 %) and thus

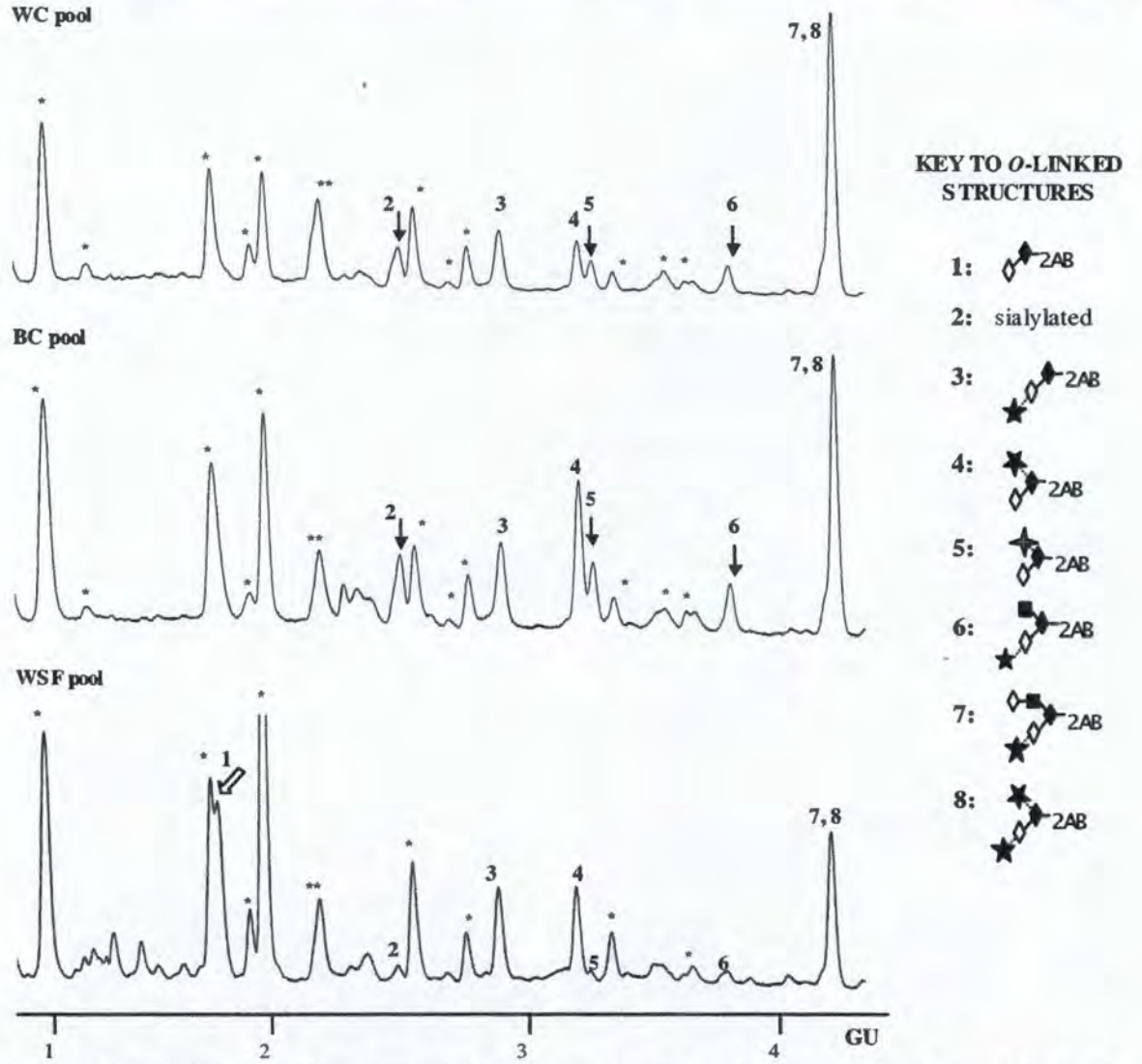

Figure 4.20: NP-HPLC profiles of *O*-linked glycans on UPTF1 pooled from white (WC) and black (BC) control subjects and white stone-formers (WSF). The solid arrows indicate structures present at significantly higher higher proportions in the control samples. The open arrow indicates a structure only present in the stone-formers' sample. Refer to paragraph 4.3.8.6 for a discussion on the structures 2 and 5. *Contaminant peaks. **Peeled product.

had a lower percentage of sialylation (72 %) than the control groups' *O*-glycans.

Table 4.13: NP-HPLC analysis of *O*-linked glycans on UPTF1 pooled from white control (WC), black control (BC) and white stone-formers (WSF)

Peak ID	GU	% AREA: [a]			Structure
		WC pool	BC pool	WSF pool	
1	1.81			28.3	[b] 
2	2.52	11.8	12.2	9.2	[c] Sialylated
3	2.91	16.4	15.3	15.2	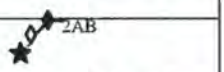
4	3.22	10.1	18.9	14.7	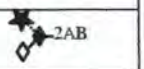
5	3.29	7.0	10.0	3.5	[d] 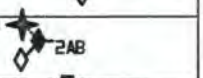
6	3.88	7.3	8.2	6.9	
7	4.38	47.3	35.4	22.1	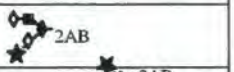
8					

[a] *Contaminant and peeled product peaks were excluded for these calculations.*
[b] *It is likely that a small amount of this structure was present in the control subjects' samples but was hidden by the contaminant peak at GU 1.78.*
[c] *WAX-HPLC showed that this structure is charged and it digests with Abs, suggesting the presence of sialic acid. Further studies are required to identify the structure (e.g. liquid chromatography – mass spectrometry).*
[d] *This structure has a slightly higher GU value than peak 5 and digests with Abs, suggesting that it may be the same structure but with a modified sialic acid (i.e. not Neu5Ac which is the most common sialic cid).*

Molecular modeling

4.3.8.9 Molecular model of UPTF1

The molecular model of UPTF1 (Figure 4.21) was generated using the calcium-bound bovine PTF1 crystal structure along with predicted *N*- and *O*-glycan sites. Figure 4.21.1 is a side view of the model and indicates the domain-like structure of the protein. Seven calcium atoms are bound to Gla residues in the Gla domain and all occupied glycan sites were located on the kringle domain. Although the site specificity of the glycans was not determined, the sizes of the major *N*-glycans were similar and the *O*-glycans were all core 1 structures, thus the conclusions drawn would not be significantly different. Both predicted *N*-glycan sites were occupied and an A2G2S2 structure was attached to residues 78 and 100. Two of the five possible *O*-glycan sites are shown occupied, namely at residues 121 and 122, and a mono-sialylated core 1 structure is attached to these sites in the model. *O*-glycans were also predicted at residues 102, 120 and 149, but these were not reasonable due to steric interactions with other glycans and the protein itself (SWISSPROT numbering, P00734). An

end-on view down the Gla domain (Figure 4.21.2) illustrates the significantly increased diameter of the glycoprotein (63 Å) compared with its unglycosylated form (36 Å). The distances between adjacent glycan chains are shown, namely 40 and 43 Å (O-N) and 60 Å (N-N).

Figure 4.21: Molecular model of UPTF1 showing *N*- and *O*-linked glycans

4.21.1: Side-on view

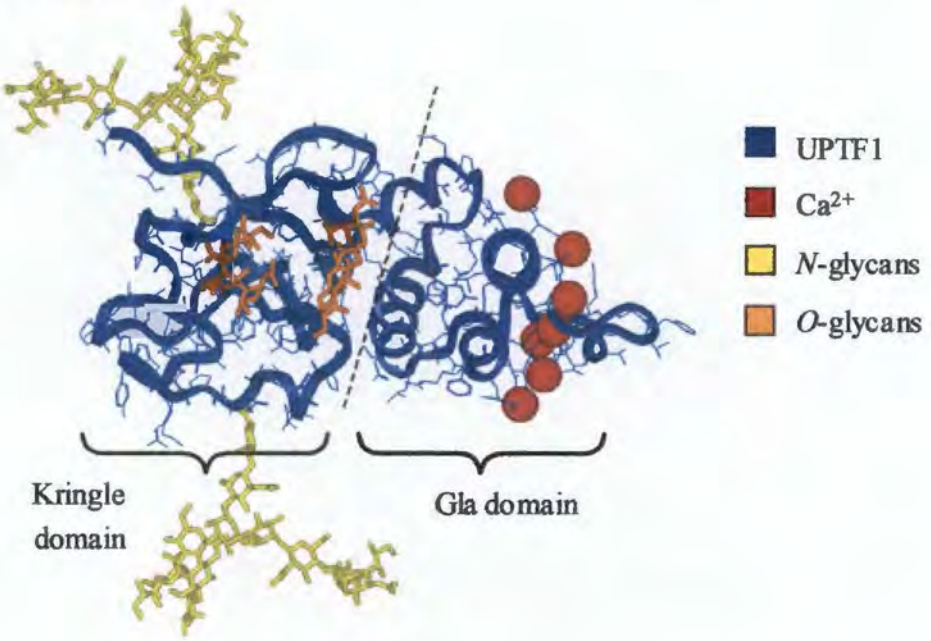

4.21.2: End-on view down the Gla domain

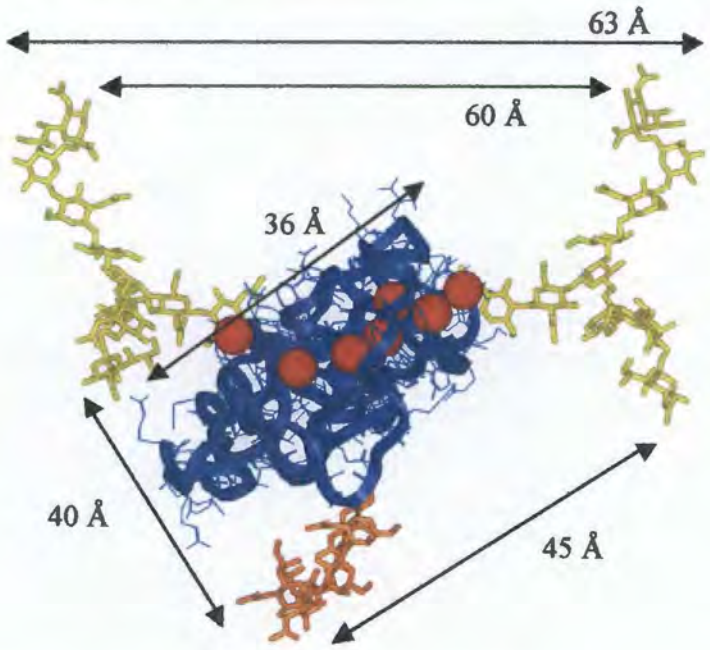

4.4 DISCUSSION

4.4.1 Primary structure

A method for the purification of UPTF1 to homogeneity was established using column chromatography and RP-HPLC in accordance with the protocol described by Ryall *et al.* (1995). Primary structural data obtained by MALDI-TOF MS, N-terminal protein sequencing and amino acid composition analysis were consistent with the reported sequence of human PTF1. These did not reveal differences between white and black subjects.

Since the Gla domain of UPTF1, by virtue of its Gla acid residues and their affinity for calcium ions, is reported to determine the protein's inhibitory activity (Grover and Ryall 1999), the number of Gla residues in WF1 and BF1 was compared. Gla is formed when glutamic acid residues acquire an additional γ-carboxyl group during post-translational modification. It is noted that WF1 contained ten Gla residues as previously reported for UPTF1 (Stapleton and Ryall 1995), whereas BF1 contained a further three such residues. This suggests that additional glutamic acids were modified on BF1. The greater number of Gla residues measured in the black population's UPTF1 may indicate a potentially greater inhibitory capacity. This would be consistent with a previous study in which nephrocalcin derived from stone-formers contained none of the Gla residues reported on normal nephrocalcin which inhibited crystallisation (Nakagawa *et al.* 1987).

2D SDS-PAGE indicated that both WF1 and BF1 have three charged variants of UPTF1 with varying degrees of γ-carboxylation, which exist at low pI values. A previous study of urinary CaOx crystals immunoblotted for PT fragments reported five charged variants in the pattern of a doublet and a triplet (Buccholz *et al.* 1999). The triplet pattern and pI were similar to the present study. Another investigator reported an approximate pI value of 4 for UPTF1 without any reference to isoforms (Stapleton *et al.* 1996). It is perhaps surprising that the observed differences in Gla from WF1 and BF1 were not reflected on 2D SDS-PAGE. It is suggested that other unknown effects may have masked these differences.

While primary structural data on WF1 and BF1 were similar, the difference in the number of Gla residues may be indicative of an enhanced inhibitory potential of BF1 which could partly account for the black population's remarkably low rate of stone formation. However, since the oligosaccharides on UPTF1 account for almost a third of its mass, and the importance of glycosylation in understanding the role of glycoproteins and their possible structure-function relationships has been shown (Rudd and Dwek 1997), a further study of the glycans on UPTF1 was undertaken.

4.4.2 Post-translational modifications

A comprehensive analysis of the *N*-linked glycans on UPTF1 of white and black subjects from both healthy and stone-forming groups was conducted. The same *N*-linked structures were observed in all four groups; only the proportions varied. The majority of the glycans (93 %) were the complex biantennary type with a high proportion of sialylation (95 %), all of which were α2-6 linked to galactose residues. Most galactose residues had β1–4 linkages, and core and outer arm fucosylation was observed. The two major structures sequenced were A2G2S1 (27 %) and A2G2S2 (43 %). Exoglycosidase digestions and WAX-HPLC both suggested that charged groups other than sialic acid might be present, although these appeared to constitute a small percentage (< 5 %) of the total glycan pool. Sulphated glycans might account for this observation since they have been reported on other urinary proteins (Hard *et al.* 1992; van Rooijen *et al.* 1998; Wakabayashi *et al.* 1999).

Two of the sialylated structures were assigned to multiple peaks, namely A1G1S1 (four peaks) and A2G2S2 (three peaks). Since differences in linkage could not account for the observations, it is possible that some of these structures contained modified sialic acid residues, *i.e.* a modification of the most commonly observed Neu5Ac. Considerable diversity exists amongst the sialic acid family and modifications can affect the hydrophilicity (and therefore the GU value) of the structures (Varki 1999). Nelsestuen reported the presence of both N-glycolylneuraminic acid and Neu5Ac on bovine PT (Nelsestuen and Suttie 1972), whereas Mizuochi detected only Neu5Ac structures (Mizuochi *et al.* 1979). However, there is evidence from the present study to suggest that such diversity may be present on UPTF1. Fraction collection of the relevant peaks followed by further characterisation (*e.g.* liquid chromatography-mass spectrometry) could validate this proposal.

Identification of sialylated A2G2 structures is consistent with a previous study of bovine PT which demonstrated extensive sialylation with sialic acids on both Gal and GlcNAc residues (Mizuochi *et al.* 1979). However, whereas all sialic acid residues in the present study were α2-6 linked to β1-4 linked galactose, Mizuochi reported α2-6 linked sialic acids with β1-4 linked galactose and α2-3 linked sialic acids with β1-3 linked galactose.

WF1 and BF1 obtained from pooled urines (of control subjects) were also characterised. These glycan pools were similar to those obtained from the individuals, suggesting that pooling is an appropriate strategy when larger amounts of protein (and therefore glycans) are required.

The analysis of *O*-linked glycans on UPTF1 revealed the presence of sialylated core 1 structures in both control groups as well as the white stone-formers. In addition, a high proportion of the core 1 structure was observed in the white stone-formers' glycan pool. The latter glycan pool therefore contained a considerably lower percentage of sialylated *O*-glycans. No previous studies have reported the presence of, or characterised, the *O*-glycans on UPTF1. Similar to the *N*-glycan results, WAX-HPLC indicated that charged groups other than sialic acids might be present; sulphated *O*-glycans are likely candidates for further testing. Additional structures were observed by WAX-HPLC which could not be identified due to the infancy of this area of glycobiology (a database of *O*-glycans was only recently published by Royle *et al.* 2002), the complexity of *O*-glycan structures due to the existence of at least eight core structures compared with one for *N*-glycans (Royle *et al.* 2002), and the lack of appropriate *O*-glycan standards.

The varying degrees of sialylation amongst the groups investigated are noteworthy. The total percentage of sialylated *N*-glycans were similar, whereas the white stone-formers had a considerably lower proportion of *O*-glycan sialylation than the two control groups. Comparison of the white and black control subjects showed a significantly higher percentage of disialylated *N*-glycans in the latter. Since these two groups had the same percentage of *O*-glycan sialylation, overall the black control group's glycans present a greater number of sialic acid residues than the white controls. It is perhaps surprising that this apparent difference in sialylation (and thus negative charge) was not observed by 2D SDS-PAGE. It is possible that the differences in sialylation were insufficient to influence the overall charge of UPTF1, or that other factors (which tended to result in a *lower* negative charge) may have opposed these effects.

Molecular modeling located the highly sialylated *N*- and *O*-glycans on the kringle domain of UPTF1. This was notable since it is the Gla domain that binds calcium ions and is responsible for the protein's inhibitory activity (Grover and Ryall 1999). It appears at first that the distance of the glycan sites to the calcium binding ones prevents the glycans' interruption of this process. However, intermolecular interactions between glycans and Gla residues/ calcium ions are possible. It is thus feasible that the glycans on UPTF1 affect its inhibitory activity. Previous studies of two urinary proteins have demonstrated a relationship between post-translational medications and protein activity. In these studies, THM from stone-formers' urine, which is a poor inhibitor of crystallisation, was shown to be less highly glycosylated than THM from normals (Knorle *et al.* 1994), while

dephosphorylation of osteopontin reduces its capacity to inhibit CaOx crystallisation (Worcester 1996).

In addition to possibly influencing UPTF1's inhibitory activity, the glycans, and in particular sialic acids (and other charged groups such as sulphates), may play a role in mediating crystal interactions with renal epithelial cells. Several studies have reported the binding of COM (Riese *et al.* 1988, Lieske *et al.* 1995, Verkoelen *et al.* 1995) and COD (Lieske *et al.* 1996) crystals to renal cell surfaces. Crystal adherence to the renal epithelium is now widely regarded as a possible mechanism of stone formation, in addition to blockage of the nephron caused by crystal aggregation (Lieske *et al.* 1999). The subsequent internalisation and dissolution of these attached crystals within lysosomal bodies may also represent a possible protective mechanism (Lieske *et al.* 1999; refer to chapter 8).

It appears that the renal cell surface presents as a negative charge (Lieske *et al.* 1996) by virtue of anionic surface molecules (Asselman and Verkoelen 2002), whereas CaOx crystals present a positively charged surface. Thus interruption of the interaction between these two oppositely charged sites is likely to occur by acting on either the cell surface and inducing a positive charge, or the crystal surface and inducing a negative charge. Either of these mechanisms would reduce crystal adhesion to the renal cell surface by way of repulsion (Lieske *et al.* 1999). A recent study in which the binding of exogenous COM crystals to cells was measured in the presence of whole urine, demonstrated that PTF1+2 (which contains UPTF1) reduces crystal adhesion by coating the surface of crystals (Kumar *et al.* 2003). It is possible that Kumar's observation was directed in part by the presence of highly sialylated glycans on UPTF1.

The negative charge on the renal cell surface is largely due to the presence of terminal sialic acids (Asselman and Verkoelen 2002), and thus several studies have focused on this monosaccharide. Sialic acid-containing cell surface glycoproteins appear to be critical determinants of crystal binding since pretreatment of cells with neuraminidase greatly reduce COM crystal binding (Lieske *et al.* 1999). Sialic acids also direct the face selective nucleation of COD crystals onto renal epithelial cell surfaces via the {001} face in favour of the {100} face in their absence (Lieske *et al.* 2001). The linkage of sialic acid also appears to be important since α2–3 linked residues on the surface of a renal cancer cell line have been shown to provide protection from COM crystal binding whereas α2–6 linked residues did not (Kramer *et al.* 2003). In another study of human collecting duct cells from six CaOx stone-formers, α2–6 linked sialic acids were more highly expressed (Hofbauer *et al.* 1998). These authors postulated that the α2–6 linkage favours crystal attachment to the

cell surface. The fact that UPTF1 contained exclusively α2–6 linked sialic acids suggests that it may mediate stone formation by attachment to the epithelial cell surface.

Thus it seems possible, and indeed highly probable, that sialic acids have an important and possibly directive role to play in the attachment of CaOx crystals to renal cell surfaces, and the possible disruption of this process. However, at present, all but one recent crystal-cell interaction study (Kumar *et al.* 2003) have used inorganic crystals, and thus the influence of urinary proteins associated with these crystals has not been rigorously investigated. Moreover, no studies have investigated protein-associated glycans but have instead focused on the role of cell surface glycans. The elucidation of the impact of specific glycans attached to the intracrystalline protein UPTF1 on crystal attachment is therefore an important study that needs to be addressed. However, it seems probable that a greater negative charge on the crystal surface of black control subjects, by virtue of an increased number of UPTF1's sialic acid residues, may provide a greater repulsive force to the negatively charged renal cell surface. This would result in diminished crystal adhesion in the black population, which could explain their relative protection from stone disease.

Further studies should address two areas. Firstly, whether the inhibitory activity of intact UPTF1 is different from the aglyco and asialo forms. And secondly, whether crystals that include the intact protein are more or less likely to attach to renal epithelial cell surfaces than crystals that contain the aglyco or the asialo forms of UPTF1. These studies will help to elucidate the role of UPTF1 and its glycans in the prevention of urolithiasis, as well as the possible protection of black South Africans from stone disease.

4.5 REFERENCES

1. Asselman M and Verkoelen CF. 2002. Crystal-cell interaction in the pathogenesis of kidney stone disease. *Curr Opin Urol* 12:271-276.

2. Atmani F and Khan SR. 2002. Quantification of protein extracted from calcium oxalate and calcium phosphate crystals induced in vitro in the urine of healthy controls and stone-forming patients. *Urol Int* 68:54-59.

3. Bradford MM. 1976. A rapid and sensitive method for the quantitation of microgram quantities of protein utilizing the principle of protein dye-binding. *Anal Biochem* 72:248-254.

4. Brandt WF, Alk H, Chauhan M, and von Holt C. 1984. A simple modification converts the spinning cup protein sequencer into a vapour-phase sequencer. *FEBS Letters* 174:228-232.

5. Buchholz NP, Kim DS, Grover PK, Dawson CJ, and Ryall RL. 1999. The effect of warfarin therapy on the charge properties of urinary crystallization of calcium oxalate in undiluted human urine. *J Bone Miner Res* 14:1003-1012.

6. Grover PK and Ryall RL. 1999. Inhibition of calcium oxalate crystal growth and aggregation by prothrombin and its fragments in vitro. *Eur J Biochem* 263:50-56.

7. Gorg A, Postel W, Domsheidt A, Gunther S. 1988. Two-dimensional electrophoresis with immobilized pH gradients of leaf proteins from barley (Hordeum vulgare): method, reproducibility and genetic aspects. *Electrophoresis* 9:681-692.

8. Guile GR, Rudd PM, Wing DR, Prime SB, and Dwek RA. 1996. A rapid higher-resolution high-performance liquid chromatographic method for separating glycan mixtures and analyzing oligosaccharide profiles. *Anal Biochem* 240:210-226.

9. Hard K, van Zadelhoff G, Moonen P, Kamerling JP, and Vliegenthart JFG. 1992. The Asn-Linked Carbohydrate Chains of Human Tamm-Horsfall Glycoprotein of One Male. Novel Sulphated and Novel N-Acetylgalactosamine-containing *N*-Linked Carbohydrate Chains. *Eur J Biochem* 209:895-915.

10. Harlos K, Boys CWG, Holland SK, Esnouf MP, and Blake CCF. 1987. Structure and order of the protein and carbohydrate domains of prothrombin fragment 1. *FEBS Letters* 224:97-103.

11. Hedgepeth RC, Yang L, Resnick MI, and Marengo SR. 2001. Expression of proteins that inhibit calcium oxalate crystallisation in vitro in the urine of normal and stone-forming individuals. *Am J Kid Diseases* 37:104-112.

12. Hofbauer J, Fang-Kircher S, Steiner G, Weiner H, Susani M, Simak R, Ghoneim MA, and Marberger M. 1998. N-acetylneuraminic acids (nana): a potential key in renal calculogenesis. *Urol Res* 26:49–56.

13. Knorle R, Schnierle P, Koch A, Buccholz NP, Hering F, Seiler H, Ackermann T, and Rutishauer G. 1994. Tamm-Horsfall glycoprotein: role in inhibition and promotion of renal calcium oxalate stone formation studied with Fourier-transform infrared spectroscopy. *Clin Chem* 40:1739-1743.

14. Kramer G, Steiner GE, Prinz-Kashani M, Bursa B, and Marberger M. 2003. Cell-surface matrix proteins and sialic acids in cell-crystal adhesion; the effect of crystal binding on the viability of human CAKI-1 renal epithelial cells. *Br J Urol* 91:554-559.

15. Kumar V, Farell G, and Lieske JC. 2003. Whole urinary proteins coat calcium oxalate monohydrate crystals to greatly reduce their adhesion to renal cells. *J Urol* 170:221–225.

16. Küster B, Wheeler F, Hunter AP, Dwek RA, and Harvey DJ. 1997. Sequencing of N-linked oligosaccharides directly from protein gels: In-gel deglycosylation followed by matrix-assisted laser desorption/ionisation mass spectrometry and normal-phase high-performance liquid chromatography. *Anal Biochem* 250:82–101.

17. Lieske JC, Toback FG, and Deganello S. 2001. Sialic-acid containing glycoproteins on renal cells determine the nucleation of calcium oxalate dihydrate crystals. *Kidney Int* 60:1784-1791.

18. Lieske J, Toback FG, and Deganello S. 1996. Face-selective adhesion of calcium oxalate dihydrate crystals to renal epithelial cells. *Calcif Tiss Int* 58:195-200.

19. Lieske JC, Deganello S, and Toback FG. 1999. Cell-crystal interactions and kidney stone formation. *Nephron* 81:8-17.

20. Lieske JC, Leonard R, and Toback FG. 1995. Adhesion of calcium oxalate monohydrate crystals to renal epothelial cells is inhibited by specific anions. *Am J Physiol* 268:F604-F612.

21. Merry AH, Neville DCA, Royle L, Matthews B, Harvey DJ, Dwek RA, and Rudd PM. 2002. Recovery of intact 2-aminobenzamide labeled O-glycans released from glycoproteins by hydrazinolysis. *Anal Biochem* 304:91-99.

22. Mizuochi T, Yamashita K, Fujikawa K, Kisiel W, and Kobata A. 1979. The carbohydrate of bovine prothrombin. *J Biol Chem* 254:6419-6425.

23. Nakagwa Y, Susan M A, Hall S L, Deganello S, and Coe F L. 1987. Isolation from human calcium oxalate renal stones of nephrocalcin, a glycoprotein inhibitor of calcium oxalate crystal growth. Evidence that nephrocalcin from patients with calcium oxalate nephrolithiasis is deficient in gamma-carboxyglutamic acid. *J Clin Invest.* 79:1782-1787.

24. Nelsestuen GL and Suttie JW. 1972. The carbohydrate of bovine prothrombin. Partial structural determination demonstrating the presence of –galactose residues. *J Biol Chem* 247:6096-6102.

25. Patel T, Bruce J, Merry A, Bigge C, Wormald M, Jaques A, and Parekh R. 1993. Use of hydrazine to release in intact and unreduced form both *N*- and *O*-linked oligosaccharides from glycoproteins. *Biochem* 32:679-693.

26. Price PA. 1983. Analysis for gamma-carboxyglutamic acid. *Meth Enzymol* 91:13-17.

27. Radcliffe CM, Diedrich G, Harvey DJ, Dwek RA, Cresswell P, and Rudd PM. 2002. Identification of specific glycoforms of major histocompatibility complex class I heavy chains suggests that class I peptide loading is an adaptation of the quality control pathway involving calreticulin and ERp57. *J Biol Chem* 277:46415-46423.

28. Riese RJ, Riese JW, Kleinman JG, Wiessner JH, Mandel GS, and Mandel NS. 1988. Specificity in calcium oxalate adherence to papillary epithelial cells in culture. *Am J Physiol* 255:F1025-F1032.

29. Royle L, Mattu TS, Hart E, Langridge JI, Merry AH, Murphy N, Harvey DJ, Dwek RA, and Rudd PM. 2002. An analytical and structural database provides a strategy for sequencing *O*-glycans from microgram quantities of glycoproteins. *Anal Biochem* 304:70-90.

30. Rudd PM and Dwek RA. 1997. Glycosylation: Heterogeneity and the 3D structure of proteins. *Crit Rev Biochem Mol Biol* 32:1-100.

31. Ryall RL, Grover PK, Stapleton AMF, Barrell DK, Tang Y, Moritz RL, and Simpson RJ. 1995. The urinary F1 activation peptide of human prothrombin is a potent inhibitor of calcium oxalate crystallization in undiluted human urine in vitro. *Clin Sci* 89:533-541.

32. Schwager SLU, Chubb AJ, Scholle RR, Brandt WF, Eckerskorn C, Sturrock ED, and Ehlers MRW. 1998. Phorbol ester-induced jutamembrane cleavage of angiotensin-converting enzyme is not inhibited by a stalk containing intrachain disulfides. *Biochem* 37:15449-15456.

33. Stapleton AMF, Dawson CJ, Grover PK, Hohmann A, Comacchio R, Boswara V, Tang Y, and Ryall RL. 1996. Further evidence linking urolithiasis and blood coagulation: Urinary prothrombin fragment 1 is present in stone matrix. *Kid Int* 49:880-888.

34. Stapleton AMF and Ryall RL. 1995. Crystal matrix protein - getting blood out of a stone. *Min Elect Metab* 20:399-409.

35. van Rooijen JJM, Kamerling JP, and Vliegenthart FG. 1998. Sulphated Di-, Tri- and Tetraantennary *N*-Glycans in Human Tamm-Horsfall Glycoprotein. *Eur J Biochem* 256:471-487.

36. Varki A. 1999. Sialic acids. In Essentials of glycobiology. Varki A, Cummings R, Esko J, Freeze H, Hart G, and Marth J, editors. Cold Spring Harbour Laboratory Press, New York. 195-209.

37. Verkoelen CF, Romijn JC, de Bruijn WC, Boeve ER, Cao L, and Schroder FH. 1995. Association of calcium oxalate monohydrate crystals with MDCK cells. *Kidney Int* 48:129-138.

38. Wakabayashi H, Natsuka S, Mega T, Otsuki N, Isaji M, Naotsuka M, Koyama S, Kanamori T, Sakai K, and Hase S. 1999. Novel proteoglycan linkage tatrasaccharides of human urinary soluble thrombomodulin. SO_4-3GlcAβ1-3Galβ1-3(+-Siaα2-6)Galβ1-4Xyl. *J Biol Chem* 274:5436-5442.

39. Walz DA, Hewett-Emmett D and Seegers WH. 1977. Amino acid sequence of human prothrombin fragments 1 and 2. *Proc Natl Acad Sci USA* 74:1969-1972.

40. Worcester EM. 1996. Inhibitors of stone formation. *Sem Nephrol* 16:474-486.

41. Zamze S, Harvey DJ, Chen YJ, Guile GR, Dwek RA, and Wing DR. 1998. Sialylated *N*-glycans in adult rat brain tissue: A widespread distribution of disialylated antennae in complex and hybrid structures. *Eur J Biochem* 258:243-270.

CHAPTER 5: UPTF1 CRYSTALLISATION STUDIES IN INORGANIC SOLUTIONS & URINE

5.1 INTRODUCTION

In an attempt to identify the potential role of urinary proteins in the black population's apparent stone immunity, the CME was isolated from the urine of black and white subjects for *in vitro* activity studies (chapter 3). The results showed that in an inorganic solution, the black group's CME inhibited crystallisation more efficiently than that of the white group. As the major protein incorporated into the CME, UPTF1 from black and white subjects was then fully characterised. Structural differences in the two group's UPTF1 were observed which suggest that their inhibitory activities may be different. Thus a comparative study of the inhibitory activity of UPTF1 from black and white subjects is required.

For the purpose of these activity studies, both inorganic media and urine were utilised. It has been claimed that aqueous solutions, synthetic urine and dilute urine do not realistically reflect the complexity of real urine (Rodgers 1999), and thus the effect of substances in such media are unlikely to reflect their activity with respect to CaOx crystallisation under physiological conditions (Fleisch 1978). However, the use of simpler inorganic media may still provide valuable information for the study of basic crystallisation processes (Ryall in Hess *et al.* 2001). Furthermore, it is possible to study the effect of a single inhibitor in isolation (Tiselius in Hess *et al.* 2001), which is not easily achieved in urine. The complexity of urine is such that innumerable interactions may interfere with the activity of a single molecule. Despite the advantages of using inorganic test solutions, the use of urine (whole or minimally diluted) is nevertheless important since it more closely approximates the solution in which kidney stones form (Ryall in Hess *et al.* 2001). Extrapolation of results to physiological conditions and thus the potential to prevent actual stone formation is more reasonable, albeit not entirely appropriate.

Thus for the purpose of this thesis, the inhibitory activities of WF1 and BF1 were compared in inorganic solutions as well as in urine in order to assess the possible contribution of UPTF1 to the black population's remarkably low incidence of kidney stones.

5.2 METHODS

5.2.1 Synthetic urine study

5.2.1.1 Synthetic urine treatment

A synthetic urine was prepared according to the method of Burns and Finlayson (1980a; paragraph 2.2.7, page 32). The solution was stored at 4 ^{0}C and was stable for a maximum of 5 days. Aliquots were filtered through a 0.22 µm filter paper immediately before use. The CaOx MSL was determined in duplicate according to the method of Ryall and co-workers (Ryall *et al.* 1985; paragraph 2.2.7 on page 32).

5.2.1.2 Effect of UPTF1 on particle size

Since it has previously been shown that macromolecules and urinary proteins including UPTF1 do not alter the MSL (Ryall *et al.* 1991, Ryall *et al.* 1995, Doyle *et al.* 1995) and since the amount of UPTF1 was limited, equal NaOx loads (30 mmol/l in excess of the previously determined MSL) were added to the control synthetic urine and protein-dosed samples to induce crystallisation. Aliquots of 10 ml were left untreated or dosed with WF1 or BF1 at final concentrations of 1.25 mg/l (approximate physiological concentration according to Ryall *et al.* 1995). This was followed by incubation at 37 ^{0}C in a shaking water bath (100 rpm) for 120 minutes. The effect of WF1 and BF1 on the particle size distribution was measured at 120 minutes using a Coulter Counter I (140 µm orifice, 2.8 - 90.0 µm particle size range, 64 channels). The following number of measurements was made for each sample: SU, n=10; SU+WF1, n=8; SU+BF1, n=10.

After completion of two of the experiments, aliquots (2 ml) of the control and protein-dosed samples were filtered through a 0.22 µm filter paper. The crystals were examined using a scanning electron microscope as previously described (paragraph 2.2.2.3 on page 28).

5.2.1.3 Effect of UPTF1 on [^{14}C]-oxalate deposition

Aliquots (25 ml) of synthetic urine were left untreated or were dosed with WF1 or BF1 at final concentrations of 1.25 mg/l. Experiments were carried out as described in paragraph 3.2.4.3 (page 51). Two separate experiments were carried out.

5.2.1.4 Statistical analysis

All data were analysed statistically by ANOVA. The results were considered statistically significant if $p \leq 0.05$. Average values and standard errors are reported for all experiments. P-values are not reported for the [^{14}C]-oxalate deposition experiment due to the small sample size.

5.2.2 Ultrafiltered urine study

5.2.2.1 Urine collection and treatment

Independent pooled urines from black and white males, each consisting of equal volumes (300 ml) of five 24-hour urine specimens in accordance with the recommendations of a study for the optimum pooling of samples (Jappie and Rodgers 2000), were prepared. Each pooled urine was filtered (0.75 μm pre-filter, 0.45 μm, 0.22 μm) and divided into two portions. One portion was retained for the MSL determination and the residual volume was ultrafiltered through a 10 kDa membrane (Millipore) in order to remove all macromolecules larger than 10 kDa including UPTF1 and retained for crystallisation studies. The ultrafiltered urine from black and white males is henceforth referred to as BUF and WUF respectively. Urine composition data (mmol/l) and physicochemical parameters were computed for each pooled urine (paragraph 2.2.1. page 26); no relative supersaturation values were computed since these are not appropriate for pooled urines. Urine composition data was analysed statistically by ANOVA and the results considered statistically significant if $p \leq 0.05$. Average values and standard errors are reported.

5.2.2.2 Cross-over experiment

The effects of WF1 and BF1 on CaOx crystallisation in ultrafiltered urine were compared using a cross-over design previously described (Craig *et al.* 1999). In this protocol, depicted in Figure 5.1 (page 108), BUF and WUF were each divided into three equal aliquots. Two aliquots of each ultrafiltrate were dosed with BF1 and WF1 at final concentrations of 1.25 mg/l, while the remaining aliquot was left unaltered and retained as a control sample.

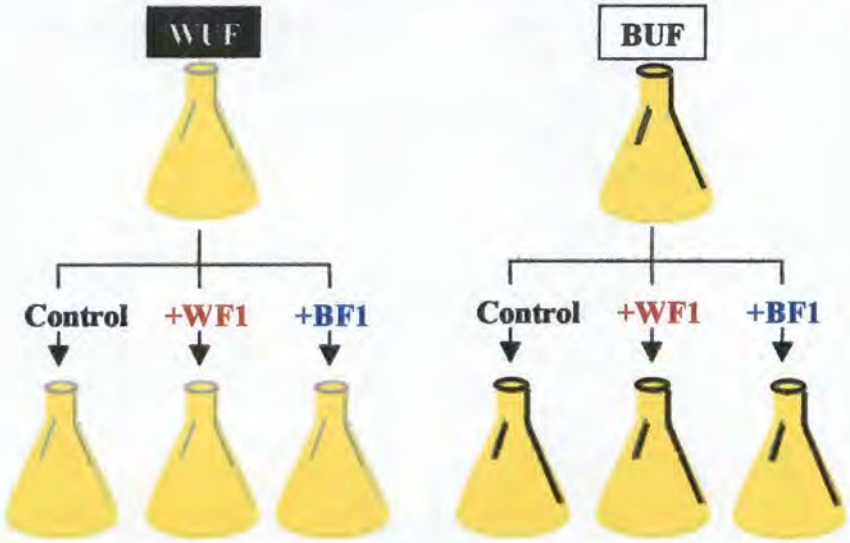

Figure 5.1: Cross-over design employed for UPTF1 crystallisation study. *WUF:* pooled, ultrafiltered urine from white males; *BUF:* pooled, ultrafiltered urine from black males; *control:* untreated ultrafiltered urine; *+WF1:* ultrafiltered urine after addition of WF1 at a final concentration of 1.25 mg/l; *+BF1:* ultrafiltered urine after addition of BF1 at a final concentration of 1.25 mg/l

5.2.2.3 Effect of UPTF1 on particle number, volume and size

The CaOx MSL of each pooled urine was determined according to the method of Ryall and co-workers (Ryall *et al.* 1985; paragraph 2.2.7, page 32). As previously described (paragraph 5.2.1.2, page 106), equal NaOx loads (30 mmol/l in excess of MSL) were added to the control and protein-dosed ultrafiltrates to induce crystallisation. This was followed by incubation at 37 ^{0}C in a shaking water bath (100 rpm) for 120 minutes. The effect of BF1 and WF1 on the particle number, particle volume and particle size distribution was measured at 120 minutes using a Coulter Counter I (140 µm orifice, 2.8 - 90.0 µm particle size range, 64 channels). The number of independent pooled urines from each population group used for the crystallisation studies are as follows: particle number and volume measurements: n=5; size measurements: n=4.

After completion of two experiments from each population group, aliquots (2 ml) of the control and protein-dosed sample urines were filtered (0.22 µm) and prepared for examination by scanning electron microscopy (paragraph 2.2.2.3, page 28).

5.2.2.4 Effect of UPTF1 on [^{14}C]-oxalate deposition

Aliquots (25 ml) of ultrafiltered urine were left untreated or dosed with WF1 or BF1 at final concentrations of 1.25 mg/l. Experiments were carried out as described elsewhere (paragraph 3.2.4.3, page 51). Three independent pooled urines from each population group were used for this experiment.

5.2.2.5 Statistical analysis

Urine composition data were analysed statistically by ANOVA and the results considered statistically significant if $p \leq 0.05$. Average values and standard errors are reported.

For the particle number, volume and size studies, protein-dosed urines were defined as being the same as their control ultrafiltrates if their difference was less than 5 %. In each of these studies, experiments that differed to the trend displayed by the majority were excluded from the average calculations. Average values and standard errors are reported. No p-values were computed since independent urine samples were used for the replicate experiments.

5.2.3 Sedimentation kinetics

5.2.3.1 Effect of UPTF1 on COM crystal slurries

Sedimentation kinetics of COM crystal slurries were tested in the absence and presence of UPTF1 isolated from the urine of white and black subjects. Crystal slurries were prepared by the addition of 1.0 mg/ml COM crystals to a buffer containing 0.010 mol/l Tris-HCl, 0.270 mol/l NaCl (pH 7.2) (Hess *et al.* 1989). Crystal slurries were equilibrated overnight (at least 16 hours) at 37 ^{0}C with stirring (1100 rpm) to ensure that equilibration saturation had been achieved after which UPTF1 was added at a final concentration of 1.25 mg/l. The slurries were then treated as described in paragraph 2.2.3.2 (page 29).

5.2.3.2 Effect of UPTF1 on COD crystal slurries

Preparation of calcium oxalate dihydrate crystals

COD crystals were prepared according to Brown *et al.* (1989), with modification to the incubation temperature and pH. These modifications were necessary since under the conditions prescribed by Brown, small percentages of COT (<10 %) were formed in the

present study. Citrate, magnesium and potassium ions were used to stabilise the dihydrate morphology. A solution containing 0.0385 mol/l $Na_3C_6H_5O_7.2H_2O$, 0.0462 mol/l $MgSO_4.7H_2O$ and 0.255 mol/l KCl was prepared in a final volume of 250 ml distilled water (solution 1). A 125 ml solution of 0.0251 mol/l $CaCl_2$ (solution 2) was then added to solution 1 with mixing. The pH of the mixture of solutions 1 and 2 was adjusted to 6.5 and left to equilibrate at 25 ^{0}C in a water bath for 10 minutes (solution 3). A 125 ml solution of 6.40 mmol/l NaOx was added to solution 3 and the mixture was left to equilibrate at 25 ^{0}C in a water bath for 10 minutes. The crystals were then collected from the final mixture by filtration (0.22 μm filters), washed with methanol and dried at 37 ^{0}C for at least 1 hour.

The crystal morphology was identified by XRD analysis (paragraph 2.2.2.1, page 27) and confirmed by TGA (paragraph 2.2.2.2, page 28). A 0.1 mg sample was also retrieved on filter paper (0.22 μm) and prepared for examination using a scanning electron microscope as described in paragraph 2.2.2.3 (page 28).

Measurement of sedimentation rate

The analogous experiment to that described in section 5.2.3.1 (page 109) was carried out, except that COD crystal slurries were used instead of COM crystal slurries.

5.2.3.3 Statistical analysis

The slope of each absorbance versus time plot was determined by linear regression analysis. The R^2 corresponding to the slope is reported for these analyses. The average slopes for the WF1 and BF1-dosed crystal slurries were compared statistically by ANOVA and considered statistically significant if $p \leq 0.05$.

5.2.4 Zeta potentials

5.2.4.1 Effect of UPTF1 on COM crystal slurries

The zeta potential of COM crystal slurries was tested before and after addition of UPTF1 isolated from the urine of white and black subjects. The experiments were carried out as described in paragraph 2.2.4.3 (page 31) except that UPTF1 (at a final concentration of 1.25 mg/l) was added to the COM crystal slurry instead of urine.

5.2.4.2 Effect of UPTF1 on COD crystal slurries

The zeta potential of COD crystal slurries was tested in the absence and presence of UPTF1 isolated from the urine of white and black subjects. The experiments were carried out as described for the COM crystal slurries above.

5.2.4.3 Statistical analysis

The average zeta potential of the WF1 and BF1-dosed crystal slurries were compared by ANOVA. The results were considered statistically significant if $p \leq 0.05$.

5.3 RESULTS

5.3.1 Synthetic urine study

5.3.1.1 Metastable limit

The average CaOx MSL plot of the synthetic urine, shown as particle number versus NaOx concentration, is presented in Figure 5.2. The data from which the plot was obtained is presented in Appendix D (Table D1, page A35). The MSL was determined as being equivalent to 45 mmol/l NaOx, as indicated by the enlarged data point below.

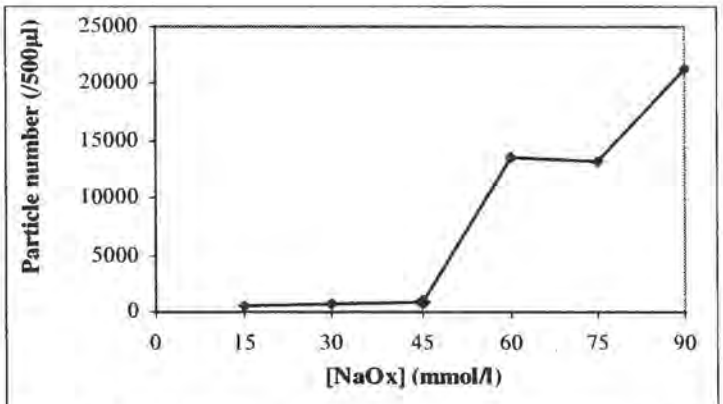

Figure 5.2: Average plot of particle number versus sodium oxalate concentration in synthetic urine

5.3.1.2 Effect of UPTF1 on particle size

Figure 5.3 shows the average particle volume-particle size distributions at 120 minutes after addition of a NaOx load. A decrease in the average particle size was observed after addition of WF1 and BF1 as indicated by a shift in the mode of the protein-dosed distributions to smaller values compared to the synthetic urine. The average particle size values are reflected in Table 5.1. The average size in the undosed synthetic urine was 17.45 µm compared with 12.60 µm and 12.09 µm after addition of WF1 and BF1 respectively. These values correspond to decreases of 27.8 and 30.7 % in particle size, respectively. The decrease in average particle size caused by both WF1 and BF1 was significant ($p < 0.01$) but no difference between WF1 and BF1 was detected ($p > 0.05$). However, a slight shift in the BF1-dosed curve towards smaller particle sizes relative to the WF1-dosed curve was evident. All of the average particle size distributions and corresponding average particle size values are presented in Appendix D, Figures D1.1 – 1.3 (page A41) and Table D2 (page A35), respectively.

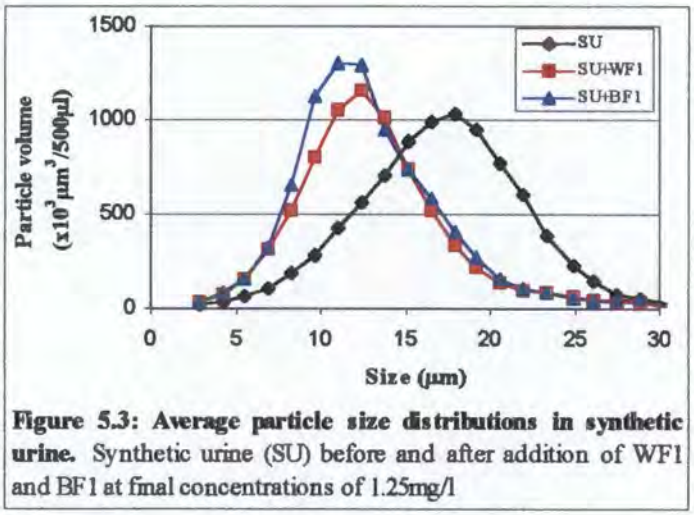

Figure 5.3: Average particle size distributions in synthetic urine. Synthetic urine (SU) before and after addition of WF1 and BF1 at final concentrations of 1.25mg/l

Table 5.1: Particle size of synthetic urine (SU) before and after addition of WF1 and BF1 at final concentrations of 1.25 mg/l

Sample	Size ave. ± SE (µm)	% Decr. wrt SU	p-value wrt SU	n-value
SU	17.45 ± 0.30			10
SU+WF1	12.60 ± 0.30	27.8	< 0.01	8
SU+BF1	12.09 ± 0.30	30.7	< 0.01	10

SU+WF1 vs. SU+BF1: p>0.05

Figure 5.4 shows scanning electron micrographs of CaOx crystals precipitated in the synthetic urine before (Figures 5.4.1 – 5.4.3) and after addition of WF1 (Figures 5.4.4 – 5.4.6) and BF1 (Figures 5.4.7 – 5.4.9). The synthetic urine typically consisted of large crystal aggregates composed of mainly small, oval-shaped COMs (<4 μm in length) (Figures 5.4.1 - 5.4.2) along with some single COM crystals. In addition, several long needle-shaped crystals (>15 μm) were observed (Figure 5.4.3). After addition of UPTF1 from both population groups, typically large bipyramidal COD crystals (10 - 15 μm in diameter) were observed. A few small single, oval-shaped COMs and long, needle-shaped crystals remained after addition of UPTF1 (SU+WF1: Figure 5.4.6; SU+BF1: Figure 5.4.9). The crystals in the protein-dosed urine were notably less highly aggregated and usually consisted of small clusters of COD crystals (SU+WF1: Figures 5.4.4 - 5.4.5; SU+BF1: Figures 5.4.7 - 5.4.8).

Figure 5.4: Scanning electron micrographs of CaOx crystals deposited in synthetic urine. The crystals were precipitated from synthetic urine: mag 3K (Fig 5.4.1), mag 5K (Fig 5.4.2), mag 8K (Fig 5.4.3); synthetic dosed with WF1: mag 8K (Fig 5.4.4), mag 10K (Fig 5.4.5), mag 7K (Fig 5.4.6); and synthetic urine dosed with BF1: mag 2.5K (Fig 5.4.7), mag 6K (Fig 5.4.8), mag 8K (Fig 5.4.9).

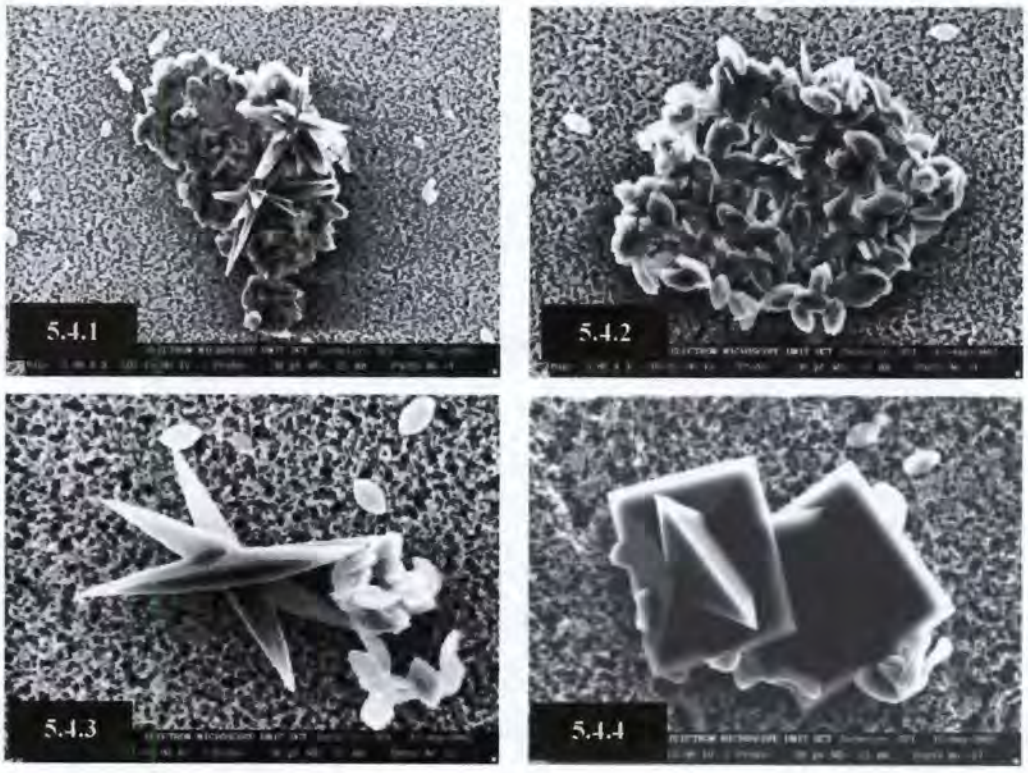

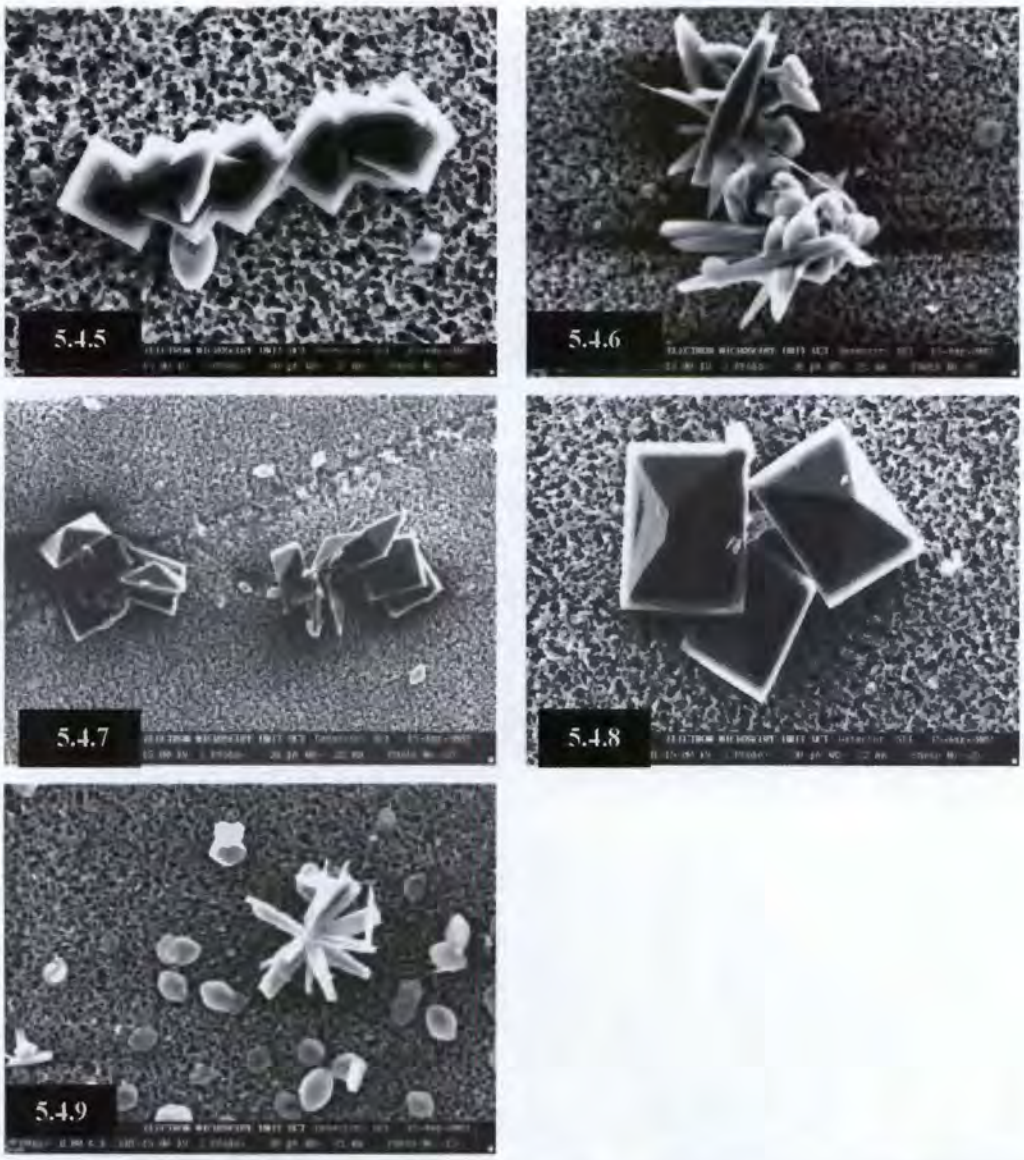

5.3.1.3 Effect of UPTF1 on [^{14}C]-oxalate deposition

Figure 5.5 shows the average increase in the deposition of precipitated [^{14}C]-oxalate during a 120-minute time course after addition of a NaOx load. It is evident that WF1 and BF1 induced a decrease in the amount of precipitated material relative to the synthetic urine control sample. After 120 minutes, the percentage precipitated [^{14}C]-oxalate decreased from 57.6 % in the synthetic urine to 46.9 and 48.4 % in the urines dosed with WF1 and BF1 respectively. These decreases correspond to growth inhibition of 18.7 and 16.0 %, respectively. The initial rate of deposition (until 60 minutes) was less in the synthetic urine dosed with BF1.

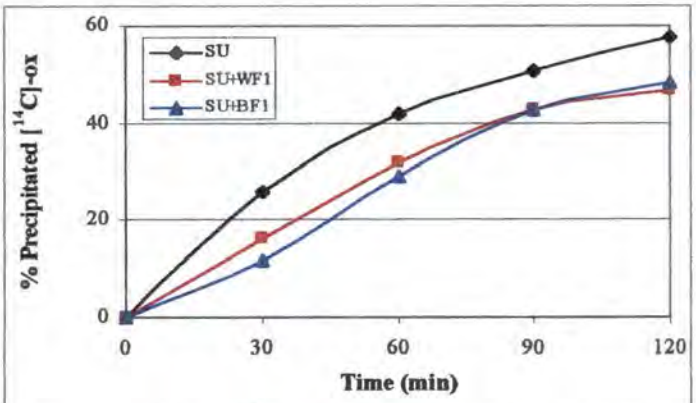

Figure 5..5: Average [^{14}C]-ox deposition rate in synthetic urine. Synthetic urine (SU) before and after addition of WF1 and BF1 at final concentrations of 1.25mg/l

The [^{14}C]-oxalate deposition curves for the two separate experiments, as well as the data from which these plots were obtained, are shown in Appendix D, Figure D2.1 -2.2 (page A41) and Table D3 (page A35), respectively.

5.3.2 Ultrafiltered urine study

5.3.2.1 Urine composition and metastable limit

The average urine composition (mmol/l) and physicochemical parameters of the pooled urines from black and white subjects are presented in Table 5.2.

Table 5.2: Average urine composition (mmol/l) and physicochemical parameters of pooled urines from white and black subjects (n=5)

Variables	White subjects (ave ± SE)	Black subjects (ave ± SE)	p-value
pH	6.30 ± 0.090	6.21 ± 0.090	NS
Volume (ml)	7006 ± 703	6437 ± 703	NS
Metastable limit (mmol/l)	48.0 ± 8.21	81.0 ± 8.21	< 0.05 *
Calcium (mmol/l)	2.26 ± 0.334	1.46 ± 0.334	NS
Chloride (mmol/l)	105 ± 12.6	104 ± 12.6	NS
Citrate (mmol/l)	1.73 ± 0.266	1.51 ± 0.266	NS
Creatinine (mmol/l)	10.6 ± 1.49	11.0 ± 1.49	NS
Magnesium (mmol/l)	2.74 ± 0.392	2.16 ± 0.392	NS
Oxalate (mmol/l)	0.150 ± 0.020	0.112 ± 0.020	NS
Phosphate (mmol/l)	20.3 ± 2.46	16.2 ± 2.46	NS
Potassium (mmol/l)	25.0 ± 4.49	26.3 ± 4.49	NS
Sodium (mmol/l)	142 ± 21.6	146 ± 21.6	NS
Uric acid (mmol/l)	2.27 ± 0.300	2.23 ± 0.300	NS

* *Significant difference between averages*

The results for all ten pooled urines are presented in Appendix D, Tables D4.1 – D4.2 (pages A36 – A37). The data from which the MSL was determined is presented in Appendix D, Table D5.1 – D5.2 (page A38), and the corresponding plots are shown in Appendix D, Figure 3.1 – 3.10 (page A42 – A43). The NaOx concentration corresponding to the MSL is shown by the turning point of the plots. It is noted that the CaOx MSL was significantly higher in the black subjects ($p < 0.05$). This is consistent with a relatively lower risk in this population group.

5.3.2.2 Effect of UPTF1 on particle number and volume

Table 5.3 and Table 5.4 show the particle number and volume data respectively measured at 120 minutes after addition of a NaOx load. For the particle number data (Table 5.3) in the white groups' ultrafiltrates, four of five experiments showed a greater increase in particle number after addition of WF1 than after addition of BF1 and one experiment showed no difference between WF1 and BF1. In the black groups' ultrafiltrates, three of five experiments showed a greater increase in particle number after addition of BF1 than after addition of WF1, one showed no difference between WF1 and BF1 and the final experiment showed a greater increase.

Table 5.3: Particle number (/500µl) of ultrafiltered urine from white (WUF) and black (BUF) subjects before and after addition of WF1 and BF1 at final concentrations of 1.25 mg/l

	WUF	WUF+WF1	WUF+BF1
Experiment 1	9203	19016	18542
Experiment 2	9202	12414	9194
Experiment 3 *	12512	14969	11258
Experiment 4	10937	19477	18489
Experiment 5	7101	14668	7928
Average ± SE:	9791 ± 912	16109 ± 1357	13082 ± 2281
	BUF	**BUF+WF1**	**BUF+BF1**
Experiment 1 *	8439	9021	14100
Experiment 2	6130	12099	12108
Experiment 3	9189	13836	18968
Experiment 4	3296	5279	8048
Experiment 5 **	12361	22179	18396
Average ± SE:	6763 ± 1326	10059 ± 1879	13306 ± 2269

** Effects of WF1 and BF1 were the same, ie. difference between particle numbers < 5%*

*** Excluded from average calculation since trend differed to that of the majority*

For the particle volume data (Table 5.4) in the white groups' ultrafiltrates, four of five experiments showed a greater increase in particle volume after addition of WF1, while the last experiment showed the opposite trend. For the black groups' ultrafiltrates, two of five

experiments showed a greater increase in particle volume after addition of BF1, two of five experiments showed no difference between WF1 and BF1, and one showed a greater increased in particle volume after addition of WF1.

Table 5.4: Particle volume ($x10^6$ μm^3/500 µl) of ultrafiltered urine from white (WUF) and black (BUF) subjects before and after addition of WF1 and BF1 at final concentrations of 1.25 mg/l

	WUF	WUF+WF1	WUF+BF1
Experiment 1	1.532	2.552	1.972
Experiment 2	2.473	4.932	2.697
Experiment 3	8.899	11.510	9.972
Experiment 4	6.121	8.806	6.953
Experiment 5 *	1.394	2.804	3.627
Average ± SE:	4.756 ± 1.699	6.950 ± 1.993	5.399 ± 1.879
	BUF	**BUF+WF1**	**BUF+BF1**
Experiment 1 **	0.904	1.614	1.646
Experiment 2	1.229	1.765	2.321
Experiment 3 **	3.177	4.356	4.165
Experiment 4	1.569	4.440	5.530
Experiment 5 *	1.672	2.782	2.377
Average ± SE:	1.720 ± 0.504	3.044 ± 0.783	3.415 ± 0.883

** Excluded from average calculation since trend differed to that of the majority*
*** Effects of WF1 and BF1 were the same, ie. difference between particle volumes < 5%*

When considering the average particle number and volume data, it is apparent that both WF1 and BF1 induced an increase in particle number and volume relative to the control, when tested in both population groups' ultrafiltrate. Furthermore, the greatest change in these parameters resulted from the addition of the UPTF1 which was endogenous to that ultrafiltrate, *i.e.* BF1 increased particle numbers and volume more than WF1 in BUF, whereas WF1 increased particle numbers and volume more than BF1 in WUF.

Table 5.5 shows the corresponding average percentage change in particle number and volume, as well as in other particle parameters which will be discussed later. The afore-mentioned trends for particle numbers are well illustrated by the percentage data. When BF1 was added to BUF, particle numbers increased by 96.7 %, whereas addition of WF1 resulted in an increase of only 48.7 %. Similarly, when WF1 was added to WUF, particle numbers increased by 64.5 %, whereas addition of BF1 resulted in an increase of only 33.6 %. The same trends were observed for particle volumes.

Table 5.5 also shows that BF1's effect on particle number and volume in BUF is considerably greater than its effect in WUF (particle number and volume increases of 96.7 and 98.6 % respectively in BUF, *vs.* 33.6 and 13.5 % respectively in WUF). However, WF1's

effect on WUF is greater than its effect in BUF with respect to particle number (particle number increases of 64.5 % in WUF *vs.* 48.7 % in BUF), but less effective than in BUF with respect to particle volume (particle volume increases of 46.1 % in WUF *vs.* 77.0 % in BUF).

Table 5.5: Percentage change in average particle parameters of ultrafiltered urine from white (WUF) and black (BUF) subjects after addition of WF1 and BF1 at final concentrations of 1.25 mg/l

	BUF experiment:		WUF experiment:	
	+WF1	+BF1	+WF1	+BF1
% Increase particle number	48.7	96.7	64.5	33.6
% Increase particle volume	77.0	98.6	46.1	13.5
% Decrease particle size	20.7	37.9	28.0	14.7
% Decrease [^{14}C]-ox deposition	30.2	43.0	33.8	21.7

5.3.2.3 Effect of UPTF1 on particle size

Table 5.6 shows the particle sizes measured at 120 minutes after addition of an oxalate load. For the particle data measured in the white groups' ultrafiltrates, three of four experiments showed a greater decrease in particle size after addition of WF1, and one experiment showed a greater decrease in particle size after addition of BF1. For the black groups' ultrafiltrates, three of three experiments showed a greater decrease in particle size after addition of BF1. The particle size distributions corresponding to each experiment is shown in Appendix D, Figures D4.1 – 4.4 (page A44) and Figures D4.5 – 4.7 (page A44), respectively.

Table 5.6: Particle size (µm) of ultrafiltered urine from white (WUF) and black (BUF) subjects before and after addition of WF1 and BF1 at final concentrations of 1.25 mg/l

	WUF	WUF+WF1	WUF+BF1
Experiment 1	16.96	11.30	14.13
Experiment 2	14.13	10.60	12.72
Experiment 3	16.96	12.72	14.13
Experiment 4 *	15.54	12.01	11.30
Average ± SE:	16.02 ± 0.94	11.54 ± 0.62	13.66 ± 0.47
	BUF	**BUF+WF1**	**BUF+BF1**
Experiment 1	14.13	11.30	9.89
Experiment 2	15.54	11.30	8.48
Experiment 3	11.30	9.89	7.07
Average ± SE:	13.66 ± 1.45	10.83 ± 0.47	8.48 ± 0.81

** Excluded from average calculation since trend differed to that of the majority*

Figure 5.6.1 and 5.6.2 shows the average particle volume – particle size distributions at 120 minutes after addition of a NaOx load to the white and black groups' ultrafiltrate, respectively. A decrease in the average particle size was observed after addition of WF1 and

BF1, indicated by a shift in the mode of the protein-dosed distributions to smaller values compared to their respective ultrafiltrate controls. The greatest decrease in particle size resulted from the addition of the UPTF1 which was endogenous to that ultrafiltrate. Thus, WF1 induced a decrease in the average size in WUF from 16.02 μm (± 0.94) to 11.54 μm (± 0.62), while addition of BF1 induced a decrease in the size to only 13.66 μm (± 0.47) (Figure 5.6.1). Similarly, BF1 decreased the average size in BUF from 13.66 μm (± 1.45) to 8.48 μm (± 0.81), while addition of WF1 decreased the size to only 10.83 μm (± 0.47) (Figure 5.6.2). These decreases are reflected as percentages in Table 5.5.

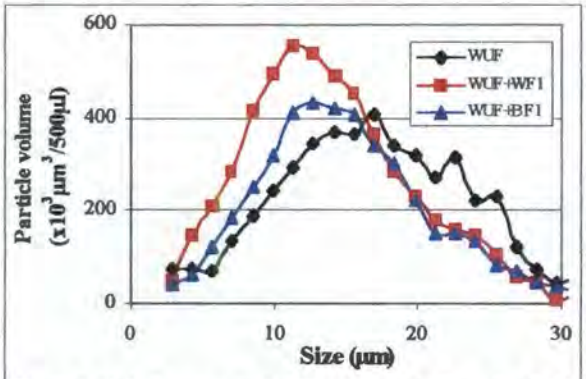

Figure 5.6.1: Average particle size distributions in WUF. Ultrafiltered urine from white males (WUF) before and after addition of WF1 and BF1 at final concentrations of 1.25mg/l

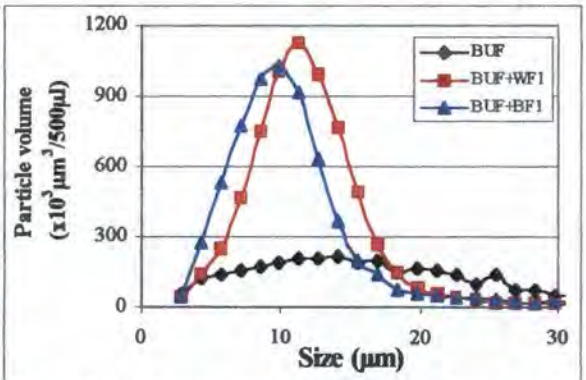

Figure 5.6.2: Average particle size distributions in BUF. Ultrafiltered urine from black males (BUF) before and after addition of WF1 and BF1 at final concentrations of 1.25mg/l

Table 5.5 (page 118) also shows that BF1's effect on particle size in BUF is considerably greater than its effect in WUF (particle size decrease of 37.9 % in BUF *vs.* 14.7 % in WUF). Similarly, WF1's effect in WUF is greater than its effect in BUF (particle size decrease of 20.7 % in BUF *vs.* 28.0 % in WUF). These trends are similar to those observed for particle number and volume.

Figure 5.7 shows scanning electron micrographs of CaOx crystals deposited after dosing with NaOx and addition of UPTF1 to each control ultrafiltrate (after 120 minutes). These micrographs are representative of the two ultrafiltrates examined from each population group. No differences between BF1 and WF1-dosed ultrafiltrates were observed. Thus in the context of the microscopy study, BF1 and WF1 will collectively be referred to as UPTF1. Crystals deposited in BUF and WUF were typically highly aggregated with only a few single

crystals (Figures 5.7.1 - 5.7.2 respectively). In contrast, both protein-dosed ultrafiltrates showed a notable decrease in the degree of aggregation (Figures 5.7.3 – 5.7.4).

Of interest is the observation that while deposits in BUF consisted of both COM and COD crystals (Figure 5.7.1), deposits in WUF were composed almost entirely of dihydrates with typically only a few, very small (<1 μm diameter) COM crystals (Figure 5.7.2). After addition of UPTF1, mainly COM crystals were observed in the blacks' ultrafiltrate (Figure 5.7.3) while the hydrate composition in the whites' ultrafiltrate was unaffected, *i.e.* COD were observed (Figure 5.7.4).

Figure 5.7: Scanning electron micrographs of CaOx crystals deposited in ultrafiltered urine. The crystals were precipitated from: blacks' ultrafiltered urine (Fig 5.7.1), blacks' ultrafiltered urine dosed with UPTF1 (final concentration 1.25 mg/l) (Fig 5.7.2), whites' ultrafiltered urine (Fig 5.7.3), whites' ultrafiltered urine dosed with UPTF1 (final concentration 1.25 mg/l) (Fig 5.7.4.). All micrograph magnifications are 4.5 K.

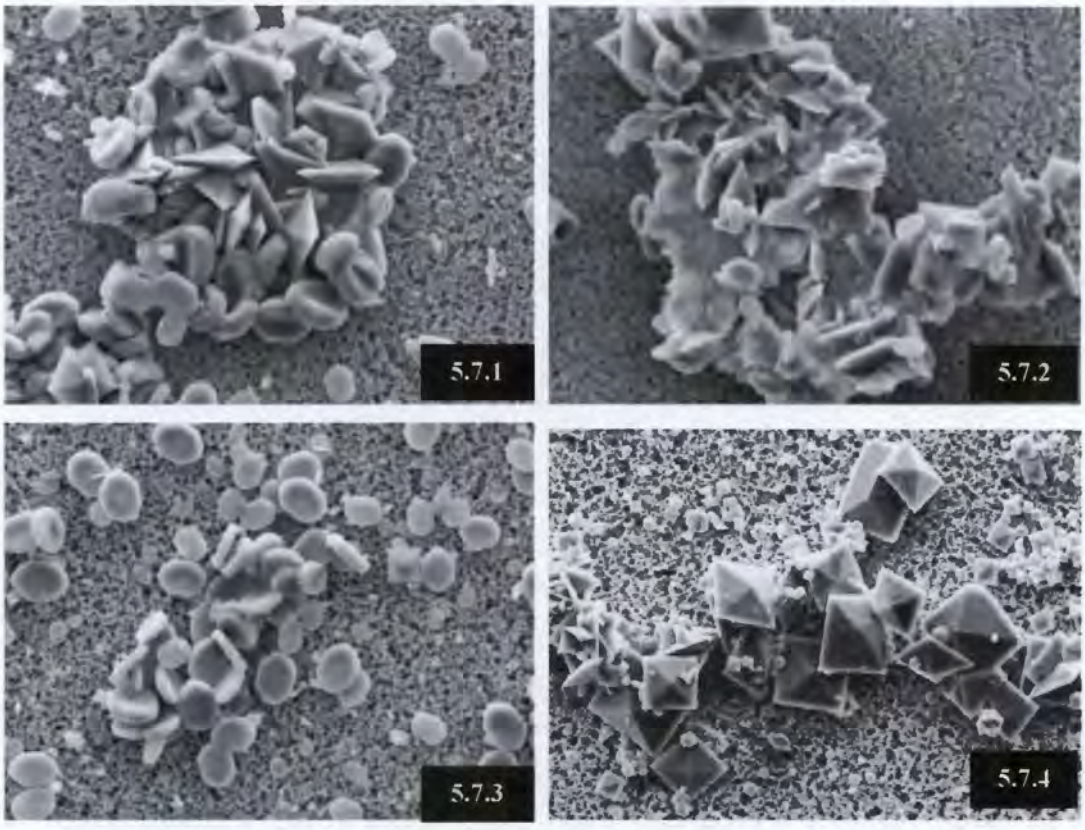

5.2.3.4 Effect of UPTF1 on [^{14}C]-oxalate deposition

Figures 5.8.1 and 5.8.2 show plots of the average increase in the deposition rate of precipitated [^{14}C]-oxalate during a 120-minute time course after addition of an oxalate load to the white

and black groups' ultrafiltrate, respectively. The average data corresponding to these plots is shown in Table 5.7. The plots of each of the individual WUF and BUF experiments is shown in Appendix D, Figures D5.1 – 5.3 (page A45) and Figures D5.4 – 5.6 (page A45), respectively. The data from which the WUF and BUF plots were obtained is presented in Appendix D, Table D6.1 (page A39) and Table D6.2 (page A39), respectively.

For the [^{14}C]-oxalate deposition measured in the white groups' ultrafiltrates, two of three experiments showed a greater decrease in deposition after addition of WF1 and one experiment showed a greater decrease after addition of BF1. In the black groups' ultrafiltrates, two of three experiments showed a greater decrease in deposition after addition of BF1 and one experiment showed a greater decrease after addition of WF1.

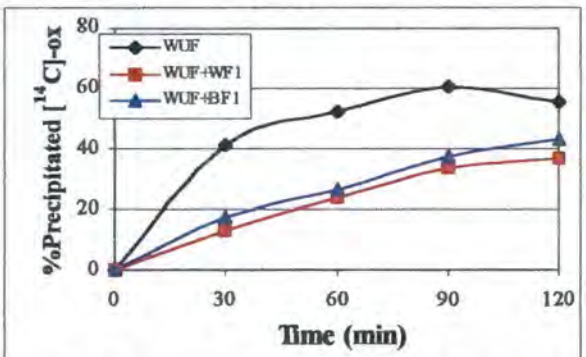

Figure 5.8.1: Average [^{14}C]-ox deposition in WUF. Ultrafiltered urine from white males (WUF) before and after addition of WF1 and BF1 at final concentrations of 1.25mg/l

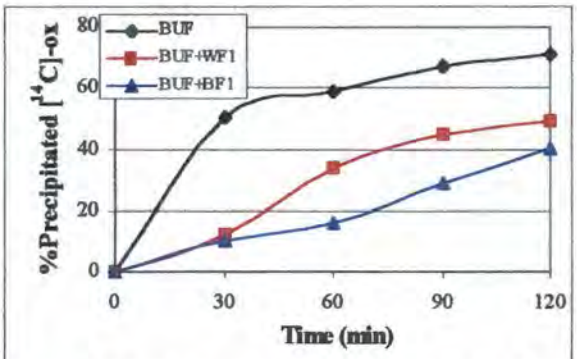

Figure 5.8.2: Average [^{14}C]-ox deposition in BUF. Ultrafiltered urine from black males (BUF) before and after addition of WF1 and BF1 at final concentrations of 1.25mg/l

Table 5.7: Average percentage precipitated [^{14}C]-oxalate in ultrafiltered urine from white (WUF) and black (BUF) subjects before and after addition of WF1 and BF1 at final concentrations of 1.25 mg/l

Time	WUF experiment:			BUF experiment:		
	WUF	WUF+WF1	WUF+BF1	BUF	BUF+WF1	BUF+BF1
0	0	0	0	0	0	0
30	41.0	13.0	17.2	50.3	12.3	10.2
60	52.4	23.9	26.7	58.6	33.9	16.2
90	60.3	33.4	37.7	67.4	45.1	28.6
120	55.5	36.8	43.4	70.9	49.5	40.4

From the average data plotted in Figures 5.8.1 and 5.8.2 above, it is evident that BF1 and WF1 decreased the amount of precipitated material, when tested in both WUF (Figure 5.8.1) and BUF (Figure 5.8.2). The greatest decrease in precipitate resulted from the addition of the UPTF1 which was endogenous to that ultrafiltrate. Thus after 120 minutes, WF1 decreased the percentage precipitated [^{14}C]-oxalate in WUF from 55.5 % to 43.4 %, while

addition of BF1 decreased the amount precipitated to only 36.8 %. These represent decreases in CaOx deposition of 33.8 and 21.7 % by WF1 and BF1 respectively relative to the whites' ultrafiltrate control (Table 5.5, page 118). Similarly, the addition of BF1 decreased the percentage precipitated in BUF from 70.9 % to 40.4 %, while addition of WF1 decreased the amount precipitated to only 49.5 %. These values correspond to decreases in CaOx deposition relative to BUF of 43.0 and 32.0 % by BF1 and WF1, respectively (Table 5.5, page 118).

5.3.3 Sedimentation rates

5.3.3.1 Effect of UPTF1 on COM crystal slurries

Figure 5.9 shows a plot of the average rate of decrease in absorbance (620 nm) of a COM crystal slurry before and after addition of WF1 and BF1. The individual experiments from which these averages were obtained are shown in Appendix D (COM: Figures D6.1.1 - D6.1.6, page A46; COM+WF1: Figures D6.2.1 – D6.2.6, page A47; COM+BF1: Figures D6.3.1 – D6.3.7, page A48).

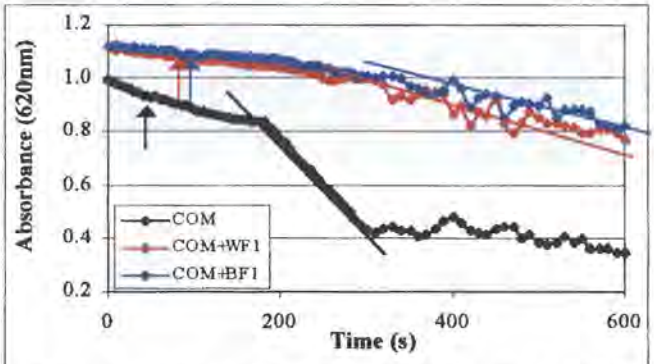

Figure 5.9: Average OD_{620} plot of COM crystal slurries. Before and after addition of WF1 and BF1 at final concentrations of 1.25mg/l

It is apparent from Figure 5.9 that the sedimentation rate of the COM crystal slurry is greatly reduced by the addition of both WF1 and BF1 while the effect of the two population groups' UPTF1 appears to be similar in this regard. This is supported by the data presented in Table 5.8. Both WF1 and BF1 significantly reduced the absorbance slope of the COM crystal slurry and thus inhibited crystal aggregation, shown by I_A indices of 78.3 and 83.1 %, respectively ($p < 0.01$). There was no significant difference between the effect of WF1 and

BF1 ($p > 0.05$). The absorbance slopes for the individual experiments from which the average slopes were obtained is shown in Appendix D, Table D7.1 (page A40).

Table 5.8: Average absorbance slope ($x\text{-}10^{-5}s^{-1}$) and inhibition of aggregation (I_A %) of COM crystal slurries before and after addition of WF1 and BF1 at final concentrations of 1.25 mg/l

Sample	Absorbance slope ave. ± SE (R^2)	I_A (%)	p-value wrt COM	n-value
COM	336 ± 8.5 (0.981)			6
COM+WF1	73 ± 8.5 (0.896)	78.3	< 0.01	6
COM+BF1	57 ± 8.5 (0.909)	83.1	< 0.01	7

COM+WF1 vs. COM+BF1: $p > 0.05$

5.3.3.2 Characterisation of CaOx crystals

The composition of CaOx crystals prepared according to the method described by Brown *et al.* (1985) was verified by XRD, TGA and SEM. Figure 5.10 shows the XRD pattern of the crystals together with the d-spacings (Å) of prominent peaks. The assignment of these peaks is shown in Table 5.9. All peaks corresponded with known COD reflections (refer to Table 2.1 on page 28 for reference values) except for the 3.42 Å peak which could not be assigned.

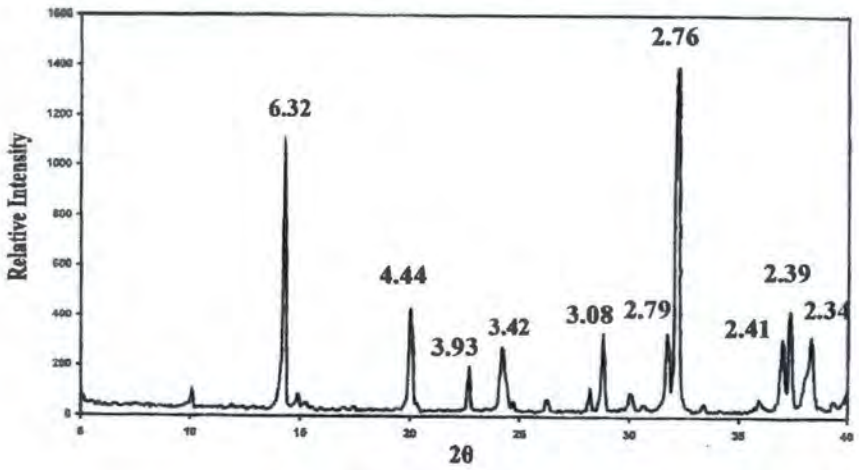

Figure 5.10: X-ray powder diffraction pattern of CaOx crystals prepared according to Brown *et al.* (1985)

Table 5.9: X-ray powder diffraction peak assignments of CaOx crystals according to Brown *et al.* (1985)

d-spacing (Å)	Assignment	
6.32	COD	100% COD
4.44	COD	
3.93	COD	
3.42	could not assign	
3.08	COD	
2.79	COD	
2.76	COD	
2.41	COD	
2.39	COD	
2.34	COD	

Figure 5.11 shows the decrease in weight (%) of the crystals as a function of temperature. The computed mass loss of 18.62 % (at an onset temperature of 106.7 ^{0}C) corresponds closely with the theoretical value of 21.96 % for the loss of two water molecules associated with one CaOx molecule.

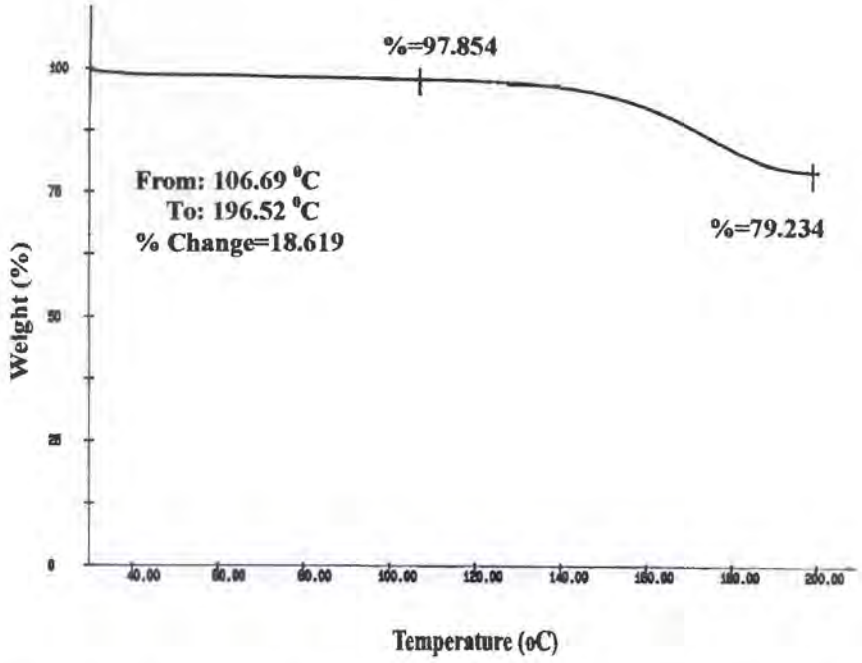

Figure 5.11: Thermogravimetric analysis of CaOx crystals prepared according to Brown *et al.* (1985)

Figures 5.12.1 – 5.12.2 show scanning electron micrographs of the CaOx crystals at different magnifications. Only small, bipyramidal crystals (~5 μm in diameter) were observed in the CaOx sample. This morphology is typical of COD crystals. Thus, all three methods used

confirmed that the crystals prepared were composed of 100 % COD, as required for the COD crystal slurry studies.

Figure 5.12: Scanning electron micrographs of CaOx crystals prepared according to Brown *et al.* (1985). The photographs were taken at the following magnifications: 9K (Fig 5.12.1) and 6K (Fig 5.12.2).

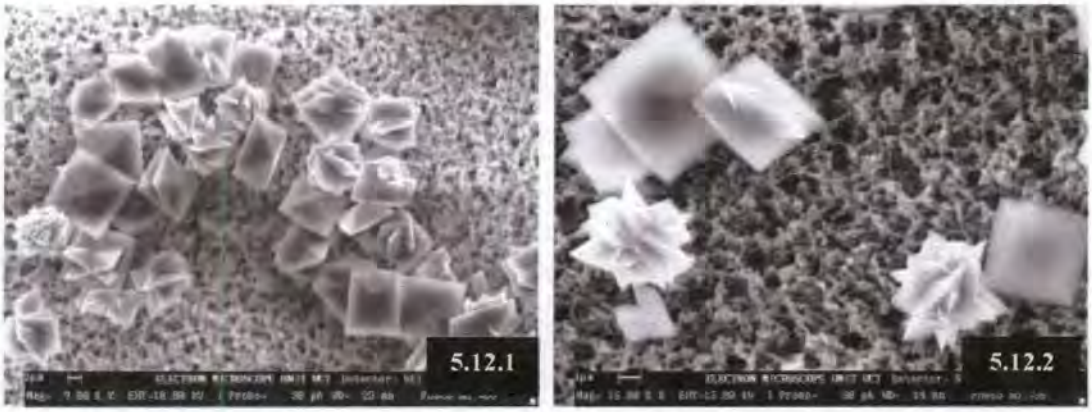

5.3.3.3 Effect of UPTF1 on COD crystal slurries

Figure 5.13 shows a plot of the average rate of decrease in absorbance (620 nm) of a COD crystal slurry before and after addition of WF1 and BF1. The individual experiments from which these averages were obtained are shown in Appendix D (COD: Figures D7.1.1 - D7.1.9, pages A49 - A50; COD+WF1: Figures D7.2.1 – D7.2.12, pages A51 – A52; COD+BF1: Figures D7.3.1 - D7.3.10, pages A53 – A54).

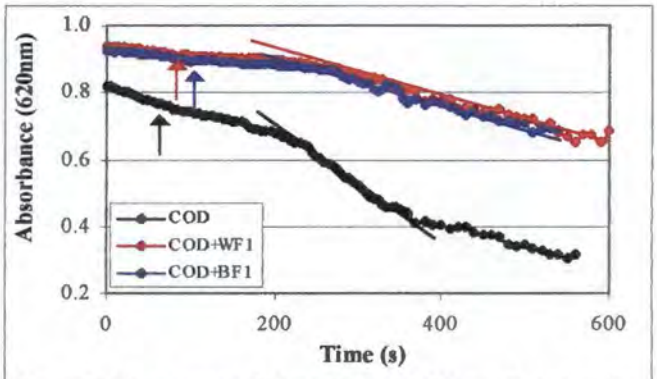

Figure 5.13: Average OD_{620} plot of COD crystal slurries. Before and after addition of WF1 and BF1 at final concentrations of 1.25mg/l

It is apparent from Figure 5.13 that the sedimentation rate of the COD crystal slurry is greatly reduced by the addition of both WF1 and BF1, while the effect of the two population groups' UPTF1 appears to be similar. This is supported by the data presented in Table 5.10. Both WF1 and BF1 significantly reduced the absorbance slope of the COD crystal slurry and therefore inhibited crystal aggregation, shown by I_A indices of 56.8 and 53.7 %, respectively ($p < 0.01$). There was no significant difference between the effect of WF1 and BF1 ($p > 0.05$). The absorbance slopes for the individual experiments from which the average slopes were obtained is shown in Appendix D (Table D7.2, page A40).

Table 5.10: Average absorbance slope ($x\text{-}10^{-5}s^{-1}$) and inhibition of aggregation (I_A %) of COD crystal slurries before and after addition of WF1 and BF1 at final concentrations of 1.25 mg/l

Sample	Absorbance slope ave. ± SE (R^2)	I_A (%)	p-value wrt COD	n-value
COD	95 ± 2.9 (0.945)			9
COD+WF1	41 ± 2.9 (0.954)	56.8	< 0.01	12
COD+BF1	44 ± 2.9 (0.913)	53.7	< 0.01	10

COD+WF1 vs. COD+BF1: $p > 0.05$

5.3.3.4 Comparative effect of UPTF1 on COM and COD crystal slurries

The ability of UPTF1 to inhibit aggregation of COM and COD crystal slurries was compared. Figure 5.14 shows the I_A indices (± SE) of the COM (shown by the solid bars) and COD slurries (shown by the open bars) after addition of both WF1 and BF1.

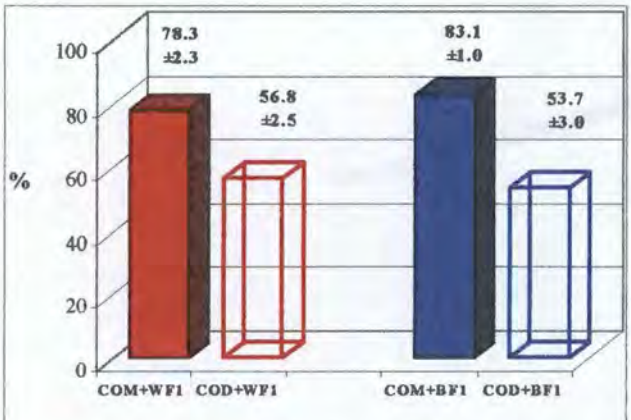

Figure 5.14: Average % inhibition by WF1 and BF1 in COM & COD slurries (final concentrations of 1.25mg/l).

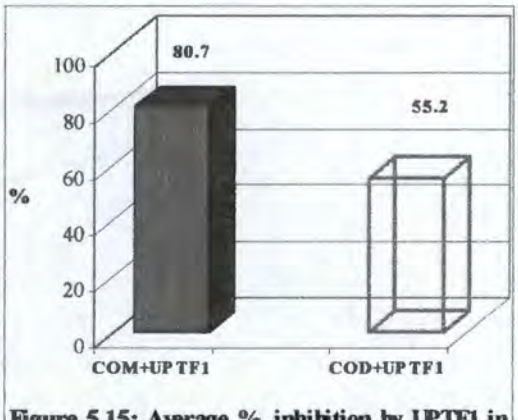

Figure 5.15: Average % inhibition by UPTF1 in COM & COD slurries (final concentration of 1.25mg/l).

It is apparent that the extent of aggregation inhibition by UPTF1 from both population groups is greater in COM than COD crystals. Since the inhibition by WF1 and BF1 was not significantly different in either crystal slurry, the I_A indices for the two groups' UPTF1 were averaged with respect to COM and COD. Thus UPTF1 collectively refers to WF1 and BF1 in Figure 5.15. The difference in inhibition by UPTF1 in COM and COD crystals is clearly shown here ($p < 0.01$).

5.3.4 Zeta potentials

5.3.4.1 Effect of UPTF1 on COM crystal slurries

Table 5.11 shows the average zeta potential (mV) values of a COM crystal slurry before and after addition of WF1 and BF1. The individual values from which the averages were calculated are presented in Appendix D (Table D8.1, page A40). These values are shown graphically in Figure 5.16 (page 128). It is evident that the addition of both WF1 and BF1 resulted in a decrease in zeta potential towards a more negative value. This is reflected by the significant decrease in zeta potential of the COM by WF1 and BF1 of 92.8 and 89.2 %, respectively ($p < 0.01$). The respective effects of WF1 and BF1 were not significantly different ($p > 0.05$).

Table 5.11: Average zeta potential of COM crystal slurries before and after addition of WF1 and BF1 at final concentrations of 1.25 mg/l

Sample	ZP ave. ± SE (mV)	% Decrease wrt COM	p-value wrt COM	n-value
COM	-16.7 ± 0.55			6
COM+WF1	-32.2 ± 0.55	92.8	< 0.01	6
COM+BF1	-31.6 ± 0.55	89.2	< 0.01	6

COM+WF1 vs. COM+BF1: $p > 0.05$

5.3.4.2 Effect of UPTF1 on COD crystal slurries

Table 5.12 below shows the average zeta potential (mV) values of a COD crystal slurry before and after addition of WF1 and BF1. The individual values from which the averages were calculated are presented in Appendix D, Table D8.2 (page A40). These values are shown graphically in Figure 5.17 below.

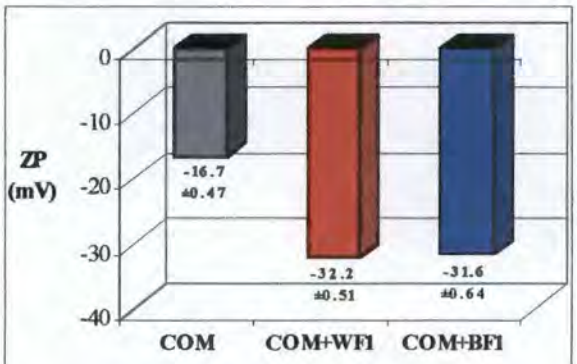

Figure 5.16: Average zeta potential of COM slurries. Before and after addition of WF1 and BF1 at final concentrations of 1.25mg/l

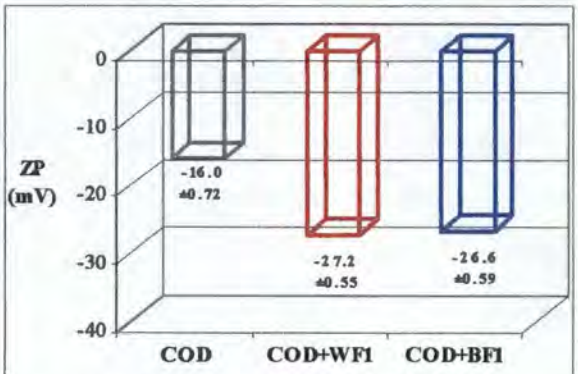

Figure 5.17: Average zeta potential of COD slurries. Before and after addition of WF1 and BF1 at final concentrations of 1.25mg/l

It is evident that the addition of both WF1 and BF1 resulted in a decrease in zeta potential towards a more negative value. This is reflected by the significant decrease in zeta potential of the COD by WF1 and BF1 of 70.0 and 66.2 %, respectively ($p < 0.01$). The respective effects of WF1 and BF1 were not significantly different ($p > 0.05$).

Table 5.12: Average zeta potential of COD crystal slurries before and after addition of WF1 and BF1 at final concentrations of 1.25 mg/l

Sample	ZP ave. ± SE (mV)	% Decrease wrt COD	p-value wrt COD	n-value
COD	-16.0 ± 0.62			6
COD+WF1	-27.2 ± 0.62	70.0	< 0.01	6
COD+BF1	-26.6 ± 0.62	66.2	< 0.01	6

COD+WF1 vs. COD+BF1: $p > 0.05$

5.3.4.3 Comparative effect of UPTF1 on COM and COD crystal slurries

The effect of UPTF1 on the zeta potential of COM and COD crystal slurries was compared. Figure 5.18 shows the average percentage decrease in zeta potential of the COM (shown by solid bars) and COD slurries (shown by open bars) after addition of both WF1 and BF1. It is apparent that the change in zeta potential towards a more negative value in the presence of UPTF1 from both population groups, indicating a greater potential for inhibition of aggregation, is greater in COM compared with COD crystals. Since the inhibition by WF1 and BF1 was not significantly different in either crystal slurry, the percentage decrease for the two proteins was averaged with respect to COM and COD. Thus UPTF1 collectively refers to

WF1 and BF1 in Figure 5.19. The difference in UPTF1 activity in COM and COD crystal slurries is clearly shown here ($p < 0.01$).

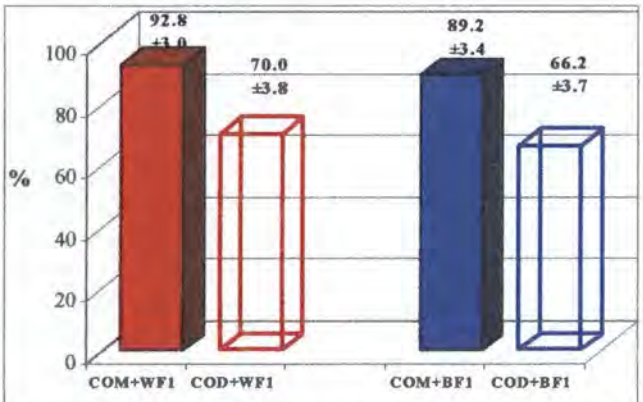

Figure 5.18: Average % decrease in zeta potential of COM & COD slurries. After addition of WF1 and BF1 at final concentrations of 1.25mg/l

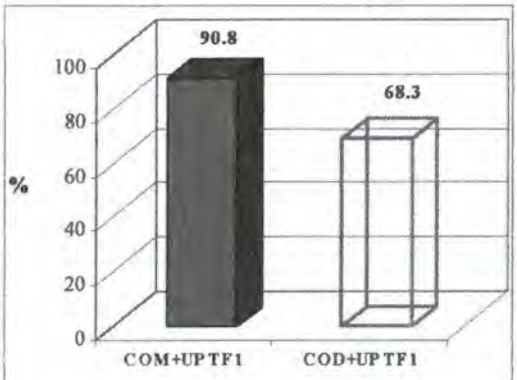

Figure 5.19: Average % decrease in zeta potential of COM & COD slurries. After addition of UPTF1 at a final concentration of 1.25mg/l

5.4 DISCUSSION

5.4.1 Synthetic urine study

The particle data obtained in synthetic urine suggests that UPTF1 inhibits crystal growth and aggregation, regardless of the population group from which it is derived. Growth inhibition is shown by the decreased amount of deposited CaOx and smaller particle sizes, while the latter observation, along with electron microscopy data, also suggests reduced crystal aggregation in the presence of UPTF1. These results represent the first report of UPTF1's inhibitory activity in an inorganic solution. In addition, when compared with WF1, BF1 appeared to result in the precipitation of more small crystals and a greater decrease in the initial rate of CaOx deposition. The formation of more small crystals is regarded as favourable since it reduces the supersaturation of CaOx (Kavanagh 1992). These observations are consistent with greater inhibition by BF1 in the synthetic urine test solution.

It is noteworthy that addition of UPTF1 derived from both population groups resulted in a change in crystal morphology, from mainly COM crystals in undosed synthetic urine to almost exclusively COD in the protein-dosed urines. A similar polymorphism has been reported previously following the addition of macromolecules to inorganic solutions (Wesson *et al.* 1998). This may be regarded as a favourable response since the higher positive charge on

COD (due to the greater number of calcium ions per unit cell) results in greater repulsive forces between crystals, and therefore favours disaggregation (Cerini *et al.* 1999). Furthermore, COD show a lower binding affinity for epithelial cell surfaces than COM crystals (Wesson *et al.* 1998), thus reducing crystal retention in the collecting ducts.

These results demonstrate that BF1 is a more efficacious inhibitor than WF1 in synthetic urine. The structural differences in UPTF1 from the two groups, in particular the black population's great number of Gla residues and higher number of sialic acid residues (chapter 4), are the most likely explanation.

5.4.2 Ultrafiltered urine study

Following the synthetic urine experiments, a more comprehensive study of UPTF1 activity was conducted in urine using a cross-over design described earlier. In this study, an increase in particle volume was observed when urine was dosed with UPTF1. An increase in *crystal* volume can occur only if the total mass of deposited crystalline material increases (through increased nucleation and/or growth). However, when crystals clump together to form a "particle", an increase in total volume can occur through two possible mechanisms. Firstly, if imperfect packing of crystals takes place during aggregation, pores containing air or fluid are created, thereby generating a larger volume for the particle as a whole. This is an *inter*crystalline process. On the other hand, a second possibility is *intra*crystalline incorporation of urinary proteins into the crystal lattice, again generating a larger volume for the particle (Ryall *et al.* 1995). The Coulter Counter simply measures the total volume of a particle, irrespective of whether there are intercrystalline pores or intracrystalline proteins. Thus, volume data obtained from this instrument may be incorrectly interpreted as *crystal* volume. This limitation can be overcome by [^{14}C]-oxalate deposition experiments which provide data about the total mass of crystalline material that has formed.

In the present study, particle volumes increased in the presence of UPTF1, but the [^{14}C]-oxalate experiments showed that the total mass of deposited CaOx did not increase. Indeed, to the contrary, the total deposited mass decreased. Thus, the observed increase in particle volume cannot be attributed to the deposition of new crystalline material. Aggregation, with concommitant generation of pores, may also be eliminated as an explanation since particle size decreased and SEM observations revealed that less aggregation had in fact occurred. The only other possible explanation for the increase in particle volume is

increased nucleation and/or intra-crystalline incorporation of UPTF1 into the CaOx crystal lattice. The former is supported by the observed increase in particle numbers, and the latter has been demonstrated previously (Fleming *et al.* 1999, Ryall *et al.* 2000, chapter 8).

The particle number and size data, [^{14}C]-oxalate deposition experiments and SEM observations suggest that the presence of UPTF1, irrespective of the population group from which it is derived, promotes the nucleation of small crystals of CaOx (increased particle numbers; smaller sizes), but inhibits their growth (decreased deposition of [^{14}C]-oxalate; smaller sizes). Inclusion of UPTF1 into the crystal lattice occurs (increase in particle volume), but these inclusions, while increasing the overall volume of the particles, are not of sufficient magnitude to increase their size. The particle number (increase) and size data (decrease) as well as SEM are also consistent with inhibition of aggregation, or promotion of disaggregation. All of these observations suggest that UPTF1 has a protective role in both population groups.

The observation that UPTF1 inhibits CaOx crystal growth and aggregation in ultrafiltered urine is in agreement with Ryall *et al.* (1995). Of some interest is the further observation that the protein promotes nucleation. As mentioned above, this is regarded as a protective factor. Cerini and co-workers (Cerini *et al.* 1999), in their study of urinary albumin in an inorganic solution, reported that an increase in the number of small crystals lowered urinary saturation and thus prevented larger crystals and aggregates from forming.

Electron microscopy results showed a difference in CaOx hydrate composition of the urine from black and white subjects. In a study on the formation of stable crystalluria, CODs were formed in the presence of a raised urinary calcium excretion (Burns and Finlayson 1980b, Hennequin *et al.* 1998, Ryall *et al.* 2001) while COM formation has been reported at lower calcium concentrations (Burns and Finlayson 1980b, Ryall *et al.* 2001). Thus, the observation that the whites' ultrafiltrate consisted of mainly CODs is consistent with their relatively higher urinary calcium concentration, while the formation of COD *and* COM in the blacks' urine is consistent with the relatively lower calcium concentration in this population group (Modlin 1967, Whalley *et al.* 1998, Rodgers and Lewandowski 2002).

Furthermore, COM crystals were present exclusively after addition of UPTF1 to the black groups' urine, while COD were present after the white groups' urine was dosed with UPTF1. The response of the former group was unexpected in light of previous reports that macromolecules result in the formation of mainly COD crystals. Moreover, the presence of

COD has been described as more protective than COM crystals (refer to page 130). However, given that the black population has a remarkably low incidence of stones, the presence of COM rather than COD crystals in their urine (both before and after dosing with UPTF1) is evidently not harmful and perhaps even an indicator of a unique protective factor in this population group.

The results of the present study clearly demonstrate a synergistic relationship between urine composition and UPTF1 activity during *in vitro* CaOx crystallisation. This relationship has not been reported previously.

A comparison of the activity of UPTF1 from the two groups shows that WF1 demonstrated a greater inhibitory activity than BF1 in *WUF*, while BF1 was superior in *BUF*. These trends are open to several interpretations, involving properties of the proteins as well as the ultrafiltrates. Factors such as the relatively lower calcium concentration of the blacks' urine (Modlin 1967, Whalley *et al.* 1998, Rodgers and Lewandowski 2002), which in turn determines their higher proportion of COM crystals, the relative binding affinities of the proteins for the CaOx hydrates which distinguish blacks and whites, and the possible presence of unidentified low molecular weight constituents in the respective ultrafiltered urines, could all play a role.

The present study of UPTF1 activity in ultrafiltered urine demonstrated several important findings. Firstly, in addition to confirming earlier findings that UPTF1 is an effective inhibitor of CaOx crystal growth and aggregation in urine, the study showed that UPTF1 promotes nucleation. The latter result has not been reported previously. Increased nucleation may be regarded as a protective mechanism. Secondly, and more importantly, a synergistic relationship between UPTF1 and urine composition was observed which influences the inhibitory capacity of the protein. The lower calcium concentration and relative supersaturation of CaOx in the black subjects' urines (Table 5.2) could have contributed to the favourable synergistic relationship between UPTF1 and urine composition in this group. Specifically, it is of considerable interest that in its endogenous urine BF1 was found to be a superior inhibitor than WF1 in its endogenous milieu (Table 5.5). This may indicate that the conformation adopted by BF1 in BUF is the most efficacious in terms of inhibitory activity.

5.4.3 Sedimentation rates and zeta potentials

The results of the ultrafiltered urine study showed the potential importance of crystal

morphology with respect to UPTF1 activity. Thus a comparative study of the activity of UPTF1 from both population groups with regard to crystal aggregation in COM and COD crystals was conducted. Since crystal morphology can be more readily controlled in an inorganic solution, synthetically prepared CaOx crystals composed of either pure COM or pure COD were used in these studies.

Both WF1 and BF1 strongly inhibited COM and COD crystal aggregation in the sedimentation rate study. Differences in the two population groups' UPTF1 activity were not detected. However, the aggregation inhibition by UPTF1 in the COM crystal slurry was considerably greater than in the COD slurry (80.7 % in COM *vs.* 55.2 % in COD).

The trend in zeta potentials was similar. While there were no detectable differences between WF1 and BF1, the decrease in zeta potential by UPTF1 towards more negative values in the COM crystal slurry, irrespective of population group, was significantly greater than in the COD slurry (90.8 % in COM *vs.* 68.3 % in COD). The decrease in zeta potential is indicative of a greater driving force towards disaggregation by action of the repulsive negative charge on the crystals (Hess and Kok 1996). A study of THM has shown that more negative zeta potentials correlate well with increased inhibitory activity (Scurr and Robertson 1986).

The sedimentation rate and zeta potential studies therefore strongly suggest that the capability of UPTF1 to disaggregate COM crystals is significantly greater than with COD crystals. In the inorganic media tested here, the interaction or binding between COM and UPTF1 therefore appears to enable greater inhibition by UPTF1.

5.4.4 Conclusions

It is clear from the present study that while UPTF1 is an effective inhibitor in both inorganic media and urine, its specific role with regard to CaOx crystallisation also varies accordingly. By investigating its inhibitory activity in several environments, valuable information was obtained on its inhibitory capacity as well as the factors necessary to facilitate and optimise this role.

Three important factors, which both independently and collectively influence UPTF1's inhibitory activity, are its calcium-binding properties (Benarous *et al.* 1976, Bloom and Mann 1978), its Gla residues (Benarous *et al.* 1976, Bloom and Mann 1978, Grover and Ryall 1999), and pH (Benarous *et al.* 1976). These factors determine the protein's conformation which, in turn, determines inhibitory activity. In a study of human PT, the parent compound from which

UPTF1 is derived, Benarous reported that the molecule had a positive affinity for calcium ions (related to the presence of Gla residues) resulting in a conformational change in the protein (Benarous *et al.* 1976). Bloom later showed the same results for the Gla-rich fragment of PT, namely PTF1 (Bloom and Mann 1978). More recent studies have confirmed that Gla residues also facilitate the *urinary* protein's exceptional affinity for calcium ions (Grover and Ryall 1999). Therefore changes in UPTF1's calcium binding ability and/or the sequence or number of Gla residues are likely to influence the protein's conformation and hence its activity. The moderately higher activity of BF1 measured in the synthetic urine may therefore be due, in part, to its greater number of Gla residues compared with the white group's UPTF1 (chapter 4).

Furthermore, a study of human PT showed optimal calcium binding in the pH range 7.4 - 8.5, with a rapid increase in binding at pH values approaching 7.4 (Benarous *et al.* 1976). The significantly higher urinary pH of blacks previously reported by our laboratory (Lewandowski *et al.* 2001), although not observed in this chapter, therefore suggests that BF1 may have a superior calcium binding capacity compared to WF1. However, the fact that BF1 was not a superior inhibitor to WF1 in all test solutions also suggests that factors other than pH interact synergistically to determine the protein's activity in urine.

Ryall's recent report that UPTF1 is preferentially included into COM rather than COD crystals (Ryall *et al.* 2001), and thus presumably binds more strongly to COM, further confirms the significance of calcium binding in the role of UPTF1. This finding may also explain the superior activity of UPTF1 in COM compared with COD crystal slurries measured in the present study. It is possible that the binding of UPTF1 to COM crystals results in a protein conformation that is more favourable for inhibition of crystallisation.

Further investigation of the relationship between CaOx crystal morphology, calcium binding and the role of UPTF1 in black and white subjects is clearly warranted. This is especially important due to the different hydrate composition of urinary CaOx crystals from the two population groups reported here. However, it is already evident that the greater inhibition by BF1 in synthetic urine, and the more favourable synergistic combination of BF1 in its parent urine compared with WF1 in its own parent urine, may be important factors in the black population's relative protection from kidney stone disease.

5.5 REFERENCES

1. Benarous R, Eloin J, and Labie D. 1976. Ca++ binding properties of human prothrombin. *Biochem* 58:391-394.

2. Bloom JW and Mann KG. 1978. Metal ion induced conformational transitions of prothrombin and prothrombin fragment 1. *Biochem* 17:4430-4438.

3. Brown P, Ackermann D, and Finlayson B. 1989. Calcium oxalate dihydrate (weddellite) precipitation. *J Crys Growth* 98:285-292.

4. a) Burns JR and Finlayson B. 1980. A proposal for a standard reference artificial urine in in vitro urolithiasis experiments. *J Urol* 18:167-169.

5. b) Burns JR and Finlayson B. 1980. Changes in calcium oxalate crystal morphology as a function of concentration. *Inves Urol* 18:174-177.

6. Cerini C, Geider S, Dussol B, Hennequin C, Daudon M, Veesler S, Nitsche S, Biostelle R, Berthezene P, Dupuy P, Vazi A, Berland Y, Daghorn J-C, and Verdier J-M. 1999. Nucleation of calcium oxalate crystals by albumin: involvement in the prevention of stone formation. *Kidney Int* 55:1776-1786.

7. Craig T-A, Brandt W and Rodgers A. 1999. Inhibitory properties of Tamm Horsfall mucoprotein isolated from two different population groups. In: Borghi L, Meschi T, Briganti A, Schanchi T and Novarini A, editors. Proceedings of the 8th European Symposium on Urolithiasis. Editoriale Bios. Cosenza, 261-264.

8. Doyle IR, Marshall VR, Dawson CJ, and Ryall RL. 1995. Calcium oxalate crystal matrix extract: the most potent macromolecular inhibitor of crystal growth and aggregation yet tested in undiluted human urine in vitro. *Urol Res* 23:53-62.

9. Fleisch H. 1978. Inhibitors and promoters of stone formation. *Kidney Int* 13:361-371.

10. Fleming DE, Doyle IR, Evans N, Marshall VR, Parkinson GM and Ryall RL. 1999. Proteins associated with calcium oxalate crystals formed in human urine are intracrystalline. In: Borghi L, Meschi T, Briganti A, Schanchi T and Novarini A, editors. Proceedings of the 8th European Symposium on Urolithiasis. Editoriale Bios. Cosenza, 359-361.

11. Grover PK and Ryall RL. 1999. Inhibition of calcium oxalate crystal growth and aggregation by prothrombin and its fragments in vitro. *Eur J Biochem* 263:50-56.

12. Hennequin C, Tardivel S, Medetognon J, Drueke T, Daudon M, and Lacour B. 1998. A stable animal model of diet-induced calcium oxalate crystalluria. *Urol Res* 26:57-63.

13. Hess B and Kok DJ. 1996. Nucleation, growth, and aggregation of stone-forming crystals. In Kidney stones: Medical and surgical management. Coe FL, Favus MJ, Pak CYC, Parks JH and Preminger GM, editors. Lippincott-Raven Publishers, Philadelphia, 3-32.

14. Hess B, Nakagawa Y, and Coe FL. 1989. Inhibition of calcium oxalate monohydrate crystal aggregation in urine proteins. *Am J Physiol* 257:F99-F106.

15. Hess B, Ryall RL, Kavanagh JP, Khan SR, Kok D-J, Rodgers AL, and Tiselius HG. 2001. Methods for measuring crystallization in urolithiasis research - why, how and when? *Eur Urol* 40:220-230.

16. Jappie D and Rodgers AL. 2000. Determination of the optimum number of subjects required for pooling of urines: statistical approach. In: Rodgers AL, Hibbert BE, Hess B, Khan SR, and Preminger GM, editors. Urolithiasis 2000. University of Cape Town, Cape Town, 92-93.

17. Kavanagh JP. 1992. Methods for the study of calcium oxalate crystallisation and their application to urolithiasis research. *Scan Micros* 6: 685-704.

18. Lewandowski S, Rodgers AL, and Schloss I. 2001. The influence of a high-oxalate / low-calcium diet on calcium oxalate renal stone risk factors in non-stone forming black and white South African subjects. *Br J Urol* 87:307-311.

19. Modlin M. 1967. The aetiology of renal stone: A new concept arising from studies on a stone-free population. *Ann Roy Coll Surg Engl* 40:155-178.

20. Rodgers AL. 1999. Aspects of calcium oxalate crystallization: theory, in vitro studies, and in vivo implementation. *J Am Soc Nephrol* 10:S351-S354.

21. Rodgers AL and Lewandowski S. 2002. Effects of 5 different diets on urinary risk factors for calcium oxalate kidney stone formation: evidence of different renal handling mechanisms in different race groups. *J Urol* 168:931-936.

22. Ryall RL, Chauvet MC and Grover PK. 2001: A space oddity. 2001. In: Kok DJ, Romijn HC, Verhagen PCMS, and Verkoelen CF, editors. Eurolithiasis: 9th European Symposium on Urolithiasis. Shaker Publishing, Netherlands, 273-274.

23. Ryall RL, Fleming DE, Grover PK, Chauvet M, Dean CJ, and Marshall VR. 2000. The hole truth: intracrystalline proteins and calcium oxalate kidney stones. *Mol Urol* 4:391-402.

24. Ryall RL, Grover PK, Stapleton AMF, Barrell DK, Tang Y, Moritz RL, and Simpson RJ. 1995. The urinary F1 activation peptide of human prothrombin is a potent inhibitor of calcium oxalate crystallization in undiluted human urine in vitro. *Clin Sci* 89:533-541.

25. Ryall RL, Harnett RM, Hibberd CM, Edyvane KA, and Marshall VR. 1991. Effects of chrondriotin sulphate, human serum albumin and Tamm-Horsfall mucoprotein on calcium oxalate crystallisation in undiluted human urine. *Urol Res* 19:181-188.

26. Ryall RL, Hibberd CM, and Marshall VR. 1985. A method for studying inhibitory activity in whole urine. *Urol Res* 13:285-289.

27. Scurr DS and Robertson WG. 1986. Modifiers of calcium oxalate crystallisation found in urine. III. Studies on the role of Tamm-Horsfall mucoprotein and of ionic strength. *J Urol* 136:505-507.

28. Wesson JA, Worcester EM, Weissner JH, Mandel NS, and Kleinman JG. 1998. Control of calcium oxalate crystal structure and cell adherence by urinary macromolecules. *Kidney Int* 33:952-957.

29. Whalley NA, Moraes MFBG, Shar TG, Pretorius SS, and Meyers AM. 1998. Lithogenic risk factors in the urine of black and white subjects. *Br J Urol* 82:785-790.

CHAPTER 6: URINARY & INTRACRYSTALLINE PROTEINS

6.1 INTRODUCTION

Earlier chapters in this thesis have described the isolation of UPTF1 from the urine of white and black South Africans, and its comprehensive characterisation (chapter 4) and testing in inhibitory activity studies (chapter 5). These investigations offered insight into the possible contribution of this urinary protein plays in the black population's relative protection from kidney stone disease.

The crystallisation inhibitor theory of stone formation suggests that the presence of certain ions, macromolecules or proteins in the urine of healthy individuals prevents the formation of stones (Robertson and Nordin 1982, Worcester 1996, Ryall 1997). An adjunct to this theory is that an abnormality in one of these inhibitors or its diminished expression may contribute to the precipitation of stone-forming salts and the resulting diseased state in stone-formers.

Thus a further area that warranted evaluation was the urinary concentration of UPTF1, and other proteins, as well as the amounts of protein associated with CaOx urine crystals in the two population groups. White stone-formers were included as a third group in this investigation.

6.2 METHODS

6.2.1 Urine treatment

Twenty-four hour urine samples were collected in plastic bottles containing a boric acid preservative from subjects on their free unrestricted diets. Ten subjects were healthy males (19 - 26 years) with no previous history of kidney stones (five white, five black). A further five subjects were white CaOx stone-formers (35 – 50 years). All of these had either passed a stone or had one surgically removed during the six months prior to commencement of the study. The urine samples from these three groups are abbreviated as WC, BC and WSF, respectively. Each urine was tested for haematuria and infection, filtered and aliquots retained

for urinalysis as previously described (paragraph 2.2.1, page 26). Urine composition data was analysed statistically by ANOVA and the results considered statistically significant if $p \leq 0.05$. Average values and SE are reported.

6.2.2 Crystal preparation

The CaOx MSL of each urine was determined as outlined before (Ryall *et al.* 1985; paragraph 2.2.7, page 32). Urines were then placed in glass beakers covered with parafilm and incubated at 37 ^{0}C with agitation (100 rpm). Thereafter, CaOx crystallisation was induced by the dropwise addition of a NaOx load (30.0 mmol/l in excess of the MSL, 0.1 ml NaOx per 100 ml urine) at 0 and 1 hour. After a further hour, the precipitated crystals were collected by filtration (0.22 µm) and washed thoroughly with distilled water to remove surface-bound proteins and extraneous urine (Ryall *et al.* 2001). A glass rod was used to remove crystals that had settled on the bottom of the beakers and the rod was rinsed thoroughly with distilled water. Crystals were dried at 37 ^{0}C for at least 30 minutes, collected from the filter paper using a metal spatula and stored in glass vials at -20 ^{0}C for later use.

6.2.3 Characterisation of urine crystals

The hydrate composition of each subject's CaOx urine crystals was identified by XRD (described in paragraph 2.2.2.1 on page 27). A sample (0.1 mg) of each was also set aside for examination using a scanning electron microscope. In this regard, crystal suspensions (0.1 - 1 mg) were prepared in plastic eppendorf tubes with distilled water (1 µg/µl) and immediately filtered onto a 0.22 µm filter paper followed by washing with 2 ml of distilled water. Filter papers were dried at 37 ^{0}C for 30 minutes and glued onto aluminium stubs and then treated as described previously (paragraph 2.2.2.3, page 28).

6.2.4 Preparation of urine and crystals for protein analysis

An aliquot (5 ml) of each urine sample was dialysed (10 kDa cut-off) extensively against distilled water and freeze-dried for analysis by SDS-PAGE and Western blotting. A sample of the CaOx crystals (10 - 20 mg) obtained from each subject was demineralised by the addition of 0.25 mol/l EDTA (pH 8.0) (1 ml per 10 mg) with stirring for 30 minutes. The resulting solution was then centrifuged at 11000 *g* for 2 minutes and the supernatant was loaded onto a P2 BioGel desalting column. Fractions were collected at 4-minute intervals and the absorbance measured at 280 nm. The first peak eluted from the column corresponded to the

protein content of the crystals; this was freeze-dried in a plastic eppendorf tube. Proteins from the urine and crystal samples were stored at -20 ^{0}C for later use.

6.2.5 SDS-PAGE

Protein samples derived from urine (0.3 - 0.5 ml) and CaOx crystals (0.9 - 2.7 mg) were dissolved in the minimum amount of distilled water and diluted 1:4 with 5x SDS reducing buffer. The proteins were resolved using 15 % polyacrylamide gels and visualised by silver staining (described in paragraph 3.2.3.1, page 49). A lower percentage of bis-acrylamide (0.2 %) was used for the WSF gels compared with the WC and BC gels (1.8 %).

6.2.6 Western blotting

Protein samples derived from urine (1 ml) and CaOx crystals (1.8 - 5.4 mg) were resolved by SDS-PAGE and transferred onto nitrocellulose membranes for immunodetection as previously described (paragraph 3.2.3.2, page 50). The primary antibody used was a rabbit anti-human PT antibody (DakoCytomation, Glostrup, Denmark) at a dilution of 1:500 with a secondary rabbit antibody (Amersham Biosciences, New Jersey, USA) at a dilution of 1:1000.

6.3 RESULTS

6.3.1 Urine composition

The average urine composition (mmol/24hr) and physicochemical data of specimens from white and black control subjects and white stone-formers are presented in Table 6.1. The values for each 24-hour urine are given in Appendix E (WC: Table E1, page A55; BC: Table E2, page A55; WSF: Table E3, page A56). Attention is drawn to the significantly lower urinary pH, and the higher creatinine and sodium excretions of the white stone-formers compared with the white control subjects ($p < 0.05$). However, the creatinine levels were all within the accepted normal range recorded in South Africa (personal communication: PathCare, Cape Town, South Africa).

Table 6.1: Average urine composition (mmol/24hr) and physicochemical parameters of white and black control subjects and white stone-formers (n=5)

Variables	WC average ± SE	BC average ± SE	WSF average ± SE	p-value: WC vs. BC	p-value: WC vs. WSF
pH	6.40 ± 0.120	6.29 ± 0.120	5.88 ± 0.120	NS	< 0.05
Volume (ml/24hr)	1076 ± 359	1246 ± 359	1877 ± 359	NS	NS
Metastable limit (mmol/l)	60 ± 22	63 ± 22	66 ± 22	NS	NS
Calcium (mmol/24hr)	3.73 ± 0.585	3.15 ± 0.585	5.46 ± 0.585	NS	NS
Chloride (mmol/24hr)	122 ± 28.0	160 ± 28.0	153 ± 28.0	NS	NS
Citrate (mmol/24hr)	2.10 ± 0.442	2.32 ± 0.442	2.77 ± 0.442	NS	NS
Creatinine (mmol/24hr)	14.3 ± 1.73	17.7 ± 1.73	18.1 ± 1.73	NS	< 0.05
Magnesium (mmol/24hr)	2.79 ± 0.629	2.73 ± 0.629	3.69 ± 0.629	NS	NS
Oxalate (mmol/24hr)	0.17 ± 0.0355	0.20 ± 0.0355	0.16 ± 0.0355	NS	NS
Phosphate (mmol/24hr)	27.4 ± 6.27	30.4 ± 6.27	33.8 ± 6.27	NS	NS
Potassium (mmol/24hr)	53.3 ± 8.84	41.4 ± 8.84	51.5 ± 8.84	NS	NS
Sodium (mmol/24hr)	62.0 ± 38.2	82.4 ± 38.2	248 ± 38.2	NS	< 0.05
Sulphate (mmol/24hr)	16.0 ± 3.90	18.0 ± 3.90	19.3 ± 3.90	NS	NS
Uric acid (mmol/24hr)	3.84 ± 0.521	3.6 ± 0.521	4.5 ± 0.521	NS	NS
RS Brushite	2.03 ± 0.300	1.27 ± 0.300	1.06 ± 0.300	NS	NS
RS Calcium oxalate	4.10 ± 0.867	3.62 ± 0.867	2.74 ± 0.867	NS	NS
RS Uric acid	1.10 ± 0.627	1.11 ± 0.627	3.09 ± 0.627	NS	NS

RS: Relative supersaturation; NS: not significant, i.e. $p > 0.05$

6.3.2 X-ray powder diffraction

The XRD patterns of crystals precipitated from each subject's urine sample along with the d-spacings (Å) of the prominent peaks is shown in Appendix E (WC: Figure E1.1 - E1.5, page A60; BC: Figure E2.1 - E2.5, page A61; WSF: Figure E3.1 - E3.5, page A62). The assignment of these peaks to particular CaOx hydrates and the corresponding estimated percentage hydrate composition of the crystals is tabulated in Appendix E (WC: Table E4, page A57; BC: Table E5, page A58; WSF: Table E6, page A59).

The CaOx hydrate composition of each subject's crystals is presented in Table 6.2

Table 6.2: Estimated hydrate composition of CaOx crystals precipitated from the urine of white and black control subjects and white stone-formers

Subject number	White subjects:		Black subjects:		White stone-formers:	
	% COM	*% COD*	*% COM*	*% COD*	*% COM*	*% COD*
1	40	60	0	100	35	65
2	0	100	50	50	70	30
3	0	100	100	0	0	100
4	0	100	60	40	0	100
5	0	100	30	70	65	35

Pure COD crystals precipitated in four of the urines from white control subjects. On the other hand, mixtures of COM and COD were the characteristic feature of crystals that precipitated from the urines of black subjects and white stone-formers.

6.3.3 Scanning electron microscopy

Figure 6.1 shows scanning electron micrographs of urine crystals obtained from five white control subjects. The predominance of bipyramidal-shaped COD crystals is clearly evident here. In fact, only one subject's urine precipitated disc-shaped COM crystals, namely WC1 (Figures 6.1.1 - 6.1.2). The COD crystals from these subjects typically ranged in diameter from 10 - 25 μm; the diameter of COM observed in WC1 was 5 - 10 μm.

Figure 6.1: Scanning electron micrographs of CaOx crystals from the urine of white control subjects. The crystals are from the following subjects: WC1, mag 8.0K (Fig 6.1.1) and mag 11K (Fig 6.1.2); WC2, mag 3.94K (Fig 6.1.3); WC3, mag 3.0K (Fig 6.1.4); WC4, mag 8.0K (Fig 6.1.5); and WC5, mag 4.05K (Fig 6.1.6).

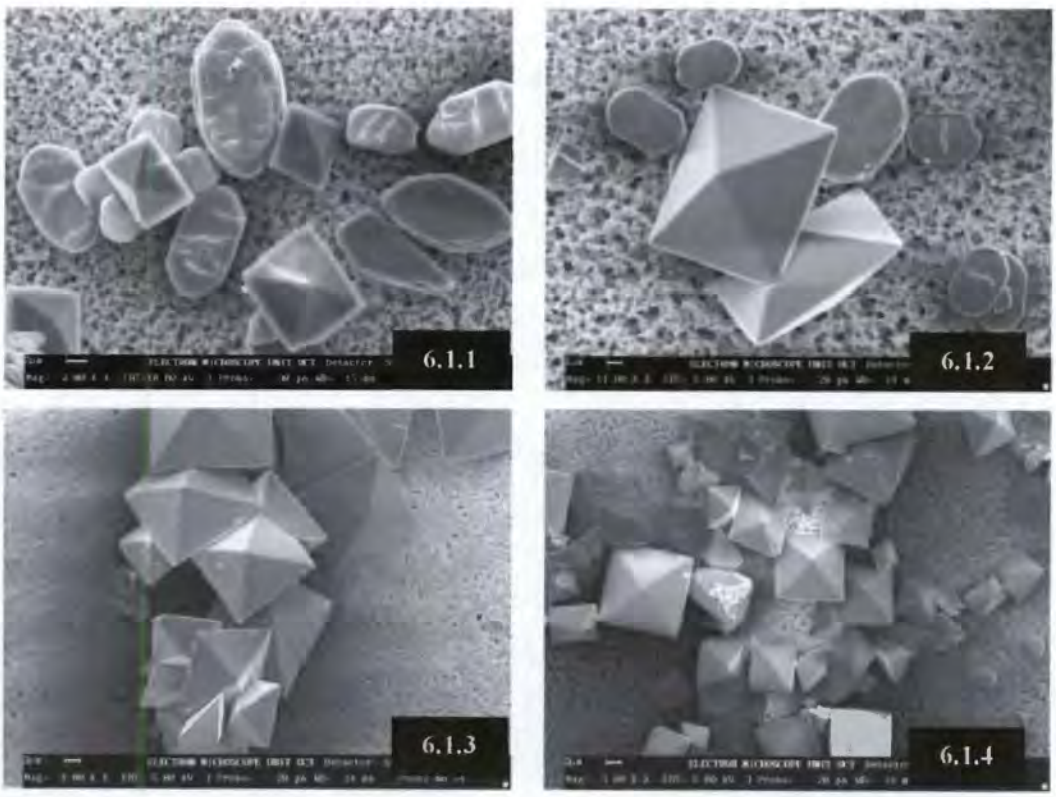

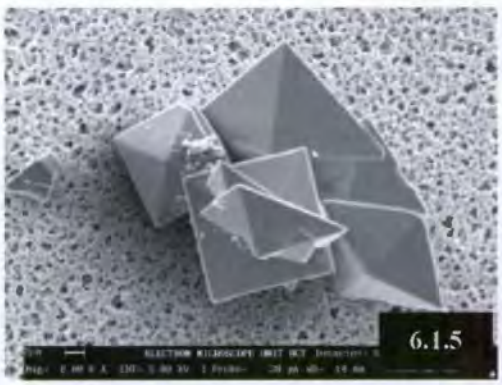

The crystals precipitated from the urine of five black control subjects are shown in Figure 6.2 below. Attention is drawn to the mixture of disc-shaped COM and bipyramidal COD crystals in this control group's urine. The exception to this trend was BC1 whose crystals were composed almost exclusively of COD (Figure 6.2.1) with a few very large plate-like trihydrate crystals (Figure 6.2.2). This CaOx hydrate is seldom observed in urine and thus its observation here is noted with interest. The size range of COM crystals typically ranged from 5 – 10 μm in diameter compared with an average diameter of 10 μm for the COD crystals. Only BC5 had larger COD crystals, which averaged 22 μm in diameter (Figure 6.2.6).

Figure 6.2: Scanning electron micrographs of CaOx crystals from the urine of black control subjects. The crystals are from the following subjects: BC1 at mag 9.0K (Fig 6.2.1) and mag 4.5K (Fig 6.2.2); BC2 at mag 6.0K (Fig 6.2.3); BC3 at mag 8.0K (Fig 6.2.4); BC4 at mag 6.12K (Fig 6.2.5); and BC5 at mag 4.0K (Fig 6.2.6).

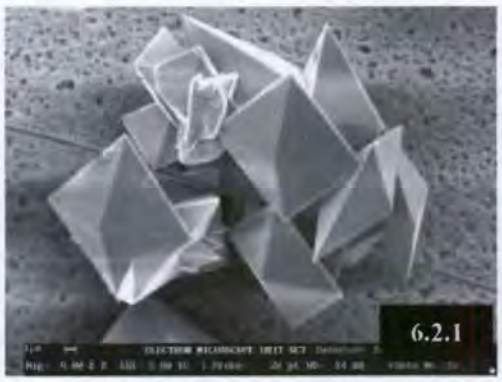

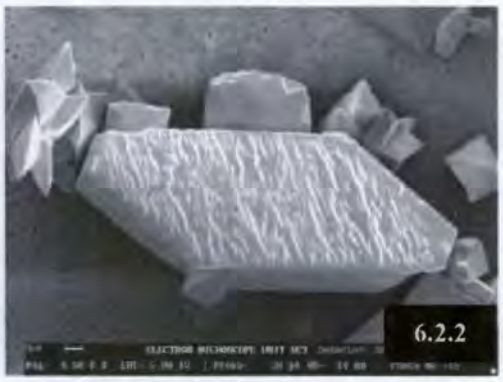

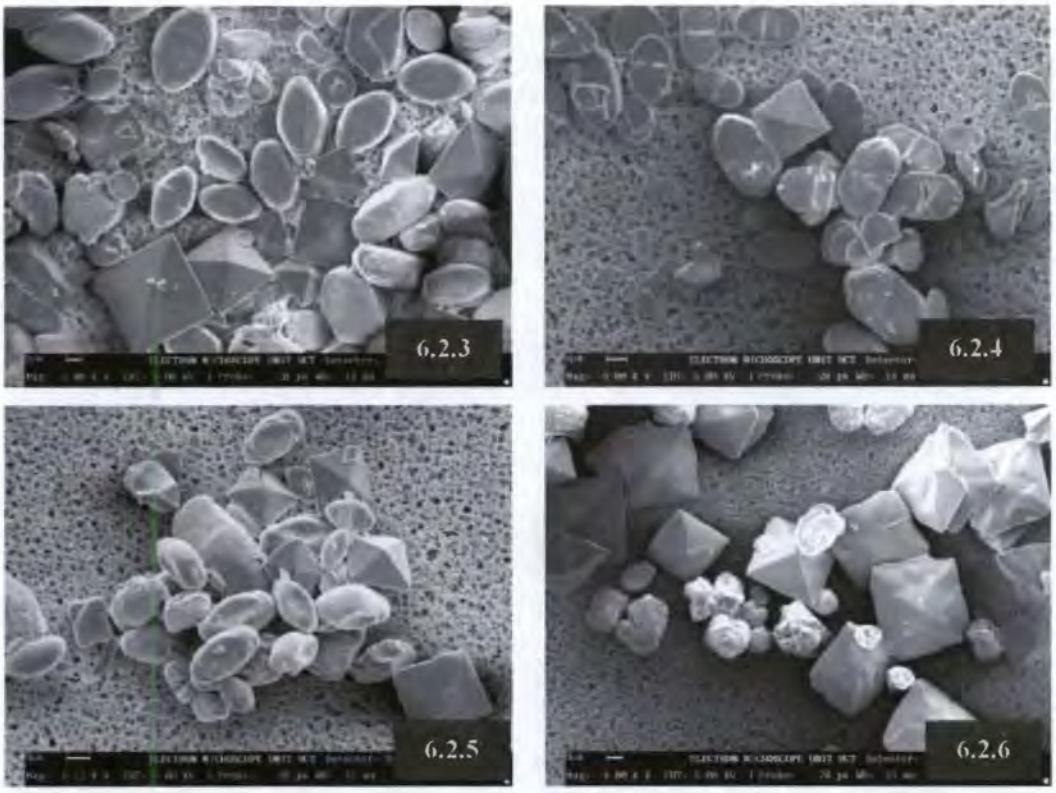

Scanning electron micrographs of urine crystals obtained from five white stone-formers are shown in Figure 6.3 below. The trend observed in these subjects' urines was towards the presence of mainly bipyramidal-shaped COD crystals, although a significant number of disc-shaped COMs were also observed in WSF1 (Figures 6.3.1 - 6.3.2), WSF2 (Figures 6.3.3) and WSF5 (Figures 6.3.7 - 6.3.8). Several large, tightly packed COD aggregates were observed in WSF4's sample as shown in a survey view of the stub (Figure 6.3.5). A close-up of these unusual aggregates is shown in Figure 6.3.6. The size of COM crystals typically ranged from 6 - 8 μm in diameter compared with an average diameter of 10 - 15 μm for the COD crystals. One stone-former (WSF1) had significantly larger COD crystals with an average diameter of 22 μm (Figures 6.3.1 – 6.3.2).

Figure 6.3: Scanning electron micrographs of CaOx crystals from the urine of white stone-formers. The crystals are from the following subjects: WSF1 at mag 7.7K (Fig 6.3.1) and mag 4.0K (Fig 6.3.2); WSF2 at mag 5.0K (Fig 6.3.3); WSF3 at mag 5.0K (Fig 6.3.4); WSF4 at mag 1.0K (Fig 6.3.5) and mag 4.0K (Fig 6.3.6); and WSF5 at mag 5.0K (Fig 6.3.7) and mag 6.0K (Fig 6.3.8).

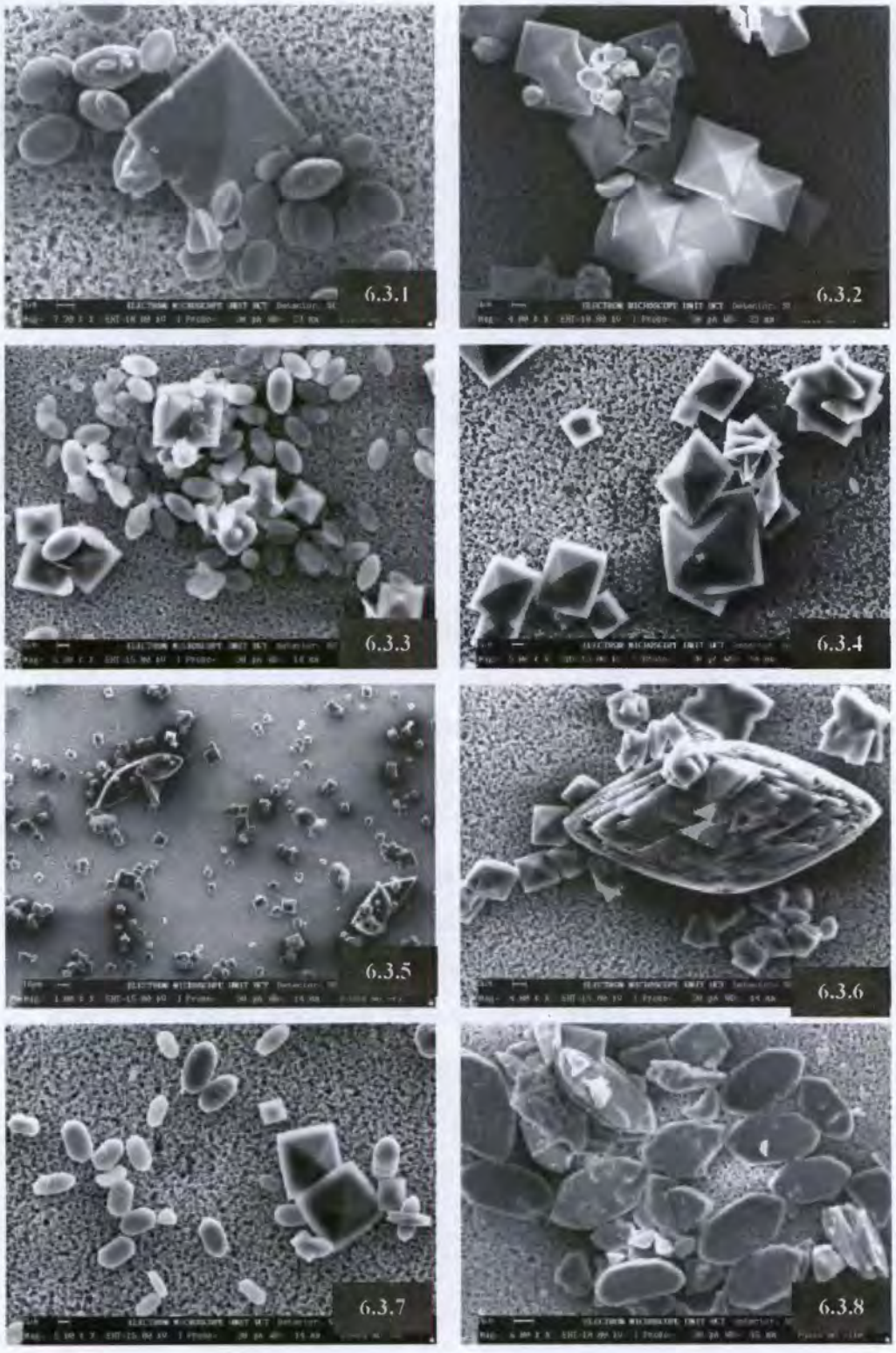

6.3.4 Protein analysis

6.3.4.1 White control subjects

The desalting chromatograms of demineralised crystals prepared from the urine of white control subjects are shown in Appendix E (Figures E4.1 – E4.5, page A63). The first peak in each chromatogram corresponds to the protein content of the crystals (confirmed by SDS-PAGE) while the second peak is the salt content (partly from the EDTA solution used for demineralisation and partly from the crystals themselves).

The SDS-PAGE of urine samples from white control subjects and the crystals precipitated from each of these samples are shown in Figures 6.4.1 and 6.4.2, respectively. The urine samples contained several proteins over a wide range of molecular weights, in contrast to the crystals which contained fewer proteins all of which were 31 kDa and larger.

Figure 6.4: SDS-PAGE of urine and CaOx urinary crystals from white control subjects. Samples were separated through a 15% polyacrylamide, 1.8% bisacrylamide SDS-PAGE. ***Figure 6.4.1.*** The patterns were obtained from urine samples as shown, *MW:* low molecular weight standard; *1:* WC1 (0.5 ml); *2:* WC2 (0.5 ml); *3:* WC3 (0.5 ml); *4:* WC4 (0.5 ml); *5:* WC5 (0.5 ml). ***Figure 6.4.2.*** The patterns were obtained from CaOx urinary crystals as shown, *MW:* low molecular weight standard, *1:* WC1 (0.9 mg); *2:* WC2 (2.7 mg); *3:* WC3 (2.7 mg); *4:* WC4 (2.7 mg); *5:* WC5 (2.7 mg); *F1:* 0.5 μg UPTF1.

Figure 6.4.1

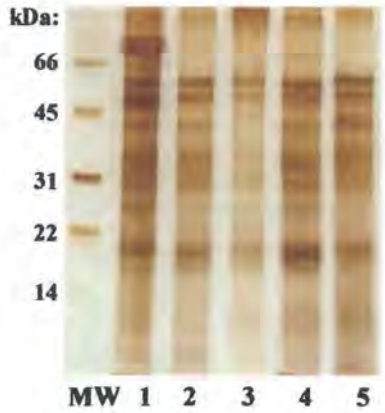

Figure 6.4.2

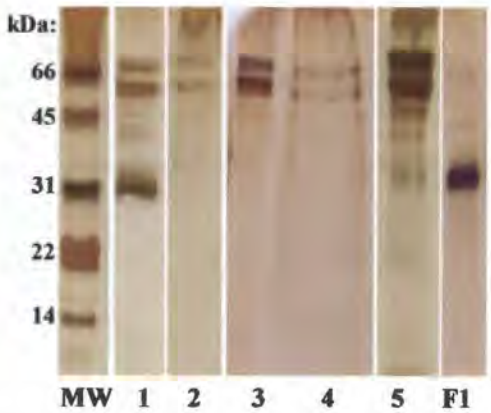

Six major bands were seen in all the urine samples with molecular weights of 18, 34, 40, 48, 53 and 58 kDa (lanes 1 - 5). In addition to these, a broad and intense band at 65 kDa was observed in WC1's urine (lane 1), which was very faint in the other control subjects. This might correspond to albumin, one of the most abundant urinary proteins. Different intensities

of the six bands were observed amongst the five subjects, with the most intense bands observed in WC1 (lane 1) and the least intense bands in WC3 (lane 3). Two additional and very faint bands below 14 kDa were found in all of the urines.

The CaOx crystals precipitated from these urines all contained significant amounts of two proteins, one at 57 and the other at 62 kDa with varying intensities (lanes 1 - 5). These bands were most prominent in the crystals from WC5 (lane 5). A third band at 32 kDa (lane 1) was observed in WC1's crystals, which had the same relative mobility as the UPTF1 standard in lane F1.

Western blots of the urine samples and CaOx crystals with a PT antibody are shown in Figure 6.5.1 and Figure 6.5.2, respectively. Four of the five white control subjects (lanes 1, 3 - 5) have a similar amount of a 31 kDa band in their urine. This band corresponds to UPTF1 as confirmed by the UPTF1 standard (Figure 6.5.2, lane F1). The fifth subject's urine contained considerably less of this band (lane 2). Comparison of the intensity of the UPTF1 bands in the urine samples with the 0.5 μg UPTF1 standard (Figure 6.5.2, lane F1) suggests that the urine samples contain approximately 0.1 μg/ml UPTF1, although this could not be quantified from the gel.

Figure 6.5: Western blot of urine and CaOx urinary crystals from white control subjects immunoblotted for prothrombin. ***Figure 6.5.1.*** The patterns were obtained from urine samples as shown, *1:* WC1 (1 ml); *2:* WC2 (1 ml); *3:* WC3 (1 ml); *4:* WC4 (1 ml); *5:* WC5 (1 ml). ***Figure 6.5.2.*** The patterns were obtained from CaOx urinary crystals as shown, *1:* WC1 (1.8 mg); *2:* WC2 (5.4 mg); *3:* WC3 (5.4 mg); *4:* WC4 (5.4 mg); *5:* WC5 (5.4 mg); *F1:* 0.25 μg UPTF1.

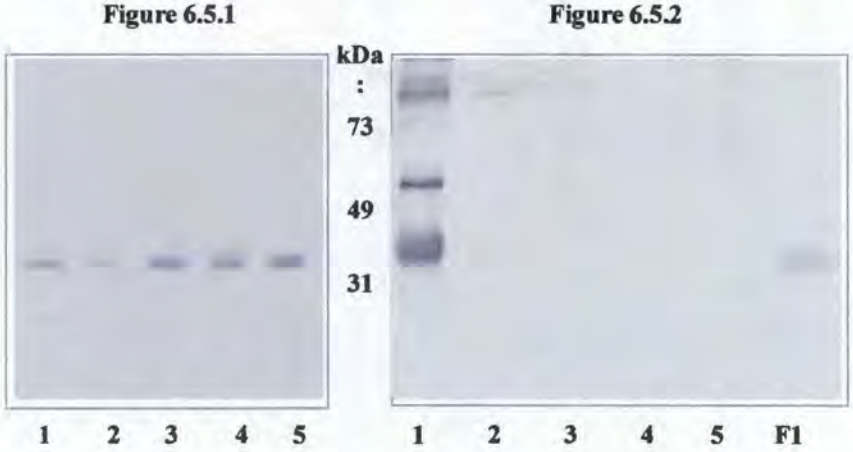

6.3.4.2 Black control subjects

The desalting chromatograms of demineralised crystals prepared from the urine of black control subjects are shown in Appendix E (Figures E5.1 – E5.5, page A64). The first peak in each chromatogram corresponds to the protein content of the crystals (confirmed by SDS-PAGE) while the second peak is the salt content (partly from the EDTA solution used for demineralisation and partly from the crystals themselves).

Figures 6.6.1 and 6.6.2 show the SDS-PAGE of urine samples and their corresponding crystals obtained from five black control subjects. As observed in the white control samples, fewer proteins were included in the CaOx crystals than were observed in the urine samples, although this distinction is less apparent in the black control subjects.

Figure 6.6: SDS-PAGE of urine and CaOx urinary crystals from black control subjects. Samples were separated by 15% polyacrylamide, 1.8% bisacrylamide SDS-PAGE. ***Figure 6.6.1.*** The patterns were obtained from urine samples as shown, *MW:* low molecular weight standard, *1:* BC1 (0.5 ml); *2:* BC2 (0.5 ml); *3:* BC3 (0.5 ml); *4:* BC4 (0.5 ml); *5:* BC5 (0.5 ml). ***Figure 6.6.2.*** The patterns were obtained from CaOx urinary crystals as shown, *MW:* low molecular weight standard, *1:* BC1 (0.9 mg); *2:* BC2 (2.7 mg); *3:* BC3 (2.7 mg); *4:* BC4 (2.7 mg); *5:* BC5 (2.7 mg);

Figure 6.6.1

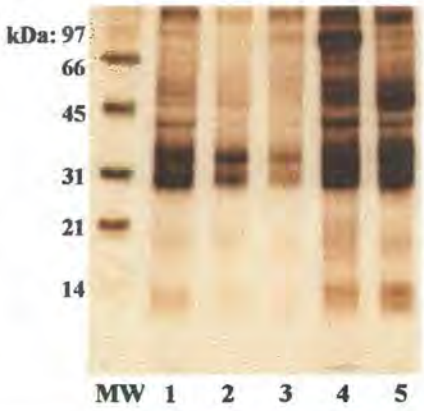

Figure 6.6.2

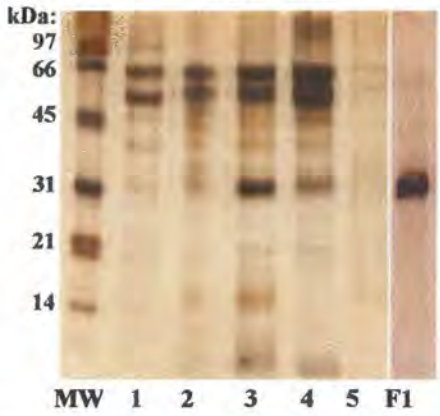

The same molecular weight bands were observed in the black controls' urine as for the whites, namely at 18, 34, 40, 48, 53, 58 and 65 kDa (lanes 1 - 5). The intensities of all of these bands differed considerably amongst the five subjects. The two bands most prominent in all of the urine samples were at 34 and 40 kDa.

The CaOx crystals precipitated from these urines all contained significant amounts of three bands at 34, 54 and 60 kDa with varying intensities (Figure 6.6.2, lanes 1 - 5). Very little

protein was included in BC5's crystals and it is likely that insufficient crystallisation occurred to allow for inclusion of protein. These three bands were most prominent in the crystals from WC5 (lane 5). The 34 kDa bands (most prominent in BC3, lane 3, and BC 4, lane 4) had the same relative mobility as the UPTF1 standard in lane F1.

Western blots of the urine samples and CaOx crystals with a PT antibody are shown in Figure 6.7.1 and Figure 6.7.2, respectively. Three of the five black control subjects (lanes 3 - 5) had a similar amount of a 31 kDa band in their urine. This band corresponds with the UPTF1 standard in lane F1 (Figure 6.7.1). One subject had a considerably higher amount of urinary UPTF1 (BC1, lane 1) while another had significantly less (BC2, lane 2). The intensity of the UPTF1 bands suggests that the urine samples contain approximately 0.1 μg/ml UPTF1 (*i.e.* lanes 3 - 5), but two- to three-fold more in some samples (lane 1). These estimates could not be quantified from the gel. A second band below UPTF1 was also observed in BC1 (lane 1) and BC4 (lane 4) probably due to degradation of UPTF1, possibly during sample processing.

Three of the subjects' crystals contained a 31 kDa band corresponding to UPTF1 (BC2 - 4, lanes 2 - 4). The amount in BC3's crystals was significantly higher than the other two subjects. Faint bands at 49 and 73 kDa corresponding to PTF1+2 and PT were also observed in BC2 and BC3's crystals.

Figure 6.7: Western blot of urine and CaOx urinary crystals from black control subjects immunoblotted for prothrombin. ***Figure 6.7.1.*** The patterns were obtained from urine samples as shown, *1:* BC1 (1 ml); *2:* BC2 (1 ml); *3:* BC3 (1 ml); *4:* BC4 (1 ml); *5:* BC5 (1 ml); *F1:* 0.5 μg UPTF1. ***Figure 6.7.2.*** The patterns were obtained from CaOx urinary crystals as shown, *1:* BC1 (1.8 mg); *2:* BC2 (1.8 mg); *3:* BC3 (1.8 mg); *4:* BC4 (1.8 mg); *5:* BC5 (1.8 mg).

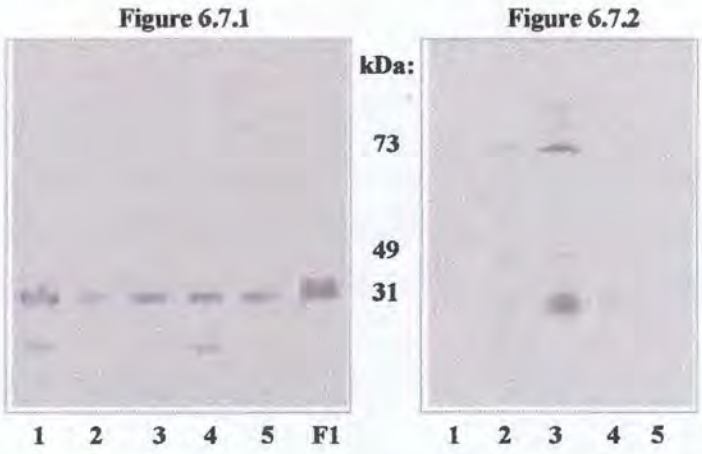

6.3.4.3 White stone-formers

The desalting chromatograms of demineralised crystals prepared from the urine of white stone-formers are shown in Appendix E (Figures E6.1 – E6.5, page A65). The first peak in each chromatogram corresponds to the protein content of the crystals (confirmed by SDS-PAGE) while the second peak is the salt content (partly from the EDTA solution used for demineralisation and partly from the crystals themselves).

The SDS-PAGE of five white stone-formers' urine samples and the CaOx crystals precipitated from these urines is shown in Figures 6.8.1 and 6.8.2, respectively. As in the control subjects' urine, similar patterns were observed amongst the individuals but with differing intensities of any given band. The major bands were observed at 20, 48, 53 and 59 kDa with a broad area containing several bands at 28 - 41 kDa (lanes 1 - 4). The most noteworthy feature of the urines' protein patterns was the relative abundance of the protein at 59 kDa which was equally evident in all of the white stone-formers' samples, possibly corresponding to albumin.

Figure 6.8: SDS-PAGE of urine and CaOx urinary crystals from white stone-formers. Samples were separated through a 15% polyacrylamide, 0.2% bisacrylamide SDS-PAGE. ***Figure 6.8.1.*** The patterns were obtained from urine samples as shown, *MW:* low molecular weight standard; *1:* WSF1 (0.3 ml); *2:* WSF2 (0.3 ml); *3:* WSF3 (0.3 ml); *4:* WSF4 (0.3 ml). ***Figure 6.8.2.*** The patterns were obtained from CaOx urinary crystals as shown, *MW:* low molecular weight standard; *1:* WSF1 (1.8 mg); *2:* WSF2 (0.9 mg); *3:* WSF3 (0.9 mg); *4:* WSF4 (1.8 mg); *5:* WSF5 (1.8 mg); *F1:* 1 µg UPTF1.

Figure 6.8.1

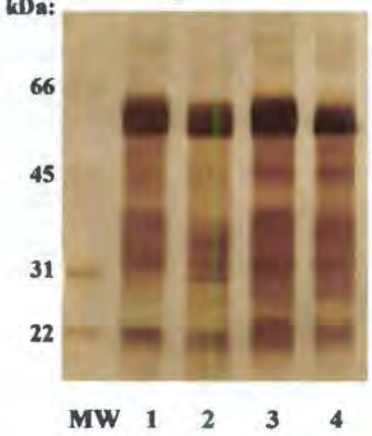

Figure 6.8.2

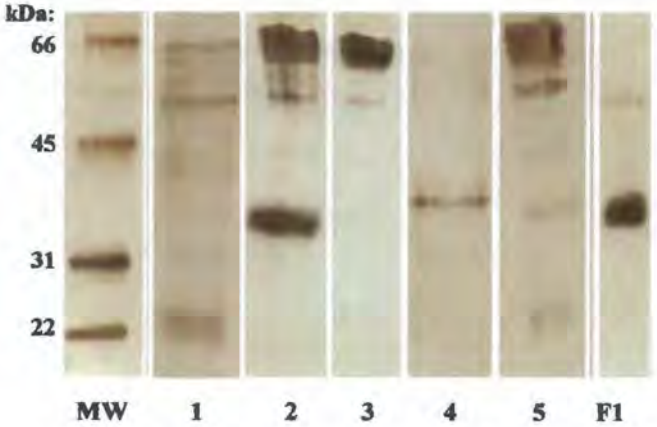

A significantly fewer number of proteins were included into the crystals (Figure 6.8.2) than their corresponding urine samples. Four of the five subjects' crystals contained bands at 58 and 68 kDa (WSF1 in lane 1, WSF2 in lane 2, WSF3 in lane 3, WSF5 in lane 5). All of

these except for WSF1 also had a prominent band at 65 kDa. These were the most prominent and characteristic of the white stone-formers' crystals. A 38 kDa band with the same mobility as the UPTF1 standard in lane F1 was observed in two of the subject's crystals (WSF2 in lane 2, WSF5 in lane 5). Two subjects had faint bands at 20 and 23 kDa (WSF1 in lane 1, WSF5 in lane 5). WSF4 had a different protein pattern to the other stone-formers with a single band at 41 kDa.

Figures 6.9.1 and 6.9.2 show Western blots of the urine samples and CaOx crystals using a PT antibody. All four stone-formers' urine (lanes 1 - 4) contained a similar amount of a 31 kDa band which corresponds with the UPTF1 standard (lane F1). Based on the intensity of these bands, the quantity or UPTF1 is approximately 0.1 μg. A notable feature of the urine blot was the presence of intense bands at a high molecular weight. These may indicate the presence of PT aggregates. Three subjects had faint bands at 73 kDa which correspond to PT (WSF2 in lane 2, WSF3 in lane 3, WSF4 in lane 4). WSF1 had a faint 49 kDa band corresponding to PTF1+2.

All of the subjects' crystals contained a 31 kDa band corresponding to UPTF1 except for WSF1. The crystals from WSF2 and WSF5 contained approximately 1 μg UPTF1 (although this could not be quantified from the gel), while WSF3 and WSF4 had considerably less. Faint bands at 49 and 73 kDa corresponding to PTF1+2 and PT were also observed in WSF2 and WSF5's crystals.

Figure 6.9: Western blot of urine and CaOx urinary crystals from white stone-formers immunoblotted for prothrombin. ***Figure 6.9.1.*** The patterns were obtained from urine samples as shown, *1:* WSF1 (1 ml); *2:* WSF2 (1 ml); *3:* WSF3 (1 ml); *4:* WSF4 (1 ml); *F1:* 0.25 μg UPTF1. ***Figure 6.9.2.*** The patterns were obtained from CaOx urinary crystals as shown, *1:* WSF1 (3.6 mg); *2:* WSF2 (3.6 mg); *3:* WSF3 (3.6 mg); *4:* WSF4 (3.6 mg); *5:* WSF5 (3.6 mg).

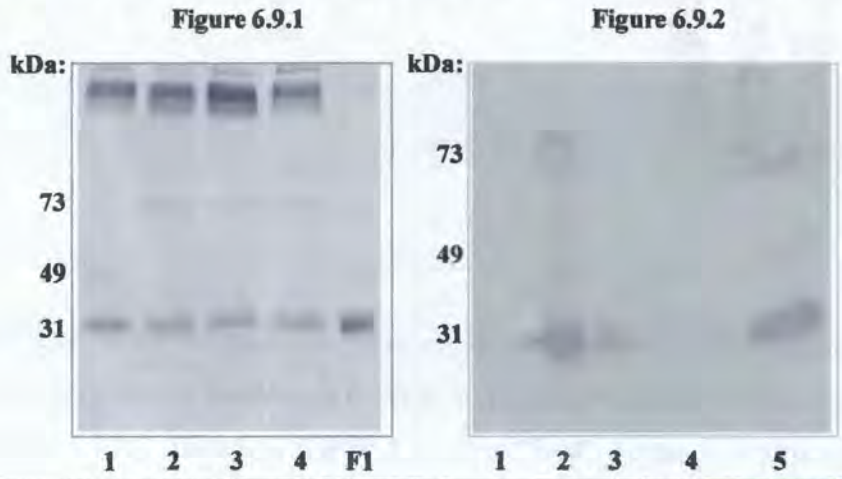

6.4 DISCUSSION

Many investigators have compared healthy and stone-forming subjects in an attempt to find factors that distinguish the two groups and thereby identify potential markers of stone formation. These studies have focused on two areas. The first area is that of urinary physicochemical parameters and the ability of urine to inhibit crystallisation. Lower urinary MSL (Ryall *et al.* 1986, Asplin *et al.* 1999), higher levels of urinary supersaturation, and reduced inhibition of COM aggregation (Tiselius *et al.* 1995) have been reported amongst male stone-formers compared with control subjects. All of these trends indicate a relatively higher risk in the former group. Growth inhibition appears to be the same in the two groups (Porile *et al.* 1996, Worcester 1996), although some differences have been reported. However, these differences were less consistently observed amongst stone formers than the different effects on aggregation inhibition (Tiselius *et al.* 1995). Robertson and Nordin (1982) reported larger particle sizes in the urine of stone-formers. However, a later study by Ryall and co-workers found the same crystals sizes in healthy and stone-forming subjects after addition of the same standard oxalate load in excess of their respective MSL (Ryall *et al.* 1986). These apparent discrepancies may be due to differences in methodology.

Secondly, studies have investigated the role of urinary proteins and in particular their relative concentrations and inhibitory properties. Reduced growth inhibition (Asplin *et al.* 1999) by stone-formers' urine proteins has been reported, as well as reduced inhibitory activity by THM (Hess *et al.* 1989) and nephrocalcin (Hess *et al.* 1989, Nakagawa *et al.* 1987) isolated from stone-formers' urine. However, conflicting results with respect to the relative amounts of protein in urine and crystal extracts have been reported. These results will be discussed in detail later.

Urine composition data in the present study indicated that the white stone-formers had a significantly lower urinary pH and a higher sodium excretion than the white control subjects. The stone-formers' lower urinary pH is surprising since an elevated urinary pH is usually regarded as risk factor for CaOx stones (Robertson and Nordin 1982). The raised urinary sodium of this group is, however, consistent with a report that increased dietary salt resulted in a greater risk of CaOx stone formation (Sakhaee *et al.* 1993). The concomitant elevation in ionic strength amongst stone-formers may have influenced the conformation and binding of urinary proteins in this group. The small sample sizes in the present study, however, prescribe that the urine composition results not be over interpreted.

In the present study, a consistent trend was observed in all urine samples. Six dominant proteins were observed in the 14 - 70 kDa molecular weight range. However, there was some variation in the relative amount of the proteins present. The distinctive major protein components amongst the three groups are noteworthy. Amongst the white subjects, no single protein was clearly dominant. In contrast, the 34 and 40 kDa bands were markedly more intense than the other protein bands in the black subjects. The identity of these proteins is unknown and requires further investigation. In the white stone-formers' urines, the 59 kDa band was the most prominent and may correspond to albumin. SDS-PAGE suggested that more total protein per millilitre of urine was observed in white stone-formers than in their control group, although this could not be quantified from the gels. Some black subjects' urine appeared to contain more total protein than the white subjects, although there was more intra-group variation amongst the former group. It is likely that in all subjects, filtration of their urine samples reduced the amount of albumin as well as selectively removing THM (Atmani *et al.* 1998). These two proteins are usually observed at approximately 66 and 80 kDa, respectively, on SDS-PAGE.

Several recent studies have reported comparative urinary protein expressions between controls and stone-formers. Hedgepeth *et al.* (2001) measured the relative density of inter-α-trypsin inhibitor trimer (220 – 240 kDa), OPN and PT-related protein bands on Western blots. No difference was found in the expression of UPTF1 from healthy and stone-forming males, in agreement with the present study. In fact, only inter-α-trypsin inhibitor trimer was differentially expressed, with significantly more of this protein in the CaOx stone-formers' urine than the control group. Stapleton reported increased PT expression in stone-formers' kidneys (Stapleton *et al.* 1993), which is consistent with the probable PT aggregation observed in the present study on Western blots of stone-formers' urine. However, lower concentrations of OPN (Yasui *et al.* 1999, Nishio *et al.* 2001) and UPTF1 (Nishio *et al.* 2001) have also been reported amongst stone-formers. There is thus no clear trend in these studies to suggest that a general elevation or lowering of protein expression occurs amongst stone-formers.

The inclination to draw firm conclusions from the urine data is tempered by the difficulties reported with the determination of certain urinary proteins. UPTF1 and OPN bind strongly to CaOx crystals (Ryall *et al.* 2001, Atmani and Khan 2002) and may therefore often be underestimated in urine due to their inevitable association with crystals that form *in vivo* or

after urine collection (Dean *et al.* 2000). Thus, the reliable quantitation of UPTF1 in controls and stone-formers, as well as other intracrystalline proteins, will only be possible once an analytical method has been developed that addresses these difficulties. This suggests that the UPTF1 determination reported by Nishio *et al.* (2001) may be unreliable.

The relative quantities of protein in the different groups are puzzling. On the one hand, the greater amounts of protein in the white stone-formers' urine compared to the white controls suggest a pathogenic role. On the other hand, it is tempting to suggest that higher levels of protein in the black control group relative to the white controls could be indicative of the inhibitory role of proteins. Perhaps the important factor to address is not the relative amounts of total protein, but rather the relative amounts of individual proteins.

Several common features were also noted in the crystal extracts in the present study. SDS-PAGE demonstrated that, with the exception of WSF4, the two protein bands near 57 and 62 kDa were present in all crystal extracts, regardless of the individual or group from which they were derived. These bands are likely to correspond to OPN on the basis of their approximate molecular weights and the similar appearance of these patterns to those obtained in another study in which the protein was identified by Western blotting (chapter 7). Similar protein patterns were observed for the white control and stone-forming subjects' crystals. In both groups, the 57 and 62 kDa bands were the major components, followed by UPTF1. The black control subjects' crystals contained notably more protein bands than the white group. In particular, more crystal extracts from black as opposed to white subjects contained UPTF1.

The prominence of UPTF1 and OPN in CaOx crystal extracts has been reported previously. Atmani and co-workers have demonstrated the presence of PT-related proteins, OPN and albumin as the major crystal components derived from controls and stone-formers (Atmani *et al.* 1996, 1998, Atmani and Khan 2002). Recently, PT-related proteins were shown to predominate in crystals from control subjects, whereas albumin predominated amongst stone-formers' crystals (Atmani and Khan 2002). Whole urine was used for all of these studies. Furthermore, Ryall *et al.* have reported the inclusion of UPTF1 and OPN as the major components of COM and COD crystals extracts, respectively (Ryall *et al.* 2001). The latter study was conducted in filtered urine which explains the absence of albumin reported by Atmani.

Inspection of the relative amounts of the two major intracrystalline protein components, UPTF1 and OPN, suggests a possible relationship between crystal morphology

and the protein(s) included therein, as Ryall has described previously (Ryall *et al.* 2001). For example, the crystals composed of 100 % COD (WC2 – WC5, BC1, WSF3) contained negligible amounts of UPTF1, but relatively large amounts of OPN. In comparison, crystals consisting of higher proportions of COM (BC3, WSF2, WSF5) contained a mixture of the two proteins. The greatest proportion of COD crystals was observed in the white control subjects, followed by the white stone-formers and the black subjects.

The trends with regard to hydrate composition are interesting in light of recent crystal-cell interaction studies in which COM crystals have been shown to attach more readily to renal epithelial cells than COD crystals (Wesson *et al.* 1998). This attachment process is believed to be a possible precursor to stone development since crystals attach to renal cells after exposure to CaOx (Lieske *et al.* 1999). The presence of mainly COD in the urine of white controls as opposed to the presence of COD and COM crystals in white stone-formers is therefore consistent with the diseased state in the latter group. However, the higher percentage of COM crystals in black subjects is inconsistent with the crystal attachment theory and thus does not provide a rational explanation for the black group's apparent immunity. Thus crystal morphology may be associated with other factors that influence the stone-forming potential in this population group. Such factors may relate to the nature and quantity of the proteins which are incorporated into the crystals themselves.

The present data showed the selective inclusion of proteins into CaOx urine crystals, a feature which was first reported by Morse and Resnick (1988) and was also shown in the CME study (chapter 3). At least six major proteins were observed in the three group's urines compared with only two major protein components in the crystal extracts. In particular, a large disparity between the urinary and intracrystalline amounts of UPTF1 was demonstrated by Western blotting. For example, subject WC4 had no detectable intracrystalline UPTF1 compared with approximately 0.5 μg UPTF1 per milligram of CaOx in WC1. These subjects appeared to have comparable urinary concentrations of the protein. This suggests that urinary proteins have different binding affinities for CaOx crystals which direct their inclusion. Thus, a clear distinction between urinary and intracrystalline proteins appears to be crucial to a discussion of the potential role of proteins in stone formation and its possible prevention.

The present study was the first to investigate urinary and intracrystalline proteins in white and black subjects. Urinary levels of UPTF1 amongst black and white control subjects as well as white stone-formers appear to be similar, although accurate and more reliable

quantitation may reveal otherwise. The apparent predominance of different urinary proteins in the three groups warrants further investigation as a possible indicator of their relative stone-forming potentials.

The distinctive CaOx crystal compositions amongst white and black subjects were noteworthy, with a higher proportion of COM crystals in the latter group. This trend appears to correspond to differences in the typical matrix proteins observed and, more specifically, the observation that UPTF1 is more consistently present in the crystals of black subjects than in the urine of white subjects (controls and stone-formers). Since the low stone incidence of stones in South African blacks is an *a priori* fact, it seems reasonable to infer that the afore-mentioned trends play a protective role in the black population. However, the role of COM is not entirely clear since a higher proportion of this hydrate was also observed amongst white stone-formers compared with their control group. Thus, further study of the relationship between crystal morphology and urinary proteins, and their role in stone formation, is required.

6.5 REFERENCES

1. Asplin JR, Parks JH, Chen MS, Lieske JC, Toback FG, Pillay SN, Nakagawa Y, and Coe FL. 1999. Reduced crystallisation inhibition by urine from men with nephrolithiasis. *Kidney Int* 56:1505-1516.

2. Atmani F, Glenton PA, and Khan SR. 1998. Identification of proteins extracted from calcium oxalate and calcium phosphate crystals induced in the urine of healthy and stone forming subjects. *Urol Res* 26:201-207.

3. Atmani F and Khan SR. 2002. Quantification of protein extracted from calcium oxalate and calcium phosphate crystals induced in vitro in the urine of healthy controls and stone-forming patients. *Urol Int* 68:54-59.

4. Atmani F, Opalko FJ, and Khan SR. 1996. Association of urinary macromolecules with calcium oxalate crystals induced in vitro in normal human and rat urine. *Urol Res* 24:45-50.

5. Dean CJ, Macardle P, and Ryall RL. 2000. The effect of the presence of calcium oxalate crystals on the measurement of prothrombin fragment 1 in urine. In: Rodgers AL, Hibbert BE, Hess B, Khan SR, and Preminger GM, editors. Urolithiasis 2000. University of Cape Town, Cape Town, 150-152.

6. Grover PK and Ryall RL. 1999. Inhibition of calcium oxalate crystal growth and aggregation by prothrombin and its fragments in vitro. *Eur J Biochem* 263:50-56.

7. Hedgepeth RC, Yang L, Resnick MI, and Marengo SR. 2001. Expression of proteins that inhibit calcium oxalate crystallisation in vitro in the urine of normal and stone-forming individuals. *Am J Kid Diseases* 37:104-112.

8. Hess B, Nakagawa Y, and Coe FL. 1989. Inhibition of calcium oxalate monohydrate crystal aggregation in urine proteins. *Am J Physiol* 257:F99-F106.

9. Lieske JC, Deganello S, and Toback FG. 1999. Nucleation, adhesion and internalisation of calcium-containing urinary crystals by renal cells. *J Am Soc Nephrol* 10:S422-S429.

10. Morse RM and Resnick MI. 1988. A new approach to the study of urinary macromolecules as a participant in calcium oxalate crystallization. *J Urol* 139:869-873.

11. Nakagwa Y, Susan M A, Hall S L, Deganello S, and Coe F L. 1987. Isolation from human calcium oxalate renal stones of nephrocalcin, a glycoprotein inhibitor of calcium oxalate crystal growth. Evidence that nephrocalcin from patients with calcium oxalate nephrolithiasis is deficient in gamma-carboxyglutamic acid. *J Clin Inves* 79:782-1787.

12. Nishio S, Hatanaka M, Takeda H, Aoka K, Iseda T, Iwata H, and Yokoyama M. 2001. Calcium phosphate crystal-associated proteins: Alpha-2-HS-glycoprotein, prothrombin fragment 1 and osteopontin. *Int J Urol* 8:S58-S62.

13. Porile JL, Asplin JR, Parks JH, Nakagawa Y, and Coe FL. 1996. Normal calcium oxalate crystal growth inhibition in severe calcium oxalate nephrolithiasis. *J Am Soc Nephrol* 7:602–607.

14. Robertson WG and Nordin BEC. 1982. Physico-chemical factors governing stone formation. In Scientific foundations of urology. Williams DI and Chisholm GD, editors. William Heinemann Medical Books Limited, London, 194-267.

15. Ryall RL. 1997. Urinary inhibitors of calcium oxalate crystallisation and their potential role in stone formation. *World J Urol* 15:155-164.

16. Ryall RL, Chauvet MC and Grover PK. 2001: A space oddity. 2001. In: Kok DJ, Romijn HC, Verhagen PCMS, and Verkoelen CF, editors. Eurolithiasis: 9th European Symposium on Urolithiasis. Shaker Publishing, Netherlands, 273-274.

17. Ryall RL, Hibberd CM, and Marshall VR. 1985. A method for studying inhibitory activity in whole urine *Urol Res* 13:285-289.

18. Ryall RL, Hibberd CM, Mazzachi BC, and Marshall VR. 1986. Inhibitory activity of whole urine: a comparison of urines from stone formers and healthy subjects. *Clin Chim Acta* 154:59-68.

19. Sakhaee K, Harvey JA, Padalino PK, Whitson P, and Pak CYC. 1993. The potential role of salt abuse on the risk for kidney stone formation. *J Urol* 150:310-312.

20. Stapleton AMF, Simpson RJ, and Ryall RL. 1993. Crystal matrix protein is related to human prothrombin. *Biochem Biophys Res Comm* 195:1199-1203.

21. Tiselius H-G, Bek-Jensen H, Fomander A-M, and Nilsson M-A. 1995. Crystallisation properties in urine from calcium oxalate stone formers. *J Urol* 154:940-946.

22. Wesson JA, Worcester EM, Weissner JH, Mandel NS, and Kleinman JG. 1998. Control of calcium oxalate crystal structure and cell adherence by urinary macromolecules. *Kidney Int* 33:952-957.

23. Worcester EM. 1996. Inhibitors of stone formation. *Sem Nephrol* 16:474-486.

24. Yasui T, Fujita K, Hayashi Y, Ueda K, Kon S, Maeda M, Uede T, and Kohri K. 1999. Quantification of osteopontin in the urine of healthy and stone-forming men. *Urol Res* 27:225-230.

CHAPTER 7: UPTF1 INCLUSION IN CALCIUM OXALATE MONOHYDRATE & DIHYDRATE CRYSTALS

7.1 INTRODUCTION

Urine chemistry studies comparing South Africa's black and white populations have revealed a few significant differences, including the former's lower urinary citrate concentration (Modlin 1967, Meyers *et al.* 1994, Whalley *et al.* 1998, Lewandowski *et al.* 2001), higher urinary oxalate concentration (Lewandowski *et al.* 2001) and lower urinary calcium concentration (Modlin 1967, Whalley *et al.* 1998, Rodgers and Lewandowski 2002). Of particular interest to the present study is the latter observation.

As demonstrated previously, urinary crystals precipitated from black subjects are composed of a mixture of COM and COD crystals compared with the predominance of COD crystals amongst the white population urine (chapter 6). This observation was not surprising since lower urinary calcium is known to favour the formation of monohydrate crystals while the dihydrate morphology predominates at higher calcium concentrations (Burns and Finlayson 1980). Of interest is a recent report by Ryall that differences in crystal morphology are associated with the selective inclusion of urinary proteins into these crystals (Ryall *et al.* 2001a). In particular, UPTF1 is the principal intracrystalline protein in COM crystals, whereas the principal intracrystalline protein in COD crystals is OPN.

An objective of this thesis was therefore to investigate the chemical conditions required to precipitate pure COM and COD crystals from the urine of black and white subjects, and to qualitatively and semi-quantitatively compares the major proteins included in the crystals.

7.2 METHODS

7.2.1 Urine treatment

Twenty-four hour urine samples were collected in plastic bottles containing a boric acid preservative. The subjects were healthy black (ages 20 – 25) and white males (ages 19 - 26) on their free unrestricted diet. Urines were tested for haematuria and infection, pooled according to population group and filtered as described in paragraph 2.2.1 (page 26). For the preliminary studies (black groups 1-3, white groups 1-3), the entire

24-hour urine from each subject (between 1 and 7 specimens) was pooled. However, for black group 4 and white group 4, an equal volume of the five urines was pooled in accordance with the recommendations of a study for the optimum pooling of samples (Jappie and Rodgers 2000). Aliquots of the pooled urines were retained for urinalysis (paragraph 2.2.1, page 26); relative supersaturations were not calculated since these are not appropraite for pooled urines. Urine composition data was analysed statistically by ANOVA and the results considered statistically significant if $p \leq 0.05$. Average values along with their standard errors are reported.

An aliquot of each pooled urine was not adjusted for its calcium concentration and was retained as a control sample, while the reminainder of the pooled sample was divided into several equal aliquots. The calcium concentration in these latter aliquots was adjusted by titration with a 1 mol/l solution of calcium chloride or by addition of distilled water to give a final range of urinary calcium concentrations between 0.5 mmol/l and 16 mmol/l. It should noted that all urinary constituents would be lowered by dilution and thus results could not be ascribed to a lowering of calcium concentration alone.

7.2.2 Crystal preparation

The CaOx MSL of each pooled urine was determined according to the method described by Ryall and co-workers (Ryall *et al.* 1985; paragraph 2.2.7, page 32). MSL determinations were repeated after adjustment of calcium concentrations. Crystals were then precipitated from these urines by addition of a standard NaOx load as decribed before (paragraph 6.2.2, page 138).

7.2.3 Characterisation of urine crystals

The composition of each batch of urine crystals was semi-quantitatively determined by XRD analysis as previously described (paragraph 2.2.2.1, page 27). Crystals (0.1 mg) obtained from black group 4 and white group 4 were also examined by scanning electron microscopy (paragraph 2.2.2.3, page 28).

7.2.4 Crystal preparation for protein analysis

Samples of CaOx crystals (10 - 20 mg) obtained from black group 4 and white group 4 were demineralised by the addition of EDTA, desalted and the resulting protein freeze-dried as previously described (paragraph 6.2.4, page 138). The protein was dissolved in distilled water to provide a final concentration of 1 mg/10 µl and stored at -20 ^{0}C in plastic eppendorf tubes for later use.

7.2.5 SDS-PAGE

Protein samples (obtained from 0.9 – 2.7 mg crystals) were dissolved in distilled water and diluted 1:4 with 5x SDS reducing buffer. The proteins were resolved by SDS-PAGE on 15 % polyacrylamide gels and detected by silver staining as previously described (paragraph 3.2.3.1, page 49).

7.2.6 Western blotting

Protein samples (obtained from 1.8 – 5.4 mg crystals) were resolved by SDS-PAGE and transferred onto nitrocellulose membranes for immunodetection as previously described (paragraph 3.2.3.2, page 50). The antibodies used were rabbit anti-human PT (DakoCytomation, Glostrup, Denmark) at a dilution of 1:500 and a rabbit polyclonal OPN antibody (Abcam, Cambridge, England) at a dilution of 1:1000. A secondary rabbit antibody (Amersham Biosciences, New Jersey, USA) was used at a dilution of 1:1000 followed by detection with 4-chloro-1-napthol.

7.3 RESULTS

7.3.1 Urine composition

Urine composition (mmol/l) and physicochemical data for pooled samples from the black and white groups are given in Tables 7.1.1 and 7.1.2, respectively (page 160). CaOx crystals were precipitated from these samples. Attention is drawn to the significantly lower urinary calcium and potassium concentrations in the black groups ($p < 0.05$).

7.3.2 X-ray powder diffraction

XRD patterns of crystals prepared at various calcium concentrations from the urines of black group 4 (Figures 7.1.1 – 7.1.4) and white group 4 (Figures 7.1.5 – 7.1.8), together with the d-spacing (Å) of prominent peaks, are shown below (page 161).

The assignment of these peaks to particular hydrates as well as the estimated percentage composition of the crystals is shown in Table 7.2.1 for black group 4 and Table 7.2.2 for white group 4 (page 162). The XRD patterns (black groups: Figures F1.1 - F1.16, pages A72 – A74; white groups: Figures F2.1 – F2.16, pages A75 - A77), peak assignments and composition (black groups: Tables F1.1 - F1.3,

pages A66 – A68; white groups: Tables F2.1 - F2.3, pages A69 – A71) of crystals prepared from black and white groups 1 – 3 are shown in Appendix F.

Table 7.1.1: Urine composition (mmol/l) and physicochemical parameters of black groups' pooled urines

Variables	Black group 1	Black group 2	Black group 3	Black group 4	Black group ave. ± SE
Number of urines	3	3	3	5	3.5
Volume for crystal preparation (ml)	50	100	80	300	133
pH	6.20	6.40	6.42	6.38	6.35 ± 0.116
Volume (ml/24hr)	4560	4890	4645	5615	4928 ± 953
Metastable limit(mmol/l)*	150	>195	>195	105	>161 ± 15.5
Calcium (mmol/l) *	1.02	0.64	1.23	2.56	1.36 ± 0.760
Chloride (mmol/l) *	43.0	53.0	88.9	70.0	63.7 ± 8.44
Citrate (mmol/l)	1.00	0.947	1.01	1.74	1.17 ± 0.784
Creatinine (mmol/l)	8.20	5.19	6.31	10.5	7.55 ± 1.09
Magnesium (mmol/l)	0.564	0.630	0.719	1.07	0.748 ± 0.716
Oxalate (mmol/l)	0.114	0.108	0.114	0.0873	0.106 ±0.0266
Phosphate (mmol/l)	12.8	4.60	10.3	18.8	11.6 ± 2.90
Potassium (mmol/l) *	10.7	10.2	17.2	17.7	14.0 ± 3.77
Sodium (mmol/l)	216	95.5	76.6	23.2	103 ± 30.8
Sulphate (mmol/l)	10.1	6.30	9.47	6.07	7.98 ± 2.06
Uric acid (mmol/l) *	1.29	0.900	1.68	2.49	1.59 ± 0.293

** Significantly different to the white groups' pooled urine average ($p<0.05$)*

Table 7.1.2: Urine composition (mmol/l) and physicochemical parameters of white groups' pooled urines

Variables	White group 1	White group 2	White group 3	White group 4	White group ave. ± SE
Number of urines	7	1	5	5	4.5
Volume for crystal preparation (ml)	50	100	200	400	188
pH	6.15	5.90	6.52	6.55	6.28 ± 0.116
Volume (ml/24hr)	8665	2350	6465	6690	6042 ± 953
Metastable limit(mmol/l)*	60	60	45	45	53 ± 15.5
Calcium (mmol/l) *	6.52	1.67	3.96	4.08	4.06 ± 0.760
Chloride (mmol/l) *	115	119	144	126	126 ± 8.44
Citrate (mmol/l)	5.99	1.07	2.21	1.90	2.79 ± 0.784
Creatinine (mmol/l)	11.9	7.70	11.3	12.0	10.7 ± 1.09
Magnesium (mmol/l)	5.37	0.574	1.98	2.56	2.62 ± 0.716
Oxalate (mmol/l)	0.226	0.0979	0.133	0.0508	0.127 ±0.0266
Phosphate (mmol/l)	23.4	13.1	26.4	19.9	20.7 ± 2.90
Potassium (mmol/l) *	40.7	19.2	38.2	37.2	33.8 ± 3.77
Sodium (mmol/l)	137	84.4	112	66.7	100 ± 30.8
Sulphate (mmol/l)	22.9	11.3	13.1	12.0	14.8 ± 2.06
Uric acid (mmol/l) *	3.09	2.38	3.50	3.20	3.04 ± 0.293

** Significantly different to the black groups' pooled urine average ($p<0.05$)*

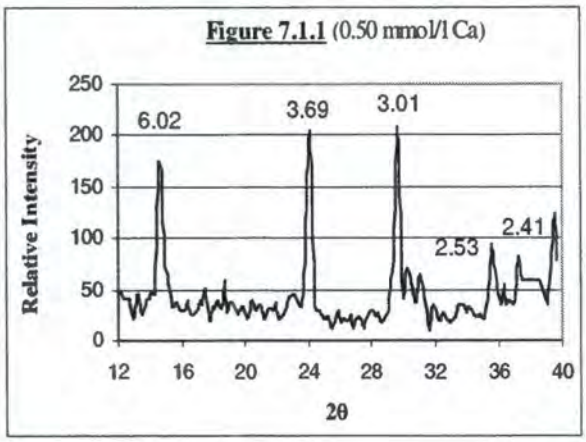

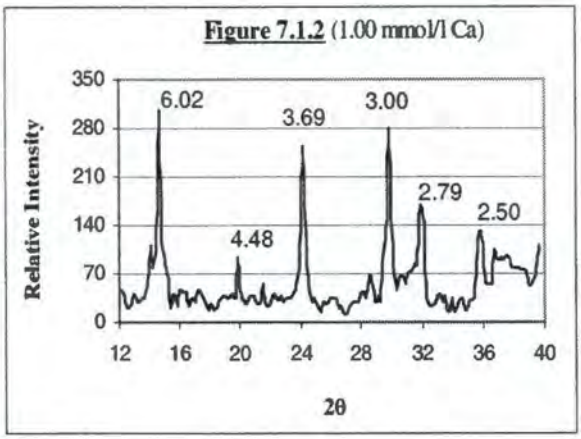

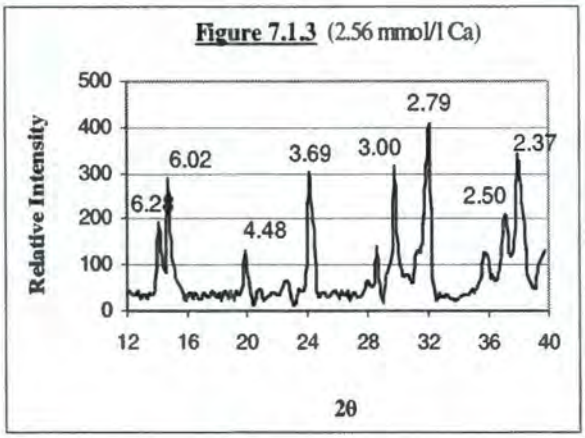

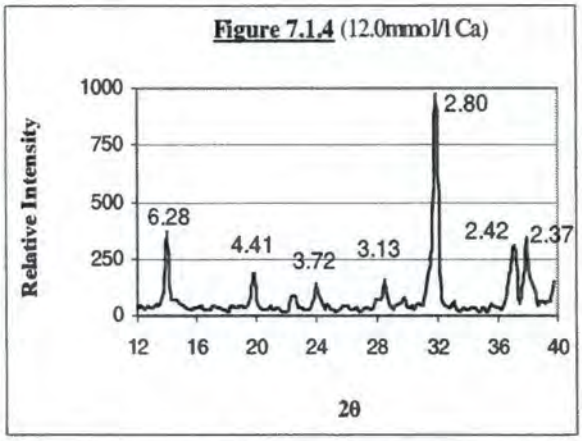

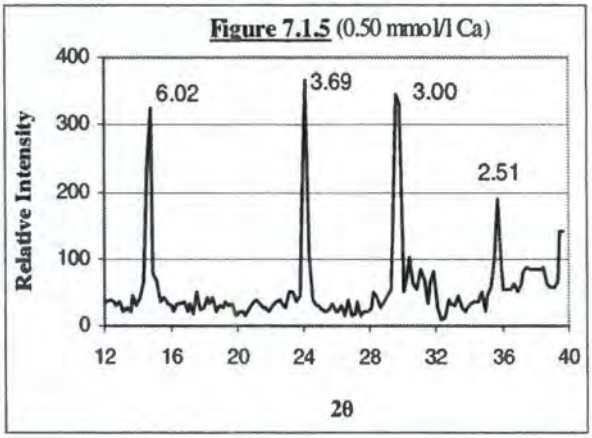

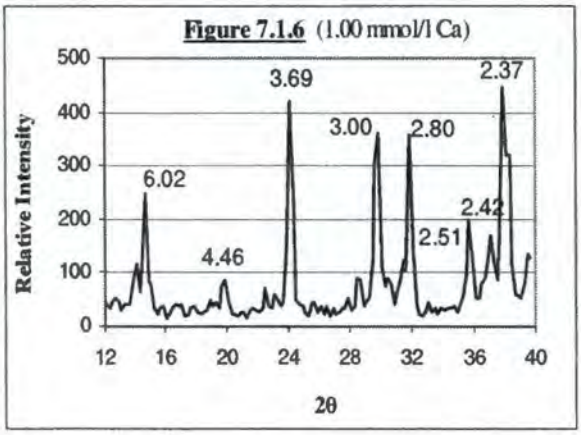

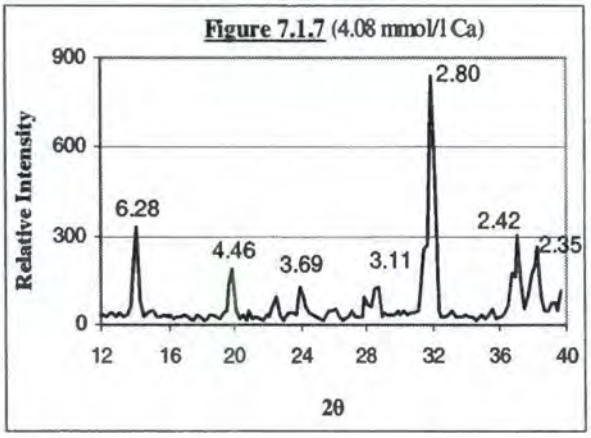

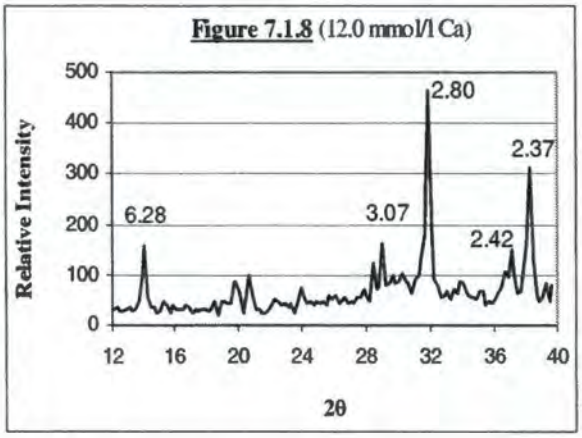

Figure 7.1: X-ray powder diffraction patterns of CaOx urine crystals. The crystals were precipitated from black group 4's urine at: 0.50 mmol/l Ca (7.1.1), 1.00 mmol/l Ca (7.1.2), 2.56 mmol/l Ca (7.1.3), 12.0 mmol/l Ca (7.1.4); and from white group 4's urine at: 0.50 mmol/l Ca (7.1.5), 1.00 mmol/l Ca (7.1.6), 4.08 mmol/l Ca (7.1.7), and 12.0 mmol/l Ca (7.1.8).

Table 7.2.1: X-ray powder diffraction peak assignments and estimated percentage composition of CaOx crystals precipitated from the urine of black group 4

Ca (mmol/l)	d-spacing (Å)	Assignment	Composition: % COM	% COD
0.50	6.02	COM		
	3.69	COM		
	3.01	COM		
	2.53	COM		
	2.41	COM	100	0
1.00	6.02	COM		
	4.48	COD		
	3.69	COM		
	3.00	COM		
	2.79	COD		
	2.50	COM	80	20
2.56*	6.28	COD		
	6.02	COM		
	4.48	COD		
	3.69	COM		
	3.00	COM		
	2.79	COD		
	2.50	COM		
	2.37	COM	55	45
12.0	6.28	COD		
	4.41	COD		
	3.72	COD		
	3.13	COD		
	2.80	COD		
	2.42	COD		
	2.37	COD	0	100

** Control urine, i.e. unadjusted Ca*

Table 7.2.2: X-ray powder diffraction peak assignments and estimated percentage composition of CaOx crystals precipitated from the urine of white group 4

Ca (mmol/l)	d-spacing (Å)	Assignment	Composition: % COM	% COD
0.50	6.02	COM		
	3.69	COM		
	3.00	COM		
	2.51	COM	100	0
1.00	6.02	COM		
	4.46	COD		
	3.69	COM		
	3.00	COM		
	2.80	COD		
	2.51	COM		
	2.42	COD		
	2.37	COM	70	30
4.08*	6.28	COD		
	4.46	COD		
	3.69	COD		
	3.11	COD		
	2.80	COD		
	2.42	COD		
	2.35	COD	0	100
12.0	6.28	COD		
	3.07	COD		
	2.80	COD		
	2.42	COD		
	2.37	COD	0	100

** Control urine, i.e. unadjusted Ca*

The percentage hydrate composition of all the black and white groups' urine crystals is summarized in Tables 7.3.1 and 7.3.2, respectively. Inspection of these trends indicates that at relatively low final calcium concentrations (0.5 mmol/l), pure COM crystals are obtained in both population groups' urine. The results further demonstrate that as the final calcium concentration increases, COD gradually replaces COM until pure COD is obtained in both groups' urine at final calcium concentrations ≥12 mmol/l. It is noteworthy that while the white groups' crystals often consisted of large percentages of COD at calcium concentrations of 8 mmol/l or lower, significant amounts of COM (40 - 50 %) were observed in the black groups' urine even at this relatively high calcium concentration.

Table 7.3.1: Estimated hydrate composition of CaOx crystals precipitated from the black groups' urine at various calcium concentrations as determined by x-ray powder diffraction

Ca	Black group 1:		Black group 2:		Black group 3:		Black group 4:	
(mM)	*% COM*	*% COD*	*% COM*	*% COD*	*% COM*	*% COD*	*% COM*	*% COD*
0.50	100	0			100	0	100	0
0.64			100*	0*				
1.00			55	45			80	20
1.02	100*	0*						
1.23					60*	40*		
2.00	65	35	55	45				
2.56							55*	45*
4.00	75	25	70	30				
8.00	40	60	50	50	45	55		
10.0					35	65		
12.0					0	100	0	100
16.0					0	100		

** Control urine, i.e. unadjusted Ca*

Table 7.3.2: Estimated hydrate composition of CaOx crystals precipitated from the white groups' urine at various calcium concentrations as determined by x-ray powder diffraction

Ca	White group 1:		White group 2:		White group 3:		White group 4:	
(mM)	*% COM*	*% COD*	*% COM*	*% COD*	*% COM*	*% COD*	*% COM*	*% COD*
0.50	100	0	100	0	100	0	100	0
1.00	100	0			100	0	70	30
1.67			100*	0*				
2.00	100	0						
3.96					0*	100*		
4.00	100	0						
4.08							0*	100*
6.52	75*	25*						
8.00	0	100	40	60				
10.0					0	100		
12.0			0	100	0	100	0	100
16.0			0	100				

** Control urine, i.e. unadjusted Ca*

7.3.3 Scanning electron microscopy

Figure 7.2 shows scanning electron micrographs of urine crystals obtained from black group 4 (Figures 7.2.1 – 7.2.4) and white group 4 (Figures 7.2.5 – 7.2.8) at various calcium concentrations. Attention is drawn to the existence of only disc-shaped COM crystals at 0.5 mmol/l calcium concentration in the urines of both population groups and their gradual replacement by bipyramidal COD crystals until only the latter are observed at a calcium concentration of 12 mmol/l. These micrographs therefore confirm the results obtained by x-ray powder diffraction. Thus, crystals prepared at the threshold concentrations of 0.5 mmol/l and 12 mmol/l were used to precipitate respectively pure COM and COD for protein analysis by SDS-PAGE and Western blotting.

Figure 7.2: Scanning electron micrographs of CaOx urine crystals. The crystals were precipitated from black group 4's urine at: 0.50 mmol/l Ca (mag 7.5K) (Fig 7.2.1), 1.00 mmol/l Ca (mag 10K) (Fig 7.2.2), 2.56 mmol/l Ca (mag 11K) (Fig7.2.3), 12.0 mmol/l Ca (mag 8K) (Fig 7.2.4); and white group 4's urine at: 0.50 mmol/l Ca (mag 9K) (Fig 7.2.5), 1.00 mmol/l Ca (mag 8K) (Fig 7.2.6), 4.08 mmol/l Ca (mag 9K) (Fig 7.2.7), and 12.0 mmol/l Ca (mag 13K) (Fig 7.2.8).

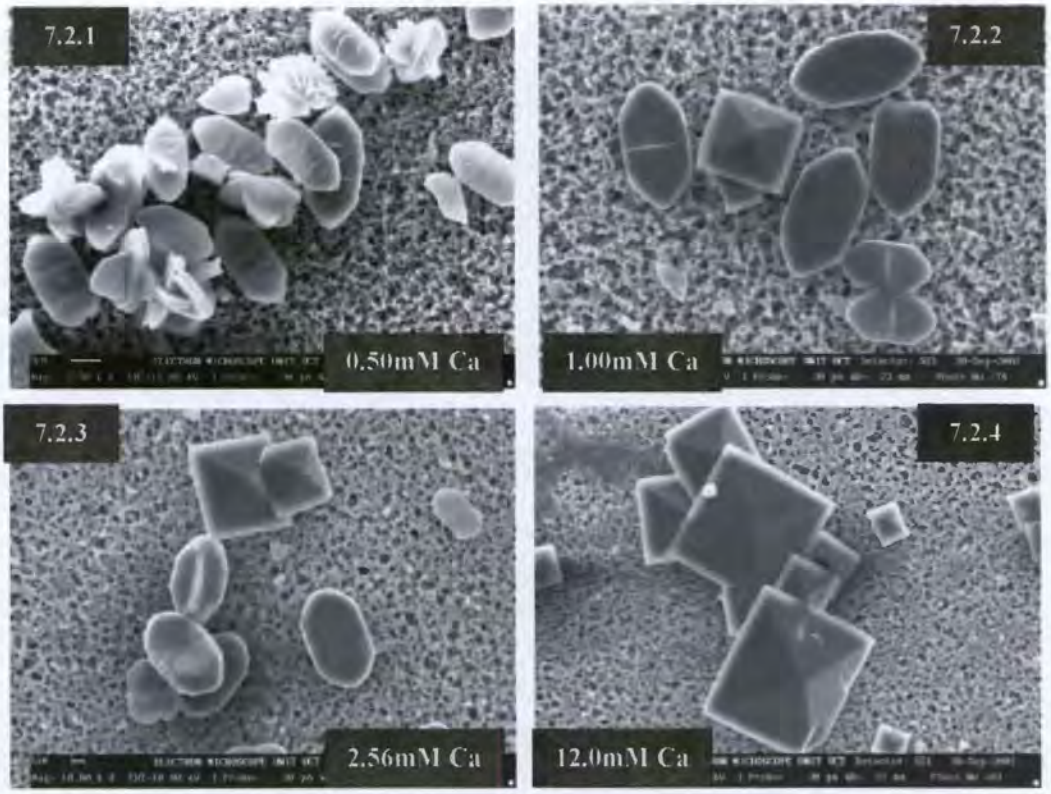

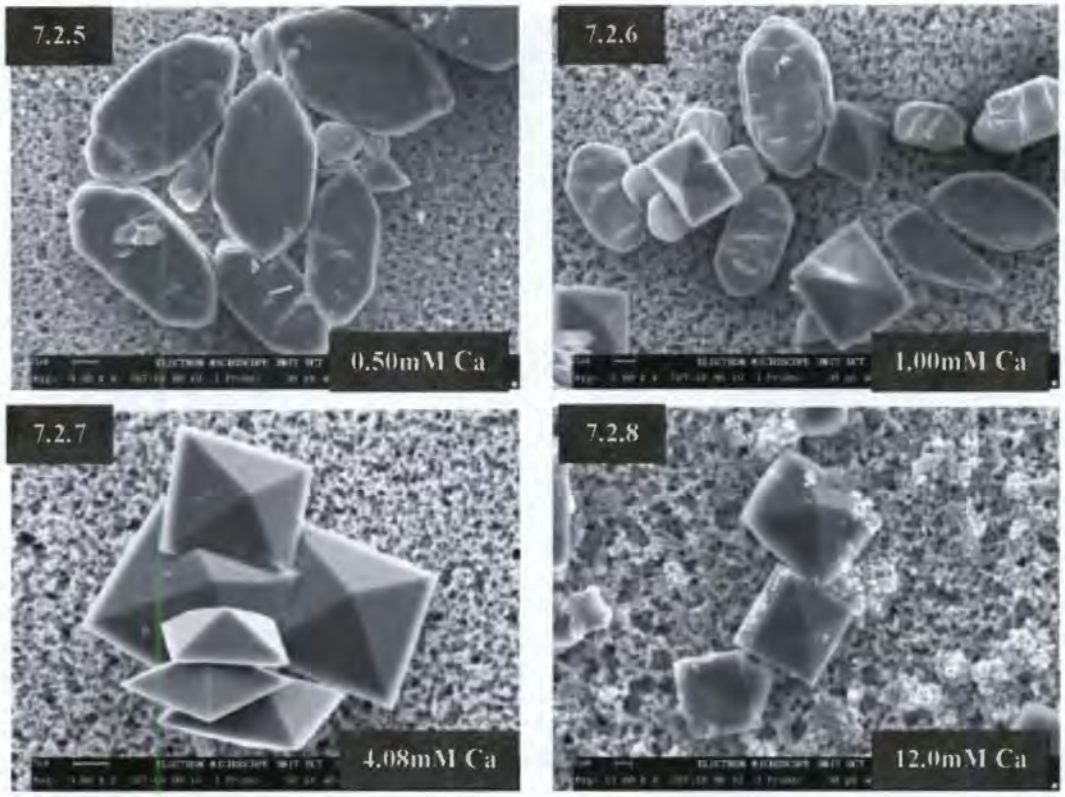

It is also evident that COMs predominate in the black groups' control urine (in which calcium was not adjusted) (Figure 7.2.3), while CODs are formed exclusively in the white groups' control urine (Figure 7.2.7). Fine lines were apparent on the {101} face of COM crystals, most notable in Figure 7.2.1 and Figure 7.2.6, which was not evident on the surface of CODs. These may be growth lines or due to the inclusion of urinary proteins, since these lines are not observed in COM crystals precipitated from ultrafiltered urine (Ryall *et al.* 2001b). The appearance of growth lines on COMs is reminiscent of y-shaped cracks due to growth by cyclic twinning in struvite (magnesium ammonium phosphate hexahydrate) crystals (Kim 1982).

7.3.4 Protein analysis

The desalting chromatograms of demineralised crystals prepared from black group 4 (Figures 7.3.1 – 7.3.3) and white group 4 (Figures 7.3.4 – 7.3.6) at various calcium concentrations are shown in Figure 7.3. The first peak in each chromatogram corresponds to the protein content of the crystals (confirmed by SDS-PAGE) while the second peak is the salt content (partly from the EDTA solution used for demineralisation and partly from the crystals themselves).

Figure 7.3: Desalting chromatograms of demineralised CaOx urine crystals. The demineralised crystals were from black group 4's urine: 0.50 mmol/l Ca and 4.3 mg (Fig 7.3.1), 2.56 mmol/l Ca and 10.9 mg (Fig 7.3.2), 12.0 mmol/l Ca and 9.35 mg (Fig 7.3.3); and white group 4's urine: 0.50 mmol/l Ca and 13.9 mg (Fig 7.3.4), 4.08 mmol/l Ca and 18.8 mg (Fig 7.3.5), and 12.0 mmol/l Ca and 23.5 mg (Fig 7.3.6).

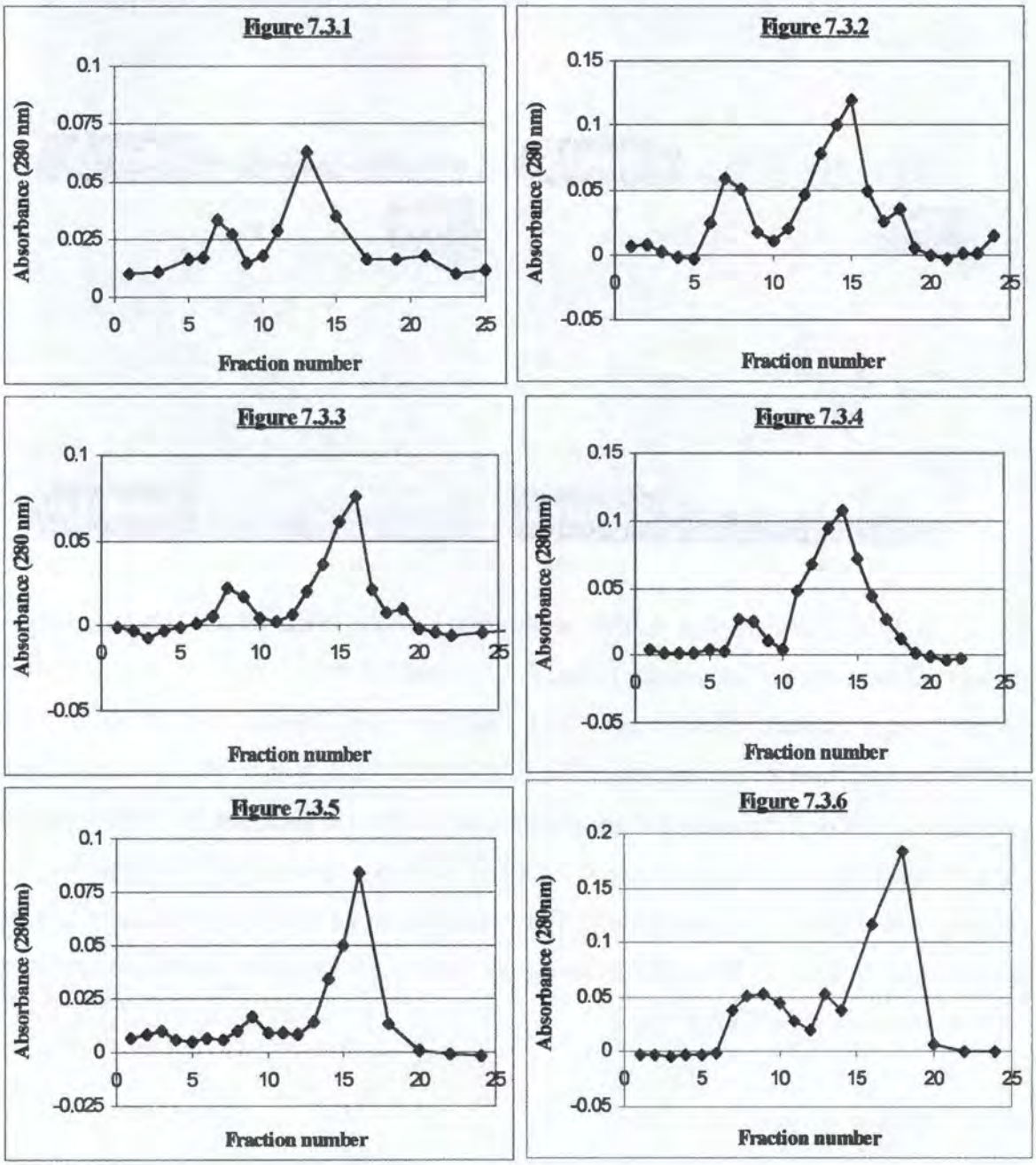

Protein patterns of the desalted crystals from black group 4 and white group 4 are shown in Figure 7.4 (black subjects: lanes 1 – 5; white subjects: lanes 6 – 10). Since these crystals were washed with thoroughly with distilled water to remove surface-bound proteins, it can be concluded that the proteins shown by gel electrophoresis are intracrystalline. The protein content of CaOx crystals prepared from the black group's urine varies markedly with hydrate type (concomitant with calcium concentration). The

pure COM crystals (lane 1) show five major bands: two low molecular weight proteins at 17 and 20 kDa, a protein at 38 kDa whose relative mobility is the same as the UPTF1 standards in lanes 4 - 5 and two higher molecular weight proteins at 62 and 66 kDa. Two faint bands at 48 and 56 kDa are also apparent. In contrast, pure COD crystals (lane 3) do not contain the low molecular weight proteins, very little of the 38 kDa band and significantly more of the proteins at 62 - 66 kDa. They also show a distinct band at 56 kDa and a faint band at 48 kDa. The mixed morphology crystals formed in the control urine (in which the calcium was not adjusted) (lane 2) contains both the 38 kDa and the high molecular weight proteins as well as a faint band at 56 kDa.

The protein content of crystals from the white group also varies with respect to hydrate type. The COM crystals (lane 6) consist almost exclusively of the 38 kDa protein whose relative mobility is the same as the UPTF1 standards in lanes 9 – 10. In contrast, the COD crystals (lane 8) are composed of higher molecular proteins at 58, 62 and 66 kDa with a faint band at 48 kDa. The same protein pattern described for lane 8 was observed in the crystals formed in the white group's control urine (in which the calcium was not adjusted) (lane 7) which were also pure CODs.

Figure 7.4: Protein patterns of CaOx urine crystals (black subjects: lanes 1 – 5; white subjects: lanes 6 – 10). Samples obtained from black group 4's urine are *MW*: low molecular weight standard; *1*: COM (0.9 mg); *2*: control urine's crystals (0.9 mg); *3*: COD (0.9 mg); *4*: 0.25 µg UPTF1; *5*: 0.5 µg UPTF1. Samples obtained from white group 4's urine are *MW*: low molecular weight standard, *6*: COM (2.7 mg); *7*: control urine's crystals (2.7 mg); *8*: COD (2.7 mg); *9*: 0.25 µg UPTF1; *10*: 0.5 µg UPTF1.

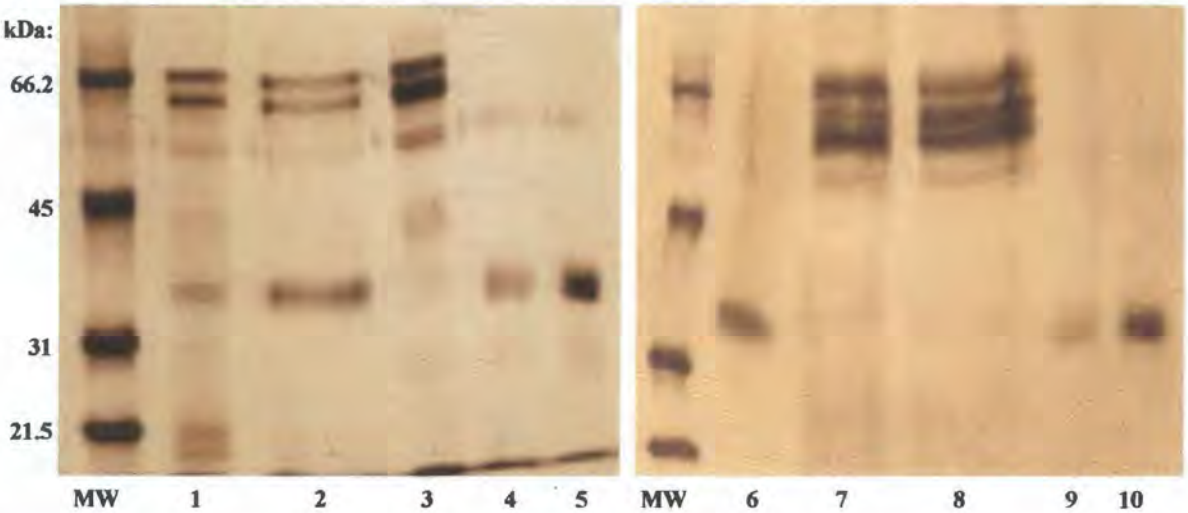

A Western blot of the CaOx urine crystals from both population groups for UPTF1 and other PT fragments is shown in Figure 7.5. Prominent bands with the same mobility as the UPTF1 standard (lane 7) appear in lanes 1, 2 and 4. Additional faint bands at 73

(lanes 1, 2 and 4) and 49 kDa (lane 2) correspond to PT and PTF1+2 (Grover and Ryall 1999), respectively.

Figure 7.5: Western blot of CaOx urine crystals immunoblotted for prothrombin. The patterns obtained from black group 4's urine are *1*: COM (1.8 mg); *2*: control urine's crystals (1.8 mg); *3*: COD (1.8 mg). Patterns obtained from white group 4's urine are *lane 4*: COM (5.4 mg); *5*: control urine's crystals (5.4 mg); *6*: COD (5.4 mg); *7*: 0.5 µg UPTF1.

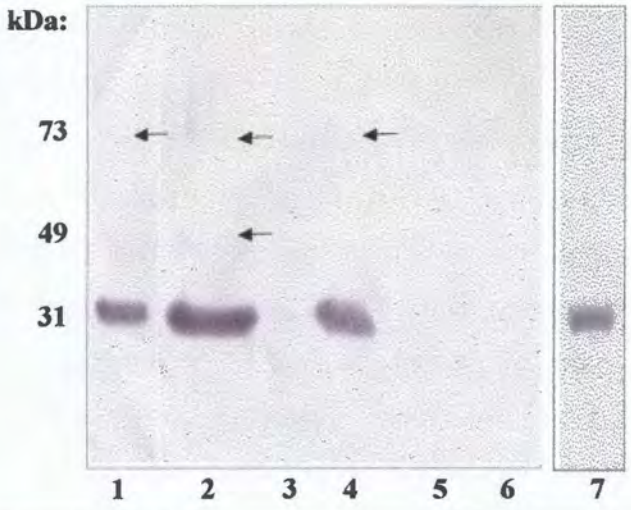

Figure 7.6 shows a Western blot of both population groups' urine crystals for OPN.

Figure 7.6: Western blot of CaOx urine crystals immunoblotted for osteopontin. The patterns obtained from black group 4's urine are *1*: COM (1.8 mg), *2*: control urine's crystals (1.8 mg), *3*: COD (1.8 mg). Patterns obtained from white group 4's urine are *4*: COM (3.6 mg), *5*: control urine's crystals (3.6 mg), *6*: COD (3.6 mg). Urine was used as a positive control, *7*: concentrated urine (1 ml).

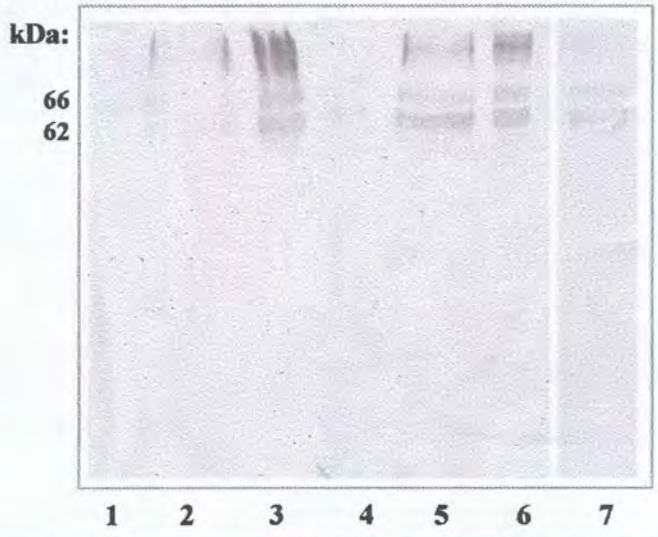

Prominent bands at 62 and 66 kDa were observed in lanes 3, 5, 6 and 7, while faint bands at the same molecular weights were observed in lane 2. The 66 kDa band corresponds to full length OPN (Atmani *et al.* 1998) and the 62 kDa band is most likely a degradation product since OPN is known to be degraded by urinary proteases (Ryall *et al.* 2001a). The higher molecular weight bands (lanes 2-3, 5-6) may be aggregates of the protein (Johnson-Tardieu *et al.* 2000). Since no purified OPN was available, urine was concentrated (lane 7) and used as a positive control.

7.4 DISCUSSION

Urine composition data confirmed previous reports that the black population has a significantly lower urinary calcium concentration than the white population (Modlin 1967, Whalley *et al.* 1998, Rodgers and Lewandowski 2002). In this study, the average urinary calcium concentration amongst the black groups' urines was 66 % lower than the white groups' urines (1.36 mmol/l *vs.* 4.06 mmol/l). The urinary calcium concentration was a relatively reliable predictor of CaOx crystal morphology. Mainly COM crystals were formed at lower calcium concentrations, but COD crystals gradually replaced these as the calcium concentration was increased. However, the actual concentrations required to produce the CaOx hydrates differed for the two population groups. Amongst the black groups, the calcium concentration required to precipitate pure COD was ≤12 mmol/l, while the required concentration was only 8 mmol/l in three of the four white groups. When comparing the hydrate composition of CaOx crystals at equal calcium concentrations (*i.e.* at 8 mmol/l calcium concentration), the white groups' crystals consistently had a higher percentage of COD than those of the black groups. Therefore, it appears that inherently different urinary compositions (and not just the calcium concentrations) may play a contributory role in determining urine crystal morphology in the two population groups. COD crystals are thermodynamically less stable than COM (Burns and Finlayson 1980). However, increased stability of the dihydrate crystal structure has been reported in the presence of citrate, magnesium and potassium (Brown *et al.* 1989). Thus, the significantly lower potassium concentration amongst the black groups in this study might have contributed to the relatively lower percentage of COD crystals in their urines.

The protein content of CaOx crystals precipitated from the urine of the two population groups was of particular interest. The COM crystals from both population

groups, formed at relatively lower calcium concentrations, contained UPTF1 (and other PT fragments), while COD crystals from both groups formed at relatively higher calcium concentrations, contained mainly OPN. These observations are in agreement with a previous study (Ryall *et al.* 2001a).

Thus, researchers interested in studying UPTF1 would be advised to adopt a modified purification procedure to the one published by Ryall and co-workers (1995). The present study showed that the amount of intracrystalline UPTF1 may be altered by manipulation of the endogenous urinary calcium concentration. The dilution of urinary calcium to lower concentrations favoured COM precipitation rather than COD, thus increasing the amount of intracrystalline UPTF1 derived per milligram of CaOx crystals from a urine sample (despite the dilution of other ions which also occurred). This strategy may be employed in a research setting if large amounts of UPTF1 are required for inhibitory activity or protein characterisation studies.

It is apparent that the different crystal structures of COM and COD (arising from different calcium concentrations) and the conformations adopted by UPTF1 and OPN, are key factors in determining the selective inclusion of urinary proteins into the respective CaOx hydrates. Indeed, Heuer suggests that intracrystalline proteins ensure that only crystals of a particular composition and shape precipitate and determine the physicochemical features of the resulting crystals (Heuer *et al.* 1992). It is therefore speculated that the conformation of UPTF1 at relatively low calcium concentrations may favour its binding, relative to OPN, to COM, which crystallises in the P21/c group (Tazzoli and Domeneghetti 1980). In contrast, the conformation of OPN at relatively higher calcium concentrations may favour its binding, relative to UPTF1, to COD, which crystallises in the I4/m space group (Sterling 1965).

Crystals obtained from the black group's control urine (Figure 7.4, lane 2) contained at least two proteins with reported inhibitory properties, namely UPTF1 and OPN. In comparison, the white group's crystals (Figure 7.4, lane 5) contained only OPN. This may be a contributing factor in the black population's lower stone incidence.

Comparison of the COM crystals from the two groups showed that while both OPN and UPTF1 were included in the black group's crystals, only UPTF1 was included in COM crystals from the white group's urine. The black group's COM crystals also contained low molecular weight proteins (17, 20 kDa), which were absent in crystals from the white group.

Western blotting showed that the black group's COM crystals contained two to three times more UPTF1 per milligram of CaOx than the white group's COM crystals. These observations suggest one of two possible conclusions: either the black group had a higher urinary UPTF1 concentration than the white group, or the former group's urine composition was more favourable for binding of UPTF1 to CaOx crystals. Since a semi-quantitative study showed that the two groups had relatively similar urinary levels of UPTF1 at their endogenous calcium concentrations (chapter 6), the strength of protein binding to CaOx crystals in the black group appeared to be a key factor in determining the higher amount of UPTF1 in this group's crystals.

The COD crystals precipitated from the black and white group's urines also differed in their protein content. While the former group's COD contained a large proportion of OPN as well as an unidentified 56 kDa protein, the white group's COD consisted almost entirely of OPN.

Although it is recognised that pretreatment of urine such as filtration and washing of urine crystals with distilled water or sodium hydroxide affects which proteins are incorporated (Atmani *et al.* 1998), the inclusion of different proteins into the same hydrate type derived from the two population groups' urines suggests that urine composition, in addition to crystal morphology, directs the capacity of particular urinary proteins to bind to CaOx crystals.

Only a select number of proteins have been found in CaOx urine crystals compared with the large number observed in urine samples by SDS-PAGE (Doyle *et al.* 1991). The most prominent crystal-associated proteins found are PT-related proteins and OPN (Atmani *et al.* 1996, 1998; Ryall *et al.* 2001a; Atmani and Khan 2002), followed by albumin (Atmani *et al.* 1996, 1998; Atmani and Khan 2002). Small amounts of α_1-microglobulin (Atmani *et al.* 1996, 1998; Atmani and Khan 2002) and inter-α-inhibitor fragments (Atmani *et al.* 1996, 1998; Dawson *et al.* 1998; Atmani and Khan 2002) have also been identified. It is possible that the unidentified proteins observed at 17 – 20 kDa in the black group's COM crystals are fragments of bikunin, itself a fragment of inter-α-inhibitor (Dawson *et al.* 1998).

Of note is the observation that SDS-PAGE showed two OPN bands for the black group's crystals, while the white group's crystals displayed three bands. Since it is well known that OPN is degraded by urinary proteases (Ryall *et al.* 2001a), this observation might suggest that less degradation of OPN occurred in the black group's urine; thus the protein may be more stable in this group's urine. Western blotting showed two OPN bands

in both groups' COD crystals, but it is possible that the lower two bands observed in the white group's crystals by SDS-PAGE were combined into one band at 62 kDa on the Western blot.

Significantly more total intracrystalline protein per milligram of CaOx crystals was included in the black group's crystals compared with the white group. This is demonstrated by the similar intensities of the two group's crystals by SDS-PAGE (Figure 7.4) despite a three-fold greater crystal load from the white group (2.7 mg *vs.* 0.9 mg for the black group).

It is widely recognised that crystal attachment to the renal epithelium may play a role in stone formation (Lieske *et al.* 1999). Ryall's studies have shown the potential of intracrystalline proteins to facilitate the erosion and dismantling (and possibly even the dissolution) of CaOx crystals by allowing urinary and intracellular proteases to penetrate the crystalline structure (Ryall *et al.* 2001b). It is thus proposed that the nature and amount of intracrystalline protein influences the probability that crystal attachment will result in stone formation (Ryall *et al.* 2001b). In light of these studies, the incorporation of greater amounts of intracrystalline protein into the black group's urine crystals may play a greater protective role in this group than the white group.

The importance of crystal morphology and urine composition to the selective inclusion and binding of urinary proteins has been clearly shown. This study has also demonstrated for the first time that CaOx crystals freshly precipitated from the black population group's urine contains a greater amount of UPTF1 than the white group (per milligram of CaOx). The black group's urine composition also appears to be more favourable for binding of UPTF1 than the white group's urine in the presence of COM crystals. Thus, the black group's urinary milieu may contain components that enhance UPTF1 binding. Further studies to identify and characterise these components are warranted.

The information presented in this chapter regarding the black group's urine composition and their intracrystalline proteins may therefore contribute to an understanding of the remarkably low incidence of kidney stones amongst the black population.

7.5 REFERENCES

1. Atmani F, Glenton PA, and Khan SR. 1998. Identification of proteins extracted from calcium oxalate and calcium phosphate crystals induced in the urine of healthy and stone forming subjects. *Urol Res* 26:201-207.

2. Atmani F and Khan SR. 2002. Quantification of protein extracted from calcium oxalate and calcium phosphate crystals induced in vitro in the urine of healthy controls and stone-forming patients. *Urol Int* 68:54-59.

3. Atmani F, Opalko FJ, and Khan SR. 1996. Association of urinary macromolecules with calcium oxalate crystals induced in vitro in normal human and rat urine. *Urol Res* 24:45-50.

4. Brown P, Ackermann D, and Finlayson B. 1989. Calcium oxalate dihydrate (weddellite) precipitation. *J Crys Growth* 98:285-292.

5. Burns JR and Finlayson B. 1980. Changes in calcium oxalate crystal morphology as a function of concentration. *Inves Urol* 18:174-177.

6. Dawson CJ, Grover PK, and Ryall RL. 1998. Inter-alpha-inhibitor in urine and calcium oxalate urine crystals. *Br J Urol* 81:20-26.

7. Doyle IR, Ryall RL, and Marshall VR. 1991. Inclusion of proteins into calcium oxalate crystals precipitated from human urine: a highly selective phenomenon. *Clin Chem* 37:1589-1594.

8. Grover PK and Ryall RL. 1999. Inhibition of calcium oxalate crystal growth and aggregation by prothrombin and its fragments in vitro. *Eur J Biochem* 263:50-56.

9. Heuer AH, Fink DJ, Laraia VJ, Arias JL, Calvert PD, Kendall K, Messing GL, Blackwell J, Rieke PC, Thompson DH, Wheeler AP, Veis A, and Caplan AI. 1992. Innovative materials processing strategies: a biomimetic approach. *Science* 255:1098-1105

10. Jappie D and Rodgers AL. 2000. Determination of the optimum number of subjects required for pooling of urines: statistical approach. In: Rodgers AL, Hibbert BE, Hess B, Khan SR, and Preminger GM, editors. Urolithiasis 2000. University of Cape Town, Cape Town, 92-93.

11. Johnson-Tardieu J, Glenton PA, Moriyama, MT, Peck AB and Kahn SR. 2000. Osteopontin expression in kidneys and urine of rats with hyperoxaluria and nephrolithiasis. In: Rodgers AL, Hibbert BE, Hess B, Khan SR, and Preminger GM, editors. Urolithiasis 2000. University of Cape Town, Cape Town, 142-143.

12. K.M. Kim. 1982. The stones. *Scan Elec Micros* 4:1635-1660.

13. Lewandowski S, Rodgers A, and Schloss I. 2001. The influence of a high-oxalate / low-calcium diet on calcium oxalate renal stone risk factors in non-stone forming black and white South African subjects. *Br J Urol* 87:307-311.

14. Lieske JC, Deganello S, and Toback FG. 1999. Cell-crystal interactions and kidney stone formation. *Nephron* 81:8-17.

15. Meyers AM, Whalley N, Zakolski WJ and Shar T. 1994. Chemical composition of the urine in the normal black and white population. In: Ryall RL, Bais R, Marshall VR, Rofe AM, Smith LH, and Walker VR, editors. Proceedings of the 7th international symposium on urolithiasis. Plenum Press, New York, 422

16. Modlin M. 1967. The aetiology of renal stone: A new concept arising from studies on a stone-free population. *Ann Roy Coll Surg Engl* 40:155-178.

17. Rodgers AL and Lewandowski S. 2002. Effects of 5 different diets on urinary risk factors for calcium oxalate kidney stone formation: evidence of different renal handling mechanisms in different race groups. *J Urol* 168:931-936.

18. a) Ryall RL, Chauvet MC, and Grover PK. 2001: A space oddity. 2001. In: Kok DJ, Romijn HC, Verhagen PCMS, and Verkoelen CF, editors. Eurolithiasis: 9th European Symposium on Urolithiasis. Shaker Publishing, Netherlands, 273-274.

19. b) Ryall RL, Fleming DE, Doyle IR, Evans NA, Dean CJ, and Marshall VR. 2001. Intracrystalline proteins and the hidden ultrastructure of calcium oxalate urinary crystals: implications for kidney stone formation. *J Struc Biol* 134:5-14.

20. Ryall RL, Grover PK, Stapleton AMF, Barrell DK, Tang Y, Moritz RL, and Simpson RJ. 1995. The urinary F1 activation peptide of human prothrombin is a potent inhibitor of calcium oxalate crystallization in undiluted human urine in vitro. *Clin Sci* 89:533-541.

21. Ryall RL, Hibberd CM, and Marshall VR. 1985. A method for studying inhibitory activity in whole urine. *Urol Res* 13:285-289.

22. Sterling C. 1965. Crystal-structure analysis of weddellite, $CaC_2O_4.(2+x)H_2O$. *Acta Cryst* 18:917-921.

23. Tazzoli V and Domeneghetti C. 1980. The crystal structures of whewellite and weddellite: re-examination and comparison. *Am Miner* 65:327-334.

24. Whalley NA, Moraes MFBG, Shar TG, Pretorius SS, and Meyers AM. 1998. Lithogenic risk factors in the urine of black and white subjects. *Br J Urol* 82:785-790.

CHAPTER 8: PROTEOLYSIS & PARTIAL DISSOLUTION OF CALCIUM OXALATE URINE CRYSTALS

8.1 INTRODUCTION

A few urinary proteins, including UPTF1, are intimately associated with the mineral constituent of CaOx crystals (Fleming *et al.* 1999, Ryall *et al.* 2000), being distributed in channels throughout the mineral phase. Ryall has thus hypothesised that in addition to their role as inhibitors of crystallisation, proteins may also fulfill another role in the prevention of urolithiasis. It has been demonstrated that urinary crystals, rich in protein, are susceptible to protease treatment whereas crystals composed of pure mineral are not. Recent studies have shown the potential of intracrystalline proteins to facilitate the dismantling of urinary crystals by providing proteases with access to their protein core (Ryall *et al.* 2000, 2001b). Thus, the inclusion of intracrystalline proteins such as UPTF1 into CaOx urinary crystals may provide an unexpected second line of protection against stone formation should such proteins unsuccessfully prevent significant crystal growth and aggregation (Ryall *et al.* 2001b).

In addition to the afore-mentioned proteolysis studies, Lieske and co-workers have also shown that dissolution of exogenous COM occurs in the acidic lysosome of renal monkey cells (Lieske *et al.* 1997). The dissolution of exogenous COD crystals incubated in urine at various dilutions has previously been reported (Akbarieh *et al.* 1987) and incubation of urinary COM crystals causes pitting and erosion, demonstrating conclusively that crystals are susceptible to attack by endogenous proteases occurring in normal, healthy urine. This is not seen in the presence of a protease inhibitor cocktail or with crystals precipitated from ultrafiltered urine (Fleming *et al.* 2000). It is probable that both dissolution and proteolysis will occur *in vivo* due to the acidic environment of cell lysosomes (pH ~5) as well as the production of proteases by these organelles.

Thus the objective of the present study was to investigate the role of both proteolysis and dissolution of urinary CaOx crystals in the white and black populations. Furthermore, since the urines of the two population groups tend to contain different CaOx hydrates (chapters 6 and 7), a comparison of the susceptibility of COM and COD to dissolution and proteolysis was warranted. The work reported in this chapter had the potential to elucidate whether the black population's urinary crystals are more susceptible

to dissolution and/or degradation, which could offer an explanation for their lower stone incidence.

8.2 METHODS

8.2.1 Preparation of CaOx urine crystals

Twenty-four hour urine samples were collected from ten healthy males (five whites, five blacks) and equal volumes from each were pooled according to population group. This was in accordance with the recommendations of a study for the optimum pooling of samples (Jappie and Rodgers 2000). The pooled urines were filtered (0.75 µm pre-filter, 0.45 µm, 0.22 µm) and an aliquot of each was retained as a control sample. The CaOx MSL of both pooled urines was determined (paragraph 2.2.7, page 32) and aliquots were retained for urinalysis (as described in paragraph 2.2.1, page 26). Relative supersaturations were not calculated since this is not appropriate for pooled urines.

The remaining urine was ultrafiltered through a 10 kDa membrane to remove all macromolecules larger than 10 kDa, including UPTF1. The ultrafiltrates from white and black subjects were each divided into three aliquots and either left unaltered, or dosed with either WF1 or BF1 (refer to Table 8.1 below) at final concentrations of 1.25 mg/l. All four samples from each population group were incubated at 37 ^{0}C in a water bath and agitated at 100 rpm. Since neither ultrafiltration nor the addition of UPTF1 alters the CaOx MSL (Doyle *et al.*1995, Ryall *et al.*1995), equal NaOx loads in excess of the filtered urines' MSL were added to all four samples from each population group. Crystallisation was induced by the addition of a NaOx load (30 mmol/l in excess of MSL, 0.1 ml NaOx per 100 ml urine) at 0 and 1 hour. After a further hour, the crystals were collected by filtration (0.22 µm) and washed briefly with 0.1 mol/l sodium hydroxide followed by thorough washing with distilled water. A shortened incubation period of 2 hours (compared with 3 hours for UPTF1 isolation) was used to ensure that a minimal layer of CaOx mineral was deposited around the intracrystalline proteins, so that they would be suitable for protease studies. The precipitated crystals were dried at 37 ^{0}C for 30 minutes and stored at -20 ^{0}C for later use.

Owing to technical difficulties with the ultrafiltration apparatus, large amounts of protein were observed (by SDS-PAGE) in the CaOx crystals from ultrafiltered urine. Negligible contamination was evident in the UF crystals dosed with UPTF1. Thus in a separate experiment, additional urines from five white and five black subjects were collected. The urines were pooled, filtered, ultrafiltered and CaOx crystals were prepared

as described above. Crystals prepared from the various urine samples are henceforth referred to by the abbreviations shown in Table 8.1 below.

Table 8.1: Abbreviations used to denote crystals prepared from white and black subjects' pooled urines before and after dosing with UPTF1 from both population groups

	White subjects' crystals	Black subjects' crystals
From filtered urine:	WF	BF
From ultrafiltered urine:	WUF	BUF
From ultrafiltered urine dosed with WF1:	WUF+WF1	BUF+WF1
From ultrafiltered urine dosed with BF1:	WUF+BF1	BUF+BF1

8.2.2 SDS-PAGE

The crystals to be analysed were demineralised and desalted as described elsewhere (paragraph 6.2.4, page 138). The protein peaks collected were freeze-dried, dissolved in distilled water and diluted 1:4 with SDS reducing buffer [62.5 mmol/l Tris-HCl (pH 8.8), 2 % SDS, 10 % glycerol, 0.05 % Bromophenol Blue and 5 % β-mercaptoethanol]. Samples were heated at 100^0C for 5 minutes and then electrophoresed on 9 - 18% gradient gels with a 4 % stacking gel [6.5 % of a 30 % acrylamide in 0.8 % bisacrylamide solution, 139 mmol/l Tris-HCl (pH 6.8), 0.11 % SDS, 1.8 % Amps, 0.22 % TEMED] using a Tris-HCl running buffer [25 mmol/l Tris-HCl (pH 8.3), 192 mmol/l glycine, 0.1 % SDS]. Electrophoresis was carried out for 10 minutes at 10 mA, followed by 60 minutes at 15 mA. The protein bands were either detected by silver staining or transferred onto nitrocellulose membranes for immunostaining. For silver staining, the gels were fixed for 30 minutes (or overnight) [40 % ethanol (v/v), 10 % acetic acid (v/v)] followed by pretreatment in a sodium acetate solution for 10 minutes [0.603 mol/l sodium acetate, 8.06 mmol/l sodium thiosulphate, 30 % ethanol, 0.52 % glutaraldehyde]. After two rinses of 5 minutes each in distilled water, the gels were incubated in a silver solution [5.88 mmol/l silver nitrate, 0.008 % formaldehyde] for 30 minutes. The silver was then washed off with two rinses of 1 minute each with distilled water and the gels were developed [0.236 mol/l sodium carbonate, 0.01 % formaldehyde]. The development was stopped by addition of a solution of EDTA [39.2 mmol/l $EDTANa_2.H_20$].

8.2.3 Western blotting

After electrophoresis, gels were soaked in blotting buffer [19.8 mmol/l Tris, 0.150 mol/l glycine, 16 % methanol, pH 8.3] for 15 minutes prior to assembly in the Bio-Rad Mini

Trans-Blot apparatus. Proteins were then transferred onto a nitrocellulose membrane in blotting buffer at 100 V for 1 hour, with cooling, followed by immunodetection. Non-specific sites on the membranes were blocked with a phosphate buffer (PBS) [145 mmol/l NaCl, 6.26 mmol/l $K_2HPO_4.3H_2O$, 1.84 mmol/l KH_2PO_4, pH 7.3] for 1 hour. The blot was then probed for UPTF1 and OPN with antibodies diluted in PBS with 3 % fat-free skim milk powder and 0.05 % Tween-20. One half of the membrane was equilibrated in a 3:1000 dilution of B19-1 IgG (Stapleton *et al.* 1996) and the other was equilibrated in a 1:2500 dilution of rat anti-human OPN IgG (Chemicon, Temecula, USA) for 1 hour. The membranes were washed with PBS (3 washes of 5 minutes each) after which the monoclonal antibodies were probed with a 1:250 dilution of goat anti-mouse IgG HRP conjugate (Bio-Rad) and 3:4000 goat anti-rat IgG HRP conjugate (Chemicon, Temecula, USA), respectively, for 1 hour. The membranes were washed three times with PBS (5 minutes per wash) and developed in a 3,3'-diaminobenzidine (DAB) solution [0.06 % DAB, 0.1 % H_2O_2] for approximately 4 minutes and washed with distilled water to stop the reaction.

8.2.4 Proteolytic digestion and partial dissolution of crystals

Prior to digestion, crystals were placed on a glass slide and fractured using a metal spatula. Crystals were viewed under a light microscope to confirm that a significant proportion had been fractured before further use. Crystals (0.25 mg) were then transferred to a glass scintillation vial and incubated at 37 ^{0}C with agitation (100 rpm) for 16 hours in a 0.5 ml solution containing 12.5 mmol/l Tris-HCl (pH 6.0) in both a saturated or unsaturated CaOx solution, and 2 units/ml of cathepsin D (Sigma), thrombin (CSL Limited) or Proteinase K (Roche). Refer to Appendix G (Table G2, page A78) for the preparation of the CaOx solutions.

Crystals before treatment (referred to as the control samples) and those incubated in the buffers alone were included. The unsaturated CaOx buffer was used to bring about partial dissolution, whereas the saturated buffer ensured minimal crystal dissolution and thus facilitated the observation of proteolysis alone.

After the 16-hour incubation period, an aliquot (0.2 ml) was removed from each scintillation vial and filtered onto a 0.22 µm filter paper. The filters were washed thoroughly with distilled water, dried at 37^{0}C for at least 30 minutes and glued onto aluminium stubs. The crystals were coated with Au/C and examined using a field emission scanning electron microscope (Philips XL30, University of Adelaide, Australia) operating

at an accelerating voltage of 10 kV and a working distance of 10 mm. A summary of the treatments for each batch of crystals is shown below (Table 8.2).

Table 8.2: Summary of treatments used for various crystals

	Control	* Unsat CaOx buffer	** Sat CaOx buffer	CathD	Throm	ProK
WF	√	√	√	√	√	√
WUF	√		√	√		
WUF+WF1	√	√		√	√	√
WUF+BF1	√	√		√	√	√
BF	√	√	√	√	√	√
BUF	√		√	√		
BUF+WF1	√	√		√	√	√
BUF+BF1	√	√		√	√	√

[a] *Unsaturated CaOx buffer to bring about partial dissolution*
; [b] *Saturated CaOx buffer to ensure minimal crystal dissolution*

8.3 RESULTS

8.3.1 Urine composition

Urine composition (mmol/l) and physicochemical parameters of the pooled urines from white and black subjects used to prepare the CaOx crystals are presented in Appendix G (Table G1, page A78).

8.3.2 SDS-PAGE and Western blotting

The SDS-PAGE of CaOx crystals prepared for proteolysis and dissolution studies is shown below (Figure 8.1). The gel confirmed that the crystals obtained from filtered urine contained a range of proteins, whereas no protein was detected in crystals from the ultrafiltered urines. A large proportion of the protein from WF and BF (Figure 8.1) was identified as UPTF1 and OPN by Western blotting (Figures 8.2.1 and 8.2.2, respectively). It is evident that BF included considerably more UPTF1 and OPN per milligram of CaOx than WF (Figure 8.2), although this could not be quantified from the gel.

SDS-PAGE demonstrated that crystals obtained after dosing ultrafiltered urine with UPTF1 (~31 kDa) also contained additional bands corresponding to PT-related proteins (Figure 8.1). These were observed at 20, 48, 60 and 72 kDa. The band at 48 kDa is PTF1+2. The bands at ~60 and higher kDa values almost certainly represent the UPTF1 dimer, and heterodimers of UPTF1, PT and other of its fragments, which are known to

form in the presence of calcium ions (Harlos *et al.* 1987). WUF+WF1 appeared to bind more PT (~72 kDa) relative to the amount of UPTF1 than the crystals from BUF dosed with UPTF1.

Multiple bands were observed in the crystals from both population groups blotted for OPN (Figure 8.2.2), which is in agreement with a previous report that the molecular weight of OPN varies widely from 20 - 75 kDa in SDS-PAGE systems (Denhardt and Guo 1993). The multiple bands observed in the present study would have resulted from degradation of OPN by urinary proteases (Ryall *et al.* 2001a). Identical OPN protein patterns have been observed by Ryall (R. Ryall, Flinders Medical Centre, Australia, personal communication).

Figure 8.1: SDS-PAGE of CaOx urine crystals. The patterns were obtained from *MW:* low molecular weight standard and the following crystals: WF, WUF, WUF+WF1, BF, BUF, BUF+WF1 and BUF+BF1. Insufficient WUF+BF1 crystals were available for SDS-PAGE.

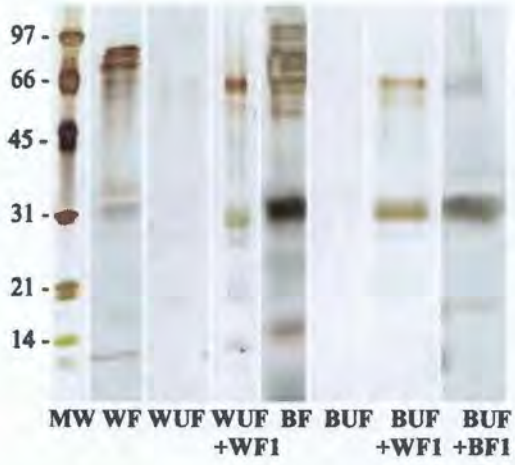

Figure 8.2: Western blot of CaOx urine crystals. The patterns were obtained from *MW:* pre-stained molecular weight marker, and crystals from white (WF) and black (BF) subjects' filtered urine immunoblotted for **(8.2.1)** UPTF1 and **(8.2.2)** osteopontin.

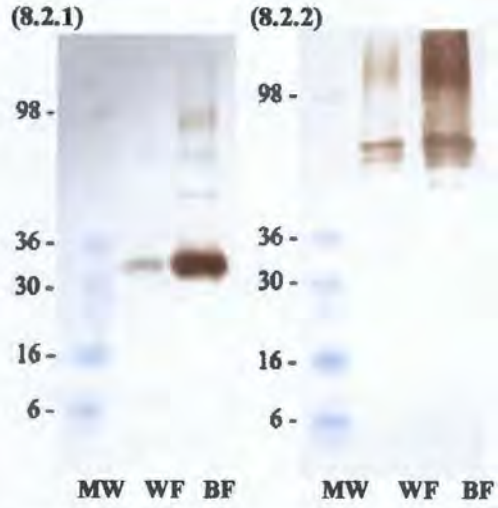

8.3.3 FESEM of control crystals

8.3.3.1 Crystals from ultrafiltered urine

Electron micrographs of the crystals precipitated from ultrafiltered urine of white and black subjects were similar and thus representative examples are shown in Figure 8.3. Before treatment, the bipyramidal COD crystals had little surface texture (Figure 8.3.1) and appeared to be solid (Figure 8.3.2). Most COM crystals were oval-shaped and had smooth surfaces (Figure 8.3.1), although a few had surface detail, particularly on the {101} face

(Figure 8.3.3). Crystal shape and texture of COM (Figure 8.3.4) and COD (Figure 8.3.5) were unaffected by incubation in the saturated CaOx buffer. Both COM (Figure 8.3.6) and COD (Figures 8.3.7 - 8.3.8) were resistant to digestion by cathepsin D.

Technical difficulties were encountered with the first batch of crystals prepared from ultrafiltered urine (UF) (described on page 176). As a result the crystals presented in Figure 8.3 do not originate from the same urines used in the remainder of the study (Figures 8.4 – 8.14). However, the appearance of UF crystals both before and after protease treatment was similar in ultrastructure to a previous report (Ryall *et al.* 2001b). Thus, in addition to the absence of protein (>10 kDa) observed by SDS-PAGE (Figure 8.1, lanes WUF and BUF), this confirmed that the UF crystals were appropriate for use as a negative control in the present study.

Figure 8.3: Field emission scanning electron micrographs of UF CaOx crystals before and after protease treatment in a saturated CaOx buffer. The crystals underwent the following treatments: control (8.3.1 – 8.3.3), saturated CaOx buffer (8.3.4 – 8.3.5), and Cathepsin D in the saturated CaOx buffer (8.3.6 – 8.3.8).

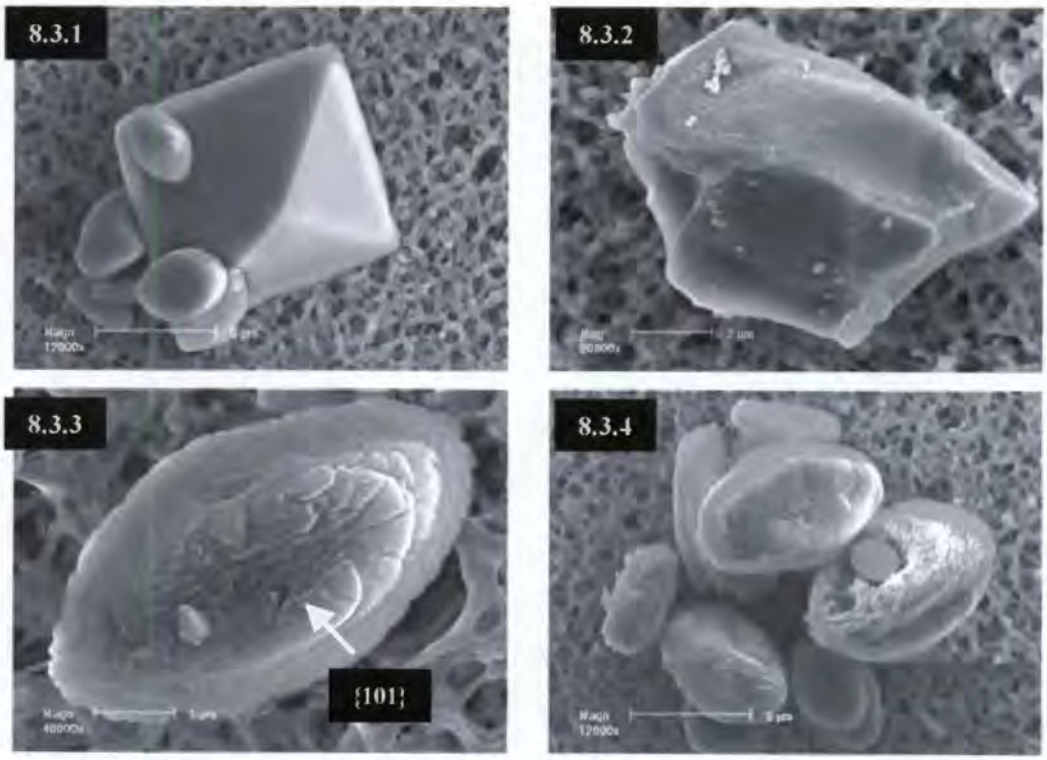

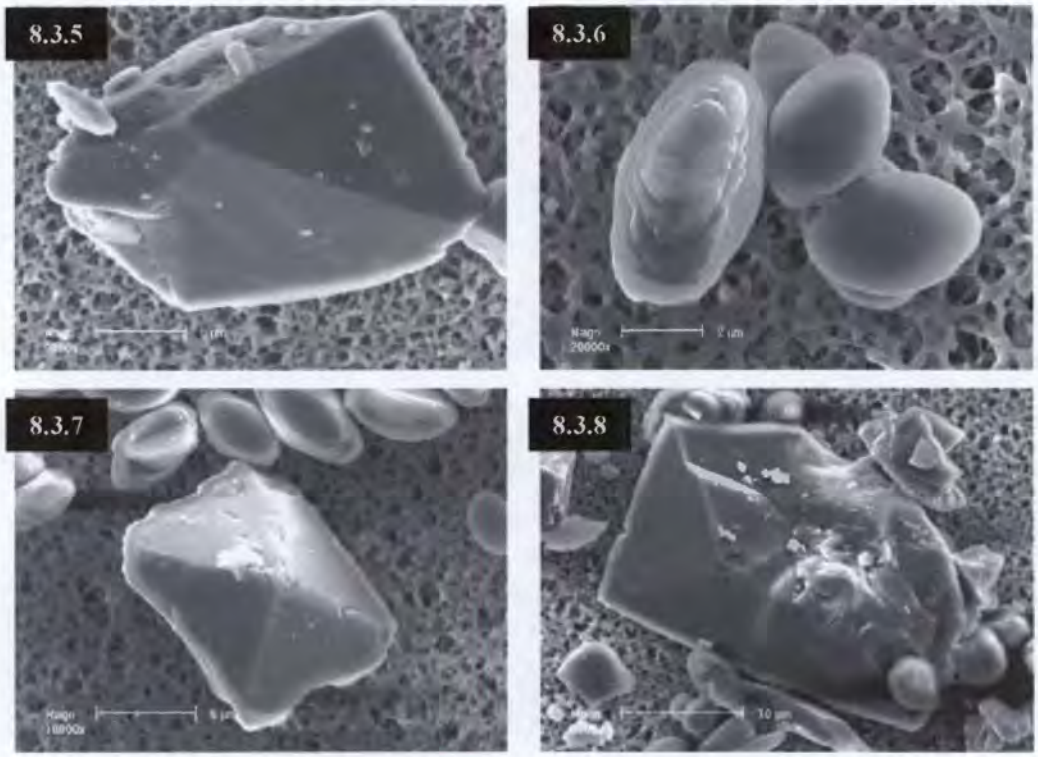

8.3.3.2 Crystals from filtered urine and ultrafiltered urine dosed with UPTF1

Crystals from white subjects

The micrographs presented in Figure 8.4 are of crystals derived from a pooled urine of white subjects. The images obtained from filtered urine and ultrafiltered urine dosed with either WF1 or BF1 are presented separately, and all are before treatment. However, since no differences between the three sets of crystals were observed, the comments are applicable to all three sets of crystals from the white subjects. A survey view of WF (Figure 8.4.1) showed the predominance of COD crystals from the white subjects, although some small COM crystals were also observed.

Several COM crystals showed the presence of surface detail on the {010} face (Figure 8.4.2) and the core of COM crystals appeared to be more porous than near the periphery (Figures 8.4.4, 8.4.6). In contrast, most COD crystals showed little evidence of erosion and were relatively smooth (Figure 8.4.5) and solid (Figures 8.4.3, 8.4.5, 8.4.7).

Figure 8.4: Field emission scanning electron micrographs of WF, WUF+WF1 and WUF+BF1 CaOx crystals before treatment. The crystals are as follows: WF (8.4.1 – 8.4.3), WUF+WF1 (8.4.4 - 8.4.5), and WUF+BF1 (8.4.6 - 8.4.7).

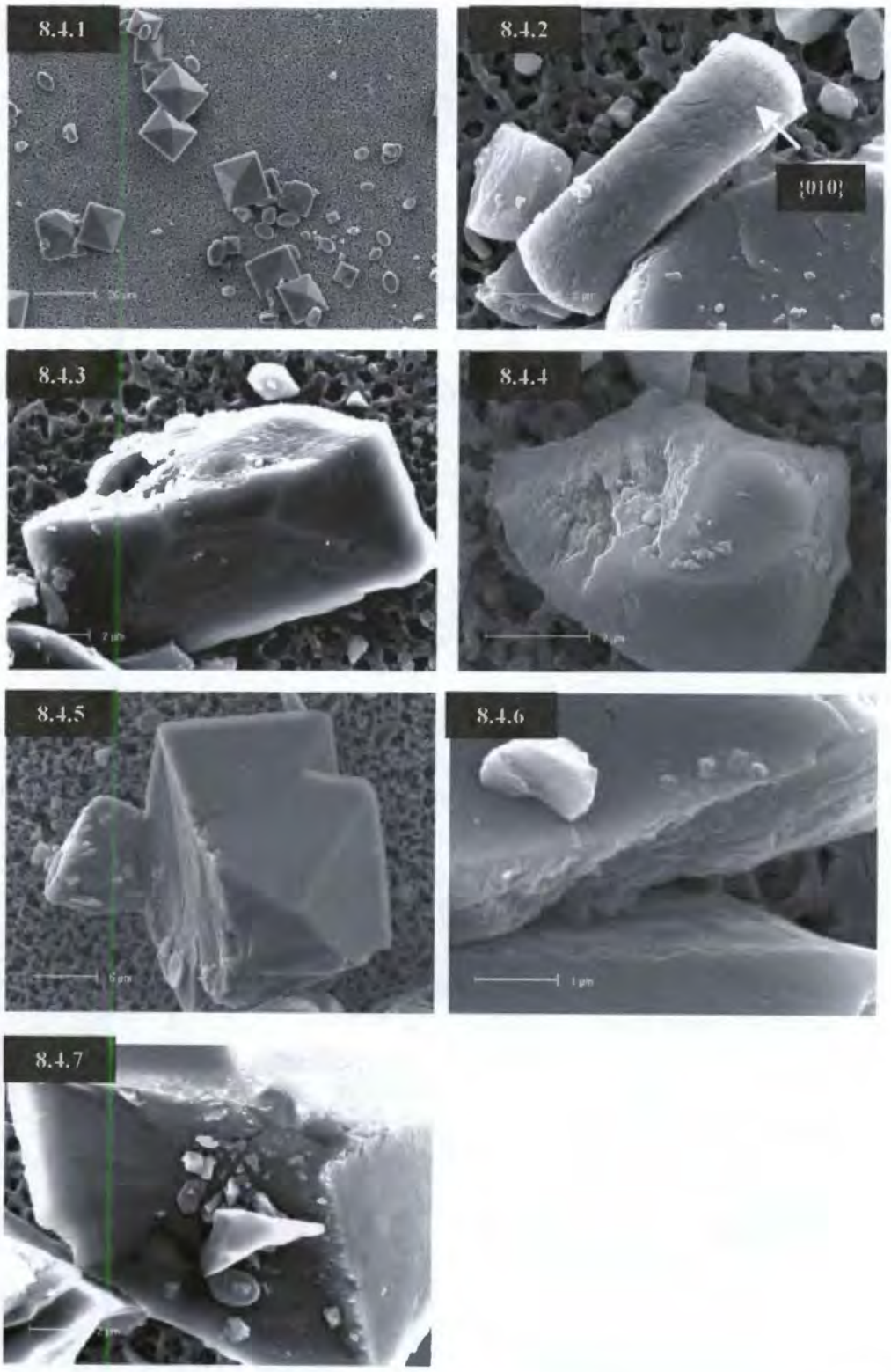

Crystals from black subjects

Figure 8.5 presents micrographs of crystals derived from a pooled urine of black subjects. The images obtained from filtered urine and ultrafiltered urine dosed with either WF1 or BF1 are presented separately, and all are before treatment. However, similarly to the white subjects' crystals described above, no differences between the three sets of crystals were observed. Thus the comments are applicable all three sets of crystals from the black subjects. A survey view of BF (Figure 8.5.1), taken at the same magnification as the WF survey image shown above (Figure 8.4.1), showed the predominance of COM crystals from the black subjects, in contrast to COD which was the principal CaOx hydrate in the urine of white subjects.

Fine fissures were observed on the {101} face (Figure 8.5.2) as well as in the interior of COM crystals (Figure 8.5.3). These observations were consistent with the binding and inclusion of urinary proteins. The exterior of COM crystals were not as smooth and well defined (Figures 8.5.5, 8.5.7) as those observed from ultrafiltered urine (Figure 8.3.6). In contrast to the COMs, most COD crystals appeared to be relatively solid (Figures 8.5.4, 8.5.6, 8.5.8). Although this was not common, some surface erosion of COD crystals was observed (Figure 8.5.8).

Figure 8.5: Field emission scanning electron micrographs of BF, BUF+WF1 and BUF+BF1 CaOx crystals before treatment. The crystals are as follows: BF (8.5.1 - 8.5.4), BUF+WF1 (8.5.5 - 8.5.6), and BUF+BF1 (8.5.7 - 8.5.8).

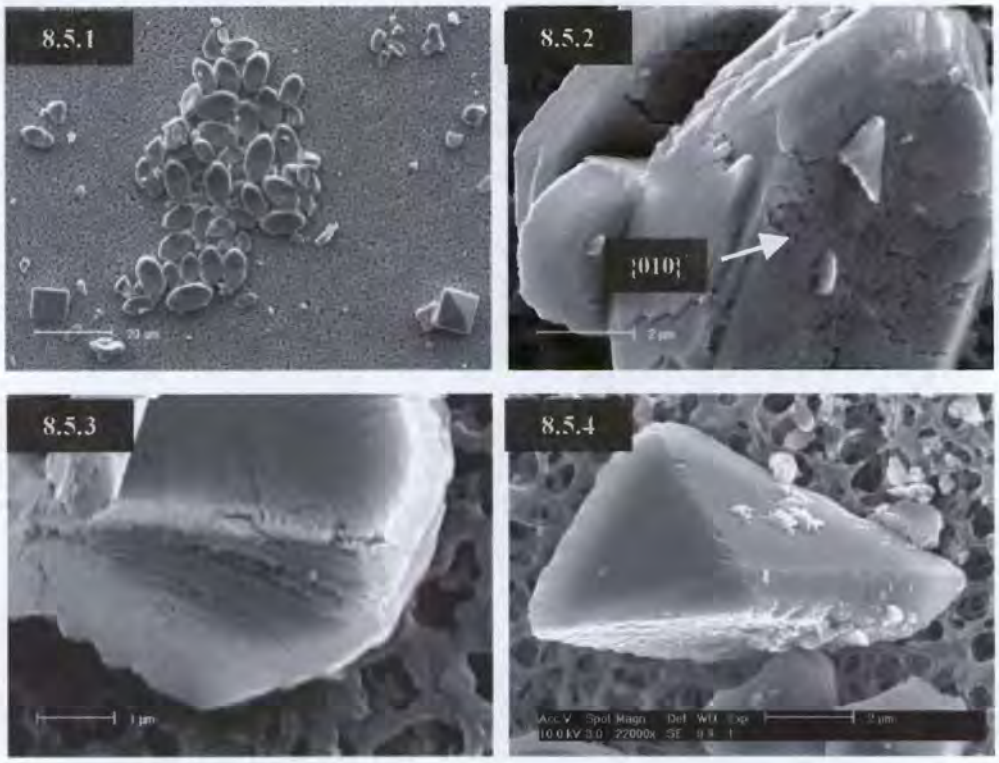

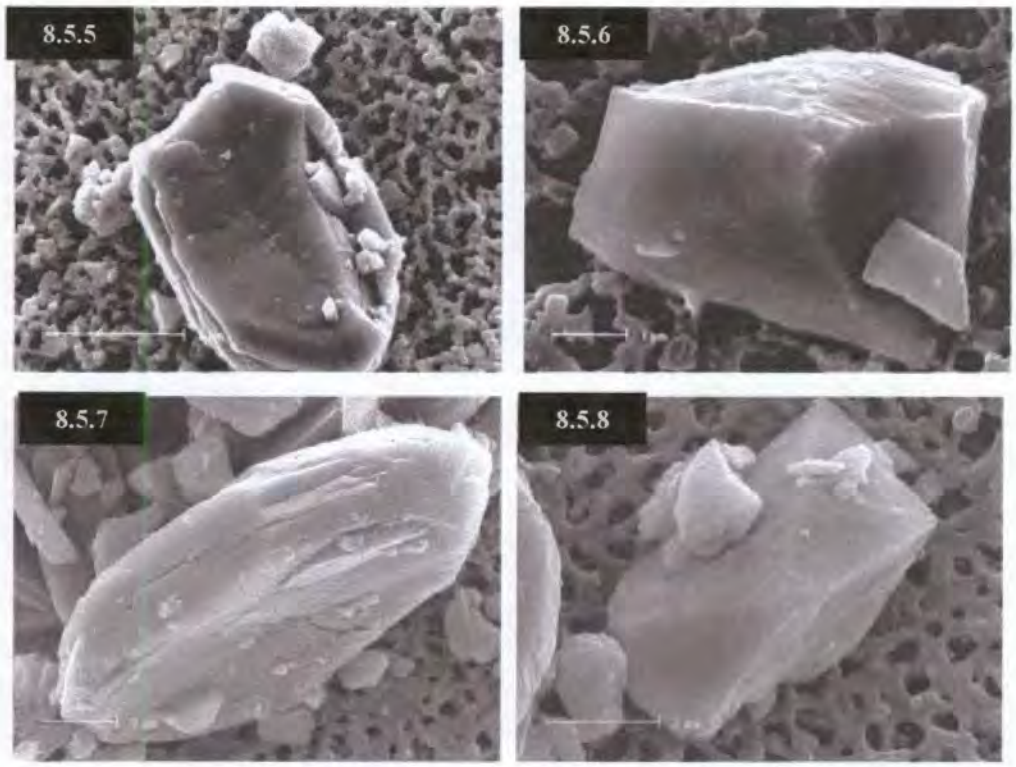

8.3.4 FESEM showing proteolysis

8.3.4.1 Crystals from white subjects

Crystals from the filtered urine of white subjects (Figure 8.6) were incubated in a saturated CaOx buffer along with various proteases in order to demonstrate proteolysis. In the presence of the buffer alone, a few COM crystals underwent partial dissolution (Figure 8.6.1), althoug h most remained intact. The edges of COD crystals were slightly eroded (Figure 8.6.2).

Figure 8.6: Field emission scanning electron micrographs of WF CaOx crystals before and after protease treatment in a saturated CaOx buffer. The crystals underwent the following treatments: saturated CaOx buffer (8.6.1 – 8.6.2); cathepsin D (8.6.3 - 8.6.4), thrombin (8.6.5 – 8.6.6) and Proteinase K (8.6.7 – 8.6.8) in the saturated CaOx buffer.

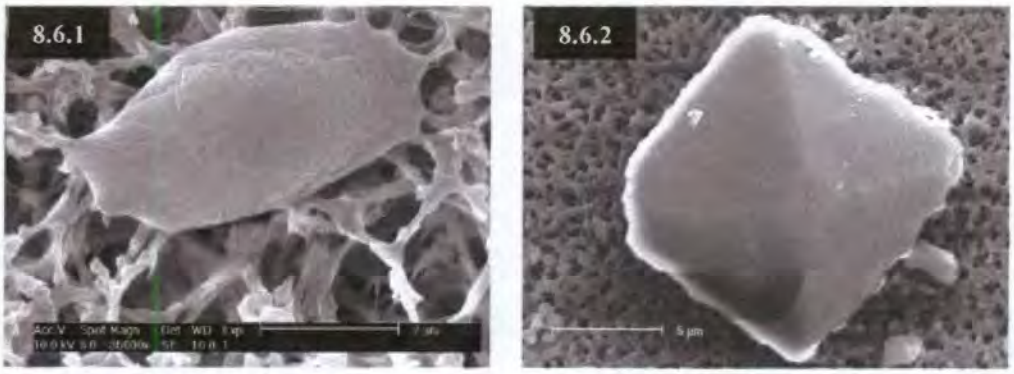

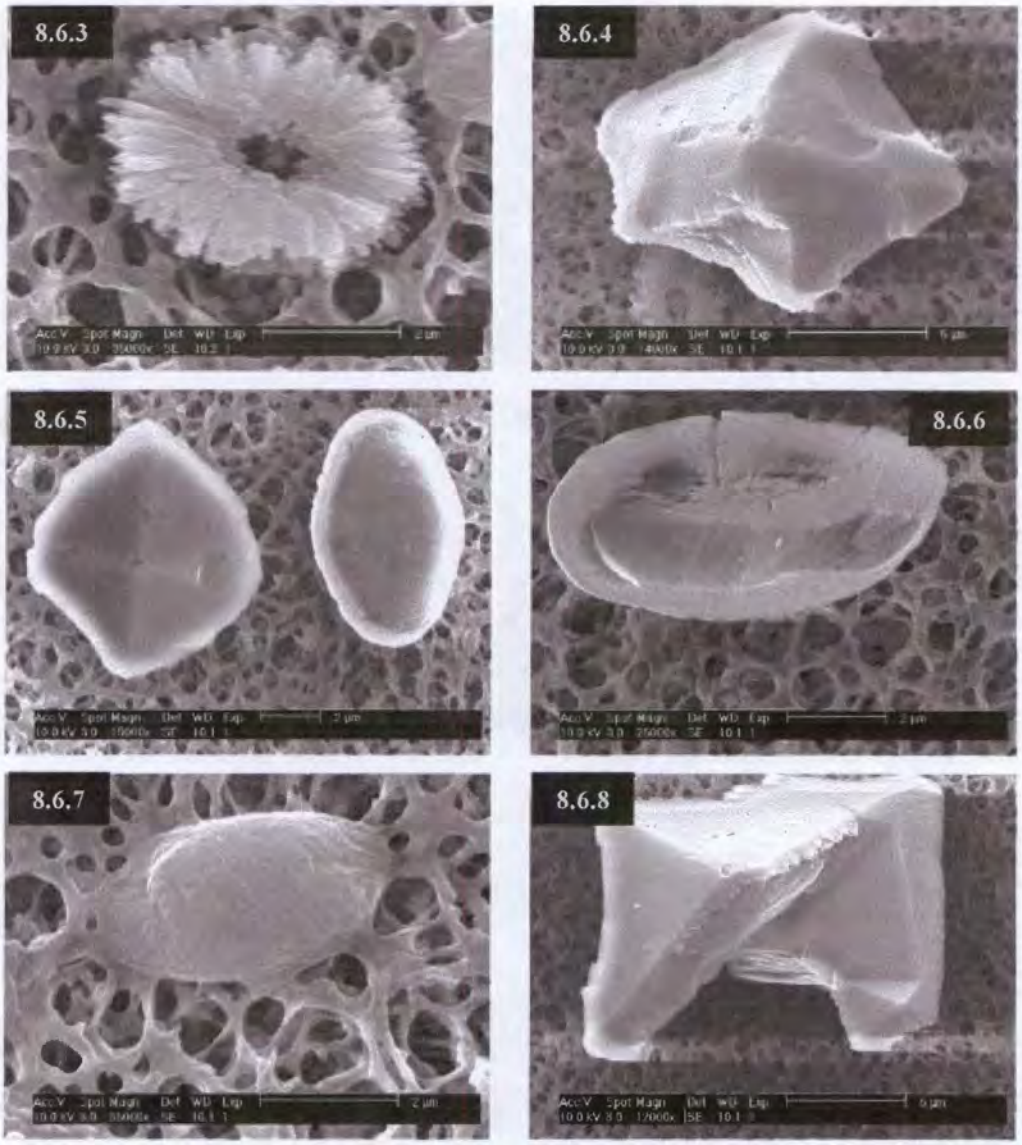

Incubation with cathepsin D resulted in varying degrees of proteolysis of COM crystals. In the most advanced cases of proteolysis, complete digestion of the core of crystals was observed (Figure 8.6.3), with the result that a doughnut-shaped exterior remained. COD crystals appeared relatively intact after treatment with cathepsin D (Figure 8.6.4). Neither COM (Figure 8.6.5 – 8.6.6) nor COD crystals (Figure 8.6.5) were notably affected by treatment with thrombin. After incubation with Proteinase K some, but not all, COM crystals showed signs of dissolution (Figure 8.6.7). The COD crystals were relatively intact except for some minor surface pitting (Figure 8.6.8).

8.3.4.2 Crystals from black subjects

Crystals from the filtered urine of black subjects after the same protease treatments are shown in Figure 8.7. In the presence of the buffer alone, most COM crystals remained

intact (Figure 8.7.1), while COD crystals developed slightly jagged edges and some erosion on the {101} faces (Figure 8.7.2).

Incubation with cathepsin D resulted in varying degrees of proteolysis. COM crystals showed evidence of slight erosion (Figure 8.7.3), while COD crystals appeared relatively intact after treatment (Figure 8.7.4). Similar to the crystals from white subjects, COM (Figure 8.7.5) and COD crystals (Figure 8.7.6) appeared resistant to treatment with thrombin. However, some crystal fragments were observed on the COM and COD crystal surfaces. COM crystals incubated with Proteinase K were unaffected (Figure 8.7.7), whereas significant surface erosion of COD crystals was observed (Figure 8.7.8). The {101} face of COD crystals were considerably more eroded then the same sample incubated in the buffer alone (Figure 8.7.2).

Figure 8.7: Field emission scanning electron micrographs of BF CaOx crystals before and after protease treatment in a saturated CaOx buffer. The crystals underwent the following treatments: saturated CaOx buffer (8.7.1 – 8.7.2); cathepsin D (8.7.3 – 8.7.4), thrombin (8.7.5 - 8.7.6) and Proteinase K (8.7.7 – 8.7.8) in the saturated CaOx buffer.

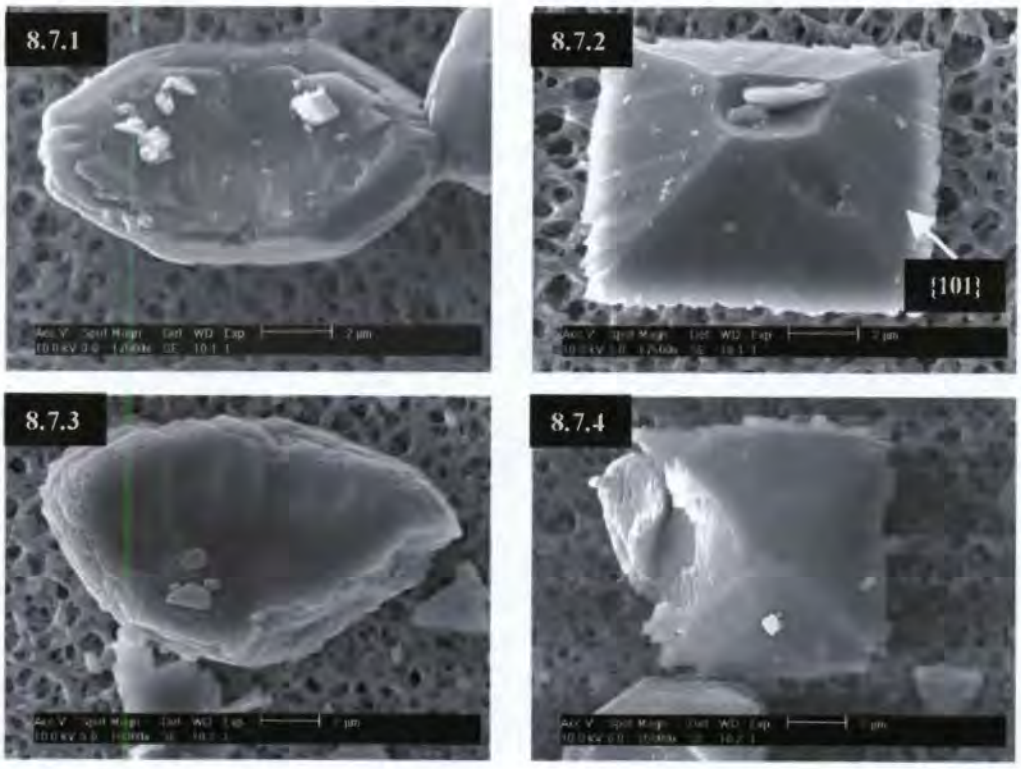

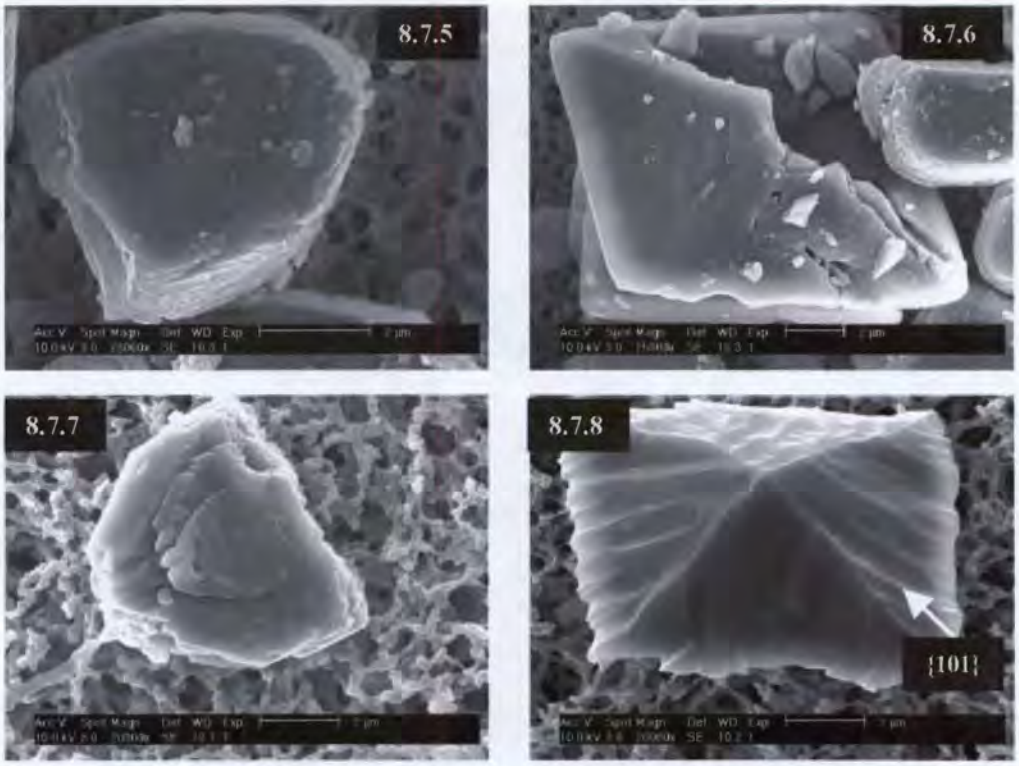

8.3.5 FESEM showing proteolysis and dissolution

Crystals prepared from filtered urine of white (WF) and black (BF) subjects, as well as both population groups' ultrafiltered urine dosed with either WF1 or BF1 (UF+WF1, UF+BF1), were treated with proteases in an unsaturated CaOx buffer. No differences were observed in crystals containing a mixture of proteins (WF, BF) and those containing mostly prothrombin fragments (UF+WF1, UF+BF1). The susceptibility of COM and COD crystals to treatment was also the same, whether from white or black subjects, although the relative proportion of the two CaOx hydrates differed in the two groups, as described before. Thus, in order to present the large number of micrographs in a manageable way, the micrographs were grouped according to their protease treatment, rather than the origin of the crystals (since these showed no differences). Furthermore, crystals derived from white and black subjects are not presented separately; representative examples are included.

8.3.5.1 Effect of cathepsin D

In the presence of cathepsin D and the unsaturated CaOx buffer, COM crystals were eroded and degraded to varying degrees. In some crystals, only surface detail on the {101} face (Figure 8.8.1) and moderate erosion (Figure 8.8.7) was evident. A cross-section of a COM crystal showed signs of fissures and porosity in the crystal interior (Figure 8.8.12). However, in other crystals, disintegration was more significant and sub-crystallites were

observed on the {010} face (Figure 8.8.2) as well as in the crystal interior (Figure 8.8.6). The COM crystal surface, which was relatively smooth before treatment (refer Figure 8.5.7 on page 185 for a typical example), was highly eroded in a few crystals and a highly porous ultrastructure was evident (Figures 8.8.3, 8.8.8). The effect of cathepsin D appeared to be most advanced in the crystal depicted in Figure 8.8.11, where numerous closely packed sub-crystalline particles were evident. Most of the core of the crystal appeared to have been excavated by the treatment.

Figure 8.8: Field emission scanning electron micrographs of CaOx crystals after incubation with cathepsin D in an unsaturated CaOx buffer. The following crystals were treated: WF/BF (8.8.1 - 8.8.5); UF+WF1 (8.8.6 – 8.8.10); UF+BF1 (8.8.11 - 8.8.14).

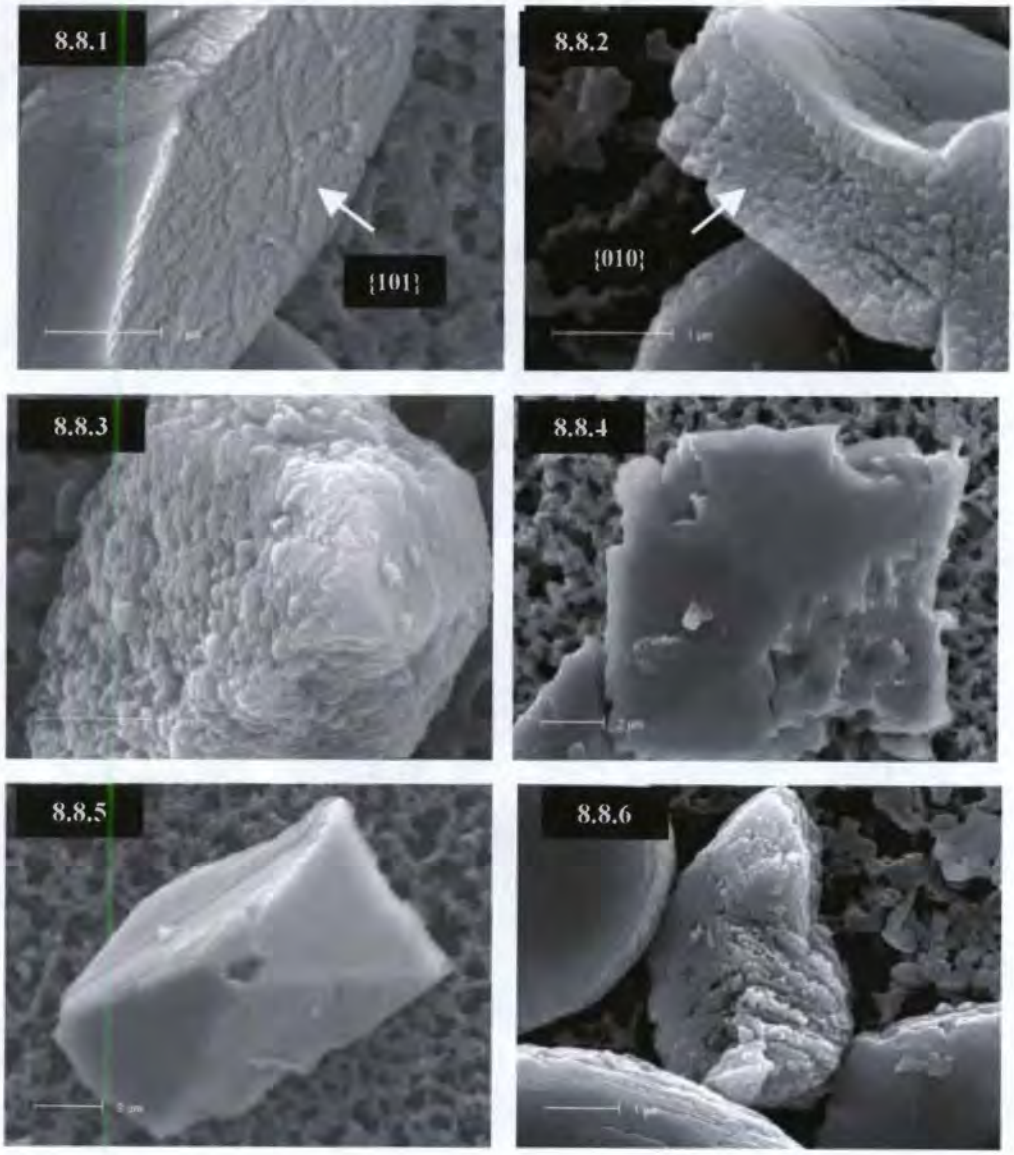

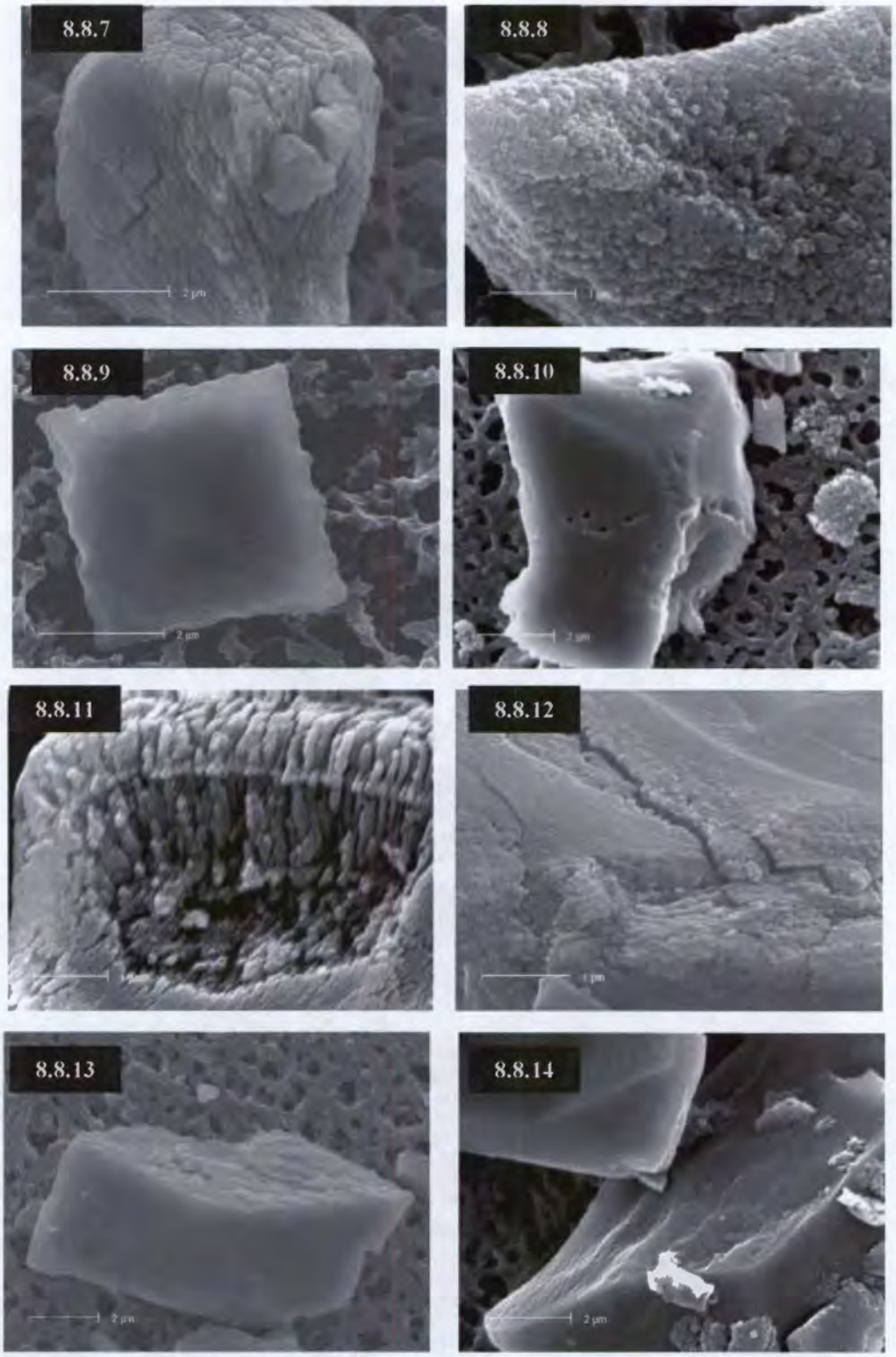

The majority of COD crystals were unaffected and appeared to be relatively smooth and solid after treatment (Figures 8.8.5, 8.8.13). However, some surface pitting and deformation (Figures 8.8.4, 8.8.10) of COD crystals was observed, along with slightly eroded edges (Figure 8.8.9). Minor etching of the surface of a few COD crystals was noted (Figure 8.8.14). Significant dissolution was not evident when the unsaturated CaOx buffer was used along with cathepsin D.

8.3.5.2 Effect of thrombin

The interior of COM crystals (Figure 8.9.2, 8.9.7, 8.9.9) appeared to be similar to those before treatment (compare Figure 8.5.3 on page 184), although porosity was evident. Some COM surfaces showed signs of erosion (Figure 8.9.6), but most were still relatively smooth and intact after treatment with thrombin in the unsaturated CaOx buffer. Sticking of crystal fragments to the surface of COM (Figures 8.9.1, 8.9.7, 8.9.9) and COD (Figure 8.9.3) crystals was frequently observed after incubation with thrombin. This may have indicated that the crystals were coated with excess protease, and also that the buffer did not dissolve these fragments. Several COD crystals had a shiny appearance (Figures 8.9.5), which may also have been indicative of a thrombin coating. Etching of COD surfaces was observed (Figures 8.9.4, 8.9.8, 8.9.10).

Figure 8.9: Field emission scanning electron micrographs of CaOx crystals after incubation with thrombin in an unsaturated CaOx buffer. The following crystals were treated: WF/BF (8.9.1 - 8.9.5); UF+WF1 (8.9.6 – 8.9.8); UF+BF1 (8.9.9 - 8.9.10).

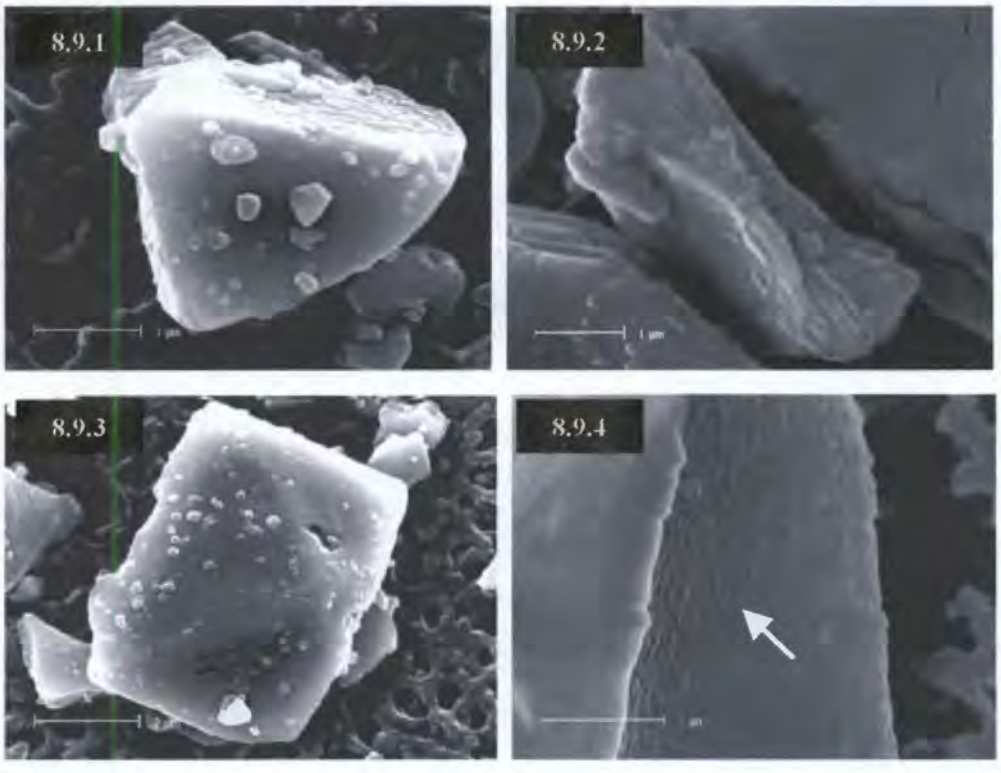

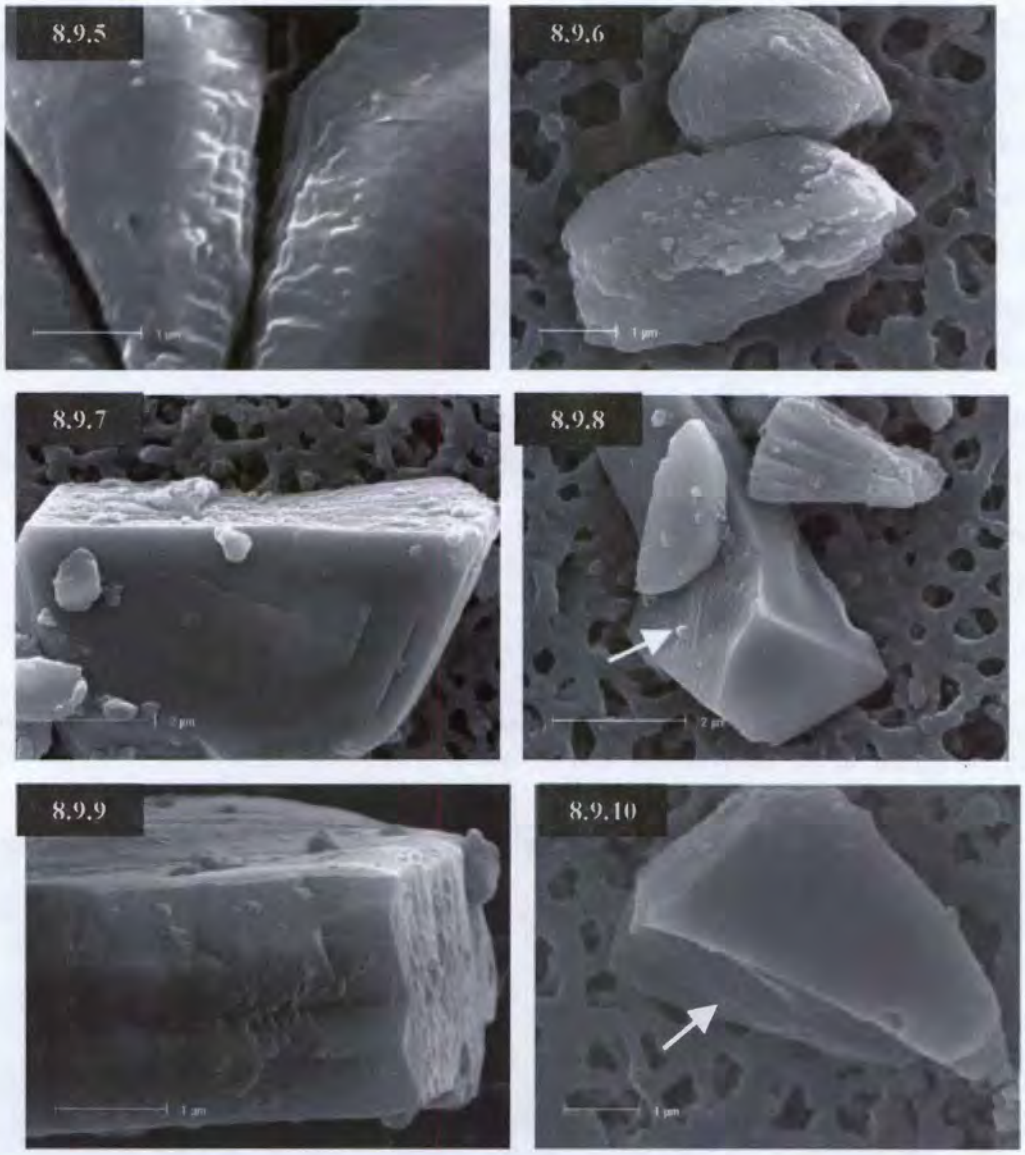

8.3.5.3 Effect of Proteinase K

Crystals incubated with Proteinase K and the unsaturated CaOx buffer showed signs of erosion and significant dissolution. While some COM crystals appeared to be unaffected (larger COM in Figure 8.10.1), some were notably deformed (Figure 8.10.7) and had apparently dissolved from the interior, being concave in appearance (Figure 8.10.2; COM in Figure 8.10.5). In the latter case, a large amount of organic material was evident on the filter papers (*e.g.* around smaller COM in Figure 8.10.1) and fewer crystals were observed than in the corresponding control samples.

Figure 8.10: Field emission scanning electron micrographs of CaOx crystals after incubation with Proteinase K in an unsaturated CaOx buffer. The following crystals were treated: WF/BF (8.10.1 - 8.10.4); UF+WF1 (8.10.5 – 8.10.6); UF+BF1 (8.10.7 - 8.10.8).

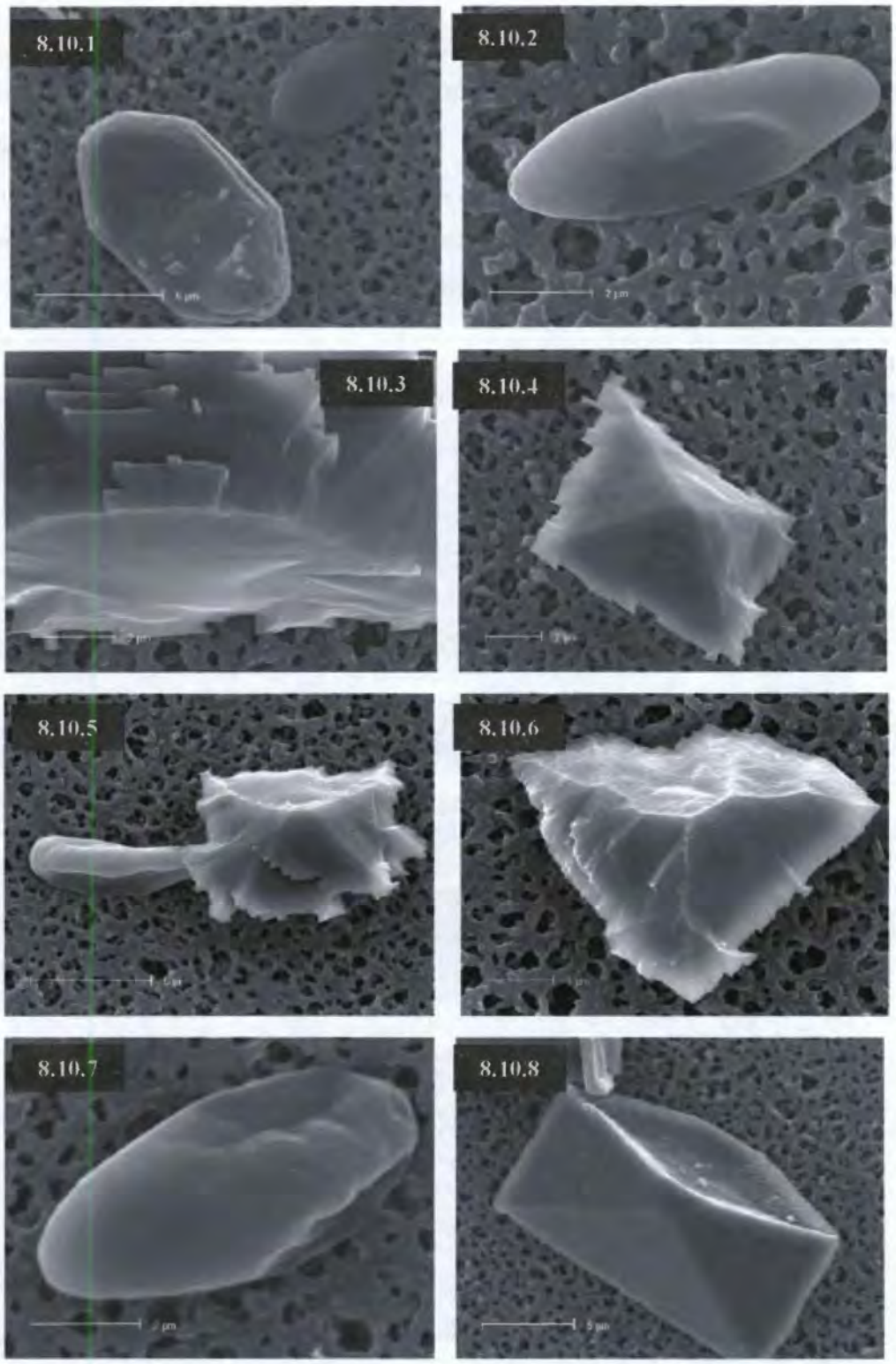

The COD crystals appeared to be relatively solid inside (Figures 8.10.3, 8.10.6, 8.10.8), but several had jagged edges (an example is shown in Figure 8.10.4). Many CODs

(Figures 8.10.5, 8.10.6), but not all (Figure 8.10.8), showed evidence of significant erosion on the crystal surfaces.

8.3.6 FESEM showing dissolution

Crystals incubated in the unsaturated CaOx buffer alone showed evidence of considerable dissolution and deformation. Since the most noteworthy feature of this study was the different effect on COM and COD crystals, this feature is depicted in the micrographs shown. No distinction is made between the batch of crystals or the population group of the subjects from which the crystals were derived.

8.11: Field emission scanning electron micrographs showing stages of COM crystal dissolution in an unsaturated CaOx buffer. (8.11.1 is a typical COM crystal before treatment)

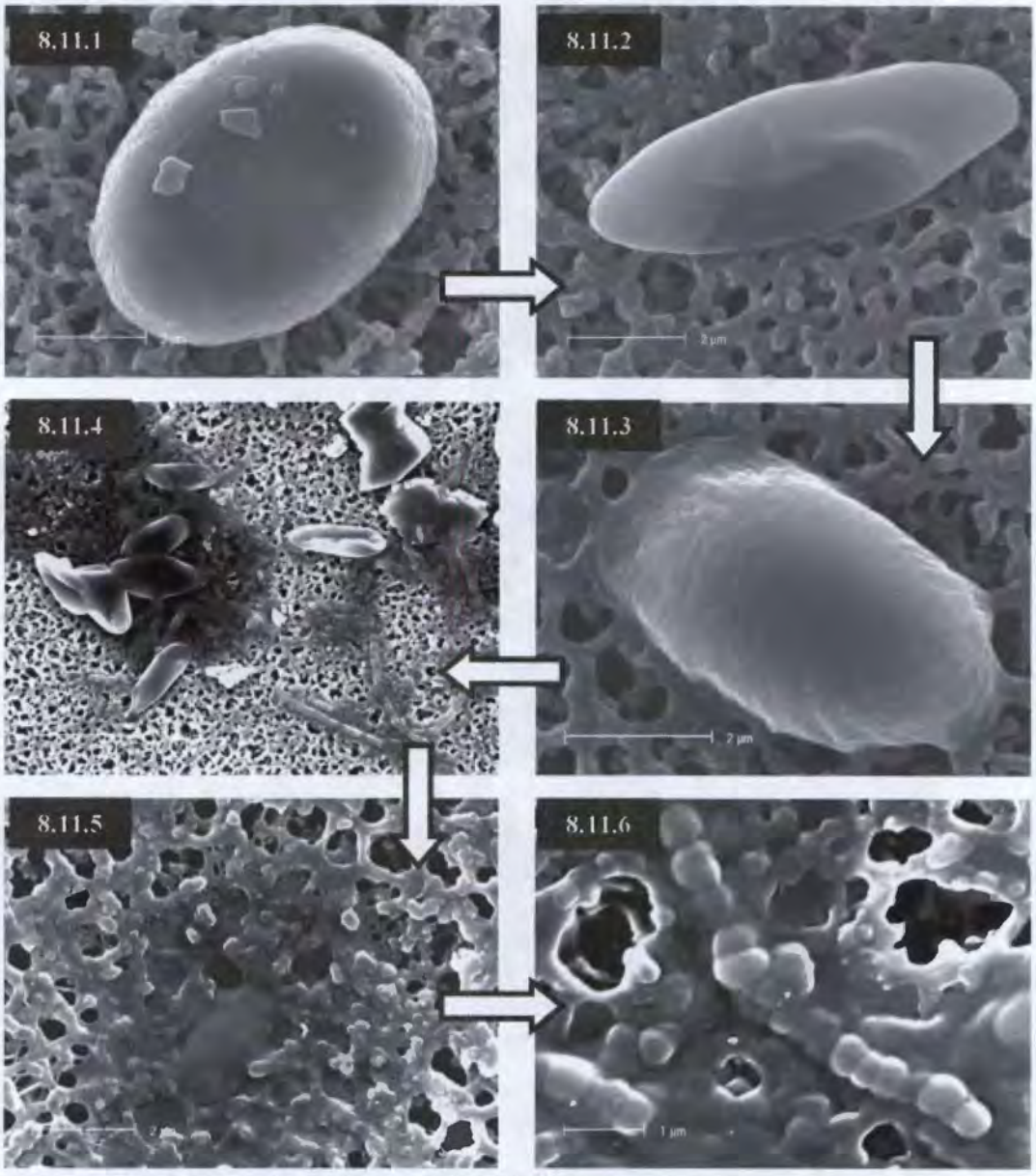

Figure 8.11 (above) shows a series of COM crystals following incubation in the unsaturated CaOx buffer alone, at various stages of dissolution. The arrows indicate the proposed pathway of dissolution from a single, intact COM (Figure 8.11.1) crystal to, possibly, its smallest fragments (Figure 8.11.6). Apparently single, whole COM crystals first showed evidence of dissolution at their inner core, being concave in appearance (Figure 8.11.2). Crystals appeared to have an organic "skin" (Figure 8.11.3), which was evident as dissolution progressed. Gradual dissolution coincided with the deposition of increasing amounts of organic material (Figure 8.11.4 - 8.11.5). Tiny, amorphous crystallites were observed and may have been the final stage of dissolution (Figure 8.11.6).

Figure 8.12: Field emission scanning electron micrographs showing COD crystal dissolution in an unsaturated CaOx buffer. (8.12.1 is a typical COD crystal before treatment)

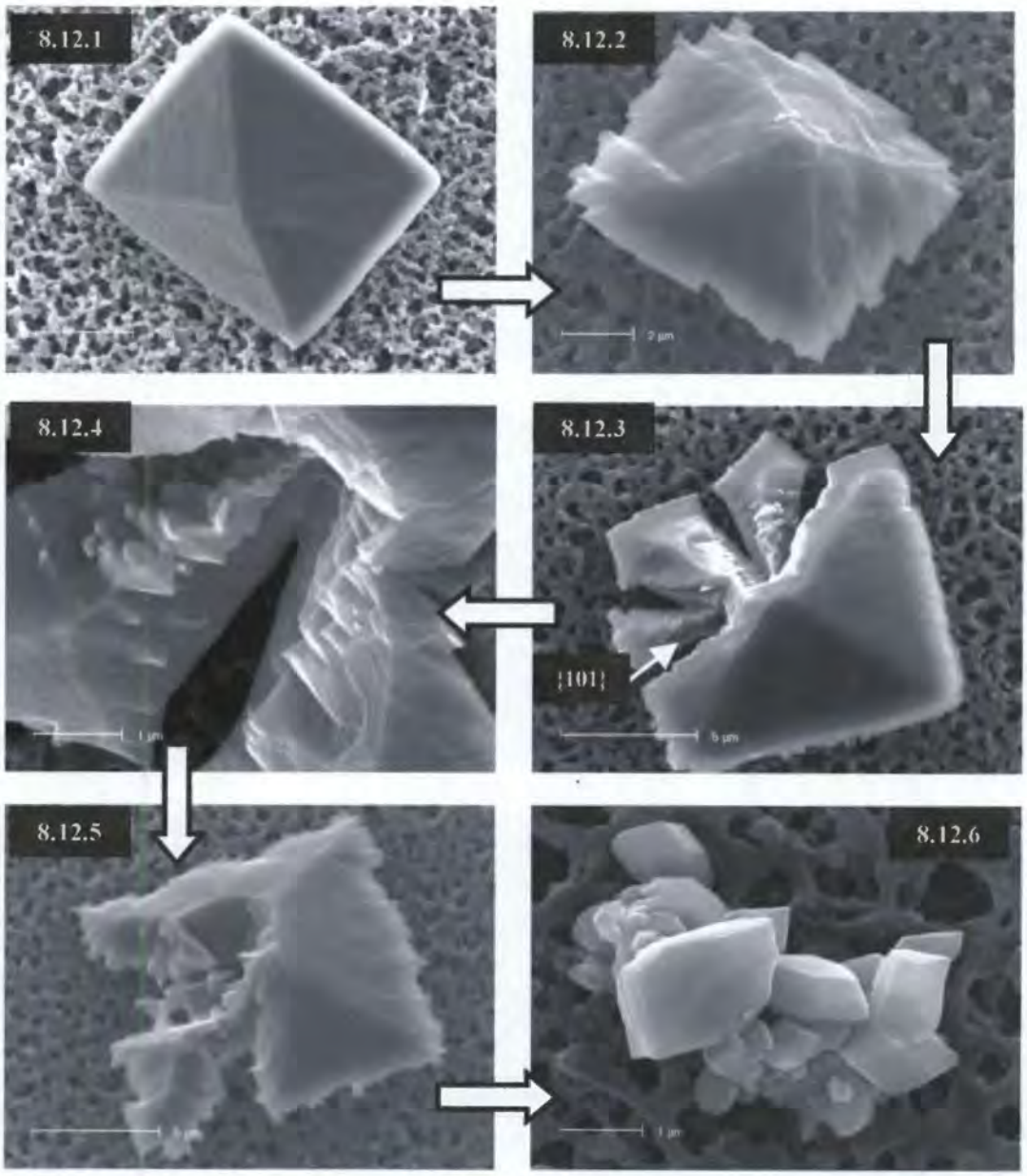

A similar series of micrographs represent COD crystals at various stages of dissolution (Figure 8.12 above). The arrows indicate the proposed pathway of dissolution from a single, intact COD (Figure 8.12.1) to, perhaps, its smallest fragment (Figure 8.12.6). Apparently single, whole COD fragmented progressively, first at their edges (Figure 8.12.2) and then on the {101} faces (Figures 8.12.3 – 8.12.4). Fracturing characteristically occurred along a common plane, namely the middle of the {101} face as depicted in Figure 8.12.3, and revealed tiny and geometrically arranged bipyramidal subunits (Figure 8.12.4). These subunits almost certainly represent crystallites. Further disruption of the crystal structure was also evident (Figure 8.12.5). Small, bipyramidal crystallites (Figure 8.12.6) were observed at, presumably, the most advanced stage of dissolution.

8.4 DISCUSSION

The proteolytic degradation of urinary CaOx crystals from both white and black subjects was demonstrated. In the presence of a saturated CaOx buffer (thus preventing significant dissolution), the addition of proteases resulted in the etching, degradation and even excavation of crystals to varying degrees. Since the crystals obtained from ultrafiltered urine appeared to have almost solid interiors and smooth surfaces, it may be assumed that the erosion observed with the crystals derived from filtered urine resulted from the removal of intracrystalline proteins. These findings are in agreement with previous reports by Ryall and co-workers (Ryall *et al.* 2000, 2001b).

Cathepsin D caused the most significant crystal erosion of the three proteases tested, and was also notably more effective in degrading COM as opposed to COD crystals. This may reflect selectivity by cathepsin D for COM-associated proteins, of which UPTF1 is predominant (Ryall *et al.* 2001a; chapter 7). In the most advanced cases of degradation, considerable excavation of the crystal interior was observed, exposing an array of tightly-packed subcrystalline particles. The removal of the core of some, but not all, COM crystals by protease treatment suggests that the protein was concentrated in the central region of the crystal and not near the edges (Ryall *et al.* 2001). This is consistent with the condensation of protein and the subsequent precipitation of mineral around it. As the urine is depleted of protein, the proportion of mineral shell surrounding it increases (Fleming *et al.* 1999).

Partial dissolution studies of COM and COD crystals permitted the observation of their unique ultrastructures, as well as stages of the fragmentation process. Whole, disc-shaped COM crystals first began to show signs of dissolution at their inner region. This was consistent with the location of protein at the centre of the CaOx crystal structure, as described above. In the latter stages of dissolution, tiny COM crystallites were observed amongst the organic material that was leached onto the filter paper. These particles may be amorphous composites of organic and inorganic material, and have been previously reported by Ryall and co-workers in COM and COD crystals (Ryall *et al.* 2000). Similar amorphous sub-units have also been reported by Addadi and co-workers in a study on biomineralisation in the marine sponge (Addadi *et al.* 1999).

The disintegration of bipyramidal COD crystals was first noted at their periphery where jagged edges appeared. Distinct fracture planes were also observed, typically in the centre of the {101} faces, and not along their edges. The strengthening of crystal planes against fracturing by proteins has been described previously in the sea urchin spine (Addadi *et al.* 1999), and would seem to be a plausible explanation in the case of urinary crystals too. The newly exposed surfaces revealed tiny, geometrically-arranged bipyramidal structures. These are likely to be the crystallites of which the apparently single COD crystals are composed.

A combination of dissolution and proteolysis was observed using an unsaturated CaOx buffer in conjunction with protease treatment. Since these two processes are likely to occur concurrently *in vivo*, these observations are probably the most physiologically relevant. Indeed, the combined effects of dissolution and proteolysis resulted in more significant erosion and degradation of CaOx crystals than in those subjected to either one of the processes alone. The effects of both thrombin and Proteinase K were most notable on COD crystals. Thrombin appeared to coat the surface of some CODs, and etching of crystal surfaces was also observed. The apparent selectivity of thrombin for COD crystals is consistent with the fact that the protease cleaves OPN (personal communication: R. Ryall, Flinders Medical Centre, South Australia), which is more abundant in COD crystals than in COM (Ryall *et al.* 2001a; chapter 7). Considerable dissolution was observed along with surface erosion of COD crystals after incubation with Proteinase K. It is possible that dissolution occurred more rapidly than proteolysis in the presence of this protease, and thus the former effects were more apparent. Furthermore, the surface erosion of COD crystals suggests selectively of Proteinase K for COD-associated proteins, although the reason for this is not apparent.

In contrast to thrombin and Proteinase K, cathepsin D facilitated considerable crystal erosion and disintegration, particularly in the case of COM crystals. Since UPTF1 is the principal protein component of COM crystals, further proteolysis studies of this protein should include cathepsin D. The results obtained in the present study with Cathepsin D are of particular interest since the protease is found in cell lysosomes and is active throughout the tubules of human nephrons (Hartz and Wilson 1997). Thus, cathepsin D could mediate the dismantling of CaOx crystals if they are internalised by renal cells *in vivo*.

In light of the apparent selectivity of the proteases tested for the different CaOx hydrates, thrombin and Proteinase K may be more appropriate for further studies of white subjects whose urines contain predominantly COD crystals, while cathepsin D should be used with black subjects, whose urines characteristically contain COM crystals.

No discernible differences in the relative response of crystals from white and black subjects to proteolysis were noted. However, in all cases, COM crystals (whether from white or black subjects) appeared to be more susceptible to degradation and dissolution than COD, possibly reflecting their unique crystal structures. The distinctive CaOx hydrates in the two population groups, as well as the relative response of these hydrates to proteolytic treatment, are thus important. Consequently, they warranted further analysis as presented below.

A study by Riese and co-workers was one of the first to report the binding of COM crystals to renal cell surfaces (Riese *et al.* 1988), an observation which others have confirmed using several renal cell lines (*e.g.* Lieske *et al.* 1995, Verkoelen *et al.* 1995). Crystal adherence to the renal epithelium is now widely regarded as a possible mechanism of stone formation, in addition to blockage of the nephron caused by crystal aggregation (Lieske *et al.* 1999). Crystal adhesion appears to be stereospecific since the association of COM with renal cells is favoured over that of COD crystals (Wesson *et al.* 1998).

Although crystal adhesion may at first appear to promote stone formation by providing a site for further crystal deposition, it is also possible that the attached crystals will be endocytosed, thus facilitating their degradation by intracellular proteases. This mechanism has been observed in cultured monkey cells treated with exogenous COM (Lieske *et al.* 1997) and COD (Lieske *et al.* 1996) crystals. These crystals were internalised and dissolved over a period of weeks within the cell lysosomes (Lieske *et al.* 1999). In fact, the proposal has been made that crystal attachment and subsequent dissolution may be an unexpected means by which to avert stone formation (Lieske *et al.* 1999). Studies

demonstrating raised lysosomal protease activity in the urine of stone-formers (Bautista *et al.* 1996) and in cultured renal cells challenged with CaOx crystals (Hackett *et al.* 1994), suggest that these mechanisms occur *in vivo*.

The distinctive morphology of urinary CaOx crystals from white and black subjects, and in particular the predominance of COM amongst the black population, could prove to be a decisive factor in their relative protection from stone disease. Although COM crystals are likely to bind more avidly to renal cells, recent evidence suggests that these crystals may be endocytosed and degraded by lysosomal proteases. Indeed, it appears, on the evidence of the present study, that this process may be more efficient with respect to COM crystals. Perhaps the degradation of internalised crystals is more efficient amongst the black population.

Further investigations comparing the attachment and dissolution of urinary crystals from white and black subjects using a renal cell culture model are required. These may elucidate the contribution of crystal adhesion and intracellular proteolysis to the exceptionally low stone incidence amongst the black population.

8.5 REFERENCES

1. Addadi L, Aizenberg J, Beniash E, and Weiner S. 1999. On the concept of a single crystal in biomineralization. In Crystal engineering: From molecules and crystals to materials. Braga D, Grepioni F, Orpen AG, editors. Kluwer Academic Publishers, Netherlands. 1-22.

2. Akbarieh M, Dubuc B, and Tawashi R. 1987. Surface studies of calcium oxalate dihydrate single crystals during dissolution in the presence of urine. *Scan Micros* 1:1397-1403.

3. Bautista DS, Denstedt J, Chambers AF, and Harris AF. 1996. Low molecular weight variants of osteopontin generated by serine proteases in urine of patients with kidney stones. *J Cell Biochem* 61:402-409.

4. Denhardt DT and Guo X. 1993. Osteopontin: a protein with diverse functions. *FASEB J* 7:1475-1482.

5. Doyle IR, Marshall VR, Dawson CJ, and Ryall RL. 1995. Calcium oxalate crystal matrix extract: the most potent macromolecular inhibitor of crystal growth and aggregation yet tested in undiluted human urine in vitro. *Urol Res* 23:53-62.

6. Fleming DE, Doyle IR, Evans N, Marshall VR, Parkinson GM and Ryall RL. 1999. Proteins associated with calcium oxalate crystals formed in human urine are intracrystalline. In: Borghi L, Meschi T, Briganti A, Schanchi T and Novarini A, editors. Proceedings of the 8th European Symposium on Urolithiasis. Editoriale Bios. Cosenza, 359-361.

7. Fleming DE, Grover PK, Chauvet MC, Marshall VR, and Ryall RL. 2000.An unexpected role of urinary proteins in the prevention of calcium oxalate urolithiasis. In Rodgers AL, Hibbert BE, Hess B, Khan SR, and Preminger GM, editors. University of Cape Town, Cape Town, 169-171

8. Hackett RL, Shevock PN, Khan SR, et al. 1994. Madin-Darby canine kidney cells are injured by exposure to oxalate and to calcium oxalate crystals. *Urol Res* 22:197–204.

9. Harlos K, Holland SK, Boys CW, Burgess AI, Esnouf MP, and Blake CC. 1987. Vitamin K-dependent blood coagulation proteins form hetero-dimers. *Nature* 330:82-84.

10. Hartz PA and Wilson PD. 1997. Functional defects in lysosomal enzymes in autosomal dominant polycystic kidney disease: Abnormalities in synthesis, molecular processing, polarity and secretion. *Bioch Mol Med* 60:8–26.

11. Jappie D and Rodgers AL. 2000. Determination of the optimum number of subjects required for pooling of urines: statistical approach. In: Rodgers AL, Hibbert BE, Hess B, Khan SR, and Preminger GM, editors. Urolithiasis 2000. University of Cape Town, Cape Town, 92-93.

12. Lieske JC, Deganello S, and Toback FG. 1999. Cell-crystal interactions and kidney stone formation. *Nephron* 81:8-17.

13. Lieske JC, Leonard R, Swift H, and Toback FG. 1996. Adhesion of calcium oxalate monohydrate crystals to anionic sites on the surface of renal epithelial cells. *Am J Physiol* 270:F192-F199.

14. Lieske JC, Leonard R, and Toback FG. 1995. Adhesion of calcium oxalate monohydrate crystals to renal epothelial cells is inhibited by specific anions. *Am J Physiol* 268:F604-F612.

15. Lieske JC, Norris R, Swift H, and Toback FG. 1997. Adhesion, internalisation and metabolism of calcium oxalate monohydrate crystals by renal epithelial cells. *Calcif Tissue Int* 58:195-200.

16. Riese RJ, Riese JW, Kleinman JG, Wiessner JH, Mandel GS, and Mandel NS. 1988. Specificity in calcium oxalate adherence to papillary epithelial cells in culture. *Am J Physiol* 255:F1025-F1032.

17. a) Ryall RL, Chauvet MC, and Grover PK. 2001: A space oddity. In: Kok DJ, Romijn HC, Verhagen PCMS, and Verkoelen CF, editors. Eurolithiasis: 9th European Symposium on Urolithiasis. Shaker Publishing, Netherlands, 273-274.

18. b) Ryall RL, Fleming DE, Doyle IR, Evans NA, Dean CJ, and Marshall VR. 2001. Intracrystalline proteins and the hidden ultrastructure of calcium oxalate urinary crystals: implications for kidney stone formation. *J Struc Biol* 134:5-14.

19. Ryall RL, Fleming DE, Grover PK, Chauvet M, Dean CJ, and Marshall VR. 2000. The hole truth: intracrystalline proteins and calcium oxalate kidney stones. *Mol Urol* 4:391-402.

20. Ryall RL, Grover PK, Stapleton AMF, Barrell DK, Tang Y, Moritz RL, and Simpson RJ. 1995. The urinary F1 activation peptide of human prothrombin is a potent inhibitor of calcium oxalate crystallization in undiluted human urine in vitro. *Clin Sci* 89:533-541.

21. Stapleton AMF, Dawson CJ, Grover PK, Hohmann A, Comacchio R, Boswara V, Tang Y, and Ryall RL. 1996. Further evidence linking urolithiasis and blood coagulation: Urinary prothrombin fragment 1 is present in stone matrix. *Kidney Int* 49:880-888.

22. Verkoelen CF, Romijn JC, de Bruijn WC, Boeve ER, Cao L, and Schroder FH. 1995. Association of calcium oxalate monohydrate crystals with MDCK cells. *Kidney Int* 48:129-138.

23. Wesson JA, Worcester EM, Weissner JH, Mandel NS, and Kleinman JG. 1998. Control of calcium oxalate crystal structure and cell adherence by urinary macromolecules. *Kidney Int* 33:952-957.

CHAPTER 9: DISCUSSION, CONCLUSIONS & A FUTURE OUTLOOK

The hypothesis of this thesis was that differences in the physical structure and/or inhibitory properties of UPTF1 from the white and black populations in South Africa contribute to the remarkably low stone incidence of kidney stones amongst the black population. As a prelude to exploring this hypothesis, a preliminary investigation of the inhibitory activity of urine from white and black subjects was conducted (chapter 2). Urine composition trends in the black population were inconclusive when compared with whites, and could not account for the former group's protection from stone disease (in fact inconsistent trends were observed in the various studies conducted in this thesis). However, urinary macromolecules from black subjects induced the formation of smaller particle sizes in synthetic urine when the urine was challenged with a sodium oxalate load. These macromolecules also demonstrated greater repulsive forces in COM crystal slurry assays, suggesting a greater potential to disaggregate the COM crystals. Both of these trends are consistent with inhibition of a greater magnitude by urinary macromolecules from the black population, which may be related to their lower incidence of stones.

Expanding on the theme of macromolecules while shifting to the primary focus of the thesis, the inhibitory activity of the CME from healthy white and black subjects was compared (chapter 3). CME reduced crystal nucleation, growth and aggregation during the early stages of CaOx crystallisation in a synthetic urine. These effects were more pronounced in the presence of the CME derived from black subjects than whites. In addition, the CME from both population groups induced the favourable nucleation or stabilisation of COD crystals. It was speculated that the apparently greater inhibition of CME from the black population might be due, in part, due to the properties of UPTF1, its principal component.

Thus, UPTF1 was isolated and purified from the urine of healthy white and black subjects and rigorously characterised (chapter 4). N-terminal sequencing, amino acid analysis and MALDI-TOF MS did not reveal differences between WF1 and BF1, and both proteins were shown to contain three charged variants with similar pI values according to 2D SDS-PAGE. However, amino acid analysis by alkaline hydrolysis demonstrated the presence of a greater number of Gla residues on BF1 than WF1. Oligosaccharide sequencing identified a high proportion of sialylated glycans on UPTF1, with a greater number of sialic acid residues present on BF1 than WF1. The *N*- and *O*-linked glycans were located on the kringle domain of UPTF1 by molecular modeling.

In addition to investigating possible structural differences, the inhibitory activity of WF1 and BF1 were compared (chapter 5). UPTF1 inhibited CaOx crystal growth and aggregation in synthetic urine, whether from white or black subjects, and these effects were greatest in the presence of BF1 during the early stages of crystallisation. Furthermore, WF1 and BF1 induced a favourable hydrate transition from COM to COD crystals in the synthetic urine. The effect of WF1 and BF1 on the crystallisation of exogenous COM and COD crystals was also examined. While the relative effects demonstrated by the two proteins could not be distinguished, sedimentation rates and zeta potential experiments suggested a greater potential for inhibition of COM rather than COD aggregation by UPTF1. In ultrafiltered urine, UPTF1 from both population groups promoted CaOx crystal nucleation, but inhibited its growth and aggregation. All of these mechanisms were regarded as protective. In a cross-over design crystallisation study, ultrafiltered urine from the two population groups was dosed with both WF1 and BF1. A synergistic relationship between UPTF1 activity and urine composition was demonstrated, and BF1 was found to be a more effective inhibitor than WF1 in their endogenous urines.

On the basis of the afore-mentioned findings, it was concluded that the relationship between UPTF1 and CaOx crystal morphology should be explored. This was motivated by the following three key points: the synergy between UPTF1 and urine; the different CaOx hydrates which predominated in the two population groups' urine; and the greater inhibition of COM rather than COD aggregation by UPTF1.

To this end, crystal morphology and the levels of urinary and CaOx matrix-associated UPTF1, as well as other urinary proteins, were compared in healthy white and black subjects and white stone-formers (chapter 6). The urinary concentrations of UPTF1 in the three groups appeared to be similar by Western blotting. However, UPTF1 and other proteins were selectively incorporated into the CaOx crystals derived from these urines. More of the black subjects' crystals contained UPTF1 than that of the whites (controls and stone-formers). These differences coincided with higher proportions of COM crystals in the urine of black subjects, compared with COD crystals which were excreted principally amongst the white subjects.

The protein content of pure COM and COD urinary crystals from healthy white and black subjects were compared both qualitatively and semi-quantitatively (chapter 7). COM crystals from black subjects contained mainly UPTF1 but also OPN, whereas the same CaOx hydrate from white subjects included exclusively UPTF1. COD crystals from both population groups included mainly OPN. In addition to the hydrate type, urine composition

appeared to influence protein binding to CaOx crystals, again drawing attention to a relationship between UPTF1 and urine composition. The total amount of intracrystalline protein (per mg CaOx) was greatest in the black subjects.

Finally, the response of CaOx crystals from healthy white and black subjects to dissolution and proteolysis was investigated (chapter 8). COM crystals, whether from white or black subjects, were notably more susceptible to dissolution, erosion and degradation than COD crystals. This observation was particularly significant in view of the predominance of COM crystals amongst the black population.

A rigorous review of the literature revealed two major pathways by which stone formation may be mediated and possibly prevented. The first of these was the long-touted mode of crystallisation inhibition. A second, and more recently proposed mode of protection was by modulating crystal adhesion to renal epithelial cells. The results and discussions presented in this thesis clearly reflected UPTF1's potential to influence both of these mechanisms; in the first instance, by way of its powerful inhibitory capacity in urine and, in the second instance, by virtue of its inclusion within the crystalline architecture and its consequent susceptibility to proteolysis.

In the context of this thesis, the important attribute of UPTF1 which has been identified is its ability to distinguish between the white and black populations. Indeed, UPTF1 derived from the urine of black subjects exhibited enhanced inhibition of CaOx crystallisation in synthetic urine and in synergy with its parent urine, in comparison with UPTF1 from the urine of white subjects. These properties are likely to be related to the greater number of Gla residues on BF1 and, possibly, the greater number of sialic acid residues on BF1, as well as a conformation in the black population's urine that is more favourable for inhibition. The greater inhibition of COM compared with COD aggregation by UPTF1 suggested that the binding affinity of UPTF1 for the CaOx hydrates may also be involved in its activity.

The abundance of urinary COM crystals amongst the black population and the concomitant higher levels of UPTF1 were noteworthy. In addition, the *total* amount of intracrystalline protein in this group was greater. The latter finding was particularly striking given recent findings that intracrystalline proteins may provide a natural defense against kidney stone formation by way of their susceptibility to intracellular proteolysis following crystal attachment and endocytosis.

Previous studies reporting the binding of COM and COD crystals to renal epithelial cells have all used crystals composed of pure mineral. However, it is now recognised that

the inclusion of proteins such as UPTF1 into CaOx crystals *in vivo* is likely to affect their physicochemical features and thus binding properties. As the major component of COM crystals from the black population, UPTF1 is likely to exert the greatest influence on the surface charge of these crystals. Thus, the larger number of sialic acid and Gla residues on BF1 compared with WF1 may provide a greater negative charge to the black population's urinary crystals. This would provide a greater repulsive force to the negatively charged renal cell surface, resulting in diminished crystal adhesion in the black population.

Consideration of all of the afore-mentioned results show that the objectives of this thesis have been met and that the original hypothesis has been validated. However, while this thesis has unearthed several new areas that allow a more enlightened understanding of the black population's remarkably low stone incidence, the present study is perhaps only the beginning. Future investigations should aim to clarify and further investigate the role of UPTF1 in the two mechanisms described above, as well as the unique properties of BF1 and its role with respect to these mechanisms. Firstly, the contribution of the glycans, and in particular sialic acids, to the inhibitory activity of UPTF1 should be investigated. This could be achieved by comparison of the aglyco and asialo forms of UPTF1 with the intact protein in an *in vitro* crystallisation study. Secondly, the role of UPTF1's glycans as possible mediators of crystal binding to renal cells should be examined by quantifying the extent of adhesion of crystals containing UPTF1 and its aglyco and asialo forms in comparison with crystals composed of pure mineral. And thirdly, the attachment and dissolution of urinary crystals from white and black subjects should be compared using a renal cell culture model. These studies have the potential to clarify the function of UPTF1's glycans and the contribution of crystal adhesion and intracellular proteolysis to the exceptionally low stone incidence amongst the black population.

The elucidation of the precise reasons for the rarity of stones amongst South Africa's black population is likely to confirm the vital role of urinary proteins in the formation of, and protection from, kidney stones. However, the complex nature of stone disease suggests that it is necessary to examine the role of proteins in conjunction with several other factors, of which diet is likely to be one. The key contribution of this thesis has been to demonstrate that, amongst these other possible factors, UPTF1 is *indeed* a potential role-player in the protection of South African blacks from CaOx kidney stone disease.

TABLES & FIGURES

Chapter 2

Table 2.1 Interplanar spacings and relative intensities of powder patterns of calcium oxalates
Table 2.2 X-ray powder diffraction peak assignments and percentage composition of CaOx crystals prepared according to Pak *et al.* (1975)
Table 2.3 Absorbance slopes and inhibition of aggregation (I_A %) of COM crystal slurry by urine at various dilutions
Table 2.4 Absorbance slopes and inhibition of aggregation (I_A %) of COM crystal slurries before and after addition of white subjects' urine (WU) at a dilution of 1:2
Table 2.5 Absorbance slopes and inhibition of aggregation (I_A %) of COM crystal slurries before and after addition of black subjects' urine (BU) at a dilution of 1:2
Table 2.6 Average zeta potential (ZP) of COM crystal slurries before and after addition of white subjects' urine (WU) at a dilution of 1:2
Table 2.7 Average zeta potential (ZP) of COM crystal slurries before and after addition of black subjects' urine (BU) at a dilution of 1:2
Table 2.8 Bradford protein assay standard curve data using bovine serum albumin (BSA)
Table 2.9 Protein concentration (μg/ml) and excretion (mg/day) of black and white subjects' urine
Table 2.10 Particle size (μm) of synthetic urine before and after addition of macromolecular urine extracts from white (WMM) and black (BMM) subjects
Table 2.11 Average composition (mmol/24hr) and physicochemical parameters of white (WC) and black (BC) subjects' urine

Figure 2.1 Typical sedimentation rate plot (or OD_{620} plot)
Figure 2.2 Typical plot of particle number versus sodium oxalate concentration to determine metastable limit (MSL)
Figure 2.3 X-ray powder diffraction pattern of CaOx crystals prepared according to Pak *et al.* (1979)
Figure 2.4 Thermogravimetric analysis of CaOx crystals prepared according to Pak *et al.* (1979)
Figure 2.5 Scanning electron micrographs of CaOx crystals prepared according to Pak *et al.* (1975)
Figure 2.6 OD620 plots of COM crystal slurries after addition of urine at various dilutions
Figure 2.7 Inhibition of aggregation by urine in COM crystal slurries at various urine dilutions
Figure 2.8 Average OD_{620} plots of COM crystal slurry. Before and after addition of urine from white (WU) and black (BU) subjects at a 1:2 dilution
Figure 2.9 Comparison of % decrease in ZP of COM crystal slurry after addition of white (WU) and black (BU) subjects' urine at a dilution of 1:2
Figure 2.10 Standard curve for Bradford protein assay using bovine serum albumin
Figure 2.11 Average of particle number versus sodium oxalate concentration in synthetic urine
Figure 2.12 Average particle size distribution. Synthetic urine before and after addition of macromolecular urine extracts from white (WMM) and black (BMM) subjects

Chapter 3

Table 3.1 Average urine composition (mmol/l) and physicochemical parameters of pooled urines from white and black subjects
Table 3.2 Particle size (μm) of synthetic urine before and after addition of CME from white (WE) and black (BE) subjects at final concentrations of 5 mg/l

Figure 3.1 SDS-PAGE of urine and CMEs from white and black subjects
Figure 3.2 Western blot of CMEs from white and black subjects
Figure 3.3 Average particle number of synthetic urine as a function of time
Figure 3.4 Average particle volume of synthetic urine as a function of time

Figure 3.5 Average particle size of synthetic urine (3.5.1 – 3.5.2)
Figure 3.6 Scanning electron micrographs of CaOx crystals deposited in synthetic urine
Figure 3.7 Average [^{14}C]-ox deposition rate of synthetic urine

Chapter 4

Table 4.1 HPLC gradient used for UPTF1 purification
Table 4.2 Specificity and final concentration of exoglycosidases
Table 4.3 MALDI-TOF of observed $[M+H]^+$ ions of UPTF1 generated by endoproteinase Lys-C or Asp-N (cysteines were protected with vinyl pyridine)
Table 4.4 Amino acid composition of WF1 and BF1 as determined by acid hydrolysis
Table 4.5 γ-Carboxyglutamic acid and glutamic acid composition of WF1 and BF1 determined by alkaline hydrolysis
Table 4.6 NP-HPLC analysis of *N*-linked glycans on UPTF1 from white control subject WC6
Table 4.7 Analysis of WAX-HPLC fractions on NP-HPLC of N-linked glycans on UPTF1 from white control subject WC6
Table 4.8 Mass data of *N*-linked glycans on UPTF1 from white control subject WC6
Table 4.9 Summary of *N*-linked glycans on UPTF1 from white control subject WC6
Table 4.10 Percentage composition of *N*-linked glycans on UPTF1 from white control subject WC6
Table 4.11 Percentage of mono- and disialylated *N*-linked glycans on UPTF1 from white and black control subjects and white stone-formers
Table 4.12 NP-HPLC analysis of *O*-linked glycans on UPTF1 pooled from 3 white stone-formers
Table 4.13 NP-HPLC analysis of *O*-linked glycans on UPTF1 pooled from white control (WC), black control (BC) and white stone-formers (WSF)

Figure 4.1 Graphical representations of monosaccharides and their linkages
Figure 4.2 Typical absorbance plot obtained of a CME sample on a desalting column
Figure 4.3 Typical HPLC chromatogram of desalted crystal matrix extract
Figure 4.4 SDS-PAGE of UPTF1 from white and black subjects
Figure 4.5 Western blot of UPTF1 from white and black subjects
Figure 4.6 2D SDS-PAGE of UPTF1 from white (4.6.1) and black subjects (4.6.2)
Figure 4.7 SDS-PAGE of crystal matrix extract from white control subject WC6
Figure 4.8 NP-HPLC profiles of N-linked glycans on UPTF1 pooled from white (WC pool) and black (BC pool) control subjects as well as from several individual white (WC1-8) and black (BC1-7) subjects
Figure 4.9 NP-HPLC profiles of N-linked glycans on UPTF1 from several white stone-formers (WSF1-6) and one black stone-former (BSF)
Figure 4.10 NP-HPLC profiles of a UPTF1 *N*-glycan pool from white control subject WC6 before and after treatment with an array of exoglycosidases
Figure 4.11 NP-HPLC profile of a UPTF1 *N*-glycan pool from white control subject WC6 before and after treatment with a fucosidase, also used in combination with a sialidase
Figure 4.12 NP-HPLC profile of a UPTF1 *N*-glycan pool from white control subject WC6 before and after digestion with two galactosidases, Btg and Spg, (in combination with other exoglycosidases) to determine the galactose linkages
Figure 4.13 NP-HPLC profile of a UPTF1 *N*-glycan pool from white control subject WC6 before and after digestion with a mannosidase
Figure 4.14 WAX-HPLC profile of *N*-linked glycans on UPTF1 from white control subject WC6 before and after digestion with a sialidase
Figure 4.15 NP-HPLC profiles of UPTF1 *N*-glycan pool from white control subject WC6 before and after separation by WAX-HPLC
Figure 4.16 NP-HPLC profile of an undigested UPTF1 *N*-glycan pool from white control subject WC6
Figure 4.17 NP-HPLC profiles of *O*-linked glycans on UPTF1 pooled from 3 white stone-formers following arrays of exoglycosidase digestions

Figure 4.18 NP-HPLC profiles of *O*-linked glycans on UPTF1 pooled from 3 white control subjects before and after exoglycosidase digestions
Figure 4.19 WAX-HPLC profiles of *O*-linked glycans on UPTF1 pooled from white control (WC) subjects and white stone-formers (WSF) before and after Abs digestion
Figure 4.20 NP-HPLC profiles of *O*-linked glycans on UPTF1 pooled from white (WC) and black (BC) control subjects and white stone-formers (WSF).
Figure 4.21 Molecular model of UPTF1 showing *N*- and *O*-linked glycans; 4.21.1: Side-on view; 4.21.2: End-on view down the Gla domain

Chapter 5

Table 5.1 Particle size (μm) of synthetic urine (SU) before and after addition of WF1 and BF1 at final concentrations of 1.25 mg/l
Table 5.2 Average urine composition (mmol/l) and physicochemical parameters of pooled urines from white and black subjects (n=5)
Table 5.3 Particle number (/500μl) of ultrafiltered urine from white (WUF) and black (BUF) subjects before and after addition of WF1 and BF1 at final concentrations of 1.25 mg/l
Table 5.4 Particle volume ($x10^3$ μm^3/500 μl) of ultrafiltered urine from white (WUF) and black (BUF) subjects before and after addition of WF1 and BF1 at final concentrations of 1.25 mg/l
Table 5.5 Percentage change in average particle parameters of ultrafiltered urine from white (WUF) and black (BUF) subjects after addition of WF1 and BF1 at final concentrations of 1.25 mg/l
Table 5.6 Particle size (μm) of ultrafiltered urine from white (WUF) and black (BUF) subjects before and after addition of WF1 and BF1 at final concentrations of 1.25 mg/l
Table 5.7 Percentage precipitated [^{14}C]-oxalate in ultrafiltered urine from white (WUF) and black (BUF) subjects before and after addition of WF1 and BF1 at final concentrations of 1.25 mg/l
Table 5.8 Average absorbance slope ($x\text{-}10^{-5}s^{-1}$) and inhibition of aggregation (I_A %) of COM crystal slurries before and after addition of WF1 and BF1 at final concentrations of 1.25 mg/l
Table 5.9 X-ray powder diffraction peak assignments of CaOx crystals prepared according to Brown *et al.* (1985)
Table 5.10 Average absorbance slope ($x\text{-}10^{-5}s^{-1}$) and inhibition of aggregation (I_A %) of COD crystal slurries before and after addition of WF1 and BF1 at final concentrations of 1.25 mg/l
Table 5.11 Average zeta potential (mV) of COM crystal slurries before and after addition of WF1 and BF1 at final concentrations of 1.25 mg/l
Table 5.12 Average zeta potential (mV) of COD crystal slurries before and after addition of WF1 and BF1 at final concentrations of 1.25 mg/l

Figure 5.1 Cross-over design employed for UPTF1 crystallisation study
Figure 5.2 Average plot of particle number versus sodium oxalate concentration in synthetic urine
Figure 5.3 Average particle size distributions in synthetic urine. Synthetic urine (SU) before and after addition of WF1 and BF1 at final concentrations of 1.25 mg/l
Figure 5.4 Scanning electron micrographs of CaOx crystals deposited in synthetic urine
Figure 5.5 Average [^{14}C]-ox deposition rate in synthetic urine. Synthetic urine (SU) before and after addition of WF1 and BF1 at final concentrations of 1.25 mg/l
Figure 5.6.1 Average particle size distributions in WUF. Ultrafiltered urine from white subjects (WUF) before and after addition of WF1 and BF1 at final concentrations of 1.25 mg/l
Figure 5.6.2 Average particle size distributions in BUF. Ultrafiltered urine from black subjects (BUF) before and after addition of WF1 and BF1 at final concentrations of 1.25 mg/l
Figure 5.7 Scanning electron micrographs of CaOx crystals deposited in ultrafiltered urine
Figure 5.8.1 Average [^{14}C]-ox deposition rate in WUF. Ultrafiltered urine from white subjects (WUF) before and after addition of WF1 and BF1 at final concentrations of 1.25 mg/l

Figure 5.8.2 Average [^{14}C]-ox deposition rate in BUF. Ultrafiltered urine from black subjects (BUF) before and after addition of WF1 and BF1 at final concentrations of 1.25 mg/l
Figure 5.9 Average OD_{620} plot of COM crystal slurries. Before and after addition of WF1 and BF1 at final concentrations of 1.25 mg/l
Figure 5.10 X-ray powder diffraction pattern of CaOx crystals prepared according to Brown *et al* (1985).
Figure 5.11 Thermogravimetric analysis of CaOx crystals prepared according to Brown *et al.* (1985).
Figure 5.12 Scanning electron micrographs of CaOx crystals prepared according to Brown *et al.* (1985).
Figure 5.13 Average OD_{620} plots of COD crystal slurries. Before and after addition of WF1 and BF1 at final concentrations of 1.25 mg/l
Figure 5.14 Average % inhibition by WF1 and BF1 in COM & COD crystal slurries (final concentrations of 1.25 mg/l)
Figure 5.15 Average % inhibition by UPTF1 in COM & COD crystal slurries (final concentration of 1.25 mg/l)
Figure 5.16 Average zeta potential of COM crystal slurries. Before and after addition of WF1 and BF1 at final concentrations of 1.25 mg/l
Figure 5.17 Average zeta potential of COD crystal slurries. Before and after addition of WF1 and BF1 at final concentrations of 1.25 mg/l
Figure 5.18 Average % decrease in zeta potential of COM & COD crystal slurries. After addition of WF1 and BF1 at final concentrations of 1.25 mg/l
Figure 5.19 Average % decrease in zeta potential of COM & COD slurries. After addition of UPTF1 at a final concentration of 1.25 mg/l

Chapter 6

Table 6.1 Average urine composition (mmol/24hr) and physicochemical parameters of white and black control subjects and white stone-formers (n=5)
Table 6.2 Estimated hydrate composition of CaOx crystals precipitated from the urine of white and black control subjects and white stone-formers

Figure 6.1 Scanning electron micrographs of CaOx crystals from the urine of white control subjects
Figure 6.2 Scanning electron micrographs of CaOx crystals from the urine of black control subjects
Figure 6.3 Scanning electron micrographs of CaOx crystals from the urine of white stone-formers
Figure 6.4 SDS-PAGE of urine and CaOx urinary crystals from white control subjects
Figure 6.5 SDS-PAGE of urine and CaOx urinary crystals from black control subjects
Figure 6.6 SDS-PAGE of urine and CaOx urinary crystals from white stone-formers
Figure 6.7 Western blot of urine and CaOx urinary crystals from white control subjects immunoblotted for prothrombin
Figure 6.8 Western blot of urine and CaOx urinary crystals from black control subjects immunoblotted for prothrombin
Figure 6.9 Western blot of urine and CaOx urinary crystals from white stone-formers immunoblotted for prothrombin

Chapter 7

Table 7.1.1 Urine composition (mmol/l) and physicochemical parameters of black groups' pooled urines
Table 7.1.2 Urine composition (mmol/l) and physicochemical parameters of white groups' pooled urines
Table 7.2.1 X-ray powder diffraction peak assignments and percentage composition of CaOx crystals precipitated from the urine of black group 4

Table 7.2.2 X-ray powder diffraction peak assignments and percentage composition of CaOx crystals precipitated from the urine of white group 4
Table 7.3.1 Composition of black groups' CaOx urine crystals as determined by x-ray powder diffraction
Table 7.3.2 Composition of white groups' CaOx urine crystals as determined by x-ray powder diffraction

Figure 7.1 X-ray powder diffraction patterns of CaOx urine crystals
Figure 7.2 Scanning electron micrographs of CaOx urine crystals
Figure 7.3 Desalting chromatograms of demineralised CaOx urine crystals
Figure 7.4 Protein patterns of CaOx urine crystals (black subjects: lanes 1 – 5; white subjects: lanes 6 – 10)
Figure 7.5 Western blot of CaOx urine crystals immunoblotted for prothrombin.
Figure 7.6 Western blot of CaOx urine crystals immunoblotted for osteopontin.

Chapter 8

Table 8.1 Abbreviations used to denote crystals prepared from white and black subjects' pooled urines before and after dosing with UPTF1 from both population groups
Table 8.2 Summary of treatments used for various crystals

Figure 8.1 SDS-PAGE of CaOx urine crystals
Figure 8.2 Western blot of CaOx urine crystals
Figure 8.3 Field emission scanning electron micrographs of UF CaOx crystals before and after protease treatment in a saturated CaOx buffer
Figure 8.4 Field emission scanning electron micrographs of WF, WUF+WF1 and WUF+BF1 CaOx crystals before treatment
Figure 8.5 Field emission scanning electron micrographs of BF, BUF+WF1 and BUF+BF1 CaOx crystals before treatment
Figure 8.6 Field emission scanning electron micrographs of WF CaOx crystals before and after protease treatment in an unsaturated CaOx buffer.
Figure 8.7 Field emission scanning electron micrographs of BF CaOx crystals before and after protease treatment in a saturated CaOx buffer
Figure 8.8 Field emission scanning electron micrographs of CaOx crystals after incubation with cathepsin D in an unsaturated CaOx buffer
Figure 8.9 Field emission scanning electron micrographs of CaOx crystals after incubation with thrombin in an unsaturated CaOx buffer
Figure 8.10 Field emission scanning electron micrographs of CaOx crystals after incubation with Proteinase K in an unsaturated CaOx buffer
Figure 8.11 Field emission scanning electron micrographs showing stages of COM crystal dissolution in an unsaturated CaOx buffer
Figure 8.12 Field emission scanning electron micrographs showing stages of COD crystal dissolution in an unsaturated CaOx buffer

Appendix A

Table A1.1 Zeta potential (ZP) of COM crystal slurries before and after addition of white subjects' urine (WU) at a dilution of 1:2
Table A1.2 Zeta potential (ZP) of COM crystal slurries before and after addition of black subjects' urine (BU) at a dilution of 1:2
Table A2 Particle number as a function of sodium oxalate concentration in synthetic urine
Table A3.1 Composition (mmol/24hr) and physicochemical parameters of white subjects' urine
Table A3.2 Composition (mmol/24hr) and physicochemical parameters of black subjects' urine

Figure A1 OD_{620} plot of COM crystal slurries
Figure A2 OD_{620} plot of COM crystal slurries after addition of white subjects' urine at a dilution of 1:2 (2.1 – 2.5)

Figure A3 OD620 plot of COM crystal slurries after addition of black subjects' urine at a dilution of 1:2 (3.1 – 3.5)
Figure A4 Particle size distributions of synthetic urine (4.1 – 4.5)
Figure A5 Particle size distributions of synthetic urine after addition of macromolecular extracts from white subjects' urine (5.1 – 5.5)
Figure A6 Particle size distributions of synthetic urine after addition of macromolecular extracts from black subjects' urine (6.1 – 6.5)

Appendix B

Table B1 Urine composition (mmol/24hr) and physicochemical parameters of pooled urines from white subjects
Table B2 Urine composition (mmol/24hr) and physicochemical parameters of pooled urines from black subjects
Table B3 Particle number as a function of sodium oxalate concentration in white subjects' pooled urines (3.1 – 3.7)
Table B4 Particle number as a function of sodium oxalate concentration in black subjects' pooled urines (4.1 – 4.7)
Table B5 Particle number (/500µl) of synthetic urine before and after addition of CME from white (WE) and black (BE) subjects at final concentrations of 5 mg/l
Table B6 Particle volume (10^6 μm^3/500µl) of synthetic urine before and after addition of CME from white (WE) and black (BE) subjects at final concentrations of 5 mg/l
Table B7 [^{14}C]-oxalate deposition expressed as a percentage precipitated [^{14}C]-oxalate in synthetic urine before and after addition of CME from white (WE) and black (BE) subjects at final concentrations of 5 mg/l

Figure B1 Particle number as a function of sodium oxalate concentration in white subjects' pooled urines (1.1 – B1.7)
Figure B2 Particle number as a function of sodium oxalate concentration in black subjects' pooled urines (2.1 – B2.7)
Figure B3 Particle number as a function of time of synthetic urine before and after addition of CME from white (WE) and black (BE) subjects at final concentrations of 5 mg/l (3.1: experiment 1, 3.2: experiment 2)
Figure B4 Particle volume of synthetic urine before and after addition of CME from white (WE) and black (BE) subjects at final concentrations of 5 mg/l (4.1: experiment 1, 4.2: experiment 2).
Figure B5 Particle size of synthetic urine before and after addition of CME from white (WE) and black (BE) subjects at final concentrations of 5 mg/l (5.1.1 – 5.1.2: experiment 1, 5.2.1 – 5.2.2: experiment 2)
Figure B6 [^{14}C]-oxalate deposition rate in synthetic urine before and after addition of CME from white (WE) and black (BE) subjects at final concentrations of 5 mg/l (6.1: experiment 1, 6.2: experiment 2)

Appendix C

Table C1 NP-HPLC analysis of *N*-linked glycans on UPTF1 from white control subjects
Table C2 NP-HPLC analysis of *N*-linked glycans on UPTF1 from black control subjects
Table C3 NP-HPLC analysis of *N*-linked glycans on UPTF1 from white (WSF) and black (BSF) stone-formers

Figure C1 MALDI-TOF spectrum of *N*-linked glycans on UPTF1 from white control subject WC6
Figure C2 QTOF spectrum of *N*-linked glycans on UPTF1 from white control subject WC6

Appendix D

Table D1 Particle number as a function of sodium oxalate concentration in synthetic urine

Table D2 Particle size (μm) of synthetic urine (SU) before and after addition of WF1 and BF1 at final concentrations of 1.25 mg/l

Table D3 [^{14}C]-oxalate deposition expressed as a percentage precipitated [^{14}C]-oxalate for synthetic urine (SU) before and after addition of WF1 and BF1 at final concentrations of 1.25 mg/l

Table D4.1 Urine composition (mmol/l) and physicochemical parameters of pooled urines from white subjects

Table D4.2 Urine composition (mmol/l) and physicochemical parameters of pooled urines from black subjects

Table D5.1 Particle number as a function of sodium oxalate concentration in ultrafiltered urine from white subjects

Table D5.2 Particle number as a function of sodium oxalate concentration in ultrafiltered urine from black subjects

Table D6.1 [^{14}C]-oxalate deposition expressed as a percentage precipitated [^{14}C]-oxalate for ultrafiltered urine from white subjects (WUF) before and after addition of WF1 and BF1 at final concentrations of 1.25 mg/l

Table D6.2 [^{14}C]-oxalate deposition expressed as a percentage precipitated [^{14}C]-oxalate for ultrafiltered urine from black subjects (BUF) before and after addition of WF1 and BF1 at final concentrations of 1.25 mg/l

Table D7.1 Absorbance slopes (x-$10^{-5}s^{-1}$) of COM crystal slurries before and after addition of WF1 and BF1 at final concentrations of 1.25 mg/l

Table D7.2 Absorbance slopes (x-$10^{-5}s^{-1}$) of COD crystal slurries before and after addition of WF1 and BF1 at final concentrations of 1.25 mg/l at final concentrations of 1.25 mg/l

Table D8.1 Zeta potential (mV) of COM crystal slurries before and after addition of WF1 and BF1 at final concentrations of 1.25 mg/l at final concentrations of 1.25 mg/l

Table D8.2 Zeta potential (mV) of COD crystal slurries before and after addition of WF1 and BF1 at final concentrations of 1.25 mg/l at final concentrations of 1.25 mg/l

Figure D1 Particle size distribution in synthetic urine (1.1) before and after addition of WF1 (1.2) and BF1 (1.3) at final concentrations of 1.25 mg/l.

Figure D2 [^{14}C]-oxalate deposition in synthetic urine before and after addition of WF1 and BF1 at final concentrations of 1.25 mg/l.

Figure D3 MSL plots of white (3.1-3.5) and black (3.6-3.10) subjects' pooled urines

Figure D4 Particle size distributions in white (4.1 - 4.4) and black (4.5 - 4.7) subjects' ultrafiltered urine before and after addition of WF1 and BF1 at final concentrations of 1.25 mg/l.

Figure D5 [^{14}C]-oxalate deposition in ultrafiltered urine from white (5.1 – 5.3) and black (5.4 - 5.6) subjects

Figure D6.1 OD_{620} plots of COM crystal slurries (6.1.1 – 6.1.6).

Figure D6.2 OD_{620} plots of COM crystal slurries after addition of WF1 (final concentration 1.25 mg/l) (6.2.1 – 6.2.6).

Figure D6.3 OD_{620} plots of COM crystal slurries after addition of BF1 (final concentration 1.25 mg/l) (6.3.1 – 6.3.7).

Figure D7.1 OD_{620} plots of COD crystal slurries (7.1.1 – 7.1.9).

Figure D7.2 OD_{620} plots of COD crystal slurries after addition of WF1 (final concentration 1.25 mg/l) (7.2.1 – 7.2.12).

Figure D7.3 OD_{620} plots of COD crystal slurry after addition of BF1 (final concentration 1.25 mg/l) (7.3.1 – 7.3.10)

Appendix E

Table E1 Urine composition (mmol/24hr) and physicochemical parameters of white control subjects

Table E2 Urine composition (mmol/24hr) and physicochemical parameters of black control subjects
Table E3 Urine composition (mmol/24hr) and physicochemical parameters of white stone-formers
Table E4 X-ray powder diffraction peak assignments and percentage composition of CaOx crystals precipitated from white control subjects' urine
Table E5 X-ray powder diffraction peak assignments and percentage composition of CaOx crystals precipitated from black control subjects' urine
Table E6 X-ray powder diffraction peak assignments and percentage composition of CaOx crystals precipitated from white stone-formers' urine

Figure E1 X-ray powder diffraction patterns of CaOx crystals precipitated from white control subjects' urine
Figure E2 X-ray powder diffraction patterns of CaOx crystals precipitated from black control subjects' urine
Figure E3 X-ray powder diffraction patterns of CaOx crystals precipitated from white stone-formers' urine
Figure E4 Desalting chromatograms of demineralised CaOx crystals precipitated from white control subjects' urine
Figure E5 Desalting chromatograms of demineralised CaOx crystals precipitated from black control subjects' urine
Figure E6 Desalting chromatograms of demineralised CaOx crystals precipitated from white stone-formers' urine

Appendix F

Table F1.1 X-ray powder diffraction peak assignments and percentage composition of CaOx crystals precipitated from the urine of black group 1
Table F1.2 X-ray powder diffraction peak assignments and percentage composition of CaOx crystals precipitated from the urine of black group 2
Table F1.3 X-ray powder diffraction peak assignments and percentage composition of CaOx crystals precipitated from the urine of black group 3
Table F2.1 X-ray powder diffraction peak assignments and percentage composition of CaOx crystals precipitated from the urine of white group 1
Table F2.2 X-ray powder diffraction peak assignments and percentage composition of CaOx crystals precipitated from the urine of white group 2
Table F2.3 X-ray powder diffraction peak assignments and percentage composition of CaOx crystals precipitated from the urine of white group 3

Figure F1 X-ray powder diffraction patterns of CaOx crystals precipitated from black males' urines at various calcium concentrations.
Figure F2 X-ray powder diffraction patterns of CaOx crystals precipitated from white males' urines at various calcium concentrations

Appendix G

Table G1 Urine composition (mmol/l) and physicochemical parameters of white and black subjects' pooled urines
Table G2 Preparation of saturated and unsaturated CaOx buffers

APPENDIX A: TABLES

Table A1.1: Zeta potential (ZP) of COM crystal slurries before and after addition of white subjects' urine (WU) at a dilution of 1:2

Sample	Zeta potential (mV)	ZP ± SE (mV)
COM	-17.9, -17.8, -17.3, -18.4, -17.9, -17.8	-17.9 ± 0.14
COM+WU1	-30.8, -30.5, -30.4	-30.6 ± 0.12
COM+WU2	-27.9, -29.8, -29.3	-29.0 ± 0.57
COM+WU3	-29.1, -29.9, -29.8	-29.6 ± 0.25
COM+WU4	-29.8, -30.2, -29.9	-30.0 ± 0.12
COM+WU5	-18.6, -16.9, -16.1	-17.2 ± 0.74

Table A1.2: Zeta potential results of COM crystal slurries before and after addition of black subjects' urine (BU) at a dilution of 1:2

Sample	Zeta potential (mV)	ZP ± SE (mV)
COM	-17.9, -17.8, -17.3, -18.4, -17.9, -17.8	-17.9 ± 0.14
COM+BU1	-22.2, -23.2, -23.3	-22.9 ± 0.35
COM+BU2	-23.5, -23.4, -23.7	-23.5 ± 0.088
COM+BU3	-23.5, -23.0, -23.5	-23.3 ± 0.17
COM+BU4	-23.1, -23.2, -23.8	-23.4 ± 0.22
COM+BU5	-22.7, -22.5, -23.3	-22.8 ± 0.24

Table A2: Particle number as a function of sodium oxalate concentration in synthetic urine

[NaOx] (mmol/l)	Particle number (/500 µl):		
	Experiment 1	*Experiment 2*	*Average ± SE*
15	3525	2902	3214 ± 312
30	1986	2002	1994 ± 8
45 *	1846	1919	1882 ± 36
60	16176	15905	16040 ± 136
75	10893	10725	10809 ± 84

** NaOx concentration equivalent to metastable limit*

Table A3.1: Composition (mmol/24hr) and physicochemical parameters of white subjects' urine

Variables	WC1	WC2	WC3	WC4	WC5	WC6	WC7	WC8	WC9	WC10	WC11	WC12	WC13	WC14
pH	6.10	5.90	6.55	6.00	6.35	5.95	6.60	5.70	6.70	6.35	6.15	5.85	6.20	6.35
Volume (ml/24hr)	1520	1080	2060	2020	2080	1160	1400	1670	2715	2130	1590	1410	2120	1880
Calcium	2.29	2.80	1.85	1.83	5.92	2.16	2.44	0.88	6.01	2.11	3.84	6.04	2.11	2.40
Chloride	117	178	269	135	199	182	107	105	192	108	133	90.0	184	118
Citrate	4.28	5.83	2.69	2.97	1.36	2.97	2.84	2.25	3.24	2.08	4.46	3.53	1.15	2.89
Creatinine	16.0	17.9	21.2	17.2	21.2	15.9	10.9	6.5	13.3	15.1	20.7	24.7	14.2	7.5
Magnesium *	3.62	2.68	2.89	3.86	6.42	2.62	3.09	1.13	3.19	3.76	4.98	8.10	3.94	3.25
Oxalate	0.12	0.13	0.30	0.25	0.23	0.18	0.13	0.13	0.21	0.14	0.11	0.10	0.18	0.15
Phosphate *	38.8	33.0	41.8	32.1	36.4	29.3	19.5	8.00	18.7	32.4	40.8	55.0	34.1	17.1
Potassium	37.4	62.9	55.3	67.2	25.8	108	48.8	38.7	63.0	72.6	66.7	64.8	72.6	54.8
Sodium	146	241	247	139	128	311	194	132	32.2	135	53.4	85.3	144	144
Sulphate	36.0	13.7	22.9	31.7	25.0	14.7	18.2	10.6	19.9	19.6	18.0	17.7	21.0	13.0
Uric acid *	3.30	3.60	5.70	3.60	6.0	4.1	2.8	1.6	2.7	4.0	4.2	5.7	4.0	2.4
RS Brushite	0.454	0.510	0.524	0.214	1.65	0.430	0.742	0.0250	0.951	0.483	1.02	1.76	0.442	0.360
RS Calcium ox	0.864	1.37	1.19	1.23	3.34	1.64	1.32	0.640	2.75	0.856	1.45	2.05	1.15	1.26
RS Uric acid	1.24	2.71	0.615	1.21	1.00	2.61	0.401	1.15	0.168	0.663	1.39	3.70	0.895	0.450

RS: Relative supersaturation

** Significantly higher than BC average ($p<0.05$)*

Table A3.2: Composition (mmol/24hr) and physicochemical parameters of black subjects' urine

Variables	BC1	BC2	BC3	BC4	BC5	BC6	BC7	BC8	BC9	BC10	BC11	BC12	BC13	BC14
pH	5.50	6.50	6.25	6.15	5.95	6.00	6.25	6.90	6.55	6.10	6.20	6.60	7.00	6.30
Volume (ml/24hr)	1630	2040	1260	980	2040	1460	940	2110	580	2470	865	2220	1195	1720
Calcium	1.20	2.62	1.32	0.48	3.90	2.82	2.54	1.62	2.40	4.07	1.42	2.07	2.14	2.19
Chloride	117	289	149	115	144	131	106	149	93.0	165	96.0	104	99.0	87.0
Citrate	4.99	5.78	2.12	1.56	4.12	3.18	2.66	5.60	2.69	1.88	2.80	5.33	4.36	2.84
Creatinine	13.9	19.0	13.5	15.5	14.9	12.6	12.6	18.8	12.7	14.1	12.5	12.2	8.50	10.5
Magnesium *	1.81	2.34	1.91	1.99	2.90	3.48	2.27	6.39	2.24	2.85	2.09	2.16	2.93	1.53
Oxalate	0.16	0.15	0.14	0.10	0.17	0.10	0.21	0.12	0.12	0.24	0.15	0.12	0.10	0.16
Phosphate *	14.3	25.3	21.3	27.3	15.1	21.8	17.0	18.8	19.6	15.6	15.2	10.0	13.1	20.8
Potassium	36.6	72.2	85.6	46.3	17.9	28.2	45.5	75.3	44.0	29.1	28.3	23.9	64.7	23.6
Sodium	166.1	380.3	180.9	143.7	121	122	159	230	91.1	124	146	40.3	44.2	44.3
Sulphate	20.7	20.6	10.1	20.1	17.0	14.7	11.1	17.9	8.16	24.9	12.1	14.0	12.0	15.3
Uric acid *	2.90	4.40	2.80	2.10	2.6	2.4	3.2	3.5	2.7	3.9	1.9	2.4	1.7	2.2
RS Brushite	0.0177	0.311	0.361	0.197	0.219	0.435	0.851	0.267	2.51	0.283	0.405	0.118	0.686	0.378
RS Calcium ox	0.454	0.588	1.01	0.376	2.10	1.34	4.03	0.357	3.89	2.73	1.81	0.577	1.08	1.68
RS Uric acid	2.82	0.529	0.928	1.09	0.999	1.15	1.42	0.173	1.02	0.933	1.02	0.233	0.120	0.512

RS: Relative supersaturation

** Significantly lower than WC average ($p<0.05$)*

APPENDIX A: FIGURES

Figure A1: OD_{620} plot of COM crystal slurry

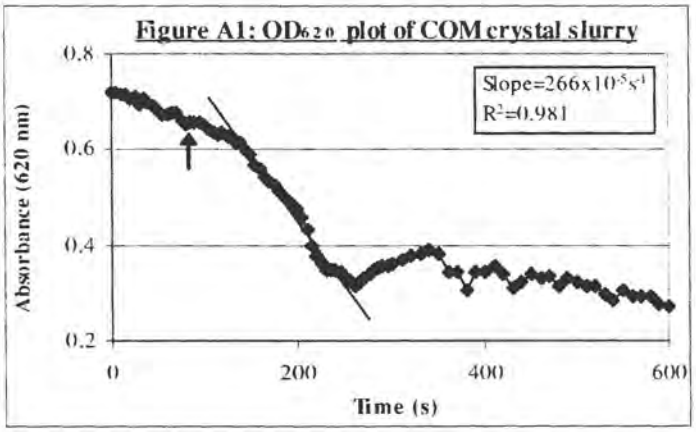

Figure A2: OD_{620} plots of COM crystal slurries after addition of white subjects' urine at a dilution of 1:2.

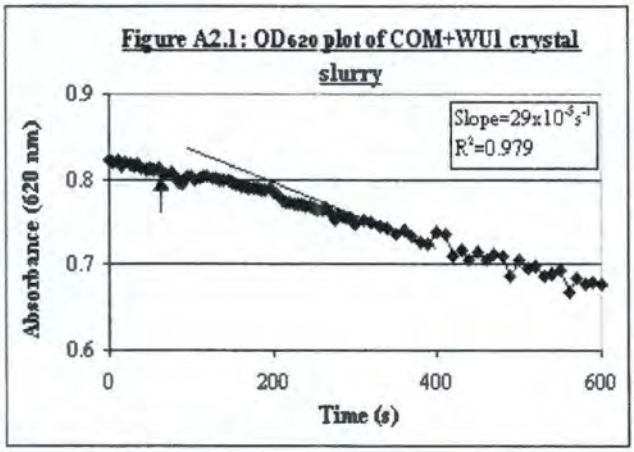

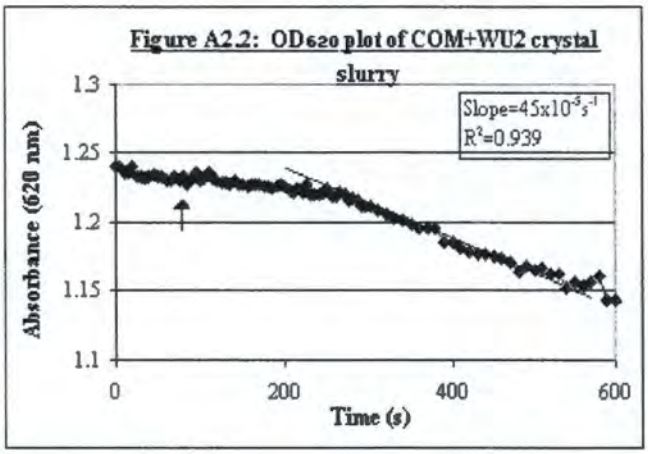

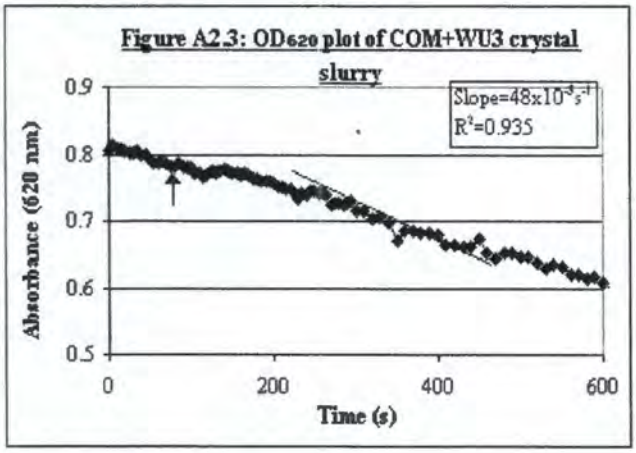

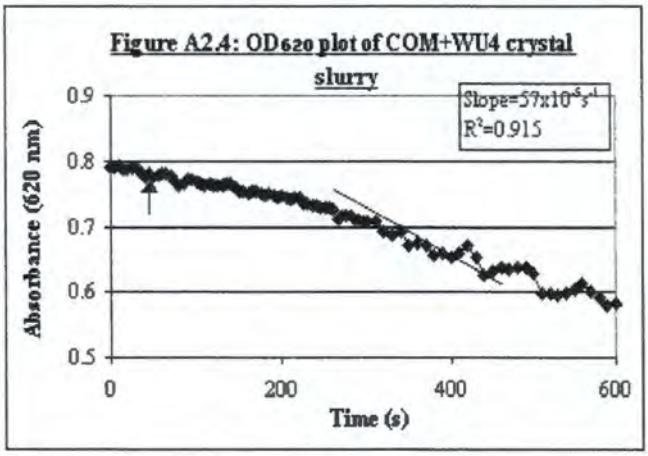

Figure A2: OD_{620} plots of COM crystal slurries after addition of black subjects' urine at a dilution of 1:2.

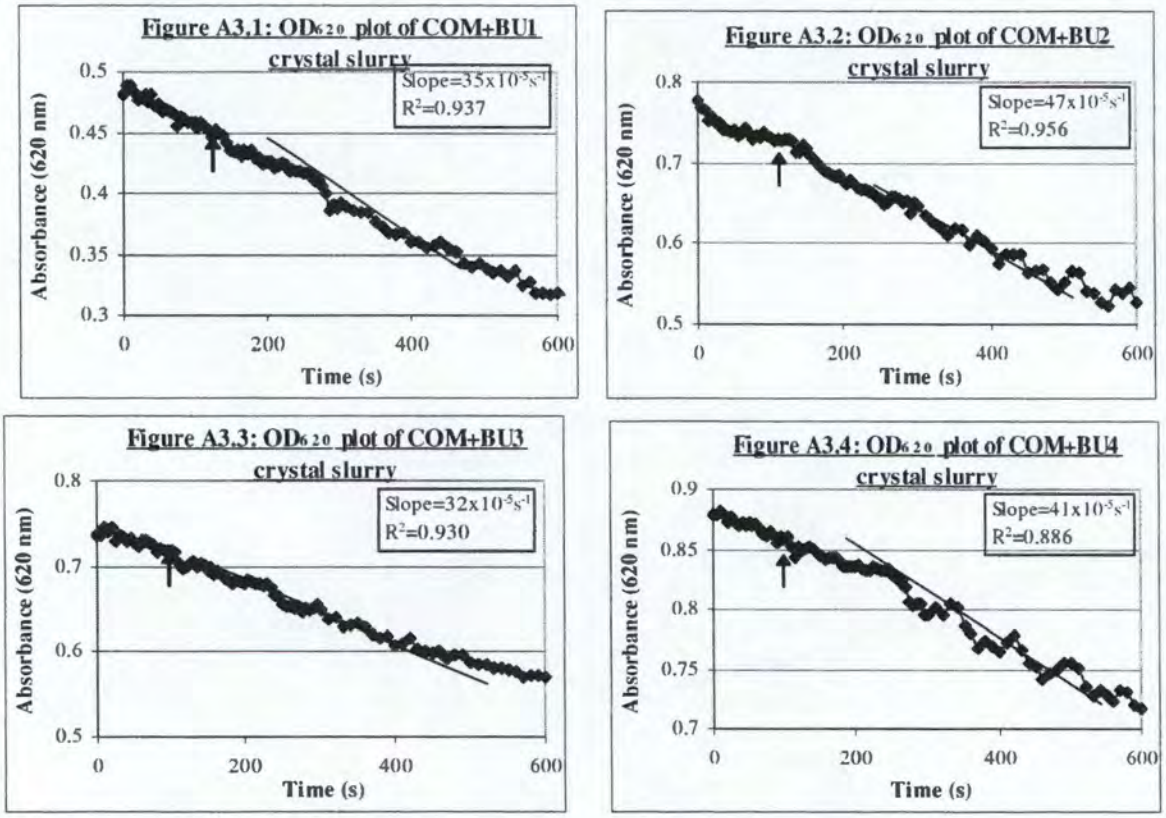

Figure A4: Particle size distributions of synthetic urine (4.1 – 4.5).

Figure A4.1: SU particle size distribution 1

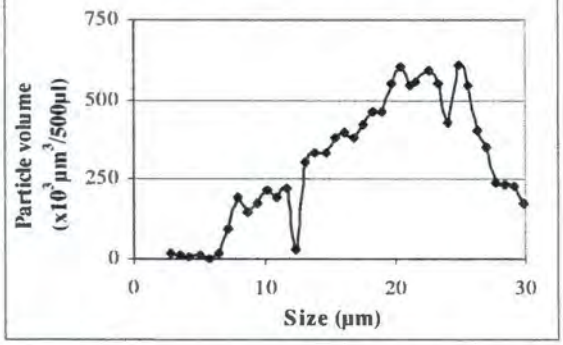

Figure A4.2: SU particle size distribution 2

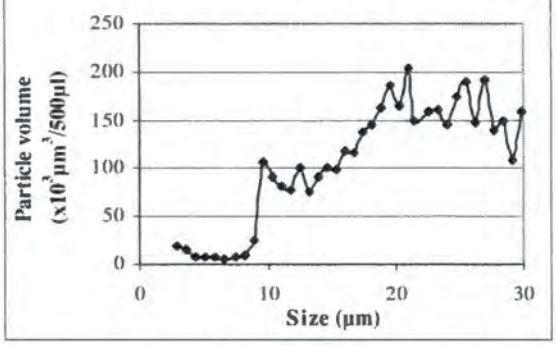

Figure A4.3: SU particle size distribution 3

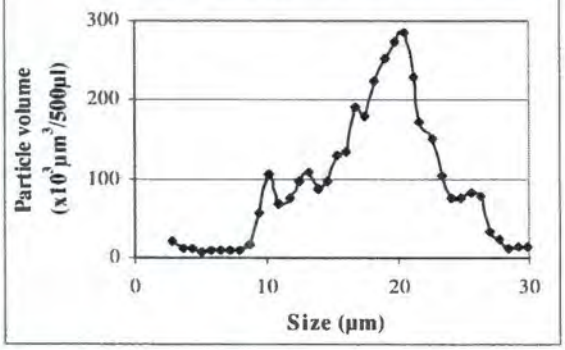

Figure A4.4: SU particle size distribution 4

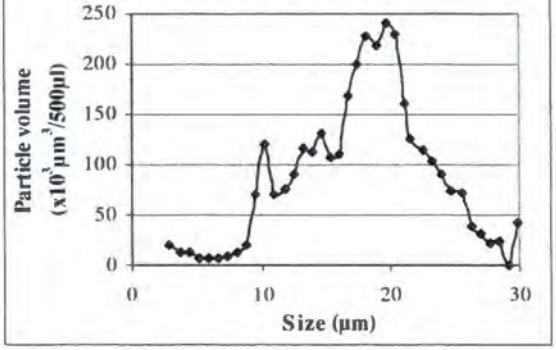

Figure A4.5: SU particle size distribution 5

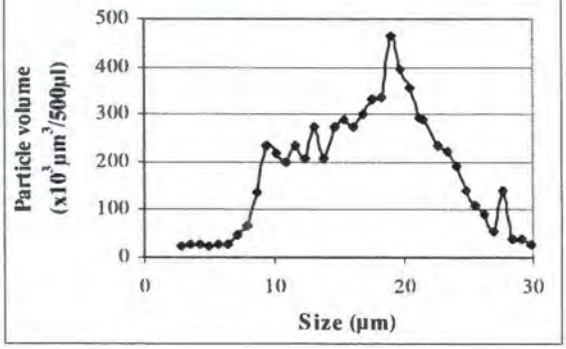

Figure A5: Particle size distributions of synthetic urine after addition of macromolecular extracts from white subjects' urine.

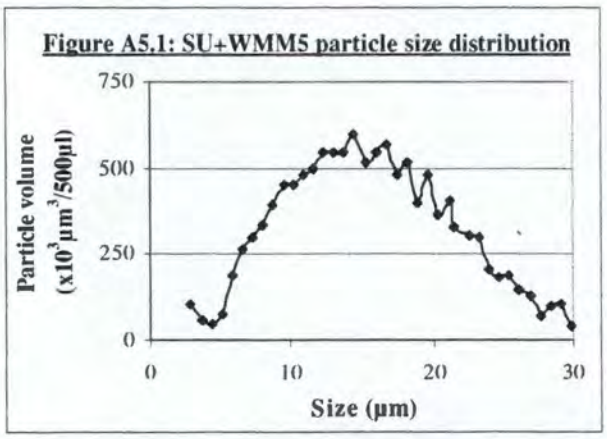

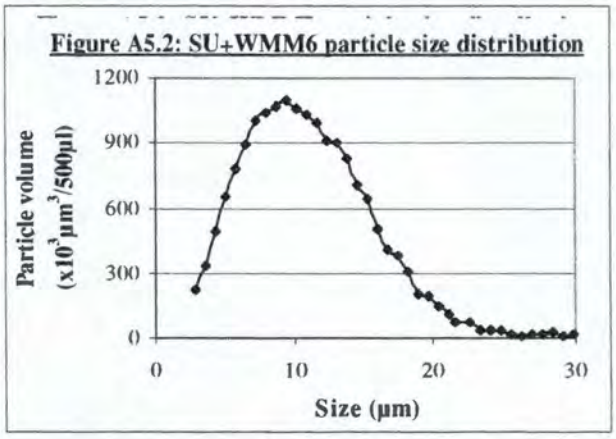

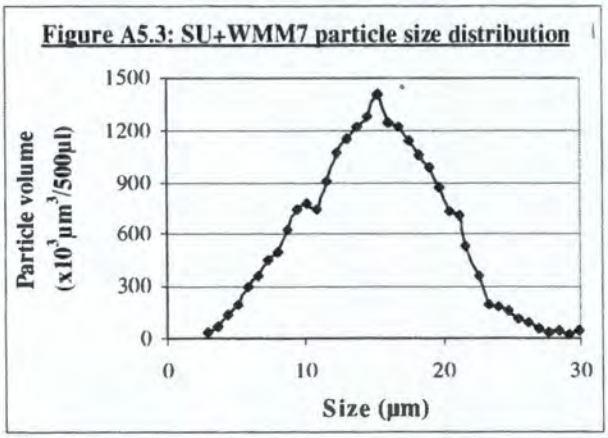

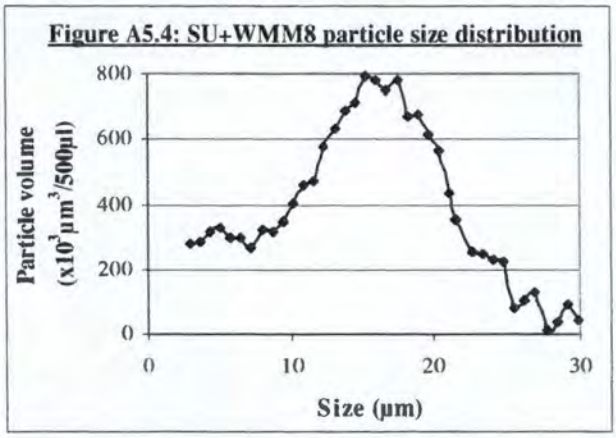

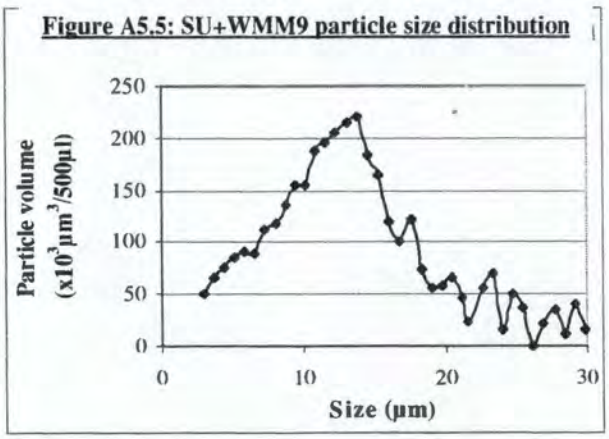

Figure A6: Particle size distributions of synthetic urine after addition of macromolecular extracts from black subjects' urine.

Figure A6.1: SU+BMM5 particle size distribution

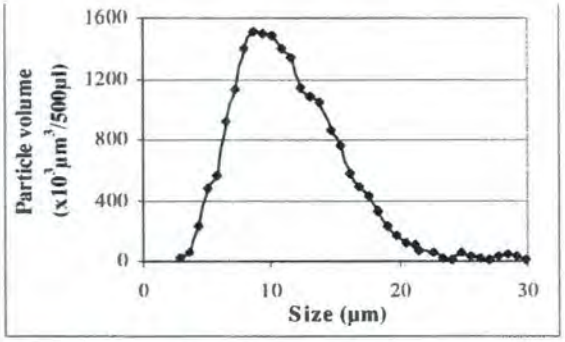

Figure A6.2: SU+BMM6 particle size distribution

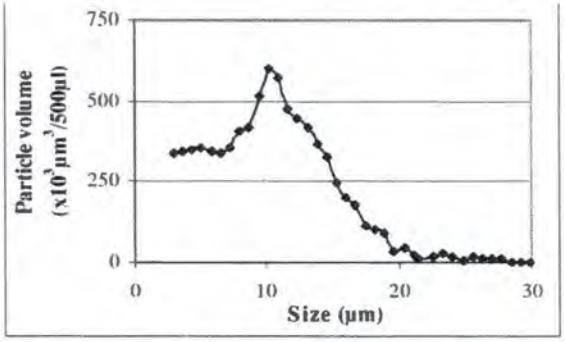

Figure A6.3: SU+BMM7 particle size distribution

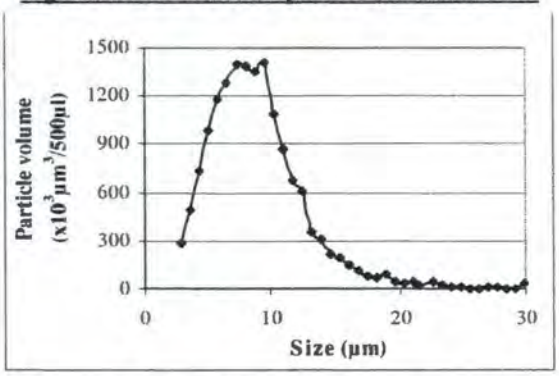

Figure A6.4: SU+BMM8 particle size distribution

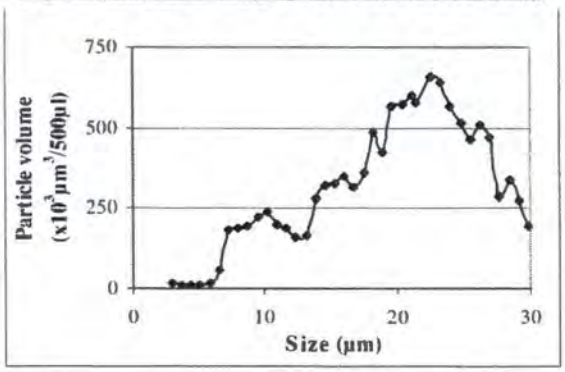

Figure A6.5: SU+BMM9 particle size distribution

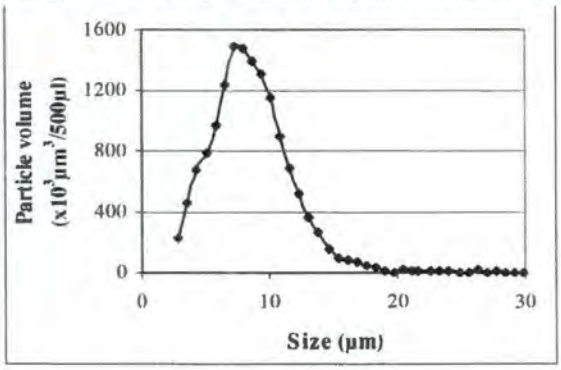

APPENDIX B: TABLES

Table B1: Urine composition (mmol/24hr) and physicochemical parameters of pooled urines from white subjects

Variables	Whites' pooled urine 1	Whites' pooled urine 2	Whites' pooled urine 3	Whites' pooled urine 4	Whites' pooled urine 5	Whites' pooled urine 6	Whites' pooled urine 7
Number of urines	6	9	13	10	11	12	5
Calcium (mmol/l)	1.97	2.94	2.55	1.65	2.88	2.97	4.19
Chloride (mmol/l)	100	104	99.0	89.0	85.0	108	135
Citrate (mmol/l)	2.17	2.69	2.69	1.94	2.07	2.42	2.69
Creatinine (mmol/l)	8.60	8.79	9.78	8.70	8.57	12.6	12.5
Magnesium (mmol/l)	2.52	3.86	4.62	1.91	2.96	2.81	3.12
Oxalate (mmol/l)	0.117	0.107	0.119	0.183	0.722	0.435	0.255
Phosphate (mmol/l)	15.1	19.1	20.1	18.3	20.0	23.0	22.0
Potassium (mmol/l)	26.9	37.9	43.2	38.5	41.5	28.7	27.3
Sodium (mmol/l)	67.4	128	174	174	128	136	204
Uric acid (mmol/l)	1.99	2.30	2.50	2.00	2.20	2.80	3.30
MSL (mmol/l)	45	45	45	45	45	30	15
pH	6.15	6.55	6.50	6.05	6.10	6.40	6.10
Volume (ml)	9135	18320	18610	16680	17040	15760	6400

RS: Relative supersaturation

Table B2: Urine composition (mmol/l) and physicochemical parameters of pooled urines from black subjects

Variables	Blacks' pooled urine 1	Blacks' pooled urine 2	Blacks' pooled urine 3	Blacks' pooled urine 4	Blacks' pooled urine 5	Blacks' pooled urine 6	Blacks' pooled urine 7
Number of urines	6	13	12	14	11	10	8
Calcium (mmol/l)	1.77	1.33	1.38	0.906	1.26	1.13	0.876
Chloride (mmol/l)	136	119	114	98.2	129	117	127
Citrate (mmol/l)	1.19	1.12	2.06	2.96	0.858	1.28	1.19
Creatinine (mmol/l)	11.6	7.82	7.10	6.74	8.88	7.32	9.09
Magnesium (mmol/l)	5.14	2.83	3.41	1.59	1.65	1.44	2.06
Oxalate (mmol/l)	0.164	0.098	0.119	0.275	0.236	0.604	0.512
Phosphate (mmol/l)	18.1	11.3	11.4	9.92	12.8	9.72	14.5
Potassium (mmol/l)	31.2	16.0	11.8	21.3	18.9	22.4	25.0
Sodium (mmol/l)	261	163	186	203	189	206	98.6
Uric acid (mmol/l)	2.24	1.90	1.80	1.88	2.50	1.60	2.10
MSL (mmol/l)	75	60	105	90	90	90	105
pH	5.60	5.60	6.00	6.40	6.00	5.80	6.00
Volume (ml)	4810	18160	18455	21975	16440	15440	12100

Table B3.1: Particle number as a function of sodium oxalate concentration in white males' pooled urine 1

[NaOx] (mM)	Particle number: Experiment 1	Experiment 2	Average
15	390	397	394
30	308	357	332
45	421	444	432
60 *	593	652	622
75	5921	6076	5998
90	14420	14718	14569

** NaOx concentration corresponding to metastable limit*

Table B3.2: Particle number as a function of sodium oxalate concentration in white males' pooled urine 2

[NaOx] (mM)	Turbidity: Experiment 1	Experiment 2	Average
15	0.54	0.50	0.52
30	0.47	0.48	0.475
45 *	1.02	1.00	1.01
60	5.5	6.0	5.75
75	8.2	9.2	8.7
90	15.6	16.6	16.1

** NaOx concentration corresponding to metastable limit*

Table B3.3: Particle number as a function of sodium oxalate concentration in white males' pooled urine 3

[NaOx] (mM)	Particle number: Experiment 1	Experiment 2	Average
15			124
30			758
45 *			946
60			12021
75			20250

** NaOx concentration corresponding to metastable limit*

Table B3.4: Particle number as a function of sodium oxalate concentration in white males' pooled urine 4

[NaOx] (mM)	Particle number: Experiment 1	Experiment 2	Average
15	0.38	0.35	0.365
30	0.45	0.48	0.465
45 *	0.97	0.95	0.96
60	4.0	4.2	4.1
75	13.7	13.8	13.75
90	13.2	13.1	13.15
105	16.0	17.1	16.55

** NaOx concentration corresponding to metastable limit*

Table B3.5: Particle number as a function of sodium oxalate concentration in white males' pooled urine 5

[NaOx] (mM)	Particle number: Experiment 1	Experiment 2	Average
15	1239	1188	1084
30	1123	1040	1082
45 *	1453	1289	1371
60	5041	5466	5254
75	21139	21486	21312

** NaOx concentration corresponding to metastable limit*

Table B3.6: Particle number as a function of sodium oxalate concentration in white males' pooled urine 6

[NaOx] (mM)	Particle number: Experiment 1	Experiment 2	Average
15	1783	1699	1743
30 *	431	420	426
45	6631	6942	6787
60	18861	18577	18719
75	20459	20410	20435
90	20666	20573	20620

** NaOx concentration corresponding to metastable limit*

Table B3.7: Particle number as a function of sodium oxalate concentration in white males' pooled urine 7

[NaOx] (mM)	Particle number: Experiment 1	Experiment 2	Average
15 *	1128	1118	1123
30	8062	7912	7987
45	17870	17893	17882
60	17649	17367	17508

** NaOx concentration corresponding to metastable limit*

Table B4.1: Particle number as a function of sodium oxalate concentration in black males' pooled urine 1

[NaOx] (mM)	Turbidity: Experiment 1	Experiment 2	Average
15	0.77	0.72	0.74
30	1.50	1.00	1.25
45	0.90	0.85	0.88
60	1.2	1.1	1.15
75 *	1.6	1.7	1.65
90	4.1	4.0	4.05
105	7.5	7.1	7.3
120	17.2	17.1	17.2

* *NaOx concentration corresponding to metastable limit*

Table B4.2: Particle number as a function of sodium oxalate concentration in black males' pooled urine 2

[NaOx] (mM)	Particle number: Experiment 1	Experiment 2	Average
15	818	917	868
30	553	639	596
45	530	580	555
60 *	632	626	629
75	6210	6477	6344
90	14819	14359	14589
105	19783	18111	18947

* *NaOx concentration corresponding to metastable limit*

Table B4.3: Particle number as a function of sodium oxalate concentration in black males' pooled urine 3

[NaOx] (mM)	Turbidity: Experiment 1	Experiment 2	Average
15	0.66	0.63	0.64
30	0.44	0.42	0.43
45	0.69	0.70	0.695
60	0.75	0.79	0.77
75	0.52	0.54	0.53
90	1.61	1.7	1.65
105 *	1.95	2.02	1.98
120	6.8	7.4	7.1
150	28	29	28.5

* *NaOx concentration corresponding to metastable limit*

Table B4.4: Particle number as a function of sodium oxalate concentration in black males' pooled urine 4

[NaOx] (mM)	Particle number: Experiment 1	Experiment 2	Average
15	508	572	540
30	538	535	536
45 *	902	1005	953
60	2003	2070	2036
75	3585	4127	3856
90	1621	2421	2021
105	7147	9528	8338
120	8128	9761	8944
150	7391	8726	8058

** NaOx concentration corresponding to metastable limit*

Table B4.5: Particle number as a function of sodium oxalate concentration in black males' pooled urine 5

[NaOx] (mM)	Particle number: Experiment 1	Experiment 2	Average
15	531	662	596
30			
45	807	874	840
60	1596	1246	1421
75	680	636	658
90 *	843	865	854
105	3753	4138	3946
120	4002	4442	4222

** NaOx concentration corresponding to metastable limit*

Table B4.6: Particle number as a function of sodium oxalate concentration in black males' pooled urine 6

[NaOx] (mM)	Turbidity: Experiment 1	Experiment 2	Average
15	0.62	0.56	0.59
30	0.68	0.58	0.63
45	1.00	0.94	0.97
60	1.08	1.03	1.06
75	1.09	1.19	1.14
90 *	1.68	1.72	1.70
105	7.4	8.1	7.75
120	27	28	27.5

** NaOx concentration corresponding to metastable limit*

Table B4.7: Particle number as a function of sodium oxalate concentration in black males' pooled urine 7

[NaOx] (mM)	Particle number: Experiment 1	Experiment 2	Average
15	775	790	772
30	655	533	644
45	1053	1194	1124
60	769	719	744
75	811	838	824
90	855	900	877
105 *	719	705	712
120	1884	2023	1954
135	2250	2263	2257

** NaOx concentration corresponding to metastable limit*

Table B5: Particle number (/500µl) of synthetic urine before and after addition of CME from white (WE) and black (BE) subjects at final concentrations of 5 mg/l

Time	*Experiment 1:*			*Experiment 2:*			*Average:*		
	SU	SU+WE	SU+BE	SU	SU+WE	SU+BE	SU	SU+WE	SU+BE
0	169	98	182	177	128	42	173	113	112
15	14754	11052	8034	13630	4206	3292	14192	7629	5663
30	15676	12193	11652	12513	6257	5164	14094	9225	8408
45	12990	11303	11848	11006	8018	6576	11998	9660	9212
60	12572	9762	11898	9028	8230	9297	10800	8996	10598

Table B6: Particle volume (10^6 µm^3/500µl) of synthetic urine before and after addition of CME from white (WE) and black (BE) subjects at final concentrations of 5 mg/l

Time	*Experiment 1:*			*Experiment 2:*			*Average:*		
	SU	SU+WE	SU+BE	SU	SU+WE	SU+BE	SU	SU+WE	SU+BE
0	0.037	0.036	0.032	0.025	0.042	0.015	0.019	0.039	0.024
15	1.637	1.266	0.590	0.928	0.556	0.556	1.283	0.911	0.573
30	1.928	1.736	1.305	1.796	1.228	0.940	1.862	1.482	1.123
45	2.08	2.500	1.654	2.333	1.972	1.559	2.207	2.236	1.607
60	2.343	2.694	2.200	2.721	2.345	2.185	2.532	2.520	2.193

Table B7: [^{14}C]-oxalate deposition expressed as a percentage precipitated [^{14}C]-oxalate in synthetic urine before and after addition of CME from white (WE) and black (BE) subjects at final concentrations of 5 mg/l

Time	*Experiment 1:*			*Experiment 2:*			*Average:*		
	SU	SU+WE	SU+BE	SU	SU+WE	SU+BE	SU	SU+WE	SU+BE
0	0	0	0	0	0	0	0	0	0
30	16.2	11.9	5.0	41.7	12.8	7.0	29.0	12.4	5.0
60	38.5	24.2	26.4	61.2	32.7	30.9	49.9	28.5	28.7
90	51.0	32.9	33.0	69.7	48.0	54.2	60.4	40.5	43.6
120	58.7	39.8	38.6	74.6	59.6	64.7	66.7	49.7	51.7

APPENDIX B: FIGURES

Figure B1: Particle number as a function of sodium oxalate concentration in white subjects' pooled urines

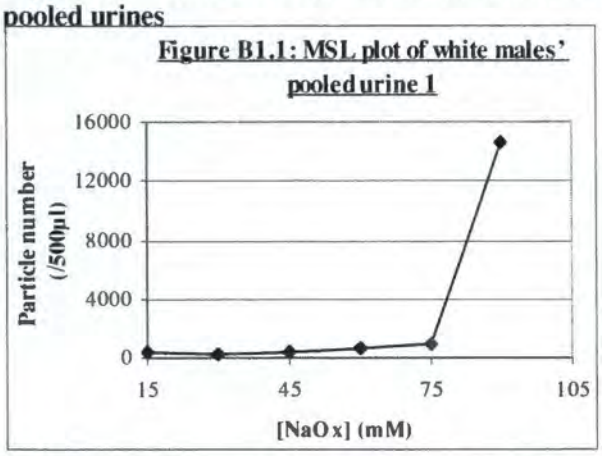

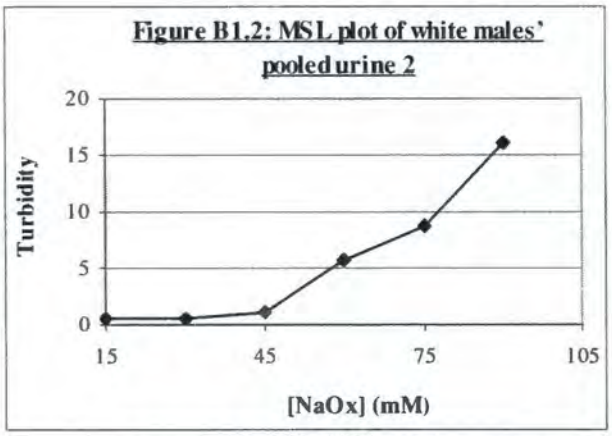

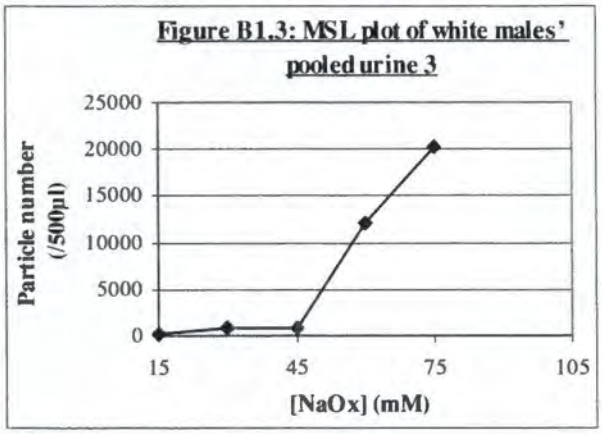

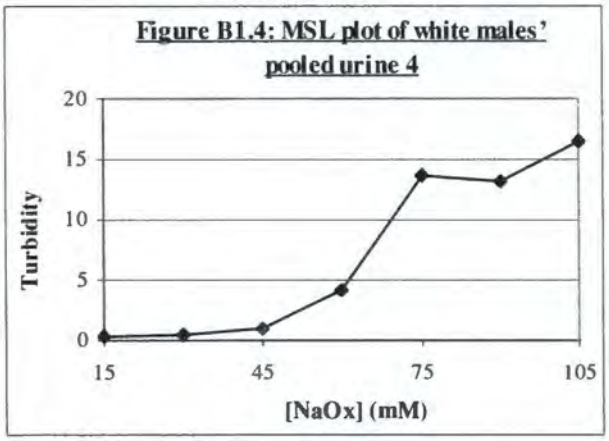

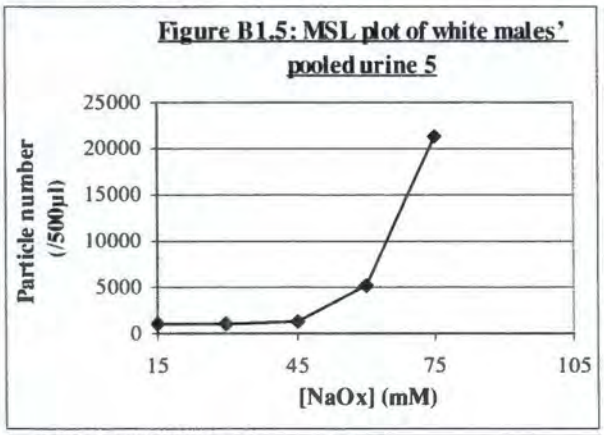

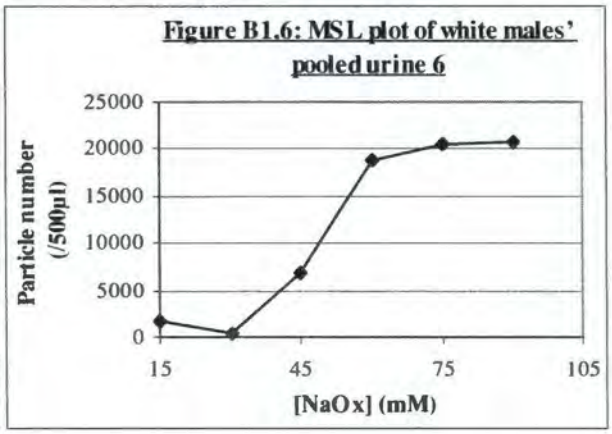

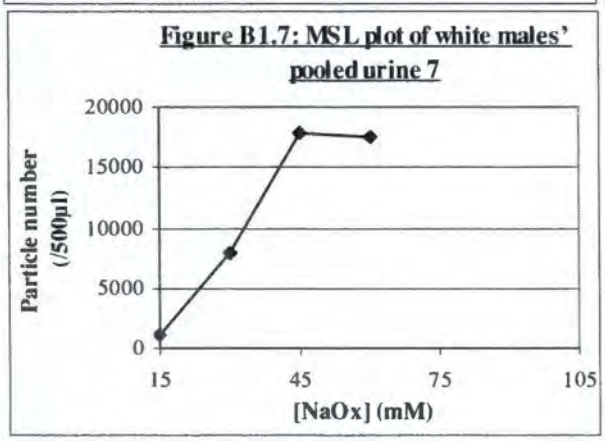

Figure B2: Particle number as a function of sodium oxalate concentration of black subjects' pooled urines

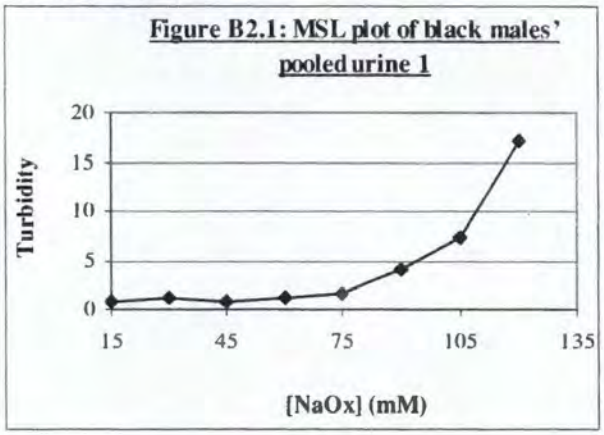

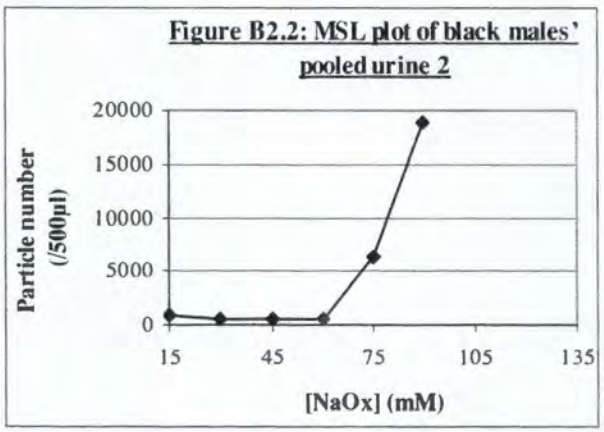

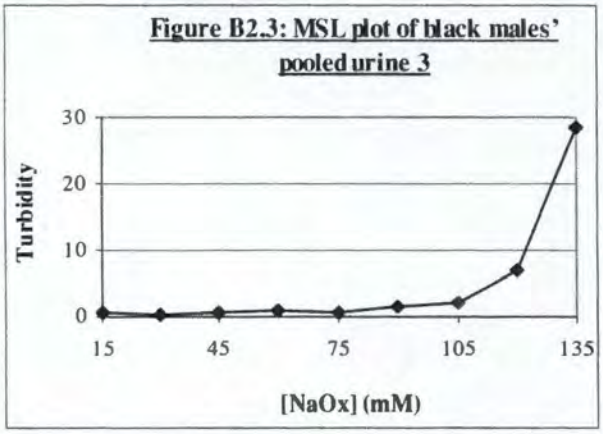

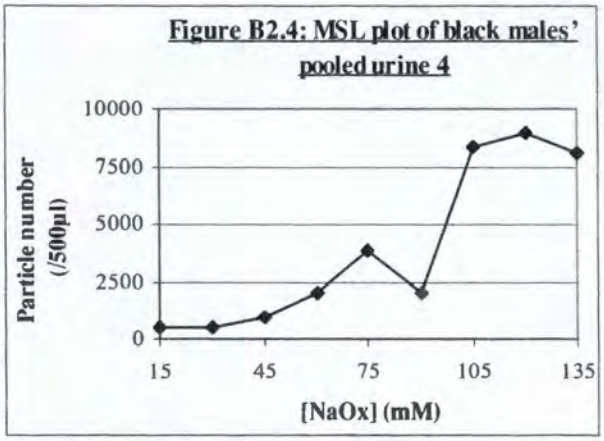

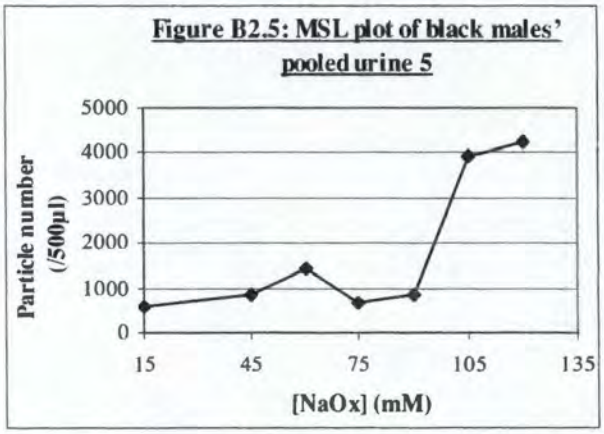

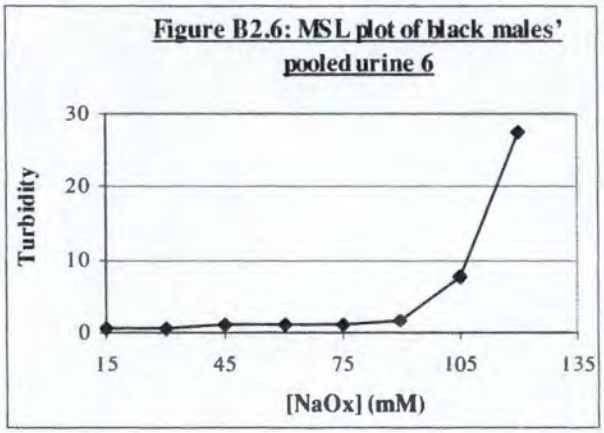

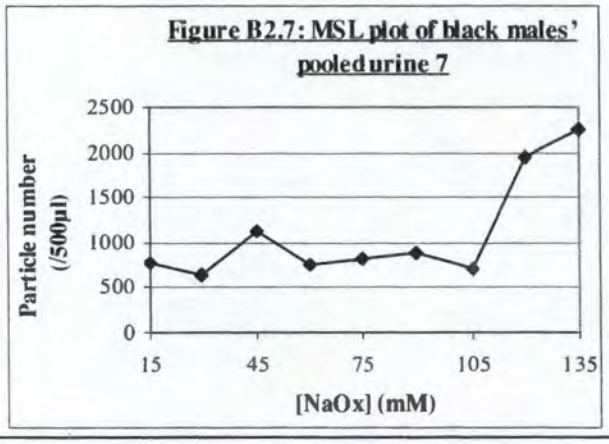

Figure B3: Particle number as a function of time of synthetic urine before and after addition of CME from white (WE) and black (BE) subjects at final concentrations of 5 mg/l (3.1: experiment 1, 3.2: experiment 2).

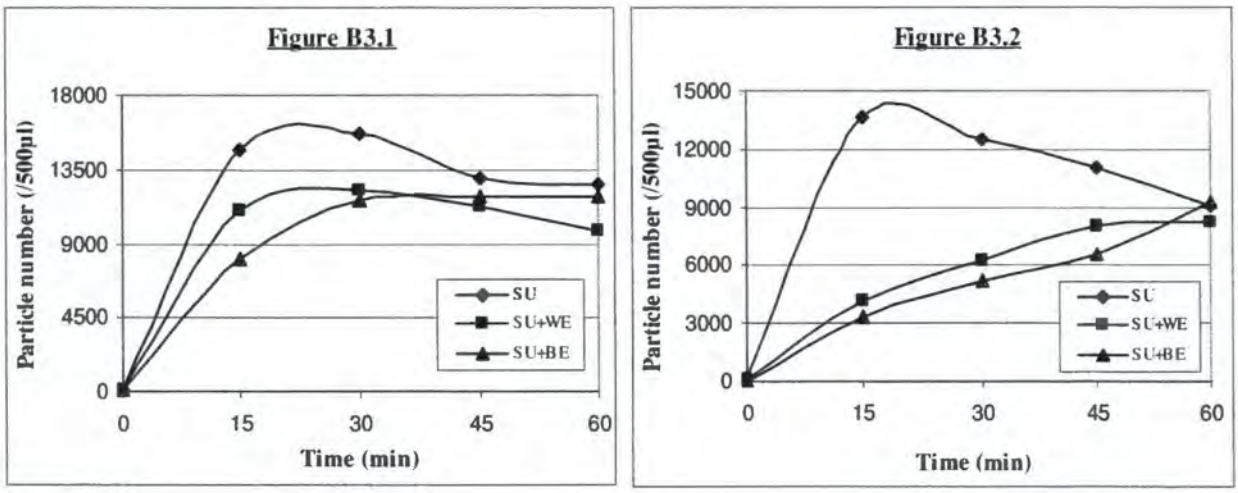

Figure B4: Particle volume of synthetic urine before and after addition of CME from white (WE) and black (BE) subjects at final concentrations of 5 mg/l (4.1: experiment 1, 4.2: experiment 2).

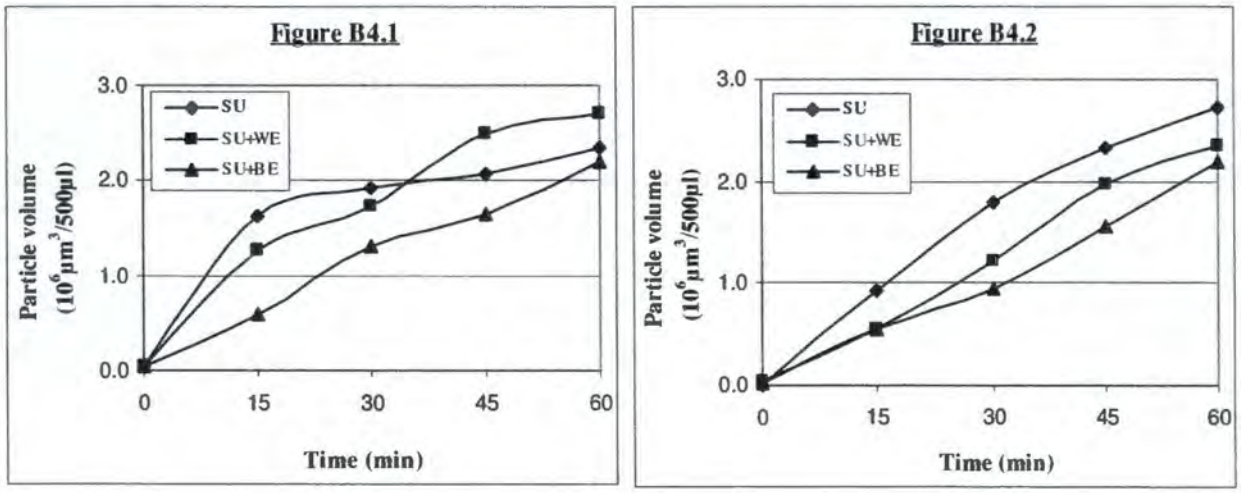

Figure B5: Particle size of synthetic urine before and after addition of CME from white (WE) and black (BE) subjects at final concentrations of 5 mg/l (5.1.1 – 5.1.2: experiment 1, 5.2.1 – 5.2.2: experiment 2).

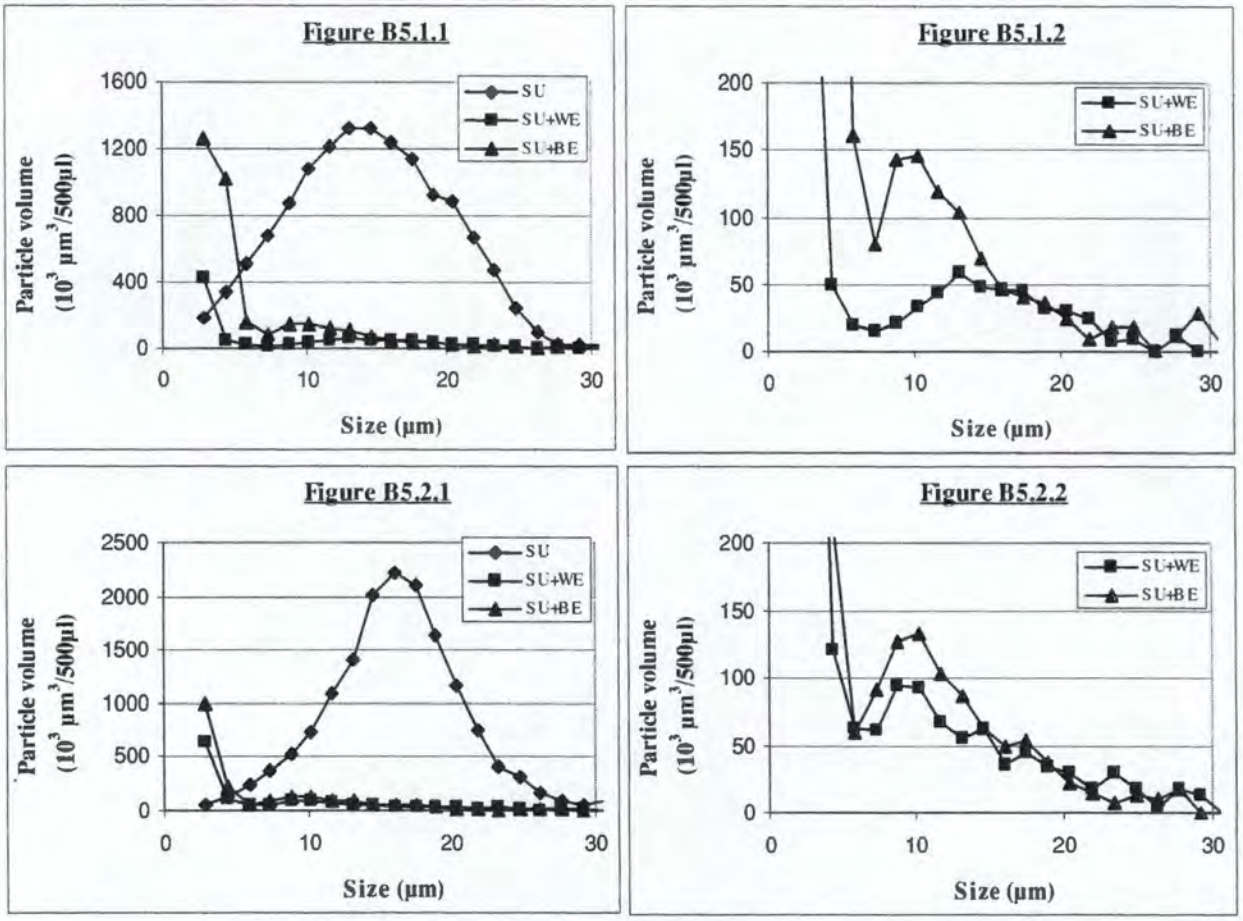

Figure B6: [^{14}C]-oxalate deposition rate in synthetic urine before and after addition of CME from white (WE) and black (BE) subjects at final concentrations of 5 mg/l (6.1: experiment 1, 6.2: experiment 2).

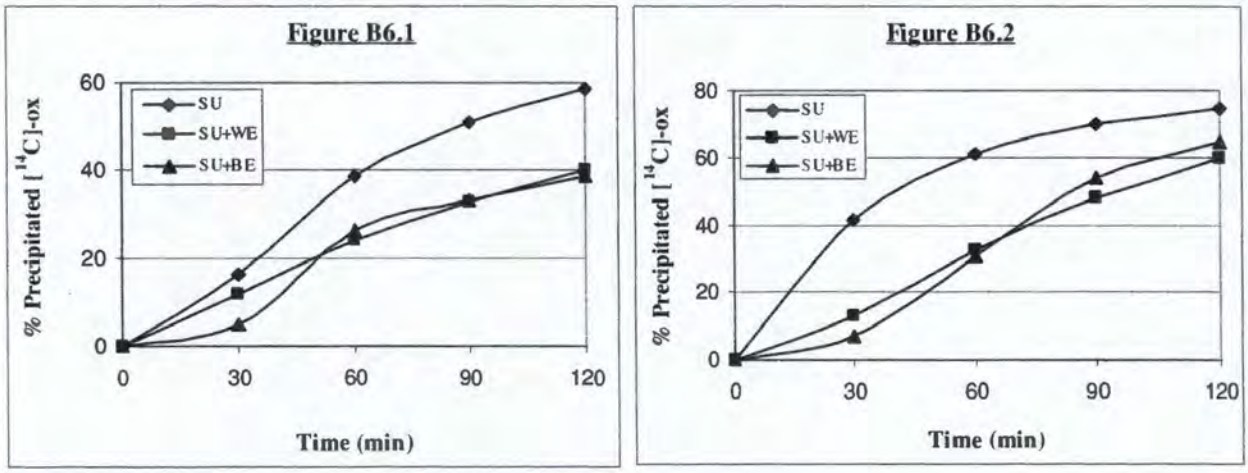

APPENDIX C: METHODS

N-LINKED GLYCAN ANALYSIS

Approximate time schedule

1.	SDS-PAGE	1 day
2.	Excise protein bands	1 hour
3.	Wash gel pieces	3 hours
4.	PNGase F digestion	overnight
5.	*N*-glycan extraction	4 - 5 hours
6.	2AB labelling & clean up	6 hours
7.	HPLC	3 ½ hour column conditioning, 3 hours per sample
8.	Exoglycosidase digestion	overnight

Sub-boiling point distilled water (SBP H_2O water)

MilliQ water has been found to contain traces of polymers and organic contaminants which give a high background signal on mass spectrometry. Samples are therefore prepared in fresh MilliQ water purified by distillation at sub-boiling point.

1. SDS-PAGE

Sample preparation

Reduce proteins by the addition of DTT as follows:

14 µl sample, 4 µl 5x Laemli sample buffer, 2 µl 0.5 mol/l DTT (7.71 mg DTT in 100 µl SBP H_2O)

Incubate at 70°C for 10 minutes.

Alkylate proteins with IA as follows.

Add 100 mmol/l IA at 10 % of the final volume (18.5 mg in 1 ml SBP H_2O).

Wrap samples in foil (IA is light sensitive) and incubate at room temperature (RT) for 30 minutes.

Note: Reduction and alkylation are necessary to separate disulphide bonded chains and to ensure optimal efficiency in digests using PNGase F.

Stock Solutions

All solutions were prepared using MilliQ water.

Protogel	:	30% acrylamide, 0.8% bisacrylamide solution
Stacking buffer	:	0.5M Tris, pH 6.6 [6g Tris in 100 ml H_2O, use HCl to adjust pH]
Gel buffer	:	1.5M Tris pH 8.8 [18.2g Tris in 100 ml H_2O, use HCl to adjust pH]
5x Running buffer	:	144g glycine, 30g Tris, 10g SDS in 2 l H_2O
Amps (10%)	:	1g Amps in 10ml H_2O
SDS (10%)	:	1g SDS in 10ml H_2O
5x Laemli sample buffer	:	0.04g Bromophenol blue, 0.625 ml stacking gel buffer pH 6.6, 1.0ml 10%SDS, 0.5ml glycerol, made up to 5 ml with H_2O
Coomassie stain	:	1.25g Coomassie R-250 (Brilliant blue), 250 ml methanol, 50 ml concentrated acetic acid, 200ml H_2O
Destain 1	:	50 % methanol, 7% concentrated acetic acid, 43% H_2O
Destain 2	:	5 % methanol, 7% concentrated acetic acid, 88% H_2O

12.5 % polyacrylamide gels (2 mini gels)

Packing gel:		***Stacking gel:***	
Protogel	5.0 ml	Protogel	0.665 ml
Gel buffer	3.0 ml	Stacking buffer	1.25 ml
SBP H_2O	4.0 ml	SBP H_2O	3.05 ml
SDS (10%)	120 µl	SDS (10%)	50 µl
Amps (10%)	120 µl	Amps (10%)	50 µl
TEMED	12 µl	TEMED	5 µl

Staining and destaining

Add Coomassie stain and leave overnight on a shaker (at low speed).

Place in "destain 1" solution for 5 minutes followed by "destain 2" solution for several hours as required.

2. EXCISE PROTEIN BANDS

Place the gel on a glass sheet over a light box and cut out the Coomassie-stained bands from the gel using a clean scalpel. Cut each band into small pieces (~1 mm^3) and transfer to 1.5ml eppendorf tube. Freeze the gel pieces for at least 2 hours; this helps break up the gel and facilitate PNGase F digestion.

3. WASHING OF GEL PIECES

Add 1 ml ACN to the eppendorf tube and vortex. Place the eppendorf in a 50 ml plastic tube on a mixer and wash for 30 minutes at RT. Discard ACN and repeat with 1 ml 20 mmol/l $NaHCO_3$ (0.168 g in 100 ml SBP H_2O, adjust to pH 7.0 with 1 mol/l HCl). Repeat the washings with ACN, followed by $NaHCO_3$ and finishing with ACN. The gel piece should move freely in the liquid so add more liquid if necessary. This removes background contamination which may interfere with 2AB labelling and subsequent mass spectrometry. The reducing and alkylating reagents as well as residual SDS are removed. Dry samples in a vacuum centrifuge.

4. PNGase F DIGESTION

The volumes given are for 15 mm^3 of gel. To the dried gel pieces add 3 µl PNGase F (1 U/µl in SBP H_2O) and 27 µl of 20 mmol/l $NaHCO_3$. Leave the samples for about 5 minutes until the gel pieces have re-swelled. Then cover the gel with additional buffer (a total of about 70 - 100 µl) until the gel is covered, and incubate at 37 ^0C for 12 - 16 hours.

5. *N*-GLYCAN EXTRACTION

After incubation in PNGase F, vortex the samples and centrifuge at 10 000 *g* for 5 minutes. In order to extract the glycans, remove and retain the supernatant and place it in a 1.5 ml eppendorf tube. Add 200 µl SBP H_2O to the gel and sonicate for 30 minutes, remove the supernatant and add to the retained supernatant. Repeat the sonication with a further two washed of SBP H_2O followed by 200 µl ACN (this shrinks the gel), 200 µl SBP H_2O and lastly 200 µl ACN. Dry the combined supernatants down to a final volume of 400 - 500 µl. Prepare AG-50 (H^+ activated) immediately as outlined below. Vortex the resin and water mixture and immediately add 50 µl resin to each sample. Place the eppendorf in a 50 ml plastic tube and mix for 5 minutes at RT to desalt. Filter the supernatant through 0.45 µm Millipore filter using a 1 ml syringe into a 1.5 ml eppendorf tube. Add 50 µl SBP H_2O to the resin remaining in the eppendorf tube and filter as before.

Dry down the sample in vacuum centrifuge and when the volume has reached 100 µl or less, transfer the supernatant to a 0.5 ml eppendorf, rinse the larger eppendorf out twice with 25 µl SBP H_2O, vortex and spin and transfer to the 0.2 ml eppendorf. Divide the sample in equal parts and dry. One half will be fluorescently labelled and the other will be retained for mass spectrometry.

AG-50 preparation: To activate AG 50W X12 200-400 mesh, put about 5 ml AG-50 in a 50 ml bottle, add 50 ml 1 mol/l HCl, shake, decant, repeat 3 times. Wash with 50 ml SBP H_2O and repeat 4 times. Check that the pH is 7 and store at 4 ^{0}C. Before use take 0.5 ml of suspension, allow to settle, remove water from above resin and discard. Add 1ml SBP H_2O, vortex and allow to settle. Remove SBP H_2O and discard. Repeat this process and remove most of the water.

6. 2AB LABELLING AND CLEAN UP

Add 5 µl of 2AB labelling mixture and vortex and spin down the sample. Incubate at 65 ^{0}C for 2 hours in a dry oven. After 30 minutes, remix and spin down the sample. Allow to cool at -20 ^{0}C for 5 minutes before applying to 3MM filter paper. Spot each labelled glycan sample onto a clean piece of filter paper about 1 cm from the bottom and allow to dry for about 20 - 30 minutes or until the spot appears dry (method for cleaning is detailed below). Run for 90 minutes in ACN. Inspect under UV light and cut out the glycan spot. Roll up the paper disc and place in a 1 ml syringe fitted with a 0.45 µm filter. Remove the plunger, insert paper disc and pipette 0.5 ml SBP H_2O into the syringe. Leave for 10 minutes and then push through the glycans into an acid washed rotary evaporator tube (abbreviated as "rotovap"). Add a further 0.5 ml double distilled H_2O, leave for 10 minutes and repeat for a total of 4 washes.

Evaporate the sample down to 50 – 100 µl and transfer to a 0.5 ml eppendorf, rinse out the rotovap tube with 50 µl SBP H_2O, vortex and centrifuge at 150 *g* for 5 minutes. Repeat twice with 50 µl SBP H_2O. Dry the labelled glycans in a vacuum centrifuge and dissolve in a final volume of 200 µl SBP H_2O.

Preparation of 3MM paper: Cut a 10 x 2.5 cm piece of paper for each sample. Was Whatman 3MM filter paper in a large volume of MilliQ H_2O for 2 washes of 15 minutes each, followed by a final wash of 15 minutes in SBP H_2O. Allow to dry completely before use.

7. HPLC

The amount of glycan required will depend on the amount of glycoprotein, the percentage glycosylation and the number of different glycans present. For the first analysis, use 1 % of the total glycan pool (*i.e.* 2/200 µl).

NP-HPLC

Make the glycans up to 20 µl with SBP H_2O and then add 80 µl ACN before analysis. Include a dextran sample as a standard. For NP-HPLC, a 4.6 x 250 mm Glycosep-N column (Glyko, England) was fitted to a Waters Alliance Separations module and monitored at a fluorescence of 420 nm following excitation at 330 nm. Solvent A was 50 mmol/l ammonium formate (pH 4.0) and solvent B was ACN. The glycans were separated with the following gradient conditions: 20 - 58 % A (0.4 ml/minute) over 152 minutes, 58 – 100 % A for 3 minutes (0.4 ml/minute), 100 % A for 5 minutes (1.0 ml/minute), 100 – 20 % A for 1 minute (1.0 ml/minute), 20 % A for 14 minutes (1.0 ml/minute) and then decreasing the flow rate to 0.4 ml/minute over 1.5 minutes. The total column time per sample is 180 minutes.

WAX-HPLC

Make the glycans up to 100 µl with SBP H_2O before analysis. Include a bovine serum fetuin sample as a standard. For WAX-HPLC, the glycans were separated according to charge density using a 7.5 x 50 mm Vydac 301VHP575 column (Anachem Limited, Luton, England). Solvent A was 0.50 mol/l formic acid (pH 9.0) and solvent B was 10 % methanol in SBP H_2O (v/v). The gradient conditions were as follows: 0 – 5 % A over 12 minutes, 5 - 21 % A over 13 minutes, 21 - 50 % A over 25 minutes, 80 – 100 % A over 5 minutes, 100 % A for 5 minutes (all at 1.0 ml/minute); then 100 – 0 % A over 1 minute, 0 % A for 11 minutes (both at 2.0 ml/minute); then continue at 1.0 ml/minute until 80 minutes. The fluorescence was monitored at 420 nm following excitation at 330 nm.

8. EXOGLYCOSIDASE DIGESTION

Dry aliquots of the 2AB labelled glycan pool (usually 1 %) in 0.5 ml eppendorf tubes. Add exoglycosidases at the final concentrations indicated in Table 4.2 (page 70) and incubate overnight at 37 ^{0}C in a circulating water bath. Use all exoglycosidases except JBM with a 10 times concentrated mix buffer (50 mmol/l sodium acetate final concentration, pH 5.5). Use JBM with a separate buffer (100 mmol/l sodium acetate, 2 mmol/l Zn, pH 5.0).

Table: Examples of exoglycosidase array preparations

Sample	Volume (µl):									
	Abs	**Amf**	**Btg**	**GluH**	**Jbh**	**Bkf**	**Jbm**	**Nani**	**buffer**	**dd H_2O**
Control	0	0	0	0		0			1	9
Abs	1	0	0	0		0			1	8
Abs+Amf	1	1	0	0		0			1	7
Abs+Amf+Btg	1	1	2	0		0			1	5
Abs+Amf+Btg+GluH	1	1	2	1		0			1	4
Abs+Amf+Btg+Jbh	1	1	2		2				1	3
Abs+Amf+Btg+GluH+Bkf	1	1	2	1		2			1	2
*Abs+Amf+Btg+GluH+Bkf+Jbm							5		1	4
Nani								1	1	8

* *The glycan pool was incubated overnight with Abs+Amf+Btg+GluH+Bkf and "cleaned up" as described below. The sample was then dried down and incubated overnight with Jbm in the Jbm buffer.*

After overnight digestion, clean up samples to remove excess enzyme. Pre-wash Amicon Micropure-EZ enzyme removers with 200 µl SBP H_2O, centrifuge at 2800 *g* for 10 minutes and discard the washings. Apply the digested glycans to the filter, centrifuge (10000 *g* for 2 minutes) and wash out the digestion tube with 20 µl SBP H_2O and apply to the filter. Centrifuge (10000 *g* for 2 minutes) and apply 100 µl SBP H_2O to the membrane. Centrifuge again (10000 g for 2 minutes) and dry down the sample under vacuum. Redissolve in 20 µl SBP H_2O and transfer to an HPLC vial. Add 80 µl ACN and inject onto the HPLC.

O-LINKED GLYCAN ANALYSIS

O-linked glycans were released by manual hydrazinolysis. This method also releases a small amount of *N*-linked glycans but these can readily be distinguished according to the elution position on HPLC.

1. Dialyse proteins overnight against 0.1 % TFA.

2. Transfer the dialysed samples to acid-washed hydrazinolysis tubes (do not fill the bulb more than half way). Put on a lid with a teflon insert which is punctured. Place the tube in a clean 50 ml plastic tube and freeze-dry overnight.
3. The sample is then cryongenically frozen (by Dr Brian Matthews, Glycobiology Institute, Oxford University).
4. Cut 47 cm lengths of Whatman 1 chromatography paper with pinking shears and make folds at 2, 6.5 and 8.5 cm. Run with SBP H_2O by descending chromatography for 24 hours and hang up the strips to dry.
5. Hydrazinolysis (Dr Brian Matthews): 60 ^{0}C for 6 hours; heat up to 60 ^{0}C at 10 ^{0}C per minute
6. Prepare an AG50 x 12(H^+) 200-400 mesh column from resin which has been activated by HCl whilst the hydrazine is being removed under vacuum. Make a column in a 1 ml Biorad disposable column [~ 0.4 ml resin]. Wash through the column with five column volumes of SBP H_2O.
7. Put the sample on ice. Add 20 µl of 0.2 mol/l sodium acetate and then add 20 µl acetic anhydride (with an acid-washed glass pipette). Leave the sample on ice for 10 minutes after shaking a little and then add a further 20 µl acetic anhydride. Leave for 50 minutes at RT. There must be sufficient acetic anhydride so that you can see phase separation; otherwise, add more acetic anhydride.
8. Desalt the sample on the AG50 and wash through with five column volumes of SBP H_2O into rotovap tubes.
9. The samples must be washed out of the tubes and dried down in eppendorf tubes. Add a drop of octanol during drying down to prevent foaming. The shaker should be on full speed with the temperature no greater than 28 °C during drying. Add 1 ml SBP H_2O and a drop of octanol, vortex, centrifuge (150 *g* for 5 minutes) and rotovap until dry. Repeat this process twice to remove the acetic anhydride. Add 0.5 ml SBP H_2O, vortex, centrifuge (150 *g* for 5 minutes) and rotovap and dry down again. Repeat with 200 µl and then 25 µl SBP H_2O at a lower rotovap speed.
10. Apply the sample to the pre-washed chromatography paper at the 8.5 cm mark. Use a further 25 µl SBP H_2O to wash out the tube and apply to the paper as well. Allow the spots to dry thoroughly.
11. Run the paper by descending chromatography in a tank with fresh solvent (~5 cm deep) and filter paper lined walls (allow time for the tank to equilibrate). Run for 48 - 72 hours with the following solvent, butanol : ethanol : SBP H_2O as 8:2:1.

12. Dry the paper and cut out from –1 cm to + 3 cm. Roll up this piece (containing the *O*-glycans) using waxed paper (so as not to handle sample) and place in a teflon 2.5 ml syringe fitted with a 0.5 µm 13mm filter on the end over an acid-washed rotovap tube.
13. In order to wash the glycans off the paper, apply 1.5 ml SBP H_2O, wait for 5 minutes and push the sample through. Repeat this procedure three times with 1.5 ml SBP H_2O and rotovap to dryness. Wash down the sides of the rotovap tube 1 ml SBP H_2O, vortex, centrifuge as before and dry on the rotovap at a moderate speed. Finally, repeat with 0.5 ml and then 0.25 ml SBP H_2O.
14. Redissolve the glycans in 25 µl SBP H_2O, centrifuge at 150 *g* for 5 minutes and transfer to an eppendorf tube. Wash out the rotovap tube with a further 3 x 25 µl SBP H_2O, centrifuging each time. Store the glycans at -20 ^{0}C until 2AB labelling.
15. Now proceed from 2AB labelling as for the *N*-linked glycans.

APPENDIX C: TABLES

Table C1: NP-HPLC analysis of *N*-linked glycans on UPTF1 from white control subjects

Peak ID	GU	% AREA:								
		WC1	WC2	WC3	WC4	WC5	WC6	WC7	WC8	Ave
1	4.43	0.1	0.1				0.2			0.1
2	4.91	0.4	0.2	0.3		1.0	0.2	0.4		0.4
3	5.06	0.3	0.1				0.1	1.2		0.4
4	5.31		0.1	0.4	1.2	1.4		1.0		0.8
5	5.45					0.6				0.6
6	5.58	0.6	0.3	0.2	0.7	1.0	0.5	2.2		0.8
7	5.83	0.5	0.1		0.5	0.9	0.3	0.8		0.5
8	5.90	1.3	0.6	0.5	1.7	1.7	0.6	1.3	0.9	1.1
9	6.03	0.8	0.9	0.4	1.2	1.4	0.8	1.1	0.3	0.9
10	6.20						0.2			0.2
11	6.28	0.6	0.4			0.9	0.3	0.5		0.5
12	6.37	1.8	1.5	0.8		0.8	1.6	2.1	1.2	1.4
13	6.58	0.7	0.6		2.7	1.7	0.8		0.4	1.2
14	6.70	1.9	1.1	0.8	2.2	1.8	1.4	2.3	1.0	1.6
15	6.80	2.2	1.7	1.5	2.5	2.9	1.8	2.4	2.1	2.1
16	7.07	2.2	1.0	0.6	0.9	1.8	1.0	1.9	1.2	1.3
17	7.16	9.8	5.4	3.4	9.6	9.1	5.8	8.8	4.9	7.1
18	7.36	1.9	1.9	1.5			2.3		0.7	1.7
19	7.49	1.8	1.8	1.9	3.6	3.4	2.1	2.8	3.0	2.6
20	7.77	1.6	1.5	1.1	1.5	1.4	1.6	1.8	1.4	1.5
21	7.88	30.7	24.1	21.6	32.4	30.4	27.3	30.7	24.5	27.7
22	8.20									
23	8.25	2.3	4.1	3.7	3.2	3.2	3.3	3.4	6.2	3.7
24	8.40	0.7	1.3	1.8	0.6	1.0	2.1	0.9	1.0	1.2
25	8.56	35.6	49.2	57.5	33.1	31.9	43.3	33.2	49.8	41.7
26	8.91	1.1	1.6	1.8	1.0	0.8	1.6	1.2	1.7	1.4
27	9.26	0.1	0.1			0.2	0.4			0.2

Table C2: NP-HPLC analysis of *N*-linked glycans on UPTF1 from black control subjects

Peak ID	GU	% AREA:							
		BC1	BC2	BC3	BC4	BC5	BC6	BC7	Ave
1	4.43							0.8	0.8
2	4.91	0.3	0.1	0.8		0.8		3.4	1.1
3	5.06	0.1	0.1						0.1
4	5.31		0.2						0.2
5	5.45					0.5	0.9	1.4	0.9
6	5.58	0.2	0.2	0.3					0.2
7	5.83	0.1	0.1			0.5	0.4	0.8	0.4
8	5.90	0.7	0.6	0.4	0.4	1.3	1.3	1.8	0.9
9	6.03	1.0	0.7	0.6	0.2	0.6	1.0	1.6	0.8
10	6.20								
11	6.28						0.4		0.4
12	6.37	1.6	1.1	1.1	1.0	1.0	1.3	2.3	1.3
13	6.58	0.7	0.6		0.2	0.5	1.0	1.2	0.7
14	6.70	1.2	1.4	1.3	0.7	1.9	2.0	2.3	1.5
15	6.80	1.7	1.6	1.5	1.1	2.8	3.0	3.4	2.2
16	7.07	1.2	0.8		0.7	1.7	2.2	2.5	1.5
17	7.16	5.7	5.5	5.2	3.2	5.0	7.1	6.0	5.4
18	7.36	1.7	2.3	1.7	1.2			0.8	1.5
19	7.49	2.3	1.6	1.8	1.7	2.6	3.3	3.4	2.4
20	7.77	1.6	1.1	1.1	1.0	1.8	2.0	2.3	1.6
21	7.88	25.3	26.8	24.4	22.7	24.6	22.0	19.1	23.6
22	8.20	3.9	0.5	4.1					2.8
23	8.25		2.8		4.9	4.6	5.3	5.2	4.6
24	8.40	1.3	0.4	0.7	0.9	1.1	1.0	1.3	1.0
25	8.56	47.8	50.3	54.3	57.8	46.0	44.4	35.8	48.1
26	8.91	1.4	0.4	0.8	2.1	1.1	0.9		1.1
27	9.26	0.2			0.2				0.2

Table C3: NP-HPLC analysis of *N*-linked glycans on UPTF1 from white (WSF) and black (BSF) stone-formers

Peak ID	GU	% AREA:									
		WSF1	WSF2	WSF3a	WSF3b'	WSF4	WSF5	WSF6a	WSF6b*	WSF Av.	BSF
1	4.43					0.2				0.2	0.1
2	4.91	1.1		1.6		0.7	0.2	1.3	1.0	1.0	
3	5.06						0.3		0.5	0.4	
4	5.31										
5	5.45			0.4		0.8	0.8			0.7	
6	5.58	0.8		1.0		0.5		0.9		0.8	0.4
7	5.83		0.8	0.4		0.5	0.4	0.6	0.5	0.5	0.2
8	5.90	1.9	1.3	0.9		1.3	1.5	1.7	0.7	1.3	0.4
9	6.03		1.2	1.1		1.2	0.9	0.8	1.6	1.1	0.5
10	6.20								0.8	0.8	
11	6.28		1.2			0.8	0.6	0.7		0.8	0.4
12	6.37	1.3	4.5	2.2	1.2	0.9	0.7	1.4	0.5	1.6	1.5
13	6.58	0.4	1.8	1.3	0.6	1.3	1.2	1.1	1.1	1.1	0.8
14	6.70	1.5	1.9	1.4	1.5	1.1	1.6	1.9	0.9	1.5	1.0
15	6.80	2.4	4.0	2.3	1.6	2.5	2.6	2.8	1.8	2.5	1.9
16	7.07	1.8			1.7	1.4	1.6	1.9	3.1	1.9	
17	7.16	6.0	14.3	9.4	7.1	10.8	10.6	9.8	1.9	8.7	8.3
18	7.36	2.3	5.0		1.0			0.8	9.7	3.8	2.4
19	7.49	2.2		3.8	4.3	3.8	3.4	3.0	3.5	3.4	2.2
20	7.77	2.0	3.9	2.5	2.4	1.3	1.4	1.5	1.5	2.1	2.0
21	7.88	26.6	24.5	22.8	23.8	32.5	33.7	33.3	32.0	28.7	23.6
22	8.20		1.8							1.8	
23	8.25	3.4	2.5	5.0	7.2	4.2	3.5	3.3	3.8	4.1	4.9
24	8.40	1.8	0.7	1.2	0.7	1.0	0.8		0.6	1.0	1.2
25	8.56	42.9	29.1	41.3	43.3	30.4	32.9	33.2	33.8	35.9	44.4
26	8.91	1.5	1.1	1.1	3.2	2.1	1.3		0.7	1.6	2.0
27	9.26		0.5	0.4	0.5	0.3				0.4	1.0

** These samples contained two bands corresponding to UPTF1 which were excised and treated separately. However, their glycan profiles were very similar and thus were pooled for subsequent analyses.*

APPENDIX C: FIGURES

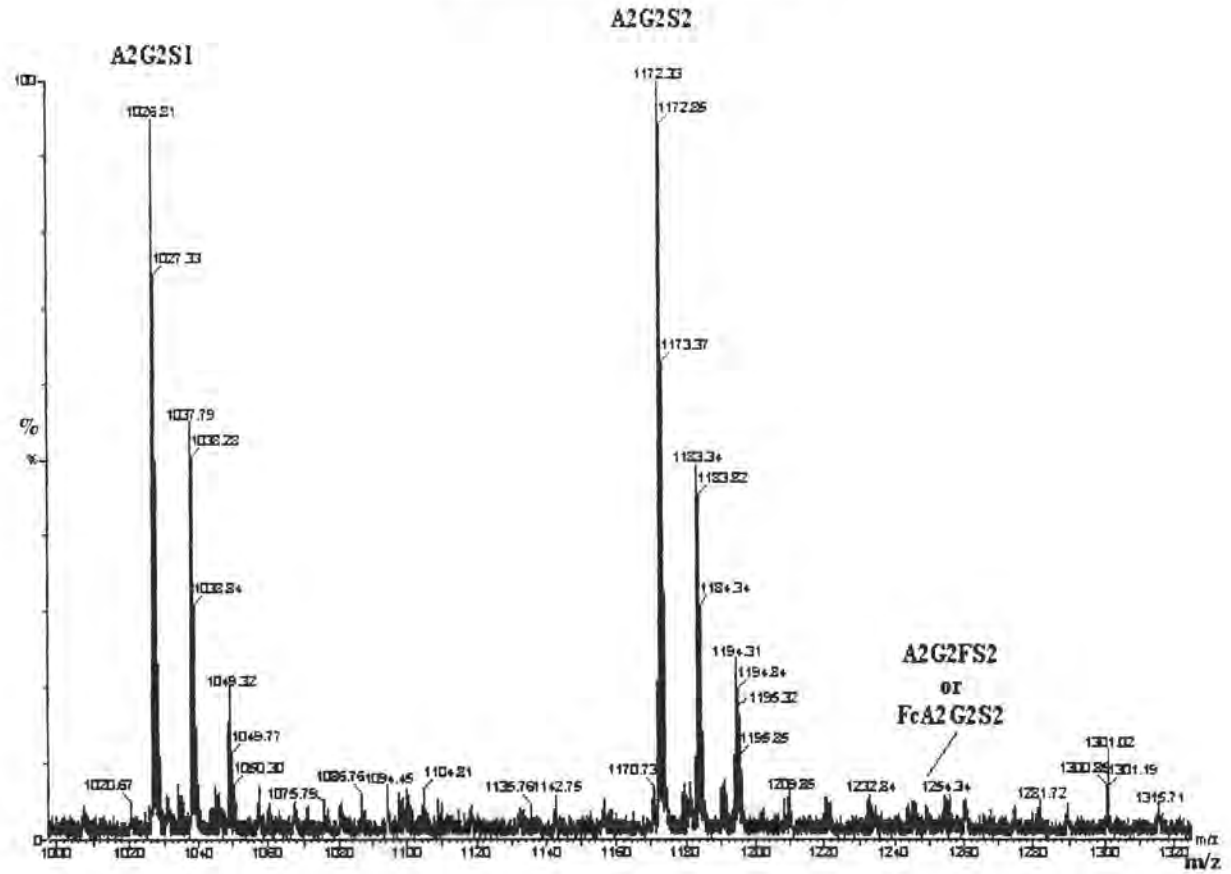

Figure C2: QTOF mass spectrum of N-linked glycans on UPTF1 from white control subject WC6

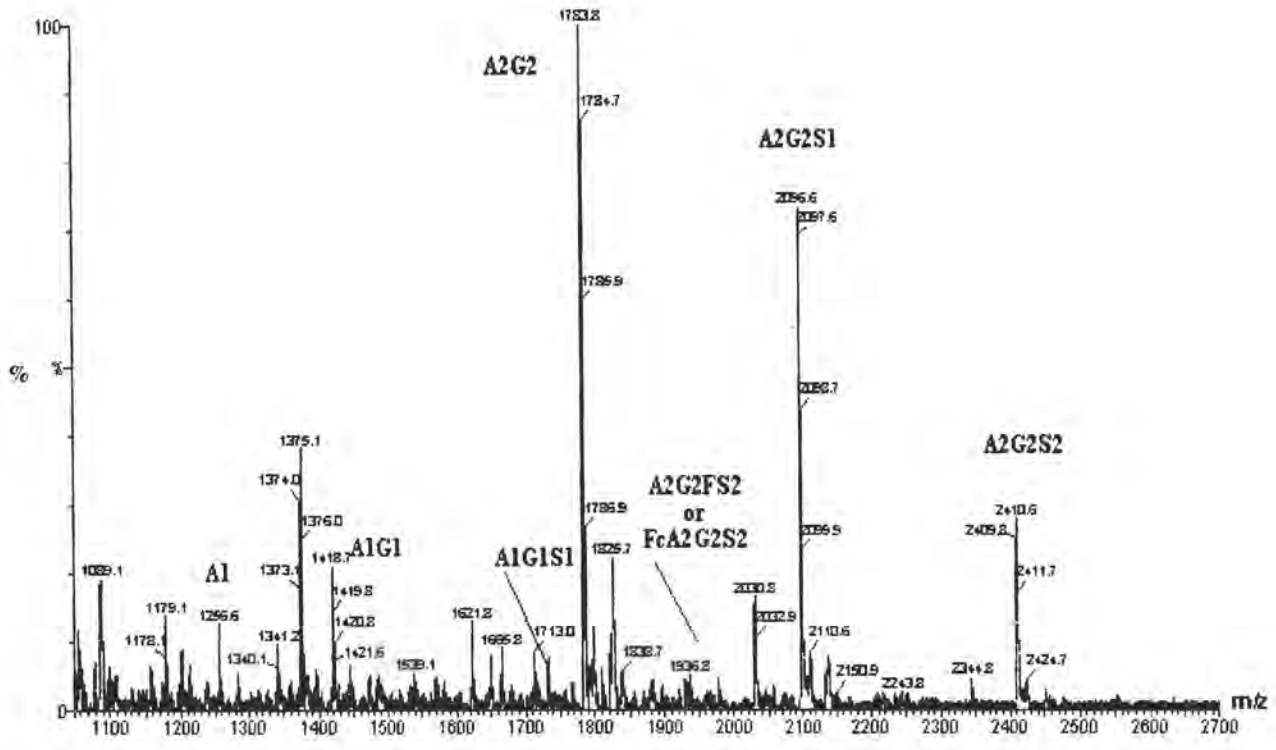

Figure C1: MALDI-TOF spectrum of N-linked glycans on UPTF1 from white control subject WC6

APPENDIX D: TABLES

Table D1: Particle number as a function of sodium oxalate concentration in synthetic urine

[NaOx] (mmol/l)	Particle number (/500 µl):		
	Experiment 1	*Experiment 2*	*Average (± SE)*
15	900	332	616 ± 284
30	984	370	677 ± 307
45 *	1119	646	902 ± 256
60	11633	15604	13539 ± 2066
75	13949	12518	13152 ± 634
90	20138	22452	21249 ± 1203

** NaOx concentration equivalent to metastable limit*

Table D2: Particle size (µm) of synthetic urine (SU) before and after addition of WF1 and BF1 at final concentrations of 1.25 mg/l

Sample	1	2	3	4	5	6	7	8	9	10	Ave.
SU	16.96	16.96	15.54	16.96	16.96	18.37	18.37	17.88	18.37	17.88	17.45
SU+WF1	13.43	11.43	12.72	12.72	14.13	12.41	11.72	12.41			12.60
SU+BF1	10.60	10.60	12.72	12.72	12.72	11.30	12.72	12.72	12.41	12.41	12.09

Table D3: [^{14}C]-oxalate deposition expressed as a percentage precipitated [^{14}C]-oxalate of synthetic urine (SU) before and after addition of WF1 and BF1 at final concentrations of 1.25 mg/l

Time	*Experiment 1:*			*Experiment 2:*			*Average:*		
	SU	SU+WF1	SU+BF1	SU	SU+WF1	SU+BF1	SU	SU+WF1	SU+BF1
0	0	0	0	0	0	0	0	0	0
30	24.2	14.9	12.8	27.1	17.4	10.6	25.7	16.2	11.7
60	42.4	35.0	32.1	41.5	28.8	26.0	42.0	31.9	29.0
90	51.4	49.4	46.1	50.0	36.0	39.2	50.7	42.5	42.6
120	57.5	50.5	55.2	57.7	43.2	41.6	57.6	46.9	48.4

Table D4.1: Urine composition (mmol/l) and physicochemical parameters of pooled urines from white males

Variables	Pooled urine 1	Pooled urine 2	Pooled urine 3	Pooled urine 4	Pooled urine 5	Ave ± SE
Calcium (mmol/l)	2.03	2.87	2.22	3.32	0.872	2.26 ± 0.334
Chloride (mmol/l)	107	138	116	101	63.9	105 ± 12.6
Citrate (mmol/l)	1.70	1.79	1.95	0.983	2.22	1.73 ± 0.266
Creatinine (mmol/l)	10.9	14.4	10.4	11.0	6.50	10.6 ± 1.49
Magnesium (mmol/l)	2.12	4.58	2.50	3.08	1.43	2.74 ± 0.392
Oxalate (mmol/l)	0.159	0.209	0.153	0.058	0.171	0.150 ± 0.020
Phosphate (mmol/l)	18.4	27.2	24.8	19.6	11.7	20.3 ± 2.46
Potassium (mmol/l)	24.6	31.2	18.9	8.68	41.7	25.0 ± 4.49
Sodium (mmol/l)	104	189	123	190	102	142 ± 21.6
Uric acid (mmol/l)	2.19	2.89	2.50	2.20	1.59	2.27 ± 0.300
Metastable limit (mmol/l)	60	45	45	30	60	48 ± 8.2
pH	6.45	5.90	6.45	6.35	6.35	6.30 ± 0.090
Volume (ml)	7345	4780	6360	9540	8060	7217 ± 703

Table D4.2: Urine composition (mmol/l) and physicochemical parameters of pooled urines from black males

Variables	Pooled urine 1	Pooled urine 2	Pooled urine 3	Pooled urine 4	Pooled urine 5	Ave ± SE
Calcium (mmol/l)	1.90	1.43	1.97	0.785	1.21	1.46 ± 0.334
Chloride (mmol/l)	92.9	109	140	61.0	116	104 ± 12.6
Citrate (mmol/l)	2.27	1.27	2.24	0.720	1.07	1.51 ± 0.266
Creatinine (mmol/l)	11.3	8.90	17.2	7.20	10.4	11.0 ± 1.49
Magnesium (mmol/l)	2.59	2.44	2.06	1.74	1.99	2.16 ± 0.392
Oxalate (mmol/l)	0.120	0.074	0.153	0.108	0.105	0.112 ± 0.020
Phosphate (mmol/l)	20.7	13.4	21.5	9.81	15.8	16.2 ± 2.46
Potassium (mmol/l)	21.5	33.5	33.8	19.6	23.0	26.3 ± 4.49
Sodium (mmol/l)	86.4	151	223	111	156	146 ± 21.6
Uric acid (mmol/l)	2.80	1.90	3.29	1.19	1.99	2.23 ± 0.300
Metastable limit (mmol/l)	60	105	60	105	75	81 ± 8.2
pH	6.00	6.35	6.40	6.10	6.20	6.21 ± 0.090
Volume (ml)	5900	5170	5680	8495	6940	6437 ± 703

Table D5.1: Particle number as a function of sodium oxalate concentration in ultrafiltered urine from white males

[NaOx]	Particle number (/500 µl):				
(mmol/l)	*Experiment 1*	*Experiment 2*	*Experiment 3*	*Experiment 4*	*Experiment 5*
15	641	394	605	1424	557
30	741	824	428	1214 *	619
45	253	846 *	382 *	9744	700
60	705 *	4279	6372	17594	1078*
75	2799	5892	10334	18408	5606
90	4573	7332	14768	21118	16680
105	3955	8080	17362		20284
120	12330				

** The corresponding NaOx concentration was equivalent to the metastable limit.*

Table D5.2: Particle number as a function of sodium oxalate concentration in ultrafiltered urine from black males

[NaOx]	Particle number (/500 µl):				
(mmol/l)	*Experiment 1*	*Experiment 2*	*Experiment 3*	*Experiment 4*	*Experiment 5*
15	189	417	286		896
30	376	926	1175	457	254
45	316	698	576	444	415
60	474 *	403	2143 *	770	838
75	12135	399	11192	1563	770
90	10428	833	21827	1975	833 *
105	6098	1468 *	16940	1121 *	2790
120	23648	10260		7703	8583
135		9759		12738	13570
150		26552		15354	15211

** The corresponding NaOx concentration was equivalent to the metastable limit.*

Table D6.1: [^{14}C]-oxalate deposition expressed as a percentage precipitated [^{14}C]-oxalate in ultrafiltered urine from white subjects (WUF) before and after addition of WF1 and BF1 at final concentrations of 1.25 mg/l

Time	*Experiment 1:*			*Experiment 2:*			*Experiment 3:*		
	WUF	WUF+WF1	WUF+BF1	WUF	WUF+WF1	WUF+BF1	WUF	WUF+WF1	WUF+BF1
0	0	0	0	0	0	0	0	0	0
30	22.7	7.3	10.6	59.4	18.8	23.7	8.5	0.7	0.0
60	39.3	19.2	22.5	65.5	28.5	31.0	11.7	4.3	1.5
90	49.6	30.4	33.8	71.1	36.3	41.6	22.6	12.8	7.9
120	55.1	36.2	38.3	55.8	37.3	48.6	30.9	23.7	22.9

Table D6.2: [^{14}C]-oxalate deposition expressed as a percentage precipitated [^{14}C]-oxalate in ultrafiltered urine from black subjects (BUF) before and after addition of WF1 and BF1 at final concentrations of 1.25 mg/l

Time	*Experiment 1:*			*Experiment 2:*			*Experiment 3:*		
	BUF	BUF+WF1	BUF+BF1	BUF	BUF+WF1	BUF+BF1	BUF	BUF+WF1	BUF+BF1
0	0	0	0	0	0	0	0	0	0
30	33.3	7.2	13.9	67.2	17.4	6.4	33.3	10.5	28.3
60	42.3	30.0	22.1	74.9	37.8	10.3	42.3	26.4	35.9
90	58.4	44.4	30.2	76.5	45.7	27.1	58.4	40.5	47.2
120	64.1	48.6	39.3	77.6	50.4	41.5	64.1	50.4	54.2

Table D7.1: Absorbance slopes ($x\text{-}10^{-5}s^{-1}$) of COM crystal slurries before and after addition of WF1 and BF1 at final concentrations of 1.25 mg/l

Sample	1	2	3	4	5	6	7	Ave. ± SE
COM	300	322	349	320	388	337		336 ± 8.52
COM+WF1	73	52	59	78	107	68		73 ± 8.52
COM+BF1	58	54	63	45	46	62	70	57 ± 8.52

Table D7.2: Absorbance slopes ($x\text{-}10^{-5}s^{-1}$) of COD crystal slurries before and after addition of WF1 and BF1 at final concentrations of 1.25 mg/l

Sample	1	2	3	4	5	6	7	8	9	10	11	12	Ave. ± SE
COD	98	96	99	99	79	89	89	93	111				95 ± 2.90
COD+WF1	44	48	52	43	34	32	41	53	41	55	31	35	41 ± 2.90
COD+BF1	55	41	35	40	57	42	49	62	43	39			44 ± 2.90

Table D8.1: Zeta potential (mV) of COM crystal slurries before and after addition of WF1 and BF1 at final concentrations of 1.25 mg/l

Sample	ZP1	ZP2	ZP3	ZP4	ZP5	ZP6	Ave. ± SE
COM	-15.5	-15.5	-17.9	-17.9	-17.4	-16.0	-16.7 ± 0.55
COM+WF1	-33.1	-30.8	-31.5	-33.9	-32.6	-31.0	-32.2 ± 0.55
COM+BF1	-31.9	-29.3	-30.3	-33.8	-32.1	-32.0	-31.6 ± 0.55

Table D8.2: Zeta potential (mV) of COD crystal slurries (COD) before and after addition of WF1 and BF1 at final concentrations of 1.25 mg/l

Sample	ZP1	ZP2	ZP3	ZP4	ZP5	ZP6	Ave. ± SE
COD	-15.2	-18.1	-17.0	-16.7	-15.7	-13.0	-16.0 ± 0.62
COD+WF1	-26.3	-27.9	-28.8	-26.4	-28.5	-25.5	-27.2 ± 0.62
COD+BF1	-28.2	-25.9	-26.3	-24.7	-28.5	-26.2	-26.6 ± 0.62

APPENDIX D: FIGURES

Figure D1: Particle size distribution in synthetic urine before and after addition of WF1 and BF1 at final concentrations of 1.25 mg/l.

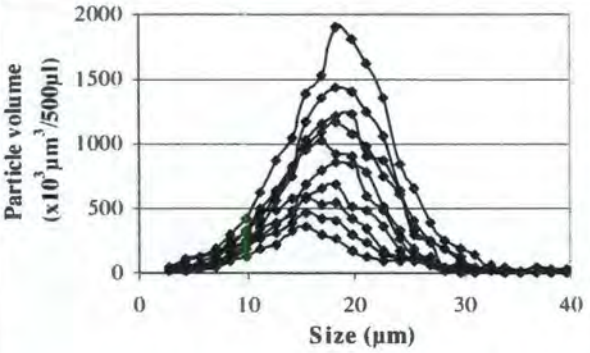

Figure D1.1: Particle size distribution in synthetic urine

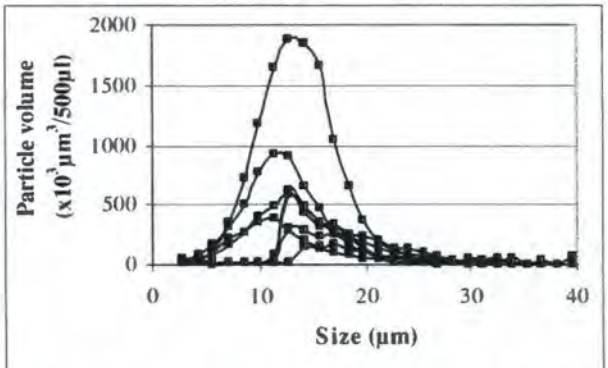

Figure D1.2: Particle size distribution in synthetic urine after addition of WF1 (final conc. 1.25mg/l)

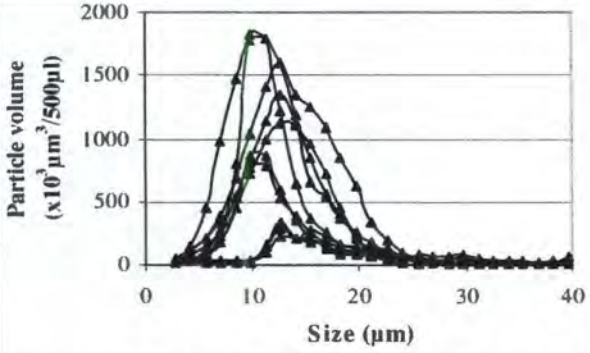

Figure D1.3: Particle size distribution in synthetic urine after addition of BF1 (final conc. 1.25mg/l)

Figure D2: [^{14}C]-oxalate deposition in synthetic urine before and after addition of WF1 and BF1 at final concentrations of 1.25 mg/l.

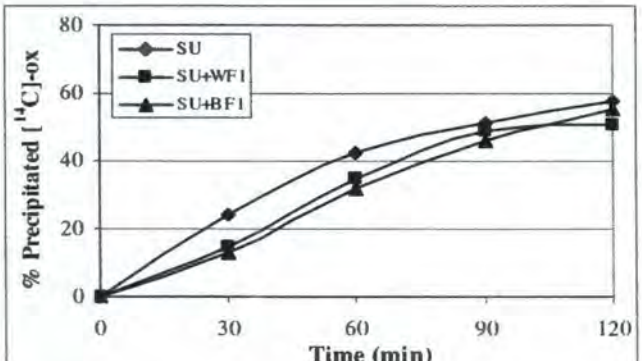

Fig D2.1: [^{14}C]-ox deposition in synthetic urine (expt 1). After addition of WF1 and BF1 at final conc. 1.25mg/l

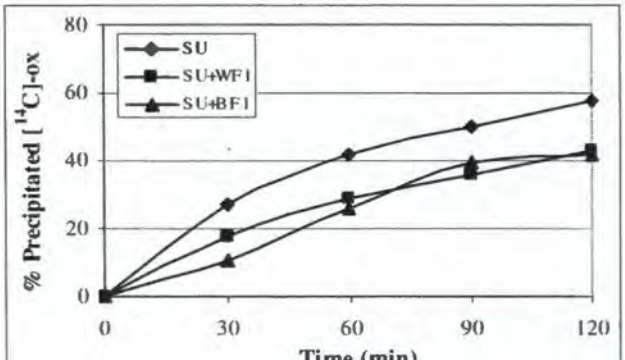

Fig D2.2: [^{14}C]-ox deposition in synthetic urine (expt 2). After addition of WF1 and BF1 at final conc. 1.25mg/l

Figure D3: MSL plots of white (3.1-3.5) and black (3.6-3.10) subjects' pooled urines

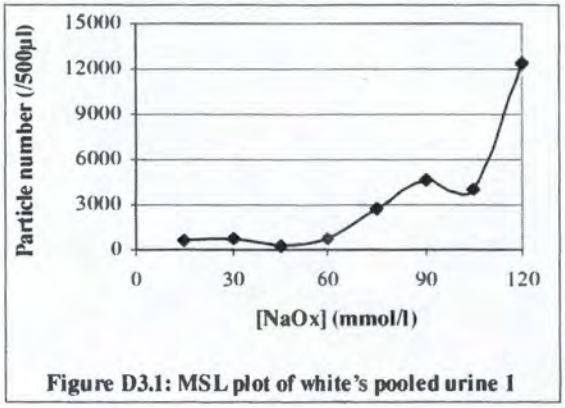

Figure D3.1: MSL plot of white's pooled urine 1

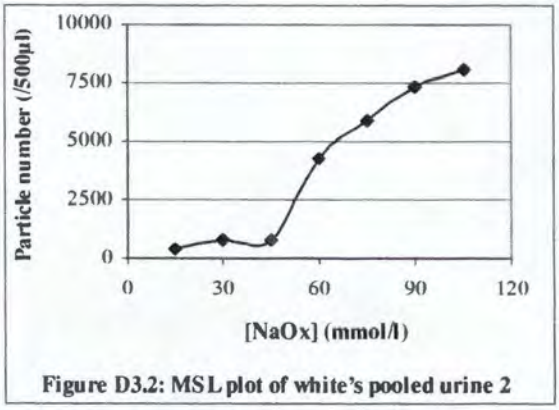

Figure D3.2: MSL plot of white's pooled urine 2

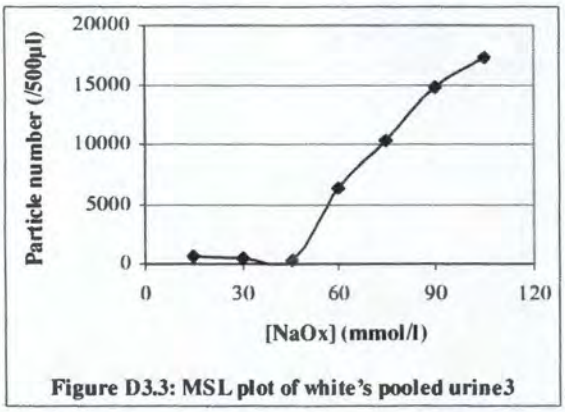

Figure D3.3: MSL plot of white's pooled urine3

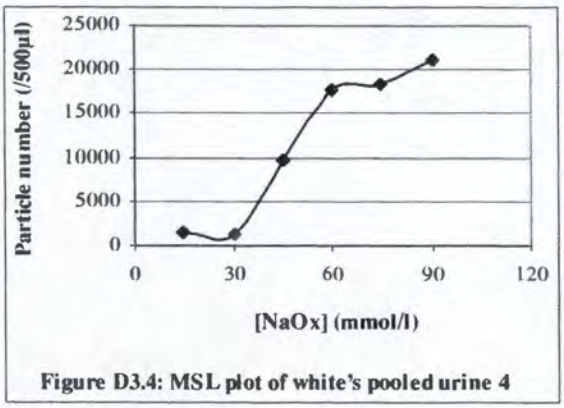

Figure D3.4: MSL plot of white's pooled urine 4

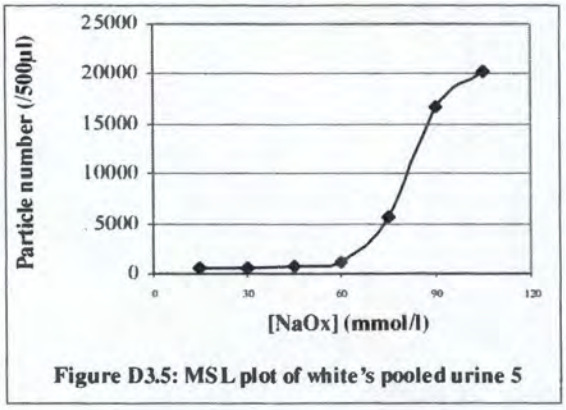

Figure D3.5: MSL plot of white's pooled urine 5

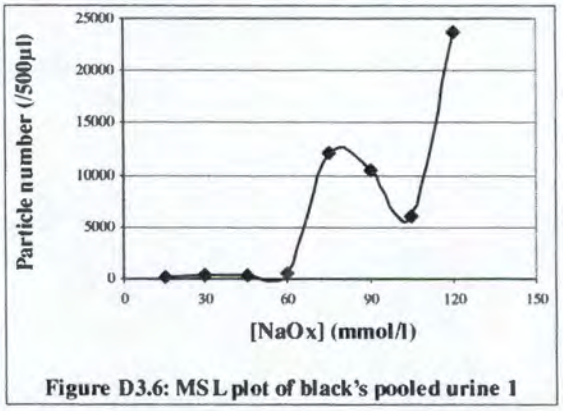

Figure D3.6: MSL plot of black's pooled urine 1

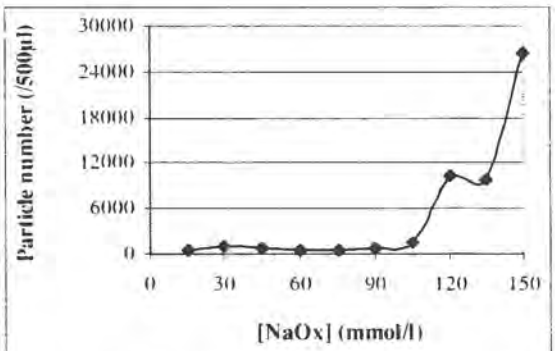

Figure D3.7: MSL plot of black's pooled urine 2

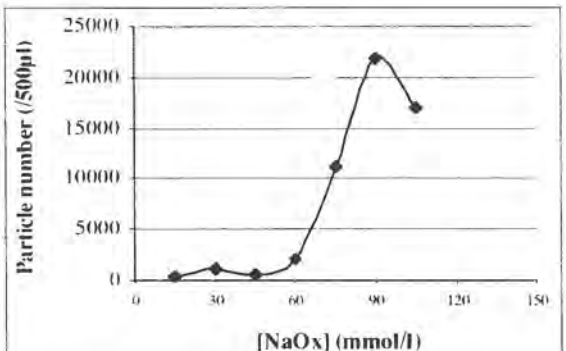

Figure D3.8: MSL plot of black's pooled urine 3

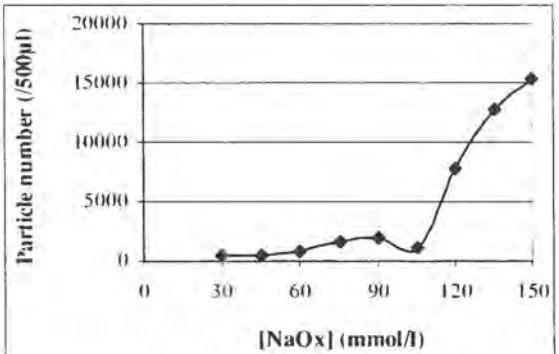

Figure D3.9: MSL plot of black's pooled urine 4

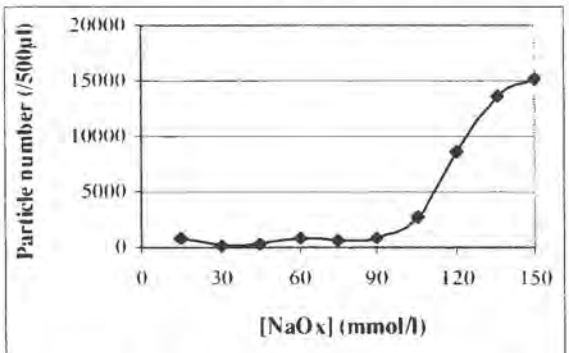

Figure D3.10: MSL plot of black's pooled urine5

Figure D4: Particle size distributions in white (4.1 - 4.4) and black (4.5 - 4.7) subjects' ultrafiltered urine before and after addition of WF1 and BF1 at final concentrations of 1.25 mg/l.

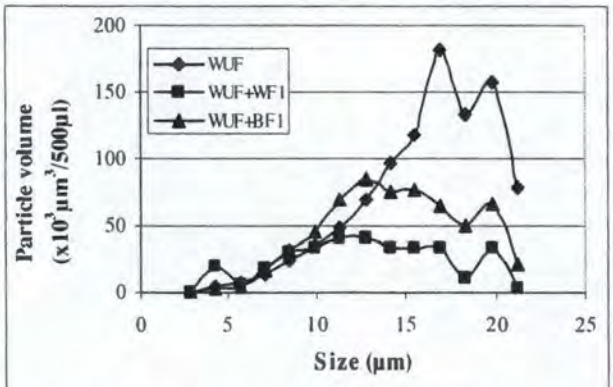

Figure D4.1: Particle size distribution in WUF (expt 1)

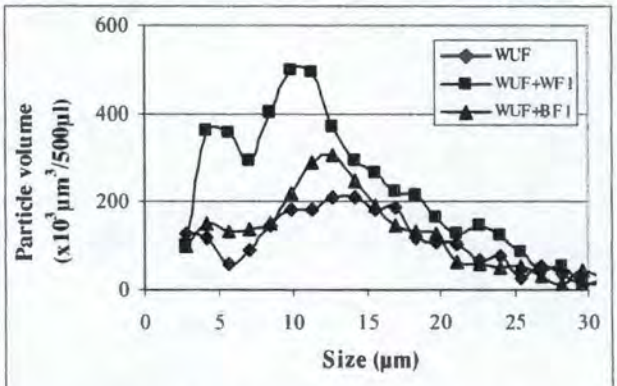

Figure D4.2: Particle size distribution in WUF (expt 2)

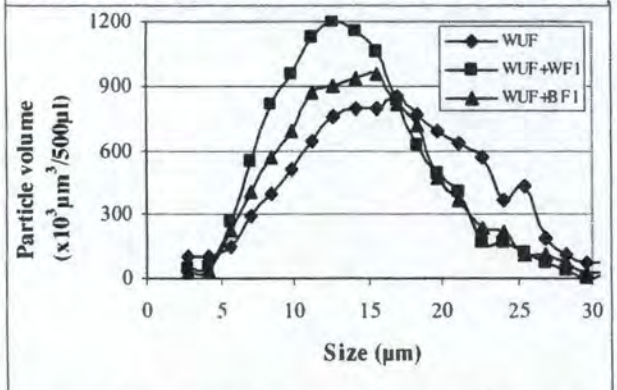

Figure D4.3: Particle size distribution in WUF (expt 3)

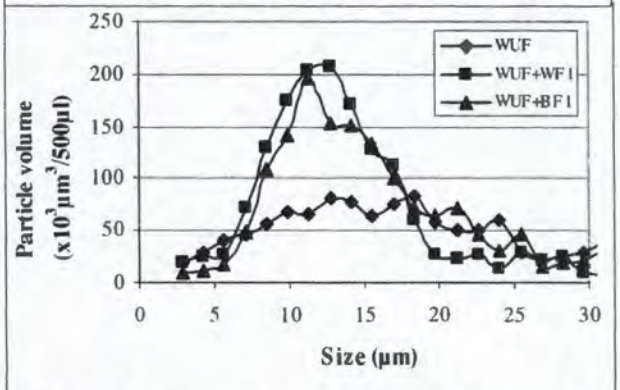

Figure D4.4: Particle size distribution in WUF (expt 4)

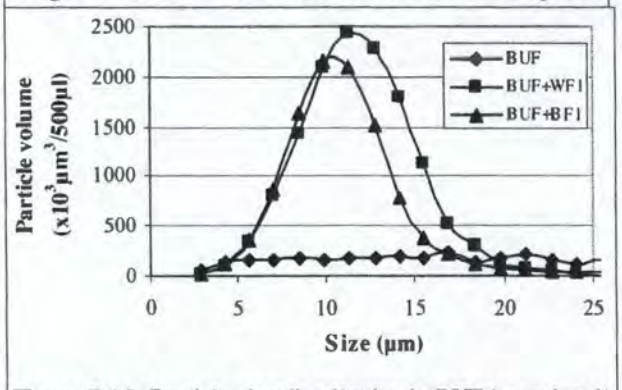

Figure D4.5: Particle size distribution in BUF (experimt 1)

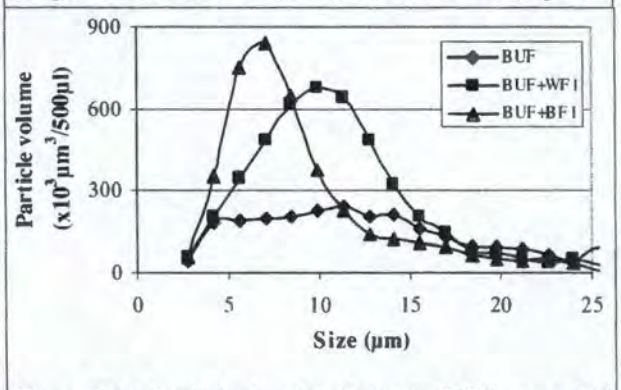

Figure D4.6: Particle size distribution in BUF (experimt 2)

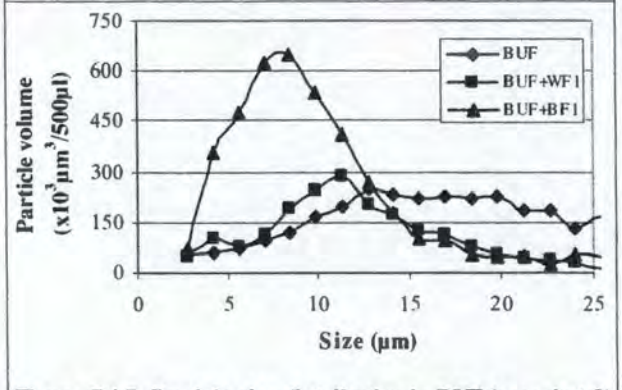

Figure D4.7: Particle size distribution in BUF (experimt 3)

Figure D5: [^{14}C]-oxalate deposition in ultrafiltered urine from white (5.1 – 5.3) and black (5.4 - 5.6) subjects.

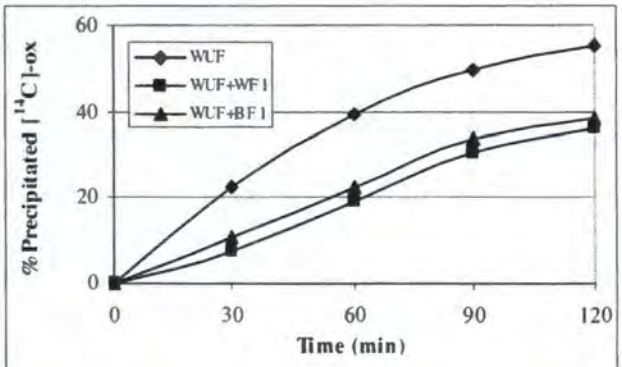

Figure D5.1: [^{14}C]-ox deposition in WUF (experiment 1)

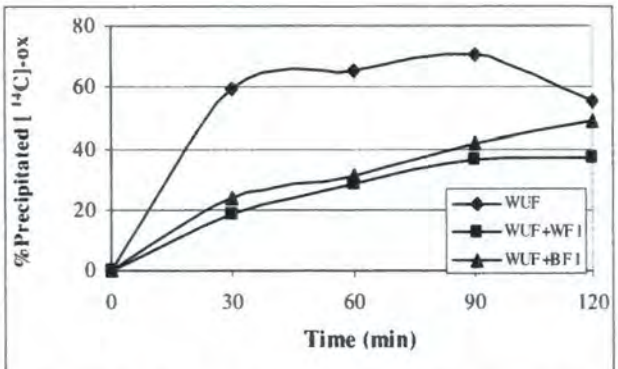

Figure D5.2: [^{14}C]-ox deposition in WUF (experiment 2)

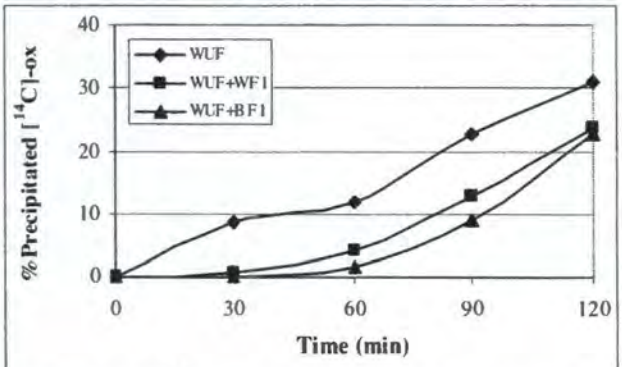

Figure D5.3: [^{14}C]-ox deposition in WUF (experiment 3)

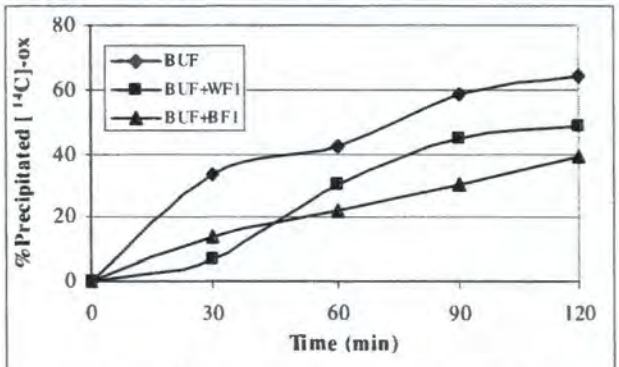

Figure D5.4: [^{14}C]-ox deposition in BUF (experiment 1)

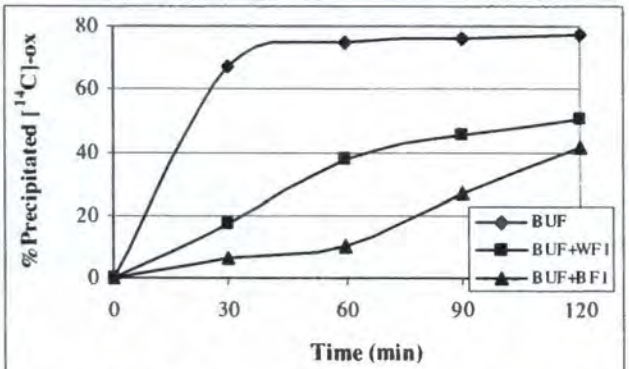

Figure D5.5: [^{14}C]-ox deposition in BUF (experiment 2)

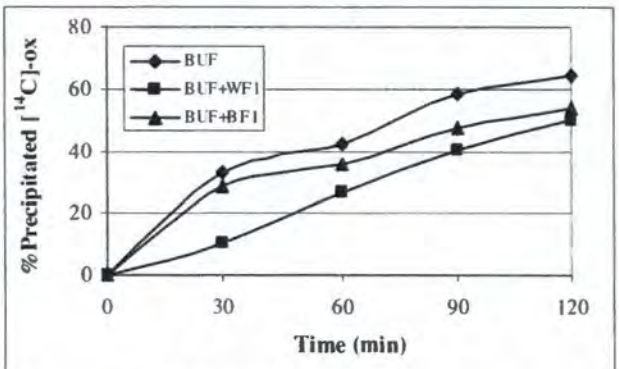

Figure D5.6: [^{14}C]-ox deposition in BUF (experiment 3)

Figure D6.1: OD_{620} plots of COM crystal slurries

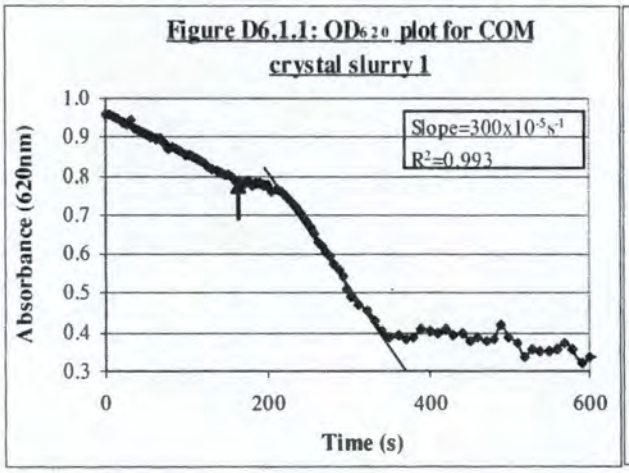

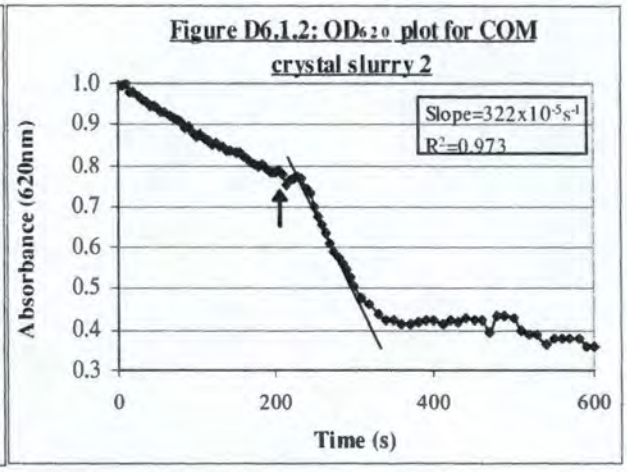

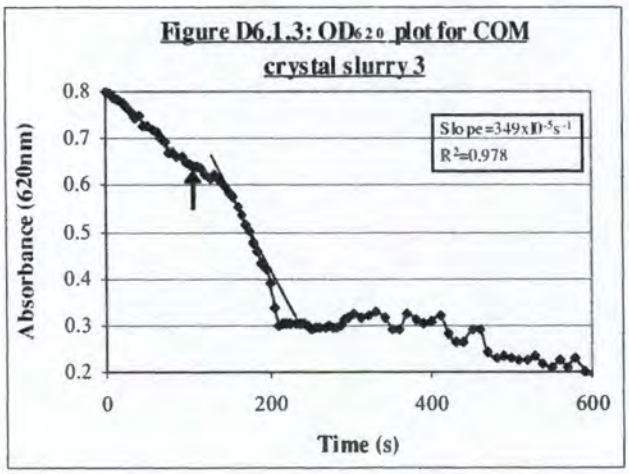

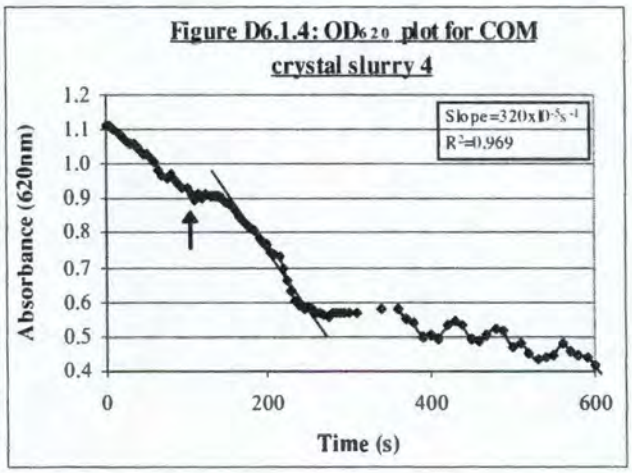

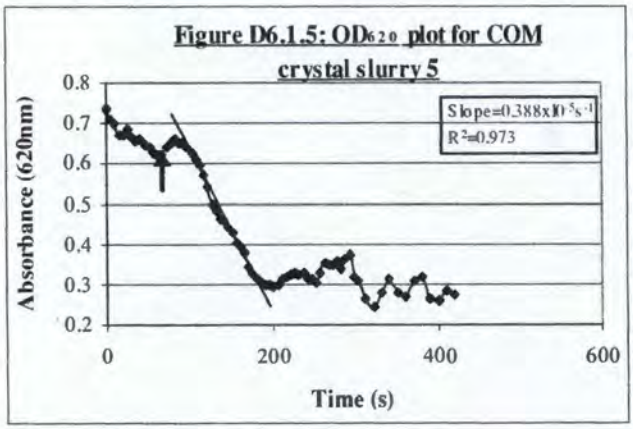

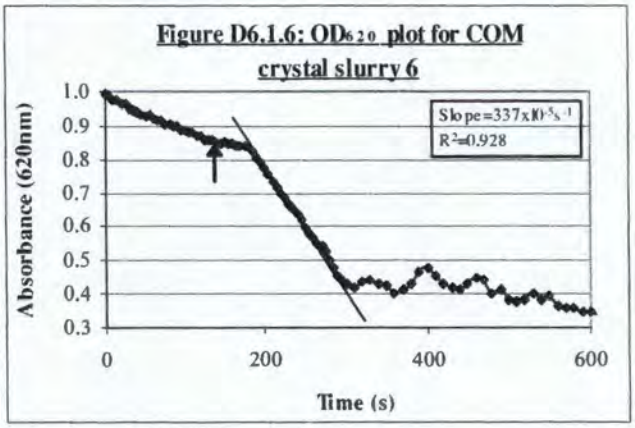

Figure D6.2: OD_{620} plots of COM crystal slurries after addition of WF1 (final concentration 1.25 mg/l)

Figure D6.2.1: OD_{620} plot for COM+WF1 crystal slurry 1

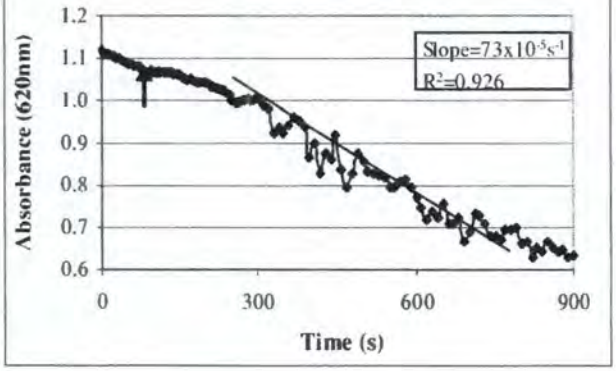

Figure D6.2.2: OD_{620} plot for COM+WF1 crystal slurry 2

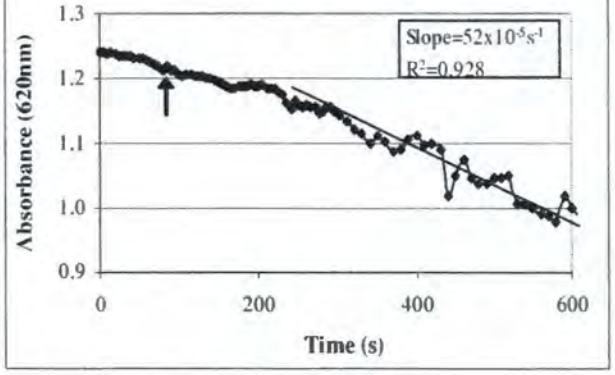

Figure D6.2.3: OD_{620} plot for COM+WF1 crystal slurry 3

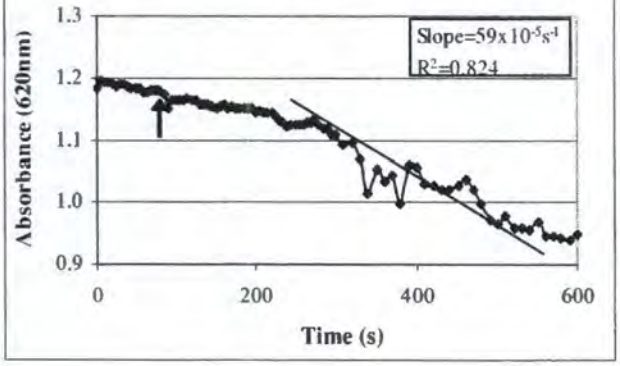

Figure D6.2.4: OD_{620} plot for COM+WF1 crystal slurry 4

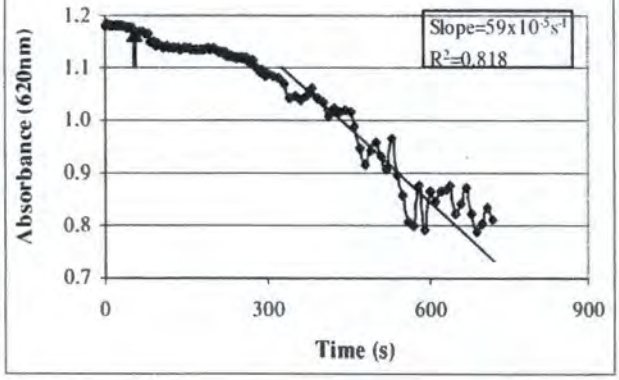

Figure D6.2.5: OD_{620} plot for COM+WF1 crystal slurry 5

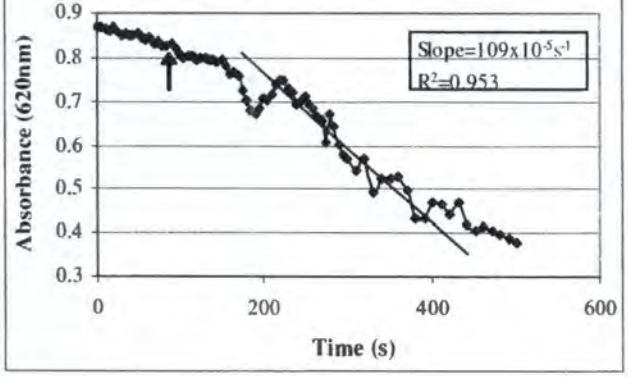

Figure D6.2.6: OD_{620} plot for COM+WF1 crystal slurry 6

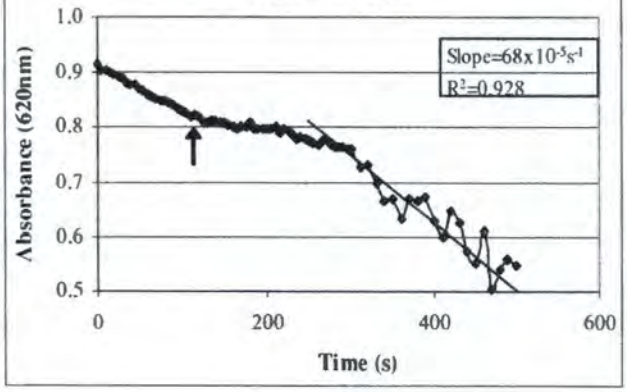

Figure D6.3: OD_{620} plots of COM crystal slurries after addition of BF1 (final conc. 1.25 mg/l)

Figure D6.3.1: OD_{620} plot for COM+BF1 crystal slurry 1

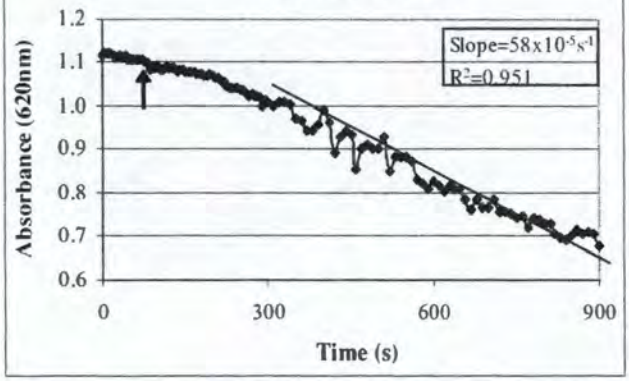

Figure D6.3.2: OD_{620} plot for COM+BF1 crystal slurry 2

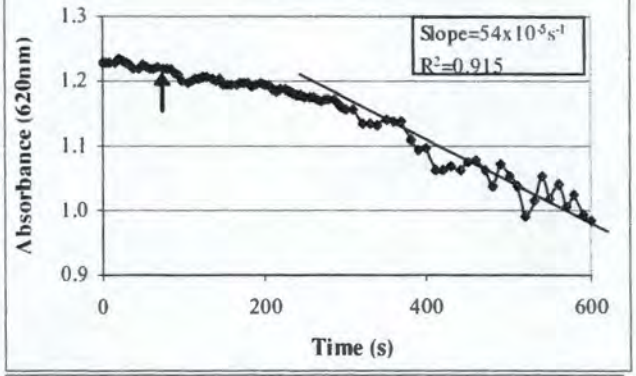

Figure D6.3.3: OD_{620} plot for COM+BF1 crystal slurry 3

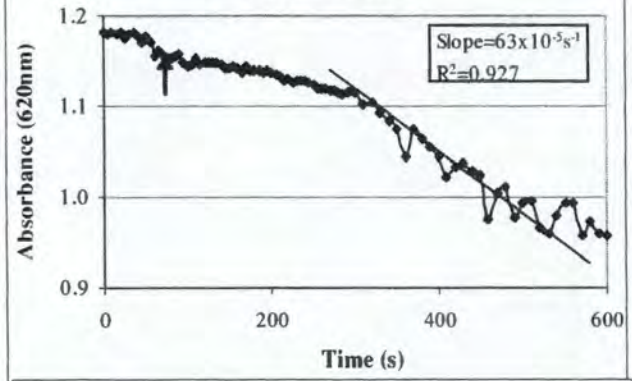

Figure D6.3.4: OD_{620} plot for COM+BF1 crystal slurry 4

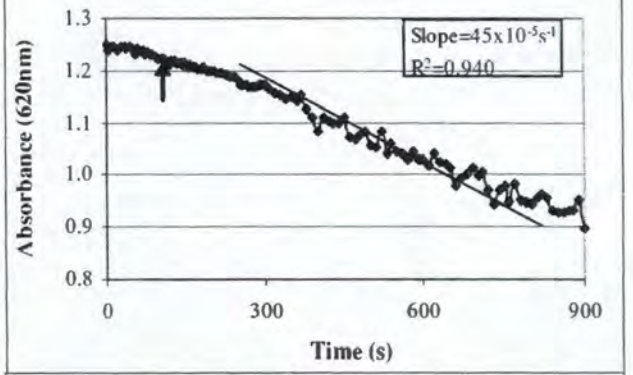

Figure D6.3.5: OD_{620} plot for COM+BF1 crystal slurry 5

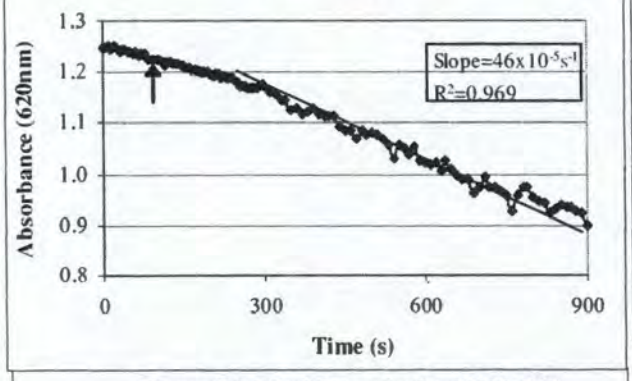

Figure D6.3.6: OD_{620} plot for COM+BF1 crystal slurry 6

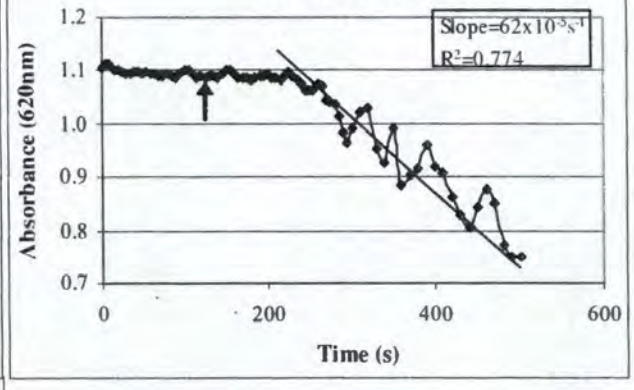

Figure D6.3.7: OD_{620} plot for COM+BF1 crystal slurry 7

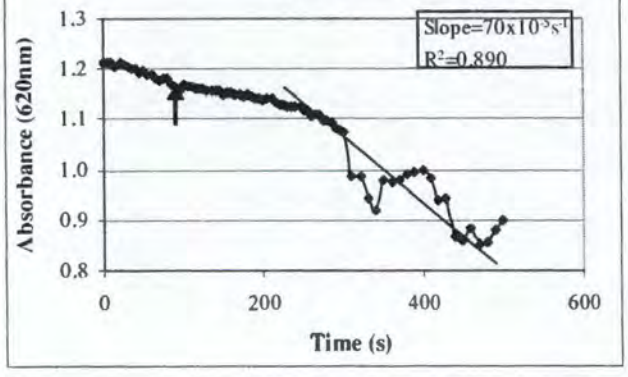

Figure D7.1: OD_{620} plots of COD crystal slurries

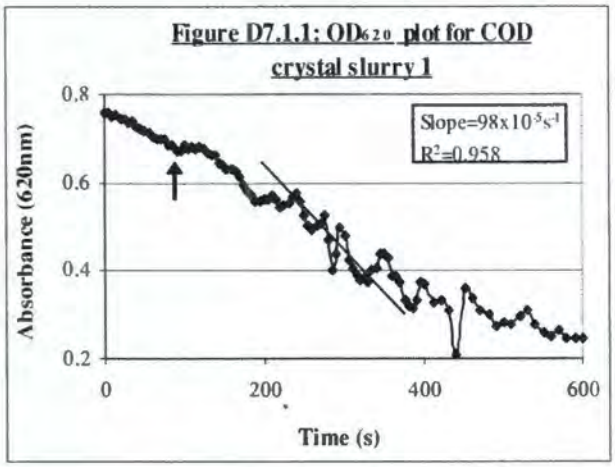

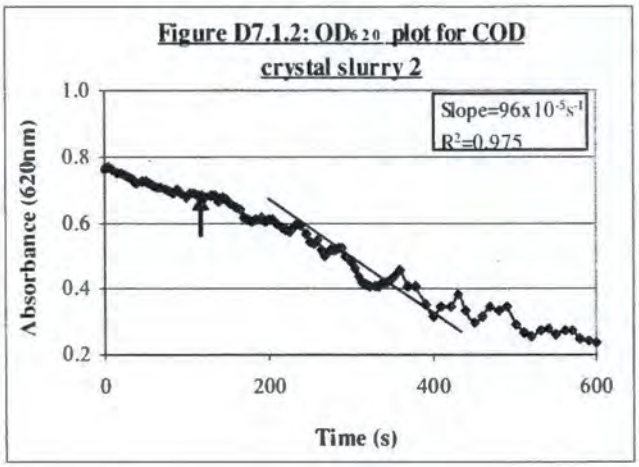

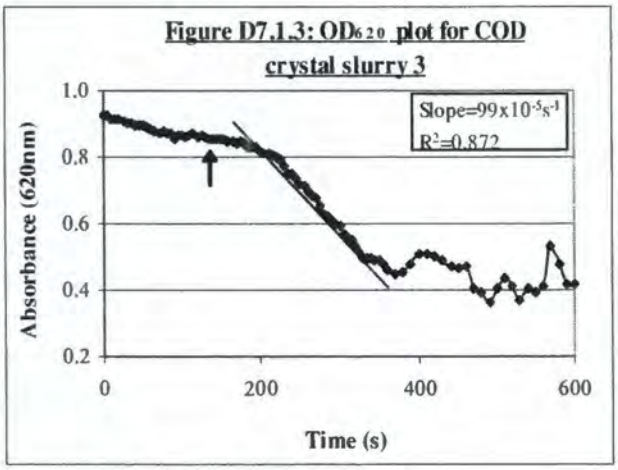

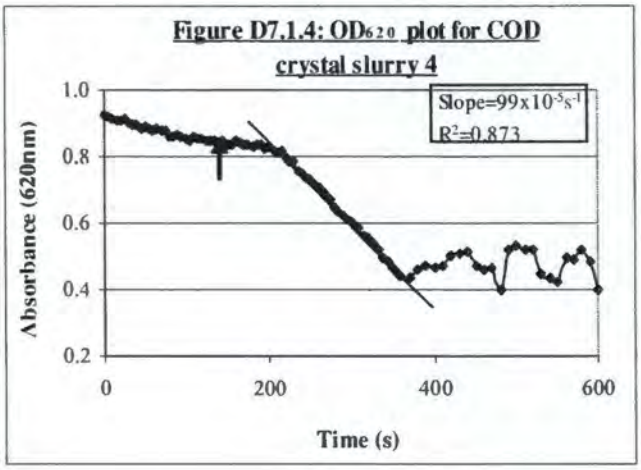

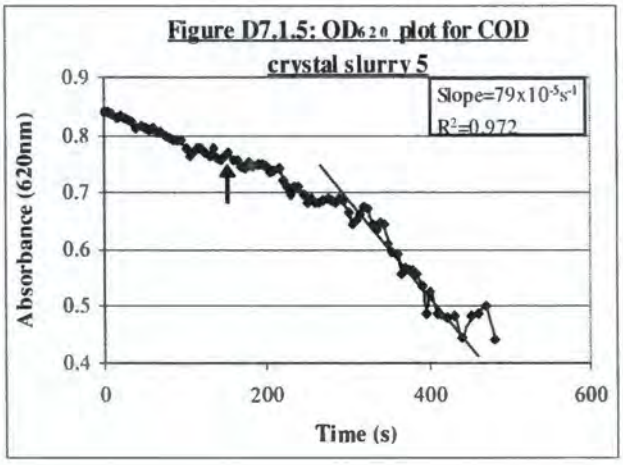

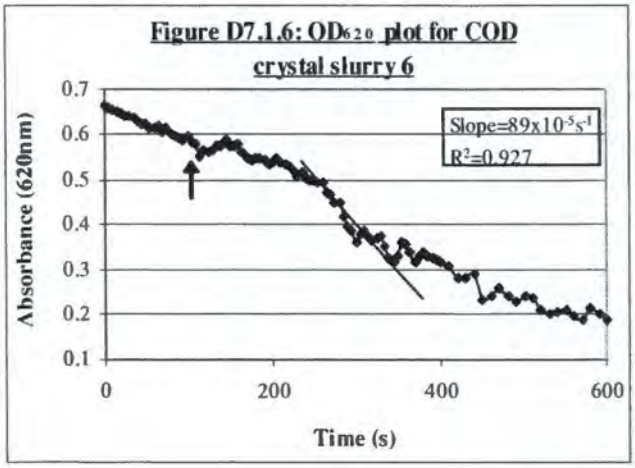

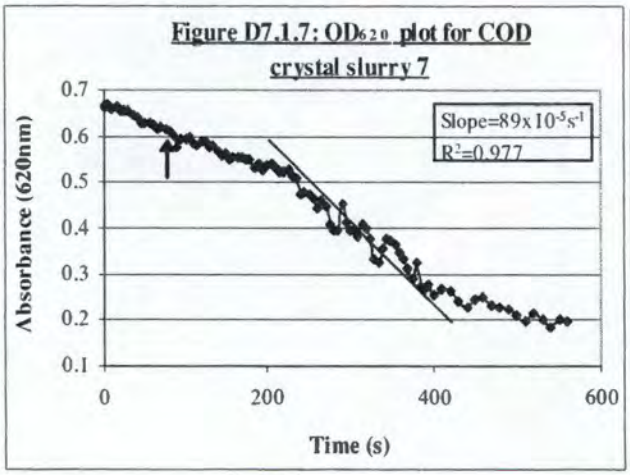

Figure D7.1.7: OD_{620} plot for COD crystal slurry 7

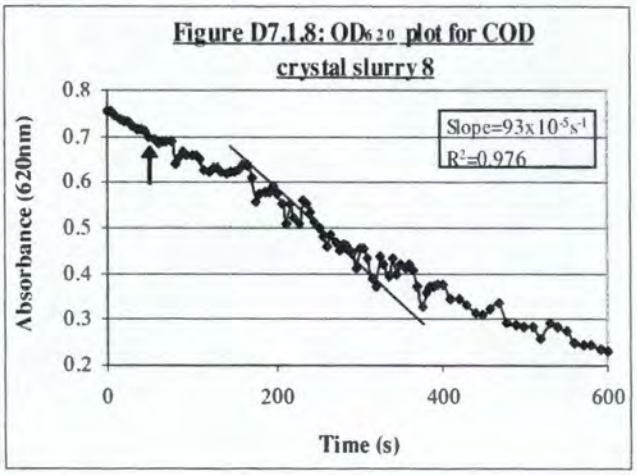

Figure D7.1.8: OD_{620} plot for COD crystal slurry 8

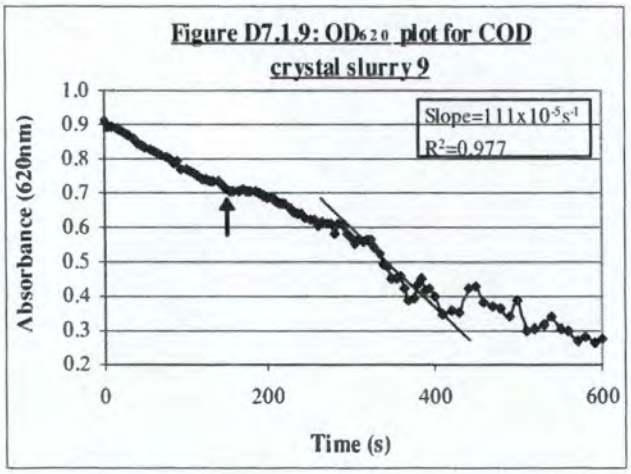

Figure D7.1.9: OD_{620} plot for COD crystal slurry 9

Figure D7.2: OD_{620} plots of COD crystal slurries after addition of WF1 (final conc. 1.25 mg/l)

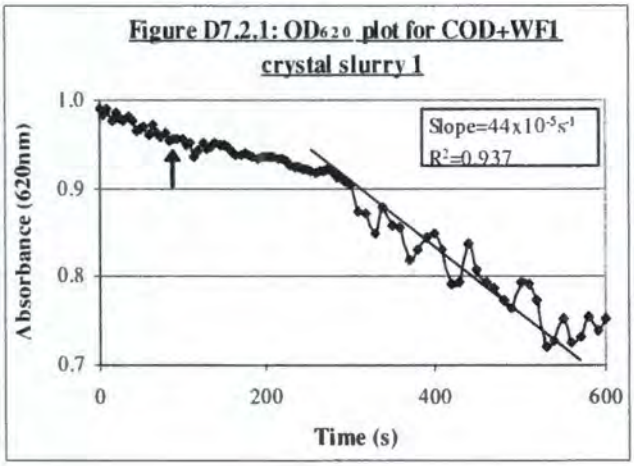

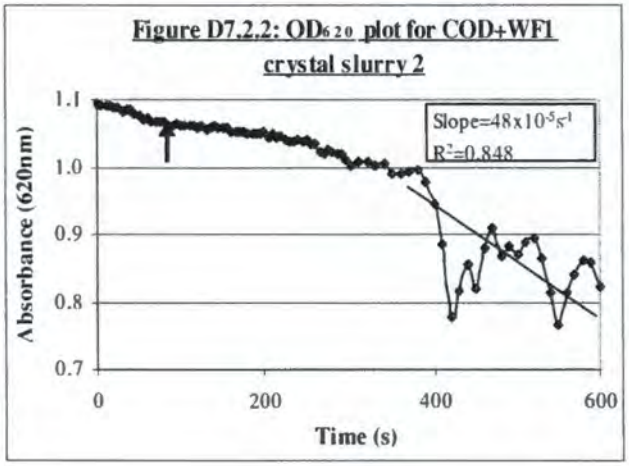

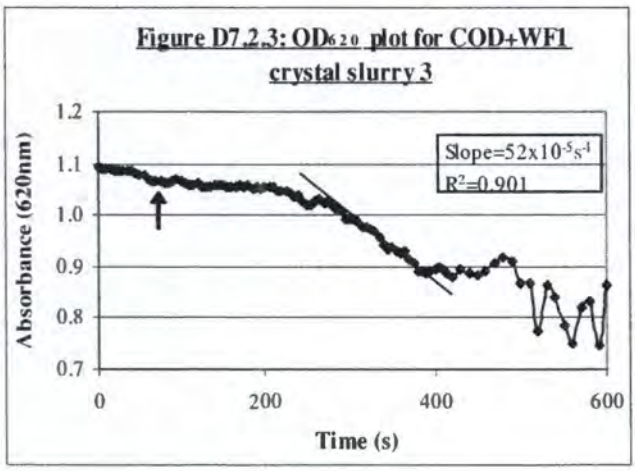

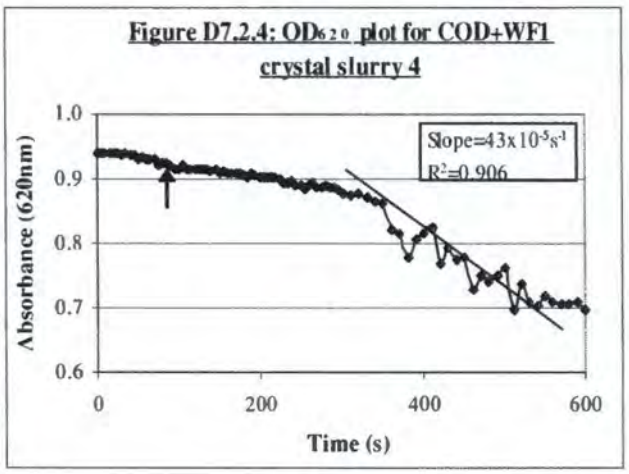

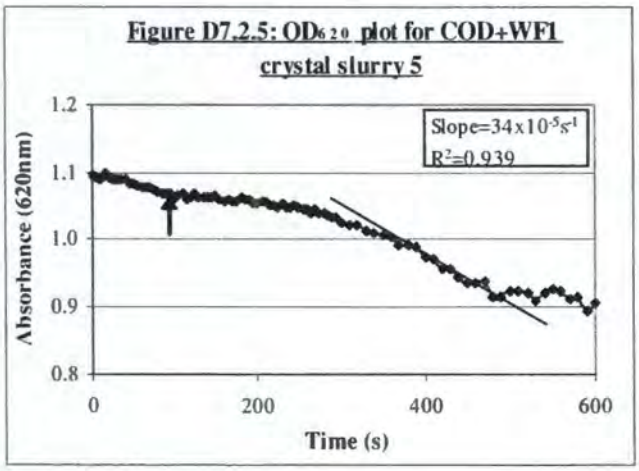

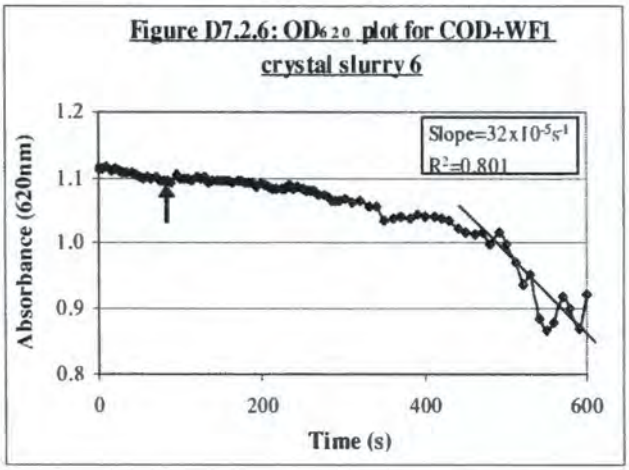

Figure D7.2.7: OD_{620} plot for COD+WF1 crystal slurry 7

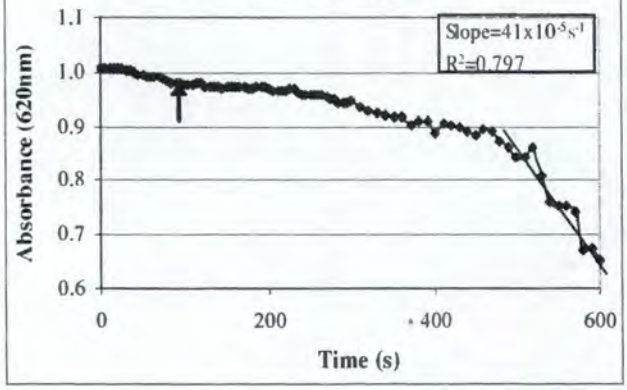

Figure D7.2.8: OD_{620} plot for COD+WF1 crystal slurry 8

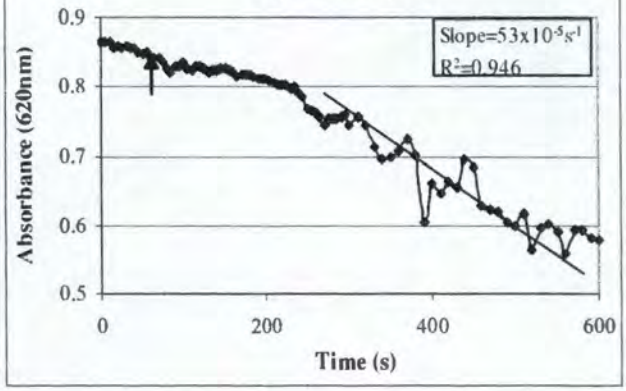

Figure D7.2.9: OD_{620} plot for COD+WF1 crystal slurry 9

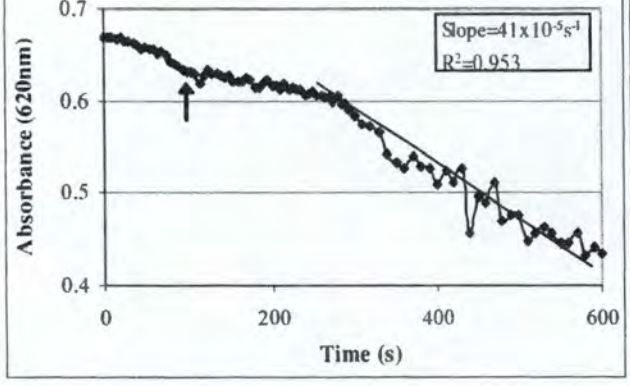

Figure D7.2.10: OD_{620} plot for COD+WF1 crystal slurry 10

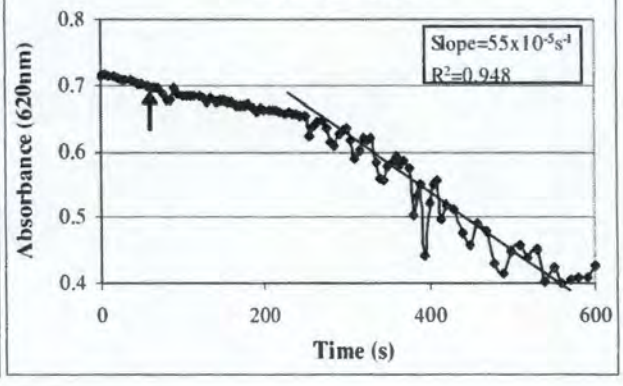

Figure D7.2.11: OD_{620} plot for COD+WF1 crystal slurry 11

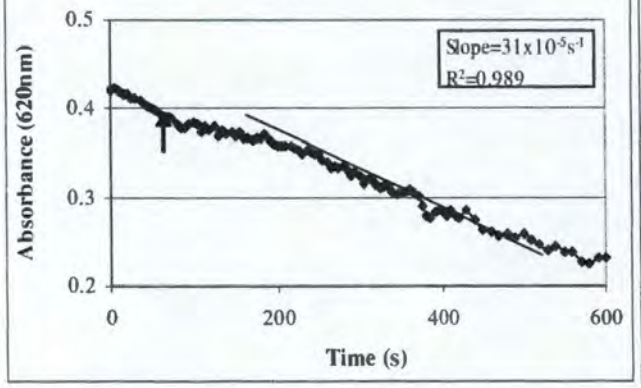

Figure D7.2.12: OD_{620} plot for COD+WF1 crystal slurry 12

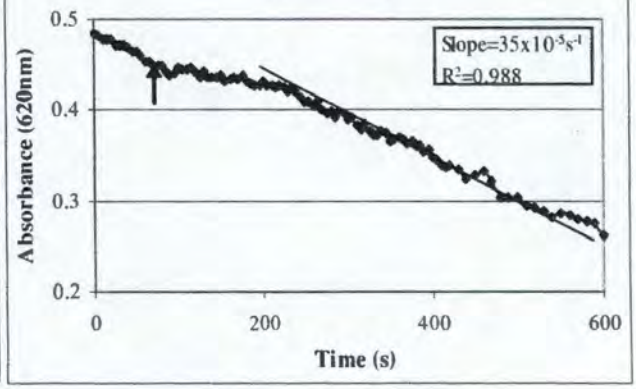

Figure D7.3: OD_{620} plots of COD crystal slurry after addition of BF1 (final conc. 1.25 mg/l)

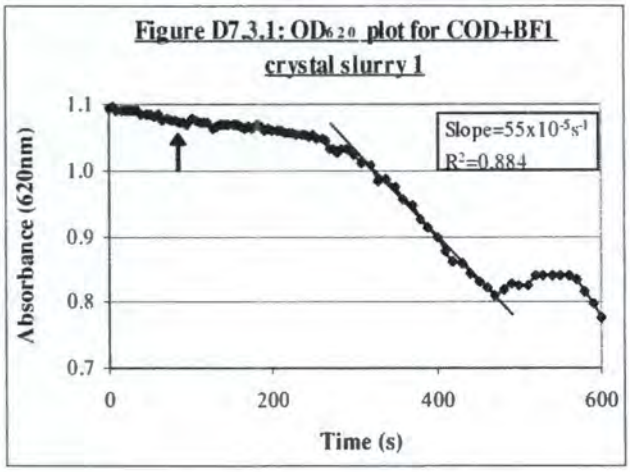

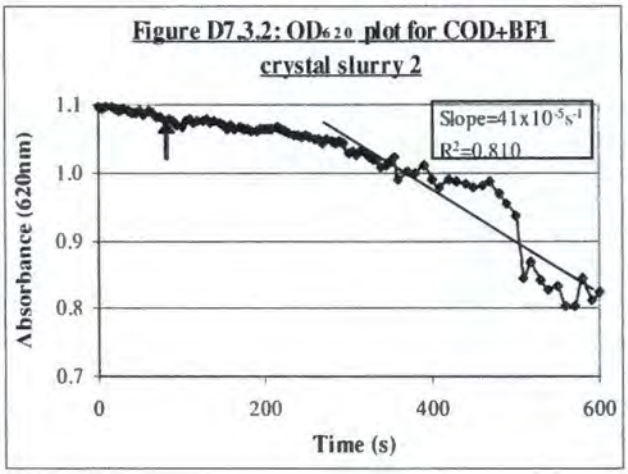

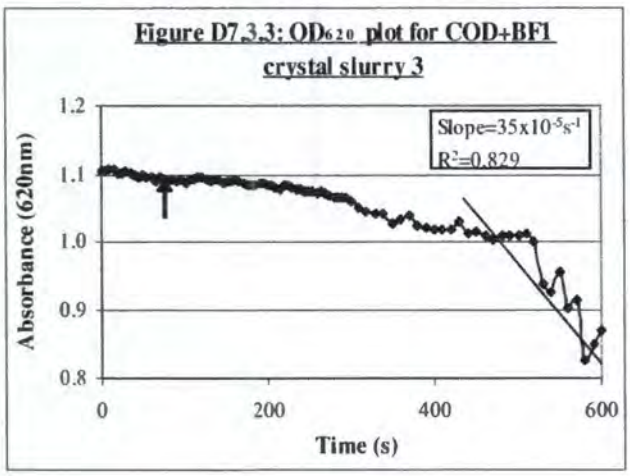

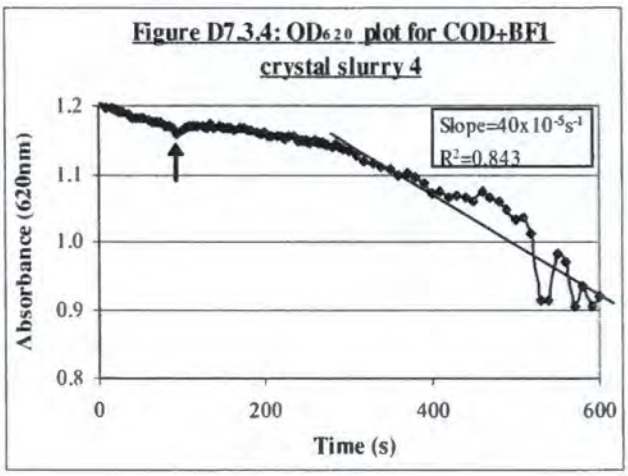

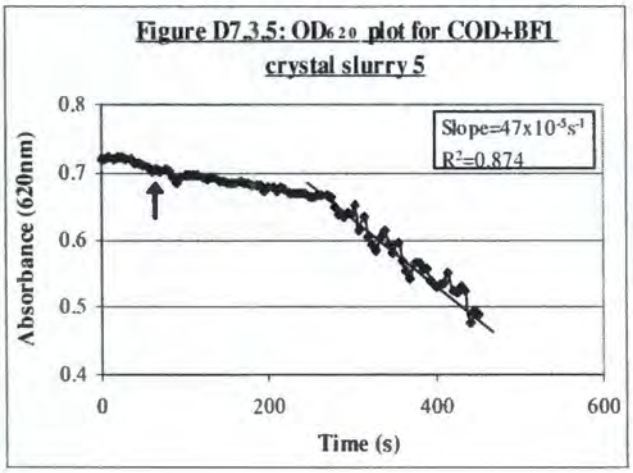

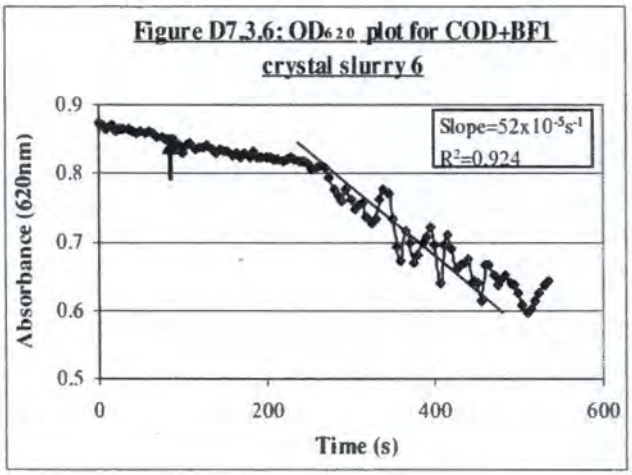

Figure D7.3.7: OD_{620} plot for COD+BF1 crystal slurry 7

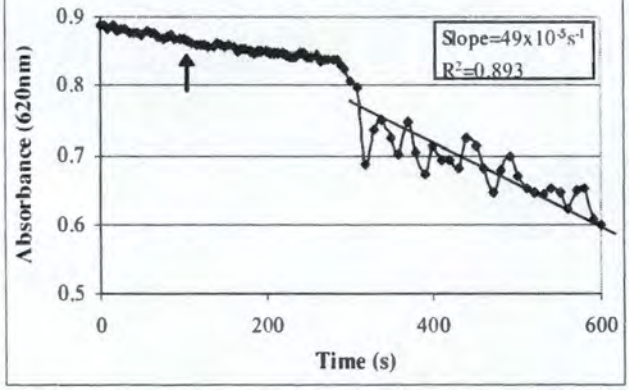

Figure D7.3.8: OD_{620} plot for COD+BF1 crystal slurry 8

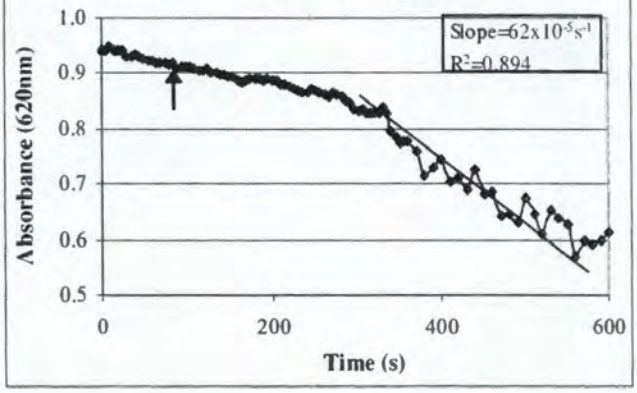

Figure D7.3.9: OD_{620} plot for COD+BF1 crystal slurry 9

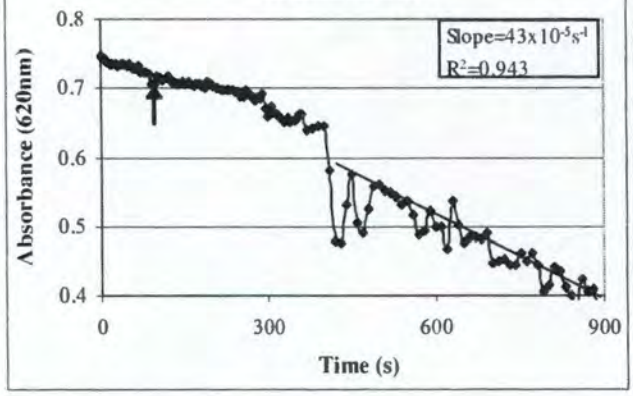

Figure D7.3.10: OD_{620} plot for COD+BF1 crystal slurry 10

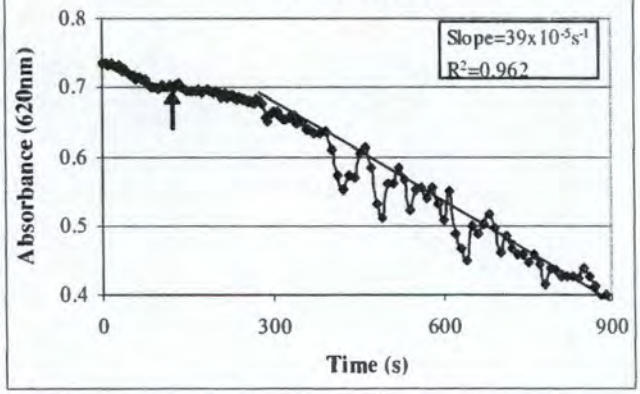

APPENDIX E: TABLES

Table E1: Urine composition (mmol/24hr) and physicochemical parameters of white control subjects

Variables	WC1	WC2	WC3	WC4	WC5	WC ave. ± SE
pH	6.62	6.10	6.38	6.52	6.38	6.40 ± 0.120
Volume (ml/24hr)	730	1270	1340	1000	1040	1076 ± 359
Calcium (mmol/24hr)	1.13	4.72	5.48	3.47	3.83	3.73 ± 0.585
Chloride (mmol/24hr)	105	152	138	105	109	122 ± 28.0
Citrate (mmol/24hr)	1.40	2.47	2.67	1.98	2.00	2.10 ± 0.442
Creatinine (mmol/24hr)	10.5	16.9	15.9	13.1	15.1	14.3 ± 1.73
Magnesium (mmol/24hr)	1.33	3.90	3.64	2.52	2.57	2.79 ± 0.629
Oxalate (mmol/24hr)	0.11	0.16	0.18	0.25	0.13	0.17 ± 0.0355
Phosphate (mmol/24hr)	15.2	35.4	24.7	32.8	28.7	27.4 ± 6.27
Potassium (mmol/24hr)	59.1	59.4	34.8	58.5	54.6	53.3 ± 8.84
Sodium (mmol/24hr)	91.3	30.9	55.8	34.7	97.5	62.0 ± 38.2
Sulphate (mmol/24hr)	10.2	18.6	10.9	6.83	33.6	16.0 ± 3.90
Uric acid (mmol/24hr)	2.5	5.3	3.8	4.0	3.6	3.84 ± 0.521
RS Brushite	0.862	1.74	2.28	3.16	2.02	2.03 ± 0.300
RS Calcium oxalate	1.16	4.02	5.18	6.96	3.06	4.10 ± 0.867
RS Uric acid	0.646	2.39	0.930	0.961	1.10	1.10 ± 0.627

RS: Relative supersaturation

Table E2: Urine composition (mmol/24hr) and physicochemical parameters of black control subjects

Variables	BC1	BC2	BC3	BC4	BC5	BC ave. ± SE
pH	6.12	6.48	6.35	6.20	6.30	6.29 ± 0.120
Volume (ml/24hr)	1380	1170	1170	1290	1220	1246 ± 359
Calcium (mmol/24hr)	3.15	3.01	2.83	3.52	3.22	3.15 ± 0.585
Chloride (mmol/24hr)	186	98	85	260	173	160 ± 28.0
Citrate (mmol/24hr)	2.25	1.89	2.51	2.38	2.55	2.32 ± 0.442
Creatinine (mmol/24hr)	23.0	11.9	11.7	23.0	18.7	17.7 ± 1.73
Magnesium (mmol/24hr)	3.33	1.56	1.24	4.53	2.98	2.73 ± 0.629
Oxalate (mmol/24hr)	0.16	0.20	0.22	0.31	0.11	0.20 ± 0.0355
Phosphate (mmol/24hr)	59.2	14.9	13.1	34.3	30.7	30.4 ± 6.27
Potassium (mmol/24hr)	55.5	29.8	16.2	37.7	67.9	41.4 ± 8.84
Sodium (mmol/24hr)	109	27.6	20.3	213	42.3	82.4 ± 38.2
Sulphate (mmol/24hr)	30.4	8.3	9.09	20.9	21.6	18.0 ± 3.90
Uric acid (mmol/24hr)	4.8	2.8	2.4	3.9	4.0	3.6 ± 0.521
RS Brushite	1.33	1.24	0.744	1.25	1.34	1.27 ± 0.300
RS Calcium oxalate	1.98	5.67	5.93	4.42	1.98	3.62 ± 0.867
RS Uric acid	1.88	0.645	0.736	1.38	1.24	1.11 ± 0.627

RS: Relative supersaturation

Table E3: Urine composition (mmol/24hr) and physicochemical parameters of white stone-formers

Variables	WSF1	WSF2	WSF3	WSF4	WSF5	WSF ave. ± SE
pH	6.30	5.55	5.80	5.50	6.25	5.88 ± 0.120
Volume (ml/24hr)	4180	560	1580	1300	1765	1877 ± 359
Calcium (mmol/24hr)	7.65	6.36	5.33	4.14	3.82	5.46 ± 0.585
Chloride (mmol/24hr)	188	77	175	226	97	153 ± 28.0
Citrate (mmol/24hr)	5.11	1.36	3.80	1.86	1.71	2.77 ± 0.442
Creatinine (mmol/24hr)	18.8	13.8	20.7	18.6	18.5	18.1 ± 1.73
Magnesium (mmol/24hr)	5.87	4.03	4.63	2.53	1.41	3.69 ± 0.629
Oxalate (mmol/24hr)	0.34	0.10	0.13	0.11	0.11	0.16 ± 0.0355
Phosphate (mmol/24hr)	18.8	20.9	48.2	36.5	44.5	33.8 ± 6.27
Potassium (mmol/24hr)	43.8	91.6	50.5	21.8	49.7	51.5 ± 8.84
Sodium (mmol/24hr)	119	368	274	352	125	248 ± 38.2
Sulphate (mmol/24hr)	21.8	10.2	22.1	20.7	21.5	19.3 ± 3.90
Uric acid (mmol/24hr)	5.8	2.0	4.5	4.8	5.2	4.5 ± 0.521
RS Brushite	0.351	2.26	0.907	0.480	1.28	1.06 ± 0.300
RS Calcium oxalate	2.77	5.62	1.88	1.86	1.57	2.74 ± 0.867
RS Uric acid	0.566	5.12	2.79	5.70	1.27	3.09 ± 0.627

RS: Relative supersaturation

Table E4: X-ray powder diffraction peak assignments and percentage composition of CaOx crystals precipitated from white control subjects' urine

Sample	d-spacing (Å)	Assignment	Composition: % COM	% COD
WC1	6.19	COD		
	4.51	COM		
	3.72	COM		
	3.15	COD		
	3.01	COM		
	2.82	COD		
	2.37	COD		
	2.35	COM	40	60
WC2	6.37	COD		
	4.51	COD?		
	3.75	COD?		
	3.15	COD		
	2.43	COD		
	2.37	COD		
	2.35	COD	0	100
WC3	6.19	COD		
	4.46	COD		
	3.69	COD		
	3.11	COD		
	2.79	COD		
	2.41	COD		
	2.35	COD	0	100
WC4	6.28	COD		
	4.51	COD		
	3.69	COD		
	2.80	COD		
	2.42	COD		
	2.37	COD	0	100
WC5	6.28	COD		
	4.46	COD		
	3.11	COD		
	2.80	COD		
	2.42	COD		
	2.35	COD	0	100

Table E5: X-ray powder diffraction peak assignments and percentage composition of CaOx crystals precipitated from black control subjects' urine

Sample	d-spacing (Å)	Assignment	Composition: % COM	% COD
BC1	6.28	COD		
	4.46	COD		
	3.72	COD		
	2.80	COD		
	2.42	COD		
	2.35	COD	0	100
BC2	6.10	COM		
	3.72	COM		
	3.01	COM		
	2.82	COD		
	2.79	COD		
	2.42	30%COM, 70%COD		
	2.35	COM	50	50
BC3	6.02	COM		
	3.69	COM		
	3.01	COM		
	2.80	COM		
	2.51	COM		
	2.35	COM	100	0
BC4	6.28	COD		
	6.02	COM		
	4.46	COD		
	3.69	COM		
	2.99	COM		
	2.80	COD		
	2.42	30%COM, 70%COD		
	2.35	COM	60	40
BC5	6.28	COD		
	4.46	COD		
	3.69	COM		
	2.79	COD		
	2.42	30%COM, 70%COD		
	2.35	COM	30	70

Table E6: X-ray powder diffraction peak assignments and percentage composition of CaOx crystals precipitated from white stone-formers' urine

Sample	d-spacing (Å)	Assignment	Composition:	
			% COM	% COD
WSF1	6.28	COD		
	6.02	COM		
	4.46	COD		
	3.69	95% COM, 5% COD		
	2.99	COM		
	2.79	COD		
	2.42	30%COM, 70% COD		
	2.35	COM	35	65
WSF2	6.10	COM		
	4.51	COD		
	3.69	95% COM, 5% COD		
	3.01	COM		
	2.80	COD		
	2.51	COM		
	2.42	30%COM, 70% COD		
	2.37	COM	70	30
WSF3	6.19	COD		
	4.41	COD		
	3.66	COD		
	2.79	COD		
	2.41	COD		
	2.35	COD	0	100
WSF4	6.37	COD		
	4.51	COD		
	3.13	COD		
	2.80	COD		
	2.42	COD		
	2.37	COD	0	100
WSF5	6.28	COD		
	6.02	COM		
	4.46	COD		
	3.67	COM		
	2.99	COM		
	2.79	COD		
	2.50	COM	65	35

APPENDIX E: FIGURES

Figure E1: X-ray powder diffraction patterns of CaOx crystals precipitated from white control subjects' urine. The subjects are WC1 (Fig E1.1), WC2 (Fig E1.2), WC3 (Fig E1.3), WC4 (Fig E1.4) and WC5 (Fig E1.5).

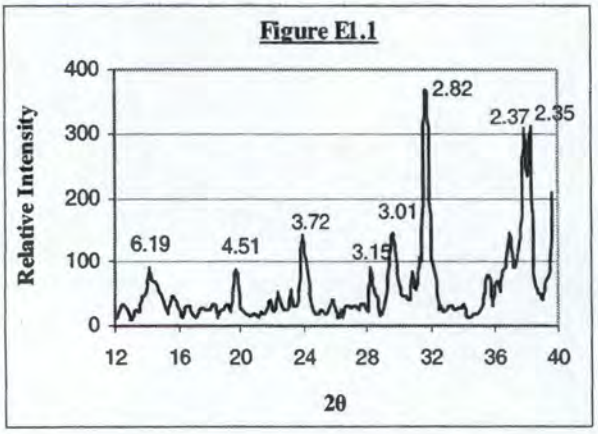

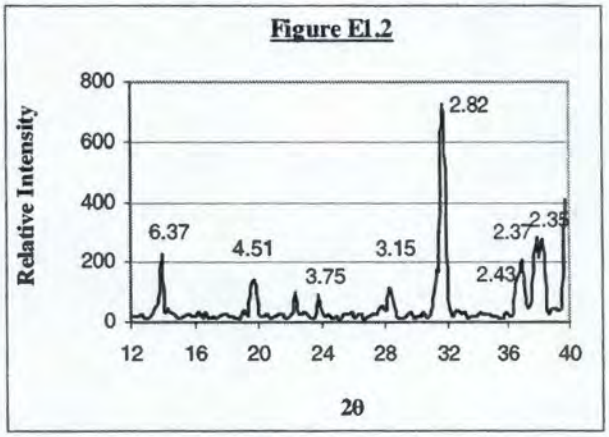

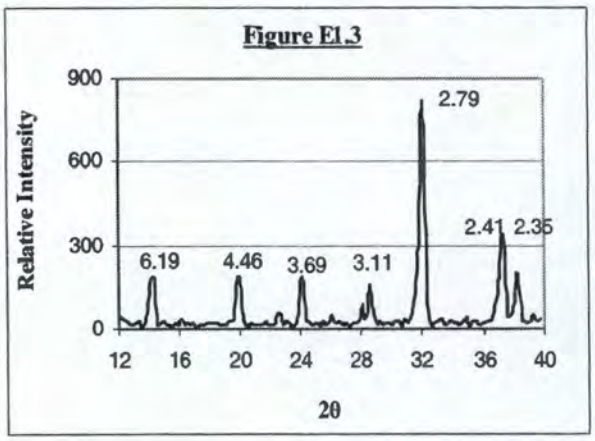

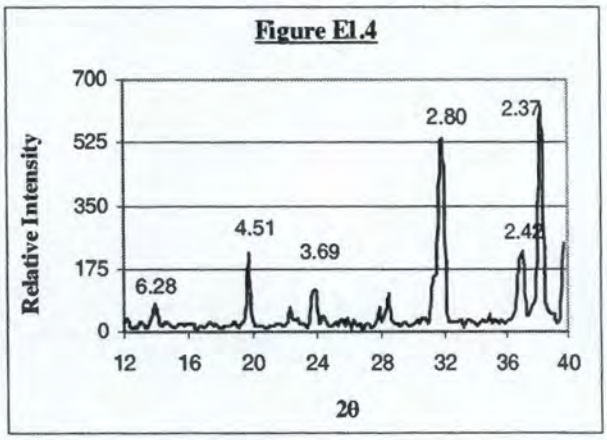

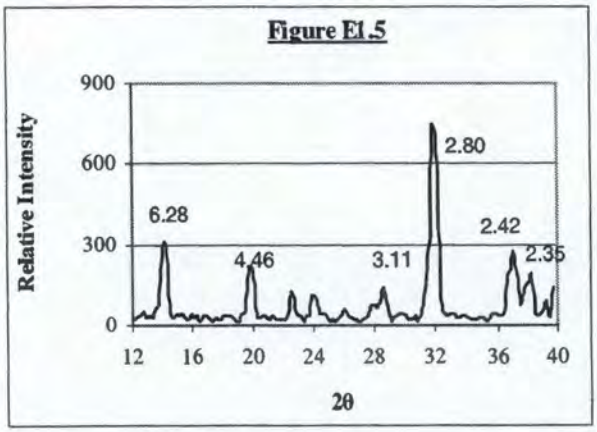

Figure E2: X-ray powder diffraction patterns of CaOx crystals precipitated from black control subjects' urine. The subjects are BC1 (Fig E2.1), BC2 (Fig E2.2), BC3 (Fig E2.3), BC4 (Fig E2.4) and BC5 (Fig E2.5).

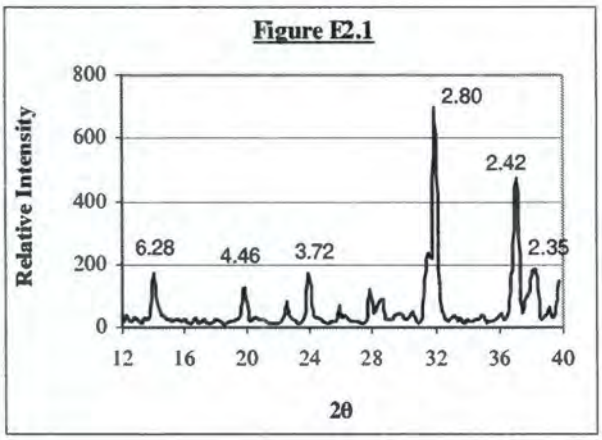

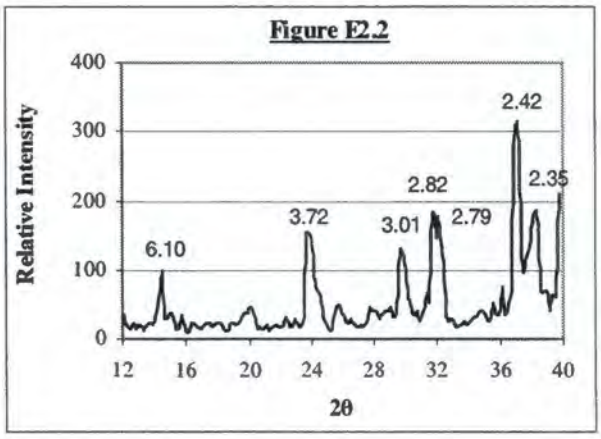

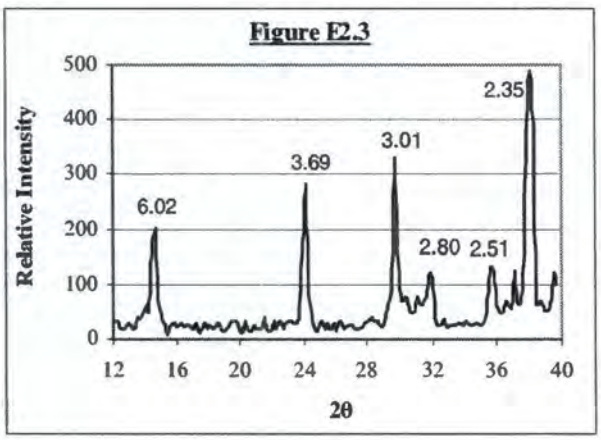

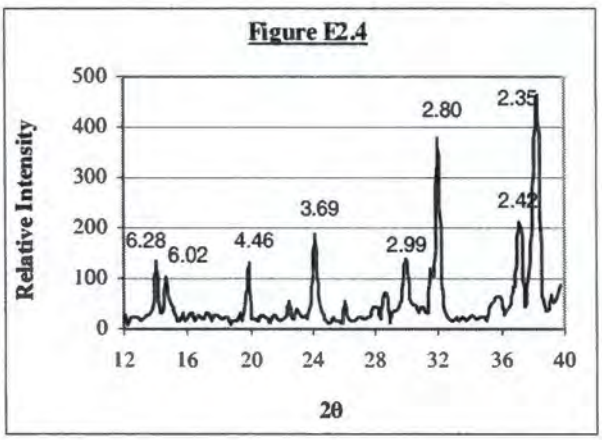

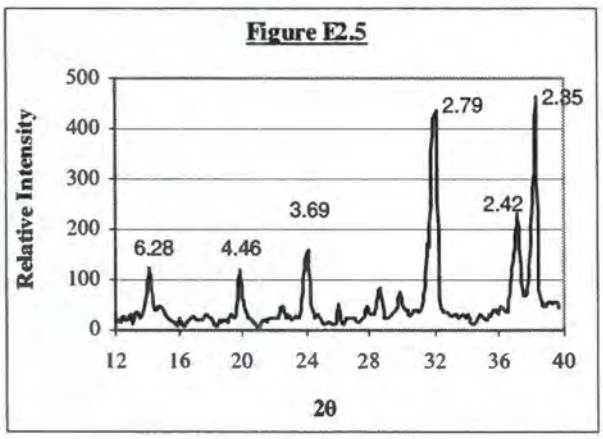

Figure E3: X-ray powder diffraction patterns of CaOx crystals precipitated from white stone-formers' urine. The subjects are WSF1 (Fig E3.1), WSF2 (Fig E3.2), WSF3 (Fig E3.3), WSF4 (Fig E3.4) and WSF5 (Fig E3.5).

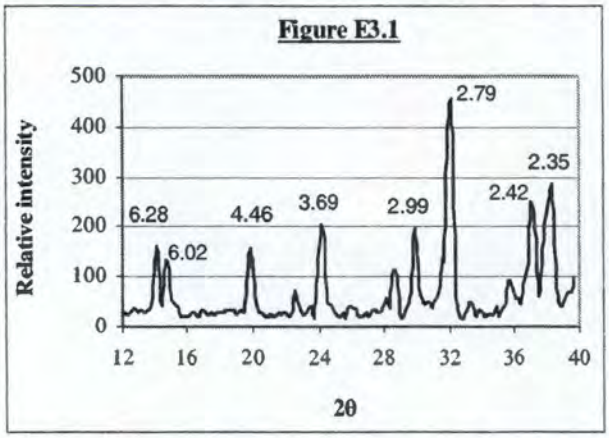

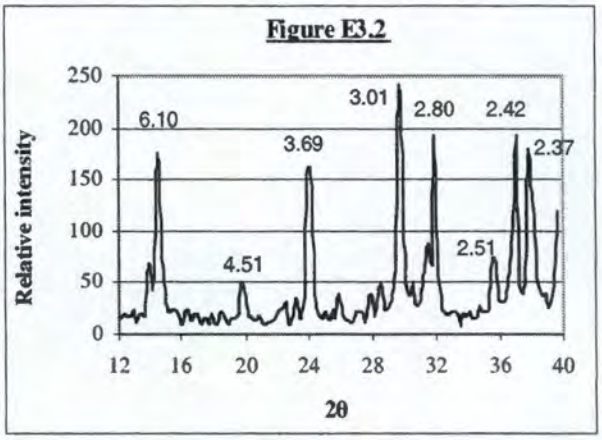

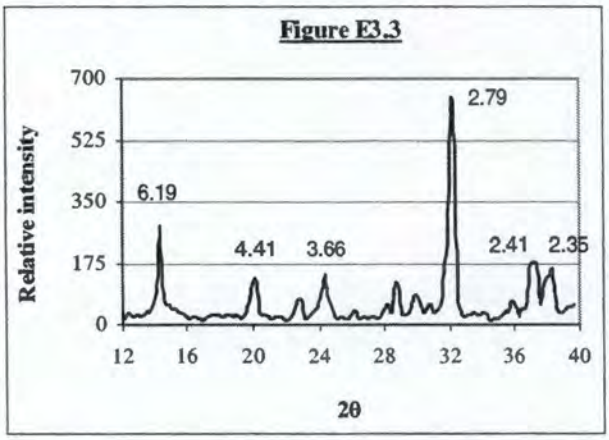

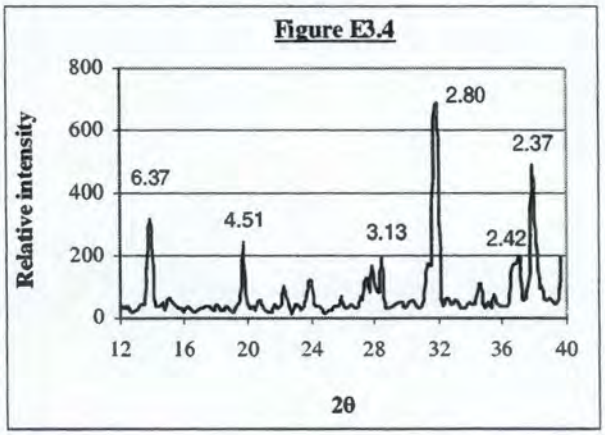

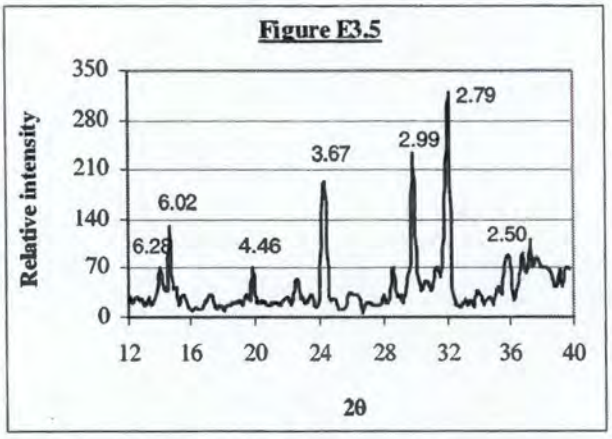

Figure E4: Desalting chromatograms of demineralised CaOx crystals precipitated from white control subjects' urine. The subjects are WC1 (Fig E4.1), WC2 (Fig E4.2), WC3 (Fig E4.3), WC4 (Fig E4.4) and WC5 (Fig E4.5).

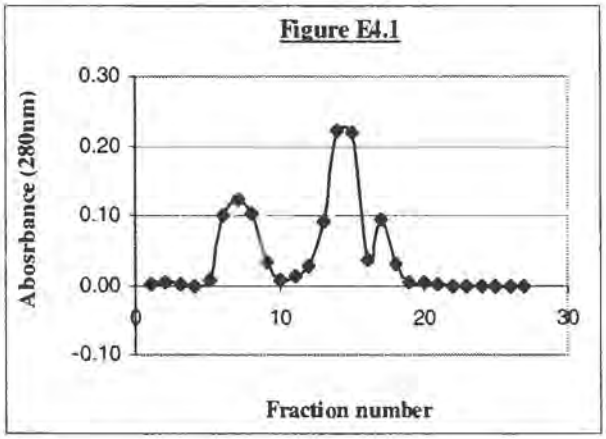

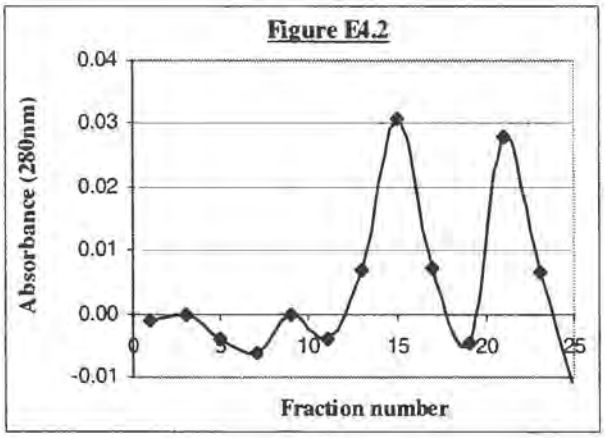

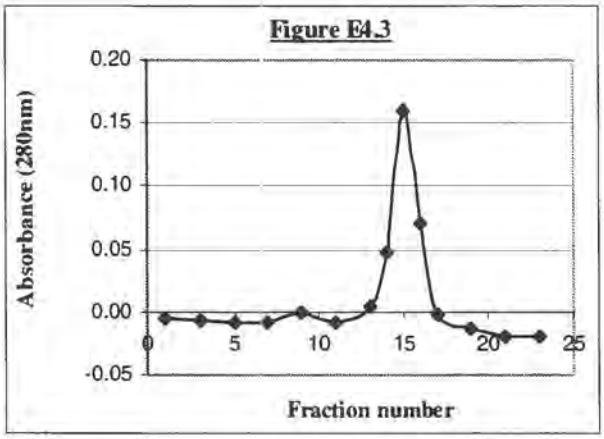

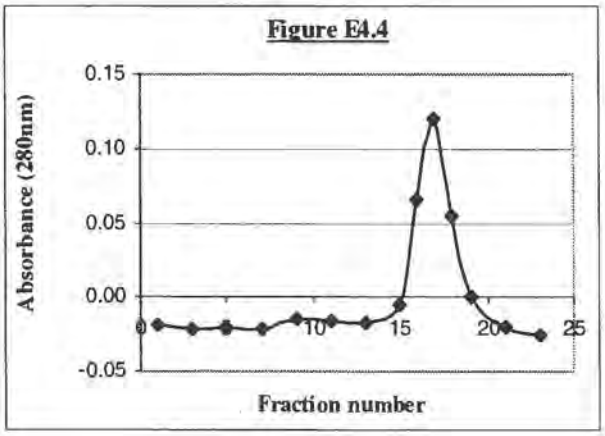

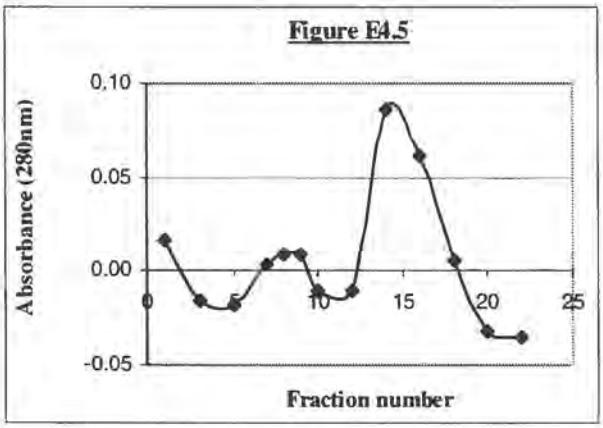

Figure E5: Desalting chromatograms of demineralised CaOx crystals precipitated from black control subjects' urine. The subjects are BC1 (Fig E5.1), BC2 (Fig E5.2), BC3 (Fig E5.3), BC4 (Fig E5.4) and BC5 (Fig E5.5).

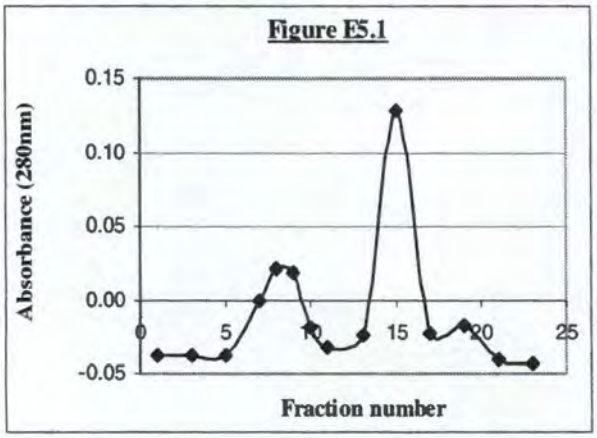

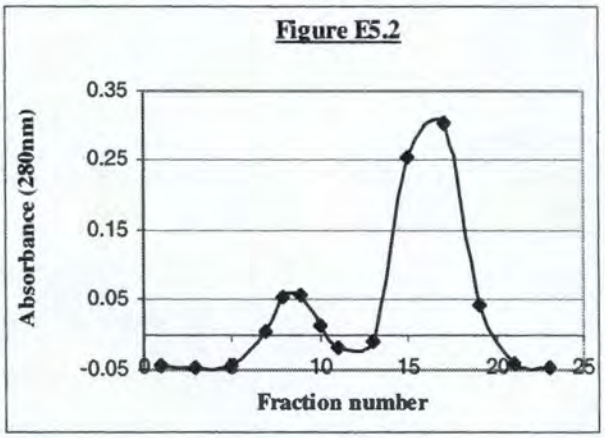

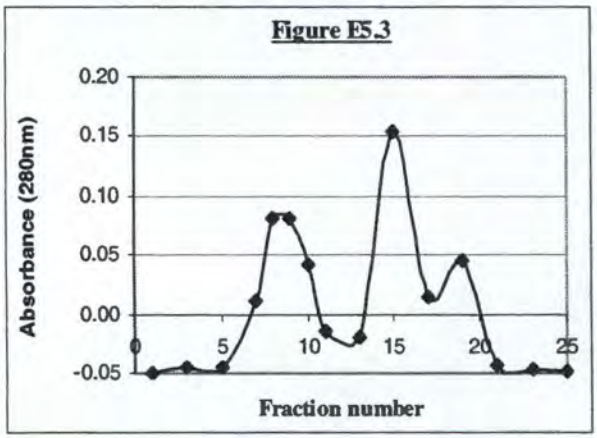

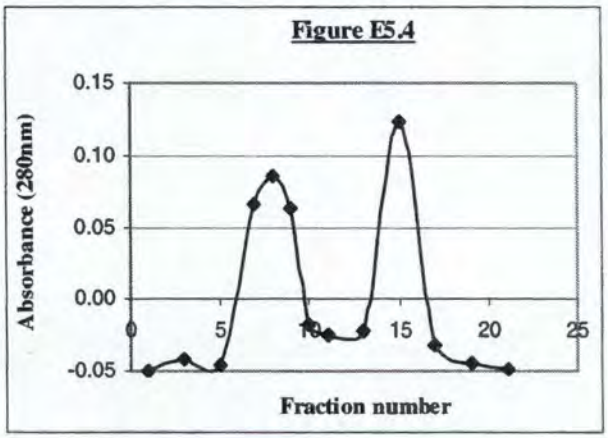

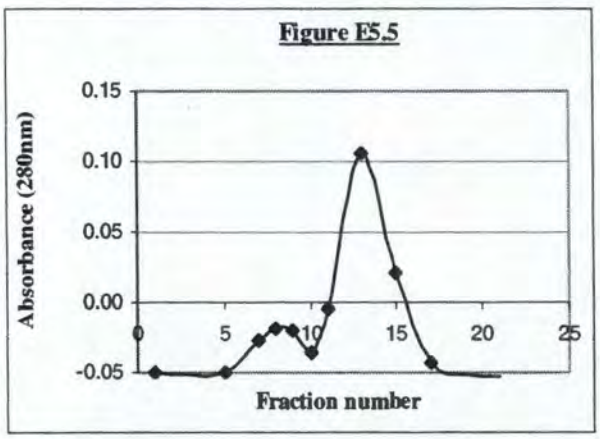

Figure E6: Desalting chromatograms of demineralised CaOx crystals precipitated from white stone-formers' urine. The subjects are WSF1 (Fig E6.1), WSF2 (Fig E6.2), WSF3 (Fig E6.3), WSF4 (Fig E6.4) and WSF5 (Fig E6.5).

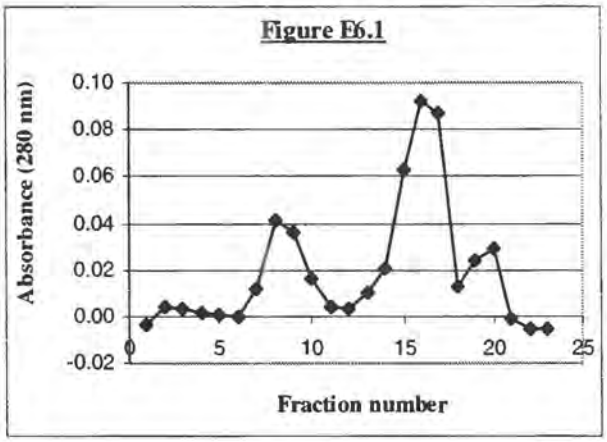

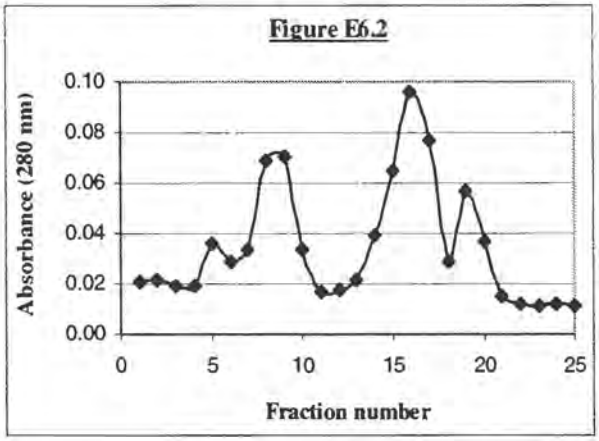

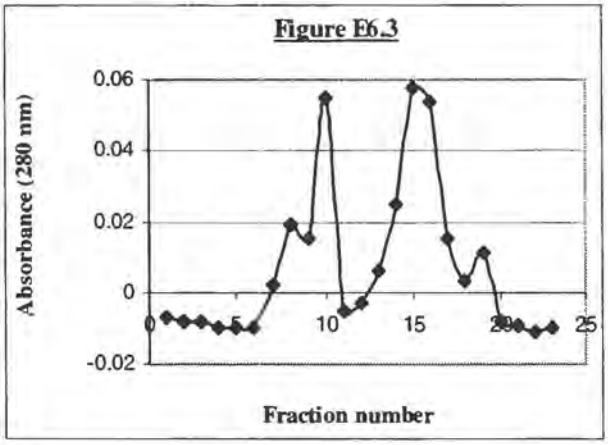

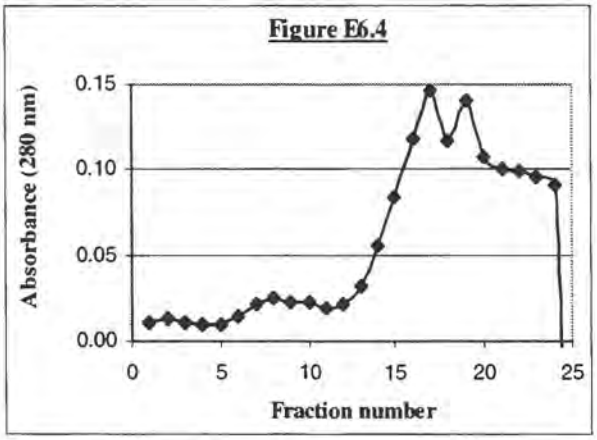

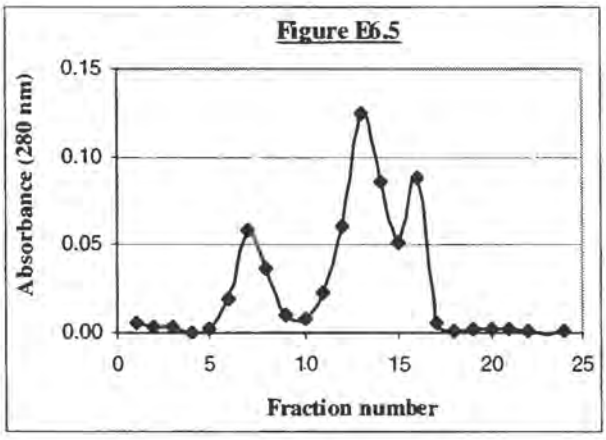

APPENDIX F: TABLES

Table F1.1: X-ray powder diffraction peak assignments and percentage composition of CaOx crystals precipitated from the urine of black group 1

Ca (mmol/l)	d-spacing (Å)	Assignment	Composition: % COM	% COD
0.50	6.02	COM		
	3.69	COM		
	2.99	COM		
	2.50	COM		
	2.40	COM	100	0
1.02*	6.02	COM		
	3.69	COM		
	2.99	COM		
	2.80	COM		
	2.51	COM	100	0
2.00	6.10	COD		
	4.51	COM		
	3.69	COM		
	3.01	COM		
	2.80	COD		
	2.51	COM	55	45
4.00	5.94	COM		
	3.66	95% COM, 5% COD		
	3.11	COD		
	3.01	COM		
	2.80	COD		
	2.51	COM	75	25
8.00	6.28	COD		
	6.02	COM		
	4.51	COD		
	3.69	COM		
	3.13	COD		
	2.99	COM		
	2.80	COD		
	2.42	30% COM, 70% COD	30	70

**Control urine, i.e. unadjusted Ca*

Table F1.2: X-ray powder diffraction peak assignments and percentage composition of CaOx crystals precipitated from the urine of black group 2

Ca (mmol/l)	d-spacing (Å)	Assignment	Composition: % COM	% COD
0.64*	6.02	COM		
	3.69	COM		
	2.99	COM		
	2.51	COM	100	0
1.00	6.19	COD		
	6.02	COM		
	3.69	COM		
	2.99	COM		
	2.80	COD		
	2.51	COD	55	45
2.00	6.19	COD		
	6.02	COM		
	4.46	COD		
	3.69	COM		
	2.99	COM		
	2.80	COD		
	2.51	COM		
	2.41	30% COM, 70% COD	45	55
4.00	5.94	COM		
	4.46	COD		
	3.69	COM		
	3.09	COD		
	2.97	COM		
	2.80	COD		
	2.35	COM	70	30
8.00	5.86	COM		
	3.69	COM		
	2.80	COD		
	2.77	COD	50	50

**Control urine, i.e. unadjusted Ca*

Table F1.3: X-ray powder diffraction peak assignments and percentage composition of CaOx crystals precipitated from the urine of black group 3

Ca (mmol/l)	d-spacing (Å)	Assignment	Composition: % COM	% COD
0.50	6.10	COM		
	3.69	COM		
	2.99	COM		
	2.47	COM	100	0
1.23*	6.37	COD		
	6.02	COM		
	4.51	COD		
	3.69	COM		
	3.11	COD		
	3.01	COM		
	2.80	COD		
	2.51	COD	60	40
8.00	6.28	COD		
	4.46	COD		
	3.69	COM		
	3.01	COM		
	2.80	COD		
	2.42	30% COM, 70% COD		
	2.37	COM	45	55
10.0	6.28	COD		
	4.46	COD		
	3.69	COM		
	3.01	COM		
	2.80	COD		
	2.45	COM	35	65
12.0	6.28	COD		
	4.46	COD		
	3.72	COD		
	3.11	COD		
	2.80	COD		
	2.42	COD		
	2.37	COD	0	100
16.0	6.19	COD		
	4.46	COD		
	3.66	COD		
	2.79	COD		
	2.42	COD		
	2.35	COD	0	100

**Control urine, i.e. unadjusted Ca*

Table F2.1: X-ray powder diffraction peak assignments and percentage composition of CaOx crystals precipitated from the urine of white group 1

Ca (mmol/l)	d-spacing (Å)	Assignment	Composition: % COM	% COD
0.50	5.94	COM		
	5.18	unassignable		
	3.63	COM		
	2.97	COM		
	2.31	COM	100	0
1.00	3.70	COM		
	3.03	COM		
	2.84	COM		
	2.46	COM		
	2.31	COM	100	0
2.00	6.19	COM		
	3.70	COM		
	3.01	COM		
	2.80	COM		
	2.53	COM	100	0
4.00	6.19	COM		
	3.70	COM		
	3.01	COM		
	2.51	COM	100	0
6.52*	6.19	COD		
	5.94	COM		
	4.41	COD		
	3.66	95% COM, 5% COD		
	2.97	COM		
	2.80	COD		
	2.41	COD		
	2.35	90% COM, 10% COD	75	25
8.00	6.19	COD		
	4.41	COD		
	3.70	COD		
	3.13	COD		
	2.80	COD		
	2.42	COD		
	2.37	COD	0	100

**Control urine, i.e. unadjusted Ca*

Table F2.2: X-ray powder diffraction peak assignments and percentage composition of CaOx crystals precipitated from the urine of white group 2

Ca (mmol/l)	d-spacing (Å)	Assignment	Composition: % COM	% COD
0.50	6.02	COM		
	3.69	COM		
	3.01	COM		
	2.51	COM		
	2.47	COM	100	0
1.67*	6.02	COM		
	4.55	COM		
	3.69	COM		
	2.99	COM		
	2.51	COM		
	2.47	COM	100	0
8.00	6.28	COD		
	6.02	COM		
	5.86	COM		
	4.46	COD		
	3.69	COM		
	3.13	COD		
	2.80	COD		
	2.41	30% COM, 70% COD	40	60
12.0	6.28	COD		
	4.46	COD		
	3.91	COD		
	3.69	COD		
	2.79	COD		
	2.35	COD	0	100
16.0	6.28	COD		
	4.46	COD		
	3.91	COD		
	3.11	COD		
	2.79	COD		
	2.41	COD		
	2.37	COD	0	100

**Control urine, i.e. unadjusted Ca*

Table F2.3: X-ray powder diffraction peak assignments and percentage composition of CaOx crystals precipitated from the urine of white group 3

Ca (mmol/l)	d-spacing (Å)	Assignment	Composition: % COM	% COD
0.50	6.10	COM		
	3.69	COM		
	3.01	COM		
	2.53	COM	100	0
1.00	6.02	COM		
	3.69	COM		
	3.00	COM		
	2.51	COM	100	0
3.96*	6.28	COD		
	4.46	COD		
	3.69	COD		
	3.11	COD		
	2.79	COD		
	2.41	COD		
	2.37	COD	0	100
10.0	6.19	COD		
	4.46	COD		
	3.69	COD		
	2.79	COD		
	2.41	COD		
	2.35	COD	0	100
12.0	6.19	COD		
	4.41	COD		
	3.69	COD		
	2.79	COD		
	2.61	unassignable		
	2.41	COD		
	2.35	COD	0	100

**Control urine, i.e. unadjusted Ca*

APPENDIX F: FIGURES

Figure F1: X-ray powder diffraction patterns of CaOx crystals precipitated from black males' urines at various calcium concentrations. The patterns are from black group 1's urine at: 0.50 mmol/l Ca (Fig F1.1), 1.02 mmol/l Ca (Fig F1.2), 2.00 mmol/l Ca (Fig F1.3), 4.00 mmol/l Ca (Fig F1.4) and 8.00 mmol/l Ca (Fig F1.5); black group 2's urine at: 0.64 mmol/l Ca (Fig F1.6).

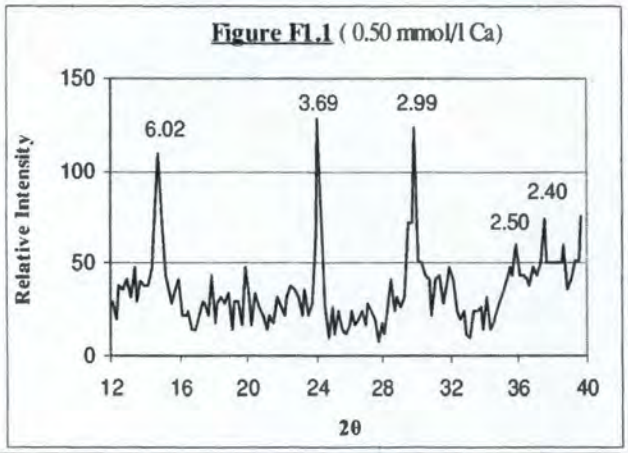

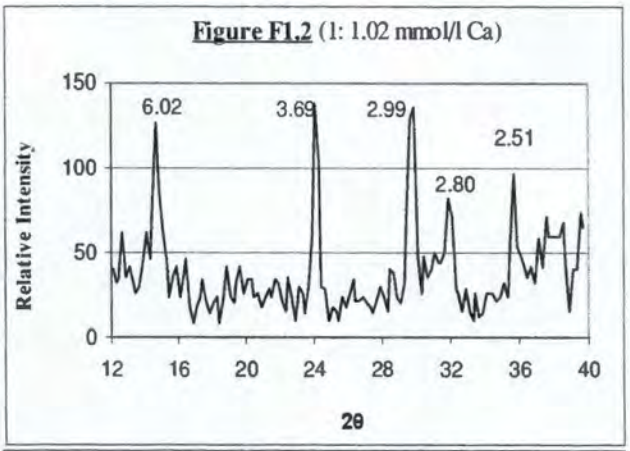

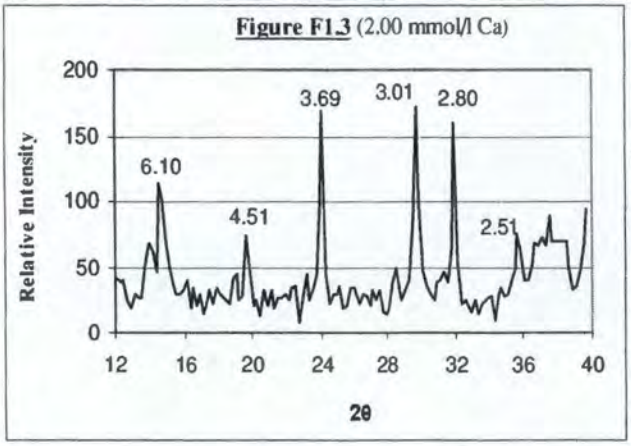

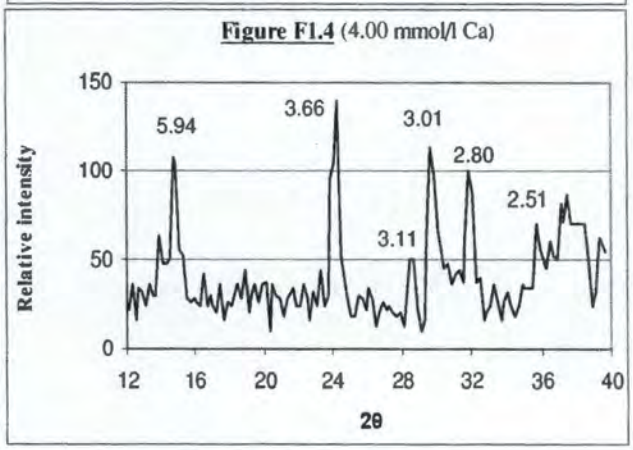

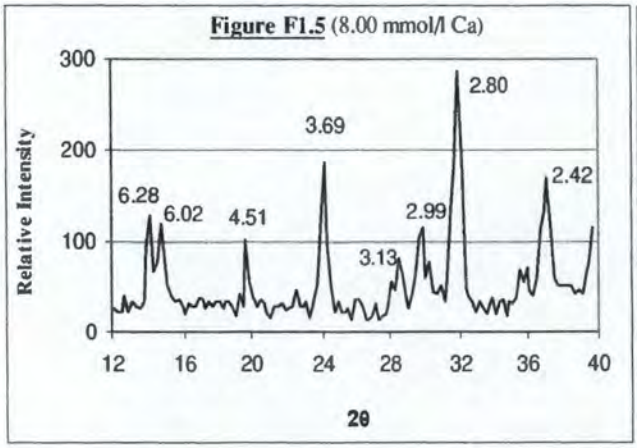

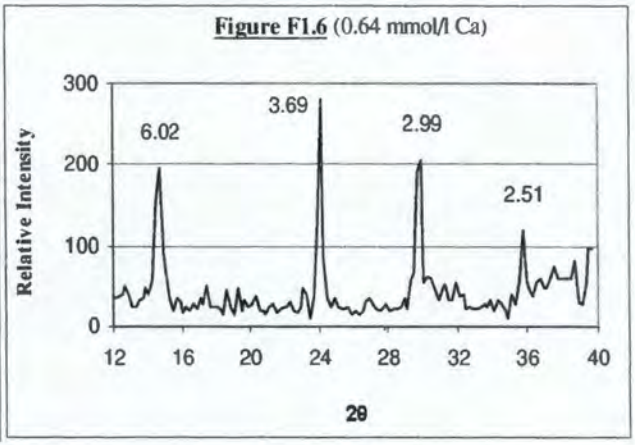

Figure F1: X-ray powder diffraction patterns of CaOx crystals precipitated from black males' urines at various calcium concentrations. The patterns are from black group 2's urine at: 1.00 mmol/l Ca (Fig F1.7), 2.00 mmol/l Ca (Fig F1.8), 4.00 mmol/l Ca (Fig F1.9) and 8.00 mmol/l Ca (Fig F1.10); black group 3's urine at: 0.50 mmol/l Ca (Fig F1.11), 1.23 mmol/l Ca (Fig F1.12).

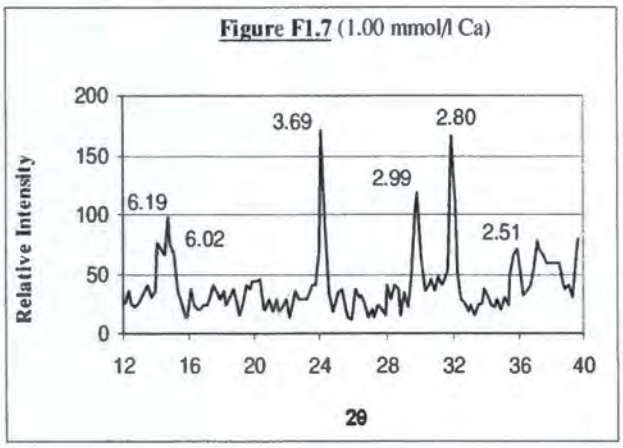

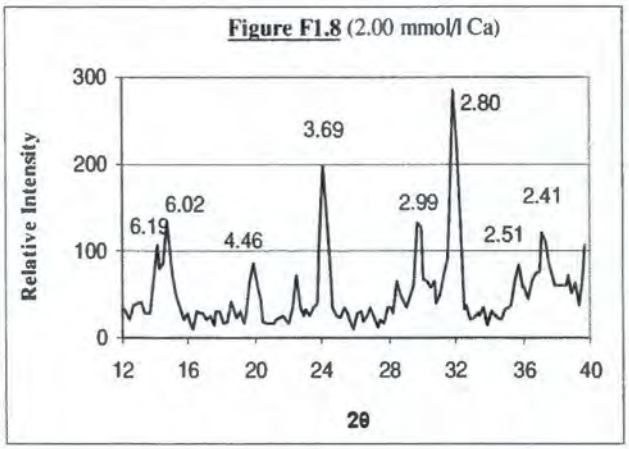

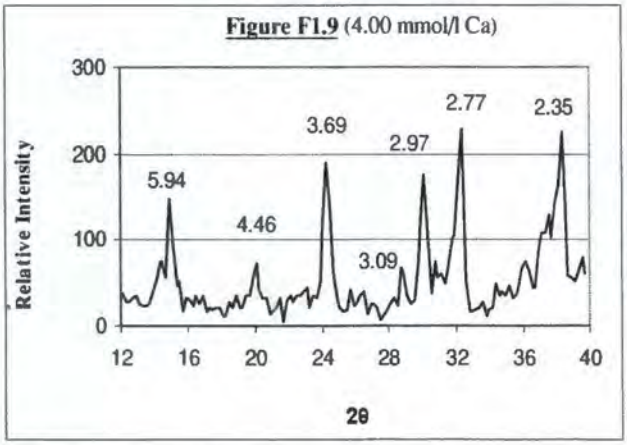

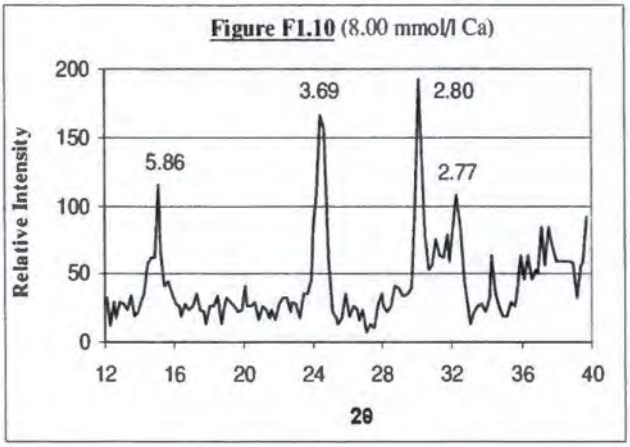

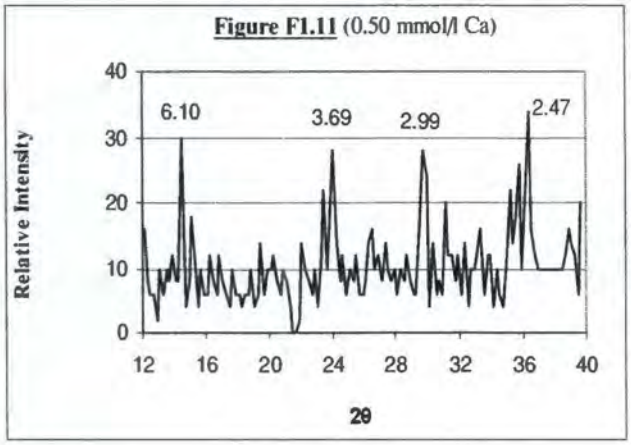

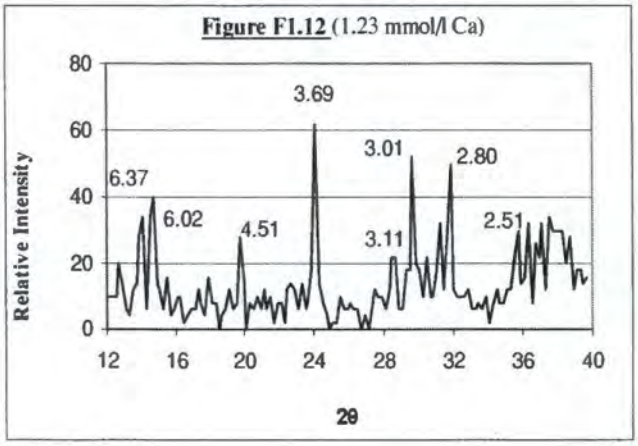

Figure F1: X-ray powder diffraction patterns of CaOx crystals precipitated from black males' urines at various calcium concentrations. The patterns are from black group 3's urine at: 8.00 mmol/l Ca (Fig F1.13), 10.0 mmol/l Ca (Fig F1.14), 12.0 mmol/l Ca (Fig F1.15) and 16.0 mmol/l Ca (Fig F1.16).

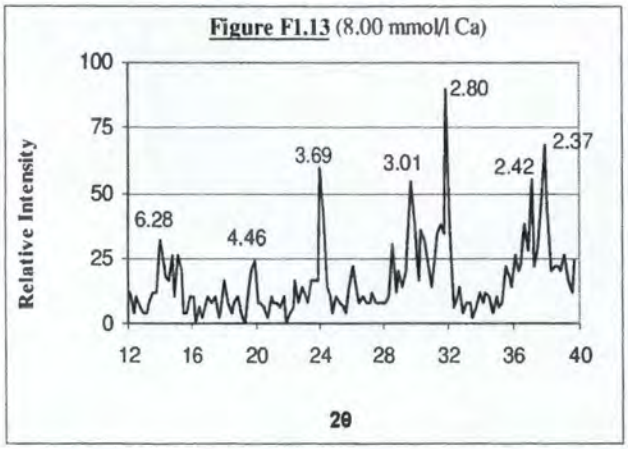

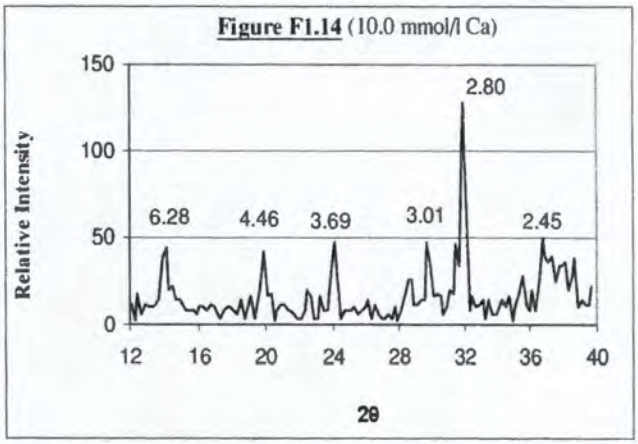

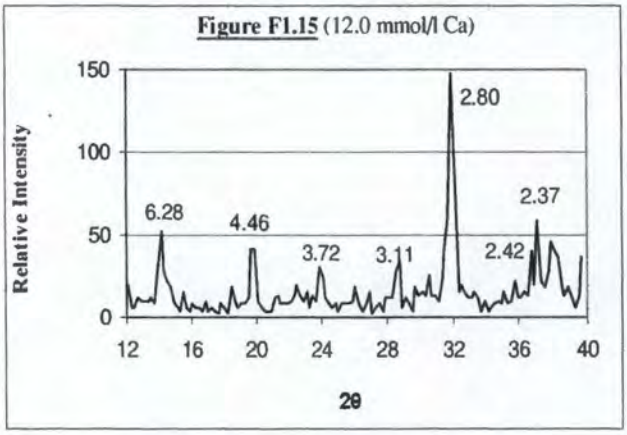

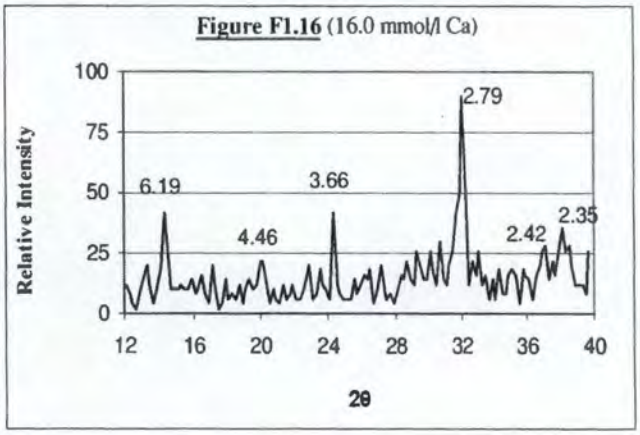

Figure F2: X-ray powder diffraction patterns of CaOx crystals precipitated from white males' urines at various calcium concentrations. The patterns are from white group 1's urine at: 0.50 mmol/l Ca (Fig F2.1), 1.02 mmol/l Ca (Fig F2.2), 2.00 mmol/l Ca (Fig F2.3), 4.00 mmol/l Ca (Fig F2.4), 6.52 mmol/l Ca (Fig F2.5) and 8.00 mmol/l Ca (Fig F2.6).

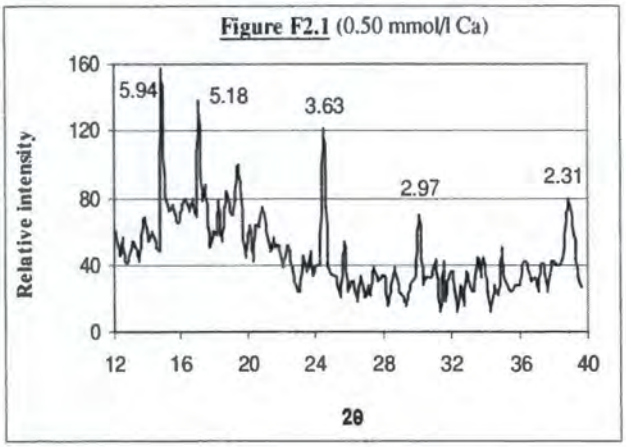

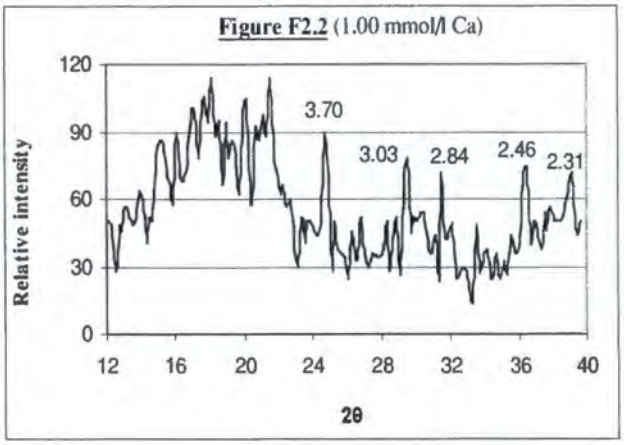

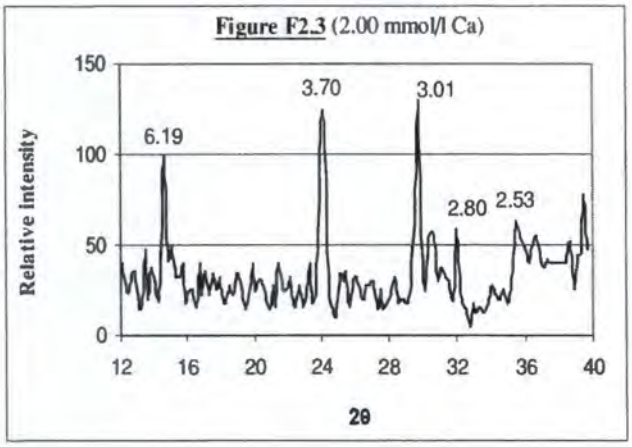

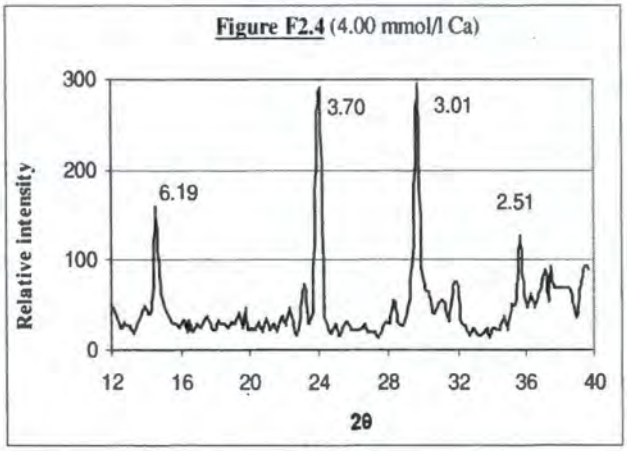

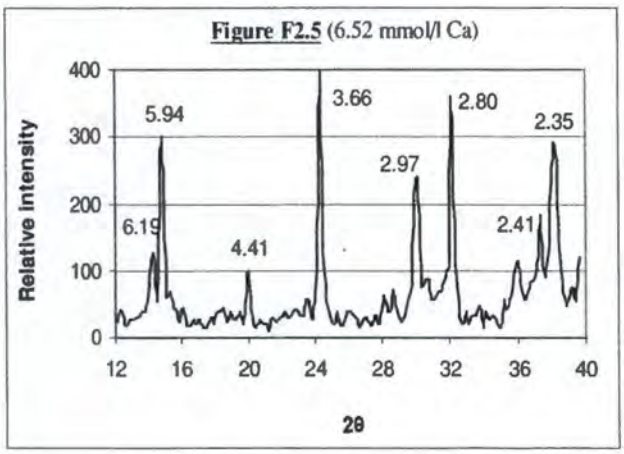

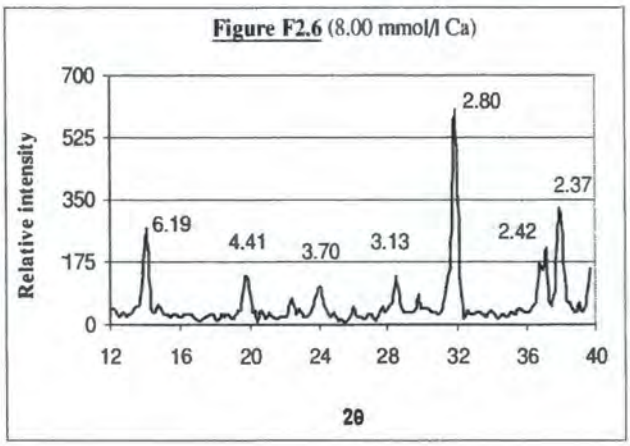

Figure F2: X-ray powder diffraction patterns of CaOx crystals precipitated from white males' urines at various calcium concentrations. The patterns are from white group 2's urine at: 0.50 mmol/l Ca (Fig F2.7), 1.67 mmol/l Ca (Fig F2.8), 8.00 mmol/l Ca (Fig F2.9), 12.0 mmol/l Ca (Fig F2.10) and 16.0 mmol/l Ca (Fig F2.11); white group 3's urine at: 0.50 mmol/l Ca (Fig F2.12).

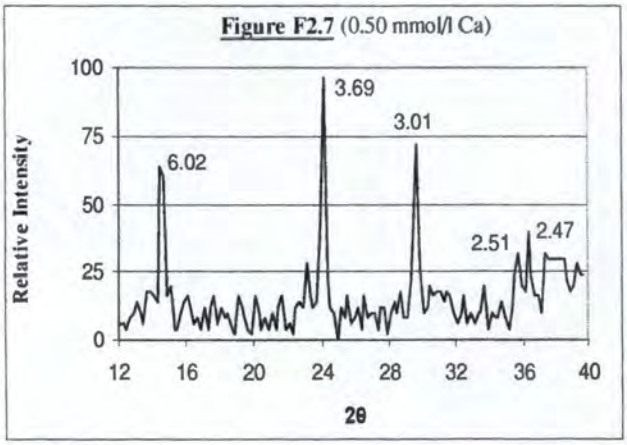

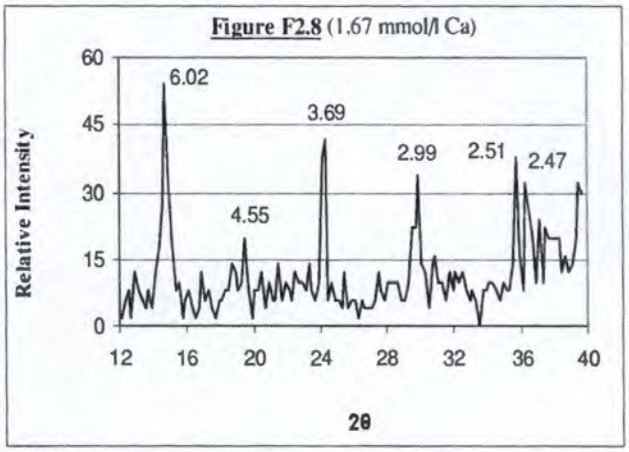

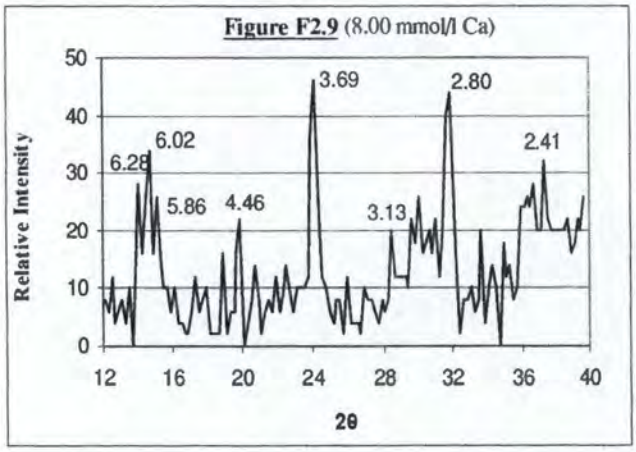

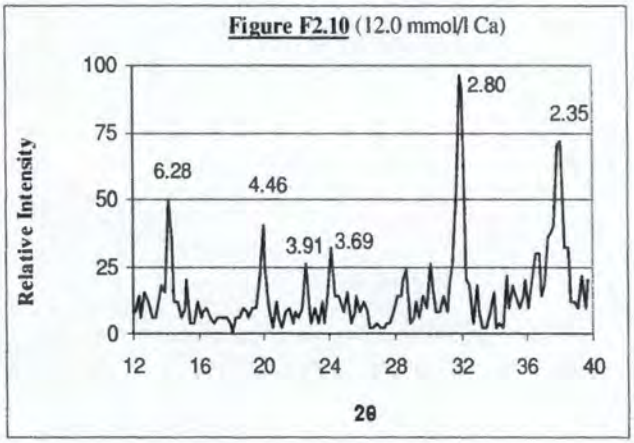

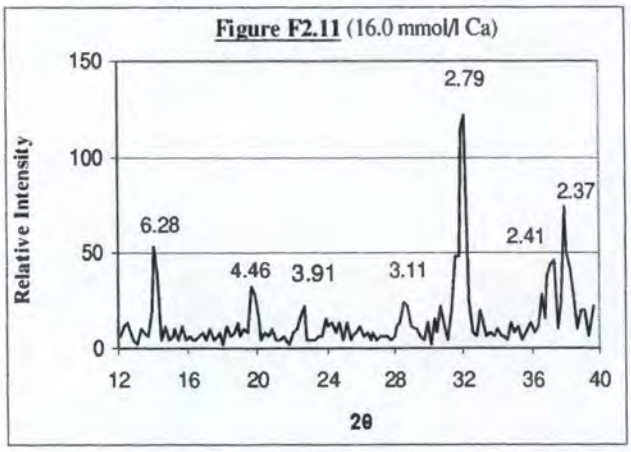

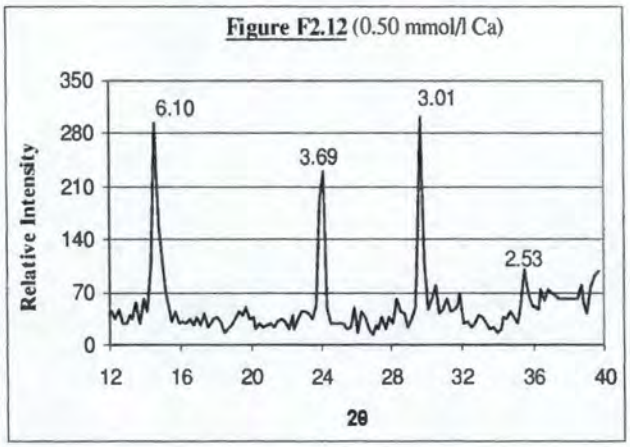

Figure F2: X-ray powder diffraction patterns of CaOx crystals precipitated from white males' urines at various calcium concentrations. The patterns are from white group 3's urine at: 1.00 mmol/l Ca (Fig F2.13), 3.96 mmol/l Ca (Fig F2.14), 10.0 mmol/l Ca (Fig 2.15) and 12.0 mmol/l Ca (Fig F2.16).

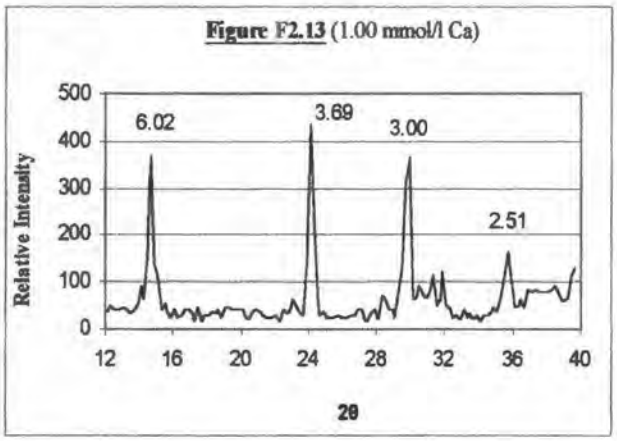

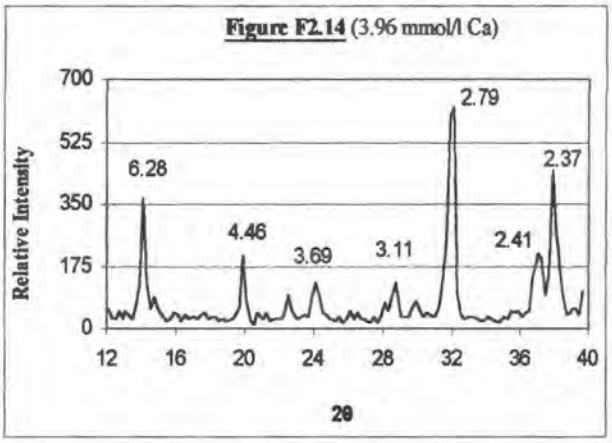

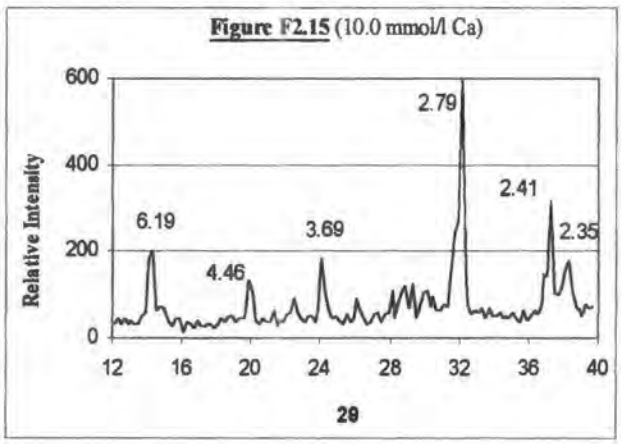

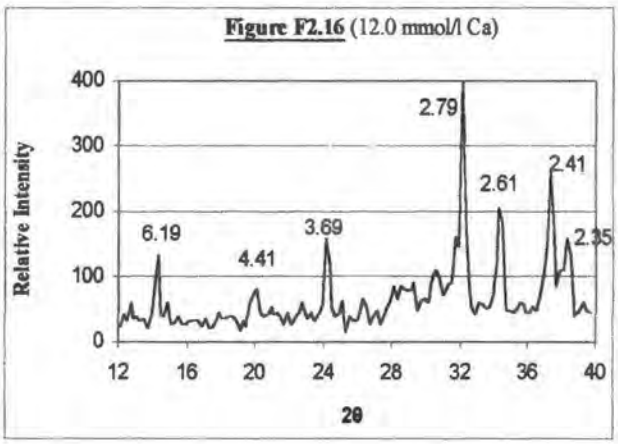

APPENDIX G: TABLES

Table G1: Urine composition (mmol/l) and physicochemical parameters of white and black subjects' pooled urines

Parameters	White subjects:		Black subjects:	
	WF, WUF+WF1 WUF+BF1	WUF	BF, BUF+WF1, BUF+BF1	BUF
pH	6.40	6.55	6.35	6.55
Volume (ml)	9480	5580	9385	7490
Metastable limit (mmol/l)	75	60	135	75
Calcium (mmol/l)	0.969	4.82	1.17	2.28
Chloride (mmol/l)	71.0	124	76.9	96.0
Citrate (mmol/l)	0.916	2.02	0.801	1.40
Creatinine (mmol/l)	7.93	13.9	5.70	8.90
Magnesium (mmol/l)	1.49	3.71	1.28	2.02
Oxalate (mmol/l)	0.112	0.142	0.199	0.116
Phosphate (mmol/l)	12.9	27.1	10.5	12.4
Potassium (mmol/l)	28.3	50.5	23.3	210
Sodium (mmol/l)	59.8	42.3	58.1	79.4
Uric acid (mmol/l)	1.91	3.58	1.69	2.10

Table G2: Preparation of saturated and unsaturated CaOx* buffers

Solution	Preparation
Saturated CaOx **	Add excess CaOx to a 10 mmol/l NaCl solution (*ca.* 10 g to 500 ml) and stir while heating to 90 ^{0}C for 15 min, agitate the solution at 37 ^{0}C and 100 rpm for 3 nights. Add Tris at a final concentration of 12.5 mmol/l, adjust the pH and store the suspension at 37 ^{0}C.
Unsaturated CaOx	Add *ca.* 10 g CaOx to a 12.5 mmol/l Tris solution (500 ml, pH 6.0) and agitate at 37 ^{0}C and 100 rpm for 3 nights. Store the suspension at 37 ^{0}C.

* *Commercially available COM crystals were used to prepare the CaOx solutions.*
** *The excess CaOx was removed by filtration (0.22 μm) at room temperature.*

APPENDIX H

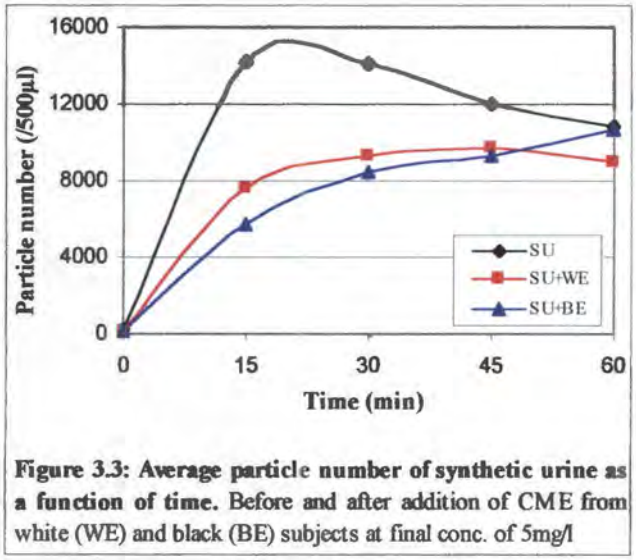

Figure 3.3: Average particle number of synthetic urine as a function of time. Before and after addition of CME from white (WE) and black (BE) subjects at final conc. of 5mg/l

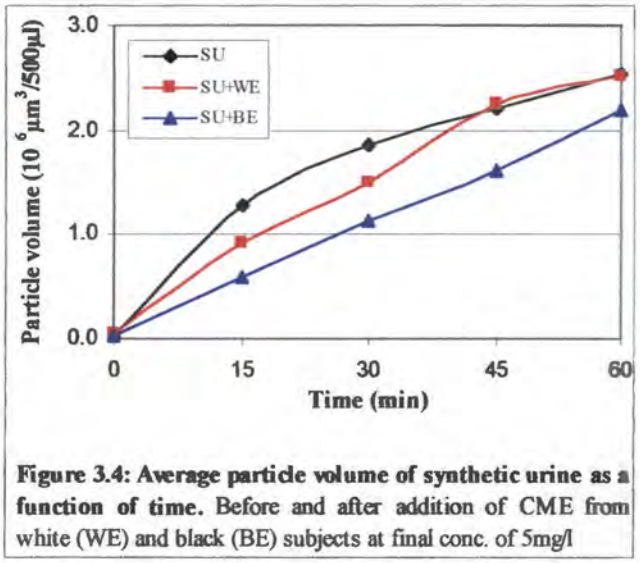

Figure 3.4: Average particle volume of synthetic urine as a function of time. Before and after addition of CME from white (WE) and black (BE) subjects at final conc. of 5mg/l

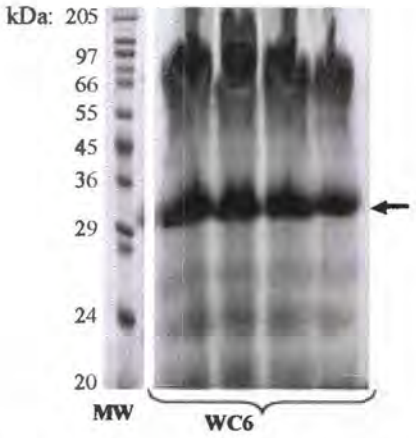

Figure 4.7: SDS-PAGE of crystal matrix extract from white control subject WC6.